

HYDROCATALYSIS: A New Energy Paradigm

for the 21st Century

by

Peter Mark Jansson, P.P., P.E.

A Thesis

**Submitted in partial fulfillment of the requirements of the
Master of Science in Engineering Degree
in the Graduate Division of
Rowan University
May 1997**



HYDROCATALYSIS: A New Energy Paradigm
for the 21st Century

by
Peter Mark Jansson, P.P., P.E.

A Thesis

Submitted in partial fulfillment of the requirements of the
Master of Science in Engineering Degree
in the Graduate Division of
Rowan University
May 1997

Approved by 
Dr. John L. Schmalzel

Approved by 
Dr. Tirupathi R. Chandrupatla

Approved by _____
Dr. Anthony J. Marchese

External Advisors

Dr. Jonathan Phillips - Pennsylvania State University
Dr. Randell L. Mills - BlackLight Power, Inc.
William R. Good - BlackLight Power, Inc.



Copyright © 1997 by Peter Mark Jansson

All rights reserved. No part of this publication may be reproduced or transmitted in any form or by any means, electronic or mechanical, including photocopy, recording, or any information storage and retrieval system now known or to be invented, without prior permission in writing from the author, except by a reviewer or other researcher who wish to quote brief passages in connection with a review written for inclusion in a magazine, newspaper, internet web page, broadcast or research for other scholarly purposes.

Library of Congress - Cataloguing in Progress

Published in the United States by
Peter Mark Jansson, P.P.,P.E.
Integrated Systems
P.O. Box 4
Tuckerton, New Jersey, 08087-0004



to *Joy*,

who encouraged me to return to college
ever since we left



HYDROCATALYSIS: A NEW ENERGY PARADIGM FOR THE 21st CENTURY

TABLE OF CONTENTS

	Page
Table of Contents	i
List of Tables	iii
List of Figures	iv
 Abstract	
Mini Abstract	
 <u>Introduction and Thesis Overview</u>	1
 <u>PART I - An Energy Technology Overview</u>	2
<i>Chapter 1 - Alternate Technology Overview</i>	4
1.1 Fossil Fuels	5
1.2 Nuclear Energy - Fission & Fusion	11
1.3 Solar Energy	14
1.4 Geothermal Energy	19
1.5 Tidal Energy	20
<i>Chapter 2 - Overview of Mills Technology</i>	21
2.1 HydroCatalysis - A Theoretical Overview	22
2.2 Astrophysical Corroboration	25
2.3 Enigmas Solved	28
2.4 Technological Embodiments	29
 <u>PART II - Analysis of Previous Experimental Results</u>	36
<i>Chapter 3 - Summary Review of Gas Phase Cell Experimental Results</i>	36
3.1 BlackLight Power Isothermal Cell	37
3.2 Penn State University Calvet	39
3.3 Jansson Calvet	41

HYDROCATALYSIS:
A NEW ENERGY PARADIGM FOR THE 21st CENTURY

TABLE OF CONTENTS
[continued]

	Page
<u>PART III - Mathematical Model</u>	52
<i>Chapter 4 - Analysis of Model Performance vs. Experimental Results</i>	52
<i>Chapter 5 - Key Learnings and Insights from Model</i>	57
<u>PART IV - Implications for the Future</u>	63
<i>Chapter 6 - Implications for the Future and Recommended Next Steps</i>	64
<u>PART V - Reference Materials</u>	66
Footnotes	67
<u>Description of Appendices</u>	72

List of Appendices

- Appendix 1. BLP Research Partners - Catalogue of Experimental Results
- Appendix 2. An Overview of Mills Theory
- Appendix 3. Jansson Astrophysical Data Calculations verifying BLP
Reported Results
- Appendix 4. BLP/AEI Experiment 15.6 - May 1996
- Appendix 5. Analysis of BLP Isothermal Calorimetry Data
- Appendix 6. PSU Calvet Test Results and Report - December 1996
- Appendix 7. Jansson Calvet Testing Protocol
- Appendix 8. Jansson Calvet Test Results - June 1997
- Appendix 9. Jansson Heat Loss Model Calibration & Performance

HYDROCATALYSIS:
A NEW ENERGY PARADIGM FOR THE 21st CENTURY

LIST OF TABLES

	Page
TABLE 1.1 - 1995 Energy Use by Fuel Type	3
TABLE 1.2 - Energy Sources and Technologies	4
TABLE 1.3 - Energy Release Processes for Fossil Fuels	5
TABLE 1.4 - Fossil Fuel Reserves and Resource Lifetimes	7
TABLE 1.5 - Energy Release Processes for Nuclear Fuels	12
TABLE 1.6 - Nuclear Fission By-Products Radioactive Half-lives	13
TABLE 2.1 - BlackLight Power Research Partners	21
TABLE 2.2 - Energy Released From Lower Energy Hydrogen	23
TABLE 2.3 - Commonly Observed Wavelengths & Mills Theory	28
TABLE 2.4 - BLP Technologies	30
TABLE 2.5 - The Search for Hydrinos	34
TABLE 3.1 - Isothermal Cell Results Summary	39
TABLE 3.2 - Penn State Calvet Cell Results Summary	40
TABLE 3.3 - Jansson Calvet Testing Objectives	41
TABLE 3.4 - Jansson Calvet Tests Completed	42
TABLE 3.5 - Jansson Calvet Testing Protocol Summary - Control	42
TABLE 3.6 - Jansson Calvet Testing Protocol Summary - Exps.	43
TABLE 3.7 - Jansson Calvet Testing - Calibration Curves	43
TABLE 3.8 - Jansson Calvet Cell Results Summary	44
TABLE 4.1 - Isothermal Cell Results - May 3-4, 1996	52
TABLE 4.2 - Isothermal Cell Heat Loss vs. Temperature	53
TABLE 6.1 - Global Reports/Observations on BLP Technology	63

Appendix 2

TABLE A.1 - Mills' Theory Predictions

TABLE A.2 - The Electron Orbitsphere

HYDROCATALYSIS:
A NEW ENERGY PARADIGM FOR THE 21st CENTURY

LIST OF FIGURES

	Page
FIGURE 1.1 - Relationship Between Energy Consumption and Economic Activity (1971)	9
FIGURE 1.2 - Per Capita GNP vs. Per Capita Energy Consumption (1987)	10
FIGURE 1.3 - Neutron Induced Fission of ²³⁵ U	11
FIGURE 1.4 - PV Historical Costs 1958-1996	18
FIGURE 2.1 - Quantized Sizes of Hydrogen Atoms	24
FIGURE 2.2 - Astrophysical Observations and Mill's Theory	27
FIGURE 2.3 - Astrophysical Data vs. Mill's Theory Illustrated	27
FIGURE 2.4 - Dewar Experimental Vessel	31
FIGURE 2.5 - Advanced Electrolytic Cell	31
FIGURE 2.6 - Non-Electrolytic Gas Phase Cell	32
FIGURE 2.7 - Isothermal Calorimeter Gas Phase Cell	32
FIGURE 2.8 - Calvet Calorimeter Gas Phase Cell	33
FIGURE 2.9 - XPS Anomalous 55 eV Peaks	35
FIGURE 3.1 - Excess Power vs. Filament Length	45
FIGURE 3.2 - Summary of 10 cm Experimental Results	46
FIGURE 3.3 - Calibration Curve 10 cm. Control	47
FIGURE 3.4 - Summary of 20 cm Experimental Results	48
FIGURE 3.5 - Calibration Curve 20 cm. Control	49
FIGURE 3.6 - Summary of 30 cm Experimental Results	50
FIGURE 3.7 - Calibration Curve 30 cm. Control	51
FIGURE 4.1 - Isothermal Cell Performance May 4, 1996	54
FIGURE 4.2 - Isothermal Model vs. Actual Performance	55
FIGURE 4.3 - Isothermal Cell Heat Loss vs. Temperature	56

Appendix 2

- FIGURE A.1 - The Electron Orbitsphere
- FIGURE A.2 - The Electron Orbitsphere

ABSTRACT

Peter Mark Jansson, P.P., P.E.
HYDROCATALYSIS: A NEW ENERGY PARADIGM FOR THE 21st CENTURY
May 1997
Dr. John L. Schmalzel, P.E. - Thesis Advisor
Graduate Engineering Department

This thesis will review the problems of worldwide energy supply, describe the current technologies that meet the energy needs of our industrial societies, summarize the environmental impacts of those fuels and technologies and their increased use by a growing global and increasingly technical economy. This work will also describe and advance the technology being developed by BlackLight Power, Inc. [BLP], a scientific company located in Malvern, Pennsylvania. BLP's technology propoerts to offer commercially viable and useful heat generation via a previously unrecognized natural phenomenon - the catalytic reduction of the hydrogen atom to a lower energy state. A review of this experimenter's laboratory data conducted as part of this research as well as that of others is provided to substantiate the fact that replication of the experimental conditions which are favorable to initiating and sustaining the new energy release process will generate controllable, reproducible, sustainable and commercially meaningful heat. By the end of the thesis the reader will have substantial information to draw a conclusion for themselves as to the potential of BLP technology to achieve commercialization and become a new energy paradigm for the next century.



MINI-ABSTRACT

Peter Mark Jansson, P.P., P.E.

HYDROCATALYSIS: A NEW ENERGY PARADIGM FOR THE 21st CENTURY

May 1997

Dr. John L. Schmalzel, P.E. - Thesis Advisor
Graduate Engineering Department

This thesis reviews the technologies used worldwide to meet the energy needs of our industrial societies. This work also describes a new technology being developed by BlackLight Power, Inc. [BLP] of Malvern, Pennsylvania. Laboratory data of the author as well as that of other scientists substantiates that the new BLP energy release process generates sustainable, commercially meaningful heat.

[illegible]

2	1	2	3	4	5	6	7	8	9	10	11	12	13	14	15	16	17	18	19	20	21	22	23	24	25	26	27	28	29	30	31	32	33	34	35	36	37	38	39	40	41	42	43	44	45	46	47	48	49	50	51	52	53	54	55	56	57	58	59	60	61	62	63	64	65	66	67	68	69	70	71	72	73	74	75	76	77	78	79	80	81	82	83	84	85	86	87	88	89	90	91	92	93	94	95	96	97	98	99	100	101	102	103	104	105	106	107	108	109	110	111	112	113	114	115	116	117	118	119	120	121	122	123	124	125	126	127	128	129	130	131	132	133	134	135	136	137	138	139	140	141	142	143	144	145	146	147	148	149	150	151	152	153	154	155	156	157	158	159	160	161	162	163	164	165	166	167	168	169	170	171	172	173	174	175	176	177	178	179	180	181	182	183	184	185	186	187	188	189	190	191	192	193	194	195	196	197	198	199	200	201	202	203	204	205	206	207	208	209	210	211	212	213	214	215	216	217	218	219	220	221	222	223	224	225	226	227	228	229	230	231	232	233	234	235	236	237	238	239	240	241	242	243	244	245	246	247	248	249	250	251	252	253	254	255	256	257	258	259	260	261	262	263	264	265	266	267	268	269	270	271	272	273	274	275	276	277	278	279	280	281	282	283	284	285	286	287	288	289	290	291	292	293	294	295	296	297	298	299	300	301	302	303	304	305	306	307	308	309	310	311	312	313	314	315	316	317	318	319	320	321	322	323	324	325	326	327	328	329	330	331	332	333	334	335	336	337	338	339	340	341	342	343	344	345	346	347	348	349	350	351	352	353	354	355	356	357	358	359	360	361	362	363	364	365	366	367	368	369	370	371	372	373	374	375	376	377	378	379	380	381	382	383	384	385	386	387	388	389	390	391	392	393	394	395	396	397	398	399	400	401	402	403	404	405	406	407	408	409	410	411	412	413	414	415	416	417	418	419	420	421	422	423	424	425	426	427	428	429	430	431	432	433	434	435	436	437	438	439	440	441	442	443	444	445	446	447	448	449	450	451	452	453	454	455	456	457	458	459	460	461	462	463	464	465	4
---	---	---	---	---	---	---	---	---	---	----	----	----	----	----	----	----	----	----	----	----	----	----	----	----	----	----	----	----	----	----	----	----	----	----	----	----	----	----	----	----	----	----	----	----	----	----	----	----	----	----	----	----	----	----	----	----	----	----	----	----	----	----	----	----	----	----	----	----	----	----	----	----	----	----	----	----	----	----	----	----	----	----	----	----	----	----	----	----	----	----	----	----	----	----	----	----	----	----	----	-----	-----	-----	-----	-----	-----	-----	-----	-----	-----	-----	-----	-----	-----	-----	-----	-----	-----	-----	-----	-----	-----	-----	-----	-----	-----	-----	-----	-----	-----	-----	-----	-----	-----	-----	-----	-----	-----	-----	-----	-----	-----	-----	-----	-----	-----	-----	-----	-----	-----	-----	-----	-----	-----	-----	-----	-----	-----	-----	-----	-----	-----	-----	-----	-----	-----	-----	-----	-----	-----	-----	-----	-----	-----	-----	-----	-----	-----	-----	-----	-----	-----	-----	-----	-----	-----	-----	-----	-----	-----	-----	-----	-----	-----	-----	-----	-----	-----	-----	-----	-----	-----	-----	-----	-----	-----	-----	-----	-----	-----	-----	-----	-----	-----	-----	-----	-----	-----	-----	-----	-----	-----	-----	-----	-----	-----	-----	-----	-----	-----	-----	-----	-----	-----	-----	-----	-----	-----	-----	-----	-----	-----	-----	-----	-----	-----	-----	-----	-----	-----	-----	-----	-----	-----	-----	-----	-----	-----	-----	-----	-----	-----	-----	-----	-----	-----	-----	-----	-----	-----	-----	-----	-----	-----	-----	-----	-----	-----	-----	-----	-----	-----	-----	-----	-----	-----	-----	-----	-----	-----	-----	-----	-----	-----	-----	-----	-----	-----	-----	-----	-----	-----	-----	-----	-----	-----	-----	-----	-----	-----	-----	-----	-----	-----	-----	-----	-----	-----	-----	-----	-----	-----	-----	-----	-----	-----	-----	-----	-----	-----	-----	-----	-----	-----	-----	-----	-----	-----	-----	-----	-----	-----	-----	-----	-----	-----	-----	-----	-----	-----	-----	-----	-----	-----	-----	-----	-----	-----	-----	-----	-----	-----	-----	-----	-----	-----	-----	-----	-----	-----	-----	-----	-----	-----	-----	-----	-----	-----	-----	-----	-----	-----	-----	-----	-----	-----	-----	-----	-----	-----	-----	-----	-----	-----	-----	-----	-----	-----	-----	-----	-----	-----	-----	-----	-----	-----	-----	-----	-----	-----	-----	-----	-----	-----	-----	-----	-----	-----	-----	-----	-----	-----	-----	-----	-----	-----	-----	-----	-----	-----	-----	-----	-----	-----	-----	-----	-----	-----	-----	-----	-----	-----	-----	-----	-----	-----	-----	-----	-----	-----	-----	-----	-----	-----	-----	-----	-----	-----	-----	-----	-----	-----	-----	-----	-----	-----	---

HYDROCATALYSIS: **A New Energy Paradigm for the 21st Century**

Introduction and Thesis Overview

This thesis will review the problems of worldwide energy supply, describe the current technologies that meet the energy needs of our industrial societies, summarize the environmental impacts of those fuels and technologies and their increased use by a growing global and increasingly technical economy. After reviewing both the renewable and non-renewable options we have as a society, this work will describe and advance the technology being developed by BlackLight Power, Inc. [BLP], a scientific company located in Malvern, Pennsylvania. BLP's technology purports to offer commercially viable and useful heat generation via a previously unrecognized natural phenomenon - the catalytic reduction of hydrogen to a lower energy state. This reduction of hydrogen to fractional quantum energy levels is based upon a radical modification to the theoretical hydrogen atom energy equation developed by E. Schrödinger and W. Heisenberg in 1926. Dr. Randell Mills of BLP has proposed that a new boundary condition, derived from Maxwell's equations, be applied to that fundamental hydrogen equation. Dr. Mills' model then would suggest a purely physical model of particles, atoms, molecules and overall cosmology. His mathematical solutions contain fundamental constants only and energy values predicted by his theoretical approach agree in a most compelling way with observations scientists have made of the universe and stars.

This source of energy is purported to comprise a significant portion of the radiant energy created by stars. The new form of hydrogen atoms with their electrons below the current "ground" state have been named "hydrinos" by their discoverer, Dr. Mills. BLP scientists believe it is this matter that comprises the significant part of the dark matter of space. It will not be the attempt of this engineering thesis to debate the merits of Dr. Mills' theory in this regard but rather to review and sometimes replicate the scientific calculations and supporting data which indicate the merits of the existence of hydrinos. This thesis will also review this experimenter's laboratory data as well as that of others that substantiates the fact that replication of the experimental conditions which are favorable to initiating and sustaining the new disproportionation process will generate controllable, reproducible, sustainable and commercially meaningful heat. It will describe the technologies currently used in the disproportionation reaction, report on the state-of-the-art for the BLP technology and state the author's opinion as to this technology's potential for successfully addressing [or solving] some of the global energy issues above. [environmental degradation from growing energy use, limits to energy supply at forecasted growth rates, etc.]



use coal for heating as well as wind and water power for grinding grains [26,000 kcal daily per capita - 30.2 kWh]. During the Industrial age of the 19th century we added the steam engine as a source of mechanical energy and increased the use of fuel energy in homes for lighting and heating [77,000 kcal daily per capita - 89.3 kWh]. Modern technological society uses the internal combustion engine for transportation, electricity for appliances and comfort which find their energy source in fossil, hydro and nuclear fuels which power steam turbines, furnaces and generators [230,000 kcal daily per capita - 266.8 kWh daily per capita].^[2] This trend indicates that as we improve the quality of life for society a commensurate increase in direct and indirect energy use is requisite. World energy and economic statistics today also demonstrate that there is a direct correlation between a nation's gross national product [GNP] and its energy consumption. The countries of Ethiopia, Mali, Malawi and Niger all have GNPs less than \$250 per capita while energy use is less than 0.4 barrels of oil per capita per year [680 kWh/year]. In contrast, the U.S., Norway, Canada and Sweden are leading economic nations with over \$10,000 of GNP per capita. They use in excess of 40 barrels of oil per capita per year [68,000 kWh].^[3] This one hundredfold increase in energy use is not a coincidence. It is characteristic of a steady evolution of society from a primitive [2.3 kWh] to technological [266.8 kWh] level of advancement and is illustrative of the critical role energy plays in increasing societal maturity, quality of life and productivity.

The sections which follow illustrate the fuels, technologies and methods used around the world to sustain this societal evolution and summarize limits on these elements which must be addressed in order to avoid major problems as the now developing nations [where over 3/4 of the world's population resides] strive to achieve western standards of living through industrialization. Table 1.1 below summarizes the current levels of energy use in the world and U.S. as of 1995.

TABLE 1.1 - 1995 Energy Use by Fuel Type
(in trillions of kilowatthours)

Energy Source		World	U.S.	U.S. % of World
Fossil Fuels	Natural Gas	22.7	6.6	29.2 %
	Petroleum	39.5	10.1	25.5 %
	Coal	26.8	6.1	22.9 %
Nuclear	Fission	7.1	2.2	30.3 %
Solar	HydroElectric	2.5	0.3	10.6 %
TOTAL		98.8	25.3	25.6 %

It is important to note that only commercially traded fuels are included in the summary data. The overview provided in Chapter 1 of this thesis presents the energy sources in an order prioritized by the contributions these sources make to industrialized society today.

Chapter 1 - Alternate Technology Overview

Prior to the announcement of the hydrocatalysis process being put forth by BlackLight Power there were fundamentally only five known sources of energy. In addition to the most commonly exploited, fossil fuels, there are nuclear [both fission and fusion], solar [in its many forms], geothermal and tidal.^[4] Table 1.2 below briefly summarizes the major energy sources available in our society.

TABLE 1.2 - Energy Sources and Technologies

Energy Source	Fuel Type	Technologies in Use
Fossil Fuels	Natural Gas Petroleum Coal Shale Oil Tar Sands	Heaters, Furnaces, Boilers, etc. Heaters, Furnaces, Boilers, etc. Heaters, Furnaces, Boilers, etc. Processing facility yields petroleum Processing facility yields petroleum
Nuclear [Fission]	Uranium	PWR creates steam / electricity BWR creates steam / electricity Breeder technology - LMFBR
Nuclear [Fusion]	Plutonium	No Technology Exists as of Yet
Solar	Hydrogen Solar Thermal	Passive & Active Water Htg. Systems Passive & Active Space Htg. Systems Power Tower/Parabolic Dishes / Troughs
	Photovoltaic	Amorphous Cells Crystalline Cells [single, multi, etc.]
	Biomass	Wood, Seaweed, algae, etc. Agricultural Crops [alcohol, waste, etc.] Municipal Solid Waste [paper primarily]
	Hydroelectric	Reservoirs, dams, water wheels, generators, pumped storage
	Wind Power Ocean Waves Ocean Thermal	Wind Mills, Sailing, Turbines [VA/HA] Pilot Systems - Compressor/Generator OTEC Design [1930, 1975]
Geothermal	Geopressured Hot Dry Rock formations Hot Water Res. Normal Grad. Res. Natural Steam Molten Magma	Heaters, Turbine/generators Heaters, Turbine/generators Water and Space Htg. Systems Heaters, Turbine/generators Heaters, Turbine/generators No Technology Exists as of Yet
Tidal	Potential Energy of Earth-Moon-Sun gravity	Reservoirs, dams, generators
Hydrocatalysis	Binding Energy of Hydrogen Atom [p^+ to e^- relationship]	Disproportionation Furnace

For each energy source the types of fuels used and the technologies in use today which convert those fuels into useful work and energy for humans is highlighted.

1.1 Fossil Fuels

In the United States fossil fuels provide 89.2% of the energy we consume. In 1995 this consisted of a combined consumption of coal equivalent to 787 million tons per year, natural gas of about 22 trillion cubic feet per year and petroleum product use of 5.9 billion barrels per year.^[5] It is clear that an industrial society like ours could not continue without these resources. Globally in 1995 our societies consumed 3441 million tons per year of coal, 75 trillion cubic feet per year of natural gas and 23.3 billion barrels per year of petroleum.^[5] The U.S. was the leader in the global use of fossil fuels [specifically petroleum] from the very beginning of its industrialization with the oil strike of Edwin L. Drake in Titusville, Pennsylvania in 1859. "By 1909, when the industry was just 50 years old, the United States was producing 500,000 barrels a day, which was more than was produced by all the other countries combined."^[6] We remained dominant in the petroleum production and manufacturing markets through 1950 when we still produced over 50% of the world's supply. The key reactions for each of the fundamental fossil fuel types are shown below in Table 1.3.

TABLE 1.3 - Energy Release Processes for Fossil Fuels

Fossil Fuel Type	Chemical Reaction[s]	By- Products
Natural Gas 85% Methane[CH ₄] 15% Ethane[C ₂ H ₆]	$\text{CH}_4 + 2\text{O}_2 \rightarrow \text{CO}_2 + 2(\text{H}_2\text{O})$	CO ₂ , CO, water, hydrocarbons and heat [exothermic reaction]
Bottled Gas Propane [C ₃ H ₈] Butane [C ₄ H ₁₀]	$2\text{C}_3\text{H}_8 + 9\text{O}_2 \rightarrow 4\text{CO}_2 + 2\text{CO} + 8(\text{H}_2\text{O})$	CO ₂ , CO, water, hydrocarbons and heat [exothermic reaction]
Petroleum Gasoline Pentane[C ₅ H ₁₂] Hexane [C ₆ H ₁₄] Heptane[C ₇ H ₁₆] Octane [C ₈ H ₁₈]	$\text{C}_8\text{H}_{18} + 12\text{O}_2 \rightarrow 7\text{CO}_2 + \text{CO} + 9(\text{H}_2\text{O})$	CO ₂ , CO, water, hydrocarbons and heat [exothermic reaction]
Coal contains carbon plus impurities	$\begin{aligned} \text{C} + \text{O}_2 &\rightarrow \text{CO}_2 + \text{CO} \\ \text{S} + \text{O}_2 &\rightarrow \text{SO}_2 \text{ [plus SO}_x\text{]} \\ \text{N} + \text{O}_2 &\rightarrow \text{NO}_2 \text{ [plus NO, NO}_3\text{, NO}_x\text{]} \end{aligned}$	CO ₂ , CO, SO ₂ , NO ₂ , water, hydrocarbons, SO _x , NO _x , particulates, etc. and heat [exothermic reaction]

It is important to note at this point that all fossil fuels release their energy to man through the chemical reduction process known as oxidation. In this reaction the energy that has been stored in carbon and hydrocarbon chains created during the early history of the earth [250-500 million years ago] is released. In this chemical reaction oxygen combines with the carbon fuel in the presence of heat to release additional heat and form water, carbon-dioxide as well as a host of other hydrocarbons and by-products.

The impact on the environment of the use of the stored chemical energy provided in fossil fuels is significant. "One example is the added burden of carbon dioxide in the earth's atmosphere, with its corresponding potential for modifying the world's climate. Other examples . . . include the acidification of the atmosphere and surface waters, . . . early deaths of thousands by sulfur dioxide in the air, . . . ozone formation, . . . problems of coal mining, . . . acid drainage, . . . carbon monoxide and other pollutants from auto traffic, . . . thermal pollution of rivers and lakes".^[7] We must add to those impacts the environmental degradation to the air, water and soil that is caused by the release of large quantities of these direct pollutants and the other heavy metals and radioactive elements stored by nature in these fuels [lead, mercury, etc.] It was not until the burning of fossil fuels during the 19th century that the element lead began being deposited in regions as remote as the arctic and continent of Antarctica. Many scientists believe that the acidification and resulting "deaths" of many high altitude lakes have been caused by the release of the pollutants generated by fossil fuel combustion [by industry, homes and in automobiles]. The increased sulfur dioxides and nitrogen oxides generated by industrialization are present in the atmosphere and lead to "the formation of acids, primarily H_2SO_4 and HNO_3 , from these pollutants and the resulting damage caused by the acidic rain formed is a story of growing importance."^[8] Presently the latest environmental alarm sounded has been that of global warming, a purported warming crisis attributable to a significant increase in the presence of so-called greenhouse gases. The earth's surface radiates thermal energy in the infrared region [approximate wavelengths of 4 to 20 μm] which keeps the global environment cooling at a steady rate. Carbon dioxide [CO_2], methane [CH_4] and nitrous oxide [N_2O] represent molecules formed by the use and manufacture of fossil fuels which trap heat at the above wavelengths, heat that would otherwise be radiated from the earth into space. "Carbon dioxide now accounts for about two-thirds of the greenhouse effect, methane about 25%."^[9] These environmental impacts caused by growing fossil fuel use are forcing many nations to rethink the role these fuels will play in the future.

The limited amount of fossil fuel resources poses a second major risk to continued expansion of the global economy. At present rates of consumption these fuels only have a limited remaining supply, on the order of decades for a few of them to less than a century in the case of coal. [See Table 1.4] In order to meet the needs of our increasingly advancing and growing societies we must find alternatives. Additionally we must preserve some of these fuels since they also serve as key chemical stores in many critical manufacturing and medicine roles in industrial society. If we conservatively grow the current rates of fossil

fuel consumption for the energy sector to include the demands that will likely be placed on the finite supply by the developing nations as the globalization megatrend continues we find that the lifetimes are much shorter still.

TABLE 1.4 - Fossil Fuel Reserves and Resource Lifetimes

Fossil Fuel Type		Proven Reserves*	Est. Remaining Lifetime**
Oil			
	Global	999×10^9 bbl	40 years
	U.S.	72×10^9 bbl	16 years ***
Natural Gas			
	Global	5185×10^{12} ft ³	60 years
	U.S.	600×10^{12} ft ³	20 years
Coal			
	Global	7.64×10^{12} tonne	200 years
	U.S.	1.5×10^{12} tonne	86 years, 66 years ****

* Remaining as of 1990
** At current consumption rates
*** Since 1948 the U.S. has imported more oil than it has exported. In 1984 the U.S. was importing 50% of its needs
**** At current consumption rate increased by 5% per year, if coal fills all U.S. energy needs when other fuels deplete

As the limits to the fuel reserves in Table 1.4 are approached the price of energy will begin to climb steadily. It is important to note that one of the key drivers to economic expansion is the readily available supply of affordable energy. Already we see a migration of industry in this country moving from the high-energy cost areas [Northeast and California] to the more inexpensive energy cost areas of the Northwest and Southern states. Many industries which were energy intensive have left the service area of Atlantic Energy [southern New Jersey] to move south over the past decade to North Carolina or another lower energy cost state for primarily energy reasons. [NOTE: economics has played the major role in corporate decisions to relocate from Atlantic Energy's region including costs associated with energy, taxes, employment and environmental compliance] We can estimate that on a global scale the trend will be the same, manufacturing [and the associated benefits of its economic engine] will move to where energy, overall manufacturing and labor costs can keep the company competitive. As industry and manufacturing leave the U.S. for less developed nations the commensurate growth in energy demand and desire for a higher standard of living on the part of those nations' workforces will all press the global

energy reserves via higher growth rates in consumption. Examples of this include the nations of Indonesia, Malaysia, Thailand and Vietnam where the annual growth in electricity demand has become double digit during the last 10 years. Were the nations of the developing world [China, India, Southeast Asia, Africa] to develop an energy appetite just a fraction as great as their technologically advanced sister countries [U.S., Canada, Japan, Norway, Sweden] the pressure on the limited global reserves and the strain on the atmosphere would become severe.

This researcher estimates that the values in Table 1.4 for the expected remaining lifetime of global fossil fuel reserves can be reduced by as much as a factor of 2 if the trend in third world energy development follows the forecasts outlined by the World Bank. As these pressures on conventional fuels drive price upward shale oil and tar sand reserves as well as many enhanced oil recovery technologies will become more economic.

An excellent illustration of the demands placed on energy by a developing, industrializing society is illustrated by the following two figures. Figure 1.1 demonstrates the relationship between energy consumption and economic activity based upon figures developed in a Scientific American article in 1971.^[10] Figure 1.2 develops similar data on per capita gross national product vs. annual energy consumption based upon World Bank data in 1987.^[11] If one observes the nation of Japan on both figures and considers the position it had in the global economy in the early 1970s contrasting it with the economic powerhouse it was becoming by the late 1980s we can see the increase in energy demand that was placed upon the global energy market in order to sustain that one country's economic advancement. Japan's population in 1961 was 89.2 million^[12] and it grew to 119.5 million in 1983.^[13] In 1971 Japan's population consumed approximately 33×10^6 Btus per capita [9,669 kWh] annually. In the short 16 years of their continued economic growth between 1971 and 1987 their energy use per capita grew to 22 barrels of oil [37,400 kWh] annually. This represents a 4 fold increase in per capita consumption and a 5 fold increase in overall national energy consumption [based upon a 1971 population of 103M and a 1987 population of 125M]. This energy growth correlates directly with their GNP growth from \$550 US [1971] to \$12,000 US [1987] and the extensive industrialization of their economy. Japan's energy consumption now is 43,285 kWh per capita [1995] and while it continues to grow, their population remains steady at 125M. Were a single, large developing nation such as India [population 936M in 1995] to undertake an economic expansion similar to Japan the impact on global fossil fuel markets would be substantial. India's per capita energy consumption in 1995 was 2,563 kWh annually, were they to reach Japan's per capita energy use it would represent a 17 fold increase in their energy use. By 2020 they would become a nation that consumes 5.7×10^{13} kWh annually [assumes continued current population growth rate and achievement of Japan's level of industrialization and commensurate per capita energy usage]. India's one year energy use in that year would represent 64% of the entire World's energy consumption in 1995 [see Table 1.1]. At those usage rates that one nation alone could consume the entire world's remaining supply of oil

in less than 30 years. In aggregate, the developed nations' growing energy consumption rates combined with their continued population growth will substantially reduce the estimates of fossil fuels' expected remaining lifetimes from those shown in Table 1.4. "There is no escaping the reality. . . fossil fuels are formed over very long time periods, and although some new deposits will certainly be discovered, there will be no significant increases in the world inventory over human history. . . the era in which we live is extraordinarily specialized and is set off from all human history and future on this planet by our use of fossil fuels. These energy resources were laid down over hundreds of millions of years during the earth's evolution, and they are now being consumed in what is essentially an instant in our occupation of the planet."^[14] Without the discovery and development of an environmentally friendly, inexpensive energy source to significantly offset the consumption of these ancient energy reserves, we will enter the new millennium only to quickly find that the standard of living developed by western civilization is not a sustainable one.

FIGURE 1.1

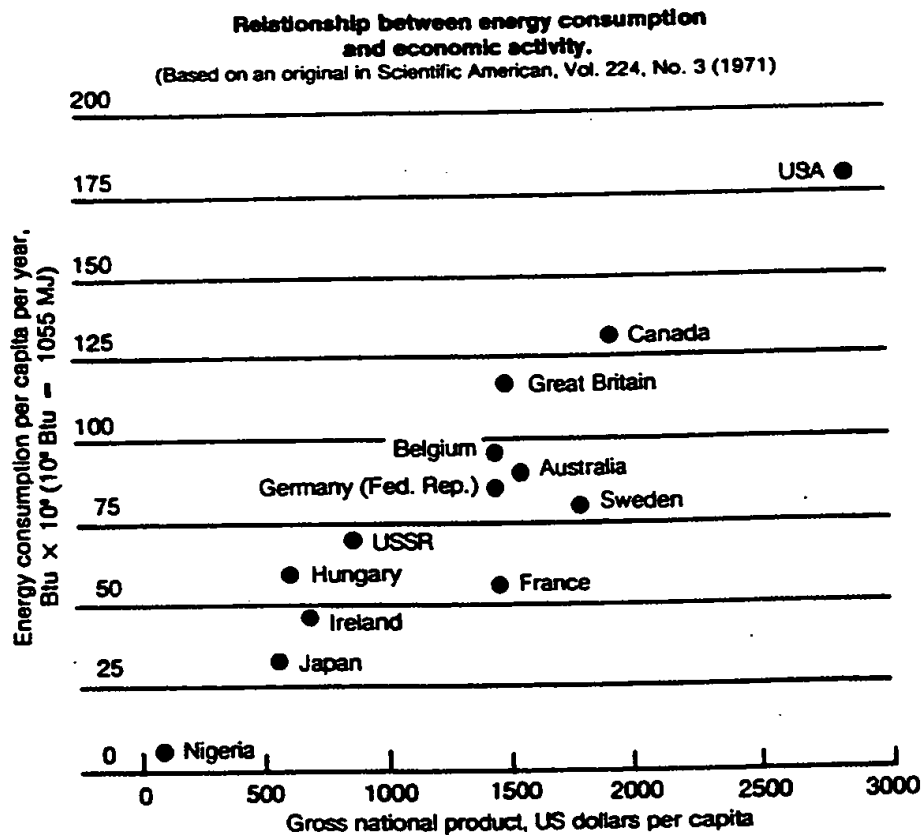


FIGURE 1.2 Per Capita GNP vs. Per Capita Energy Consumption

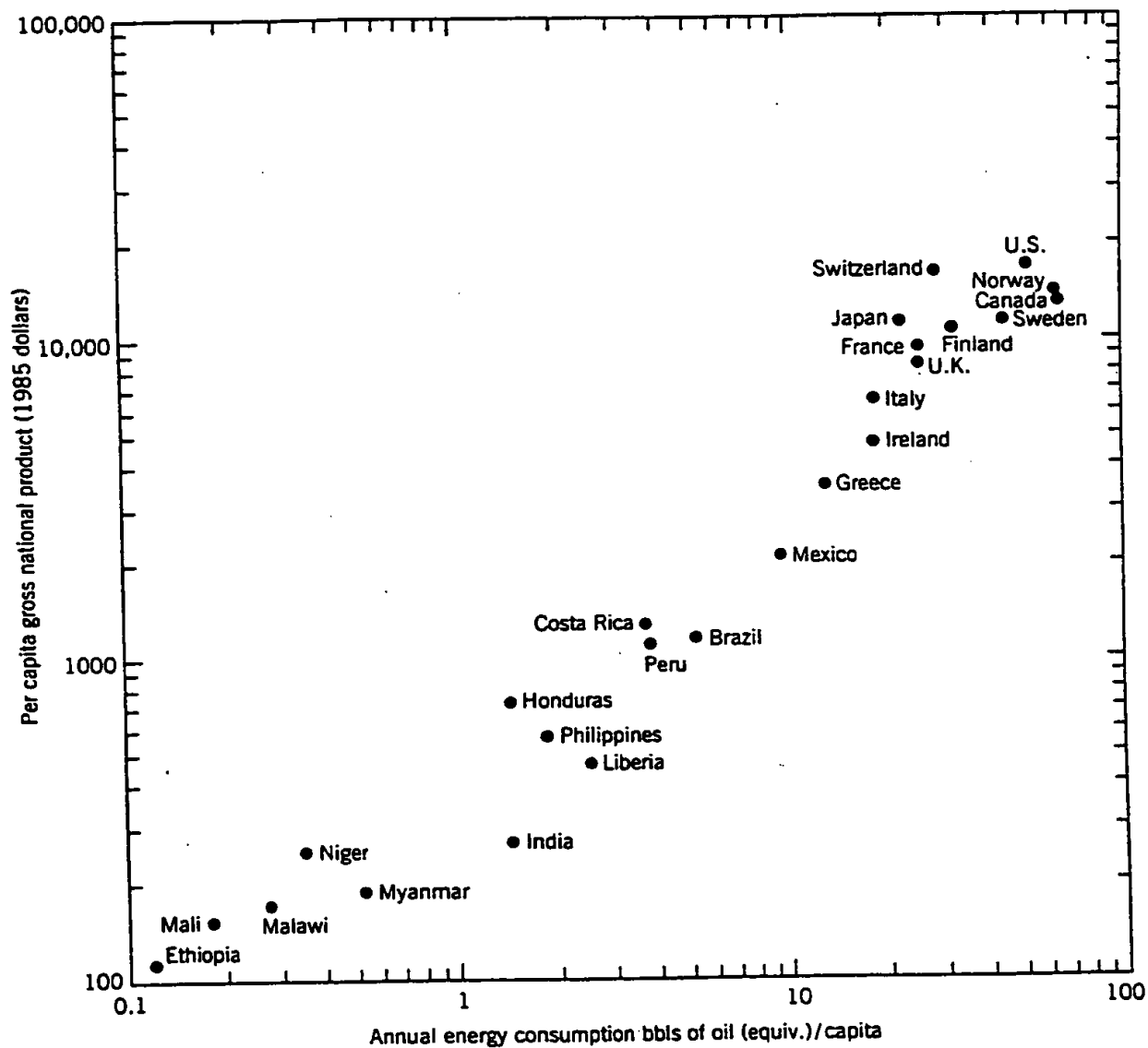
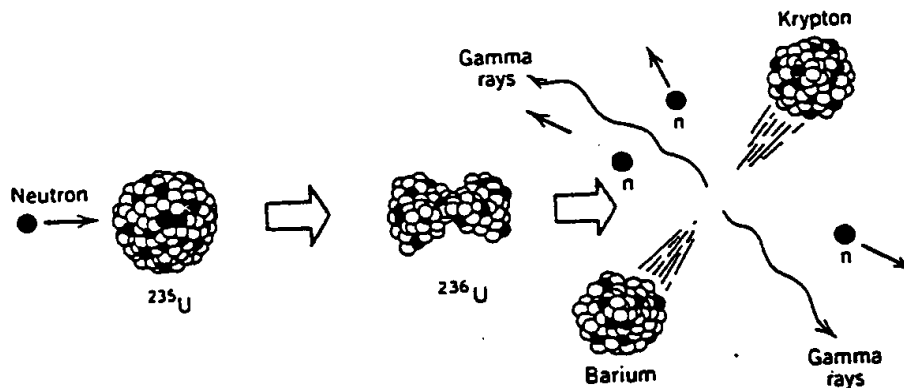


Figure 1.15 Per capita gross national product in 1985 dollars and per capita energy consumption per year in terms of the equivalent barrels of oil. (Source: World Bank [1987]. Adapted from E. S. Cassedy and P. Z. Grossman *Introduction to Energy, resources technology and society* Cambridge: Cambridge University Press [1990].)

1.2 Nuclear Energy - Fission and Fusion

While the fissionability of uranium was first discovered in 1938 it was not until Enrico Fermi constructed a sustainable nuclear reactor in 1942 that the usefulness of this technology for energy production was truly demonstrated. In a parallel way in which chemical [electronic] bonds between carbon atoms are broken down through chemical combustion with oxygen, the breaking of nuclear bonds via a fission reaction is caused by the bombardment of a radioactive uranium atom's nucleus with neutrons. This bombardment, upon successful collision, causes the nucleus of the uranium atom [^{235}U] to become a highly excited uranium atom [^{236}U], this atom rapidly separates [or fissions] into smaller pieces forming new nuclei as a result. This is more clearly illustrated in Figure 1.3 below. The energy released via this nuclear reaction is equal to Einstein's famous equation $E = mc^2$. To put this in perspective, the energy available within a ton of coal that is chemically released through combustion [ie; breaking down all of the carbon bonds] is 7056 kWh. Were that same ton of coal to be converted to energy via a nuclear reaction the energy available is 22.7 trillion kWh, this is 3.2 billion times more energy.

FIGURE 1.3 Neutron Induced Fission of ^{235}U



This process of working on the nuclear bonds of the atom, rather than the chemical bonds of molecules releases a significant amount of the nuclear binding energy within the atom. What makes this a sustainable chain reaction is the creation of additional neutrons [see fission reaction in Table 1.5] from the fission reaction which can then go and impact additional uranium nuclei to keep the bombardment occurring without external neutron input. Control rods used in commercial nuclear power plants provide a moderating effect

on the reaction by absorbing excess neutrons in order to slow or to bring the reaction to a stop. The process outlined above is used in both pressurized water reactors [PWR] used significantly in nuclear submarines and power plants as well as in boiling water reactors [BWR] used widely for commercial applications.

TABLE 1.5 - Energy Release Processes for Nuclear Fuels

Nuclear Process	Nuclear Chain Reaction[s]	Energy Release
Fission	$n + {}^{235}\text{U}_{143} \rightarrow {}^{236}\text{U}_{144} \rightarrow {}^{144}\text{Ba}_{88} + {}^{89}\text{Kr}_{53} + 3n$	+ 177 MeV
Breeder	$n + {}^{238}\text{U} \rightarrow {}^{239}\text{U} \rightarrow {}^{239}\text{Np} \rightarrow {}^{239}\text{Pu} + >1n$	+ 177 MeV
Fusion	${}^1\text{H}_0 + {}^1\text{H}_0 \rightarrow {}^2\text{H}_1 + \beta^+ + \nu + \text{energy} \quad (1)$ ${}^1\text{H}_0 + {}^2\text{H}_1 \rightarrow {}^3\text{He}_1 + \text{energy} \quad (2)$ ${}^3\text{He}_1 + {}^3\text{He}_1 \rightarrow {}^4\text{He}_2 + 2{}^1\text{H}_0 + \text{energy} \quad (3)$ $4{}^1\text{H}_0 \rightarrow {}^4\text{He}_2 + 2\beta^+ + 2\nu + \text{energy}$	

Detailed descriptions of the nuclear energy process is not within the scope of this research but rather an overview of these technologies and their associated economic and environmental risks are described below.

The breeder reactor is a concept not yet fully commercialized which takes advantage of the fact that free neutrons are not only capable of inducing fission via a conversion of ${}^{235}\text{U}$ to ${}^{236}\text{U}$, but are also as equally capable of converting a ${}^{239}\text{U}$ atom into ${}^{239}\text{Pu}$. This is very valuable since ${}^{239}\text{Pu}$ is also a fissionable material capable of acting as a fuel in standard nuclear reactors. If the design of a breeder reactor could be optimized to create additional ${}^{239}\text{Pu}$ while also creating uranium fission it would be a reactor that created its own fuel and would significantly increase the lifetime of nuclear fuel materials.

Fusion is a nuclear reaction that occurs commonly on the stars and in the case of our sun is likely the source of approximately 60% of the energy it provides. This estimate is based upon observed solar neutrino flux as measured by the Gallex solar neutrino detector in Italy.^[15] As shown in Table 1.5 above according to the Standard Solar Model fusion begins with the combining of two hydrogen nuclei (protons) to form a deuterium nucleus. The process then continues to build a heavier helium nucleus all the while releasing large amounts of the nuclear binding forces within the atom. For a more complete explanation of this process the reader is referred to pages 108-111 of *"Energy and Problems of a Technical Society"*^[16], which is an excellent summary of energy technology information

referred to often in this paper. Due to the very high temperatures involved, the limits of current materials and the fact that proof of the scientific feasibility of the essential reactions has not yet been established it is unlikely that significant additional funding will go into the development of fusion. The Tokamak Fusion Test Reactor [TFTR] located at the Princeton University Plasma Physics Lab was designed to answer some of these fundamental questions. It appears that after significant resources have been invested in this test those questions will still not be sufficiently addressed. The TFTR was shut down on April 3, 1997 "many say prematurely ... for lack of money".^[17]

In the U.S. during the last decade no new nuclear power facilities have been opened, ordered or planned. This is due in large part to 4 primary developments during the past 15 years. These facilities have become very expensive to build and meet all Nuclear Regulatory Commission [NRC] standards, the issue of nuclear waste storage has yet to be resolved by the utilities and the Federal government, there was and continues to be significant public opposition to this technology and there have been key nuclear accidents which have increased the financial risks and liabilities to investors and owner / operators of such facilities. When nuclear advocates were espousing the virtues of this technology in the 1960's and 1970's it was believed that the energy would be so cheap that utilities would not need to meter customers any longer. As the technology was deployed, many safety features were required "along the way" by the emerging NRC which wanted to assure the safety of the technology. This often led to major cost overruns and units that were intended to come on line for \$1,000 - 1,500 per kilowatt escalated to often over \$4,000 per kilowatt. Many units in the Northeastern and Western regions of the U.S. were never finished due to these massive costs. This is clearly one of the key reasons utilities are not interested in the technology today. Another reason is the longevity of hazardous nuclear radioactive wastes. Table 1.6 below indicates the lifetimes of radioactive materials generated as by-products from the nuclear industry.

TABLE 1.6 - Nuclear Fission By-Products Radioactive Halfives^[18]

Radionuclide	T _{1/2} [Halfife]	Decay Particle
²³³ U [uranium-232]	1.59 x 10 ⁸ years	α
²³⁹ Pu [plutonium-239]	2.41 x 10 ⁴ years	α
³ H ₂ [hydrogen-3, tritium]	12.35 years	β ⁻
⁹⁰ Sr [strontium-90]	29 years	β ⁻
¹³¹ I [iodine-131]	8.04 days	β ⁻
¹³⁷ Cs [cesium-137]	30.17 years	β ⁻
⁸⁵ Kr [krypton-85]	10.72 years	β ⁻

It is clear that wastes from the nuclear industry will need to be kept away from the human population and environment for excessive lengths of time [often exceeding many generations]. Although this was known in the early years of this technology, as of today, after over 20 years as an active industry, the government and utilities have yet to find an acceptable long-term high level waste repository. It is unlikely that the nuclear industry in the U.S. will see any significant expansion during the next few decades. In Sweden recently the government ratified its 17 year old promise to remove all nuclear reactors from service in its country by 2010. The first two reactors will be officially removed from service in 1998 and 2001 "before their technical life expires".^[19] This leaves only France, Japan and a few developing nations that will be expanding their commitments to nuclear fission as a viable energy source for the future.

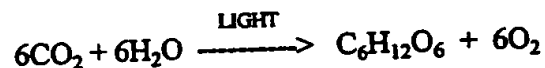
1.3 Solar Energy

Without a doubt the most widespread form of energy in the universe is the energy radiated from the stars. Specifically in our solar system, the Sun is the source of nearly all forms of useful energy. From the fossil fuels first formed by carbon fixing organisms [plants and animals] in the presence of solar energy 250-500 million years ago to the hydroelectric plants operating on major rivers, the Sun is responsible for creating the potential energy each represents. This section will briefly summarize all of the primary forms of solar energy and prioritize their discussion from the most economical and technologically ready to the forms that are the least economical and require the most additional development. It is important to note that although significant attention is given to these sources of energy because of their potential for the future, at the present time solar energy in all of its forms represents less than 3% of the World's commercially traded forms of useful energy. Of that small fraction over 90% represents the use of solar energy in the form of hydropower.

The most developed form of solar energy is hydroelectricity. The hydrologic cycle driven by the sun evaporates over 5.5 quadrillion cubic feet of water from the earth every year. This same energy falls back to the earth in the form of rain and the potential energy of water at higher elevations. Of the more than 100 quadrillion kilowatthours of energy in the hydrologic cycle only a very small portion is harnessable. Most precipitation falls back into the oceans with only a fractional amount falling upon dry land at higher elevations where its potential energy becomes available for exploitation via rivers, dams, waterwheels and hydroelectric generating facilities. World energy usage statistics indicate that in 1995 we were providing approximately 2.3 trillion kilowatthours^[20] of our global society's energy needs through hydroelectric sources. This represents approximately 2.5% of all energy consumed. Man's use of falling water to displace human and animal energy dates back over 2000 years. Hydropower also played a major role in the industrialization of western

Europe the 16th century when waterwheels served as the primary powerhouses. While many believe the potential for exploiting more hydropower is great there are environmental considerations and social concerns that make extensive expansion unlikely. Due to the need to create large dams and reservoirs to harness hydropower there is often substantial displacement of people as well as restriction of the normal ecology of the river. While it represents a significant capital investment, where it can be practically developed hydropower remains an economic source of electricity.

The most widely known and experienced form of solar energy is biomass. A significant majority of the World's now 5.8 billion people^[21] come in contact with this fuel on a daily basis. The biomass category represents fuelwood, charcoal, agricultural products and waste [alcohol, dung, mill residues, rice hulls, straw, etc.] as well as the less recognized biomass of industrial society - municipal solid waste [mostly paper and packaging materials]. Least recognized in the category of biomass is the harvesting of ocean biologic life [seaweed, algae, etc.] for fuel production. "Noncommercial biomass fuels ... already supply more than 10 percent of total global energy needs and a much higher percentage of the energy needs in developing nations, albeit with low levels of efficiency and service quality."^[22] This source does not appear in Table 1.1 since very little biomass is commercially traded on the global level. The sun plays the critical role in the creation all the biomass fuels either directly through photosynthesis or indirectly via man's or animal's use of a product the sun's energy created [ie; foodstuffs, paper, etc.]. Besides using biomass for meeting heating and other human energy needs probably the most common use is in the food we eat. Vegetables, fruits and other animals all received their energy from the solar source as well through the process of photosynthesis shown below:



The energy release processes for biomass are very similar to fossil fuels where the biomass is directly burned in the presence of oxygen to release the energy of carbon chains and form CO_2 , H_2O , etc. Continued use of biomass is inevitable, expanded use of wood and woodwaste as a fuel in the U.S. is likely as well. Without specialized biomass growing and harvesting techniques and efficient fuel conversion systems it will be quite a few years into the future before these fuels will become economic on a large scale and find a major place in the growing global energy market. The energy densities of biomass fuels are relatively low, on the order of lignite to peat coal resources, and this also presents barriers to commercial development.

Another widely experienced form of solar energy is the direct heating of the sun known as solar thermal energy. From the highly technological systems we have created [passive and active solar space and water heating systems] to the primitive habit of laying out in the sun for a siesta or tan, the human race daily takes advantage of the direct warming

available from the sun. Many societies still use the sun for drying grains [such as rice] as a critical step in their agricultural process. In the U.S. the most prevalent form of solar thermal energy use is in passive and active heating systems for homes as well as heating systems for hot water. During the late 1970s and early 1980s the Federal government provided significant tax incentives for renewable energy systems. This led to many domestic solar hot water heating systems being installed throughout the country. These systems typically consist of a solar collector device that traps incoming short wavelength incident solar radiation and upon collision with a dark, metallic 'absorber' plate the light energy is converted directly to heat [or mechanical molecular vibrational energy] in the absorber plate. This collector is typically called a flat-plate solar collector. The absorber plate typically has an antifreeze solution which runs through it [i.e. it acts as a heat exchanger to move the incoming solar energy it absorbs into the fluid] and this fluid is used to capture, move and store the solar energy for use either in a hot water system or for heating a home or building. Another example of solar thermal energy systems is the focusing collector which comes in various shapes, sizes and configurations. From the Solar One power tower demonstration in Barstow, California which had a commercial production of 10 megawatts, to modular, parabolic dish and trough systems that collect watts to kilowatts of power, directly focusing the sun's energy on a light-absorbing surface can create commercially meaningful heat. The drawbacks with all of these systems was that they were never economically attractive. Most solar thermal heating systems have between a 15 and 30 year simple economic payback. Without significant social policy change or government subsidy these types of heating and energy production systems will not be commercially significant.

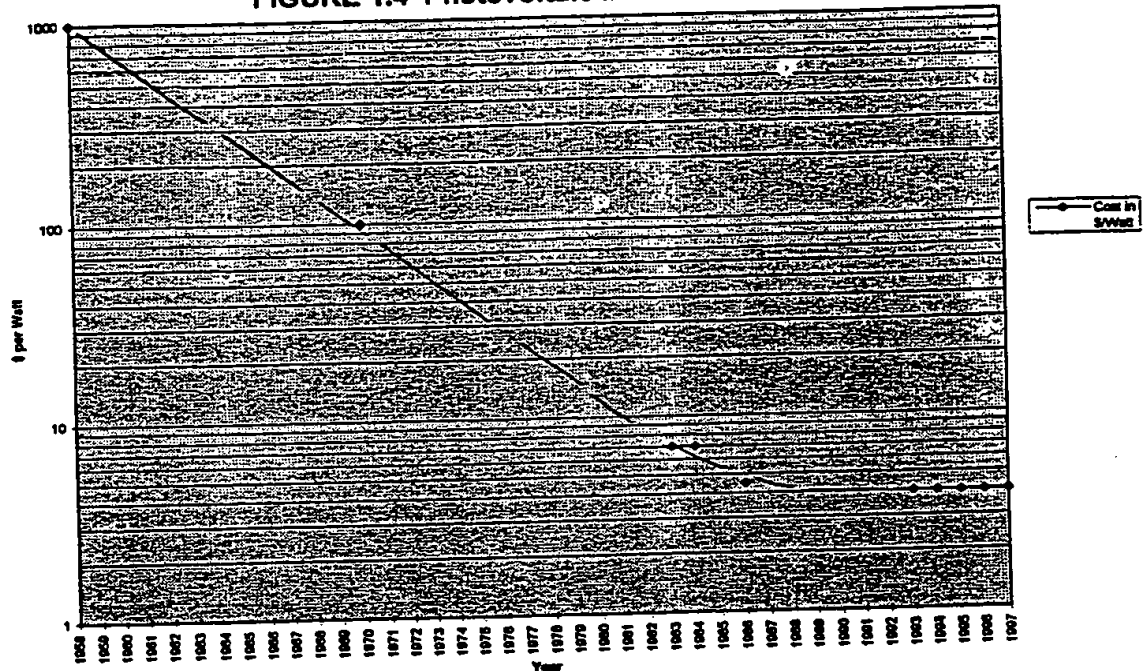
Another solar resource is wind power. In 1995 it was estimated that geothermal, wind and solar of all types accounted for nearly 5% of the world's primary electricity generation [ie; 0.5% of the world's total energy resources]. This resource was used from the most ancient of times by mariners in their quest for increasing the speed of their then human powered vessels to the applications of water pumping and grain grinding by animals in Europe and America in the 19th and 20th centuries. Wind power is still used in many locations throughout the world for these purposes. As an electricity generating source wind power first began to find its way into the marketplace in the 1970s and 1980s in both Europe and the U.S. While we know that the mechanical motion of air is a direct consequence of solar heating of the planet it has always been a challenge to economically extract the energy in this air movement. Modern wind turbines are designed to remove the kinetic energy in the wind and use that energy to turn a generator to provide electricity. They do this by placing their aerodynamically efficient blades into the wind to enable the mechanical force of the wind to cause those blades to rotate and sweep over a large area. Present technologies include vertical axis wind turbines as well as horizontal axis wind turbines; manufacturing is dominated by the latter at the present. The energy that can be removed by a wind turbine is proportional to the area its blades sweep out as well as the cube of the wind velocity. For this reason most turbines are mounted on towers to place

them more aloft where higher wind regimes are present. In areas of moderate to high annual wind speed, wind turbine generators are able to create electricity at approximately \$.05 per kWh assuming a 20 year equipment life. It is difficult to find areas where local citizens are willing to allow wind facilities to be located at the present time and it is also increasingly difficult to find investors willing to tie up their capital for a project that produces electricity at a higher cost than where the electricity market is at present [i.e. \$.02-.03 per kWh].

A widely acclaimed technology that showed promise in the 1980s of becoming a major player in the solution to the energy crisis is photovoltaics. These are semiconductor devices made of materials that are designed and oriented in such a way as to convert light energy [photons] directly into electrons at efficiencies of 5-30%. PV devices being developed commercially employ similar physics in their operation. The photovoltaic effect is created when incoming photons interact with electrons in a semiconductor material so as to create a charge carrier pair; an electron and a "hole". Each PV device is constructed with positively and negatively doped layers so as to maximize the cell's ability to separate the charge carriers and keep them separated so as to induce a voltage across the cell as long as the incoming light is present to induce this voltage. The photovoltaic effect was first discovered by 17 year old French physicist Edmund Becquerel in the 1850s when he was experimenting with batteries. He noticed that his batteries were able to provide significantly more energy in the presence of light than when shaded in the darkness. He noted this in his journal but it wasn't until Albert Einstein's work in 1905 that the principles behind the photoelectric effect were described scientifically. This technology's potential lay dormant for another 50 years until the space race began. After Russian scientists launched Sputnik in 1957 and the U.S. had fallen behind in the race they wanted to assure that their first satellite would 'last longer'. As a result in 1958 the Vanguard satellite was launched by the U.S. powered with not only a battery, but a battery recharged on-board by the world's first commercial application of photovoltaic cells. [Sputnik lost its battery energy and floated useless in space after only a few months] Those cells, costing over \$1000 per watt kept the Vanguard satellite's batteries charged for years of successful operation.

Since that time the cost of photovoltaic [called PV] cells continued to plummet driven by advances in technology, increased manufacturing volume and increasing demand for satellite applications, remote power applications as well as commercial electricity uses. Figure 1.4 shows the progressive decline in PV cell prices as advances in technology continued through the 1980s. By the late 1980s as Federal research monies for renewables decreased during the Republican Administration, the commensurate investment in and advancement of PV technology subsided. Current pricing for PV cells has not substantially changed from those present in 1989

FIGURE 1.4 Photovoltaic Module Prices



In addition to the photovoltaic modules that are made up of cells configured to provide adequate current and voltage, a PV system requires balance of system components. These components are module mounting and wiring peripherals, a DC to AC inverter for typical interface with home wiring and the installation [roof or ground mount, etc.] of the entire system. In 1996 these were estimated to cost \$2 per watt, \$1 per watt for the inverter and \$1 per watt for balance of system hardware and installation. This would bring a total PV system's cost to \$6-7 per watt installed. To put this in perspective, a typical home could use a 4kW system which cost \$24,000 to install. This system would provide approximately 6,000 kilowatthours of useful energy each year at present electricity rates this \$750 per year savings represents a simple payback of 32 years. Near term growth in economic expansion of the PV market for utility connected customers appears unlikely. Market research conducted by the author and his colleague indicate that until installed PV prices reach \$0.6-1.3 per watt, no major changes in the demand for PV by the grid-connected market is likely.^[23] There are many different types of PV cells that have been attempted from single crystalline to multi crystalline to amorphous cells. In the last five years only minor additional improvements to the technologies have been made leading to a flattening of the price curve at \$4 per watt since 1990 [see Figure 1.4].

Probably the forms of solar energy with the least potential for future development and expansion are ocean thermal and wave power. The ocean is a source and sink for energy of many types. It is probably the vast dihydrogen oxide resource of the ocean that

keeps the temperature, environment and atmosphere of the planet moderated and suitable for human life. In that same environment thermal gradients and atmospheric disturbances cause currents, waves and temperature differences around the world. Ocean Thermal Energy Conversion [OTEC], is a technology that was conceived of in 1880 by d'Arsonval. OTEC takes advantage of the thermal gradient which exists in the sea and is especially pronounced around the tropical regions where surface water temperatures can get very high. This approach to energy generation uses ammonia as a working fluid. This fluid runs an evaporator-condensor cycle where cold water from deep in the ocean condenses the ammonia vapor while warm water on the ocean surface is used as a heat source to boil the ammonia to give it the vapor pressure needed to drive a gas turbine. The gas turbine in turn drives an electric generator. In 1930 the first demonstration plant was constructed in Cuba; since that time no additional plants or demonstrations have been constructed. The islands in the tropic zones may have potential for this technology at some point in the future but presently the technology is very expensive which has limited its development. Wave energy systems are not commercially available at the present, but it is believed that the difference in wave heights may be commercially exploited at some point in the future. Ocean currents may provide a significant potential source of energy as well but no commercial technologies currently exist to harness it effectively. Similarly to OTEC, ocean current systems will be further hindered by the fact that where the energy source is located is often far from where the demand for energy exists.

1.4 Geothermal Energy

If you have ever sat or swam in a natural hot spring you are familiar with one of the benefits of Nature's outpourings of geothermal heat. While less dramatic than the volcanos or geysers, low temperature geothermal sources make up a significant portion of the global geothermal resource. The most widely used type of geothermal resource for energy generation is the natural steam reservoirs. By 1990 the U.S. was generating "over 2800 MW_e at 4 to 6 cents per kWh"^[24] from these reservoirs in the western states. While the U.S. potential for geothermal is estimated at 22,675 QBtu [this compares with an annual U.S. energy use of 82 QBtu] there has been little additional exploitation of these reserves since the removal of Federal tax subsidies in the 1980s. The most economical and expanding market for geothermal energy applications exist in the residential and commercial sectors. Geothermal heating and cooling systems use the earth as a heat source and sink with an electric heat pump to move heat into or out of the conditioned space. Geothermal heatpumps move 3-4 kWh of energy for every one kWh of energy they consume. This technology was perfected in Sweden and is seeing extensive application in the U.S. and other industrialized countries. In many applications it represents the least costly heating and cooling system on an annual energy as well as operation and maintenance cost basis. The use of geothermal energy in these applications is likely to expand.

1.5 Tidal Energy

There are presently no commercial tidal facilities in the United States and only three tidal power systems in the world. These facilities operate on principles that are very similar to those of hydroelectric stations. They require a reservoir, a dam and a series of turbine generators. In the case of tidal systems they are capturing the kinetic energy that exists in the movement of tidal waters into and out of an estuary or man-made reservoir four times each day. The energy is being created by the gravitational interaction of the Sun, the Moon and the Earth which causes this motion in the seas daily. In the lower 48 continental U.S. the tidal variations range from 2 to 16 feet between mean high and mean low waters. In the U.S. the potential for tidal power represents less than 15,000 MW. The global potential for the most favorable tidal power sites is about 63,000 MW, or about 1/50th the world's potential for hydroelectric power.^[25] The three tidal facilities in operation worldwide are a 1-MW plant on the White Sea in Russia [1969], a 240-MW plant on the Rance River in France [1966], and most recently a 20-MW plant on the Bay of Fundy in Canada.

Chapter 2 - An Overview of Mill's Technology

This chapter will focus specifically on the hydrocatalysis technology developed by Dr. Randell Mills of BlackLight Power, Inc.. After providing an overview of the theory behind the design of the various technologies I will move to a review of the astrophysical data which supports Dr. Mills' claim that fractional state hydrogen is common and abundant throughout the universe. I will highlight some key enigmas that Dr. Mills' theory solves and review the current technological devices that capture energy from this new found fuel source. Table 2.1 below summarizes the significant government, corporate and university research centers that have partnered to corroborate many of BLP's experimental findings.

TABLE 2.1 - BlackLight Power Research Partners

LABORATORY

Government

Idaho National Engineering Laboratory

SDIO-Wright Patterson AFB

Chalk River National Lab [Canada]

NASA - Lewis

Brookhaven National Lab

University

Lehigh University - Zettlemoyer Center for
Surface Studies

M.I.T. Lincoln Laboratory

Pennsylvania State University

Ursinus College

Moscow Power Engineering Institute

Laboratory for Electrochemistry of Renewed
Electrode-Solution Interfaces [LEPGER]

Corporate

Thermocore, Inc.

Air Products & Chemicals

Westinghouse Electric Corporation

Charles Evans & Associates Laboratories

Schrader Analytical & Consulting Laboratory

BlackLight Power Laboratories

WORK PERFORMED

Electrolytic Cell [850% VI]

X-ray Photoelectron Spectroscopy

Diffusion Cell

Electrolytic Cell [130% VI DC]

Electrolytic Cell [170% VI DC]

Electrolytic Cell

X-ray Photoelectron Spectroscopy

Electrolytic Cell [400% VI DC]

Gas Cell [>2000% H₂ Energy]

Electrolytic Cell

Electrolytic Cell [250% VI DC]

Electrolytic Cell

Electrolytic Cell [2100% VI AC]

Mass Spectroscopy

Electrolytic Cell [150% VI DC]

TOF-SIMS

Mass Spectroscopy

Electrolytic Cells [2100% VI AC]

Gas Cells [2 - 50 watt Energy]

Mass Spectroscopy

Gas Chromatography

In the column entitled "Work Performed" I have summarized the types of devices tested or work performed in each laboratory. In all cases these labs provided data and results which were consistent with the results anticipated by the Mills theory [i.e. excess heat production, hydrino or dihydrino signatures, etc.]. The numbers in brackets, where provided, show the energy output to energy input ratio confirmed by the lab. I gathered this data by reading and summarizing the reports produced by the labs themselves. A detailed bibliography of the reports generated by these partnerships, plus others I was able to catalogue has been provided in Appendix 1. It is important to note that all of the work in Table 2.1 is very recent, having been completed during the last five years. The four subsections of Chapter 2 are as follows: Section 2.1 will briefly describe the theory Dr. Mills developed leading to the design of the various BLP technologies. Section 2.2 will summarize and analyze some of the astrophysical data which supports Dr. Mills' claims with that this new form of hydrogen is prolific throughout the universe, Section 2.3 will describe a few of the enigmas that Dr. Mills' theory solves, and Section 2.4 will provide a brief synopsis of the state of the art of current BLP technological devices that demonstrate energy production from the new found fuel source.

2.1 Hydrocatalysis - A Theoretical Overview

The catalytic reduction of atomic hydrogen below its ground state of $n=1$ has been postulated by Dr. Randell Mills of BlackLight Power, Inc. There is substantial data that has been gathered confirming an unexplainable amount of energy being released from hydrogen; these energy values are well in excess of any known chemical reaction with hydrogen and were observed by others when reproducing BLP experiments. In addition, new electronic signatures corresponding to the expected [ie; calculated] energy values for low energy hydrogen via mass spectroscopy, gas chromatography, x-ray photoelectron spectroscopy and extreme ultraviolet spectroscopy have been identified. A non-trivial number of independent laboratories and research centers have been involved in the confirmations described in the above findings. In addition, a sound theoretical basis for the phenomenon has been postulated by Dr. Mills which unifies field theory with a completely classical approach to physics. Mills theory holds at its foundations inviolate the classical laws of physics, including all of those listed below:

- 1] Conservation of mass-energy
- 2] Conservation of Linear and Angular Momentum
- 3] Maxwell's Equations
- 4] Newton's Laws of Mechanics
- 5] Einstein's Special Relativity
- 6] Einstein's General Relativity

The postulated reduction of hydrogen to fractional quantum energy levels represents a radical departure from currently held quantum theory. But when it comes to

the classical laws of physics the Mills' theory rather than contradicting current models actually builds upon them. Dr. Mills' approach is fundamentally based upon the theoretical hydrogen atom energy equation developed by E. Schrödinger and W. Heisenberg in 1926 shown below. ^[26]

$$E_n = -e^2 / n^2 8\pi\epsilon_0 a_H = -13.598\text{eV} / n^2 \quad (1a)$$

$$n = 1, 2, 3, \dots \quad (1b)$$

Dr. Mills has proposed that a new boundary condition, derived from Maxwell's equations, be applied to Schrödinger's original equation. When it is applied to the fundamental hydrogen equation the Mills' model suggests a purely physical model which applies for all of known nature. This same model applies on the microscale [i.e. particles, atoms, molecules] and through the macroscale [i.e. planets, stars, galaxies and the overall universe]. A more detailed overview of Mills' theory for the interested reader was developed by this researcher and is provided in Appendix 2. The modification Dr. Mills' theory would make predicts that equation (1b) above be replaced with equation (1c) below which allows for lower than $n=1$ non-radiative valence states for the hydrogen atom.

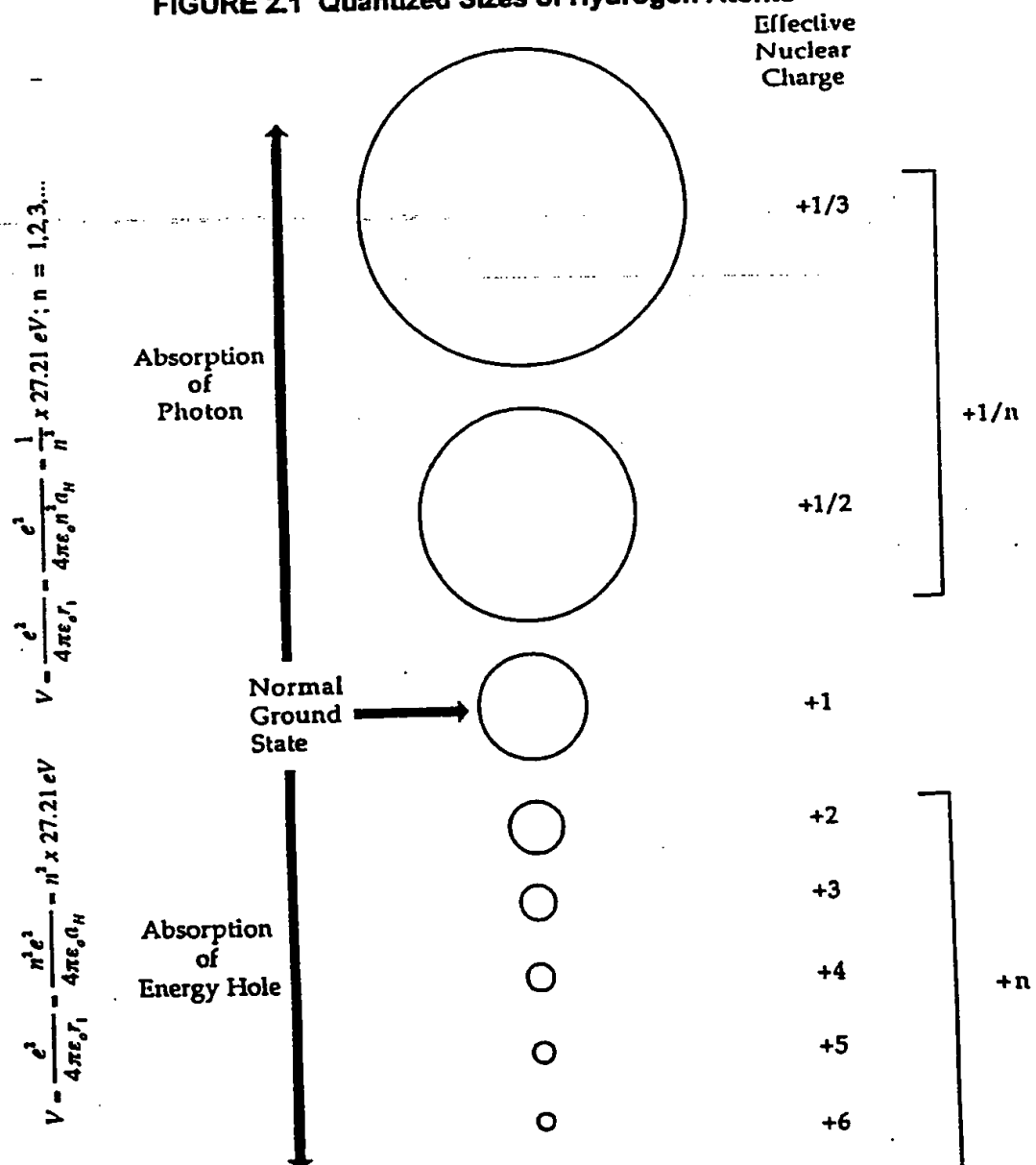
$$n = 1, 2, 3, \dots, \text{ and } n = 1/2, 1/3, 1/4, \dots \quad (1c)$$

His mathematical solution uses fundamental constants only and the energy values predicted by his theoretical approach agree in a most compelling way with observations scientists have made of the universe and stars. The new form of fractional valence states of the hydrogen atoms [named "hydrinos" by their discoverer, Dr. Mills] are able to radiate meaningful amounts of energy as they undergo electron relaxation to lower energy states [see Table 2.2].

TABLE 2.2 - Energy Released From Lower Energy Hydrogen

n	R [radius]	Energy Released (eV)	
		$r = \infty$ to $r = R$	$\Delta E_{\text{final}} - \Delta E_{\text{initial}}$
1	a_H	13.6	—
1/2	$a_H/2$	54.4	40.8 [1 \rightarrow 1/2]
1/3	$a_H/3$	122.4	68.0 [1/2 \rightarrow 1/3]
1/4	$a_H/4$	217.7	95.3 [1/3 \rightarrow 1/4]
1/5	$a_H/5$	340.1	122.4 [1/4 \rightarrow 1/5]
1/10	$a_H/10$	1360	258.4 [1/9 \rightarrow 1/10]
1/100	$a_H/100$	136keV	2706.4 [1/99 \rightarrow 1/100]

FIGURE 2.1 Quantized Sizes of Hydrogen Atoms



The radical new model Dr. Mills has proposed [i.e. that there exist stable forms of hydrogen in fractional energy states below the accepted ground state, $n=1$] with its commensurate fractional radii between the electron and proton [i.e. $n=1/2$, $n=1/3$, $n=1/4$, etc.] are shown on the next page. The model being proposed will hereinafter be referred to as "Mills Theory".

It is important to emphasize at this point that the transitions described are *not nuclear*. This is a chemical reaction that only effects the binding energy of the hydrogen atom's electron. The fundamental energy release mechanisms in this process are *hydrocatalysis* and *disproportionation*. Hydrocatalysis occurs when a hydrogen atom with its electron at its normal ground state or a lower ground state [ie; $n \leq 1$] reacts with a catalyst having a net enthalpy of 27 eV. Energy is released per equation (1d). Disproportionation occurs when a lower energy state hydrogen atom [ie; $n < 1$] collides with another lower energy state hydrogen atom [ie; $n < 1$] which results in the ionization of one atom [ionization energy is a multiple of 27 eV] and the transition of the electron of the other atom to a stable, lower energy level. Energy is released per equation (1e) when the atom which ionizes has its electron at its $n = 1/2$ state.

$$E = (1/n_f^2 - 1/n_i^2) \times 13.6 \text{ eV} \quad (1d)$$

$$E = (1/n_f^2 - 1/n_i^2) \times 13.6 \text{ eV} - 54.4 \text{ eV} \quad (1e)$$

The interested reader is referred to Appendix 2 for more detail on Mills theory.

2.2 Astrophysical Corroboration

The theoretical model proposed by Mills might remain an interesting approach to unifying physics but be written off as a theory of no import were it not for the fact that the laboratory of the universe provides a prodigious amount of data which appears to support his predictions. For example, his theory predicts that the electronic transition of atomic hydrogen below its ground state of $n=1$ is a widespread phenomena which provides a significant amount of the energy radiated by all stars. The theory also predicts this transition reaction occurs in the atmosphere of some of the larger planets [Jupiter and Saturn] as well as in the dark regions of space. Hydrogen is the most abundant element in the universe, and if it also is able to exist in a stable form in lower energy states it must be measurable and detectable. There is substantial observational data confirming that possibility. One source is the extreme ultraviolet spectrometer data collected and analyzed by Simon Labov and Stuart Bowyer of the Center for Extreme Ultraviolet [EUV] Astrophysics at UC-Berkeley.^[28] They designed and had launched a diffuse, grazing

incidence EUV spectrometer into space from White Sands Missile Range in the spring of 1986. They analyzed their data and published it in the *Astrophysical Journal* in the spring of 1991. Their data is remarkable in many ways; 1] it was not believed that such data could be collected, 2] they observed and validated significant emission features and signatures from the dark regions of space, 3] they achieved a very high statistical confidence that the data was real [in many cases >99% confidence] and 4] their explanations for what these emission signatures must be postulate that an unexplainably high temperature [million degree gases] must exist in what was otherwise believed to be a vastly cold region.

Upon review of this data the scientists of BLP, being chemists by background believed that "hot interstellar gas" view of dark space was not very plausible. They undertook to view this data in light of the fundamentals of the Mills' theory which predicts that lower energy hydrogen can collide with other lower energy hydrogen atoms and undergo an energy transition to a lower non-radiative energy state. These transitions radiate at specific energy levels and wavelengths as predicted by equations (1d) and (1e) as described above. While the Labov and Bowyer's interpretation of these signatures originating from hot interstellar gases [Fe_{XIX} , Fe_{XI} , O_V , etc.] is more widely accepted by astrophysicists, other scientists see the explanation as less plausible.

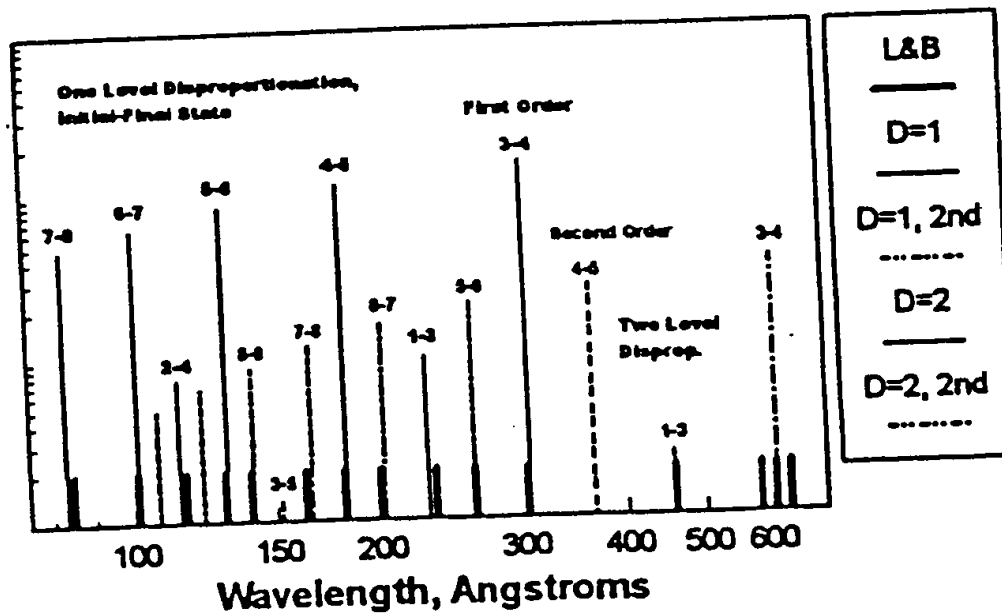
The BLP assignment of these and many other planetary, stellar and interstellar radiation signatures to a calculated amount of energy being released from hydrogen atoms undergoing collisional effected transitions to lower energy states appears to be much more plausible. When the data is analyzed and one views the assignments of the probable hydrogen transitions and sees the reasonableness of such a theoretical match it appears to be much more than a remarkable coincidence. The analysis provided by BLP in Table 1 [on page xiii of the Forward] as well as page 424 of the text on the theory^[27] shows a match between the background data and theoretical transitions for nearly all of the transitions that are probable to the $n = 1/8$ state of hydrogen. I have reproduced these calculations in Appendix 3 and provide a summary of one of those spreadsheets on the page that follows as Figure 2.2.

Perhaps an even more compelling way to view this data is in the manner developed by Jim Kendall, P.E., a Ph.D. Nuclear Engineer from Technology Insights [a technology assessment firm from southern California]. He graphically stacked the Labov and Bowyer data side by side with Mills theory predictions as shown in Figure 2.3 to reveal a correlation which is most persuasive.

FIGURE 2.2 - Astrophysical Observations and Mills Theory

Raw Extreme UV Background Spectral Data *							
OBSERVED DATA			Fractional State		MILLS PREDICTED		
Peak	Wavelnth A	Energy eV	Calc eV	1/nf	1/ni	Wavelnth A	Energy eV
1	84.8	146.2	146.2	8	7	82.9	149.6
2	101.5	122.2	122.2	7	6	101.3	122.4
3	116.8	106.2	106.2	4	2	114.0	108.8
4	129.6	95.6	95.7	6	5	130.2	95.2
5	139.6	88.8	88.8	4	2	141.6	87.6 He scattered
6	163.2	75.9	76.0	8	7	165.8	74.8 2nd order Peak 1
7	181.7	68.3	68.2	5	4	182.3	68.0
8	200.6	61.8	61.8	7	6	202.6	61.2 2nd order Peak 2
9	233.8	53.0	53.0	3	1	227.9	54.4
10	261.2	47.5	47.5	5	4	265.0	46.8 He scattered
11	302.5	41.0	41.0	4	3	303.9	40.8
12	459.1	27.0	27.0	3	1	455.9	27.2 2nd order Peak 9
13	584.0	21.2	21.2	4	3	584.9	21.2 Helium Resonance
14	607.5	20.4	20.4	4	3	607.8	20.4 2nd order Peak 11
15	633.0	19.7	19.6	4	3	633.0	19.6 He scattered
16				3	2	911.7	13.6

FIGURE 2.3 - Astrophysical Data vs. Mills Theory Illustrated



The analysis completed by this researcher in Appendix 3 corroborates the findings of BLP in regard to the extreme ultraviolet data in the background of space [above] as well as from our star, the Sun, as well as from a stellar flare on AU Mic and star EQ Pegasi. Dr. Mills' text also provides many other sources of astrophysical data which produce information that regularly display the lower energy hydrogen transition energies that would be most likely from a probabilistic standpoint. Table 2.4 on the page that follows lists the most commonly occurring wavelengths and energies in all of the data described above [ie; data that appeared in at least 3 of the 4 sources cited] and the match I have calculated for that data by equation (1e) above.

TABLE 2.3 - Commonly Observed Wavelengths & Mills Theory Predictions

Wavelength A	Mills Theory Wavelength & Hydrogen Transition A	Initial Stage → Final Stage	# of sources of 4
911.8	912.3	1/2 → 1/3	1*
302.8-304	303.9	1/3 → 1/4	3
261.2-265	265.0	1/4 → 1/5 He scattered	3
182-183	182.3	1/4 → 1/5	4
129.1-130	130.2	1/5 → 1/6	4
122.2-123	122.6	1/6 → 1/7 He scattered	3
101-101.3	101.3	1/6 → 1/7	4
89-90	89.0	1/7 → 1/8 H scattered	3
81-81.1	81.1	1/3 → 1/5 H scattered	3

* NOTE: Only one source, the solar spectral data, included observations above the 600 Å wavelength

2.3 Enigmas Solved

Perhaps the two most compelling enigmas that the Mills theory resolves are solar problems. They are; an inadequate solar neutrino flux and a solar coronal temperature that is inexplicably too hot. For two decades we have known that the standard solar model predicts that the primary energy source of our star is the nuclear fusion of hydrogen atoms. The problem is that scientists have been unable to account for an appreciable amount of the solar neutrino flux that would be predicted by assuming all of the Sun's radiant energy is from fusion. The Gallex solar neutrino detector in Italy sees only 60% of the neutrinos that the standard solar model would predict.^[29] The Homestake detector reports neutrino flux of 2.1 ± 0.03 SNU or only 27% of the standard solar model's 7.9 ± 2.6 SNU.^[30-32] Where

then, if not fusion, could the rest of the Sun's energy be coming from? A similar problem exists with the description of all of the Sun's energy coming from nuclear fusion when we consider the temperature gradient from the surface of the Sun into space. The photosphere [visible surface layers] of the Sun is 6000 K, "whereas the temperature of the corona [solar atmosphere] based upon the assignment of the emitted X-rays to highly ionized heavy metals is in excess of 1,000,000 K."^[33] The Mills theory is able to explain both of these seeming mysteries by postulating the disproportionation of hydrogen atoms in the atmosphere of the Sun. This transition of hydrogen to lower energy states as previously discussed gives rise to significant non-nuclear radiant energy [ie; transitions of hydrogen to the $n = 1/100$ level yield energy densities (139 keV) on the order of nuclear reactions]. The disproportionation reaction takes place in the coronal region of the Sun giving rise to the much higher temperatures there. Together the Mills theory makes sense of what otherwise could only be explained by difficult-to-believe concepts. The standard solar model has no answers for this enigma but two theories attribute the higher coronal temperature to "the conversion to heat energy by the dissipation of the energy in electric currents or magnetohydrodynamic [MHD] waves."^[34] If the corona consists of an "almost fully ionized plasma contained in closed magnetic field loops or of plasma expanding outwards along open magnetic field lines"^[35] it is quite a stretch and additional complication to propose the electric currents or MHD.

Another key enigma solved is that of the total mass or matter in the universe. For years physicists have been wrestling with the fact that either "black holes" or an unidentified "dark matter" must exist out there in space in order to explain why our calculated mass of the universe can not be obtained by adding up all of the radiative and observable matter. We need more mass to explain the observation that galaxies rotate at a higher angular velocity than possible with only the observed [visible] matter providing the stabilizing gravitational attraction.^[36] Is it too much a stretch for the logical mind to postulate that if over 95% of the known matter of the universe consists of hydrogen that the large amount of "missing matter" may also be some non-radiative form of hydrogen? Mills theory predicts that stars consume hydrogen and convert it into lower energy state hydrogen as the "ash" residue of the reaction. This ash is non-radiative, microscopically smaller than ground state hydrogen and is believed by Mills to be ubiquitous throughout the universe. It would appear to be an excellent candidate for the undiscovered, yet ubiquitous dark matter of the universe.

2.4 Technological Embodiments

This final section of Chapter 2 is devoted to devices and apparatus that have been designed and operated by BLP scientists in order to prove that the catalytic reduction of atomic hydrogen below its ground state of $n=1$ is not only achievable but is repeatable,

predictable and consistent. Table 2.4 below indicates the types of devices that have been designed and developed by BLP scientists to demonstrate the phenomenon.

TABLE 2.4 - BLP Technologies

Device	Type	Other
Dewar Flask	Electrolytic Cell	
Electrolytic Cell	Electrolytic Cell	DC electricity
Electrolytic Cell	Electrolytic Cell	AC electricity
Non-Electrolytic Cell	Gas Phase	
Glass Lamp	Gas Phase	
Isothermal Calorimeter	Gas Phase	
Calvet Calorimeter	Gas Phase	Oven Moderated
Nickle Hydride Wire Cell	Gas Phase	Water Cooled
Quartz Firebrick Cell	Gas Phase	
Test Cell 1	Gas Phase	Steady State Flow

Furthermore, all of the devices in the above table exhibit the ability to generate anomolous heat that is inexplicable by any known chemical or nuclear reactions. These devices generate heat with no flux or radioactive materials, reduction or consumption of known chemical or molecular reactions or bonds and follow directly from the Mills theory. The specific devices are in essence the embodiment of his concepts for bringing hydrogen atoms into contact with a catalyst in order to begin the hydrocatalysis and subsequent disproportionation reactions. The devices developed by BLP are both test and demonstration units.

The two and one-half pages following below provide illustrations of some of the key BLP technological embodiments. Figure 2.4 illustrates the dewar experimental vessel. Figure 2.5 shows the typical arrangement for one of BLP's advanced electrolytic cells. Figure 2.6 illustrates the device developed by the BLP joint venture with Thermacore -- a non-electrolytic first generation gas phase cell. Figure 2.7 illustrates the isothermal calorimeter and Figure 2.8 is a typical Calvet calorimeter arrangement. I am focusing on these few devices to keep the reader directed to the specific technological embodiments of the Mills theory that demonstrate that the production of excess and anomalous heat from each apparatus is conditional upon bringing all of the elements of Mills' theoretical requirements to the experiment. If any one of the key elements is

missing, the experiment functions as a typical control with no excess heat being produced.

FIGURE 2.4 - Dewar Experimental Cell

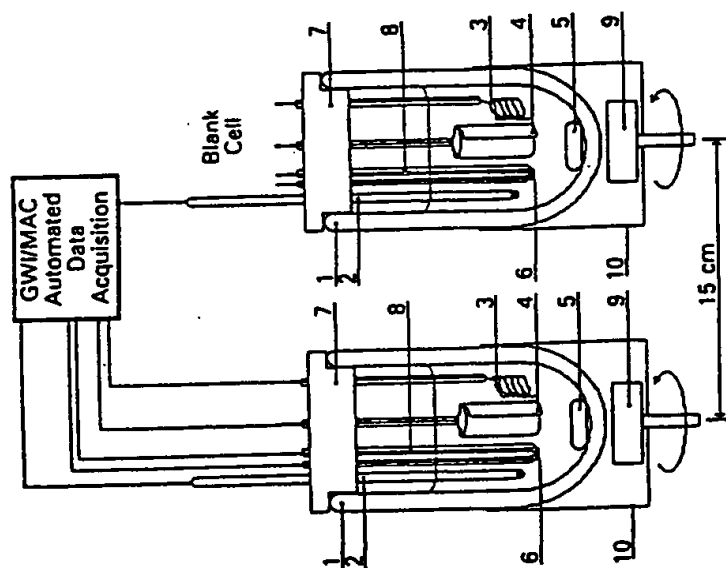


Fig. 5. Experimental calorimeter setup: (1) vacuum-jacketed dewar, (2) thermistor, (3) platinum anode, (4) nickel cathode, (5) magnetic stirring bar, (6) resistor-heater, (7) Styrofoam stopper lined with Parafilm, (8) Teflon tubing, (9) magnetic stirrer, and (10) aluminum cylinder.

FIGURE 2.5 - Advanced Electrolytic Cell

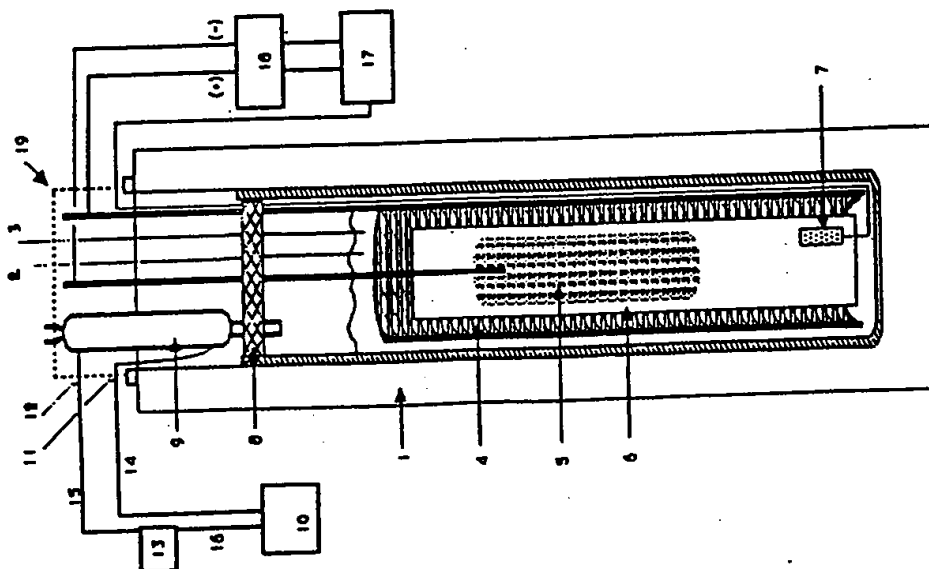


Fig. 1. The calorimeter/electrolysis cell: 1 = vacuum jacketed dewar, 2 = electrolyte thermistor, 3 = conductivity sensor, 4 = nickel anode, 5 = nickel cathode, 6 = Teflon spacer, 7 = resistor heater, 8 = Teflon cap, 9 = condenser, 10 = peristaltic pump, 11 = inlet reservoir, 12 = outlet thermistor, 13 = condenser inlet tubing, 14 = condenser outlet tubing, 15 = reservoir to pump tubing, 16 = power supply, function generator, power meter, 17 = oscilloscope, 18 = insulated cap.

FIGURE 2.6 - Non-Electrolytic Gas Phase Cell

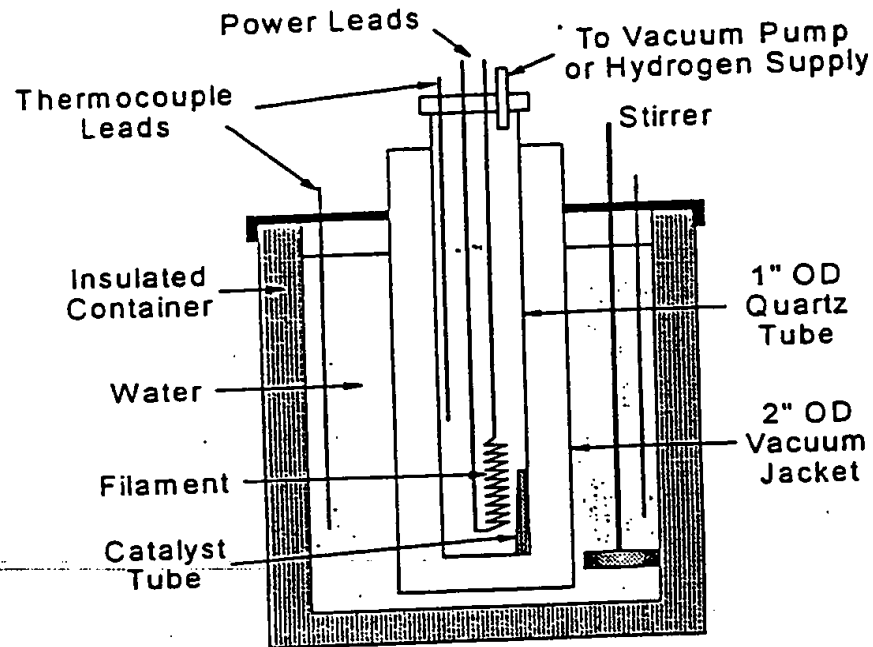


FIGURE 2.7 - Isothermal Calorimeter Gas Phase Cell

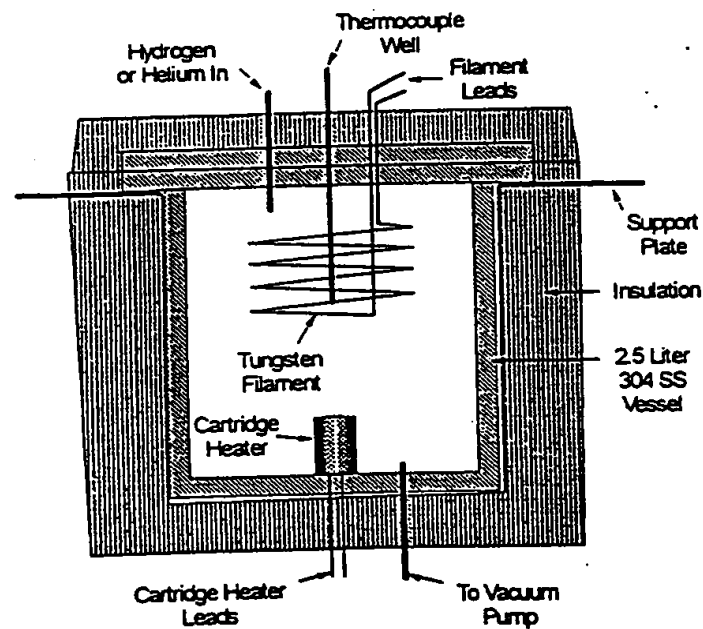
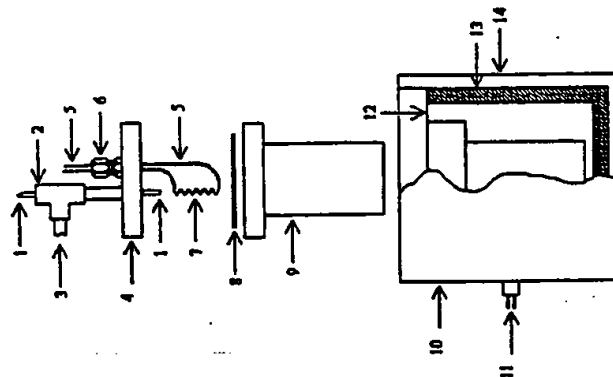


FIGURE 2.8 - Calvet Calorimeter Gas Phase Cell

Figure 1. Schematic of the Gas Cell for the Calvet Calorimeter and Cross Sectional View of the Calvet Calorimeter. 1 - (1/16)" OD stainless steel tube (to hydrogen supply), 2 - stainless steel tee union, 3 - (1/4)" OD stainless steel tube (to vacuum manifold), 4 - cell lid, 5 - filament leads, 6 - Conax-Buffalo gland, 7 - precision resistor, 0.1 mm OD tungsten filament, or nickel hydride filament treated with catalyst, 8 - copper ring gasket, 9 - cell body, 10 - Calvet Calorimeter, 11 - thermopile signal output, 12 - thermal shunt, 13 - thermopile, 14 - insulated calorimeter base.



In the case of the electrolytic cells it is very important that the hydrogen atoms be formed on the cathode contact with the right concentration of the catalytic ions in order for the heat generation phenomenon to be replicated. In the case of the gas cells a small, partial atmosphere of hydrogen gas, a small partial pressure of the catalytic ions as well as a mechanism to cause hydrogen dissociation all need to be present for the reaction to commence and continue. The experiments and subsequent demonstration units were designed specifically to assure that the mean free path for the hydrogen atoms [once formed] to interact with and collide with the catalytic ions was appropriate to favor the collision and catalytic reaction prior to hydrogen atom recombination into H_2 .

Each of the cells illustrated above were able to regularly, consistently and repeatedly generate heat in amounts that were far in excess of the any known chemical reaction for hydrogen and any other known elements. In the case of the vacuum gas cells this reaction was developed and maintained using only very small amounts of hydrogen gas, a filament to dissociate H_2 into its atomic form and a catalyst with the appropriate resonant enthalpy of 27 eV. Part II of this thesis will highlight the performance of BLP's isothermal cell, Penn State University's Calvet cell experiments as well as the experiments of this researcher in the Calvet cell at BLP laboratories.

To more fully document the BLP theory that lower energy hydrogen [hydrino formation] was the source of the heat in the reaction, the residue "ash" as it were from the reaction gases from both the electrolysis and vacuum cells was collected. According to Mills theory this "ash" should contain the lower energy form of hydrogen postulated by

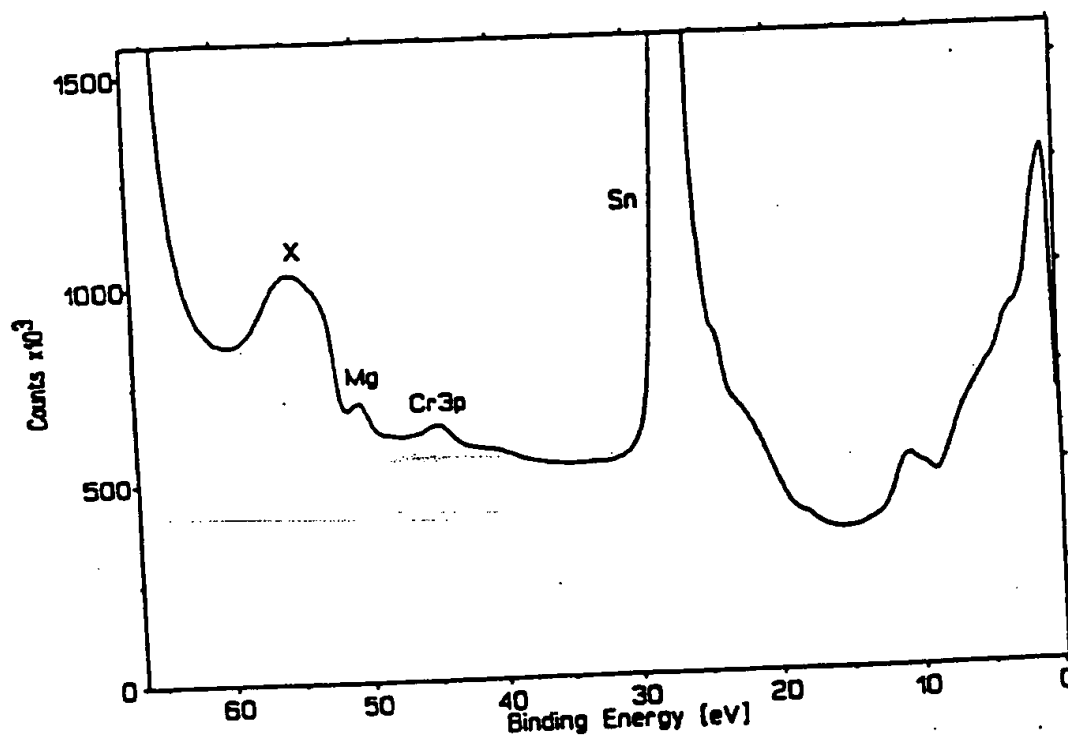
BLP. The difficulties of capture make this effort quite a challenge since the atoms being searched for will have significantly smaller diameters than the smallest of all atoms. BLP and four other scientific laboratories began this search a few years ago. They used the methods of mass spectroscopy, gas chromatography and X-ray photoelectron spectroscopy [XPS]. Table 2.5 below highlights the results of those investigations thus far.

TABLE 2.5 - The Search for Hydrinos

Device	Results/Observations	Investigating Laboratory
Mass Spectroscopy	Large signal with ionization energy in calculated range of dihydrino	BLP Laboratory Air Products & Chemicals Lab Schrader Analyt. & Cons. Lab
Gas Chromatography	Significant signal peaks which can be associated with $n=1/2$, $1/3$ and $1/4$ dihydrino molecules	BLP Laboratory
X-Ray Photoelectron Spectroscopy [XPS]	Signal Peaks associated with the binding energy of $n=1/2$, $1/3$ and $1/4$ hydrino molecules	Lehigh University - Zettlemoyer Center for Surface Studies Idaho National Engineering Lab Clark Evans & Associates

Figure 2.9 which follows on the final page of Part I illustrates the location of an anomalous peak near 55 eV binding energy which was detected by Zettlemoyer Center for Surface Studies at Lehigh University, Charles Evans & Associates and Idaho National Engineering Laboratories [INEL] in separate analyses of BLP and INEL samples. BLP asserts that the $n=1/2$ state of hydrogen, which has a calculated binding energy of 54.4 eV, is the source for the peaks in each independent study. At present all other potential known sources of a peak at that energy level [i.e. Fe_{3p}] have been ruled out as a source.

FIGURE 2.9 - XPS Anomalous 55 eV Peaks



PART II - Analysis of Previous Experimental Results

As noted in Chapter 2 [Table 2.1] there have been a substantial number of tests of BLP electrolytic cells. This researcher was not able to find any documented results from tests that had been performed on BLP cells which indicated that the cells did not operate in a manner to generate the anomalous heat predicted by BLP scientists. However, due to the controversial nature of electrolytic cell and the close association of the work with the continuing debate regarding cold fusion claims I have directed my research toward reviewing the test results which have been achieved in the gas phase cells. It is worthy of note at this point that there continue to be significant publications in Fusion Technology where well respected scientists are continuing to claim excess heat in so called "cold fusion" cell experiments. Of particular note is a recent technical paper in the March 1997 Fusion Technology journal. The authors [from Shell Research / CNAM Laboratoire des Sciences Nucléaires in Paris, France] describe how they have detected and verified that they are creating excess energy from hydrogen "7300 times higher than the most exothermic known reaction" at a high confidence level [99%]. They also detect missing hydrogen in their exhaust samples. Further, they present their postulate that the source of the additional energy is from "the formation of a tightly bound state of hydrogen...In such bound states, the electron is much closer to the proton than in normal hydrogen. This could explain both a high energy of formation and a greater than normal capacity to diffuse through any material" ^[37] All of these findings are consistent with the Mills theory. Part II of this thesis will focus on summarizing the results of two of the gas phase cell experimental results developed to date noting with special interest the experiments conducted by this researcher in section 3.3. In each case the gas phase cells produce a statistically significant [ie; beyond the error range and accuracy of the measuring device] amount of unexplainable heat. In the experiments the heat generated is well beyond the most energetic of chemical reactions known for hydrogen. I will attempt to explain, when possible potential reasonable alternative explanations for the repeatedly observed phenomenon. Often, however, there is no reasonable explanation other than the potential for a new energy source resulting from the interaction of hydrogen and the catalyst materials in the cells. After summarizing all of the gas phase cell experiments, the results of a singular isothermal cell test will be reviewed in detail [the experimental results from this cell formed the basis for the computer modeling work detailed in Chapter 4]. Results from the Penn State University cell will be reviewed and then the closing section will summarize the results of my work with Mr. William Good, the Chief Scientist and Director of Research & Development at BLP.

Chapter 3 - Summary Review of Gas Phase Cell Experimental Results

Table 2.4 illustrated seven gas phase cell experimental devices. I will provide a detailed explanation the operation of two of these devices in sections 3.1 through 3.3. I will place special focus [sections 3.2 and 3.3] on the Calvet device [see Figure 2.8] which is the most accurate in measuring the heat generated in a BLP reaction. Prior to the announcement of the hydrocatalysis process developed by BlackLight Power the

paradigm for hydrogen as a fuel revolved around its energetic reaction with oxygen. In nature, water [H_2O] is a very abundant, stable and versatile molecule. Hydrogen is very energetically bound to oxygen, and requires significant energy to break these these stable bonds to yield H_2 . After they are broken, hydrogen in its molecular form [H_2] is also stable, but reacts well and energetically with many other elements to form a plethora of molecules and compounds. The basic principle being tested with the gas phase cells of BLP is the ability of the hydrogen atom, once dissociated from its molecular form, to undergo electronic transition to lower energy levels [as described in Chapter 2] when it collides with a catalyst. All of the experiments therefore that will be described in the next three sections are configured to provide a reaction chamber [capable of operating at vacuum or near vacuum pressures], a means for hydrogen to be introduced to the chamber, a catalytic material to be introduced in the reaction chamber, a means for dissociating the hydrogen molecule into its atomic form, and a method for measuring heat generated by the reaction. Fundamentally the two cells reviewed in Chapter 3 are identical in nearly all respects except for the method for measuring or determining meaningful heat generation. The Calvet cell utilizes very accurate thermopiles to measure the heat flowing out of the vessel into the constant temperature oven. The isothermal cell uses the laboratory environment as the 'stable' external temperature and assumes the internal cell temperature represents a steady state heat loss previously measured by control runs to yield an 'estimate' of the additional power [anomalous heat] being provided by the reaction in a more indirect way. The Calvet cell experiments yield heat on the order of 6% to 12% more than energy being provided by the reaction than that used in the reaction zone [0.6 to 1.2 watts over a 10 watt filament power]. The isothermal cell experiments indicate heat gains of 52% to 171% over the energy being provided to the reaction zone [43 to 55 watts over a 32-86 watt input power]. It is the isothermal cell experiments that are of the greatest interest to this researcher since they portend the greatest potential for creating commercially significant heat. Section 3.1 focuses specifically on that BLP technological embodiment.

3.1 BlackLight Power Isothermal Cell

In the laboratory of BLP in Malvern, Pa. this researcher observed an experimental test on May 1, 1996 which was quite intriguing. A stainless steel vessel of 2 liters in volume was evacuated to a pressure of 1150 millitorr. [760 torr = 1 atm.]. This vessel was being maintained at a steady state temperature of 275° C by way of a cartridge heater consuming 97.1 watts located in the base of the vessel [see Figure 2.8]. The only materials inside this vessel were a 200 cm tungsten filament [0.01 cm. diameter] supported by 4 ceramic rods connected by 1/8th inch stainless steel tees and 3 grams of KNO_3 catalyst. Hydrogen was introduced into the system at a pressure of 1 atmosphere, the valve to the vacuum was opened and the pressure reduced to 2 torr minutes later. When the vacuum vessel comprised a closed system it had a steady state pressure of 1150 mtorr. When the power to the tungsten filament was turned on and raised to 15 watts the cartridge heater turned off and did not come back on for about one half hour. The temperature rose from

275° C to about 285° C during this period. When the cartridge heater did begin cycling again to maintain the vessel temperature at approximately 275° C it did so at a steady state energy consumption rate of 48.5 watts. [The details of this experiment are found in Appendix 4] The filament wattage was successively increased to 25 watts, 35 watts and 40 watts in three additional steps during which the cartridge heater energy decreased to 17.2 watts, 5.7 watts and 0 watts respectively. The vessel continued to maintain a temperature of 288-289° C without any energy being provided by the cartridge heater. The filament steady state power consumption was 40 watts indicating that something [presumably the Hydrocatalytic effect] occurring within the vessel appeared to be providing the additional 57 watts of heating that was necessary to keep the vessel at temperature. If one assumes that all the data being gathered on this closed system [i.e; energy in, temperature, pressure and chemicals involved] are accurate, then this appears to be a compelling illustration of this technology's capability. Table 3.1 illustrates a significant number of BLP experimental and control runs on their isothermal calorimeters.

I have summarized the results for each of the runs but the reader is encouraged to review the detailed data in Appendix 5. The Appendix includes all of the detailed experimental data as well as the analysis completed by this researcher. It is clear from the few control studies that the isothermal cell exhibits different behavior when it is operating on filament power versus cartridge heater power. As shown in experiments 15.5 and 15.8 the isothermal cell uses significantly less power with the filament than that required on the cartridge heater. This researcher believes that this apparent 25-54% savings may be due to four factors in the following order of significance; 1] The relative distances between the heating sources and the thermocouple [The filament was closer in proximity to the thermocouple and therefore had greater radiant coupling], 2] Radiant coupling of the filament with the thermocouple may have resulted in the thermocouple being at a higher temperature than actual temperature. [This condition would allow the cell to cool down and thus reduce to some degree its heat loss and associated energy requirements]. 3] Increased stratification may have occurred under filament power [i.e.; convective mixing of gases may not have occurred sufficiently allowing stratification. With the upper regions of the cell warmer than the lower regions of the cell heat loss would have decreased across the entire cell surface]. 4] In the case when the cartridge heater was the only source of power, heat loss through the bottom of the cell may have been higher, thus the thermocouple in the cell will need to see greater power from the cartridge heater in order to cycle off the power. It is important to note that another way of considering this last point is that the filament provided all of its heat interior to the cell most efficiently, while the cartridge heater entered through and was connected to the bottom surface of the calorimeter allowing a larger percentage of its heat energy to leave the cell without affecting thermocouple temperature.

Nonetheless, it is important to note that experiments 15.4, 15.6, 15.9 and 15.10 all create anomalous heat far beyond the cartridge/filament differential calculated by the control experiments. From the heat loss model developed on these cells in Part III of this

thesis it appears that the isothermal cells are able to create at least tens of watts of useful power even in their very primitive development state.

TABLE 3.1 - Isothermal Cell Results Summary

Experiment #	Temp (C)	Pressure (Torr)	Watts [Heater]	Watts [Filament]	Excess Heat [Watts]	Power Gain [%]
15.4	259	2.0	95.2	45.7	49.5	108.3%
15.5 control	273	low atm	94.3	61.3	33.0	53.8%
	273	2.0	94.3	75.7	18.6	24.5%
15.6	271	1.4	92.0	43.6	48.4	111.0%
15.8 control	261	low atm	87.3	62.5	24.8	39.7%
15.9	280	1.7	103.5	41.7	61.8	48.2%
15.10	264	1.6	92.7	32.2	60.5	187.9%
15.12	284	0.02	106.0	97.8	8.2	8.3%
15.13	319	1.9	131.2	83.6	47.6	56.9%

It is recommended that the isothermal cells be outfitted with external temperature measurement thermistors and that a full set of controls and experiments be carried out on these cells. From this work we can develop heat loss calibration curves under various temperature and pressure regimes. In addition, each cell should be blanketed with a standard jacket to reduce heat loss variability from experiment to experiment. From a very high temperature the cell should be turned off and a heat loss decay model be fit to its heat loss rate over time. This empirical model could then be used as a second source of validation for the calculated excess energy created in the hydrocatalytic reaction within the vessel.

3.2 Penn State University Calvet

In late 1996 Dr. Jonathan Phillips, Professor of Chemical Engineering at the Pennsylvania State University, and Julian Smith, his graduate research assistant undertook significant control experiments and tests on the heat generation of gas phase Hydrocatalysis. A complete copy of their report and findings is provided in Appendix 6. The Calvet cell

that they used is shown in Figure 2.9. The Calvet calorimeter cell is configured much like the isothermal cell described above but it includes much more accurate direct measurement of heat flux out of the reaction vessel. This measurement device is accurate to within 0.5% in recording energy flow. Unfortunately, in order to gain this extremely high accuracy one must place this vessel into a very controlled environment and into a thermopile base. This makes a large device very costly. The size of the Calvet cells used by Penn State are 20 cubic centimeters. The tests were conducted during the period of October - December 1996 in Penn State Chemical Engineering Department laboratories. The following excerpt from the report summarizes their key work and findings; "In three separate trials between 10 and 20 K Joules were generated at a rate of 0.5 Watts, upon the admission of approximately 10^{-3} moles of hydrogen to the 20 cm^3 Calvet cell containing a heated platinum filament and KNO_3 powder. This is equivalent to the generation of 1×10^7 J/mole of hydrogen as compared to 2.5×10^5 J/mole of hydrogen anticipated from standard hydrogen combustion. Thus, the total heats generated appear to be two orders of magnitude too large to be explained by conventional chemistry, but the results are completely consistent with the Mills' model." [38]

It is noteworthy that in all cases the Penn State tests [summarized in Table 3.2] were terminated by removing the hydrogen from the reaction vessel by opening the valve to the vacuum and pumping the gas from the vessel. It is not clear how long these reactions would have continued if the vessel was not emptied of the hydrogen gas. The method used by PSU included bringing their Calvet reactor cell to steady state in a controlled environment oven with only a platinum filament and small vessel of KNO_3 present within the reactor vessel. They would zero out the Calvet output at this point and then admit hydrogen to observe the reaction that this precipitated. Their experiments showed a significant exothermic reaction upon the admission of hydrogen which could not be replicated upon the admission of helium [which they used as a control gas for their experiments]. In all cases this exothermic reaction was curtailed by the researchers once the total energy that had been produced was significantly greater than that available in known chemical reactions of hydrogen.

TABLE 3.2 - Penn State Calvet Cell Results Summary

Experiment #	Temperature (°C)	Pressure (Torr)	Total Time (minutes)	Total Energy (Joules)	Excess Heat (milliWatts)
BL1218CD	250	170	612	21,560	586.8
BL1220BC	250	180	364	13,003	595.9
BL1221AB	250	120	284	10,293	604.7

3.3 Jansson Calvet

In early 1997, this researcher approached Mr. William R. Good, Research Director of BLP to discuss the possibility of replicating the isothermal cell work at BLP to determine more conclusively the primary parameters of the gas phase reaction. It was this researchers intent to determine the effect of filament surface area on excess heat formation as well as begin parameterizations of other key variables such as reaction zone volumes, gas partial pressures, temperature, and other variables. BLP was most gracious in offering their Calvet cells for any experiments I would choose to run. The isothermal cells could be used as a follow-up in the event that the data from the Calvet work indicated a significant isothermal cell demonstration was feasible. In as much as it is believed that the formation of excess energy is caused by hydrogen atoms colliding with catalyst ions or hydridos, I undertook to prove that increasing filament surface area would increase atom generation rate and thus increase power output from the Calvet cell. The protocol for my experiments is included as Appendix 7. A copy of my control and experimental results are included as Appendix 8. My original intent was to reproduce the Penn State experimental results and then go on to vary only the filament length in two subsequent experiments. If this could be done successfully, I believe it would demonstrate that specific parameters of the reaction could be controlled and engineered. We followed the PSU protocol in all aspects except reaction vessel pressure; this was because it appeared we were unable to demonstrate the excess heat effect at the 150-1000 torr range where the PSU reaction had operated successfully. We were successfully able to replicate numerous times the anomalous heat gain results in the 50-200 mtorr pressure regime. When we completed many of our post-experimental calibrations without the KNO_3 catalyst we believe we were able to identify excess heat that was being generated from the small amount of hydrogen that was off gasing from the platinum filament. This is my present interpretation of the results I obtained. Presently I can not offer an alternative expalantion for the consistent excess heat activity when only the filaments and KNO_3 catalyst are present in the experiments. Table 4.3 below summarizes my testing objectives.

TABLE 3.3 - Jansson Calvet Testing Objectives

- * Replication of PSU Results
 - * Vary Filament Length [10cm , 20 cm , 30 cm]
 - * Analyze Results for Consistency and Patterns
 - * Determine if Effect Appears Engineerable
 - * Develop New Technical Skills and Knowledge
-

Table 3.4 below summarizes the 9 experiments and controls that I performed during the period of February 27 through May 5 1997. Each was conducted according to the primary protocol summarized in Appendix 7.

TABLE 3.4 - Jansson Calvet Tests Completed

- * 20 cm Experiments
 - 1 control
 - 2 experiments
 - February 27 - March 21, 1997
- * 10 cm Experiments
 - 1 experiment / post control-calibration run
 - March 25 - April 13, 1997
- * 30 cm Experiments
 - 1 control
 - 4 experiments
 - March 22 - 25, 1997
 - April 13 - May 5, 1997

The following tables [3.5 & 3.6] summarize the testing protocol which was followed for each of the controls and experiments conducted in the BLP laboratories:

TABLE 3.5 - Jansson Calvet Testing Protocol Summary - Control

- Prepare Calvet Reactor Vessel
 - ◆ Install Filament and Vacuum Test
 - Place Calvet in Thermopile Cup
 - ◆ Vacuum test, connect leads, insulate
 - Bring Oven & Calvet to Steady State
 - ◆ 250° C, vacuum cell to remove all H₂O, etc.
 - Start DAS, Turn On Power, Close Vac.
 - ◆ 0,1,5,6,10,11,15,16, etc. watts to steady state
 - Wait Until Steady State is Achieved
 - Observe Changes in V_c
-

TABLE 3.6 - Jansson Calvet Testing Protocol Summary - Experiments

- Prepare Calvet Reactor Vessel
- ◆ Install Filament, KNO_3 , Vacuum Test
- Place Calvet in Thermopile Cup
- ◆ Vacuum test, connect leads, insulate
- Bring Oven & Calvet to Steady State
- ◆ 250°C , vacuum cell to remove all H_2O , etc.
- Start DAS, Turn On Power, Close Vac.
- ◆ 0,1,5,6,10,11,15,16, etc. watts to steady state
- Wait Until Steady State is Acheived
- ◆ Stable V_c , W_{in} , V_f , KNO_3 vapor pressure
- Observe Changes in V_c
- Inlet H_2 to Double Current Pressure*
- Wait 5 min. and Vacuum Down to $< 0.1 \text{ T}$
- Observe Changes in V_c

NOTE: V_c is the Calvet calorimeter voltage indicative of heat output, W_{in} is the total energy being consumed by the filament within the Calvet, V_f is the Voltage associated with the energy being dissipated by the filament [allows us to know I^2R losses], and vapor pressure is measured in mTorr.
* in all cases it was not necessary to add additional H_2 in order to observe an elevated V_c

Table 3.7 below illustrates the calibration curves and linear regression analysis fits which I obtained for each of the control runs used in calculating the excess heat from each experiment.

TABLE 3.7 - Jansson Calvet Testing - Calibration Curves

- | | | |
|------------------------------------|--|----------------|
| ■ 10 cm | | |
| ◆ $V_c = 0.2016 (W_{in}) - 0.0806$ | | $R^2 = 0.9966$ |
| ■ 20 cm | | |
| ◆ $V_c = 0.2333 (W_{in}) - 0.0605$ | | $R^2 = 0.9996$ |
| ■ 30 cm | | |
| ◆ $V_c = 0.2297 (W_{in}) + 0.5188$ | | $R^2 = 1.0000$ |

Pages 45-51 graphically and tabularly depict the results of the many days [over 555 hours] of analyzed Calvet cell experiments and controls. The results begin with a summary slide and then summarize the data by 10 cm., 20 cm. and 30 cm. experimental and control runs. These are labeled Figures 3.1, 3.2, 3.3, 3.4, 3.5, 3.6 and 3.7. Table 3.8 below is a numerical summary of the results obtained for all KNO_3 experiments as well as KNO_3 plus hydrogen experiments. All excess heat calculations for the experiments is based upon the difference between the Calvet output power anticipated via the control runs contrasted with the actual input power used to generate that Calvet voltage output during the experimentals. All controls and experimentals were completed in a closed system in an oven with temperature of 250 °C. In all cases the vacuum integrity of the reaction vessel was maintained throughout the entire run of the experiments.

Table 3.8 Jansson Calvet Cell Results Summary

Filament Length [cm]	Excess Power Generated [Watts]			Hours of Operation	Total Energy Produced [W-hrs]	% Over * Chemical
	Mean	Max	Min			
10	0.581	0.635	0.523	297.97	173.013	234,387
20	0.818	1.231	0.337	125.22	102.464	138,090
30	1.572	2.092	0.635	131.95	207.467	278,151

* - % Over Chemical - is the amount of energy generated by the reaction divided by the energy that would have been created had all of the hydrogen available at anytime in the experimental apparatus been consumed in the most energetic chemical reaction calculated [ie; hydrogen combining with oxygen to form water - H_2O] expressed in percent.

The energy produced by these experiments significantly exceeds that which could be released by any known or potential chemical reaction by several orders of magnitude. The value shown in the table above is extremely conservative in that it was determined assuming the following; 1] all potential hydrogen in the system was converted with perfect efficiency into water, 2] all of the impurities in the platinum wire [99.99% pure] were hydrogen, 3] all hydrogen admitted at any time into the reaction chamber reacted within the vessel, even though it was rapidly brought under vacuum pressure and drawn out early in each experiment. Even when these conservative assumptions are applied, there remains a significant and large amount of energy that is unaccounted for. This ranges from about 1,400 to 2,800 times the amount of energy that was available at any time to the system assuming it was able to be perfectly released in a chemical reaction. These results would appear to be entirely consistent with Mills theory.

Figure 3.1

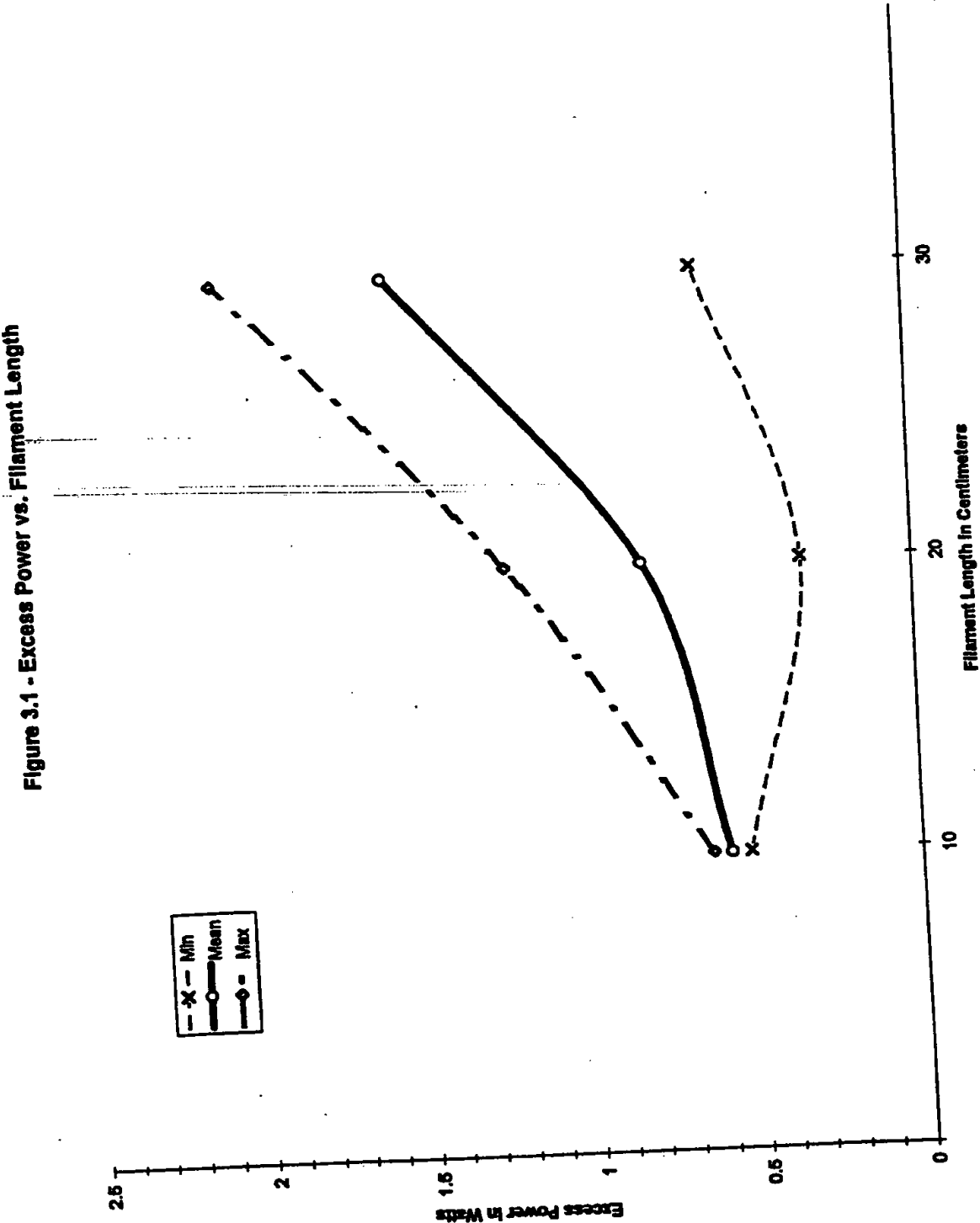


Figure 3.2

Figure 3.2 - Summary of 10cm

[illegible]

Figure 3.3

Figure 3.3 - Calibration Curve - 10 cm Control

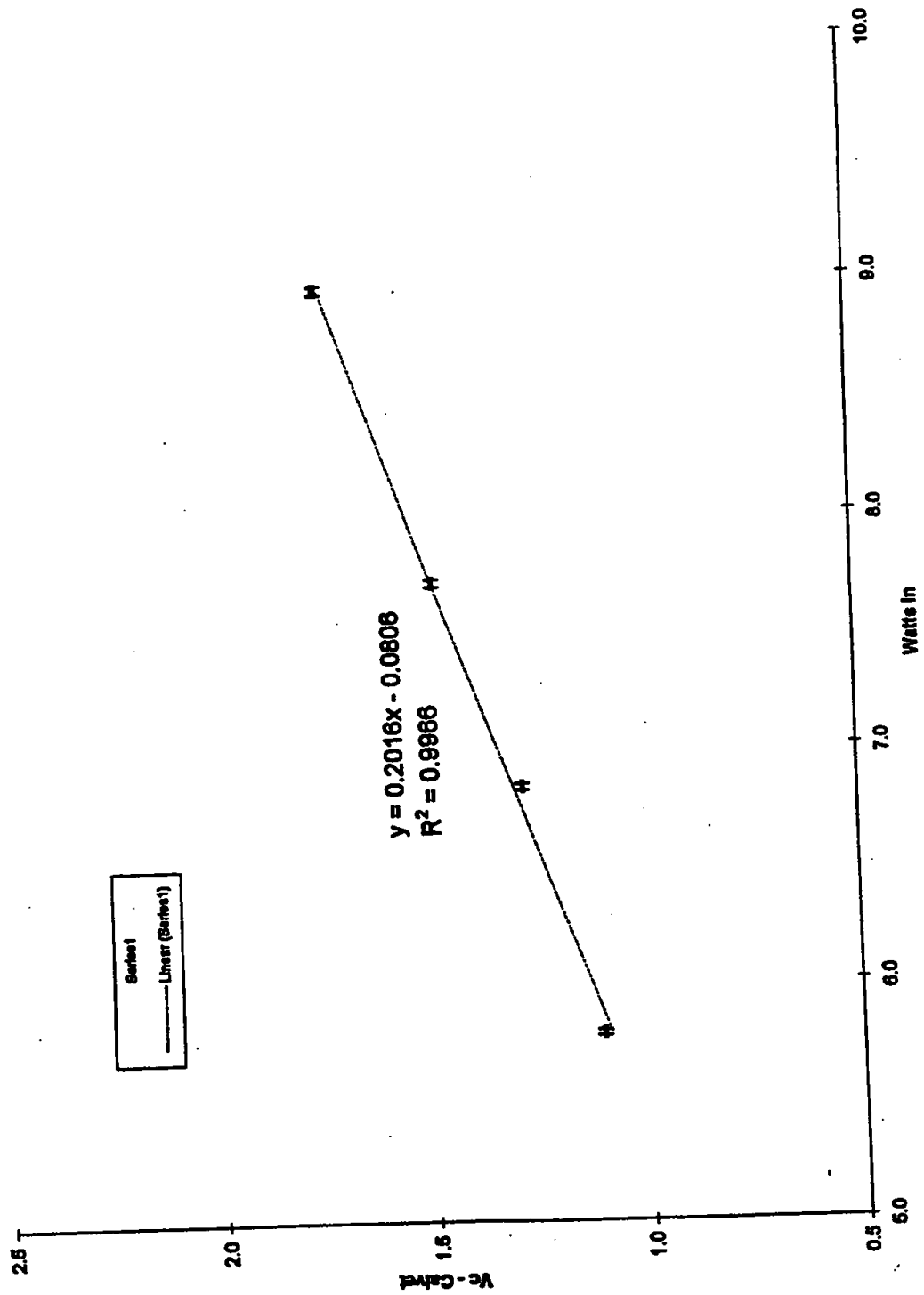


Figure 3.4

[illegible]

Figure 3.5

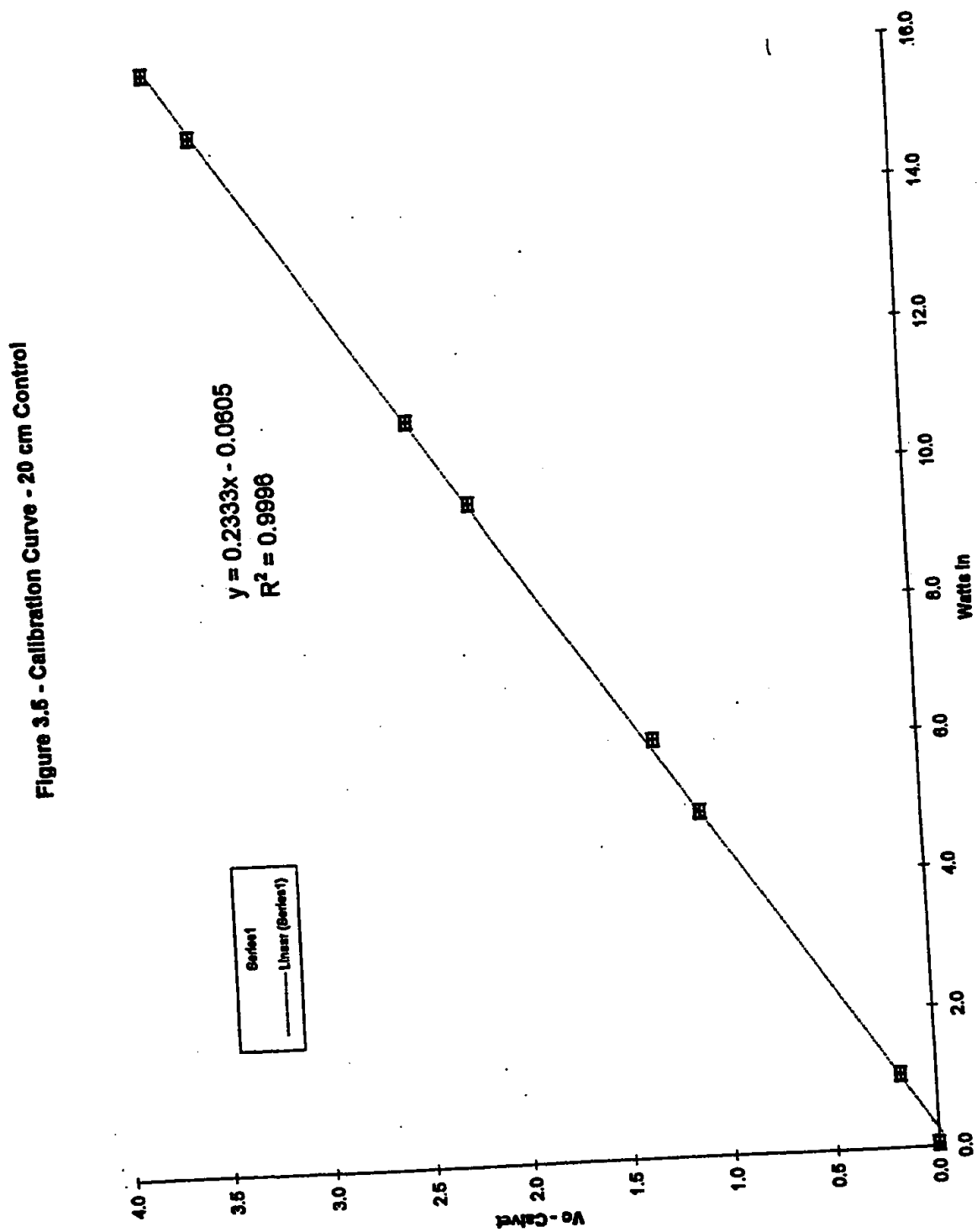
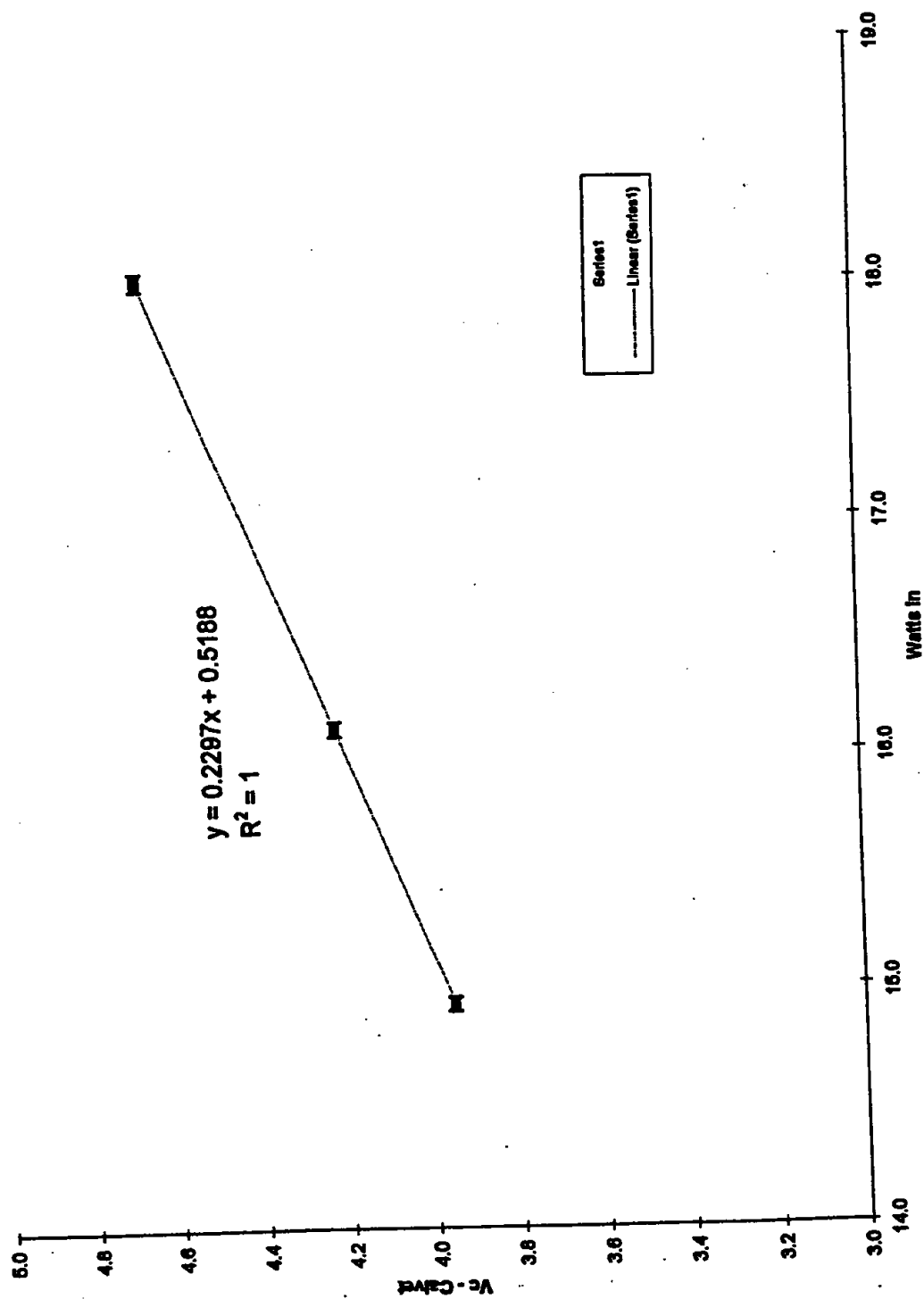


Figure 3.6

[illegible]

Figure 3.7

Figure 3.7 - Calibration Curve - 30 cm Control



PART III - Mathematical Simulation Model

In order to assess the commercial potential of the BlackLight Power technology I performed some mathematical simulation modeling on one of their most promising devices. The isothermal cell described in Section 3.1 produced meaningful excess power on the order of 50-60 watts and at meaningful temperatures 250-320 °C. The simulation model I developed attempts to recreate the heat loss profile of the isothermal cell in order to assess how much energy theoretically would be required to maintain the cell at any temperature level. I developed this method as a theoretical modeling method to cross-check the calibrations and excess energy results achieved by the experiments on the isothermal cell. Chapters 4 and 5 below provide the results of the simulation model as well as my insights and lessons learned from the exercise. In addition, I developed a comprehensive testing protocol which, if implemented, could conclusively prove the energy gain of the isothermal cell and provide additional documentation for its performance.

Chapter 4 - Analysis of Model Performance vs. Experimental Results

In order to model thermally the heatloss for the BLP Isothermal Calorimeter I used the data provided from the BLP Experiment 15.6 witnessed by AEI employees on May 3,1996. The method of operation of the Isothermal Cell is provided in Section 3.1. The experiment which we observed operated according to BLP's predictions, previous experiments and protocol. We were able to observe the results detailed in Appendix 9. A summary of that test has been provided on Table 4.1 below.

TABLE 4.1 - Isothermal Cell Results: May 3-4, 1996

TIME	CRITICAL TEMPERATURES - °C			PRESS. MILLTORR	FILAMENT WATTS	HEATER WATTS	EXCESS WATTS
	CELL	ROOM	AT				
10:45 AM	279.50	28.42	251.08	1150	0	96.99	0.01
					0	97.07	-0.07
					0	97.32	-0.32
11:10 AM	285.09	28.04	257.05	1400	15	48.54	33.46
11:15 AM					15	48.94	33.06
11:45 AM					15	49.26	32.74
11:50 AM	288.86	27.88	260.98	1400	25	16.23	55.77
12:05 PM					25	17.75	54.25
12:15 PM					25	17.78	54.22
12:20 PM	289.24	27.45	261.79	1700	35	5.73	56.27
2:10 PM					42	0.00	55.00
2:15 PM							
2:25 PM							

At approximately 2 A.M. on the morning of May 4, 1996 the filament inside the Isothermal Cell which we were testing burnt out. This caused a significant and dramatic fall in cell temperature. The Isothermal Cell at that point in the experiment was receiving all of its input power and cell heating from the tungsten filament and the associated heat of reaction from the believed Hydrocatalytic reduction of the hydrogen gas at the near vacuum pressure [1.2-1.7 torr] within the cell. Figure 4.1 on the following page illustrates the dramatic drop in cell temperature which was observed when the filament ceased to operate. The intent of my simulation model was to develop mathematical formulae that could match the heat loss profile of the cell while it underwent this steady state cooling toward room temperature and also match in to the calibration tests conducted at the 260-320 °C temperature levels. I pursued this approach assuming simplistically that all significant heat loss was achieved via conduction $[U \cdot A \cdot \Delta T]$ and that radiative and convective heat losses from the Isothermal Cell were minimal. With this approach I was able to get an excellent correlation at the lower temperature regime of operation $[\leq 160 \text{ }^{\circ}\text{C}]$ - see Figure 4.2] with a good fit at the higher temperature profile $[\geq 260\text{-}320 \text{ }^{\circ}\text{C}]$ - see Figure 4.3].

From those two pieces of the model I was able to develop an estimate of the heat loss of the Isothermal Cell at its entire range of operation in the tests conducted by BLP. This data is summarized below on Table 4.2.

TABLE 4.2 - Isothermal Cell Heat Loss vs. Temperature*

Cell Temperature [°C]	Calculated Heat Loss [watts]
27	0.0
50	9.3
75	19.3
100	29.4
125	39.5
150	49.6
175	59.6
200	69.8
225	79.8
250	89.9
275	100.0
300	110.1
325	120.2

* - assumes ambient temperature is 27 °C

FIGURE 4.1 - Isothermal Cell Performance - May 4, 1996

M. Custer
5/6/96

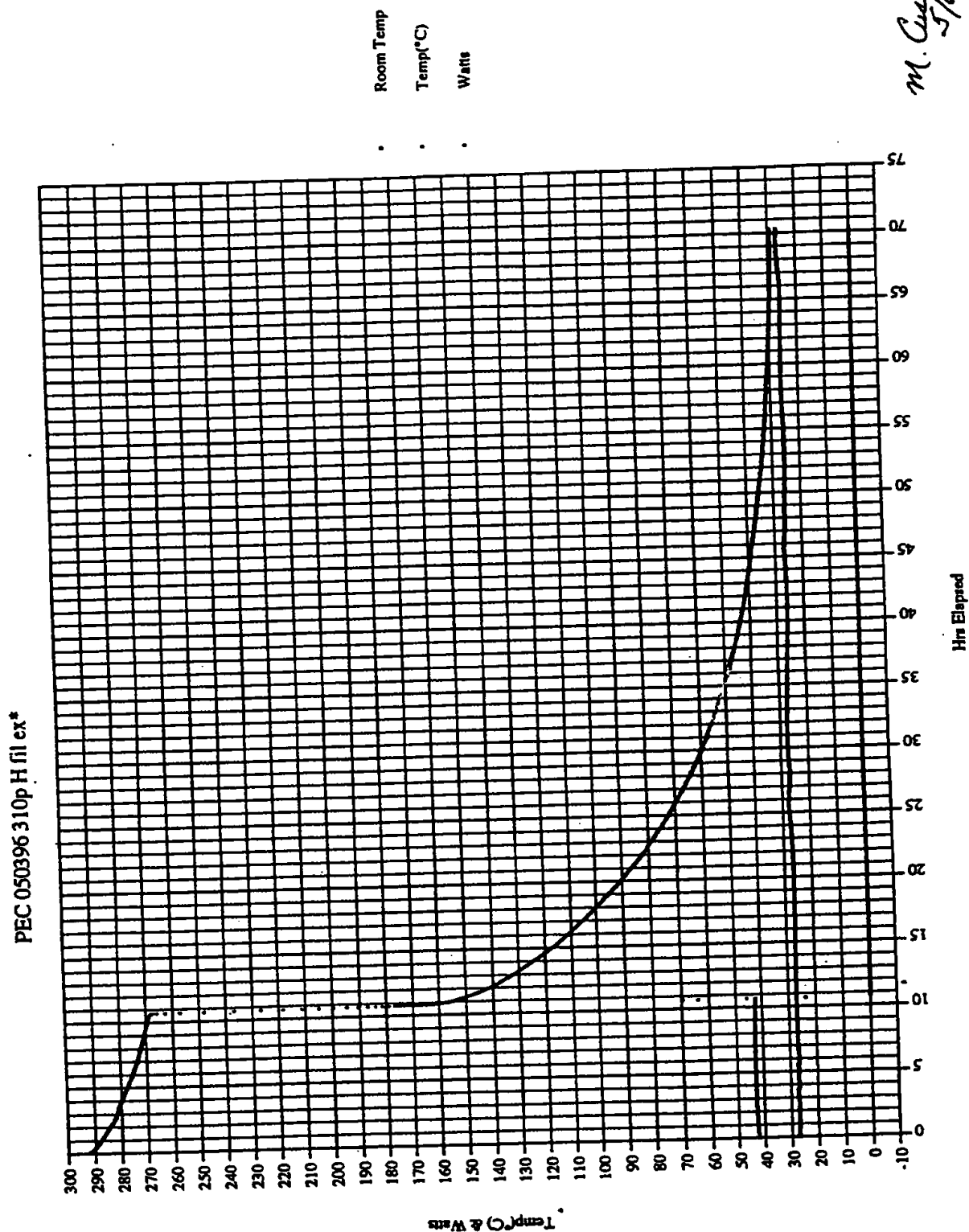
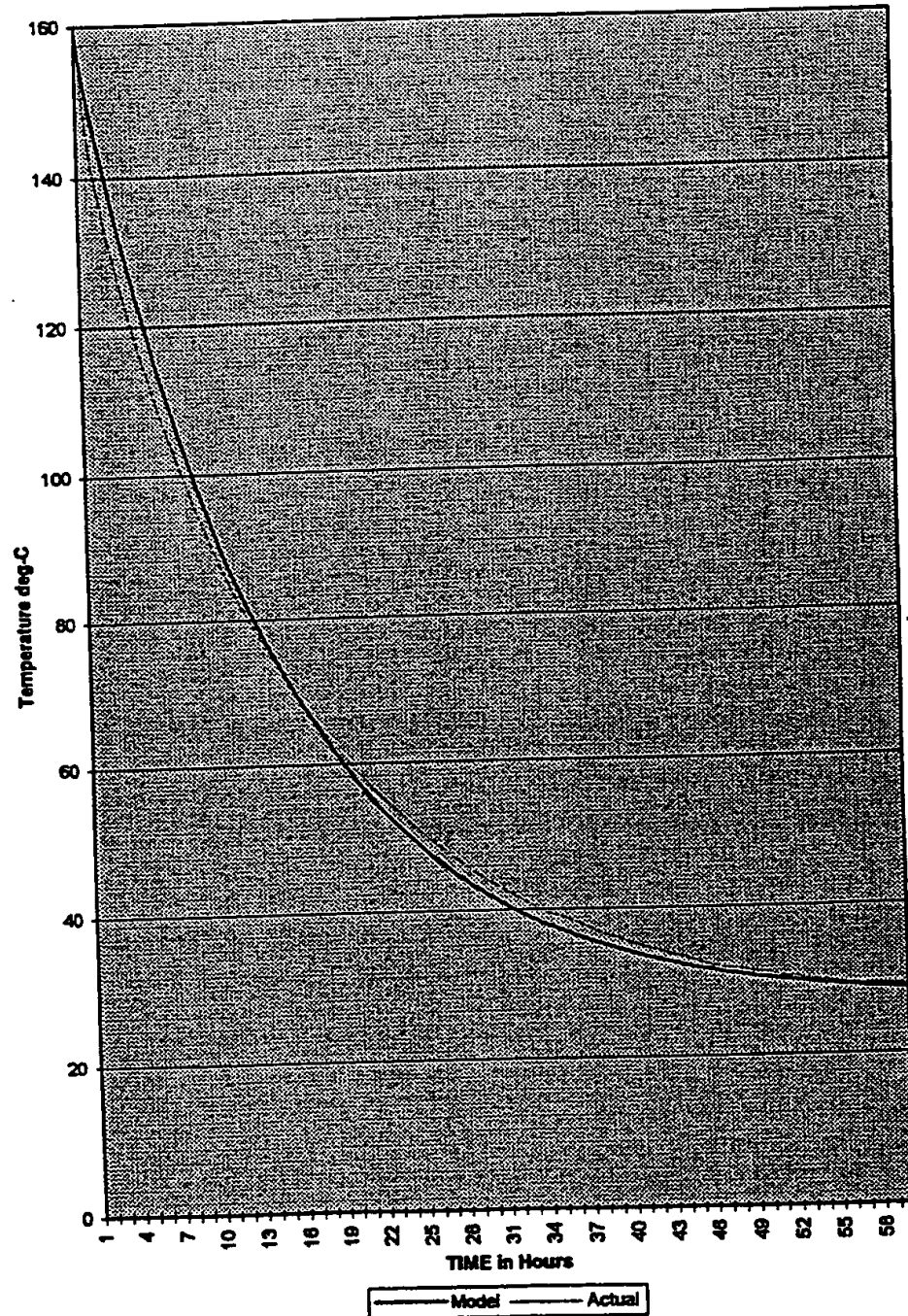


FIGURE 4.2 - Isothermal Cell Model vs. Actual Heat Loss

Model vs. Actual Data



Isothermal Cell - Heat Loss



Chapter 5 - Key Learnings and Insights From Simulation and Model

What does all this modeling tell us? The specific experiment that we reviewed in order to develop the model can now be looked at with a greater degree of detail and understanding. We know that the Isothermal Cell was able to maintain a temperature measured by the thermocouple at between 280-290 °C. While under cartridge heater power it took 97-103 watts to maintain this temperature [our model says it should have taken approximately 102-106 watts]. When the hydrogen gas was exposed to the filament the thermocouple reading said that the temperature was maintained at approximately the same level. However, in this case the filament was using only 42 watts at steady state. If we were to estimate from the simulation model what the Isothermal Cell temperature would have to be in order for its steady state heat loss to be satisfied with only 42 watts of input power we would see that the equivalent temperature was 132 °C. It is hard to believe the cell was operating at this low of a temperature during the experiment since our heat loss model was well able to accurately track the heat loss of the cell from when the filament burnt out all the way up to 160 °C with an extremely high degree of accuracy. While these learnings indicate that the cell was in fact producing anomalous heat, it must be pointed out that due to cell variability observed between experimental runs and control runs and also between similar experiments the accuracy of heat measurement in the Isothermal Cell is not fully quantified and known. Due to the significant number of BLP experimental and control runs on their isothermal calorimeters the summary results highlighted in Table 3.1 it is most probable that the cell in fact produces heat consistently. Due to the variability of the few control studies that were run by BLP demonstrating that the Isothermal cell exhibits different behavior when it is operating on filament power versus cartridge heater power, more control studies are needed. As discussed in section 3.1 this researcher believes that some of the variability between cell heating source performance may be due to the four factors described in Section 3.1 [i.e.; the relative distances between the heating sources and the thermocouple, etc.] Nonetheless, it is important to note that this experiment does appear to create anomalous heat far beyond the cartridge/filament differential calculated by the control experiments. From the heat loss model described above it appears that this isothermal cells was able to create at least 10-30 watts of useful power even in its early development state.

Included on the pages that follow I have outlined a proposed testing protocol for the Isothermal Cells which I believe will conclusively demonstrate their performance or lack of performance. In that protocol I recommend that the isothermal cells be outfitted with external temperature measurement thermistors and that a full set of controls and experiments be carried out on these cells. From this work we can develop heat loss calibration curves under various temperature and pressure regimes. In addition, each cell should be blanketed with a standard jacket to reduce heat loss variability from experiment to experiment. From a very high temperature the cell should be turned off and a heat loss decay model be fit to its heat loss rate over time. This empirical model can then be used as a second source of validation for the calculated excess energy created in the hydrocatalytic reaction within the vessel.

ISOTHERMAL CALORIMETER

Definitive and Conclusive Testing Protocol

SETUP:

- Develop and Install Standard Insulation Jacket [2-4" min. thickness]
- Install 2 Internal [Top and Bottom] Thermocouples and/or Thermistors
- Install 6 External Thermistors top, bottom, each 90 degrees alternate up down 1/3
- Measure total weight, and total volume of isothermal vessel
- Develop computer controlled program to initiate steps 1-3 of each protocol

Control Run #1 - He at 1 atmosphere

1. Measure all relevant temperature, pressure parameters and time for following protocol:

USING ONLY CARTRIDGE HEATER

- 10 watts in for 1-4 hours or until steady state is achieved
- up power to 20 watts in for another 1-4 hours or until steady state temperatures are reached
- up power to 30 watts in [until steady state temps]
- up power to 40 watts in [until steady state temps]
- continue..... in 10 watt increments noting all temps and time
- up to 200 watts in or until cell temps are over 400 °C
- Shut off all power and monitor temperature decline vs. time

2. Measure all relevant temperature parameters and time for following protocol:

USING ONLY 200 CM. FILAMENT

- 10 watts in for 1-4 hours or until steady state is achieved
- up power to 20 watts in for another 1-4 hours or until steady state temperatures are reached
- up power to 30 watts in [until steady state temps]
- up power to 40 watts in [until steady state temps]
- continue..... in 10 watt increments noting all temps and time
- up to 200 watts in or until cell temps are over 400 °C
- Shut off all power and monitor temperature decline vs. time

3. Measure all relevant temperature parameters and time for following protocol:

USING FIRST CARTRIDGE HEATER FOR 10 WATTS THEN FILAMENT FOR NEXT 10 WATTS

- 10 watts in for 1-4 hours or until steady state is achieved
- up power to 20 watts in for another 1-4 hours or until steady state temperatures are reached
- up power to 30 watts in [until steady state temps]

up power to 40 watts in [until steady state temps]
continue..... in 10 watt increments noting all temps and time
up to 200 watts in or until cell temps are over 400 °C

Control Run #2 - H₂ at 1 atmosphere

1. Measure all relevant temperature parameters and time for following protocol:

USING ONLY CARTRIDGE HEATER

10 watts in for 1-4 hours or until steady state is achieved
up power to 20 watts in for another 1-4 hours or until steady state temperatures are reached
up power to 30 watts in [until steady state temps]
up power to 40 watts in [until steady state temps]
continue..... in 10 watt increments noting all temps and time
up to 200 watts in or until cell temps are over 400 °C
Shut off all power and monitor temperature decline vs. time

2. Measure all relevant temperature parameters and time for following protocol:

USING ONLY 200 CM. FILAMENT

10 watts in for 1-4 hours or until steady state is achieved
up power to 20 watts in for another 1-4 hours or until steady state temperatures are reached
up power to 30 watts in [until steady state temps]
up power to 40 watts in [until steady state temps]
continue..... in 10 watt increments noting all temps and time
up to 200 watts in or until cell temps are over 400 °C
Shut off all power and monitor temperature decline vs. time

3. Measure all relevant temperature parameters and time for following protocol:

**USING FIRST CARTRIDGE HEATER FOR 10 WATTS THEN
FILAMENT FOR NEXT 10 WATTS**

10 watts in for 1-4 hours or until steady state is achieved
up power to 20 watts in for another 1-4 hours or until steady state temperatures are reached
up power to 30 watts in [until steady state temps]
up power to 40 watts in [until steady state temps]
continue..... in 10 watt increments noting all temps and time
up to 200 watts in or until cell temps are over 400 °C

Control Run #3 - He at 2 Torr

1. Measure all relevant temperature parameters and time for following protocol:

USING ONLY CARTRIDGE HEATER

10 watts in for 1-4 hours or until steady state is achieved
up power to 20 watts in for another 1-4 hours or until steady state temperatures are reached
up power to 30 watts in [until steady state temps]
up power to 40 watts in [until steady state temps]
continue..... in 10 watt increments noting all temps and time
up to 200 watts in or until cell temps are over 400 °C
Shut off all power and monitor temperature decline vs. time

2. Measure all relevant temperature parameters and time for following protocol:

USING ONLY 200 CM. FILAMENT

10 watts in for 1-4 hours or until steady state is achieved
up power to 20 watts in for another 1-4 hours or until steady state temperatures are reached
up power to 30 watts in [until steady state temps]
up power to 40 watts in [until steady state temps]
continue..... in 10 watt increments noting all temps and time
up to 200 watts in or until cell temps are over 400 °C
Shut off all power and monitor temperature decline vs. time

3. Measure all relevant temperature parameters and time for following protocol:

**USING FIRST CARTRIDGE HEATER FOR 10 WATTS THEN
FILAMENT FOR NEXT 10 WATTS**

10 watts in for 1-4 hours or until steady state is achieved
up power to 20 watts in for another 1-4 hours or until steady state temperatures are reached
up power to 30 watts in [until steady state temps]
up power to 40 watts in [until steady state temps]
continue..... in 10 watt increments noting all temps and time
up to 200 watts in or until cell temps are over 400 °C

Control Run #4 - H₂ at 2 Torr

1. Measure all relevant temperature parameters and time for following protocol:

USING ONLY CARTRIDGE HEATER

10 watts in for 1-4 hours or until steady state is achieved
up power to 20 watts in for another 1-4 hours or until steady state temperatures are reached
up power to 30 watts in [until steady state temps]
up power to 40 watts in [until steady state temps]

continue..... in 10 watt increments noting all temps and time
up to 200 watts in or until cell temps are over 400 °C
Shut off all power and monitor temperature decline vs. time

2. Measure all relevant temperature parameters and time for following protocol:

USING ONLY 200 CM. FILAMENT

10 watts in for 1-4 hours or until steady state is achieved
up power to 20 watts in for another 1-4 hours or until steady state temperatures are reached
up power to 30 watts in [until steady state temps]
up power to 40 watts in [until steady state temps]
continue..... in 10 watt increments noting all temps and time
up to 200 watts in or until cell temps are over 400 °C
Shut off all power and monitor temperature decline vs. time

3. Measure all relevant temperature parameters and time for following protocol:

**USING FIRST CARTRIDGE HEATER FOR 10 WATTS THEN
FILAMENT FOR NEXT 10 WATTS**

10 watts in for 1-4 hours or until steady state is achieved
up power to 20 watts in for another 1-4 hours or until steady state temperatures are reached
up power to 30 watts in [until steady state temps]
up power to 40 watts in [until steady state temps]
continue..... in 10 watt increments noting all temps and time
up to 200 watts in or until cell temps are over 400 °C

Control Run #5 - Near Vacuum [< 25 mTorr]

1. Measure all relevant temperature parameters and time for following protocol:

USING ONLY CARTRIDGE HEATER

10 watts in for 1-4 hours or until steady state is achieved
up power to 20 watts in for another 1-4 hours or until steady state temperatures are reached
up power to 30 watts in [until steady state temps]
up power to 40 watts in [until steady state temps]
continue..... in 10 watt increments noting all temps and time
up to 200 watts in or until cell temps are over 400 °C
Shut off all power and monitor temperature decline vs. time

2. Measure all relevant temperature parameters and time for following protocol:

USING ONLY 200 CM. FILAMENT

10 watts in for 1-4 hours or until steady state is achieved
up power to 20 watts in for another 1-4 hours or until steady state temperatures
are reached
up power to 30 watts in [until steady state temps]
up power to 40 watts in [until steady state temps]
continue..... in 10 watt increments noting all temps and time
up to 200 watts in or until cell temps are over 400 °C
Shut off all power and monitor temperature decline vs. time

3. Measure all relevant temperature parameters and time for following protocol:

USING FIRST CARTRIDGE HEATER FOR 10 WATTS THEN
FILAMENT FOR NEXT 10 WATTS

10 watts in for 1-4 hours or until steady state is achieved
up power to 20 watts in for another 1-4 hours or until steady state temperatures
are reached
up power to 30 watts in [until steady state temps]
up power to 40 watts in [until steady state temps]
continue..... in 10 watt increments noting all temps and time
up to 200 watts in or until cell temps are over 400 °C

Conduct Full Experiment Series

Repeat Series of Experiments [ie; 15.6, 15.9, 15.10, etc.] w/ 200 cm. filament to isolate
optimal zones of operation for maximizing excess heat generation effect. Track power
dissipation per surface area on filament.

Replace filament with tungsten of greater surface area. First increase diameters, then
increase roughness. Assure 100% and 200-500% changes in area.

Increase total areas of tungsten filament in reactor vessel by 1000% via curled filament
etc.

Use parameters above to design meaningful 1-5 kW water heater design
and 1-20 kW space heater design

PART IV - Implications for the Future

The world energy market represents over 100 trillion kilowatthours of equivalent energy consumed each year and traded for well in excess of \$1 trillion. It is clear that the BLP process is in a very early stage of development and is not likely to impact this market in any significant way before the turn of the century. However, the experimental evidence reviewed and the data developed by this thesis indicates that there is an extremely high probability that the effect predicted by Dr. Mills' work in his unified field theory and the laboratory devices developed by William R. Good and his BLP associates in the laboratory may play a major role in the future of the energy industry. Gas and electrolytic phase cells and devices currently capable of releasing heat on the order of 1-20 times energy input show promise for significant technical expansion as more focus and scientific and engineering resources are brought to bear on the task. BlackLight Power currently raised over \$10M in additional investment through its final private placement offering which will make it possible for them to hire additional scientists and engineers for this very purpose. Across the world others are beginning to note with interest the reproducible and predictable production of anomalous heat via test cells that incorporate hydrogen and appropriate catalytic materials [see Table 6.1] While the "cold fusion scandal" has created a stigma which has made it difficult for the academic community to perform a complete and unbiased analysis of the claims the many researchers have made over the past few years, it appears clear that the dike holding this information back is about to burst. Table 6.1 is a brief snapshot of but a few claims that have been documented by credible scientists in industry and academia in the last few years.

TABLE 6.1 - Global Reports/Observations on BLP Technology

Journal	Observed Data / Reported Results *	Researcher(s) & Affiliation
FUSION TECHNOLOGY March 1997	2,500 times energy out of hydrogen, hydrogen is lost in reaction, new form of tightly bound hydrogen is the model proposed to explain energy and loss results	DuFour, Foos, Millot and DuFour of Shell Research/CNAM Laboratoire des Sciences Nucleaires, Paris, France
JOURNAL of ELECTRO- ANALYTICAL CHEMISTRY (1993) and (1991)	Significant heat production from electrolytic cells and the observation of a dideutrin molecule with a higher ionization energy similar to the Mills energy predictions	Miles, Bush, Lagowski, Ostrom and Miles of China Lake Naval Air Warfare Center Weapons Division, US
3rd Conference on Cold Fusion - October 1992	Significant excess heat production from cell with mass spec data indicating a dideutrin molecule [i.e.; lower energy deuterium molecule via Mills]	Yamaguchi and Nishioka of the NTT Basic Research Laboratories and IMRA Europe S.A.

* - see footnotes 39 - 43

Within the next five years there will be a significant increase in awareness of the factual information surrounding the experiments conducted by many on hydrogen technologies which are taking advantage of the natural effect first observed by Dr. Mills. The data provided in this thesis is but a brief summary of the wealth of work that has already been performed in this area of science. Most academicians I have spoken with regarding the work of Dr. Mills and Mr. William Good are annoyingly critical and pessimistic before even asking to hear the details of their experiments or supporting data. It does not surprise this researcher that it has taken at least five years for Dr. Mills work to begin to gain the recognition that it needs to have for appropriate peer review and true academic critique. It is hoped that this thesis work will draw attention to the need for a balanced and open debate on the legitimacy of the BLP claims, which though they seem extensive are also grounded in excellent technical and theoretical research.

Chapter 6 - Implications for the Future and Recommended Next Steps

A new energy paradigm will not be quickly embraced by those currently in decision-making positions in the energy industry. Literally trillions of dollars have been invested over the past fifty years in the current energy infrastructure and its early retirement could cause major economic disruption. However, the deregulation of the gas industry over the past decade combined with the current efforts to deregulate the electric industry have positioned at least the U.S. and much of the U.K. energy industry for the major competitive forces and shifts that the introduction of a new technology like BLP would cause. Cogeneration and independent power producer competition have already ushered in the pre-competitive era for most in the electric industry while the gas, oil and other traded energy commodities have been fiercely competitive for some time. Nonetheless, there is little to gain for the established energy providers to accelerate the adoption of a new energy technology based upon hydrogen. Adopting a 'wait and see' strategy not only minimizes the risk of embarrassment should the technology prove to have little commercial potential, but also could stall or delay the day when the technology is ready and able to compete directly with the energy providers for their customers. History has shown that only a few in business adopt the Peter F. Drucker strategy of creating their future. [Drucker quote; "The only way to control the future is to create it"] Most are content to watch it being created around them and then getting involved once it is clear what the winning technologies are likely to be. In the case of a paradigm shift as radical as the one proposed by Dr. Mills and BLP, waiting could be a devastating business strategy. This researcher has advised his energy company to become involved from the beginning and other companies should also follow this advice. Knowing how quickly the technology may develop and emerge best positions the energy company to plan for the timely deployment, divestiture and or disposition of its assets that may be most at risk should commercialization move on a fast or slower track. This closing section of my thesis however, is not dedicated to what the energy industry should do as next steps but rather to what BLP should do in the near future to solidify their position with this technology and maximize the benefits for their shareholders for the investment

they have made in developing this technology. The following list of recommended next steps is brief and succinct, but should assure BLP success in their endeavors if completed in a timely manner.

Recommended Next Steps

1. Clarify the Vision, Mission and Purpose of BlackLight Power, Inc. and communicate it clearly to all employees, contractors and owners. Align all corporate and employee goals and compensation strategies with the attainment of these. Identify the corporate competencies needed to execute the goals and mission of organization.
2. Focus on maximizing the intellectual property developed, owned and applied by BLP employees [individually and as a group]. Maximize new patent filings for all supportive device technologies and innovations. [If overarching patents fail, supporting patents will still protect the embodiments of the BLP effect in most apparatus] Maximize the technical and journal papers published and defended during years 1-5.
3. Focus on Communicating the BLP Vision, Mission and Purpose to all appropriate audiences and keep an adequate supply of current, accurate and appropriate information flowing to the media and necessary constituents.
4. Focus on Identifying and Quantifying the Key Parameters controlling the Hydrocatalysis and Disproportionation effects including the isolated optimization of each as well as their interactions with each other. [ie; dissociation surface area, partial pressures -catalyst vs. hydrogen atoms, mean free paths, temperature regimes, volumetric proportionalities, time dependence, etc.] This should be completed for all key embodiments gas phase, electrolytic phase, etc.
5. Develop a self-contained, self-sustaining "Hot Black Box" which irrefutably demonstrates the ability that BLP has to control all key parameters and engineer the optimization of the effect for commercial application and manufacturing. This must not be left to others to develop, it should be the work and competence of BLP at the end of the day in order to maintain a competitive advantage in this field.
6. Develop the BLP management model and compensation strategy. Hire sufficient numbers of management and staff with the necessary competencies to successfully execute items 1- 5 during the first 18 months after sufficient funding is achieved.

PART V - Reference Materials

The data reviewed in this thesis was substantial and unfortunately only a brief overview was able to be provided in the limited space. Many items referenced can be easily obtained from the author or from a librarian. This section is devoted to making that exercise more simple. The reference materials have been divided into two sections. First, a straightforward list of all Footnotes cited in the text grouped by their section or subsection number is available on the next three pages. Second, where key information was substantial and of primary relevance to the thesis but could not be afforded adequate coverage in the text, Appendices were developed to provide the needed reference support. Placing them at the end of this thesis allowed the continuity of idea flow without distracting the reader from the key points being made. The full list of relevant supporting appendices is shown on the page before they begin as the final page in Part V.

References Provided in this Thesis

Footnotes	Pages 67-71
Description of Appendices	Pages 72-73
Full Appendices Follow	

THESIS FOOTNOTES [continued]

PART I Chapter 1. Section 1.1 - Fossil Fuels [continued]

- 10 Nesbit, William, *"World Energy- Will There Be Enough in 2020?"*, Decisionmakers Bookshelf, Vol. 6, Edison Electric Institute, © 1979, ISBN 0-931032-06-7
- 11 Kraushaar, Jack J., Ristinen, Robert A., *"Energy and Problems of a Technical Society"*, 2nd Edition, John J. Wiley & Sons, Inc., © 1984, 1993, ISBN 0-471-57310-8, Figure 1.15, p. 21
- 12 *"World Book Encyclopedia J-K"*, Field Enterprises Educational Corporation, © 1961, Library of Congress Cat. No. 61-5169, p. 32a
- 13 Weinfeld, Steven G., *"Funk & Wagnalls New Encyclopedia - Volume 14"*, Funk & Wagnalls, ©1986, Library of Congress Cat. No. 72-170933, ISBN 0-8343-0072-9, p. 402
- 14 Kraushaar, Jack J., Ristinen, Robert A., *"Energy and Problems of a Technical Society"*, 2nd Edition, John J. Wiley & Sons, Inc., © 1984, 1993, ISBN 0-471-57310-8, pp. 2-3

PART I Chapter 1. Section 1.2 - Nuclear Energy - Fission & Fusion

- 15 Schwarzschild, B., *Physics Today*, October 1990, pp. 17-20
- 16 Kraushaar, Jack J., Ristinen, Robert A., *"Energy and Problems of a Technical Society"*, 2nd Edition, John J. Wiley & Sons, Inc., © 1984, 1993, ISBN 0-471-57310-8, pp. 108-111
- 17 Associated Press, *"Princeton reactor's closure casts doubt on fusion prospects"*, The Press of Atlantic City, March 30, 1997
- 18 Kraushaar, Jack J., Ristinen, Robert A., *"Energy and Problems of a Technical Society"*, 2nd Edition, John J. Wiley & Sons, Inc., © 1984, 1993, ISBN 0-471-57310-8, Table 4.1, p. 95
- 19 *"Barsebäck to Close Down by 2001"*, The Swedish Press, March 1997, p. 9



THESIS FOOTNOTES [continued]

PART I. Chapter 1. Section 1.3 - Solar Energy

- 20 Energy Info Home Page, <http://www.energyinfo.co.uk:80/wstats.html>, World Fuel Consumption by Country, pp. 1-2, ©1996 by EnergyInfo, last modified April 26, 1996
- 21 U.S. Census Bureau - World POPClock Web Page, <http://www.census.gov/cgi-bin/ipc/popclockw>, International Programs Center, World Population projected to 2/24/97 at 7:09:44 PM EST
- 22 Energy Info Home Page, <http://www.energyinfo.co.uk:80/wstats.html>, World Fuel Consumption by Country, pp. 1-2, ©1996 by EnergyInfo, last modified April 26, 1996
- 23 P.M. Jansson and R.A. Michelfelder, "*Market-Driven Photovoltaic System Economics for Grid-Connected Residential and Commercial Customers*", 14th European Photovoltaic Solar Energy Conference, Barcelona, Spain, June 30 - July 4, 1997

PART I. Chapter 1. Section 1.4 - Geothermal Energy

- 24 Kraushaar, Jack J., Ristinen, Robert A., "*Energy and Problems of a Technical Society*", 2nd Edition, John J. Wiley & Sons, Inc., © 1984, 1993, ISBN 0-471-57310-8, p. 204

PART I. Chapter 1. Section 1.5 - Tidal Energy

- 25 Kraushaar, Jack J., Ristinen, Robert A., "*Energy and Problems of a Technical Society*", 2nd Edition, John J. Wiley & Sons, Inc., © 1984, 1993, ISBN 0-471-57310-8, p. 210, Table 7.8

PART I. Chapter 2. Section 2.1 - Theoretical Description

- 26 Mills, Randell L., "*The Grand Unified Theory of Classical Quantum Mechanics*", Black Light Power, © September 1996, Library of Congress Cat. No. 96-70686, ISBN 0-9635171-2-0, p. x
- 27 Mills, Randell L., "*The Grand Unified Theory of Classical Quantum Mechanics*", Black Light Power, © September 1996, Library of Congress Cat. No. 96-70686, ISBN 0-9635171-2-0, p. 138

THESIS FOOTNOTES [continued]

PART I. Chapter 2. Section 2.2 - Astrophysical Corroboration

- 28 Labov, S.E., Bowyer, S., "Spectral Observations of the Extreme Ultraviolet Background", The Astrophysical Journal, 371:810-819 © 20 April 1991, The American Astronomical Society
- 29 Schwarzschild, B., Physics Today, October 1990, pp. 17-20
- 30 Bahcall, J., et. al., "Solar neutrinos: a field in transition", Nature, 334, 11 1988, pp. 487-493
- 31 Taubes, G., Science, 256, 1992, pp. 1512-1513
- 32 Taubes, G. Science, 256, 1992, pp. 731-733

PART I. Chapter 2. Section 2.3 - Enigmas Solved

- 33 Mills, Randell L., "The Grand Unified Theory of Classical Quantum Mechanics", Black Light Power, © September 1996, Library of Congress Cat. No. 96-70686, ISBN 0-9635171-2-0, p. 426
- 34 Phillips, Kenneth J.H., "Guide to the Sun", Cambridge University Press, © 1992, ISBN 0-521-39483, p. 166
- 35 Phillips, Kenneth J.H., "Guide to the Sun", Cambridge University Press, © 1992, ISBN 0-521-39483, p. 367
- 36 Chown, Marcus, "Dark matter is still the only game in town", New Scientist, January 7, 1995, p. 15

PART II. Chapter 4

- 37 DuFour, J., Foos, J., Millot, J.P., DuFour, X., "Interaction of Palladium / Hydrogen and Palladium / Deuterium to Measure the Excess Energy Per Atom for Each Isotope", Fusion Technology, Volume 31, March 1997, pp 198-209

PART II. Chapter 4. Section 4.2 - Penn State University Calvet

- 38 Phillips, Jonathan, "Report on Calorimetric Investigations of Gas-Phase Catalyzed Hydrino Formation", Department of Chemical Engineering, Penn State University, Final Report for period of October - December 1996, p. 1

THESIS FOOTNOTES [continued]

PART IV

- 39 DuFour, J., Foos, J., Millot, J.P., DuFour, X., *"Interaction of Palladium / Hydrogen and Palladium / Deuterium to Measure the Excess Energy Per Atom for Each Isotope"*, Fusion Technology, Volume 31, March 1997, pp 198-209
- 40 Miles, M.H., Bush B.F., Ostrom, G.S., Lagowski, J.J., *"Helium Production During the Electrolysis of D₂O in Cold Fusion Experiments"*, Journal of Electroanalytical Chemistry, 301, p. 271 (1991)
- 41 Miles, M.H., Hollins, R.A., Bush B.F., Lagowski, J.J., Miles, R.E.J., *"Correlation of Excess Power and Helium Production During D₂O and H₂O Electrolysis using Palladium Cathodes"*, Journal of Electroanalytical Chemistry, 346, p. 99 (1993)
- 42 Notoya, R. and M. Enyo, *"Proceedings of the Third Annual Conference on Cold Fusion, Nagoya, Japan"* October 21-25, 1992, H. Ikegami, Editor, Universal Academy Press, Inc., Tokyo, ©1992, pp. 421-426
- 43 Yamaguchi, E. and Nishioka, T., *"Direct Evidence for Nuclear Fusion Reactions in Deuterated Palladium"*, Proceedings of the Third Annual Conference on Cold Fusion, Nagoya, Japan, October 21-25, 1992, p. 179

DESCRIPTION OF APPENDICES

Appendix 1. BLP Research Partners - Catalogue of Experimental Results

This researcher compiled a log of numerous experiments and studies that had been performed on BLP technologies over the past 5 years. These are summarized by title, author, report name, date of work and subject matter in this appendix.

Appendix 2. An Overview of Mills Theory

The theory of Dr Mills is rather complex in that it unifies all of the aspects of a new classical quantum mechanics, Maxwell's Equations, Einstein's Special and General Relativity as well as the fundamental classical theories and models of physics. A more full description of his theory is provided in this appendix.

Appendix 3. Jansson Astrophysical Data Calculations Verifying BLP Reported Results

Specific calculations provided by Dr. Mills in his text as part of demonstrating that data being collected from space is able to validate that the theoretical results of his model are sound have been made by this author. The Excel spreadsheet has produced the tables found in this appendix.

Appendix 4. BLP/AEI Experiment 15.6 - May 1996

Atlantic Energy witnessed testing of the Isothermal Cell at the BLP Laboratories in Malvern, Pa. On May 4-6, 1997. The actual lab notes from that experiment and associated calculations done by Atlantic Energy staff to verify the results observed are provided in this appendix

Appendix 5. Analysis of BLP Isothermal Calorimetry Data

Analysis of the Isothermal cell experiments was conducted by this researcher to see if the results that were being observed were consistent with heat loss modeling estimates. The actual data provided by the BLP data logger was reviewed to see if excess heat of formation was actually occurring. This appendix summarizes these results.

Appendix 6. PSU Calvet Test Results and Report - December 1996

This appendix contains the full research report completed by Pennsylvania State University on their tests of the BlackLight technology via a Calvet calorimeter.

Appendix 7. Jansson Calvet Testing Protocol

This appendix describes the protocol that was used in the control and experimental runs performed in BlackLight Power's laboratory facility during February through May 1997 by Peter Mark Jansson, P.P.,P.E.

DESCRIPTION OF APPENDICES [continued]

Appendix 8. Jansson Calvet Test Results June 1997

The results of the experimental and control runs are provided in more detail in this appendix. While the Lab Note Book has not been included each day of experiments that were analyzed in the summary data provided in the thesis are shown explicitly. Each data set name is listed as well.

Appendix 9. Jansson Heat Loss Model Calibration & Performance

Specific mathematical modeling of the Isothermal cell was developed by this researcher to see if the results that were being observed were consistent with those that a heat loss model could predict. The calibration of the model was made via actual data provided by the BLP data logger and produced results which indicated excess heat of formation was actually occurring. This appendix summarizes these results.



THESIS - APPENDIX ONE



Appendix 1 - Catalogue of Relevant Publications and Experimental Results

This appendix provides a brief overview of relevant publications and printed experimental results that this researcher was able to acquire, review and summarize. I have not made an exhaustive search for electrolytic cell experimental data since it is extremely lengthy. The catalogue begins on the page which follows and forms the essence of this appendix.



Appendix 1 - Catalogue of Relevant Publications and Experimental Results

<u>Paper/Report - Author</u>	<u>Publication Status</u>	<u>Purpose/Results/Conclusions</u>
<i>HydroCatalysis Technical Assessment</i> TECHNOLOGY INSIGHTS San Diego, CA 618-455-9500	PC - Confidential presented to Pacificorp printed 30 August 1996	Independent Technology Assessment
<i>The Grand Unified Theory of Classical Quantum Mechanics</i> R.L. Mills BLACKLIGHT POWER CORP Malvern, PA 610-651-4938	BlackLight Power published September 1996	Presentation and Defense of Theory w/ Experiments
<i>The Grand Unified Theory</i> R.L. Mills and J.J. Farrell HYDROCATALYSIS POWER CORP Malvern, PA 610-651-4938	Science Press published 1989	Presentation and Defense of Theory
<i>Excess Heat Production by the Electrolysis of an Aqueous Potassium Carbonate Electrolyte and the Implications for Cold Fusion</i> R.L. Mills and S.P. Kneizys HYDROCATALYSIS POWER CORP Malvern, PA 610-651-4938	Fusion Technology Vol 20., 65-81 published 1991	Experimental Electrolytic Cell Results
<i>Dihydrino Molecule Identification</i> R.L. Mills, W.R. Good and R.M. Schaubach* HYDROCATALYSIS POWER CORP Malvern, PA 610-651-4938 * - of THERMACORE, INC.	Fusion Technology Vol 25., 103 published 1994	Experimental Electrolytic Cell Results Dihydrino Identification
<i>Fractional Quantum Energy Levels of Hydrogen</i> R.L. Mills and W.R. Good HYDROCATALYSIS POWER CORP Malvern, PA 610-651-4938	Fusion Technology Vol 28., 1897-1719 published 1995	Experimental Electrolytic Cell Results Hydrino and Dihydrino Identification

Appendix 1 - Catalogue of Relevant Publications and Experimental Results

<u>Paper/Report - Author</u>	<u>Publication Status</u>	<u>Purpose/Results/Conclusions</u>
<i>Nascent Hydrogen an Energy Source</i> N.J. Gemhart, R.M. Schaubach WRIGHT PATTERSON - AFB Malvern, PA 610-651-4936	SBIR Phase I Project Report 11-1124 published March 1994	Experimental Permeation Cell Results
<i>Report on Calorimetric Investigations of Gas-Phase Catalyzed Hydrido Formation</i> S. Kurtz, J. Phillips and J. Smith Penn State Univ., PA 814-863-4809	PSU -Confidential presented to BLP prepared December 1996	Penn State Gas Phase Calvet Calorimetry
<i>A Calorimetric Investigation of the Reaction of Hydrogen with Sample PSU #1</i> M.C. Bradford and J. Phillips Penn State Univ., PA 814-863-4809	PSU -Confidential presented to BLP prepared 1994	Penn State Solid Oxide Catalyst Calvet Calorimetry
<i>Additional Calorimetric Examples of Anomalous Heat from Mixture of K/Carbon and Pd/Carbon</i> J. Phillips and Shim, H. Penn State Univ., PA 814-863-4809	PSU - Confidential presented to BLP prepared 1996	Penn State Spillover Catalyst Calvet Calorimetry
<i>Additional Examples of Anomalous Heat: Hydrogen Mass Balance</i> J. Phillips Penn State Univ., PA 814-863-4809	PSU - Confidential presented to BLP prepared 1996	Penn State Spillover Catalyst Calvet Calorimetry
<i>Replication of the Apparent Excess Heat Effect in a Light Water -- Potassium Carbonate -- Nickel Electrolytic Cell</i> J. M. Niedra and I.T. Myers	NASA - Lewis Technical Memorandum 107167 prepared 1996	NASA Investigation & Experiments - Electrolytic Cell

Appendix 1 - Catalogue of Relevant Publications and Experimental Results

<u>Paper/Report - Author</u>	<u>Publication Status</u>	<u>Purpose/Results/Conclusions</u>
<i>Evaluation of Heat Production from Light Water Electrolysis Cells of HydroCatalysis Power Corp.</i> S.H. Peterson	Westinghouse STC Report prepared 23 February 1984	Westinghouse Investigation of Electrolytic Cells
<i>Excess Energy Cell Final Report</i> C. Haldeman, et. al. Cambridge, MA	M.I.T. Lincoln Labs Meeting Viewgraphs printed / reviewed 1985	M.I.T. Lincoln Labs Experimental Electrolytic Cell Results
<i>Calorimetry for a NI/K_2CO_3 Cell</i> M.T. Crawl-ivanco, R.P. Tremblay, H.A. Boniface and J. Hilborn CHALK RIVER LABORATORIES Chalk River, ON	Proprietary/EPRI AECL Research Chemical Engineering Branch printed June 1984	Experimental Electrolytic Cell Results

as of: 31 May 1997



THESIS - APPENDIX TWO



Appendix 2 - An Overview of Mills Theory

The section which follows is but a brief description of a theory that has clearly been years of development work on the part of Dr. Randell Mills. I refer the reader to his complete text on ***"The Grand Unified Theory of Classical Quantum Mechanics"***. Dr. Randell Mills received his BA in Chemistry from Franklin & Marshall College in 1982 where he graduated summa cum laude. He went on to graduate from Harvard Medical School receiving his MD in 1986 while simultaneously developing his theoretical model for unification while taking electrical engineering courses at M.I.T. He is the creator and owner of many medical patents and the recipient of many academic awards. He has published many technical papers and presented his Grand Unified Theory in 1989. The following year [1990] he went on to form the HydroCatalysis Power Corporation [now BlackLight Power]. Since that time he has been demonstrating the proof of his theory by using it to design devices that use proprietary catalysts to reduce hydrogen to the lower energy states predicted by his model of the hydrogen atom. This he has done successfully in many types of apparatus. Concurrently he has filed patents in the U.S. and 23 foreign countries. A patent was awarded in Australia in 1996.

Dr. Mills is President of BlackLight Power [BLP], presently a small, high technology firm and laboratory located in Malvern, Pennsylvania. It is a privately held company with numerous entrepreneurial investors but has at least two major utility owners [PacifiCorp from the western U.S. and Atlantic Energy from the eastern U.S.] BLP is currently being courted by additional U.S. utilities and major U.S. energy equipment manufacturers. While significant data and experiments conducted by BLP and others appear to demonstrate conclusively the reproducibility of their new heat generation effects it would seem that the timing of their discovery was not conducive to its being objectively reviewed and granted widespread academic review for authenticity. The 1990-1991 debunking of "cold fusion" and the sharp criticism that still comes to scientists and academicians who research these claims has placed a cold, wet blanket on the hot findings that continue to be generated by the scientific team from BLP. This researcher believes that the "Pons and Fleischmann experience" has increased resistance in the academic community to objective investigation of the BLP findings and claims.

Table 2.1 in the thesis text summarizes the significant government, corporate and university research centers that have corroborated BLP's findings. At the present time the company's Board has voted to allow only one more private offering before an independent public offering planned sometime in the next 1 to 2 years. To date it is important to note that the work developed by BLP has been primarily funded by its investors with limited government research funding. The total effort to bring the company to its current state of technological development has cost its private owners less than a few million dollars over the past seven years. This needs to be contrasted with the billion dollar expenditures over the past few decades for particle accelerators, nuclear research and investigations into the claims of cold fusion.

To Dr. Mills' credit his theory holds at its foundations inviolate the classical laws of physics, including all of those listed below:

- 1] Conservation of mass-energy
- 2] Conservation of Linear and Angular Momentum
- 3] Maxwell's Equations on Electromagnetics
- 4] Newton's Laws of Mechanics
- 5] Einstein's General Relativity
- 6] Einstein's Special Relativity

His theory produces the same equation for the principle energy levels of the hydrogen atom as both Bohr and Schrodinger but only Mills theory gets there through a derivation from first principles. Bohr's model [1913] represented the electron as a point particle whose circular orbit around the nucleus of the hydrogen atom was maintained by a perfect balancing of the coulombic force of attraction [positive proton nucleus (e^+) and negative electron (e^-) satellite] between the two particles and the centrifugal force of the electron. However, the non-radiation of the electron charge at such an orbit velocity led to this postulation being in defiance of Maxwell's Equations on electromagnetics. While "his model was in agreement with the observed hydrogen spectrum it failed for the helium spectrum and could not account for chemical bonds in molecules."^{A1} Schrodinger's model [1926] was a totally mathematical view of the electron which he developed based upon de Broglie's wave postulate for electron motion. His famous wave equation has an infinite number of ways in which it can be solved. In order to create a solution for the electron he applied a boundary condition which in essence stated that as the radius of the electron's orbit approaches infinity [$r \rightarrow \infty$] his wave function approaches zero [$\Psi \rightarrow 0$]. The problems of creating a classical or physical interpretation of Schrodinger's wave equation have been significant over the years and so, as a result, physicists have drifted more and more to a purely mathematical view of the interaction of physics at the atomic level, with no adequate physical description of particle behavior. This has set up a duality in the application of the laws of physics. The classical laws are used at the macro level but at the micro level probability and statistics reign. "According to the Copenhagen interpretation, every observable state exists in a state of superposition of possible states and observation or the potential for knowledge causes the wavefunction corresponding to the possibilities to collapse into a definite state"^{A2} It was these difficulties in the accepted physics of quantum mechanics that led Dr. Mills to seek an alternative. Through his theory, he sought physical laws which were exact on all spatial scales. Dr. Mills did not give the electron the wave nature adopted by Schrodinger and suggested by de Broglie and the Davisson-Germer experiment but developed closed-form calculations that use only the fundamental constants of physics already accepted and understood that predict these aspects of the electron.

Table A.1 below outlines the aspects of physics which Dr. Mills' theory can directly calculate with its closed form equations.

TABLE A.1 - Mills' Theory Predictions

one electron atom w/ 4 quantum numbers
the Rydberg constant
the ionization energies of 1,2 & 3 electron atoms
equation of the electron in free space
electron g factor
excited states of the electron
parameters of pair production
bond energies, vibrational energies, rotational
energies and bond distances of hydrogen
-type molecules and molecular ions
equation of the expansion of the universe
the masses of atomic particles [leptons,
quarks and nucleons]
beta decay energy of the neutron
theory of alpha decay

spin/nuclear hyperfine structure
the stability of atoms
equation of the photon
results of Stern-Gerlach experiment
spin angular momentum energies
results of the Davisson-Germer experiment
hyperfine structure interval of positronium
Quantum Hall effects
the Aharonov-Bohm effect
equations of gravitation
the gravitational constant
the basis for the antigravitational force
magnetic moments of nucleons
the binding energy of deuterium
the chemical bond energies of molecules

Mills theory begins with the classical, fundamental laws of physics [see 1-6 above] and then applies a boundary condition on the electron significantly different than Schrodinger. His boundary condition is that a bound electron can not radiate energy at 13.6 eV. "The mathematical formulation for zero radiation is that the function that describes the motion of the electron must not possess spacetime Fourier components that are synchronous with waves traveling at the speed of light. The permissible solutions for the electron function are derived as a boundary value problem with the application of the nonradiative boundary condition."^{A3} By using only the classical laws of physics, mathematics and this one new boundary condition [NOTE: this boundary condition is essentially required to satisfy Maxwell's equations] a totally new view of the electron emerges. The result of this theory by Dr. Mills also leads to the unification of all of the standard classical laws of physics. These can be solved mathematically, discretely and without the need to resort to the arbitrary gauging constants developed by presently accepted quantum theory in order to "get the theory to fit" observed data. Dr. Mills calls this new electron perspective and new classical view an **electron orbitsphere**. The orbitsphere solution to the electron's mathematical function produces many interesting features some of which are highlighted in Table 2.3 below. For a complete summary of the features described by Mills' theory the reader is referred to pages 22-26 of Dr. Mills' text.

TABLE A.2 - The Electron Orbitsphere

bound electron orbitspheres are described completely by a charge-density [mass-density] function that can exist only at specified distances from the nucleus

the function which totally describes an electron orbitsphere's motion is composed of two functions
1) a spin function and 2) a modulation function

electron orbitsphere radii are calculated by setting its centripetal force equal to the electric and magnetic forces of the orbitsphere

the electron orbitsphere behaves like a resonator cavity capable of absorbing photons of discrete frequencies [solutions to Maxwell's equations for excitation modes in this cavity give rise to four quantum numbers]

excited electron orbitsphere states are unstable because the incoming photon disturbs the charge-density function creating a doublet function that has spacetime Fourier components synchronous with waves travelling at the speed of light, thus it is radiative

the photon is an orbitsphere with electric and magnetic field lines along orthogonal great circles

when an electron orbitsphere is ionized its radius goes to infinity and it becomes a plane wave

atom's energy is stored in their electric and magnetic fields, chemical bonding occurs when the total energy of the atoms can be lowered by forming equipotential orbitals with geodesic motion and the nonradiative boundary condition can be met

lower electronic states exist below *conventional* [$n = 1$] ground state, hydrogen atoms can react with a catalyst having a net enthalpy of 27 eV inducing them to electronically relax and decrease their radii with the emission of electromagnetic energy consistent with each of their change in total energy state [ie; electric and magnetic field energies]

This thesis will not review the many mathematical formulations and proof calculations of Mills theory which is fully elaborated in his text. However the following illustrations may help the reader grasp more succinctly the new orbitsphere model proposed by Mills. Figures A.1 and A.2 below represents a physical view of Mills' model of the electron orbitsphere a spinning, two-dimensional spherical surface.

FIGURE A.1

Figure 1.4 B. The current pattern of the orbitsphere shown with 8.49 degree increments of the infinitesimal angular variable $\Delta\alpha(\Delta\alpha')$ from the perspective of looking along the x axis.

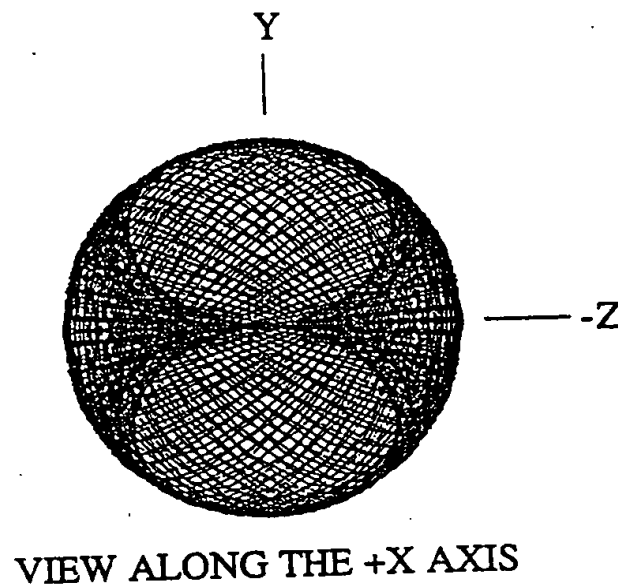


Figure 1.4 C. The current pattern of the orbitsphere shown with 8.49 degree increments of the infinitesimal angular variable $\Delta\alpha(\Delta\alpha')$ from perspective of looking along the y axis.

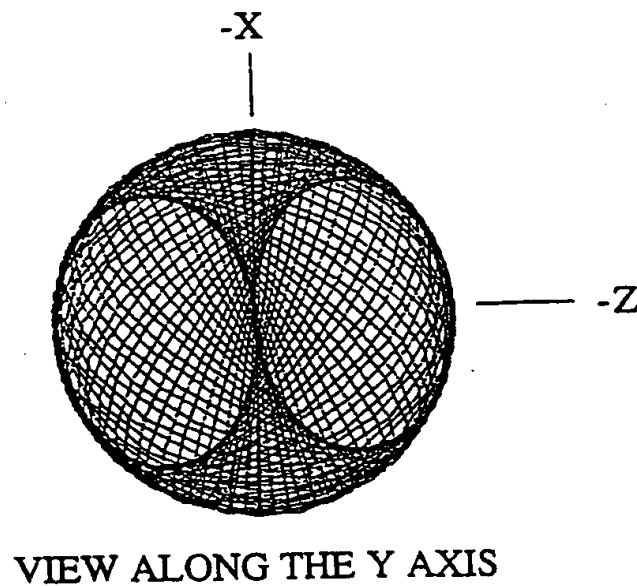
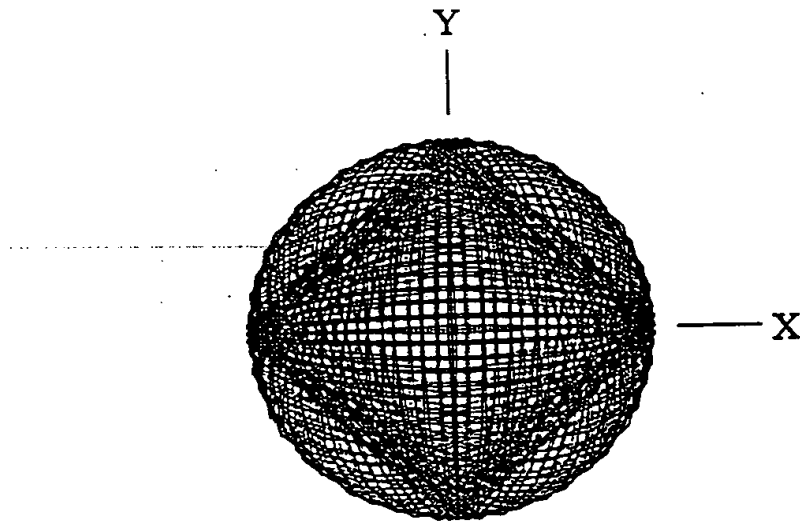


FIGURE A.2

Figure 1.4 A. The current pattern of the orbitsphere shown with 8.49 degree increments of the infinitesimal angular variable $\Delta\alpha(\Delta\alpha')$ from the perspective of looking along the z axis.



VIEW ALONG THE Z AXIS

In closing this overview of Mills' theory it is important to note that while the scientific community has been searching for a more classical unified field theory that could stand up to rigorous mathematical scrutiny for some time, there has not yet been a widespread review of his work by academia. The few academic reviews that have been made on the merits, potential flaws or criticisms of Mills' work have come out glowingly in favor of his findings. This researcher believes that because Dr. Mills' is an outsider and not considered an expert in these fields that it will take much longer for his work to be widely discussed in academic circles. Mills theory is compelling and may offer just what Albert Einstein was looking for when he uttered his famous words denouncing the then emerging quantum theory "God does not play dice with the universe".

APPENDIX 2 FOOTNOTES

- [A1] Mills, Randell L., *"The Grand Unified Theory of Classical Quantum Mechanics"*, BlackLight Power, © September 1996, Library of Congress Cat. No. 96-70686, ISBN 0-9635171-2-0, p. 7
- [A2] Mills, Randell L., *"The Grand Unified Theory of Classical Quantum Mechanics"*, BlackLight Power, © September 1996, Library of Congress Cat. No. 96-70686, ISBN 0-9635171-2-0, p. 9
- [A3] Mills, Randell L., *"The Grand Unified Theory of Classical Quantum Mechanics"*, BlackLight Power, © September 1996, Library of Congress Cat. No. 96-70686, ISBN 0-9635171-2-0, p. 22



THESIS - APPENDIX THREE



Mills Prediction vs. Data

Raw Extreme UV Background Spectral Data *							
Peak	OBSERVED DATA		Fractional State		MILLS PREDICTED		
	Wavelnth	Energy	Calc	nf	ni	Wavelnth	
	A	eV	eV			A	eV
1	84.8	146.2	146.2	8	7	82.9	149.6
2	101.5	122.2	122.2	7	6	101.3	122.4
3	116.8	106.2	106.2	4	2	114.0	108.8
4	129.6	95.6	95.7	6	5	130.2	95.2
5	139.6	88.8	88.8	4	2	141.6	87.6
6	163.2	75.9	76.0	8	7	165.8	74.8
7	181.7	68.3	68.2	5	4	182.3	68.0
8	200.6	61.8	61.8	7	6	202.6	61.2
9	233.8	53.0	53.0	3	1	227.9	54.4
10	261.2	47.5	47.5	5	4	265.0	46.8
11	302.5	41.0	41.0	4	3	303.9	40.8
12	459.1	27.0	27.0	3	1	455.9	27.2
13	584.0	21.2	21.2			584.9	21.2
14	607.5	20.4	20.4	4	3	607.8	20.4
15	633.0	19.7	19.6	4	3	633.0	19.6
16				3	2	911.7	13.6
				1.60E-19	6.63E-34	3.00E+08	
				eV	h	c	
Raw Extreme UV Solar Spectral Data **							
	OBSERVED DATA		MILLS PREDICTED				
	Wavelnth	O-M	Wavelnth	nf	ni	A	
	A	delta	A				eV
	1215.7			2	1	911.74	13.6
	911.8			2	1	-911.74	-13.6
	911.8	0.01%	911.74	3	2	911.74	13.6
	584.5			1	1	-227.93	-54.4
	373.7	0.03%	373.60	3	1	373.60	33.2
	303.784	-0.04%	303.91	4	3	303.91	40.8
	280.2	-0.12%	280.54	3	1	280.54	44.2
	280.8	0.09%	280.54	3	1	280.54	44.2
	264.8	-0.08%	265.01	5	4	265.01	46.8
	228	0.03%	227.93	3	1	227.93	54.4
	215.16	0.29%	214.53	5	4	214.53	57.8
	182.16	-0.10%	182.35	5	4	182.35	68.0
	167.5	-0.05%	167.59	6	5	167.59	74.0
	152.15	45.52%	82.89	4	1	82.89	149.6
	145.9	0.01%	145.88	6	5	145.88	85.0
	141	-0.40%	141.56	4	2	141.56	87.6
	129.87	-0.29%	130.25	6	5	130.25	95.2
	125.5	-0.20%	125.76	4	2	125.76	98.6
	122.2	-0.28%	122.54	7	6	122.54	101.2
	114	0.03%	113.97	4	2	113.97	108.8
	110.5	-0.01%	110.51	7	6	110.51	112.2
	101.3	0.00%	101.30	7	6	101.30	122.4
	96.7	0.13%	96.58	8	7	96.58	128.4

Page 2

THESIS - APPENDIX FOUR



5/1/96 @ 7:00 pm

115.9

- @ 3m KNO_3 soln was coated onto ^{inner} sides of vessel & dried on with a heat gun.
- @ 3g of dried powderized KNO_3 was sprinkled onto the bottom of the cell.
- 200 cm tungsten filament (0.01 cm diam) wrapped @ 4 ceramic rods supported by 1/8" SS tees.
- opened valve to vacuum pump.
- turned on cartridge heater to @ 250°C on temp controller.

Started PEC 050196 Tp V

5/2/96 @ 10:00 am - filament read high $\sqrt{2}$ across both buffer/gland ends indicating an incomplete circuit.

@ 11:05 pm - cartridge htr was turned off.

@ 1:30 pm - cell was dismantled hot & filament was replaced.

@ 2:30 pm - opened valve to vacuum.

@ 2:45 pm - turned on cartridge htr.

started PEC : comp crashed.

started PEC 050296 830p V (cycle disabled)

5/3/96 @ 9:30 am

Temp Controller: Time on = 26.52 / 26.62 / 26.80 / 26.65 (Avg) (81.2%)
 Total Time = 32.47 / 32.94 / 33.06 / 32.82
 $W_{in} = \frac{(100.97)^2}{80} \times \frac{26.65}{32.82} = 103.48 \text{ W}$
 Temp = 279.49
 RT = 27.72
 Pres = 109 mbar

@ 9:45 am - closed valve to vacuum, pressurized cell w/ H_2 to @ ATM on gauge.

@ 9:48 am - closed valve to vac when cell pressure

Continued on Page

Read and Understood By

Steve Ballay 5/3/96
 Signed Date

WHL
 Signed

5/3/96
 Date

PROJECT ATLANT ENERGY TEST

Notebook No. _____
Continued From Page 60

5/3/96 @ 9:48 am (cont.)
was @ 2 torr.

@ 10:45 am

Temp Controller: Time on = 22.42 / 21.77 / 22.18 / 22.12
Total Time = 29.15 / 28.28 / 28.78 / 28.74
Temp = 279.50 (11)
RT = 28.42
Pres = 1150 mtorr

$$126.1 \text{ W} \times \frac{22.12}{28.74} = 97.05 \text{ W}$$

@ 10:10 am - turned on filament to @ 15 W.

$$V = 26.06, I = 0.289 \times 2, W = 15.11$$

@ 11:15 am - first time cart. htr. clicks ~~back~~ on since increasing filament wattage

@ 11:45 am

Temp Controller: Time on = 7.99 / 8.08 / 8.14 / 8.07 (38.6)
Total Time = 20.94 / 21.00 / 21.12 / 21.02
Temp = 285.09
RT = 28.04
Pres = 1400 mtorr

$$W_{in} = 127.2 \times \frac{8.07}{21.02} = 48.47 \text{ W}$$

$$97.05 - 48.47 - 15.11 = 33.47 \text{ W} \times 5$$

Watts
to Fil
(Control)

Watts
to Fil on
to 15 W

Fil W

@ 11:50 am - increased filament wattage to @ 25 W.

$$V = 36.15, I = 0.35 \times 2, W = 25.31$$

@ 12:05 pm - first time ^{art.} htr clicks on since increasing filament wattage.

Continued on Page

Read and Understood By

Art & Belin 5/3/96 Wm O 5/3/96

Date

5/3/96 @ 12:15 pm

Temp Controller:

Time on = 5.61 | 6.05 | 6.05 | 5.90
Total Time = 43.69 | 43.09 | 43.00 | 43.26 (13.1)

$$W_{in} = 126.4 \times \frac{5.90}{43.26} = 17.24 W$$

Avg
Temp = 27.88
RT = 288.86
Pres = 1400 wt. mm

$$97.05 - 17.24 - 25.31 = 54.50 W \times S$$

(Control) cart. htr
cart. htr w/o fil
w/ fil on to 25 W

@ 12:20 pm - increased filament wattage to @ 35 W.

$$V = 45.02, I = 0.39 \times 2, W = 35.12$$

@ 2:10 pm - first time cart. htr. clicks on since increasing filament wattage.

@ 2:15 pm

Filament $V = 44.93, I = 0.40 \times 2, W = 35.94$

Temp Controller: Time on = 5.66
Total Time = 125.93

$$W_{in} = \frac{(100.97)^2}{80} \times \frac{5.66}{125.93} = 5.73 W$$

4.5%
Temp = 289.24
RT = 27.45
Pres = 1700 wt.

$$97.05 - 5.73 - 35.94 = 55.38 W \times S$$

(Control) cart. htr
cart. htr w/o fil
w/ fil on to 35 W

Continued on Page

Read and Understood By

Steve Ballinger 5/3/96
Signed DateVNL
Signed5/3/96
Date

PROJECT ATLANTIC E. TEST

Notebook No. 62
Continued From Page

6:

5/3/96 @ 2:25pm - increased filament wattage to @ 401

@ 2:40pm - disconnected watt meter from cartridge heater & connected it to the filament. Computer data acquisition system crashed. Polaroid & video tape pictures were ~~taken~~ taken of the on screen temperature trace of the experiment ^{from} morning 5/3/96 to present.

started PEC 050396 310p H fil

3:30pm Sealed Door with signed tape

PLAN: VIDEO TAPE BREAKING SEAL
on Monday. ~~Disassemble~~ Cool
vessel down. OPEN U/ ATLANTIC
Personnel present Monday Afternoon

WRLD 5/3/96

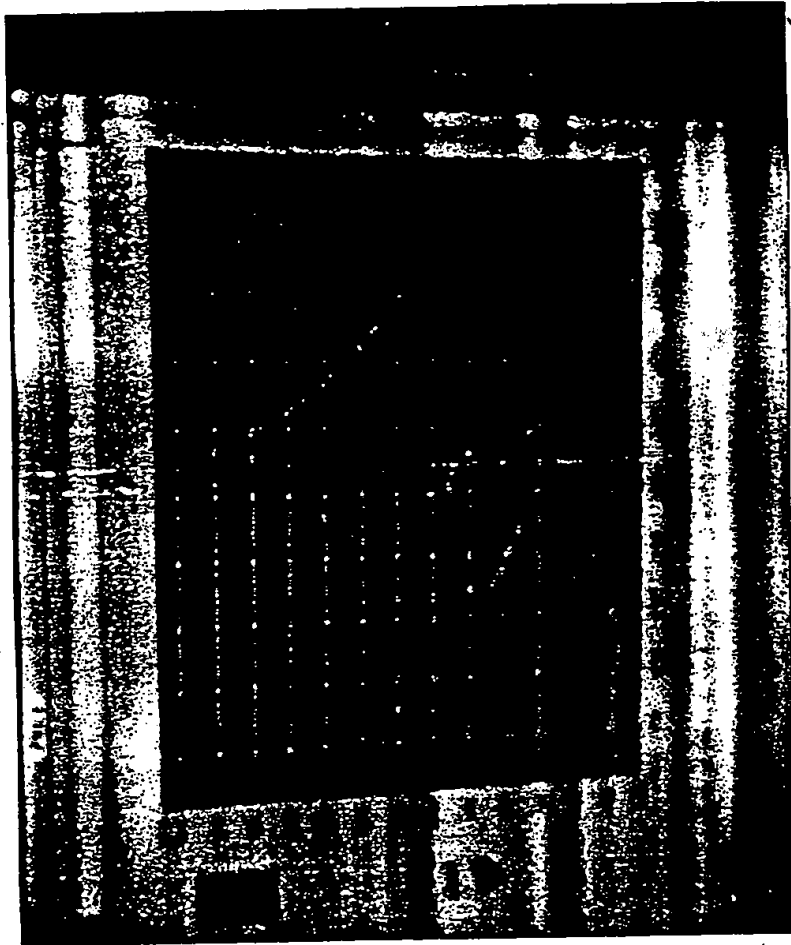
WATT METER is monitoring filament power.
cartridge heater Power supply is off.

WRLD
Jeta Mah Jones
Matt Custer
for Mark

Continued on Page

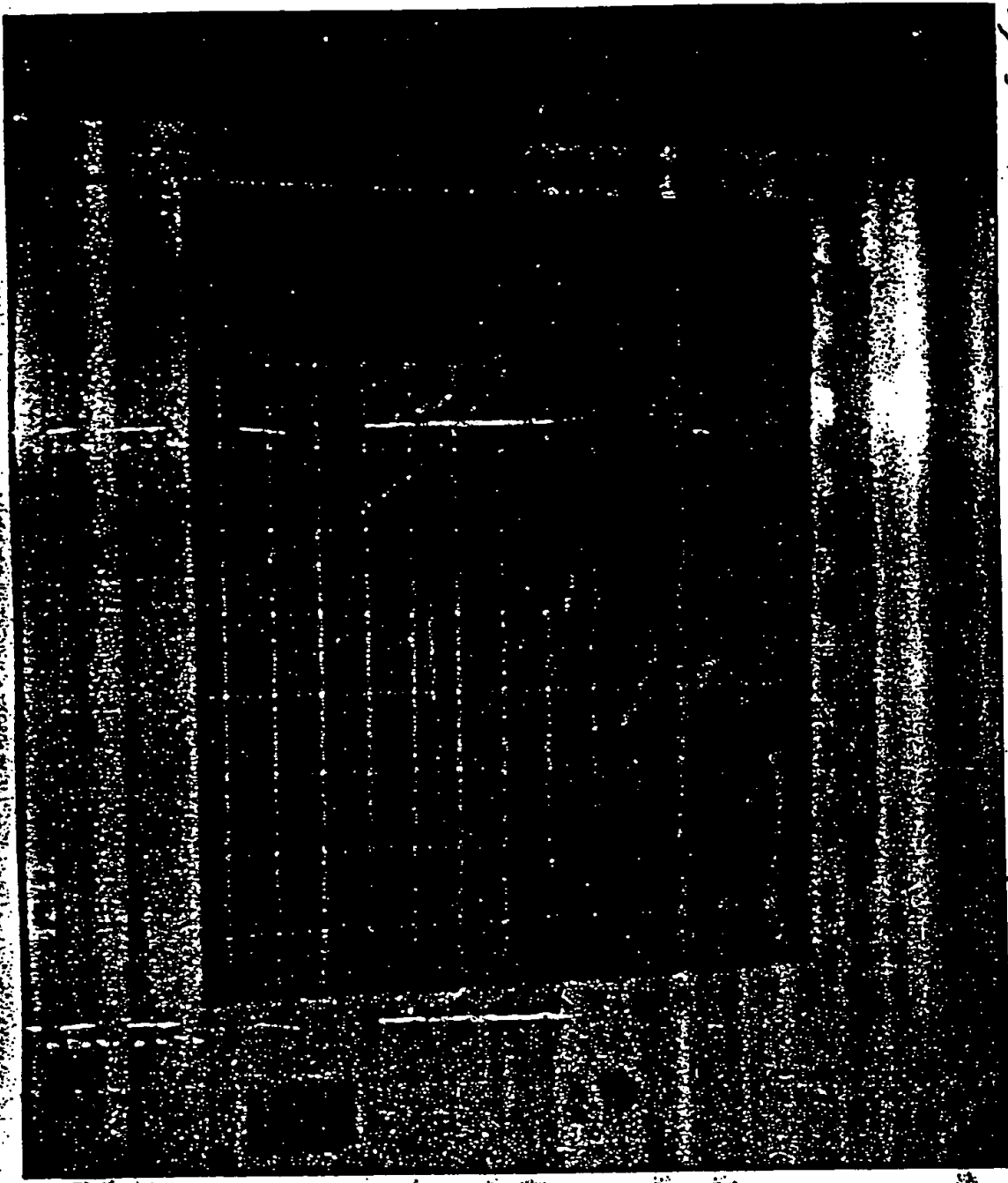
Read and Understood By

Mr. Bellin 5/3/96 WRLD 5/3/96
Date



Witnessed: Matt Custer 5/3/96
TEST RUN BEGAN 10:45 AM 5/3/96

PHOTO TAKEN 2:50 PM 5/3/96
Start Bollinger 2:51 PM 5/3/96



5/3/96

Witnessed: Matt Cuatrecasas

5/3/96

TEST RUN BEGAN 10:45 AM

5/3/96

2:50 PM

PHOTO TAKEN -
1.0 x 1.0 in

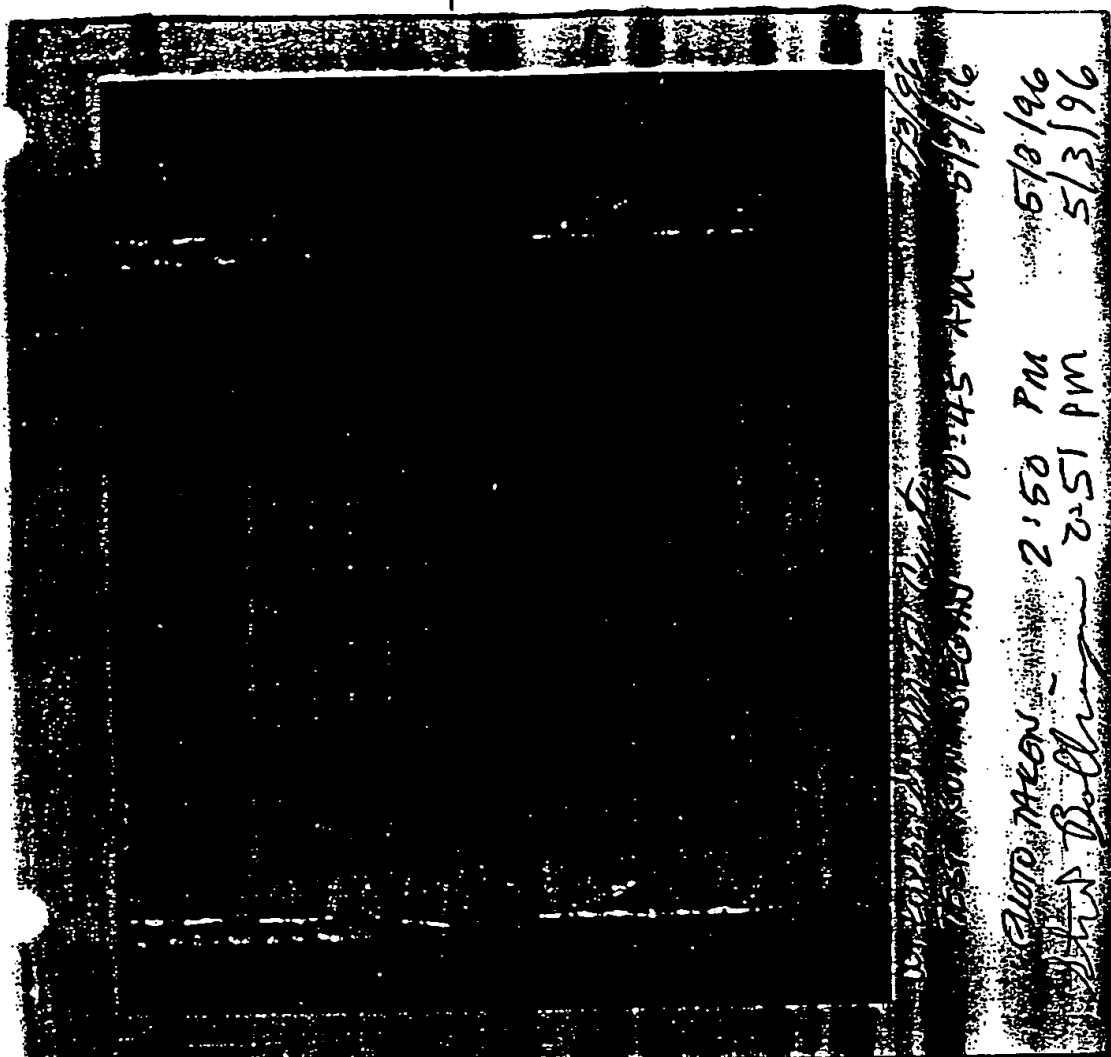
302

296

244

279

LABVIB



10:45 AM 5/3/96
10:45 AM 5/3/96

ELITE TAKEN 2:50 PM 5/3/96
2:51 PM 5/3/96

2926° 3:04 May 3



The following is a list of the column headings and their meanings for the PEC data spreadsheet:

Column 1, Time(sec)-the time in seconds for each data point from the initial time (To) when the data acquisition system was started

Column 2, Room Temperature-room temperature measured on the data acquisition board

Column 3, Temperature(°C)-cell temperature in °C measured from the type K thermocouple which is positioned in a thermocouple well in the top flange of the vessel

Column 4, Watts-wattage going into either the cartridge heater or filament (depending on which it is connected to) at each of the data points

Column 5, Hours Elapsed-the time in hours elapsed from the initial time (To) when the data acquisition system was started; this number is calculated by dividing the corresponding seconds in column 1 by 3600 in order to convert from seconds to hours.

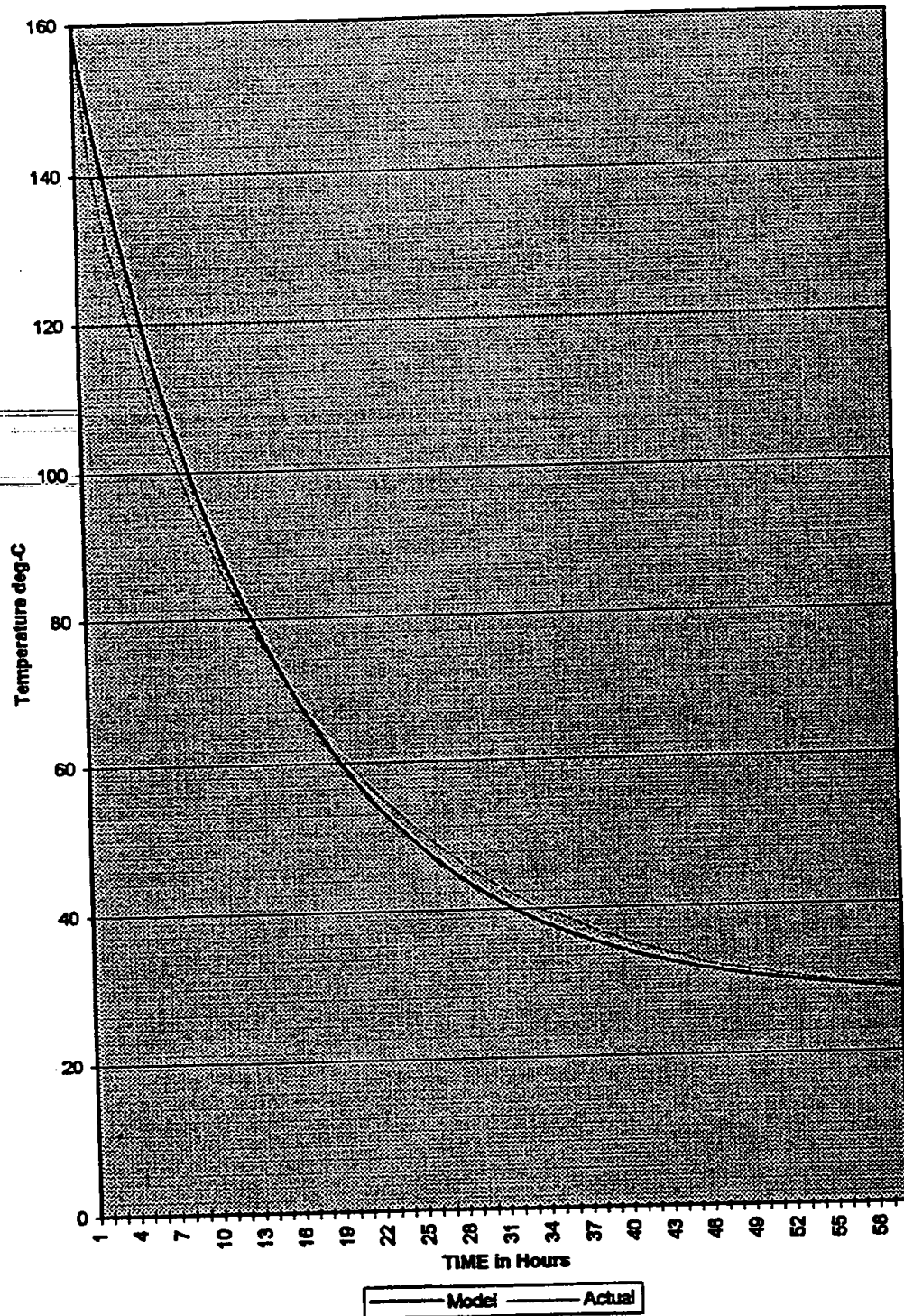
Ex. $50 \text{ sec} (x) 1 \text{ min} / 60 \text{ sec} (x) 1 \text{ hr} / 60 \text{ min} = 50 / 3600 \text{ (hr)} = 0.014 \text{ hours}$

Data = Excel
Graphics = Pic

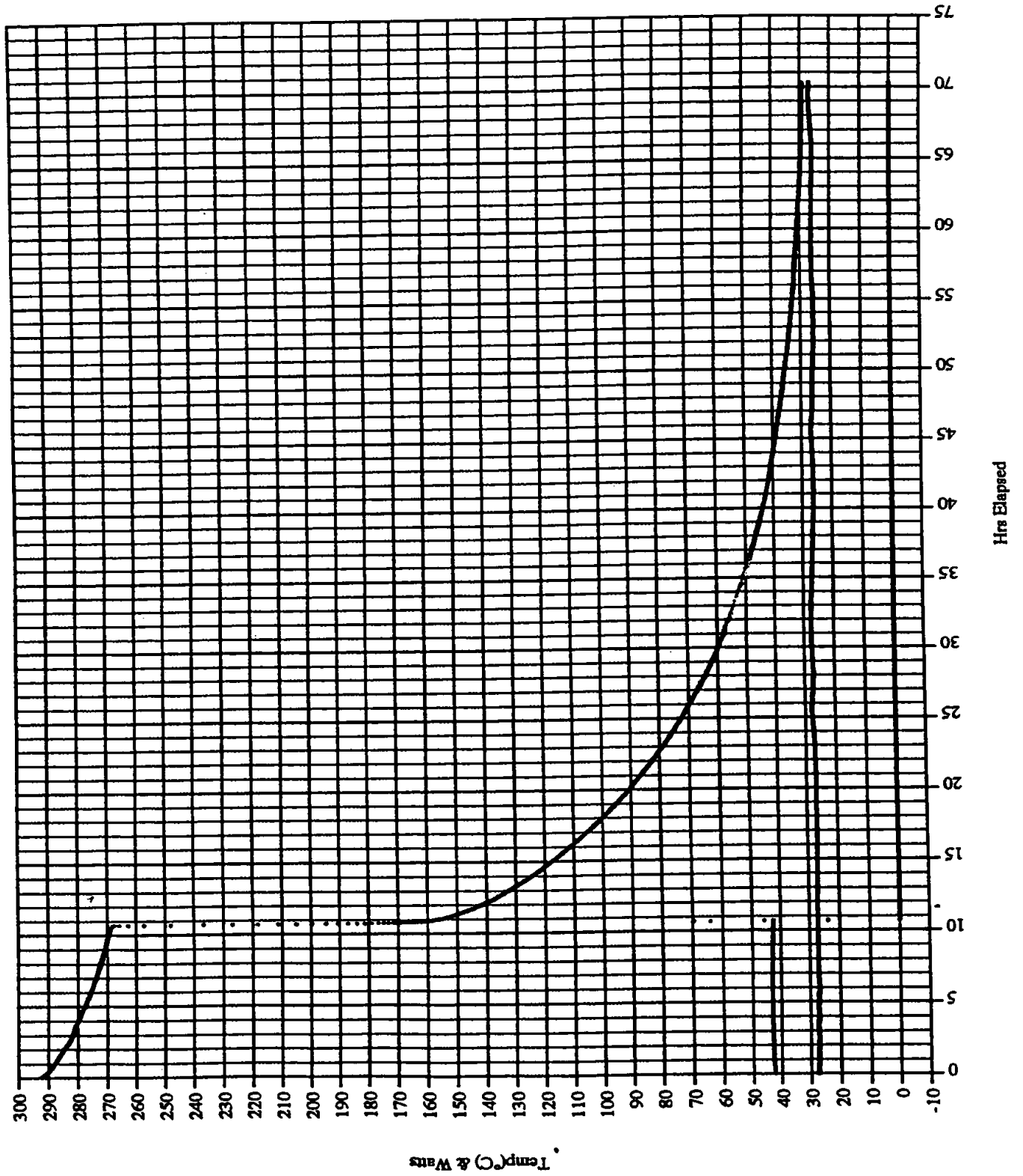
36887	27.082	268.98	42.563	10.24639
36907	27.082	269.07	42.635	10.25194
36927	27.082	268.99	42.655	10.2575
36948	27.081	268.88	42.544	10.26333
36968	27.08	268.9	42.546	10.26889
36988	27.081	268.92	42.614	10.27444
37008	27.083	268.87	42.626	10.28
37028	27.08	268.9	42.551	10.28556
37048	27.082	268.86	42.634	10.29111
37068	27.083	268.91	42.552	10.29667
37088	27.081	268.85	42.641	10.30222
37108	27.082	268.91	42.635	10.30778
37128	27.082	268.93	42.561	10.31333
37148	27.08	268.78	42.543	10.31889
37168	27.08	268.81	42.527	10.32444
37188	27.079	268.93	42.528	10.33
37208	27.079	268.78	42.565	10.33556
37228	27.077	268.82	42.609	10.34111
37248	27.078	268.72	42.651	10.34667
37268	27.079	268.91	42.596	10.35222
37288	27.078	268.84	42.542	10.35778
37308	27.076	268.6	42.524	10.36333
37328	27.077	268.74	42.568	10.36889
37349	27.078	268.82	42.642	10.37472
37369	27.077	268.73	42.58	10.38028
37389	27.078	268.84	42.523	10.38583
37409	27.077	268.77	42.593	10.39139
37429	27.08	268.76	42.61	10.39694
37449	27.078	268.71	42.51	10.4025
37469	27.076	268.64	42.537	10.40806
37489	27.076	268.73	42.619	10.41361
37509	27.078	268.7	42.565	10.41917
37529	27.079	268.69	42.507	10.42472
37549	27.078	268.66	42.54	10.43028
37569	27.078	268.59	42.62	10.43583
37589	27.077	268.59	42.532	10.44139
37609	27.078	268.63	42.543	10.44694
37629	27.078	268.67	42.624	10.4525
37649	27.078	268.51	42.53	10.45806
37669	27.079	268.59	42.493	10.46361
37689	27.079	268.47	42.503	10.46917
37709	27.078	268.56	42.528	10.47472
37729	27.08	268.51	42.577	10.48028
37750	27.077	268.41	42.613	10.48611
37770	27.079	268.52	42.493	10.49167
37790	27.077	268.46	42.493	10.49722
37810	27.078	268.5	42.539	10.50278
37830	27.078	268.46	42.592	10.50833
37850	27.077	268.43	42.586	10.51389
37870	27.076	268.36	42.479	10.51944
37890	27.076	268.48	42.478	10.525

Heat Loss Model - Vers 1.1 Chart 2

Model vs. Actual Data



PEC 050396 310p H fil ex*



Room Temp
Temp(°C)
Watts

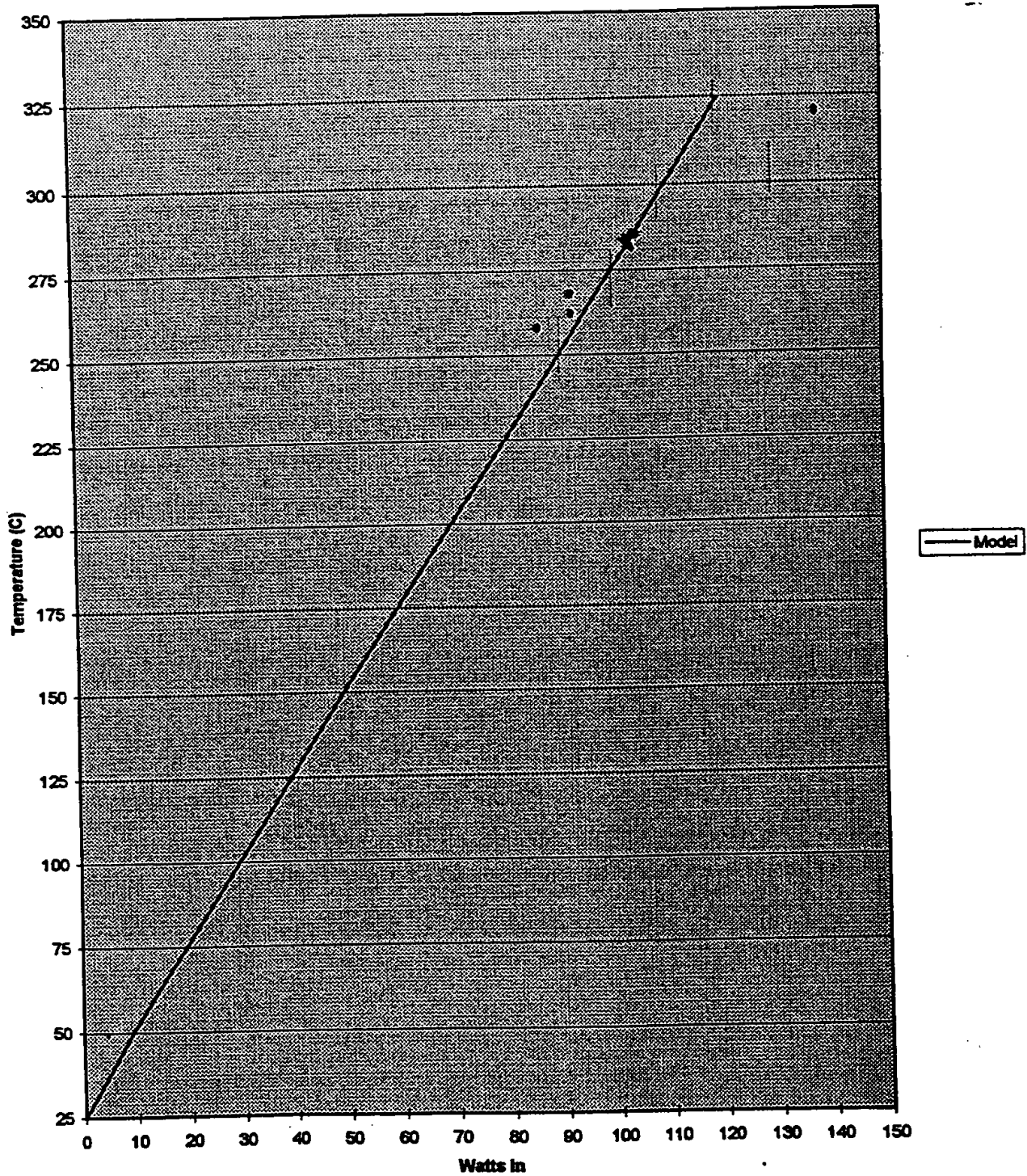
M. Custer
5/6/96

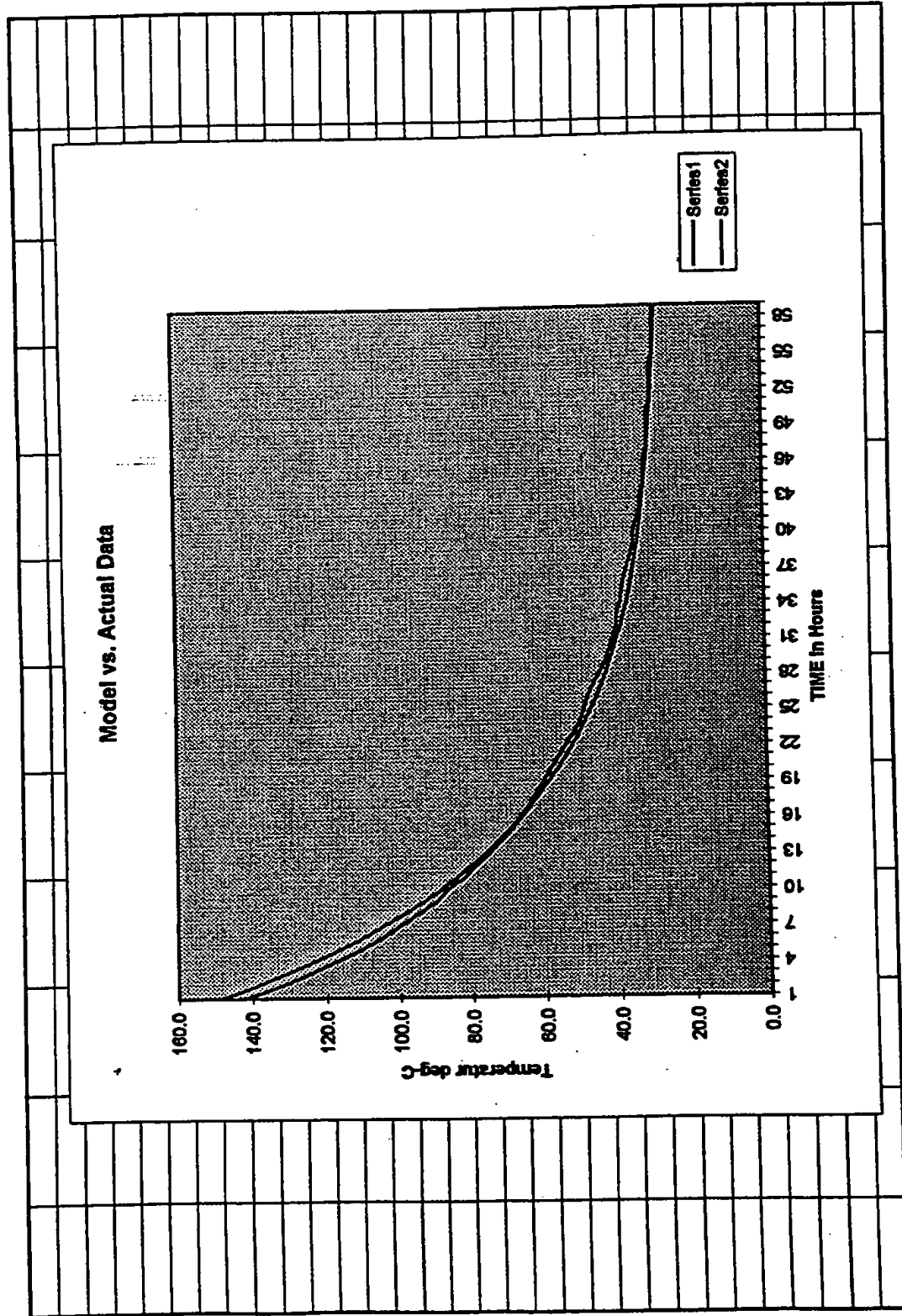
THESIS - APPENDIX FIVE



BLP Isothermal Cell Model Chart 3

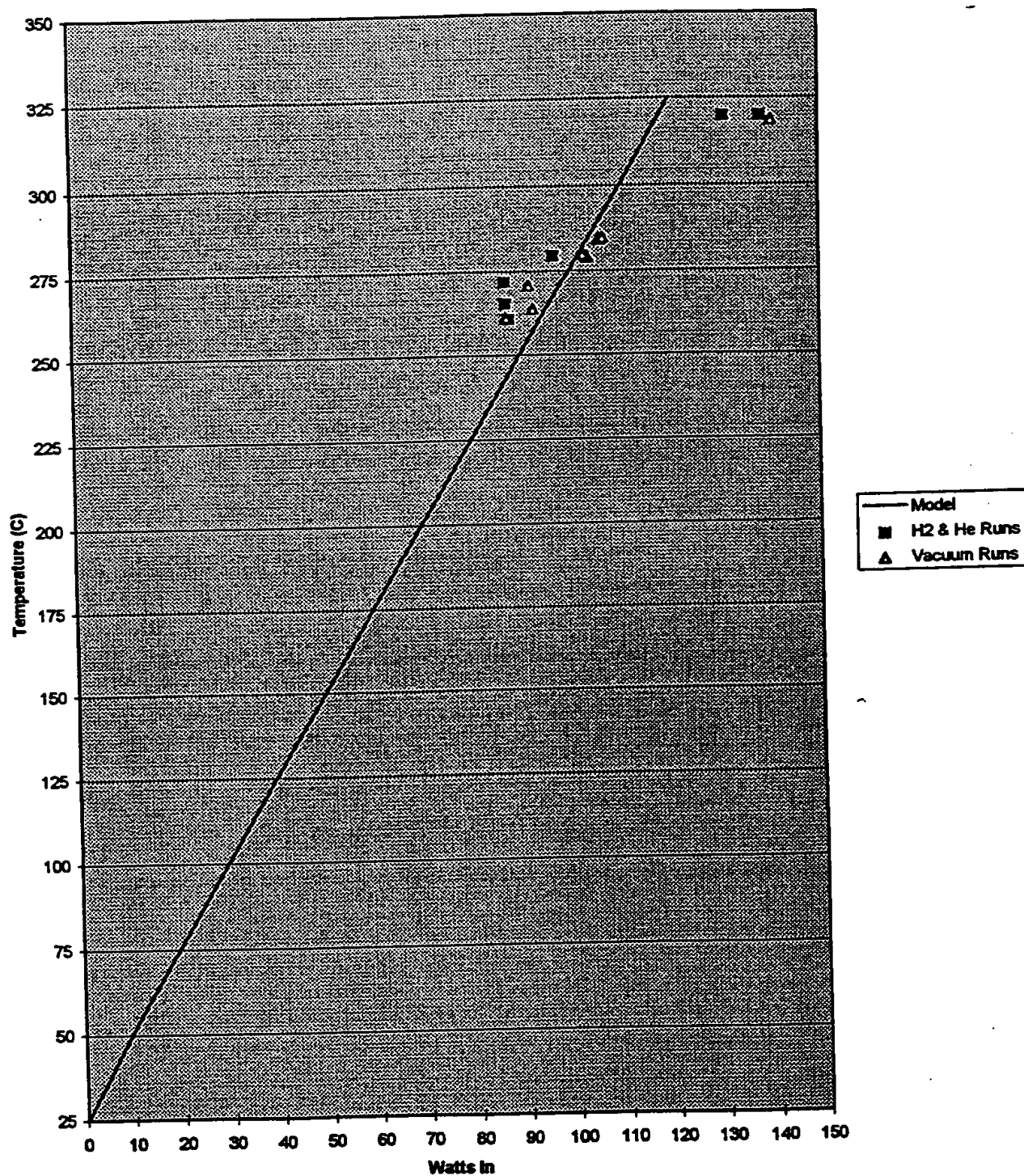
Isothermal Cell - Heat Loss





BLP Isothermal Cell Model Chart 3

Isothermal Cell - Heat Loss

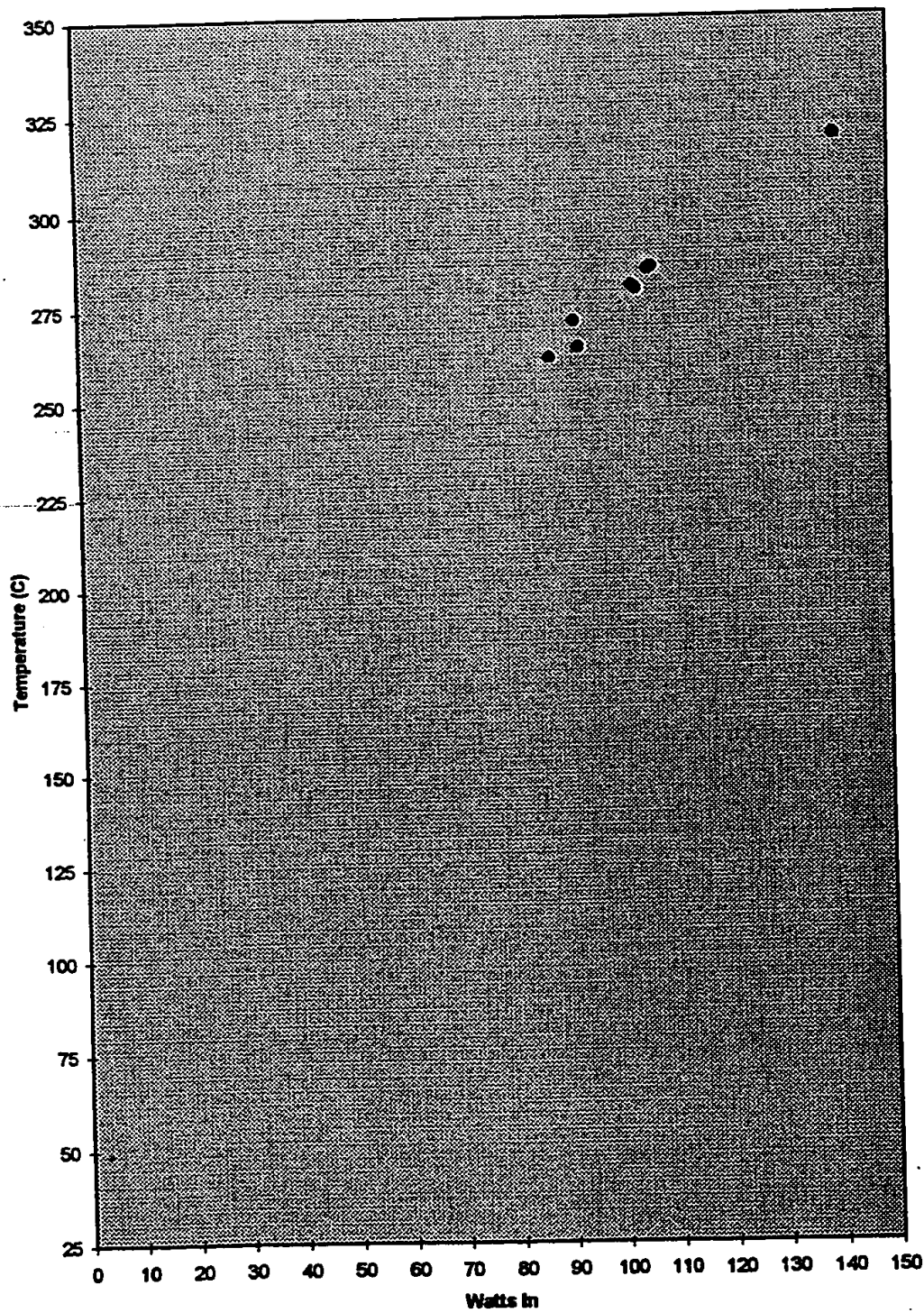


BLP Isothermal Cell Model

ALL RUNS WITH ISOTHERMAL CALORIMETER				
Experimental Run	Cell Pressure (mtorr)	Temperature (C)	Steady State Watts	Gas
			Cartridge Heater Only	
15.6	38	270.73	91.95	V
	1800	271.79	87.07	H2
15.8	48	261.07	87.29	V
	1350	260.82	87.85	H2
15.9	109	279.49	103.48	V
	1150	279.5	97.05	H2
15.10	56	263.72	92.71	V
	1600	265.41	87.16	H2
15.12	21	284.33	106.02	V
	20	284.72	106.71	V
15.13	2000	319.91	138.29	He
	35.5	318.45	140.45	V
	1900	319.83	131.22	H2
16.2	22.3	279.01	103.7	V
	22	279.97	102.96	V
VACUUM RUNS ONLY WITH ISOTHERMAL CALORIMETER				
Cell Pressure (mtorr)	Temperature (C)	Steady State Watts		
		Cartridge Heater Only		
38	270.73	91.95	V	
48	261.07	87.29	V	
109	279.49	103.48	V	
56	263.72	92.71	V	
21	284.33	106.02	V	
20	284.72	106.71	V	
35.5	318.45	140.45	V	
22.3	279.01	103.7	V	
22	279.97	102.96	V	
GAS RUNS ONLY WITH ISOTHERMAL CALORIMETER				
Cell Pressure (mtorr)	Temperature (C)	Steady State Watts		
		Cartridge Heater Only		
1800	271.79	87.07	H2	
1350	260.82	87.85	H2	
1150	279.5	97.05	H2	
1600	265.41	87.16	H2	
2000	319.91	138.29	He	
1900	319.83	131.22	H2	

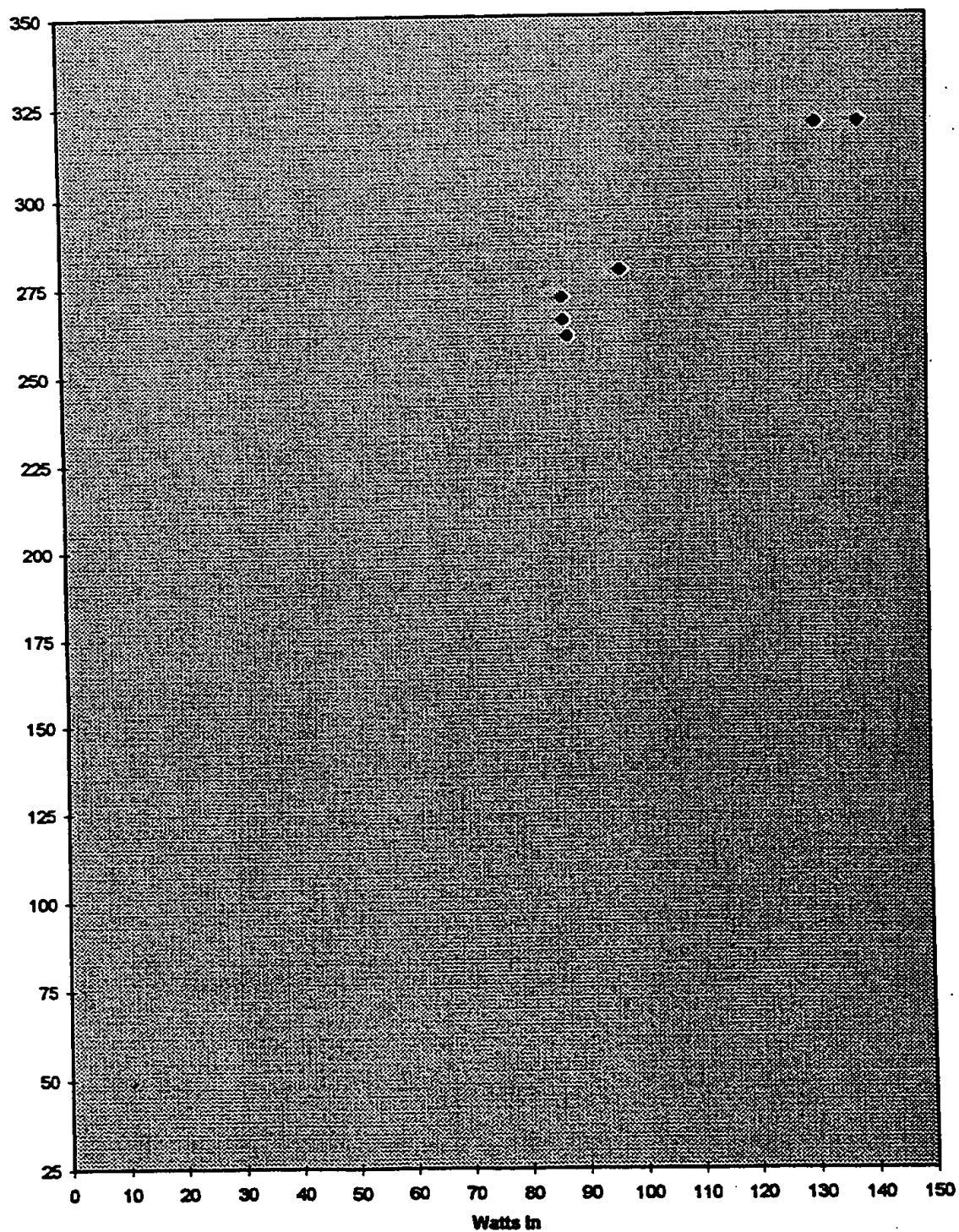
BLP Isothermal Cell Model Chart 1

Isothermal Cell - Vacuum



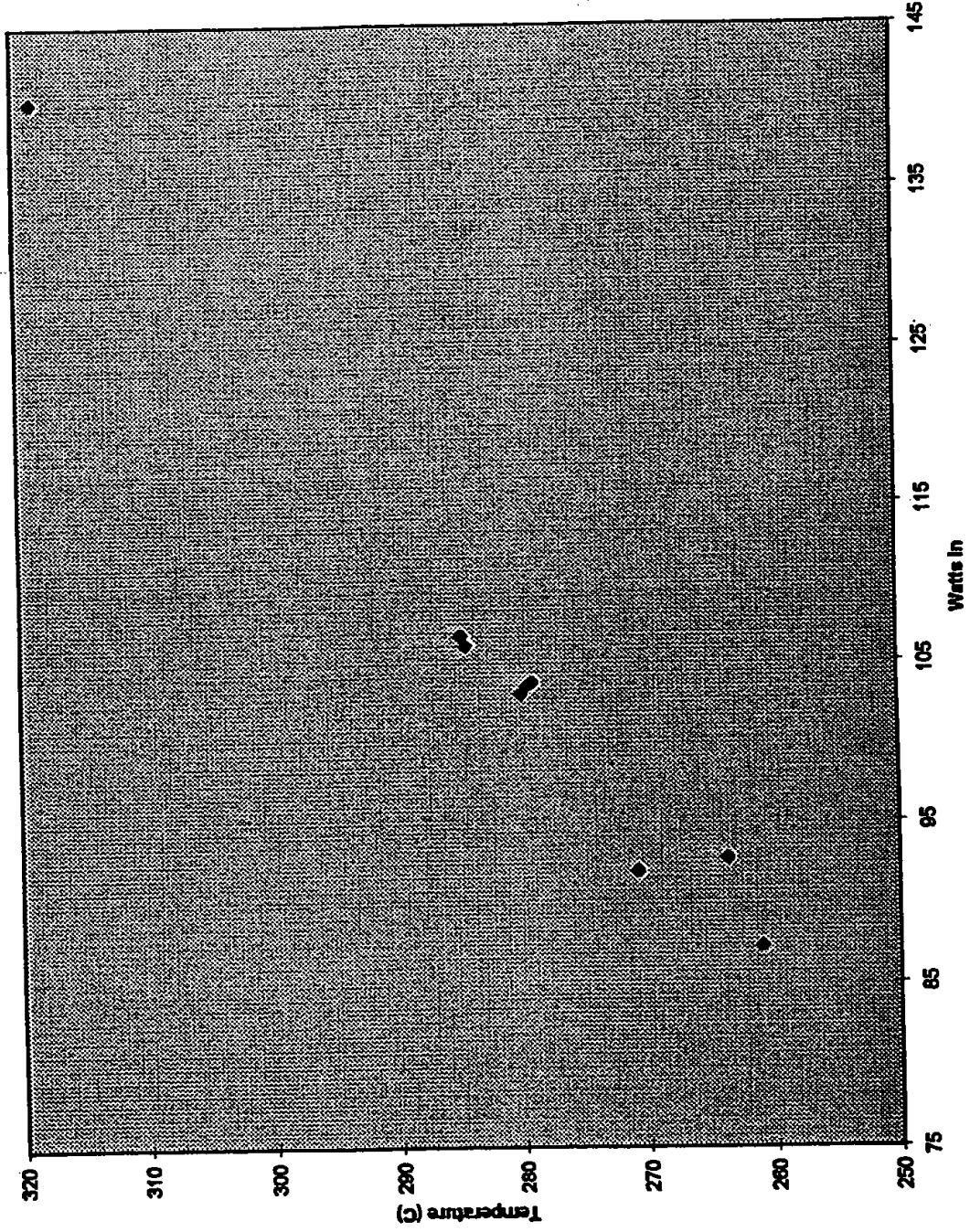
BLP Isothermal Cell Model Chart 2

Isothermal Cell - Gas 1500-2000 mtorr



BLP Isothermal Cell Model Chart 1

Isothermal Cell - Vacuum



Dear Peter,

Here is the data for the isothermal calorimeter which you requested. I tried to give you the most complete and representative data for our work on the isothermal calorimeter. The data includes one control and one experiment for a short (66 cm) tungsten filament, and also one control and five experiments for a longer (200 cm) tungsten filament. Varying diameters of tungsten filament were used for the 200 cm experiments and these diameters are noted. Other variables and data are listed under each experiment number (15.x) and description.

If you have any questions about the data, give me a call.

Sincerely,


Stev Bollinger

Analysis of Raw Lab Data

Analysis of BlackLight Power Gas Phase Cells									
BLP & Major US University									
Power Inputs & Outputs [watts]									
CHW FW TOTW EHW EHCW									
Temperature									
Gas Cell Characteristics									
Volume Pressure									
Filament Characteristics [cm-cm2]									
Length Diameter Surface Area									
Type									
BLP-15.3	H2 Run?	?	?						
BLP-15.4	H2 Run?	68.04	?						
BLP-15.5	Control	68.04	?						
BLP-15.6	H2 Run	200	0.01	6.2831853	2000				
	KNO2								
	KNO2								
	KNO2								
BLP-15.7	H2 Run?	200	0.01	6.2831853	2000				
BLP-15.8	Control	200	0.01	6.2831853	2000				
	?								
	?								
	?								
BLP-15.9	H2 Run	200	0.01	6.2831853	2000				
	KNO2								
	KNO2								
	KNO2								
BLP-15.10	H2 Run	200	0.01	6.2831853	2000				
	KNO2								
	KNO2								
	KNO2								
BLP-15.11	Control	200	0.025	15.70796325	2000				
BLP-15.12	Control	200	0.025	15.70796325	2000				
	VAC								
	VAC								
	VAC								
	VAC								
BLP-15.13	Control	200	0.025	15.70796325	2000				
	He								
	He								
BLP-15.13	H2 Run	200	0.025	15.70796325	2000				

Analysis of Raw Lab Data

[illegible]

Review of Iso Cal Data*

Confidential	Isothermal Calorimeter Data					15.9-KNO ₂ , 200 cm(0.01 cm dia) tungsten filament				
						status	Temp(°C)	Wcart htr	Wfil	Wtotal
15.4-KNO ₂ , 66 cm(0.01 cm dia) tungsten filament						vac 0.109 torr	279.49	103.48	0	103.48
status						H ₂ 1.15 torr	279.5	97.05	0	97.05
vac 0.075 torr						H ₂ 1.7 torr	289.24	5.73	35.94	41.67
H ₂ 1.6 torr										
H ₂ 2.0 torr										
H ₂ 2.0 torr										
H ₂ >2.0 torr										
15.10-KNO ₂ , 200 cm(0.01 cm dia) tungsten filament						status	Temp(°C)	Wcart htr	Wfil	Wtotal
status						vac 0.056 torr	263.72	92.71	0	92.71
vac 0.086 torr						H ₂ 1.6 torr	265.41	87.16	0	87.16
H ₂ >2.0 torr						H ₂ 1.6 torr	275.7	1.82	30.36	32.18
H ₂ >2.0 torr										
H ₂ 2.0 torr										
H ₂ low ATM										
15.12-KNO ₂ , 200 cm(0.025 cm dia) tungsten filament						status	Temp(°C)	Wcart htr	Wfil	Wtotal
status						vac 0.021 torr	284.33	106.02	0	106.02
vac 0.038 torr						vac 0.019 torr	288.49	62.15	35.091	97.24
H ₂ 1.8 torr						vac 0.020 torr	284.72	106.71	0	106.71
H ₂ 1.35 torr						vac 0.0208 torr	288.54	54.96	42.85	97.81
15.6-KNO ₂ , 200 cm(0.01 cm dia) tungsten filament										
status										
vac 0.038 torr										
H ₂ 1.8 torr										
H ₂ 1.35 torr										
15.8-(control), empty 200 cm(0.01 cm dia) tungsten filament										
status										
vac 0.048 torr										
H ₂ 1.35 torr										
H ₂ low ATM										
15.13-KNO ₂ , 200 cm(0.025 cm dia) tungsten filament						status	Temp(°C)	Wcart htr	Wfil	Wtotal
status						vac 0.0355 torr	318.45	140.45	0	140.45
vac 0.075 torr						vac 0.020 torr	323.36	82.59	46.638	129.23
H ₂ 1.6 torr						H ₂ 1.9 torr	319.83	131.22	0	131.22
H ₂ 1.6 torr						H ₂ 1.6 torr	328.48	38.5	47.77	86.27
H ₂ 1.9 torr						H ₂ 1.9 torr	331.03	8.79	74.798	83.59
He 2.0 torr						He 2.0 torr	318.91	138.29	0	138.29
He 2.0 torr						He 2.0 torr	326.24	60.71	47.194	107.90



THESIS - APPENDIX SIX



Final report for period October-December 1996
In fulfillment of Service Contract with HydroCatalysis Power Corp. (now BlackLight Power, Inc.)

REPORT ON CALORIMETRIC INVESTIGATIONS OF GAS-PHASE CATALYZED HYDRINO FORMATION

Submitted by
Prof. Jonathan Phillips*
and Julian Smith
Department of Chemical Engineering
Penn State University
University Park, PA 16802

Ph: (814) 863-4809
Fax: (814) 865-7846

Professor Stewart Kurtz
Department of Electrical Engineering
Penn State University
University Park, PA 16802

Ph: (814) 863-8407
Fax: (814) 863-8561


Jonathan Phillips


Julian Smith


Stewart Kurtz

*Corresponding Author



SUMMARY

Tests for heat production associated with hydrino formation were carried out with two types of calorimeters during the period October-December 1996. Experiments carried out in a modified Calvet system yielded extremely exciting results. Specifically, initial results are apparently completely consistent with the Mill's Hydrino formation hypothesis. In three separate trials between 10 and 20 K Joules were generated at a rate of 0.5 Watts, upon the admission of approximately 10^{-3} moles of hydrogen to the 20 cm³ Calvet cell containing a heated platinum filament and KNO₃ powder. This is equivalent to the generation of $1 \cdot 10^7$ J/mole of hydrogen, as compared to $2.5 \cdot 10^5$ J/mole of hydrogen anticipated from standard hydrogen combustion. Thus, the total heats generated appear to be two orders of magnitude too large to be explained by conventional chemistry, but the results are completely consistent with the Mill's model. It must be noted that although the results presented in this report are very exciting, they require further verification. Moreover, it should be noted that some control studies are not yet complete.

Also included is a brief report on an attempt to replicate the Calvet cell results on a larger scale using the water bath calorimeter (described in some detail in an earlier report). Unfortunately, no evidence of 'excess heat production' was found. This can be linked to a failure to maintain the catalyst ions (K⁺) in the vapor phase. Specifically, it is hypothesized that the KNO₃ catalyst evaporated from the containing pot at the reactor center, where the temperature is high, and deposited on the reactor walls, which are cold due to immediate contact with the calorimeter water bath. (That is, the catalytic material is 'cryo-pumped' by the cold walls.) Indeed, at the conclusion of the experiment, when the reactor was removed from the water bath, the walls of the quartz reactor were observed to be white in the general vicinity of the pot which contained the KNO₃.

INTRODUCTION

Experiments were conducted to test the hypothesis that in the gas phase potassium ions will catalyze the conversion of hydrogen atoms to hydrino atoms. These experiments were initially carried out in a Calvet cell as this type of calorimeter is highly sensitive and accurate. Moreover, the conditions of the calorimeter are controlled.

RM's theory of hydrino formation requires that both K^+ ions and H-atoms are present in the gas phase. In order to generate gaseous K^+ ions, KNO_3 is placed in a small (2cc) quartz 'boat' inside the calorimeter cell. The boat is heated, to increase the vapor concentration of KNO_3 , with a platinum filament, which is wound around the boat. A second function of the platinum filament is to generate H-atoms. It is well known that hydrogen molecules in contact with a heated filament will decompose, yielding a relatively high H-atom concentration in the boundary layer around the filament. Thus, according to RM's model, in a cell containing KNO_3 in the boat and vapor phase hydrogen, there is a small region in the boundary layer around the heated metal filament which should contain sufficient concentrations of both H-atoms and K^+ ions for hydrino formation to occur.

Calorimetric considerations require that a stable baseline exists before the heat generating process is initiated. Thus, signal change away from the baseline can be correlated to the onset of the process under investigation. In the present experiments the cell was run with KNO_3 in the boat and the filament fully 'powered'. The calorimeter was allowed to equilibrate until a steady baseline existed. The 'hydrino formation' process was initiated by then adding gaseous hydrogen. Good calorimetric practice also requires that adequate control studies be carried out. Also required are repeated electric calibrations.

In the present work, data is presented which indicates that significant heat evolved upon the introduction of hydrogen to the Calvet calorimeter cell. In contrast, no heat was evolved upon the admission of helium. Repeated calibrations were also conducted. Thus, it appears that The RM

hypothesis is supported by the present results. A more definitive statement must await repeats of these experiments, and the results of a few additional control experiments.

An attempt was also made to employ the water bath calorimeter (see previous report to HPC) to detect excess heat. Indeed, the positive results of the Calvet study present a staggering challenge to conventional physics. Challenges of this magnitude require enormous experimental support. Thus, evidence of excess heat production from a second type of calorimeter would be useful. Unfortunately, the experiment failed to yield any evidence of excess heat. However, there is reason to believe that catalyst concentration was low and thus the failure to observe excess heat does not disprove the Mill's hypothesis.

EXPERIMENTAL SYSTEM

Calvet Calorimeter. The Calvet-type calorimeter employed in this study is similar to one described in the literature (attached) and is also described in earlier reports to HPC (now BLP). In essence a stainless steel cup of almost exactly 20 cm³ volume is placed in a calorimeter well such that the cup is surrounded by thermopiles on its sides and bottom. The cup and calorimeter are surrounded by a thick layer of insulation, and the entire device is placed inside a commercial convection oven. In all cases experiments were conducted with the oven temperature set to 250 C.

Reaction cell. For these experiments the top of the calorimeter cup/reactor cell was fitted with a Conflat knife edge flange. The top element of the flange is connected to a gas supply system outside the convection oven with a 0.5 cm OD ss tube, and with two welded vacuum high current copper feedthroughs. The feedthroughs were connected on the cup side of the flange to a coiled section of 0.25 mm platinum wire approximately 18 cm in length. Fitted inside the coiled platinum was a small quartz boat into which 200 mg of powdered KNO₃ were placed.

Plumbing. On the outside of the oven the gas feed through is connected to a line leading to hydrogen and helium tanks, a pressure gauge, and a standard vacuum roughing pump. It is notable that the gas lines were all well insulated, both inside the oven, and for about 50 cm outside the oven.

The plumbing system was so arranged that the cell could be evacuated, and then isolated from the pump in such a way that hydrogen or helium could be added directly from high purity gas tanks. Great care was taken before the experiments were initiated to evacuate and flush the gas lines several times. It was also determined that the lines held gas pressure, with no loss in pressure, for several days. That is, there were no leaks.

Water Bath Calorimeter. This instrument is described in detail in the previous report to HPC. Two minor modifications were made for the present experiment. First, to facilitate the decomposition of hydrogen, the center section of the mandrel was wrapped with a 60 cm length (about 8 cm of mandrel) of 0.25 mm diameter platinum wire. Second, in the center of this section the same quartz boat (again filled with about 200 mg of catalyst) used in the Calvet system, wrapped with the same coil of platinum wire, was inserted into the circuit. (The experiment described was carried out after the completion of the Calvet system experiments.)

RESULTS

Calvet Calorimeter. The Calvet studies suggest large amounts of heat are generated upon the admission of hydrogen to the cell. In contrast, virtually no heat is observed upon admission of helium to the cell.

Calibration. The first tests performed on the Calvet system were electrical calibration experiments. The system was set-up for full experimentation: KNO_3 was in the boat, the system was evacuated, and 10 watts of steady power were supplied to the platinum coil. After a steady baseline was achieved (approximately 10 hours after the oven was adjusted to 250 C), the cell was isolated from the pump and the pressure allowed to equilibrate (approximately 100 Torr). This did not appear to impact the baseline in any fashion. The power supply was then adjusted to deliver an additional 1 watt (11 watt rather than 10) for a specified time period. The power was then returned to the original 10 watt setting. A typical response curve is shown in Figure 1. The area under the response curve can be used to obtain a calibration constant which relates signal area increase to the number of extra Joules delivered. This was done in four cases (Table I). As can be seen, there is some error ($\pm 15\%$) in the calculated calibration constant.

Control Studies. Helium was admitted, approximately 10 psig, to the cell to test the impact of a change in pressure, and heat transfer characteristics on the response of the cell. The helium was admitted after the cell had been isolated from the pump for a considerable time and a steady pressure (approximately 100 Torr) achieved. As can be seen in Figure 2a, the response was a short-lived small increase in output signal, followed by a relatively short time period during which the signal gradually returns to the original baseline. Within an hour the signal returned to the original baseline, with some drift evident.

The response of the system is expected. The helium increases the rate of heat transfer away from the platinum filament, and heated boat. Thus, the initial addition of helium to the system results in a temporary increase in the amount of heat reaching the thermopiles. That is, the boat and the filament cool off, until such time as the boat and filament have reached their new steady state temperatures. The steady state temperature of boat and filament are a function of heat transfer mechanism. After the admission of helium most heat transfer is occurring by convection to the walls. Before the admission of helium a considerable fraction is by radiation. Radiative transfer of 10 watts requires a higher filament/boat temperature than does convective heat transfer.

Figure 2b illustrates again the impact of adding pressure, or removing gas, from the system. Upon the addition of helium there is a very short lived increase in heat reaching the thermopiles. Upon pumping there is a period of time, perhaps an hour, during which the heat signal goes below the baseline. This is consistent with the model in that pumping makes convective and diffusive heat transfer minimal. Virtually all heat transfer is by radiation, which requires that the filament/boat temperature increase. It takes some time for this new steady-state temperature to be reached.

Hydrogen Admission. Hydrogen admission was carried out in much the same fashion as helium admission. The cell reached an equilibrium pressure, approximately 100 Torr, and then hydrogen at 10 psig was admitted to the cell. The valve to the hydrogen source, which was a steel line 4 meters by 0.6 cm OD, was closed off by a valve in front of the regulator during admission. Moreover, it was open for only a couple of seconds in each case. This was done on three separate

occasions, and the signal that evolved in response to these three processes is recorded in Figures 3, 4 and 5. One other observation recorded was that the pressure decreased gradually over time, such that after about an hour the pressure returned to the original equilibrium pressure of the cell. It must also be noted that the heat production was ended deliberately in all three cases by pumping the system to 5×10^{-3} Torr. It is clear 'excess heat' evolution would have continued in all cases if the system had not been evacuated.

It is expected that in the absence of reaction that the response of the cell to the addition of hydrogen would be similar to that observed for helium. Indeed, given that pressure measurements suggest that most hydrogen is adsorbed, or in some other fashion removed from the cell after an hour, even heat transfer effects should be totally transitory. Even in the event of reaction no more than a small heat signal is expected. Indeed, a high end estimate is that 25 cm^3 of hydrogen at a temperature of 300 K and a pressure of 2 atmospheres entered the cell. This is equivalent to 2×10^{-3} moles of hydrogen. If all of that hydrogen interacted with oxygen to form water only 510 J would be generated. It is possible to imagine that the hydrogen could interact with nitrogen in KNO_3 to form ammonia. Even less energy would evolve from this process. Thus, the largest heat peak might be expected to be 0.5 watts for 1000 seconds (approx. 17 minutes). A block of this size is marked on Figure 3.

It is clear from figures 3, 4 and 5 that hydrogen admission to the cell apparently leads to far more energy evolution than can be explained by any conventional chemical process. It is interesting in this regard to graphically contrast the response of the system to helium admission to the response to that for hydrogen admission. This is done on Figure 6 in which Figure 3 and Figure 2a are superimposed.

Water Bath Calorimeter. Studies conducted with the water bath calorimeter do not indicate the evolution of any excess heat. As shown in Figure 7 the increase in temperature almost exactly parallels the increase predicted on the basis of the amount of energy added to the system and the known heat capacity of water.

Do the results of the experiment refute the RM hypothesis? No. At the conclusion of the experiment the large cell was removed from the water bath and a white coating was seen on the walls in the vicinity of the pot which contained the KNO_3 . This suggests that the KNO_3 was rapidly cryopumped by the walls, and that the gas phase concentration of catalyst was too low to be effective.

DISCUSSION

The evidence presented in this report clearly suggests that an extraordinary phenomenon takes place upon the admission of hydrogen to a cell containing a heated platinum filament and KNO_3 . This phenomenon appears to generate a tremendous amount of 'excess' heat. Still, the author of this report urges that a cautious approach be taken at present. Additional experimental work is required. A partial list of proposed additional experiments is given below:

- 1) A control experiment consisting of admission of hydrogen to a cell in which 10 watts of power is applied to a platinum filament, but no KNO_3 is present.
- 2) Hydrogen is admitted to a cell containing a platinum filament and KNO_3 in a boat, but no power is applied to the filament.
- 3) The experiments are run as described in the present report, but the boat containing KNO_3 is at the bottom of the cell, rather than in the center of the platinum coil.
- 4) The hydrogen admission experiments described above are repeated BUT continued for times sufficient to return the signal to the original baseline.

In addition, modifications in the apparatus should be made. First, insulation should be added to improve the stability of the baseline. Second, a quality pressure gauge should be attached to a known volume outside the oven such that all uncertainty regarding the number of moles of hydrogen admitted to the cell can be eliminated. Third, the plumbing should be re-arranged to facilitate 'capture' of gas for analysis using gas chromatography. Fourth, provision should be made to permit pressure to be recorded as a function of time.



Typical Calibration Experiment: 1 W Input, 20 Mins

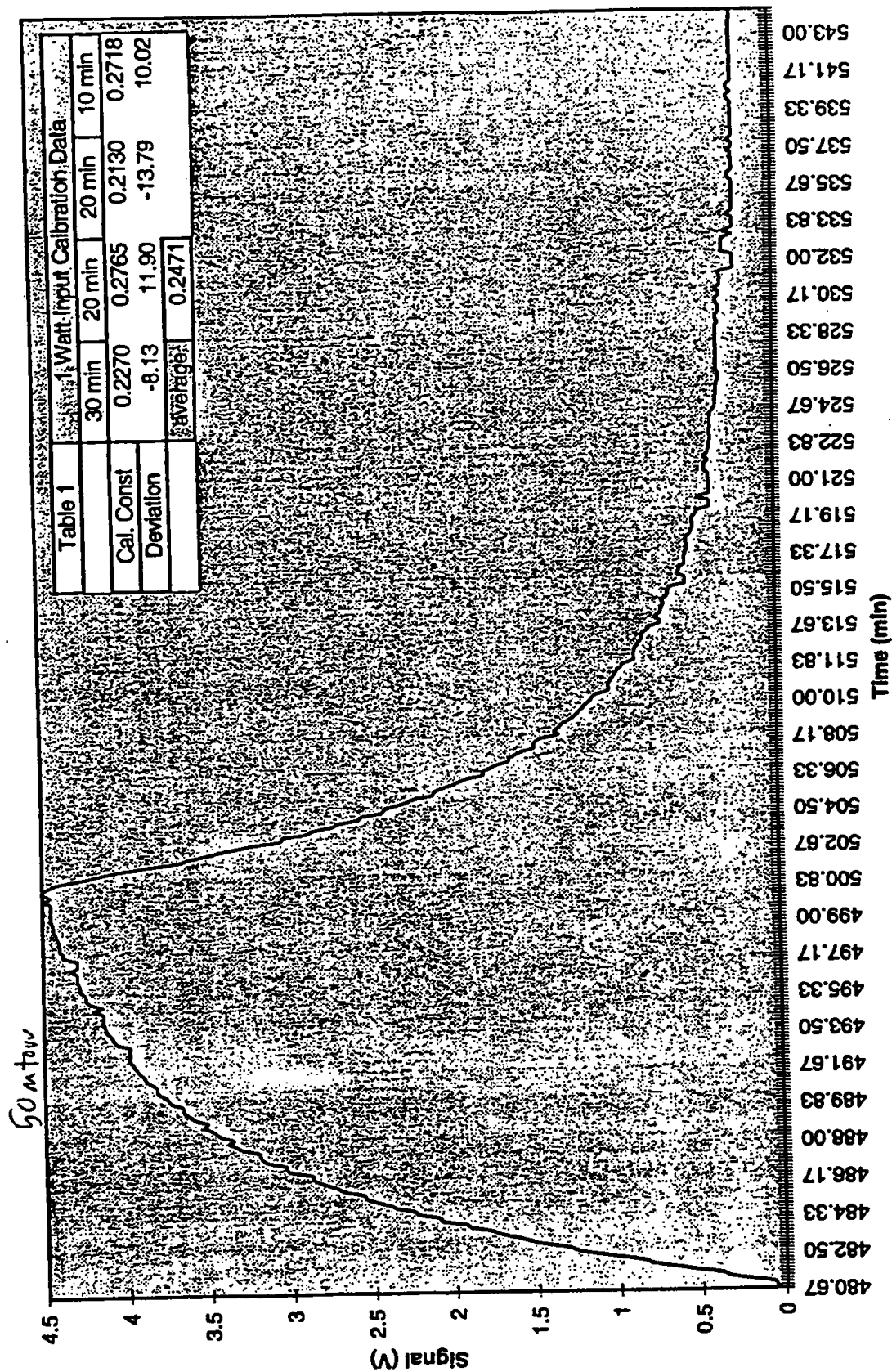


Figure 1

Heat Production, KNO3 w/ Helium Injection (BL1220A)

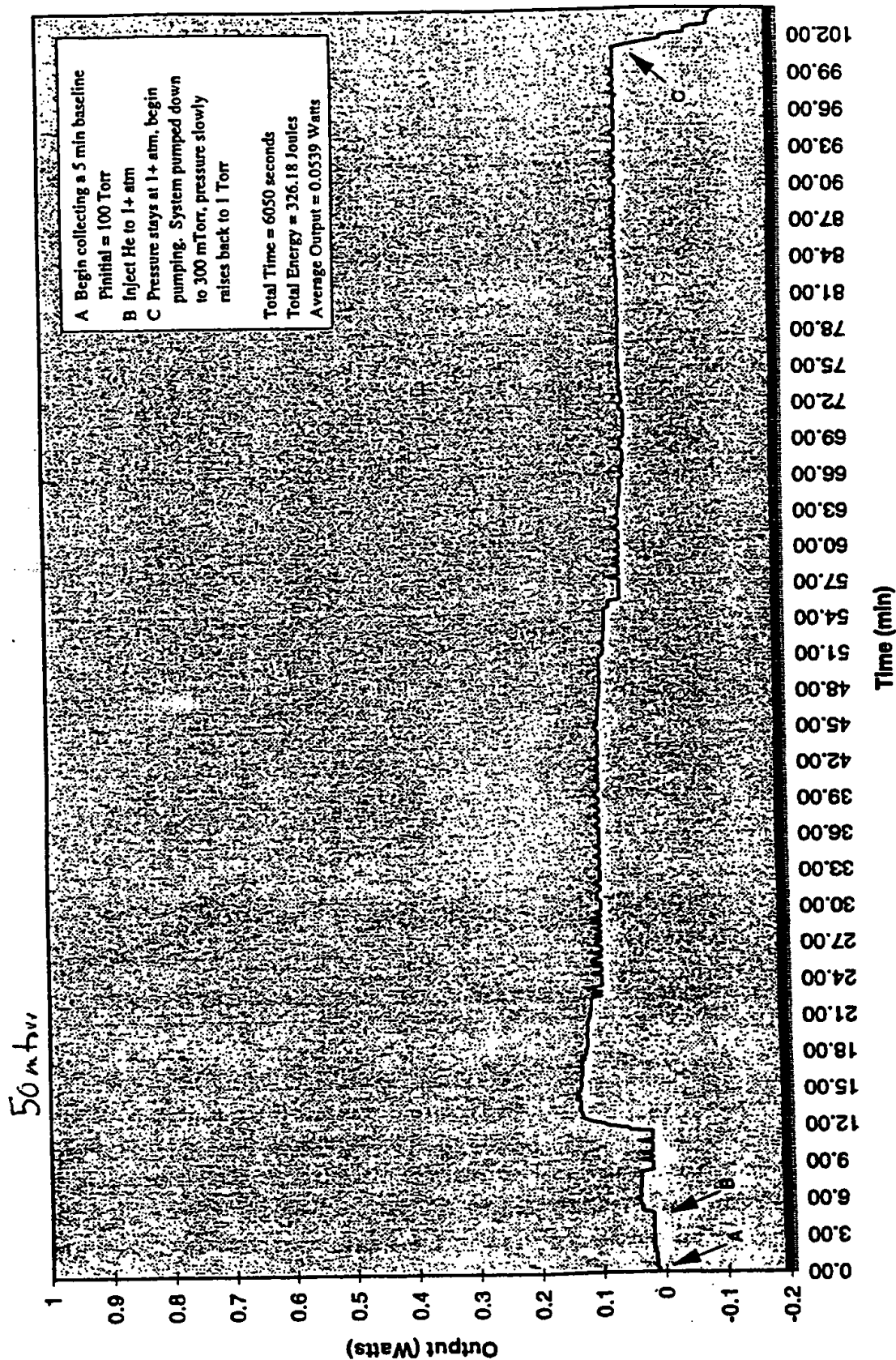
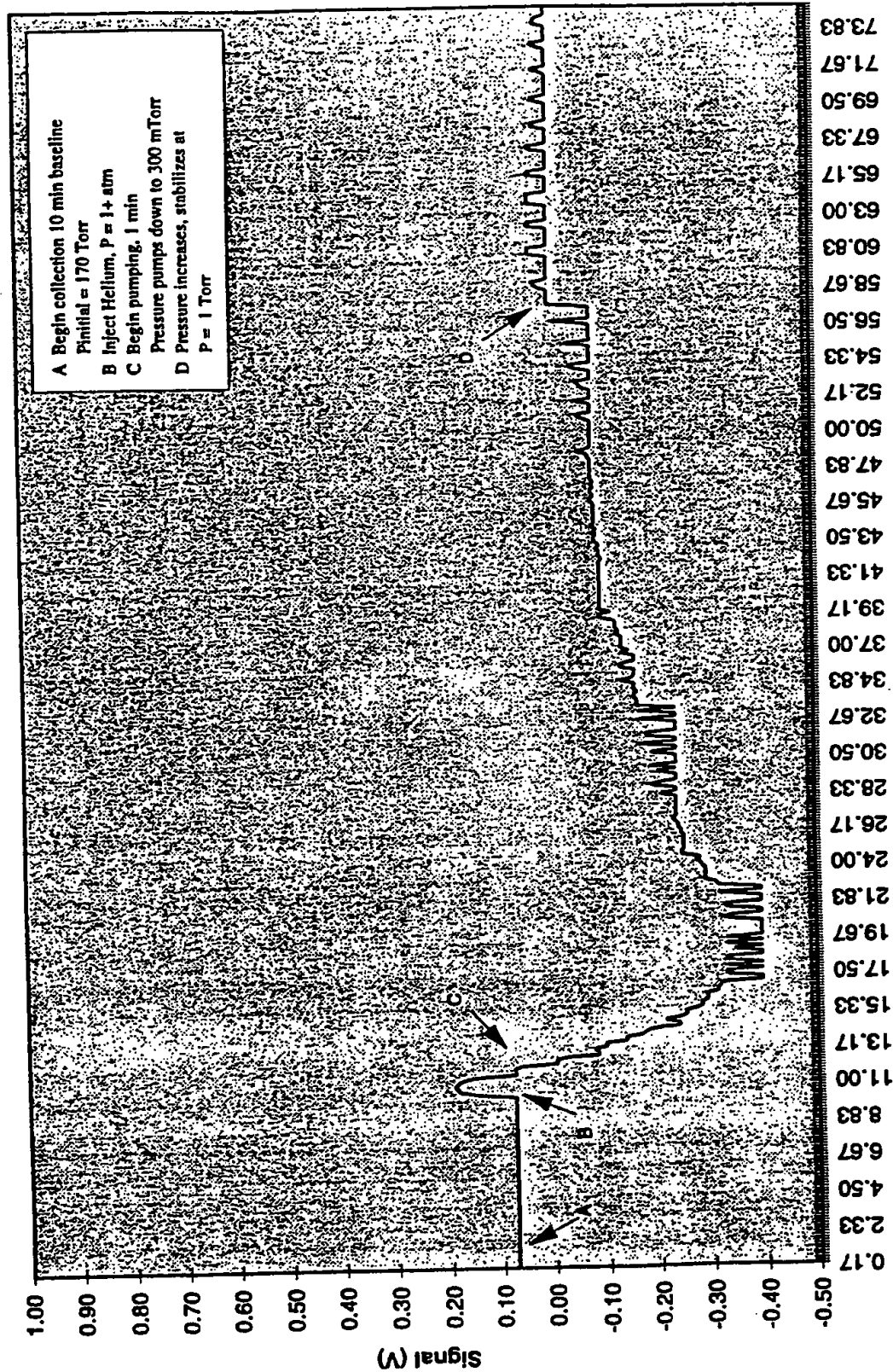


Figure 2A

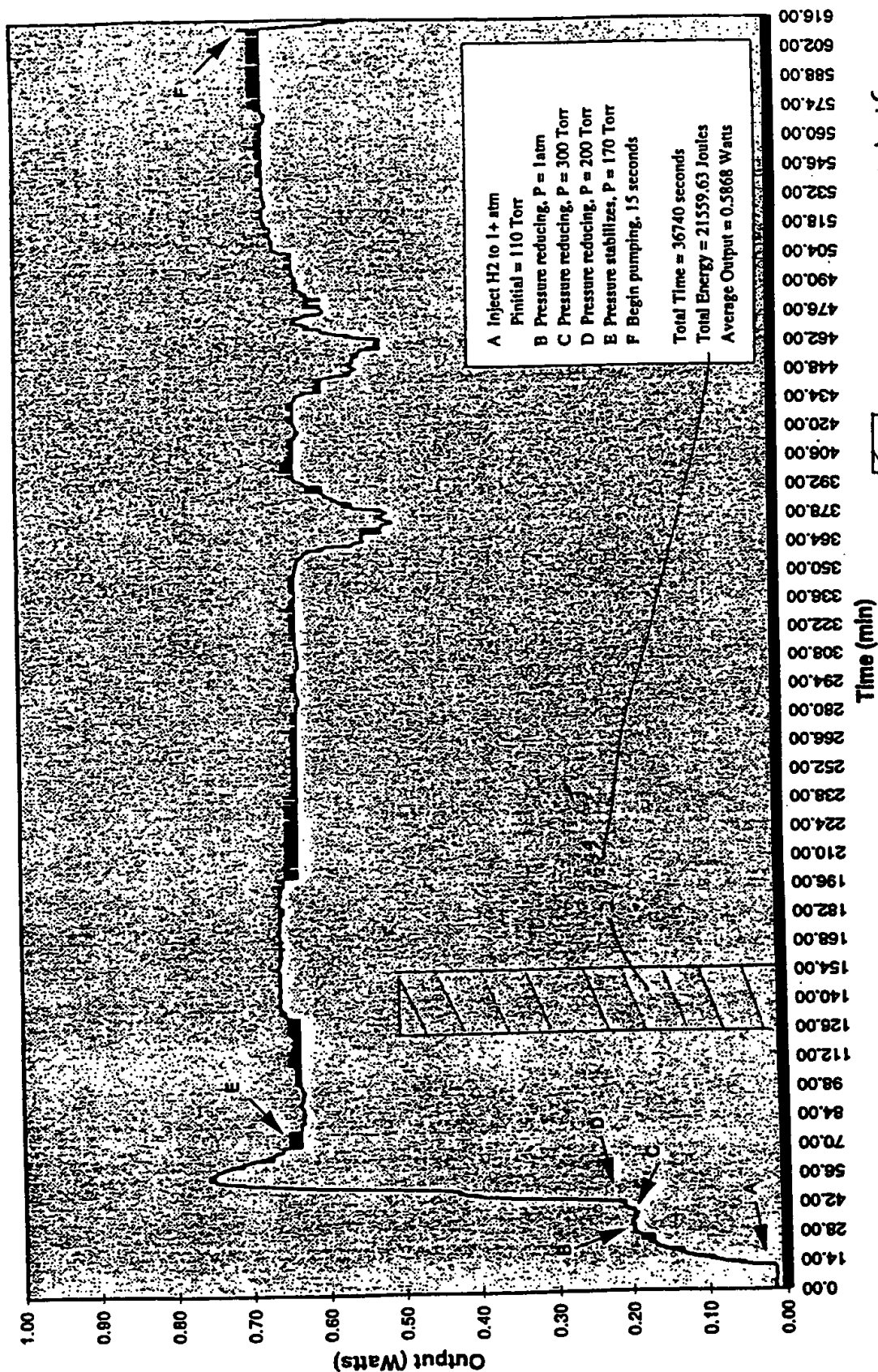
Heat Production, KNO3 w/ Helium Injection (BL1219B)



Constant power power supply

Figure 2B

Heat Production, KNO3 w/ H2 Injection (BL1218CD)



20cc H_2 70×10^{-3} moles

Figure 3

Heat Production, KNO3 w/ H2 Injection (BL1220BC)

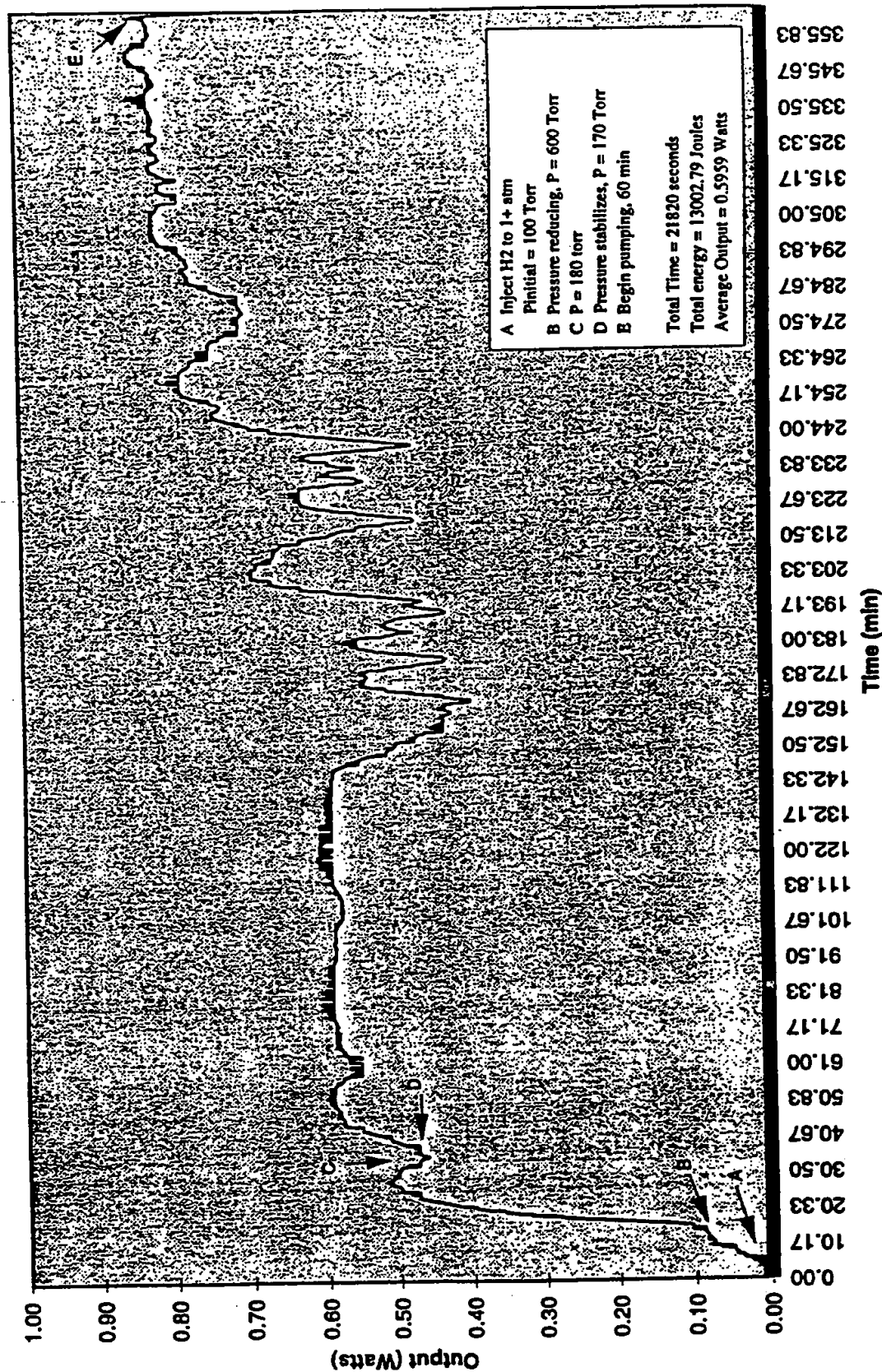


Figure 4

Heat Production, KNO₃ w/ H₂ Injection (BL1221AB)

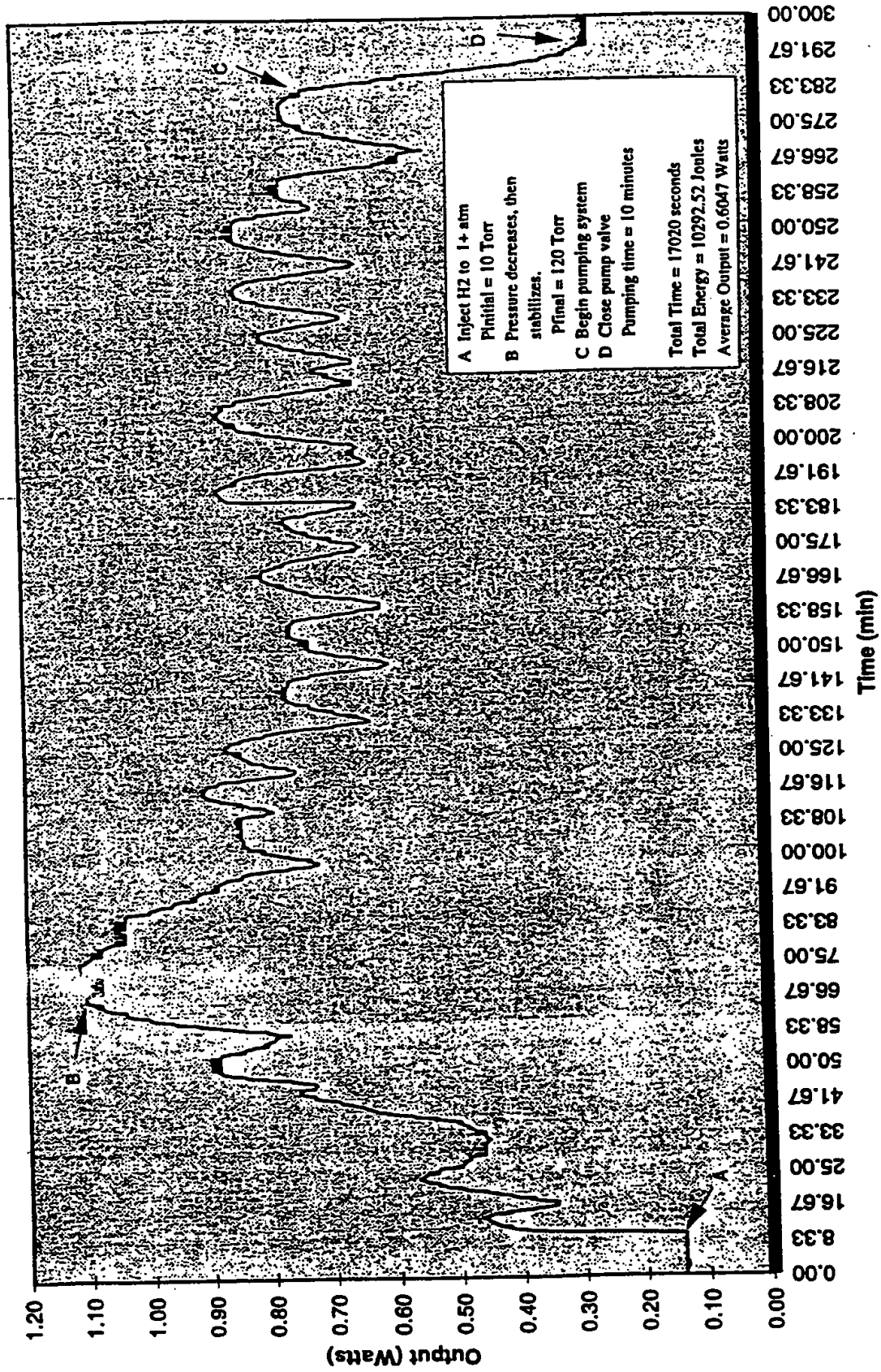


Figure 5

Heat Production, KNO3 w/ H2 and He Injection (BL1218CD,BL1219B)

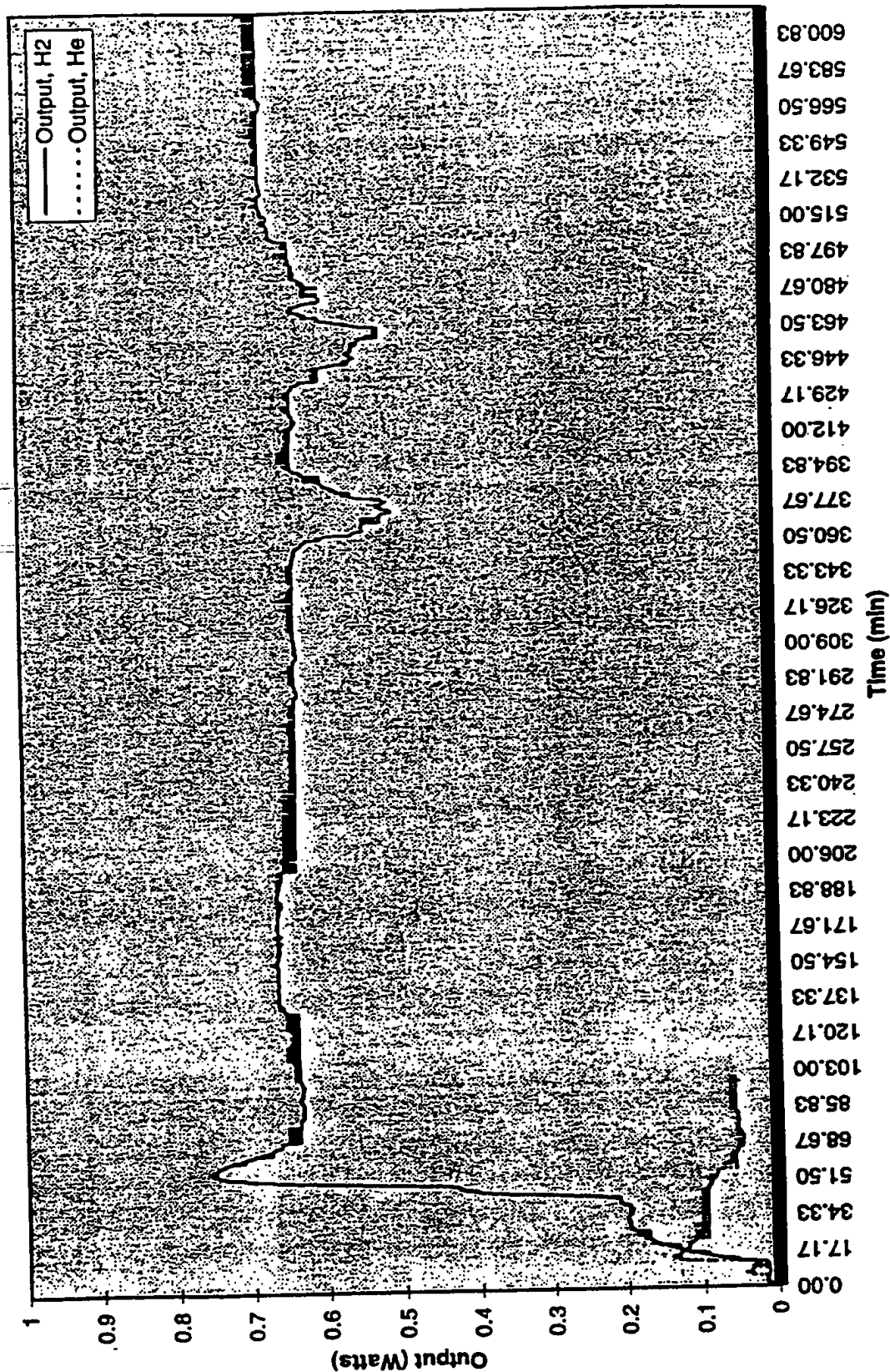


Figure 6



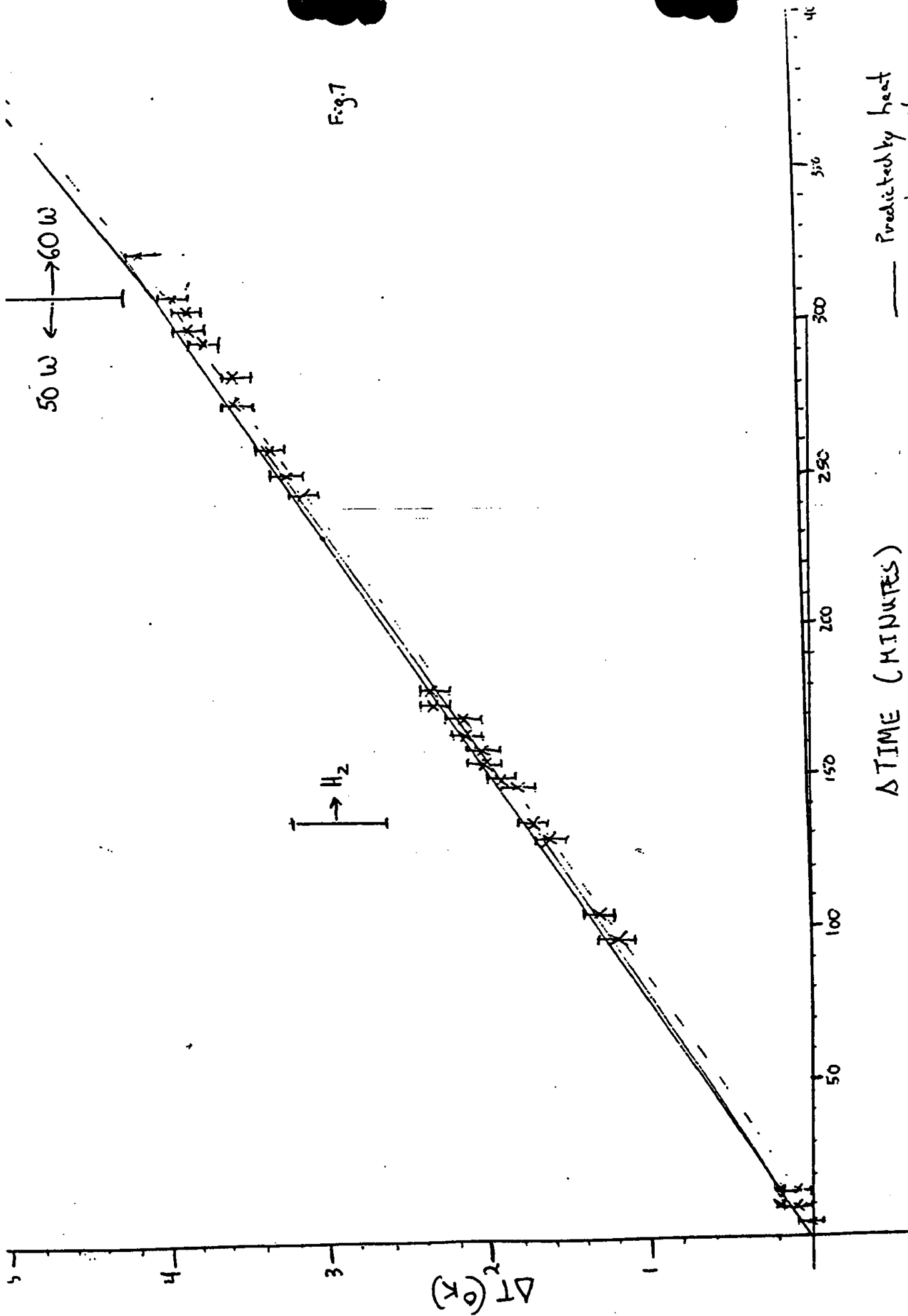


Fig. 7

$\Delta TIME (MINUTES)$

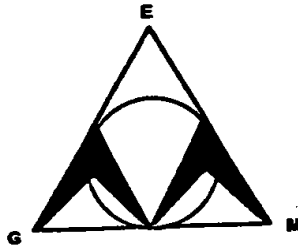
— Predicted by heat capacity
 --- Best-eye-bull fit...

Summary. Runs as predicted by heat capacity within a 10 minute (warm-up) off-set.

THESIS - APPENDIX SEVEN



FINAL
REVISED 12 APRIL 1997



BLACKLIGHT POWER CORPORATION

**EXPERIMENTAL PROTOCOL
FOR
CALVET HEAT MEASUREMENTS
OF A HIGH TEMPERATURE
VAPOR PHASE CELL**

EXPERIMENTS BY P.M. JANSSON, P.P., P.E.
B.S.C.E. MASSACHUSETTS INSTITUTE OF TECHNOLOGY '78
FOR M.S.E. THESIS AT ROWAN UNIVERSITY '97

**TO DETERMINE FILAMENT SURFACE AREA EFFECTS
ON HEAT GENERATION**

3 March 1997 - 20 April 1997

Experiments Conducted in Laboratory of:

BLACK LIGHT
P O W E R inc.

Great Valley Corporate Center
41 Great Valley Parkway
Malvern, PA 19355



CALVET HEAT MEASUREMENTS OF THE HIGH TEMPERATURE VAPOR PHASE CELL

Objective

A number of experimental observations from BlackLight Power and Pennsylvania State University lead to the conclusion that atomic hydrogen can achieve fractional quantum states that are at lower energies than the traditional "ground" ($n=1$) state which form the basis of a new hydrogen energy source. Certain inorganic ions which are proprietary to the BlackLight Power serve as transition catalysts which resonantly accept energy from hydrogen atoms and release the energy to the surroundings. The reaction of hydrogen to lower-energy states is referred to as a transition reaction. The transition catalyst should not be consumed in the reaction. It accepts energy from hydrogen and releases the energy to the surroundings. Thus, the transition catalyst returns to the original state. And, the energy released from hydrogen atoms is very large compared to conventional chemical reactions including the combustion of hydrogen. Multiple cycles of catalysis are possible with increasing amounts of energy with successive cycles of transitions.

The goal of this project is to perform precise Calvet calorimetric measurements of a hydrogen gas energy reactor wherein the predicted exothermic reaction of electronic transitions of hydrogen to lower energy states could be measured. This new reaction occurs in the gas phase of atomic hydrogen. If successful, the experiments should produce statistically significant excess heat much greater than any known chemical reactions for hydrogen. The experiment will also vary the size [length] of the platinum filament used in the reactor to dissociate the hydrogen molecules to make hydrogen atoms available for the anticipated catalytic transition to reduced energy states. The intent will be to demonstrate that heat generation from this reaction will be directly related to available hydrogen atoms, which should be generated at different rates by varying filament size while keeping all other controllable parameters constant [ie; filament temperature, partial pressure of the catalyst, partial pressure of the H_2 gas, vessel temperature and pressure, etc.]

Vapor Phase Energy Cell

The hydrogen gas energy reactor wherein the exothermic reaction of hydrogen occurs in the gas phase comprises a vacuum vessel; a source of hydrogen; a means to control the pressure and flow of hydrogen into the vessel; a material to dissociate the molecular hydrogen into atomic hydrogen, and a transition catalyst. The hydrogen transitions occur by contact of the hydrogen with the transition catalyst such that the resonant energy transfer occurs. The catalytic reaction rate is maximized in the gas phase. The gaseous transition catalyst includes ions that sublime, boil, and/or are volatile at the elevated operating temperature of some regions of the gas energy reactor. In this project, the source of hydrogen atoms in the gas phase comprises an external tank of pressurized hydrogen gas at room temperature conditions.

Volatilized Transition Catalyst, K^+ / K^+ , in a Gas Cell for a Calvet Calorimeter

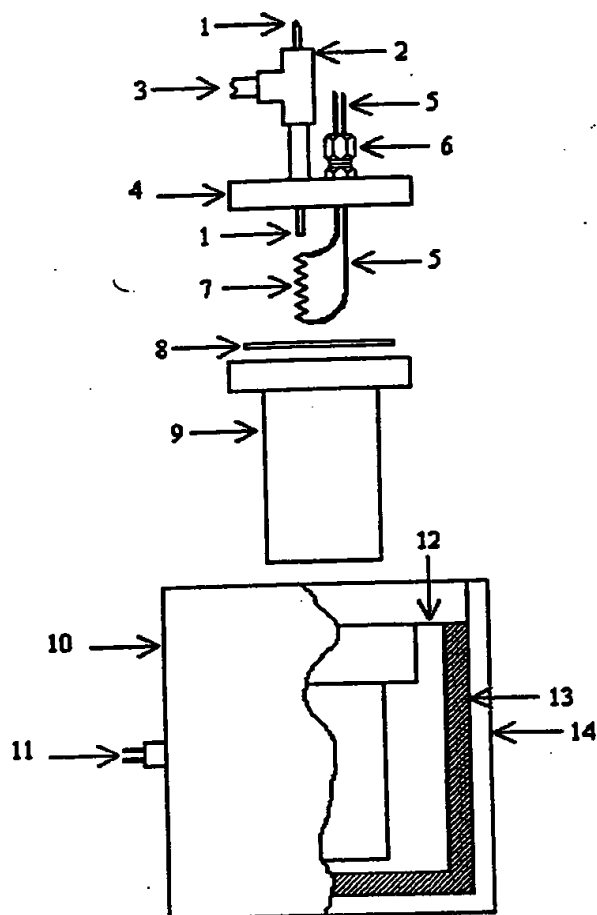
The transition reaction occurs in the gas phase. Gas phase hydrogen atoms are generated with a high purity platinum filament. The general cell schematic is shown in Figure 1. The cell comprises a 20 cc stainless steel vessel capable of containing a vacuum or a pressure

above atmospheric. The cell is maintained at an elevated isothermal temperature by a forced convection oven. The operating temperature of the convection oven [and gas cell when no filaments are energized] is 250°C. The cell is used in the vertical position and is inserted into a thermopile [13]. The flange [4] is sealed with a copper gasket [8] that has had its surface oxidized and softened by direct heating with a propane torch or oven. The flange has a two hole Conax-Buffalo gland [6] for the leads [5] of the filament that is present during the calibration of the cell and varied in length for the experiments 1-3 of the reaction vessel. The flange [4] also has a 1/4" vacuum port through which the hydrogen is passed. The vacuum port connects to a Tee [3], a OE bellows valve, a pressure gauge, and then the hydrogen supply. The elbow port of the Tee [3] is attached to vacuum gauges, a bellows valve, and then a vacuum pump. The filament is platinum wire [0.25 mm. diameter] of 99.99% purity. The lengths of the filament [and resulting surface areas] are varied 20cm, 10cm and 30cm for experiments 1 through 3 respectively.

A small ceramic vessel is secured at the base of the Calvet cell [by a nickle wire stand] which contains the catalyst potassium nitrate (KNO_3). A vacuum is pulled on the cell while the oven is brought to operating temperature. The appropriate power is dissipated in the filament at an established rate calculated to keep the filament surface temperature constant [10watts for 20cm., 5 watts for 10cm., 15 watts for 30cm.] The oven maintains the surrounding ambient temperature at 250°C. The catalyst's vapor pressure is observed as a function of temperature, and once Calvet cell reaches its steady state output at the supplied input energy, the vacuum pump is stopped and the catalyst pressure within the outlet tube [3] is observed to be constant in the range of about one-hundred to two-hundred torr. Hydrogen gas is then added to the cell to bring its overall total static pressure including the hydrogen pressure measured in the outlet tube [3] by the vacuum gauge to be 3 times the stable pressure of the catalyst (KNO_3). The data is recorded with a Macintosh based computer data acquisition system (Apple Quadra 800) and the following National Instruments, Inc. hardware: Lab-NB Data Acquisition Board; Back-Plane with amplifiers: (2) 10 mV to 5 V and (2) 50 mV to 5 V.

NOTE: Minor Edits to Figure 1 below need to be made.

Figure 1. Schematic of the Gas Cell for the Calvet Calorimeter and Cross Sectional View of the Calvet Calorimeter. 1 - (1/16)" OD stainless steel tube (to hydrogen supply), 2 - stainless steel tee union, 3 - (1/4)" OD stainless steel tube (to vacuum manifold), 4 - cell lid, 5 - filament leads, 6 - Conax-Buffalo gland, 7 - precision resistor, 0.1 mm OD tungsten filament, or nickel hydride filament treated with catalyst, 8 - copper ring gasket, 9 - cell body, 10 - Calvet Calorimeter, 11 - thermopile signal output, 12 - thermal shunt, 13 - thermopile, 14 - insulated calorimeter base.



Sequence of Controls and Experiments

Control #1

Install 20 cm Platinum [Alfa] filament, 0.25mm diameter in Reaction Vessel
Warm up oven Temperature 250°C.
Filament input wattage = 0
Vacuum down pressure in Reaction Vessel below 10 mtorr to remove moisture.
Stabilize Oven and Vessel Temperature to 250°C.
Close all valves and vacuum pump.
Inlet H₂ gas to 650 torr pressure.
Run Calibration #1 through full sequence allowing Calvet Cell to reach steady state output [Vc]
for each power level shown below:
0 watts, 10 watts, 11 watts, 5 watts, 6 watts, 15 watts, 16 watts, 0 watts, 1 watt.
Develop 'BEFORE' Calibration Curve.

Experiment #1

Install New 20 cm Platinum [Aldrich] Filament [99.99% purity], 0.25 mm diameter
Weigh approx. 0.25 grams of KNO₃ and place in ceramic boat
Support boat via nickle wire support legs
Reassemble reaction vessel
Pressure check Calvet and all gas & vacuum lines
Insulate Calvet Calorimeter close oven
Warm up oven Temperature 250°C.
Filament input wattage = 0
Vacuum down pressure in Reaction Vessel below 10 mtorr to remove moisture.
Close all valves and vacuum pump.
Stabilize Oven and Vessel Temperature to 250°C.
Observe catalyst vapor pressure steady state [100-200 torr]
Begin Experiment #1 by Increasing Filament Power Level to that shown below:
10 watts
Inlet H₂ gas to bring vessel to 3 times overall catalyst steady state pressure. [Ie; if catalyst pressure is 200 torr add 400 torr of H₂ gas to bring Calvet to 600 torr.
Wait 5 minutes for mixing to occur.
Slowly vacuum down Vessel to 30-70 mtorr level until excess heat formation commences.
Keep Vessel under vacuum to maintain 'active' pressure regime [ie; 38 mtorr, 70 mtorr, etc.]
Stabilize Readings and Develop Experimental Data Curves.
Save Data Acquisition System [DAS] file daily, using the same standard naming convention: tpdte[mmddyy] time[930a] watt[7w] id[h]
Take 1 or 2 new data points [controls] to develop specific curve after reaction ceases.
OPTION 1: Close valve to Vacuum to quench reaction if required.
OPTION 2: Repeat experiment if it is believed that catalyst pressure is inadequate or hydrogen atom generation is compromised

Experiment #2

Install New 10 cm Platinum [Aldrich] Filament [99.99% purity], 0.25 mm diameter
Weigh approx. 0.25 grams of KNO₃ and place in ceramic boat
Support boat via nickle wire support legs
Reassemble reaction vessel
Pressure check Calvet and all gas & vacuum lines
Insulate Calvet Calorimeter close oven
Warm up oven Temperature 250°C.
Filament input wattage = 0
Vacuum down pressure in Reaction Vessel below 10 mtorr to remove moisture.
Close all valves and vacuum pump.
Stabilize Oven and Vessel Temperature to 250°C.
Observe catalyst vapor pressure steady state [100-200 torr]
Begin Experiment #1 by Increasing Filament Power Level to that shown below:
5 watts
Inlet H₂ gas to bring vessel to 3 times overall catalyst steady state pressure. [ie; if catalyst pressure is 200 torr add 400 torr of H₂ gas to bring Calvet to 600 torr.
Wait 5 minutes for mixing to occur.
Slowly vacuum down Vessel to 30-70 mtorr level until excess heat formation commences.
Keep Vessel under vacuum to maintain 'active' pressure regime [ie; 38 mtorr, 70 mtorr, etc.]
Stabilize Readings and Develop Experimental Data Curves.
Save Data Acquisition System [DAS] file daily, using the same standard naming convention: t[mmddyy] time[930a] watt[7w] id[h]
Take 1 or 2 new data points [controls] to develop specific curve after reaction ceases.
OPTION 1: Close valve to Vacuum to quench reaction if required.
OPTION 2: Repeat experiment if it is believed that catalyst pressure is inadequate or hydrogen atom generation is compromised

Experiment #3

Install New 30 cm Platinum [Aldrich] Filament [99.99% purity], 0.25 mm diameter
Weigh approx. 0.25 grams of KNO₃ and place in ceramic boat
Support boat via nickle wire support legs
Reassemble reaction vessel
Pressure check Calvet and all gas & vacuum lines
Insulate Calvet Calorimeter close oven
Warm up oven Temperature 250°C.
Filament input wattage = 0
Vacuum down pressure in Reaction Vessel below 10 mtorr to remove moisture.
Close all valves and vacuum pump.
Stabilize Oven and Vessel Temperature to 250°C.
Observe catalyst vapor pressure steady state [100-200 torr]

Begin Experiment #1 by Increasing Filament Power Level to that shown below:

15 watts

Inlet H₂ gas to bring vessel to 3 times overall catalyst steady state pressure. [Ie; if catalyst pressure is 200 torr add 400 torr of H₂ gas to bring Calvet to 600 torr.

Wait 5 minutes for mixing to occur.

Slowly vacuum down Vessel to 30-70 mtorr level until excess heat formation commences.

Keep Vessel under vacuum to maintain 'active' pressure regime [ie; 38 mtorr, 70 mtorr, etc.]

Stabilize Readings and Develop Experimental Data Curves.

Save Data Acquisition System [DAS] file daily, using the same standard naming

convention: t[update[mmddyy] time[930a] watt[7w] id[h]

Take 1 or 2 new data points [controls] to develop specific curve after reaction ceases.

OPTION 1: Close valve to Vacuum to quench reaction if required.

OPTION 2: Repeat experiment if it is believed that catalyst pressure is inadequate or hydrogen atom generation is compromised

Control #2

Install New3 20 cm Platinum [Aldrich] filament [99.99% purity], 0.25mm diameter in Vessel

Warm up oven Temperature 250°C.

Filament input wattage = 0

Vacuum down pressure in Reaction Vessel below 10 mtorr to remove moisture.

Stabilize Oven and Vessel Temperature to 250°C.

Close all valves and vacuum pump.

Inlet H₂ gas to 650 torr pressure.

Vacuum down to 40-100 mtorr range.

Run Calibration #2 through full sequence to steady state at each power level shown below:

0 watts, 10 watts, 11 watts, 5 watts, 6 watts, 15 watts, 16 watts, 0 watts, 1 watt. [add any new points determined via Experiments 1-3 then repeat sequence above]

Develop 'AFTER' Calibration Curve.

Compare Calibration Curves 'Before' and 'After'

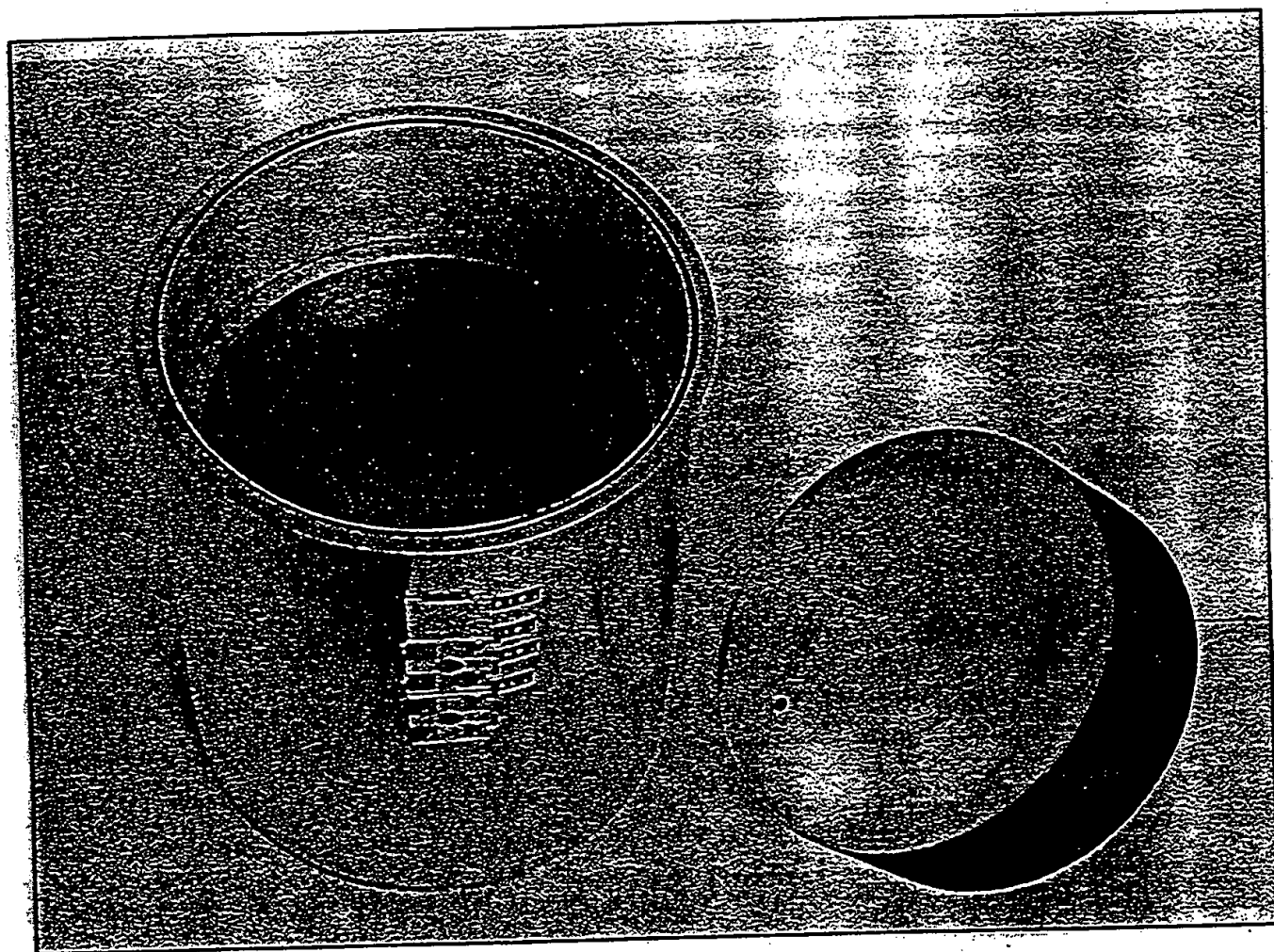
Analyze and Report on Results Based upon above

final revised 12 April 1997

developed by: William Good - BlackLight Power

Peter Jansson - Atlantic Energy

RADIOISOTOPE MICROCALORIMETERS



CR-100 7" Thermoelectric Enclosure

The series CR-100 Microcalorimeters provide an accurate measurement of radioisotope heat release rates.

PRINCIPLE

The thermal gradient calorimeter transfers all the heat developed in a reaction to its surrounding heat sink at a constant temperature. The calorimeter walls thermoelectrically transduce sample heat release into an electrical signal which is directly proportional to the energy release of the source. Transient as well as steady state energy releases may be measured.

FEATURES

- Whole body heat release measurements
- Microwatt to kilowatt sample output
- High sensitivities and repeatability
- Linear output
- Transient and steady state response
- Wide temperature range
- Simple "in-situ" recalibration
- No excitation required

SPECIFICATIONS

Sample chamber volume range:
1 in³ to 3000 in³

Sensitivities:
to 15 milliwatts per millivolt

Temperature range:
Cryogenic to 600°F

Response times:
10 sec. to 10 min.

Vacuum:
to 10⁻⁶ torr.

Output impedance range:
10Ω to 7500Ω

Accuracies:
to 0.5%

Repeatability:
0.01%

Power supply:
not required

Materials:
Aluminum, stainless steels, copper, composites

CONSTRUCTION

The calorimeter walls are composed of a thin, high temperature thermopile structure containing thousands of junctions. One set of junctions is in thermal contact with one wall surface, and the other set is in contact with the opposite surface. As heat flows through the walls, (Fig. 1) a temperature difference is established between both sets of thermopile junctions, thus generating a voltage which is directly proportional to the heat flow. The large number of thermopiles develop extreme sensitivity to minute heat flows. Calorimeters are constructed in a range of designs incorporating large sample chambers for high heat fluxes (cover) or small sample chambers capable of measuring low heat releases (Figure 2).

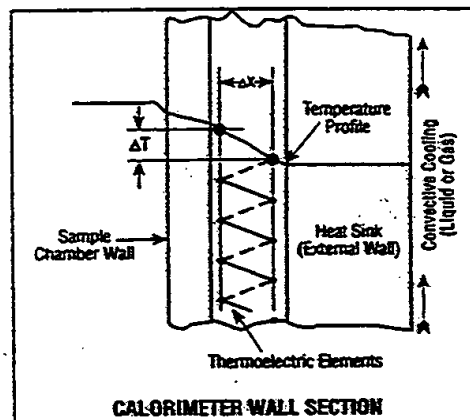


Figure 1

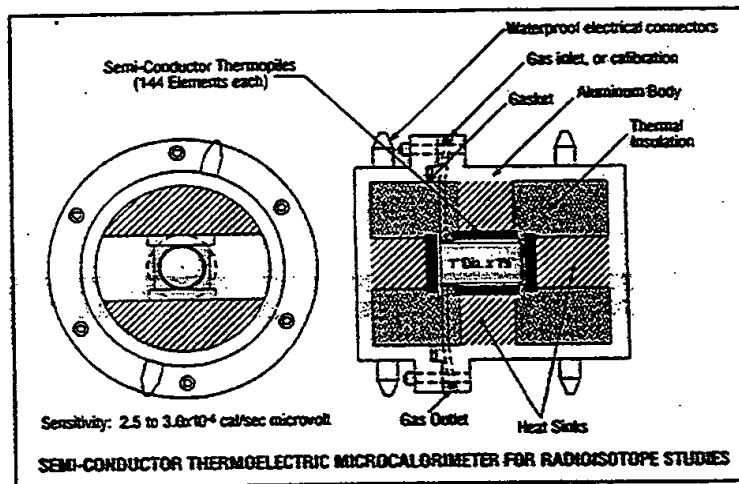


Figure 2

CALIBRATION

Each calorimeter is calibrated at a base temperature of 70° F by a known, electrical heat source in thermal equilibrium with the system.

The calibration constant is expressed in terms of wattage input versus millivolt output. A temperature correction curve is also supplied for use at elevated temperatures.

APPLICATIONS

The CR-100 Series calorimeters are designed to measure both microcaloric and macrocaloric heat release from pure or mixed radioisotopes. The magnitude of the generated signal is strictly proportional to the mean intensity of the sample.

Other applications include: physical, chemical and biological thermogenesis, specific heats, heats of fusion and reaction.

EXAMPLE OF OPERATION

Reactive materials are placed in a suitable container within the calorimeter sample chamber and permitted to reach equilibrium. To decrease the equilibrium time, it is desirable to heat sink the container to the sample chamber wall. The calorimeter should be situated in a constant temperature environment cooled either by gas or liquids. The time required for the calorimeter assembly to attain thermal equilibrium is a function of the conductivity and size of the sample, the thermal contact at the sample chamber wall, calorimeter wall characteristics, and the external cooling rate.

At thermal equilibrium, the output signal will reach a mean steady state value which is proportional to the total heat release from the sample. With the known calibration constant (milliwatts/millivolt), the total heat liberation rate is accurately determined. For radioisotopes with mean decay rates greater than calorimeter response time, the signal is proportional to radioisotope sample decay (Figure 3).

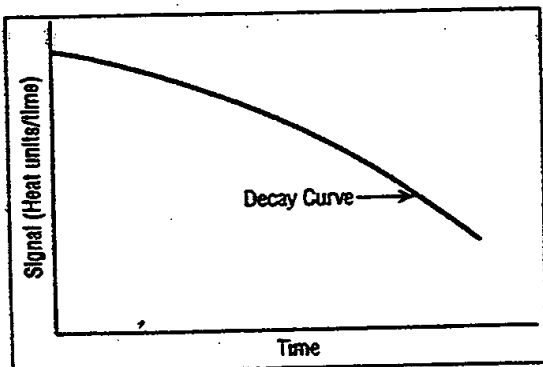


Figure 3

MICROWATT DETERMINATIONS

To measure microwatt heat flow accurately, it is necessary to provide a stable, cooling environment.

However, most constant temperature cooling baths exhibit small fluctuations which may generate signals the same order of magnitude as those produced by the sample. To avoid this large noise to signal ratio, a temperature compensated enclosure has been developed (Figure 4). This double

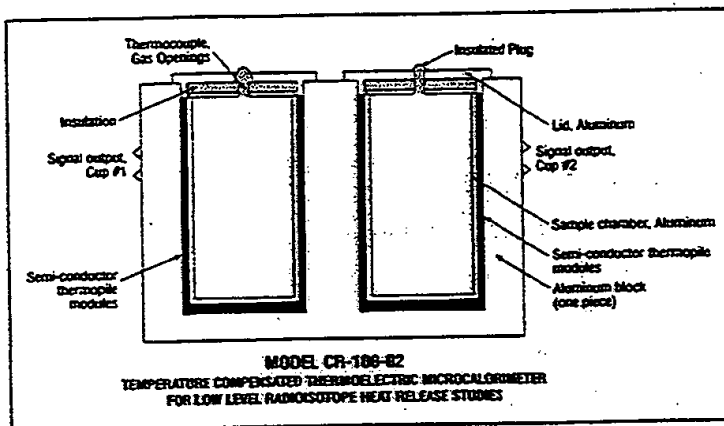


Figure 4

cup system contains both an active and passive chamber having matched sensitivities in opposition. Thus, spurious, external temperature fluctuations are compensated for, and only the heat release from the sample source is detected.

COMPENSATED MICROCALORIMETER SPECIFICATIONS

Sample chamber series:

1"-6" Dia. x 1"-12" Depth

Sensitivity:

10-15 milliwatts/millivolt

Materials:

Aluminum, composites, semi-conductor elements

Calibration:

1% Acc.

Sample chamber matching:

Within 1/2%

Internal resistance:

10-7500Ω

Readout required:

Millivolt potentiometer/Recorder

Environmental requirements:

Ambient temperature operation/Constant temperature bath

STANDARD MODELS, SINGLE CHAMBER

Model Number	Internal Dimensions		External Dimensions		Accuracy %	Sensitivity, Milliwatts per Millivolt	Nominal Output Resistance	Temperature F° (Note 1)	63% Response Time, Min.
	Diameter, In.	Depth, In.	Diameters, In.	Length, In.					
CA-100-1	1	1	3	3	1%	15	4	250*	1
CA-100-2	2	4	4	6	1%	15	10	250*	1
CA-100-4	4	8	5	12	1%	250	2000	600	3
CA-100-8	8	16, 32	9	21	1%	250	4000	600	3
CA-100-C	Custom	Custom	Custom	Custom	1%	250	Varies	600	Varies

* Models CR-100-1 and CA-100-2 are also available for 600°F operating temperature at reduced sensitivities.

READOUT INSTRUMENTATION

Suitable readouts for all CR-100 models include: millivolt potentiometers/recorders, data loggers, or conventional D.C. millivolt meters.

OTHER ITI THERMAL INSTRUMENTS

Thermal Conductivity Apparatus, Heat Flux Meters, HEAT-PROBE™, Accelerator target Calorimeters, Radiometers, Thermal Flux Standards.

ORDERING INFORMATION

Delivery6-8 weeks, ARO
 Shipping weight5 to 200 lbs
 Termsnet 30 days to established customers
 FOBDel Mar, California

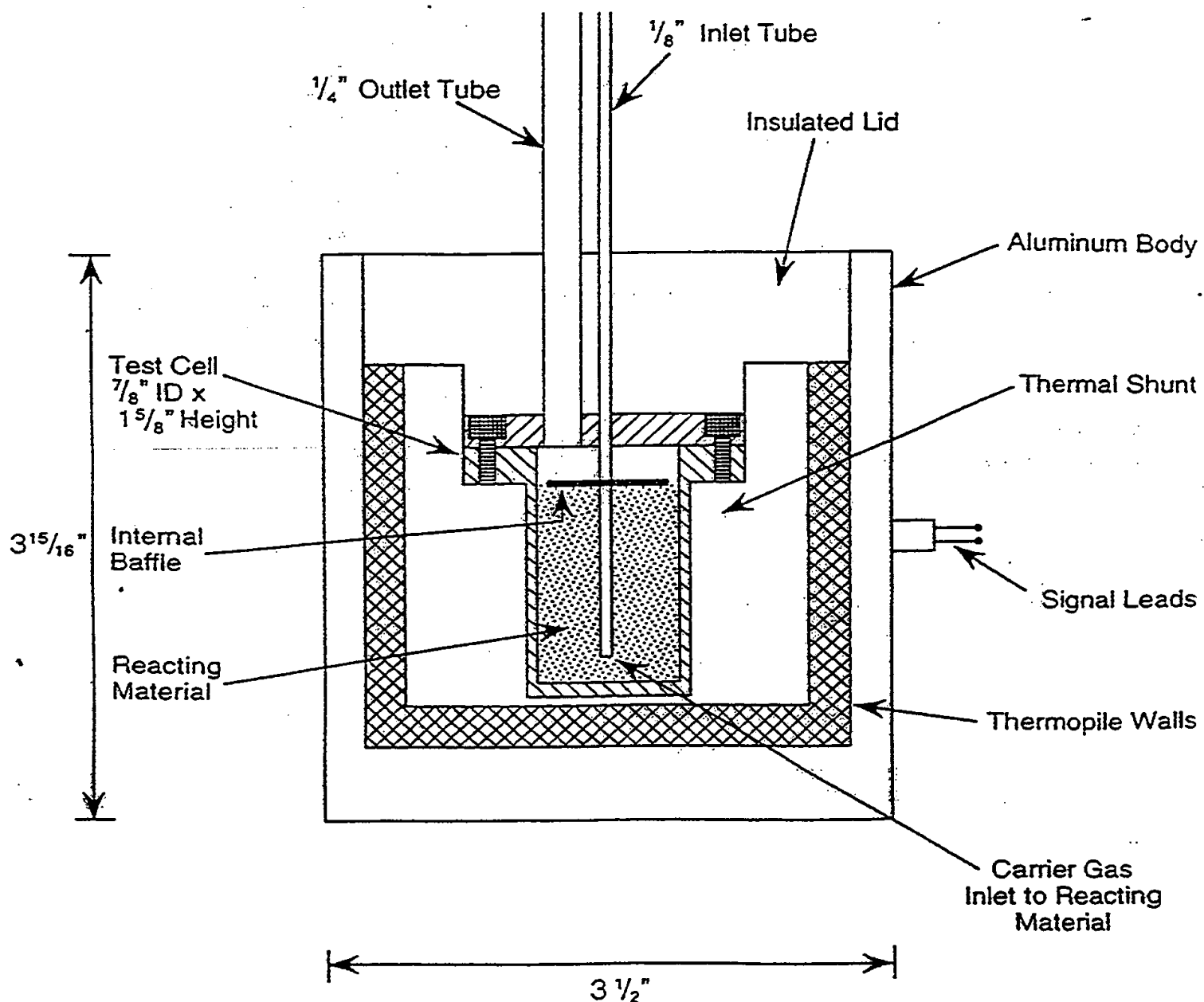
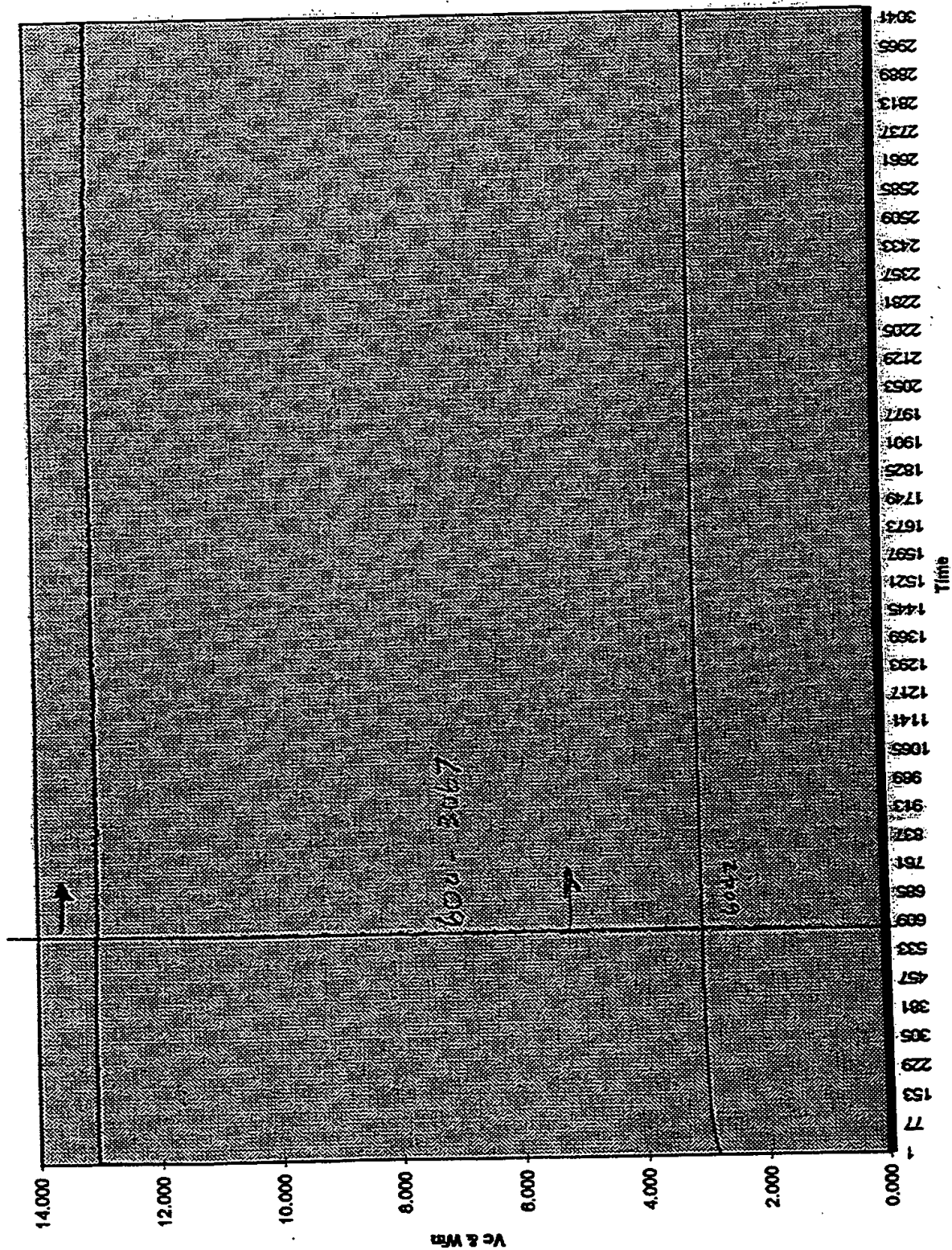


Figure 1. Scale Drawing of Calorimeter Assembly



Win	Predicted Vc	Given Vc	Estimated	Watts Out	Watts of power
0	-0.0605	3.076			
1	0.1728				
2	0.4061			13.444	watts of power
3	0.6394			13.04	watts of input power
4	0.8727			0.404	excess watts
5	1.106				
6	1.3393				
7	1.5726				
8	1.8059				
9	2.0392				
10	2.2725				
11	2.5058				
12	2.7391				
13	2.9724				
14	3.2057				
15	3.439				
16	3.6723				



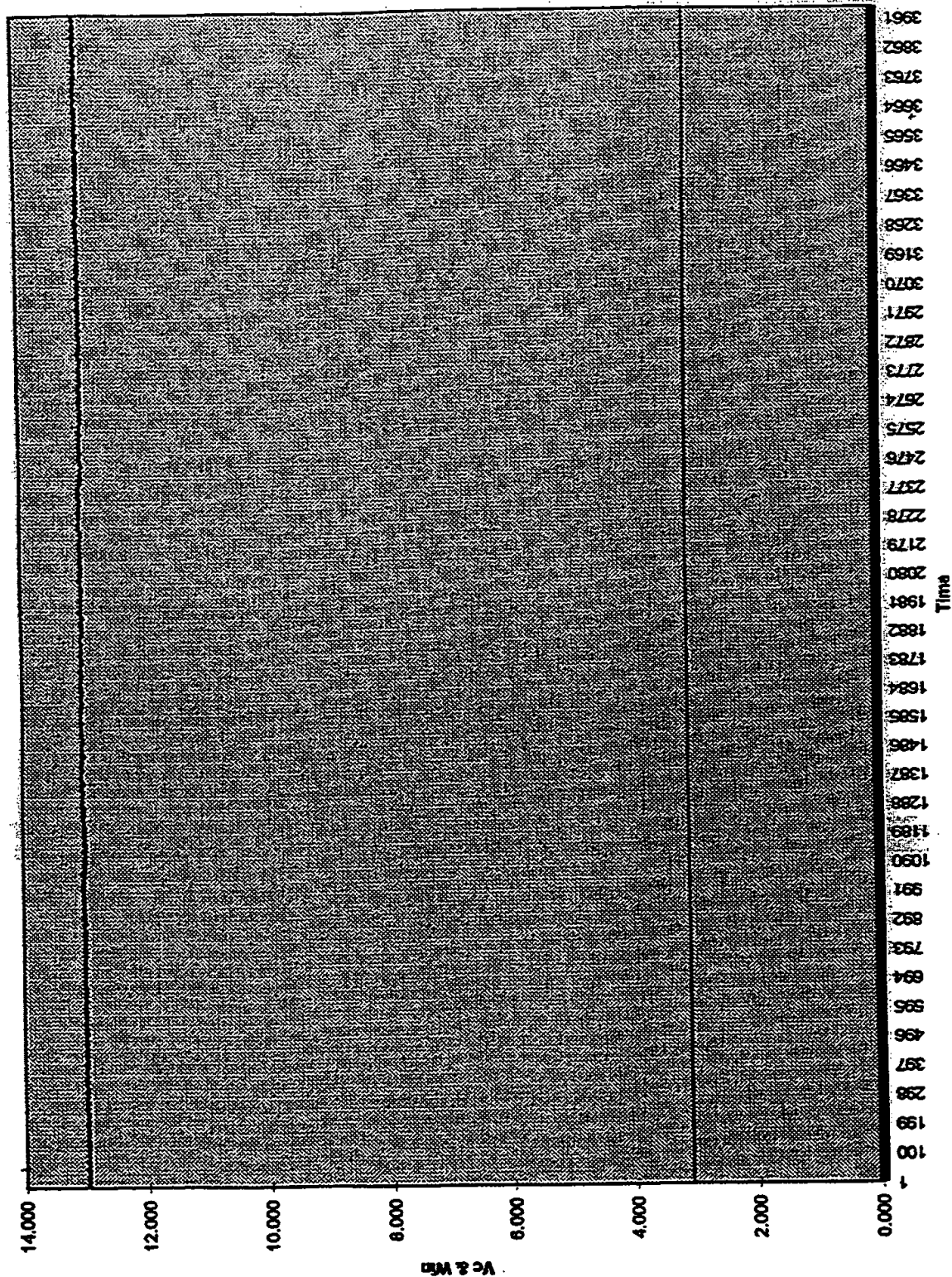
Win
Vo

30773

6.870 hr

Time [sec]	Vc	Vc'	x	Win	Vc	Statistics from 2 to 5280 [14,698 hrs]							
						Vc	Win	Average	Std Dev	Min	Max		
32	3.083	0.617	0.280	13.003	3.083			3.078	0.018	3.021	3.082		
42	3.083	0.617	0.280	12.996	3.083			13.007	0.034	12.777	13.077		
52	3.083	0.617	0.280	12.996	3.083								
62	3.083	0.617	0.280	12.996	3.083								
72	3.083	0.617	0.280	12.982	3.083								
82	3.083	0.617	0.280	13.015	3.083								
92	3.084	0.617	0.280	13.017	3.084								
102	3.084	0.617	0.259	12.973	3.084								
112	3.084	0.617	0.280	12.983	3.084								
122	3.084	0.617	0.280	12.979	3.084								
134	3.084	0.617	0.259	12.971	3.084								
143	3.083	0.617	0.280	13.015	3.083								
153	3.083	0.617	0.280	13.008	3.083								
163	3.083	0.617	0.280	13.013	3.083								
173	3.083	0.617	0.259	12.973	3.083								
183	3.083	0.617	0.280	12.984	3.083								
193	3.083	0.617	0.280	13.010	3.083								

Win	Predicted Vc	Given Vc=	
0	-0.0605	3.078	
1	0.1728	Estimated	
2	0.4061	Watts Out	13.453 watts of power
3	0.6394	Actual =	13.007 watts of input power
4	0.8727		0.446 excess watts
5	1.106		
6	1.3393		
7	1.5726		
8	1.8059		
9	2.0392		
10	2.2725		
11	2.5058		
12	2.7391		
13	2.9724		
14	3.2057		
15	3.439		
16	3.6723		



Time [sec]	Vc	Vc'	x	Win	Vc	Statistics from 130 to 400 [0.762 hrs]	Statistics from 890 to 1120 [1.198 hrs]	Statistics from 1550 to 1735 [0.616 hrs]	Statistics from 2 to 1735 [4.838 hrs]	Max
37	3.03	0.607	0.257	12.851	3.03	Average	Average	Average	Average	Max
47	3.03	0.607	0.258	12.921	3.03	Vc	Vc	Vc	Vc	2.844
57	3.03	0.606	0.258	12.882	3.03	Win	Win	Win	Win	12.932
67	3.028	0.606	0.258	12.893	3.028					
77	3.028	0.606	0.26	12.885	3.028					
87	3.028	0.606	0.26	13.006	3.028					
97	3.028	0.606	0.26	12.982	3.028					
107	3.028	0.606	0.26	12.99	3.028					
117	3.028	0.606	0.26	12.983	3.028	Vc	Vc	Vc	Vc	3.113
127	3.028	0.606	0.259	12.958	3.028	Win	Win	Win	Win	13.188
137	3.028	0.606	0.259	12.928	3.028					
147	3.03	0.607	0.258	12.88	3.03					
157	3.03	0.606	0.257	12.855	3.03					
168	3.028	0.606	0.259	12.934	3.028					
178	3.028	0.606	0.259	12.983	3.028	Vc	Vc	Vc	Vc	3.075
188	3.028	0.606	0.259	12.972	3.028	Win	Win	Win	Win	13.087
198	3.028	0.606	0.258	12.884	3.028					
208	3.028	0.606	0.259	12.925	3.028					
218	3.028	0.606	0.259	12.938	3.028					
228	3.028	0.606	0.259	12.984	3.028	Vc	Vc	Vc	Vc	
238	3.028	0.606	0.258	12.912	3.028	Win	Win	Win	Win	
248	3.028	0.606	0.259	12.992	3.028					
258	3.028	0.606	0.26	12.991	3.028					
268	3.028	0.606	0.26	12.975	3.028					

	Win	Predicted Vc								
	0	-0.0605	Given Vc =	3.016						
	1	0.1728	Estimated							
	2	0.4061	Watts Out	13.187	watts of power					
	3	0.6394	Actual =	13.015	watts of input power					
	4	0.8727		0.172	excess watts					
	5	1.106								
	6	1.3393								
	7	1.5726								
	8	1.8059								
	9	2.0392								
	10	2.2725								
	11	2.5058								
	12	2.7391								
	13	2.9724								
	14	3.2057								
	15	3.439								
	16	3.6723								

Time [sec]	Vc	Vc'	x	Win	Vc	Statistics from 130 to 400 [0.752 hrs]					
37	3.030	0.607	0.257	12.851	3.030	Average	Std Dev	Min	Max		
47	3.030	0.607	0.258	12.921	3.030	Vc	2.802	0.011	2.792	2.844	
57	3.030	0.608	0.258	12.882	3.030	Win	12.779	0.097	12.601	12.932	
67	3.029	0.608	0.258	12.893	3.029						
77	3.029	0.608	0.260	12.985	3.029						
87	3.029	0.608	0.260	13.008	3.029						
97	3.029	0.608	0.260	12.992	3.029	Statistics from 690 to 1120 [1.198 hrs]					
107	3.029	0.608	0.260	12.990	3.029	Average	Std Dev	Min	Max		
117	3.029	0.608	0.260	12.983	3.029	Vc	3.100	0.012	3.087	3.113	
127	3.029	0.608	0.259	12.958	3.029	Win	13.151	0.021	13.091	13.188	
137	3.029	0.608	0.259	12.928	3.029						
147	3.030	0.607	0.258	12.880	3.030						
157	3.030	0.608	0.257	12.855	3.030	Statistics from 1650 to 1735 [0.616 hrs]					
168	3.029	0.608	0.259	12.934	3.029	Average	Std Dev	Min	Max		
178	3.029	0.608	0.259	12.983	3.029	Vc	3.073	0.001	3.071	3.075	
188	3.029	0.608	0.259	12.972	3.029	Win	13.020	0.052	12.380	13.087	
198	3.029	0.608	0.258	12.984	3.029						
208	3.029	0.608	0.259	12.926	3.029						

March 5 - March 10, 1997

Win	Predicted Vc	Given Vc	
0	-0.0605	2.802	
1	0.1728	Estimated	
2	0.4061	Watts Out	12.270 watts of power
3	0.6394	Actual =	12.779 watts of input power
4	0.8727		-0.509 excess watts
5	1.106		
6	1.3393		
7	1.5726		
8	1.8059		
9	2.0392		
10	2.2725		
11	2.5058		
12	2.7391		
13	2.9724		
14	3.2057		
15	3.439		
16	3.6723		

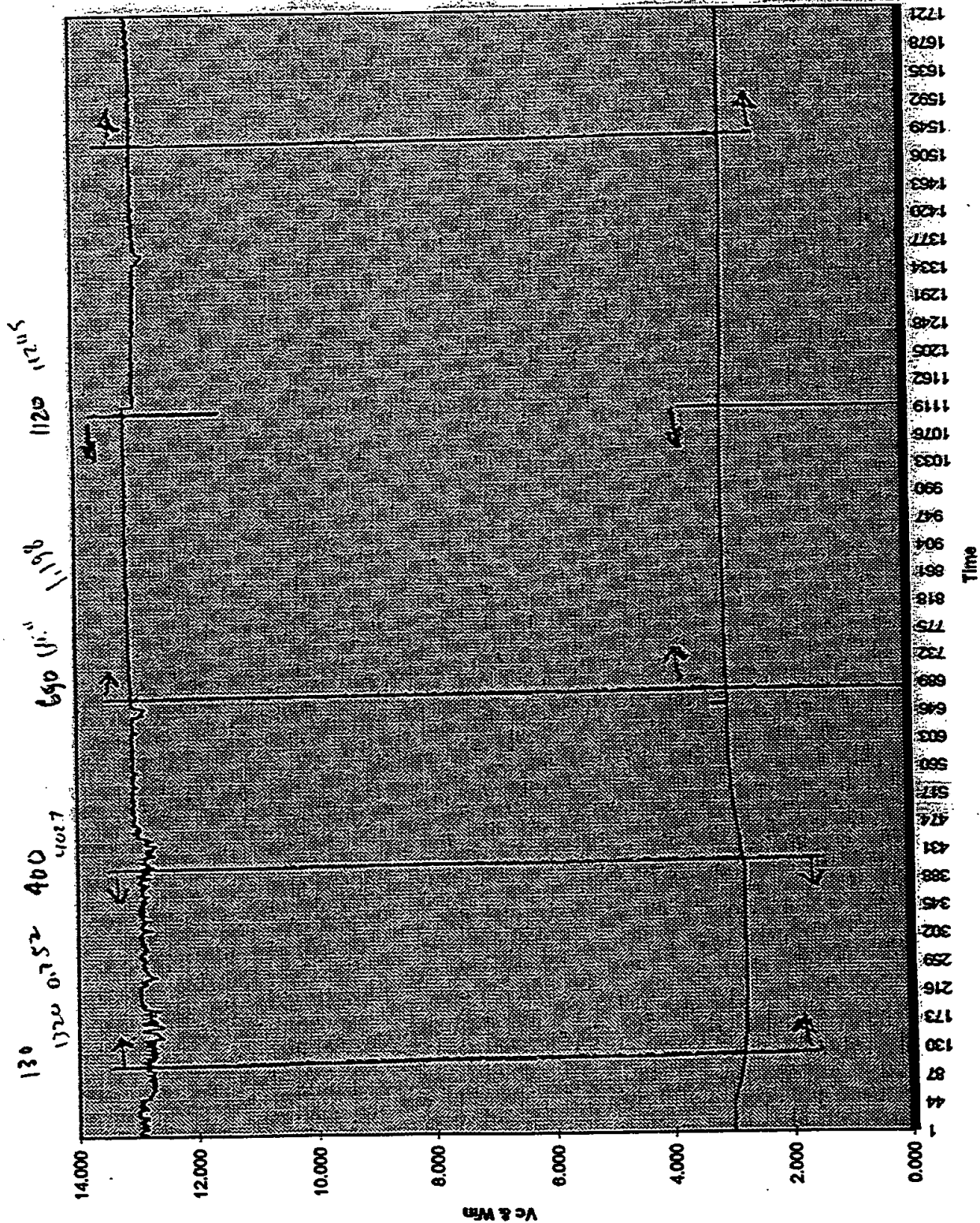
March 5 - March 10, 1997

Win	Predicted Vc	Given Vc=					
0	-0.0605	3.1					
1	0.1728	Estimated					
2	0.4061	Watts Out	13.547	watts of power			
3	0.6394	Actual =	13.151	watts of input power			
4	0.8727		0.396	excess watts			
5	1.106						
6	1.3393						
7	1.5726						
8	1.8059						
9	2.0392						
10	2.2725						
11	2.5058						
12	2.7391						
13	2.9724						
14	3.2057						
15	3.439						
16	3.6723						

March 5 - March 10, 1997

Win	Predicted Vc	Given Vc	
0	-0.0605	3.073	
1	0.1728	Estimated	
2	0.4061	Watts Out	13.432 watts of power
3	0.6394	Actual =	13.020 watts of input power
4	0.8727		0.412 excess watts
5	1.106		
6	1.3393		
7	1.5726		
8	1.8059		
9	2.0392		
10	2.2725		
11	2.5058		
12	2.7391		
13	2.9724		
14	3.2057		
15	3.439		
16	3.6723		

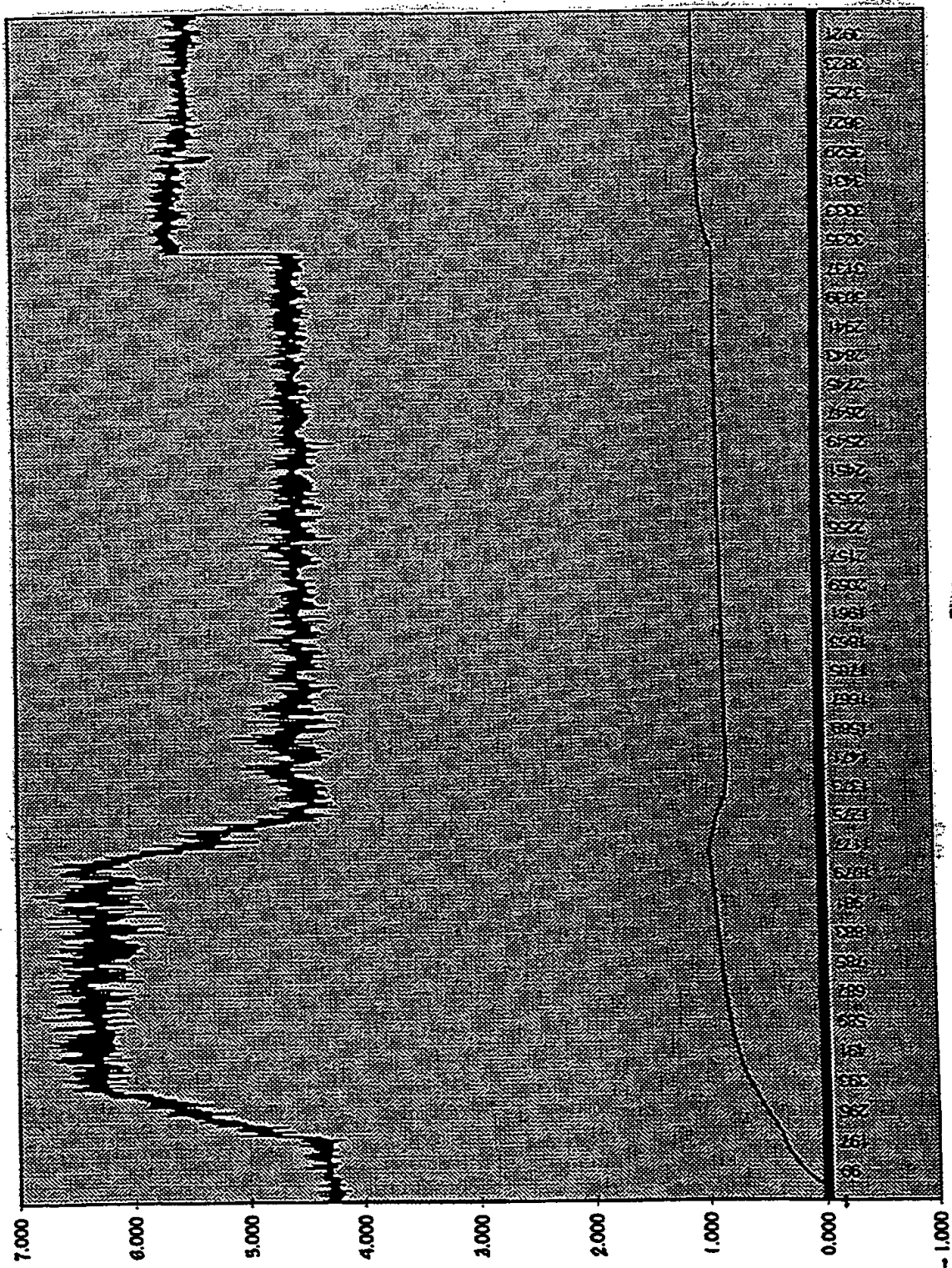
TP032197 Chart 1



TP032697

Time [sec]	Vc		Vc'	x	Win	Vc		Statistics from 6000-8700 [7.516 hrs]					Min	Max
	Vc					Win		Vc	Win	Average	Std Dev			
69	0.000	0.000	0.000	0.058	2.923	0.000	0.000			1.102	0.004		1.089	1.121
79	0.000	0.000	0.000	0.001	0.034	0.000	0.000							
89	0.000	0.000	0.000	0.024	1.190	0.000	0.000			5.791	0.122		5.272	7.004
99	0.000	0.000	0.000	0.082	4.082	0.000	0.000							
110	0.000	0.000	0.000	0.087	4.372	0.000	0.000							
120	0.000	0.000	0.000	0.086	4.276	0.000	0.000							
130	0.000	0.000	0.000	0.085	4.244	0.000	0.000							
140	0.000	0.000	0.000	0.085	4.247	0.000	0.000							
150	0.000	0.000	0.000	0.085	4.272	0.000	0.000							
160	0.000	0.000	0.000	0.085	4.258	0.000	0.000							
170	0.000	0.000	0.000	0.085	4.232	0.000	0.000							
180	0.000	0.000	0.000	0.085	4.252	0.000	0.000							
190	0.000	0.000	0.000	0.086	4.325	0.000	0.000							
200	0.000	0.000	0.000	0.086	4.318	0.000	0.000							
210	0.000	0.000	0.000	0.086	4.280	0.000	0.000							

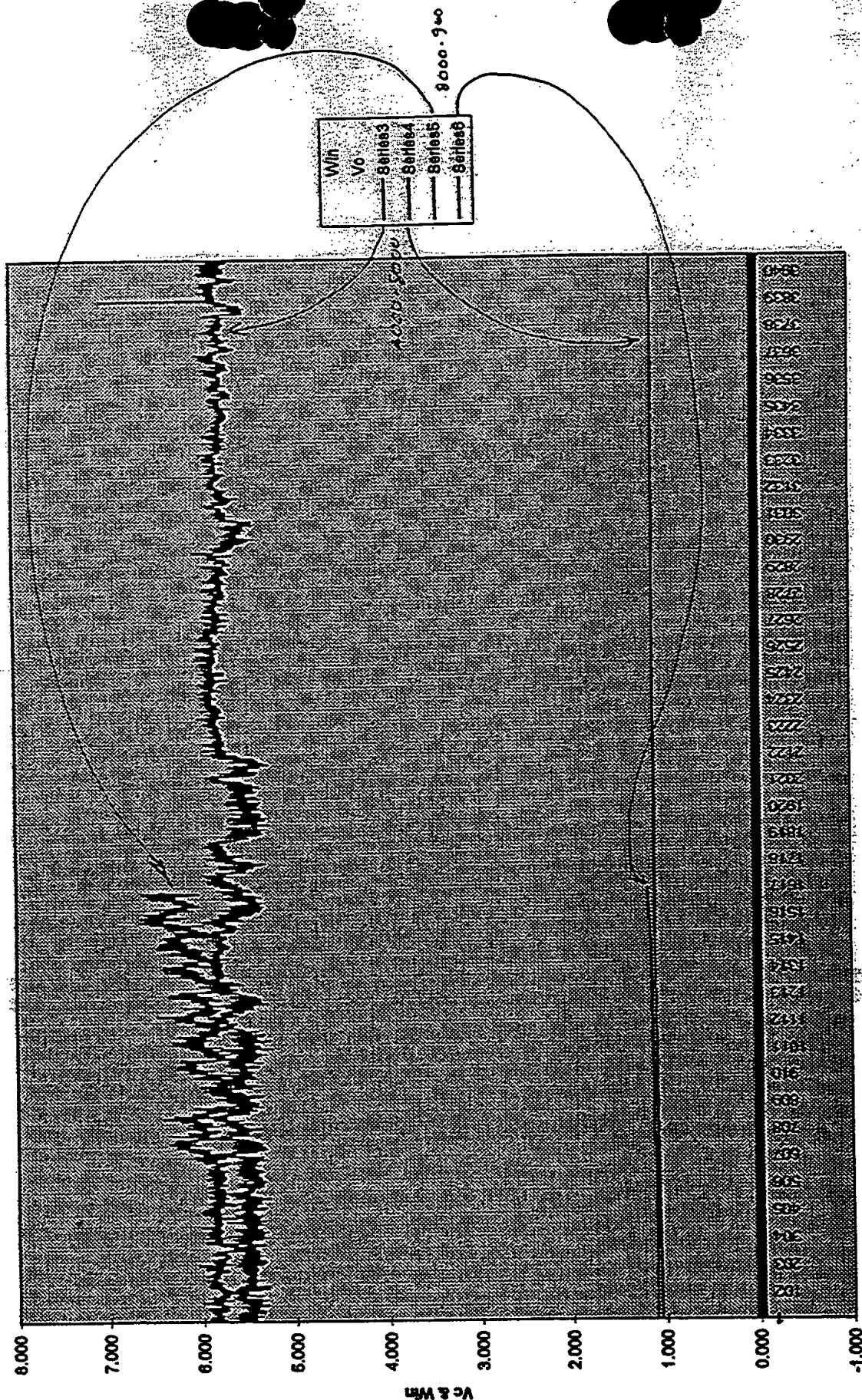
No Hydrogen



Win
Vo

FROM 1-4000

TP032697 Chart 1



30 Centimeter Calibration Run

GRAPHING of 30 CM Control Experimental Points								
Vc	Win	Vc-SD	Win-SD	Date	%-Vc-SD	%-Win-SD	Hours	
3.951	14.943	0.004	0.013	29-Apr	0.10%	0.09%	2.539	
3.951	14.940	0.001	0.010	30-Apr	0.03%	0.07%	1.676	
4.221	16.123	0.001	0.008	30-Apr	0.02%	0.05%	0.590	
4.663	18.041	0.002	0.007	30-Apr	0.04%	0.04%	0.808	

TP042997

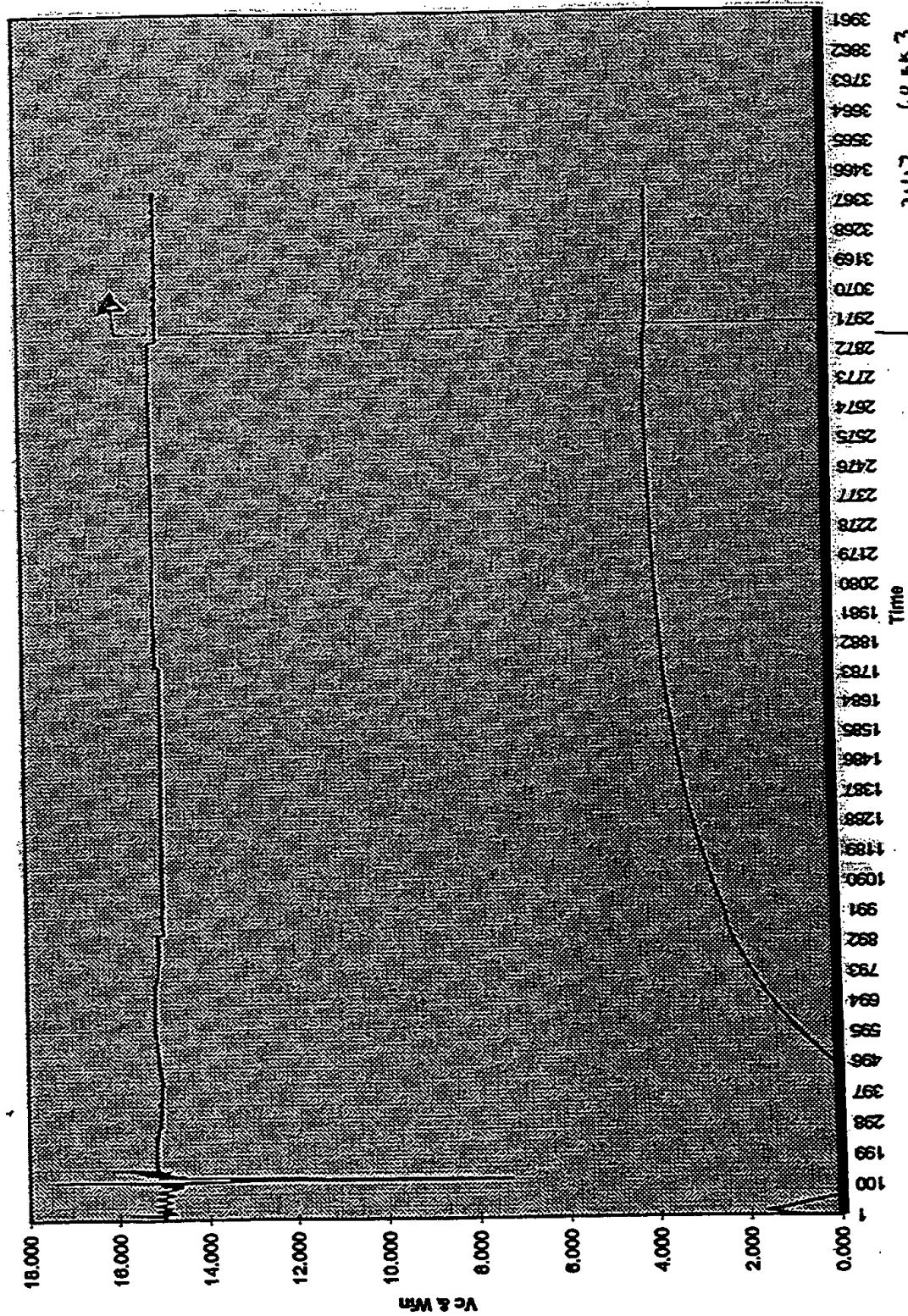
Statistics for 2991 - 3417 (2.632 hrs)									
Win	P[H]	P[L]	x	Win	Vc	Average	Std. Dev	Vc	Win
15.044	0.549	0.179	0.00	15.044	0.836	3.951	0.004	0.004	
14.983	0.548	0.176	0.00	14.983	0.908	14.943	0.013		
14.999	0.538	0.170	0.00	14.999	0.971				
15.019	0.536	0.168	0.00	15.019	1.029				
15.003	0.529	0.166	0.01	15.003	1.084				
14.957	0.529	0.166	0.03	14.957	1.139				
14.977	0.531	0.164	0.04	14.977	1.190				
14.997	0.530	0.165	0.08	14.997	1.241				
14.971	0.528	0.164	0.09	14.971	1.294				
14.972	0.554	0.168	0.11	14.972	1.343				
15.041	0.517	0.160	0.14	15.041	1.388				
14.980	0.536	0.168	0.17	14.980	1.431				
14.969	0.535	0.164	0.21	14.969	1.476				
14.980	0.542	0.165	0.24	14.980	1.514				
15.002	0.533	0.164	0.27	15.002	1.548				

30 cm Control

$V_c = 3.951$

$W_{in} = 14.943$

Plot of V_c & W_{in} vs. Time



3417 - 68553
2961
59411
2.539

TP043087

Time [sec]	Vc	Vc'	Win	P[H]	P[L]	Vfil	Win	Vc	Statistics from Points		
									Average	Std Dev	
60	3.949	0.780	14.930	0.375	0.151	2.358	14.930	3.949	3.951	0.001292	
80	3.950	0.780	14.932	0.375	0.158	2.352	14.932	3.950	14.940	0.010438	
100	3.950	0.780	14.958	0.354	0.147	2.352	14.958	3.950			
120	3.950	0.780	14.952	0.355	0.152	2.352	14.952	3.950			
141	3.951	0.780	14.948	0.362	0.152	2.353	14.948	3.951			
160	3.951	0.780	14.930	0.398	0.169	2.353	14.930	3.951			
180	3.951	0.780	14.914	0.416	0.185	2.353	14.914	3.951			
200	3.951	0.780	14.913	0.415	0.184	2.353	14.913	3.951			
220	3.951	0.780	14.934	0.374	0.167	2.362	14.934	3.951			
240	3.951	0.780	14.938	0.368	0.150	2.353	14.938	3.951			
260	3.951	0.780	14.932	0.343	0.149	2.353	14.932	3.951			
280	3.951	0.780	14.935	0.361	0.148	2.353	14.935	3.951			
300	3.951	0.780	14.934	0.369	0.166	2.353	14.934	3.951			
320	3.951	0.780	14.921	0.317	0.141	2.353	14.921	3.951			
341	3.951	0.791	14.927	0.388	0.162	2.353	14.927	3.951			

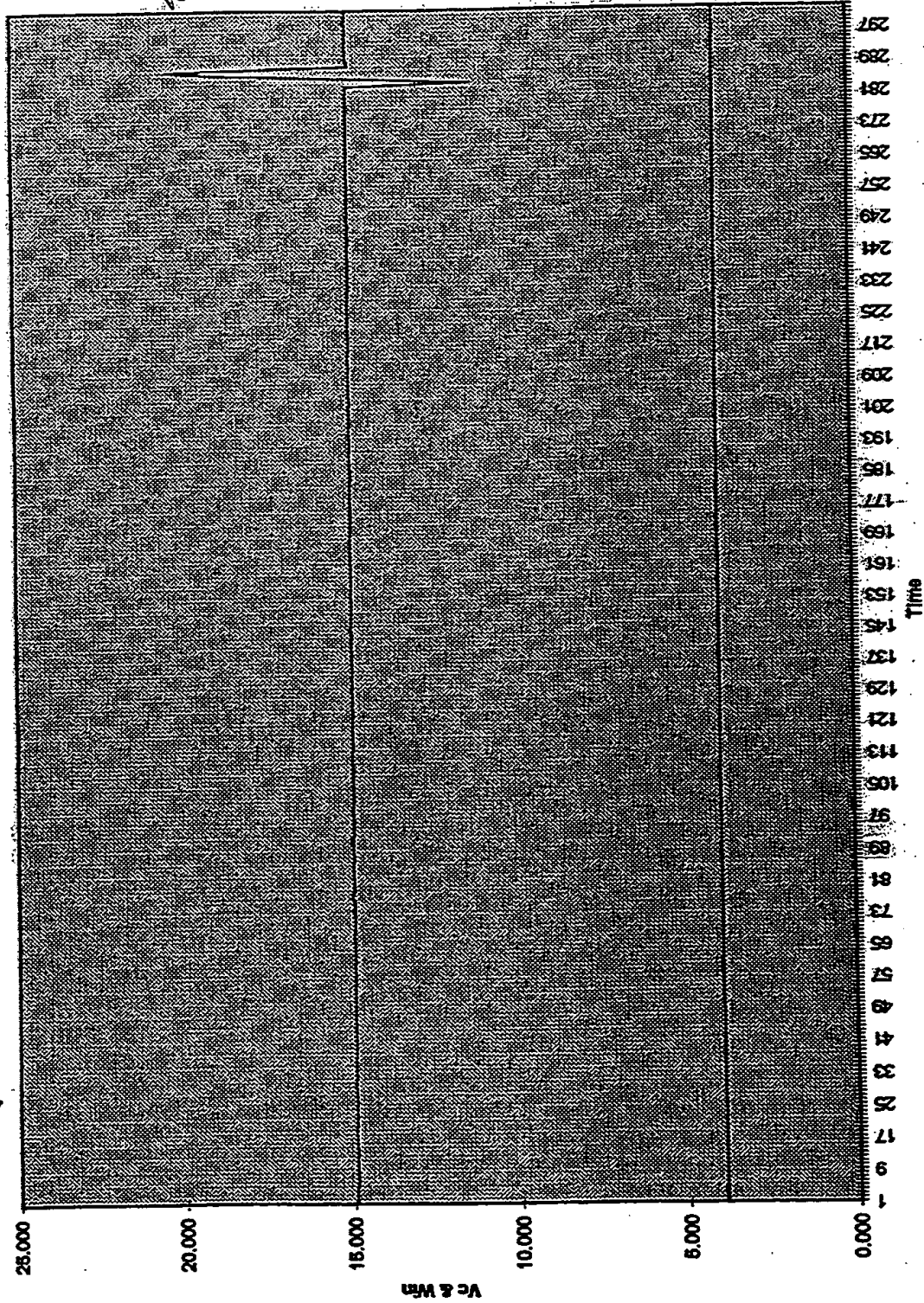
30 cm control

$V_c = 3.951$

$W_{in} = 14.940$

TP043097 Chart 1

April 30, 1997 - 1.7 hours



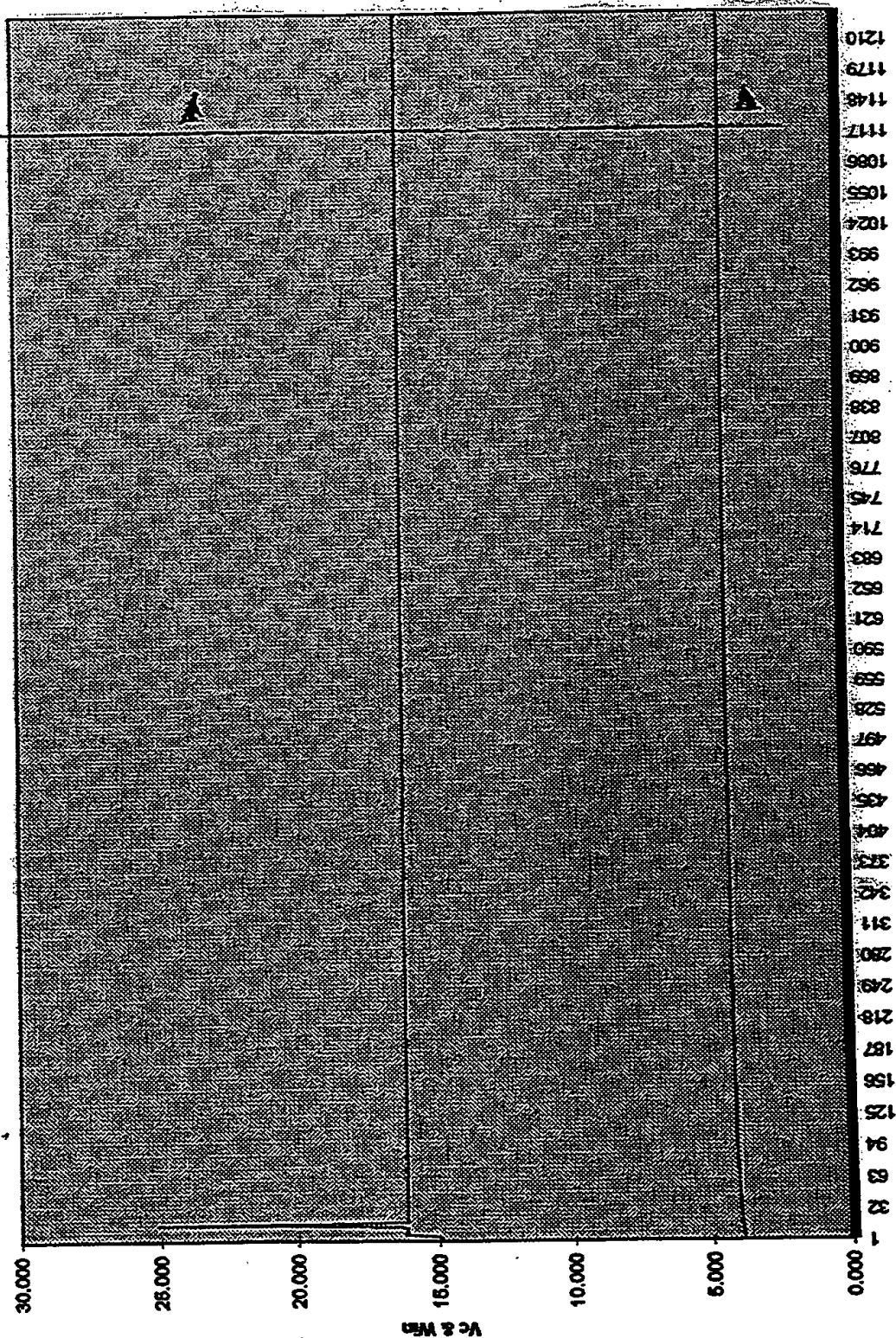
Time [sec]	Vc	Vc'	Win	P[H]	P[L]	Vll	Win	Vc	Statistics from Points 1133 to 1239 (0.500 hrs)		
									Average	8td Dev	
123	3.948	0.790	14.934	0.375	0.154	2.361	14.934	3.948	4.221	0.001	
143	3.948	0.790	14.931	0.379	0.157	2.350	14.931	3.948			
163	3.948	0.790	14.949	0.376	0.156	2.350	14.949	3.948	16.123	0.008	
183	3.948	0.790	14.952	0.382	0.149	2.350	14.952	3.948			
203	3.948	0.790	14.942	0.375	0.153	2.350	14.942	3.948			
223	3.948	0.790	15.487	0.376	0.153	2.350	15.487	3.948			
243	3.950	0.790	16.131	0.385	0.152	2.351	16.131	3.950			
263	3.955	0.791	16.147	0.381	0.154	2.355	16.147	3.955			
283	3.982	0.793	16.159	0.399	0.158	2.362	16.159	3.982			
303	3.989	0.794	16.170	0.378	0.152	2.367	16.170	3.989			
323	3.975	0.795	16.163	0.387	0.154	2.373	16.163	3.975			
343	3.981	0.796	16.145	0.381	0.155	2.378	16.145	3.981			
363	3.986	0.797	16.154	0.393	0.153	2.382	16.154	3.986			
383	3.991	0.798	16.151	0.376	0.152	2.386	16.151	3.991			
404	3.996	0.799	16.421	0.381	0.152	2.390	16.421	3.996			
424	4.000	0.800	20.443	0.388	0.155	2.394	20.443	4.000			
444	4.004	0.801	25.080	0.373	0.152	2.398	25.080	4.004			
464	4.009	0.802	19.705	0.377	0.152	2.401	19.705	4.009			
484	4.012	0.803	16.115	0.379	0.152	2.405	16.115	4.012			

30 cm Control

 $V_c = 4.221$ $W_{in} = 16.123$

April 30, 1997 - 16 watt point

1133 - 1239

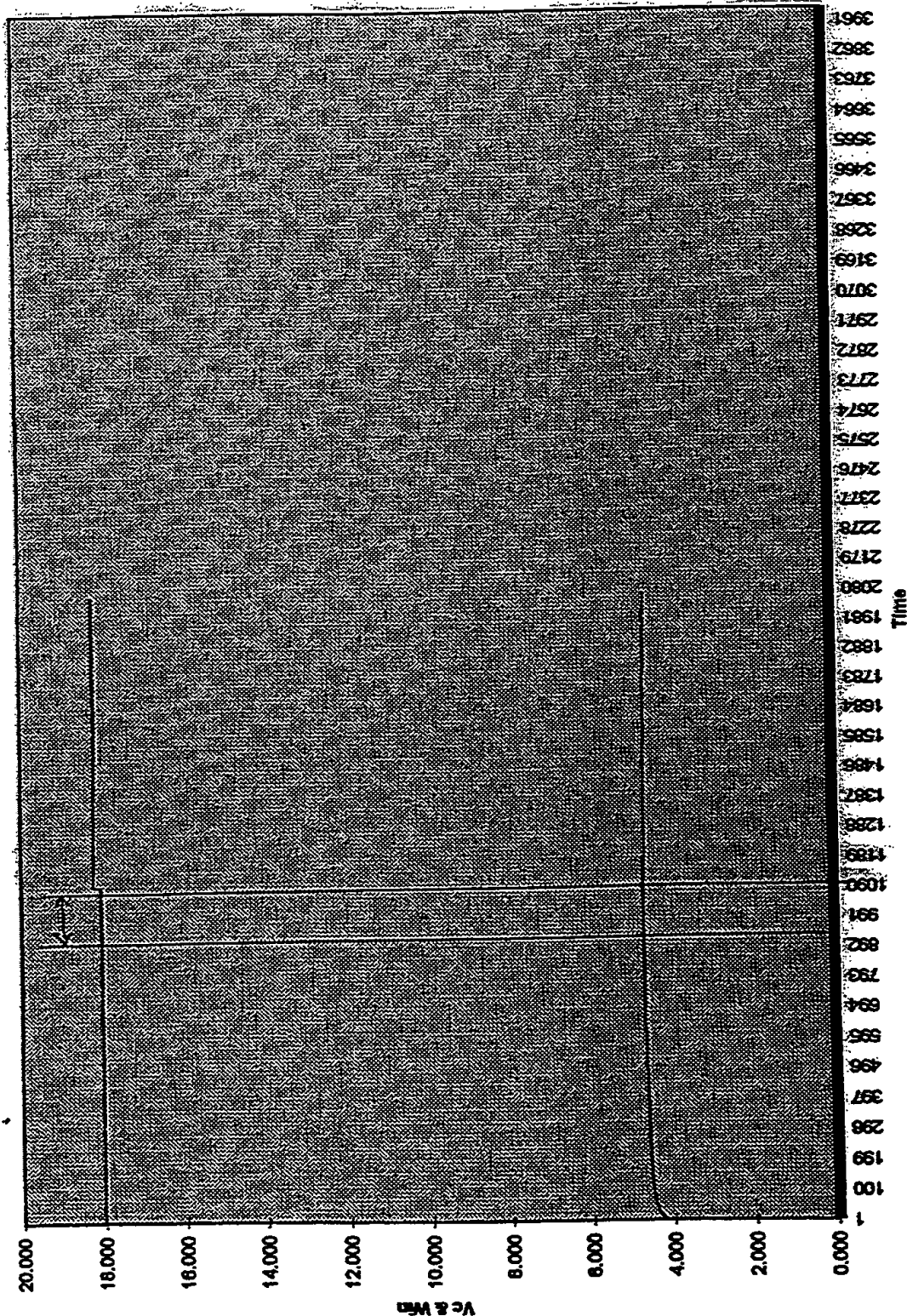


Time [sec]	Vc	Vc'	Win	P[H]	P[L]	Vfil	Win	Vc	Statistics from Points 986 - 1100 [0.808 hrs]		
									Average	Std Dev	
54	4.222	0.845	16.128	0.439	0.154	2.587	16.129	4.222	4.663	0.002	
74	4.222	0.845	17.170	0.394	0.143	2.588	17.170	4.222	18.041	0.007	
108	4.224	0.845	18.035	0.418	0.148	2.588	18.035	4.224			
114	4.233	0.847	18.040	0.435	0.151	2.598	18.040	4.233			
134	4.245	0.849	18.045	0.437	0.153	2.605	18.045	4.245			
154	4.256	0.851	18.038	0.389	0.143	2.615	18.038	4.256			
174	4.265	0.853	18.031	0.417	0.149	2.623	18.031	4.265			
195	4.274	0.855	18.022	0.415	0.149	2.630	18.022	4.274			
215	4.281	0.856	18.028	0.420	0.149	2.637	18.028	4.281			
235	4.288	0.858	18.036	0.424	0.151	2.643	18.036	4.288			
255	4.295	0.859	18.036	0.409	0.146	2.649	18.036	4.295			
275	4.301	0.860	18.023	0.419	0.149	2.654	18.023	4.301			
295	4.308	0.862	18.019	0.416	0.151	2.659	18.019	4.308			
315	4.314	0.863	18.025	0.418	0.150	2.665	18.025	4.314			
335	4.319	0.864	18.033	0.405	0.148	2.670	18.033	4.319			
355	4.325	0.865	18.039	0.423	0.152	2.674	18.039	4.325			
375	4.331	0.866	18.041	0.408	0.148	2.679	18.041	4.331			

30 cm Control

 $V_c = 4.663$ $W_{in} = 18.041$

April 30, 1997 18 watt point



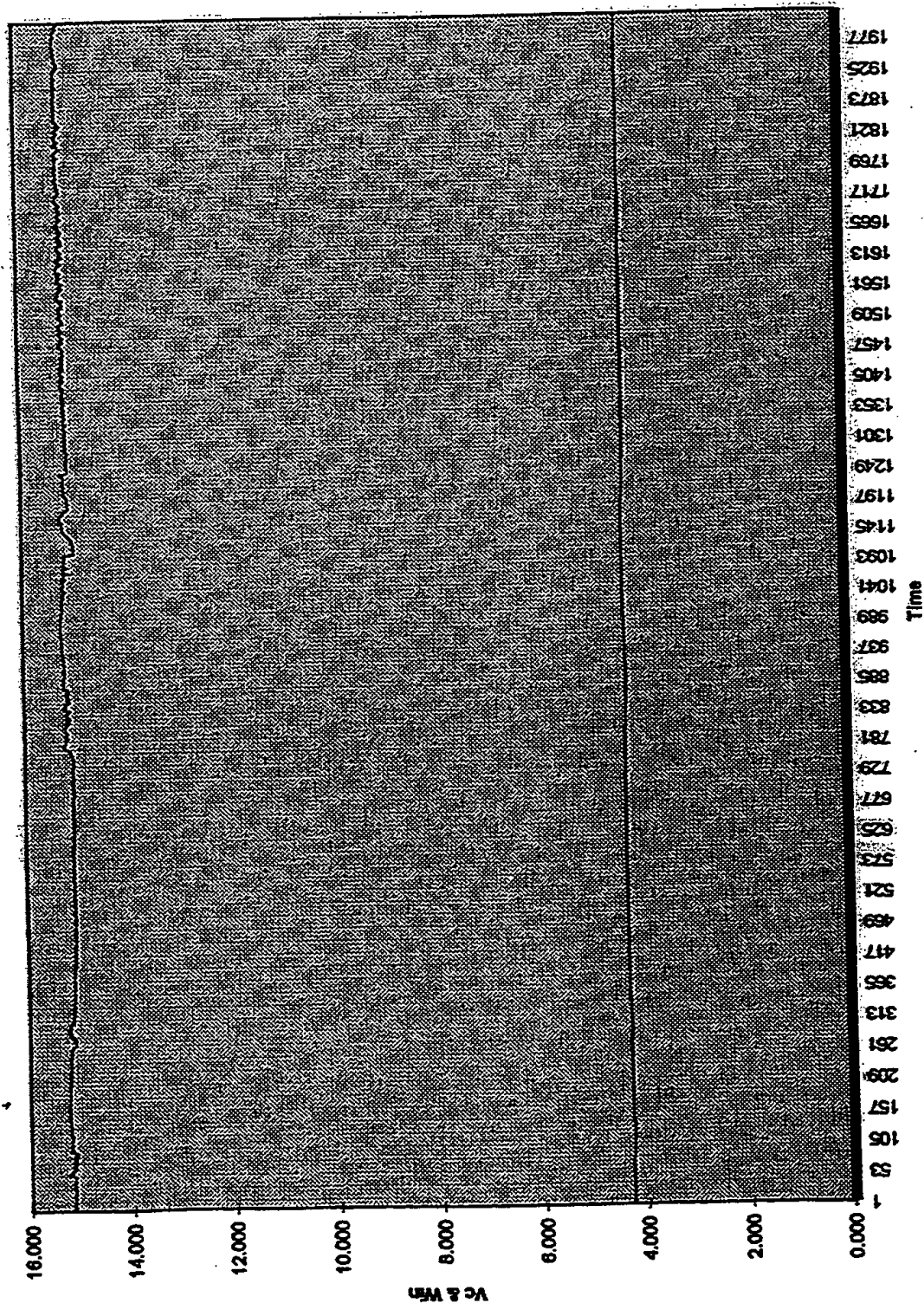
Summary of Exo. Power Produced

Summary of 30 cm Experimental Results								
Date(s) of Run	Hours Issl	Excess Power (watts)	Pressure	Additional H ₂ O				
14-Apr	6.632	1.181	132.8-176.2T	No				
15-Apr	15.160	1.459	0.38-5.49T	Yes				
16-Apr	12.080	1.689	0.388-0.691T	Yes				
17-Apr	21.273	1.335	0.386-0.693T	Yes				
18-Apr	6.916	0.635	0.349-0.676T	Yes				
23-Apr	11.572	1.954	0.428-0.692T	No				
24-Apr	23.461	2.092	0.352-0.692T	No				
25-Apr	13.507	2.067	< 1.312T	No				
3-May	6.237	1.264	0.335-0.443T	No				
4-May	11.355	1.135	0.453-0.679T	Yes				
5-May	4.777	1.079	0.447-0.696T	Yes				
					Average of Points			
					1.445			
					0.635	Minimum		
					2.092	Maximum		
					0.461	Std. Deviation		
					31.91%	Std. Deviation %		

Time [sec]	Vc	Vc'	Win	p[H]	p[L]	Vf	Win	Vc	Statistics for 8011 - 8033 [5.632 hrs]				Max
									Vc	Average	Std Dev	Mln	
86	0.000	0.000	0.674	1.007	0.125	0.008	0.674	0.000					
96	0.000	0.000	2.634	0.997	0.128	0.000	2.634	0.000		4.268	0.015	4.240	4.294
106	0.000	0.000	0.150	1.035	0.124	0.000	0.150	0.000	Vc	15.141	0.081	14.970	15.268
116	0.000	0.000	0.070	1.037	0.125	0.000	0.070	0.000	Win				
126	0.000	0.000	0.068	1.020	0.128	0.000	0.068	0.000					
137	0.000	0.000	1.083	1.045	0.125	0.000	1.083	0.000					
146	0.000	0.000	11.892	1.068	0.125	0.000	11.892	0.000					
156	0.000	0.000	14.905	1.085	0.128	0.000	14.905	0.000					
167	0.000	0.000	15.142	1.287	0.124	0.000	15.142	0.000					
177	0.004	0.001	15.016	1.481	0.115	0.000	15.016	0.004					
187	0.041	0.008	14.941	1.568	0.127	0.000	14.941	0.041					
197	0.087	0.017	14.970	1.730	0.118	0.000	14.970	0.087					
207	0.133	0.027	14.995	1.739	0.125	0.000	14.995	0.133					
217	0.177	0.035	14.998	1.849	0.123	0.000	14.998	0.177					
227	0.219	0.044	14.987	1.899	0.124	0.000	14.987	0.219					
237	0.258	0.052	14.991	1.944	0.122	0.000	14.991	0.258					
247	0.295	0.059	14.992	2.007	0.121	0.000	14.992	0.295					
257	0.331	0.068	14.993	2.015	0.126	0.000	14.993	0.331					
267	0.365	0.073	15.007	2.087	0.122	0.000	15.007	0.365					
277	0.398	0.080	15.003	2.089	0.124	0.000	15.003	0.398					
287	0.430	0.086	15.003	2.162	0.122	0.000	15.003	0.430					
297	0.461	0.092	15.002	2.158	0.125	0.000	15.002	0.461					
307	0.491	0.098	15.012	2.179	0.124	0.000	15.012	0.491					
317	0.521	0.104	15.007	2.230	0.122	0.000	15.007	0.521					
327	0.560	0.110	14.998	2.244	0.124	0.000	14.998	0.560					

[illegible]

April 14, 1997 - 16 watt warmup



Series1
Series2

PH 132.5 - 601
PH 178.2T

TP041597

Time [sec]	Vc	Vc'	Win	p[H]	p[L]	Vf	Win	Vc	Statistics for 2 - 5445 [15:160hrs]					Max
									Vc	Win	Average	Std Dev	MIn	
82	4.292	0.859	15.242	243.980	99.976	2.658	15.242	4.292			4.331	0.023	4.283	4.380
92	4.292	0.859	15.244	243.980	99.976	2.646	15.244	4.292						
102	4.292	0.859	15.239	244.000	99.976	2.646	15.239	4.292			15.137	0.083	14.954	15.269
112	4.291	0.859	15.248	244.000	99.976	2.645	15.248	4.291						
122	4.291	0.859	15.251	244.040	99.976	2.645	15.251	4.291			12.44		0.360	549.01
132	4.291	0.859	15.256	244.030	99.976	2.645	15.256	4.291						
142	4.290	0.859	15.249	244.040	99.976	2.645	15.249	4.290						
153	4.290	0.859	15.256	244.070	99.976	2.645	15.256	4.290						
162	4.290	0.859	15.264	244.090	99.976	2.645	15.264	4.290						
172	4.290	0.859	15.257	244.110	99.976	2.645	15.257	4.290						
182	4.290	0.859	15.256	244.130	99.976	2.644	15.255	4.290						
192	4.290	0.859	15.255	244.170	99.976	2.645	15.255	4.290						
202	4.290	0.859	15.248	244.190	99.976	2.645	15.248	4.290						
212	4.290	0.859	15.251	244.220	99.976	2.645	15.251	4.290						
223	4.290	0.859	15.250	244.270	99.976	2.645	15.250	4.290						
233	4.290	0.859	15.252	244.310	99.976	2.644	15.252	4.290						

[illegible]

Time [sec]	Vc	Vc'	Win	p[H]	p[L]	Vf	Win	Vc	Statistics for 4192-8540 [12,060: hrs]					
									Vc	Win	Average	Std Dev	Min	Max
125	4.335	0.868	15.176	0.446	0.154	2.691	15.176	4.339						
135	4.335	0.868	15.179	0.445	0.154	2.680	15.179	4.339		Vc	5.075	0.027	5.040	5.135
145	4.335	0.868	15.184	0.437	0.156	2.679	15.184	4.339		Win	18.146	0.039	18.058	18.283
155	4.335	0.868	15.176	0.453	0.155	2.679	15.176	4.339						
165	4.335	0.868	15.173	0.463	0.153	2.679	15.173	4.339		p[H]	0.486	0.029	0.366	0.591
175	4.334	0.868	15.180	0.452	0.154	2.679	15.180	4.339						
185	4.334	0.868	15.176	0.434	0.156	2.679	15.176	4.338						
195	4.334	0.868	15.199	0.448	0.163	2.679	15.199	4.338						
205	4.334	0.868	15.198	0.450	0.150	2.678	15.198	4.338						
215	4.334	0.868	15.195	0.466	0.133	2.679	15.195	4.338						
225	4.334	0.868	15.200	0.495	0.133	2.679	15.200	4.338						
235	4.334	0.868	15.540	0.506	0.133	2.679	15.540	4.338						
245	4.334	0.868	17.450	0.542	0.134	2.679	17.450	4.339						
255	4.336	0.868	18.067	0.548	0.132	2.680	18.067	4.340						
265	4.340	0.869	18.145	0.558	0.138	2.683	18.145	4.344						
275	4.347	0.870	18.136	0.608	0.132	2.689	18.136	4.351						
285	4.355	0.872	18.130	0.697	0.130	2.697	18.130	4.359						
295	4.364	0.874	18.093	0.617	0.133	2.704	18.093	4.368						

Win	Predicted Vc	Given Vc=	5.075
14.5	3.849	Estimated	
15.0	3.964	Watts Out	19.835 watts of power
15.5	4.079	Actual =	18.146 watts of input power
16.0	4.194		1.689 excess watts
16.5	4.309		
17.0	4.424		
17.5	4.539		
18.0	4.653		
18.5	4.768		

Time [sec]	Vc	Vc'	Win	p[H]	p[L]	Vi	Win	Vc	Statistics for 2.7640 (21.27 hrs)			
									Average	Std Dev	Min	Max
76	4.999	1.010	18.141	0.526	0.147	3.302	18.141	5.050				
86	4.999	1.010	18.139	0.517	0.155	3.295	18.139	5.049	Vc	0.056	4.884	5.051
96	4.999	1.010	18.143	0.487	0.160	3.294	18.143	5.050	Win	0.061	17.755	18.326
106	4.999	1.010	18.139	0.514	0.152	3.284	18.139	5.049				
116	4.999	1.010	18.147	0.536	0.148	3.284	18.147	5.049	p[H]	0.492	0.385	0.603
126	4.999	1.010	18.151	0.481	0.158	3.284	18.151	5.049				
136	4.999	1.010	18.149	0.543	0.146	3.284	18.149	5.049				
146	4.999	1.010	18.153	0.487	0.158	3.284	18.153	5.049				
156	4.999	1.010	18.150	0.516	0.150	3.294	18.150	5.050				
166	4.999	1.010	18.150	0.497	0.156	3.294	18.150	5.050				
176	4.999	1.010	18.153	0.532	0.149	3.295	18.153	5.050				
186	4.999	1.010	18.153	0.510	0.152	3.295	18.153	5.050				
196	4.999	1.010	18.149	0.497	0.157	3.295	18.149	5.050				
206	4.999	1.010	18.148	0.461	0.155	3.295	18.148	5.050				
216	4.999	1.010	18.142	0.543	0.146	3.295	18.142	5.050				
226	4.999	1.010	18.145	0.489	0.156	3.295	18.145	5.050				
236	4.999	1.010	18.151	0.533	0.148	3.295	18.151	5.050				

Time [sec]	Vc	Vc'	Win	p[H]	p[L]	Vf	Win	Vc	Statistics for 2-2455 (C.916 hr)			
									Average	Std Dev	Min	Max
55	4.801	0.961	17.938	0.504	0.132	3.093	17.938	4.801	4.791	0.009	4.776	4.816
65	4.801	0.961	17.939	0.509	0.130	3.086	17.939	4.801	17.964	0.046	17.886	18.105
75	4.801	0.961	17.975	0.505	0.133	3.086	17.975	4.801	Win			
85	4.801	0.961	17.961	0.501	0.135	3.086	17.961	4.801	p[H]	0.030	0.349	0.576
95	4.802	0.961	17.952	0.508	0.131	3.086	17.952	4.802				
105	4.802	0.961	17.931	0.510	0.131	3.086	17.931	4.802				
115	4.802	0.961	17.911	0.490	0.133	3.086	17.911	4.802				
125	4.802	0.961	17.895	0.505	0.128	3.086	17.895	4.802				
135	4.802	0.961	17.895	0.499	0.132	3.086	17.895	4.802				
145	4.801	0.961	17.900	0.506	0.130	3.085	17.900	4.801				
155	4.801	0.961	17.908	0.508	0.130	3.085	17.908	4.801				
165	4.800	0.961	17.899	0.492	0.131	3.084	17.899	4.800				
175	4.800	0.961	17.910	0.510	0.129	3.084	17.910	4.800				
186	4.799	0.961	17.907	0.491	0.132	3.084	17.907	4.799				
195	4.799	0.961	17.910	0.508	0.130	3.084	17.910	4.799				
205	4.798	0.960	17.921	0.500	0.132	3.083	17.921	4.798				
215	4.798	0.960	17.931	0.502	0.130	3.082	17.931	4.798				

April 29 - May 1, 1997

[illegible]

Time [sec]	Vc	Vc'	Win	p[H]	p[L]	Vf	Win	Vc	Statistics for 2437 - 4515 [11.572 hrs]					Max	
									Average	Std Dev	MIn	Vc	Win		p[H]
109	0.000	0.000	0.064	0.507	0.138	0.005	0.064	0.000	4.431	0.040	4.318	4.478			
129	0.000	0.000	0.063	0.508	0.137	0.000	0.063	0.000	15.078	0.015	15.018	15.110			
149	0.000	0.000	0.070	0.515	0.138	0.000	0.070	0.000	0.508	0.021	0.425	0.582			
169	0.000	0.000	0.062	0.530	0.139	0.000	0.062	0.000							
190	0.000	0.000	0.069	0.531	0.138	0.000	0.069	0.000							
209	0.000	0.000	0.061	0.531	0.146	0.000	0.061	0.000							
229	0.000	0.000	0.070	0.522	0.276	0.000	0.070	0.000							
249	0.000	0.000	0.068	0.534	0.287	0.000	0.068	0.000							
269	0.000	0.000	8.831	0.523	0.292	0.000	8.831	0.000							
289	0.000	0.000	15.024	0.577	0.351	0.000	15.024	0.000							
309	0.000	0.000	15.068	0.653	0.485	0.000	15.068	0.000							
329	0.015	0.003	14.928	0.708	0.563	0.000	14.928	0.015							
349	0.098	0.019	14.910	0.741	0.595	0.000	14.910	0.098							
369	0.177	0.035	14.940	0.750	0.610	0.000	14.940	0.177							
389	0.250	0.050	14.969	0.755	0.620	0.000	14.969	0.250							
409	0.317	0.063	14.992	0.842	0.641	0.000	14.992	0.317							
429	0.381	0.076	15.029	0.767	0.634	0.000	15.029	0.381							

[illegible]

Time [sec]	Vc		Vc'	Win	p[H]	p[L]	Vf	Win	Vc	Statistics for 2 - 42.5 (23.44 l/wt)			
	Vc	Vc								Average	Std Dev	Min	Max
58	4.470	4.470	0.894	15.091	0.500	0.134	2.801	15.091	4.470	4.457	0.012	4.440	4.484
78	4.470	4.470	0.894	15.094	0.508	0.132	2.801	15.094	4.470	15.053	0.035	14.937	15.114
98	4.470	4.470	0.894	15.083	0.509	0.133	2.801	15.083	4.470	p[H]	0.038	0.352	0.582
118	4.471	4.471	0.894	15.081	0.527	0.131	2.801	15.081	4.471				
138	4.471	4.471	0.894	15.077	0.552	0.137	2.801	15.077	4.471				
158	4.471	4.471	0.894	15.082	0.526	0.136	2.801	15.082	4.471				
178	4.471	4.471	0.894	15.075	0.513	0.134	2.801	15.075	4.471				
198	4.471	4.471	0.894	15.078	0.539	0.137	2.801	15.078	4.471				
218	4.471	4.471	0.894	15.073	0.503	0.130	2.801	15.073	4.471				
238	4.471	4.471	0.894	15.077	0.526	0.136	2.801	15.077	4.471				
258	4.471	4.471	0.894	15.071	0.508	0.134	2.801	15.071	4.471				
279	4.471	4.471	0.894	15.060	0.518	0.136	2.801	15.060	4.471				
299	4.471	4.471	0.894	15.065	0.492	0.131	2.802	15.065	4.471				
319	4.471	4.471	0.894	15.066	0.521	0.136	2.802	15.066	4.471				
339	4.471	4.471	0.894	15.078	0.500	0.131	2.801	15.078	4.471				
359	4.472	4.472	0.895	15.079	0.509	0.133	2.802	15.079	4.472				
379	4.472	4.472	0.895	15.086	0.507	0.134	2.802	15.086	4.472				

[illegible]

TP042597

Time [sec]	Vc	Vc'	Win	p[H]	p[L]	Vf	Win	Vc	Statistics for 2 - 1457 [13.507 hrs]			
									Average	Std Dev	Min	Max
98	4.447	0.889	15.005	1.205	0.046	2.805	15.005	4.447				
131	4.446	0.889	15.005	1.275	0.071	2.790	15.005	4.446				4.447
165	4.445	0.889	14.985	0.648	0.202	2.767	14.985	4.445	Vc	0.002	4.441	
198	4.445	0.889	14.998	0.051	0.253	2.759	14.998	4.445	Win	0.045	14.922	15.111
231	4.445	0.889	15.015	0.017	0.245	2.760	15.015	4.445	p[H]	0.374	0.000	1.312
265	4.445	0.889	15.042	0.152	0.270	2.759	15.042	4.445	pressure data is erratic			
298	4.445	0.889	15.041	0.103	0.259	2.759	15.041	4.445				
332	4.444	0.889	15.055	0.110	0.126	2.783	15.055	4.444				
365	4.444	0.889	15.093	1.122	0.062	2.791	15.093	4.444				
398	4.444	0.889	15.097	0.551	0.211	2.763	15.097	4.444				
432	4.443	0.889	15.075	0.008	0.182	2.771	15.075	4.443				
465	4.443	0.889	15.089	0.005	0.145	2.776	15.089	4.443				
499	4.444	0.889	15.067	0.008	0.145	2.778	15.067	4.444				
532	4.444	0.889	15.038	0.325	0.043	2.795	15.038	4.444				
566	4.445	0.889	15.016	1.175	0.080	2.788	15.016	4.445				
599	4.445	0.889	15.011	0.403	0.239	2.761	15.011	4.445				
632	4.445	0.889	15.000	0.014	0.212	2.766	15.000	4.445				

[illegible]

TP050397

Time [sec]	Vc	Vc'	Win	p[H]	p[L]	V/2	Win	Vc	Statistics for 3085 - 4205 [6.237 hrs]				
									Average	Std Dev	Min	Max	
64	2.491	0.498	15.086	0.408	0.152	3.620	15.086	2.491	4.282	0.008	4.250	4.273	
84	2.508	0.502	15.089	0.448	0.160	3.621	15.089	2.508	15.032	0.009	15.011	15.057	
104	2.524	0.505	15.084	0.392	0.148	3.620	15.084	2.524	3.624	0.003	3.619	3.632	
124	2.541	0.508	15.083	0.410	0.148	3.619	15.083	2.541	p[H]	0.015	0.335	0.443	
144	2.557	0.512	15.077	0.397	0.146	3.620	15.077	2.557					
164	2.574	0.515	15.072	0.379	0.145	3.618	15.072	2.574					
185	2.591	0.518	15.085	0.393	0.146	3.618	15.085	2.591					
204	2.607	0.521	15.084	0.386	0.147	3.619	15.084	2.607					
224	2.622	0.525	15.085	0.381	0.145	3.620	15.085	2.622					
244	2.637	0.528	15.083	0.420	0.151	3.621	15.083	2.637					
264	2.652	0.531	15.081	0.421	0.153	3.621	15.081	2.652					
284	2.667	0.534	15.057	0.414	0.150	3.621	15.057	2.667					
304	2.682	0.537	15.083	0.420	0.150	3.621	15.083	2.682					
324	2.697	0.540	15.080	0.385	0.146	3.620	15.080	2.697					
344	2.712	0.543	15.059	0.396	0.145	3.619	15.059	2.712					
364	2.726	0.545	15.059	0.418	0.153	3.621	15.059	2.726					
384	2.738	0.548	15.060	0.396	0.146	3.619	15.060	2.738					

[illegible]

TP050497

Time [sec]	Vc	Vc'	Win	p[H]	p[L]	Vf/2	Win	Vc	Statistics for 1712 - 5789 [11.355 hrs]					
									Vc	Win	Average	Std Dev	Min	Max
42	4.310	0.862	15.090	0.370	0.253	3.619	15.090	4.310			4.200	0.008	4.188	4.219
53	4.312	0.862	15.096	0.353	0.256	3.620	15.096	4.312		Vc	14.891	0.013	14.868	14.981
63	4.313	0.863	15.089	0.370	0.259	3.618	15.089	4.313		Win	0.578	0.029	0.453	0.679
73	4.314	0.863	15.090	0.399	0.255	3.619	15.090	4.314		p[H]	3.525	0.004	3.518	3.544
83	4.315	0.863	15.094	0.392	0.262	3.619	15.094	4.315		Vf/2				
93	4.315	0.863	15.089	0.388	0.258	3.619	15.089	4.315						
103	4.315	0.863	15.094	0.367	0.267	3.619	15.094	4.315						
113	4.315	0.863	15.095	0.362	0.255	3.619	15.095	4.315						
123	4.314	0.863	15.095	0.374	0.256	3.618	15.095	4.314						
133	4.314	0.863	15.113	0.399	0.269	3.619	15.113	4.314						
143	4.315	0.863	15.109	0.380	0.267	3.619	15.109	4.315						
153	4.315	0.863	15.113	0.395	0.268	3.619	15.113	4.315						
163	4.315	0.863	15.112	0.368	0.270	3.619	15.112	4.315						
173	4.315	0.863	15.108	0.389	0.270	3.619	15.108	4.315						
183	4.315	0.863	15.111	0.392	0.273	3.620	15.111	4.315						
193	4.314	0.863	15.118	0.392	0.272	3.619	15.118	4.314						
203	4.314	0.863	15.114	0.382	0.273	3.619	15.114	4.314						

[illegible]

TP050597

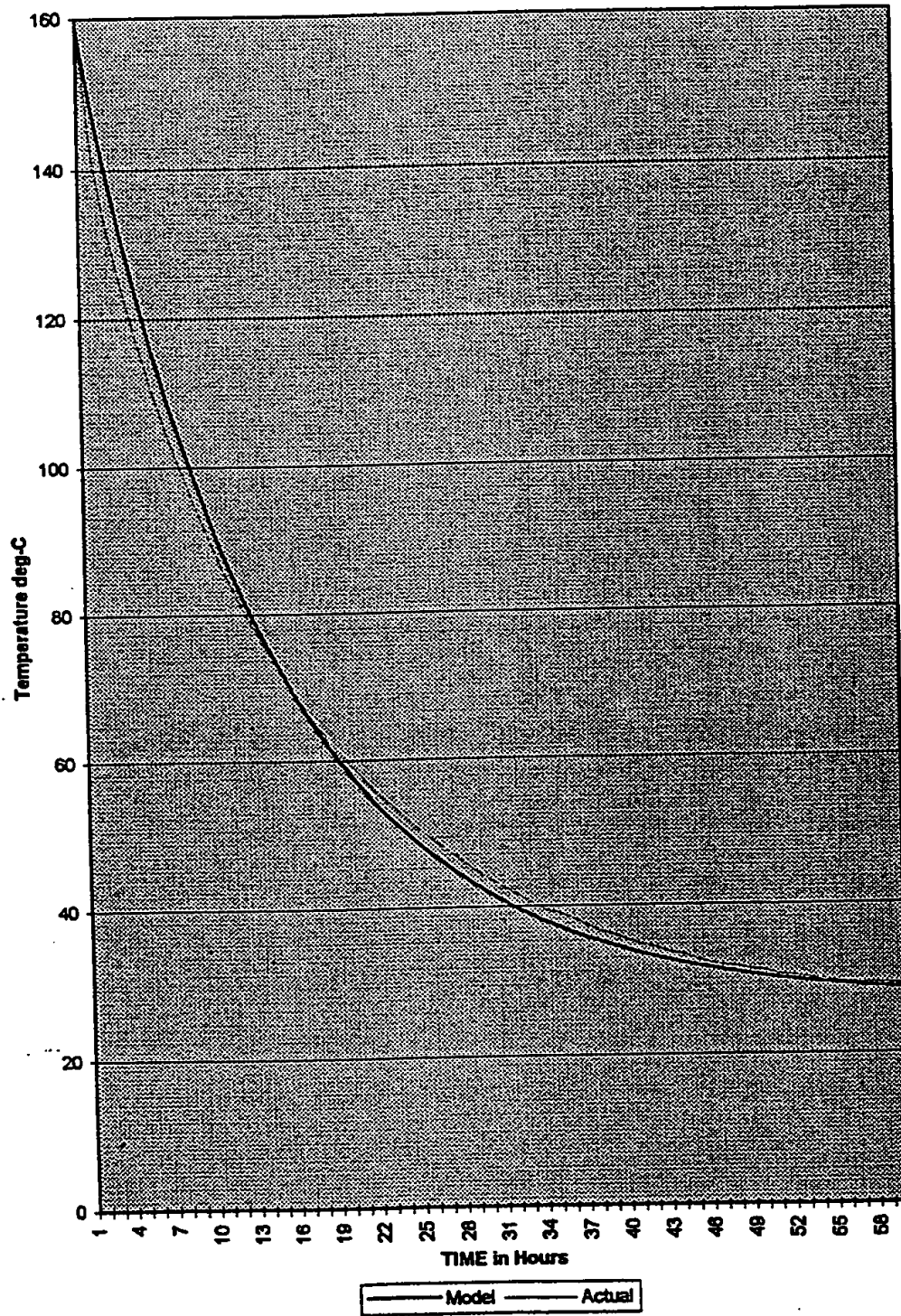
Time [sec]	Vc	Vc'	Win	p[H]	p[L]	Vf/2	Win	Vc	Statistics for 2 - 8 s (4.777 hrs)			
									Average	Std Dev	Min	Max
56	4.190	0.838	14.878	0.535	0.136	3.526	14.878	4.189	4.187	0.005	4.175	4.199
76	4.189	0.838	14.878	0.574	0.141	3.526	14.878	4.189	14.891	0.026	14.857	15.004
96	4.189	0.838	14.877	0.559	0.138	3.526	14.877	4.189	3.522	0.003	3.505	3.537
116	4.188	0.838	14.872	0.587	0.141	3.527	14.872	4.188	0.538	0.024	0.447	0.596
136	4.188	0.838	14.876	0.577	0.141	3.527	14.876	4.188				
156	4.188	0.838	14.883	0.592	0.142	3.527	14.883	4.188				
177	4.188	0.838	14.881	0.596	0.144	3.527	14.881	4.188				
197	4.189	0.838	14.888	0.514	0.134	3.528	14.888	4.189				
217	4.189	0.838	14.895	0.571	0.142	3.529	14.895	4.189				
237	4.190	0.838	14.897	0.550	0.139	3.530	14.897	4.190				
257	4.190	0.838	14.892	0.556	0.140	3.530	14.892	4.190				
277	4.191	0.838	14.885	0.552	0.139	3.530	14.885	4.191				
297	4.192	0.838	14.886	0.567	0.143	3.531	14.886	4.192				
317	4.192	0.838	14.901	0.561	0.142	3.531	14.901	4.192				
337	4.193	0.839	14.907	0.563	0.141	3.532	14.907	4.193				
357	4.194	0.839	14.908	0.558	0.141	3.534	14.908	4.194				
377	4.195	0.839	14.902	0.569	0.139	3.533	14.902	4.195				

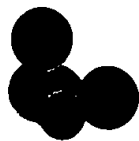
[illegible]

THESIS - APPENDIX NINE



Model vs. Actual Data





111
112
113
114

Heat Loss Model - Vers 1.1

Heat Loss Model for HPC Test 15.9 - May 3-4, 1996										Kc=	40850	UA=	0.85	
Temperature - degrees C		Delta - T		Heat Loss Predictions		Model Fit		Temp.						#VALUEI
Time	Cel.	Ambient		Next Per.	Best	Vs.	Error	Error - C						
(secs)				Predicted	Prediction	Actual	%							
				268.1										
38211	268.1	27.1	241											
38271	268.0	27.1	240.9											
38331	267.9	27.1	240.8	267.9			0.00%						Unable to Replicate	
38391	265.6	27.1	238.5	265.6			0.00%						Precipitous Drop In	
38451	248.0	27.1	220.9	248.0			0.00%						Internal Temperature	
38511	218.3	27.1	191.2	218.3	Start Model		0.00%							
38571	199.5	27.1	172.4	218.1	218.1		9.30%	18.6						
38632	187.0	27.1	159.9	217.8	217.8		16.48%	30.8						
38692	178.9	27.1	151.8	217.6	217.6		21.62%	38.7						
38752	173.3	27.1	146.2	217.3	217.3		25.42%	44.0						
38812	169.2	27.1	142.1	217.1	217.1		28.32%	47.9						
38872	166.5	27.1	139.4	216.9	216.9		30.25%	50.4						
38932	164.2	27.1	137.1	216.6	216.6		31.93%	52.4						
38993	162.6	27.1	135.5	216.4	216.4		33.09%	53.8						
39053	161.5	27.1	134.4	216.2	216.2		33.85%	54.7						
39113	160.5	27.1	133.4	215.9	215.9		34.53%	55.4						
39173	159.7	27.1	132.6	215.7	215.7		35.06%	56.0						
39233	158.8	27.1	131.7	215.5	158.8	Match Pt.	0.00%	0.0						
39293	158.4	27.1	131.3	158.6	158.6		0.15%	0.2						
39353	157.6	27.1	130.5	158.5	158.5		0.55%	0.9						
39414	157.2	27.1	130.1	158.3	158.3		0.70%	1.1						
39474	156.6	27.1	129.5	158.1	158.1		0.99%	1.5						
39534	156.4	27.1	129.3	158.0	158.0		1.01%	1.6						
39594	156.2	27.1	129.1	157.8	157.8		1.04%	1.6						
39654	155.5	27.1	128.4	157.7	157.7		1.39%	2.2						
39714	155.3	27.1	128.2	157.5	157.5		1.41%	2.2						
39774	154.8	27.1	127.7	157.3	157.3		1.63%	2.5						
39835	154.6	27.1	127.5	157.2	157.2		1.66%	2.6						
39895	154.2	27.1	127.1	157.0	157.0		1.82%	2.8						
39955	153.8	27.1	126.7	156.8	156.8		1.98%	3.0						
40015	153.7	27.1	126.6	156.7	156.7		1.94%	3.0						

Heat Loss Model - Vers 1.1

40075	153.2	27.1	126.1	156.5	156.5	153.2	2.15%	3.3		
40135	152.8	27.1	125.7	156.4	156.4	152.8	2.33%	3.6		
40196	152.5	27.1	125.4	156.2	156.2	152.5	2.42%	3.7		
40256	152.2	27.1	125.1	156.0	156.0	152.2	2.52%	3.8		
40316	151.9	27.1	124.8	155.9	155.9	151.9	2.62%	4.0		
40376	151.9	27.1	124.8	155.7	155.7	151.9	2.51%	3.8		
40436	151.5	27.1	124.4	155.6	155.6	151.5	2.67%	4.1		
40496	151.3	27.1	124.2	155.4	155.4	151.3	2.70%	4.1		
40556	150.9	27.1	123.8	155.2	155.2	150.9	2.87%	4.3		
40616	150.8	27.1	123.7	155.1	155.1	150.8	2.83%	4.3		
40677	150.5	27.1	123.4	154.9	154.9	150.5	2.93%	4.4		
40737	150.2	27.1	123.1	154.8	154.8	150.2	3.03%	4.6		
40797	150.0	27.1	122.9	154.6	154.6	150.0	3.08%	4.6		
40857	149.7	27.1	122.6	154.4	154.4	149.7	3.16%	4.7		
40917	149.5	27.1	122.4	154.3	154.3	149.5	3.19%	4.8		
40977	149.2	27.1	122.1	154.1	154.1	149.2	3.30%	4.9		
41038	149.0	27.1	121.9	154.0	154.0	149.0	3.33%	5.0		
41098	148.8	27.1	121.7	153.8	153.8	148.8	3.38%	5.0		
41158	148.5	27.1	121.4	153.6	153.6	148.5	3.46%	5.1		
41218	148.2	27.1	121.1	153.5	153.5	148.2	3.57%	5.3		
41278	148.0	27.1	120.9	153.3	153.3	148.0	3.60%	5.3		
41338	147.8	27.1	120.7	153.2	153.2	147.8	3.63%	5.4		
41398	147.6	27.1	120.5	153.0	153.0	147.6	3.67%	5.4		
41459	147.3	27.1	120.2	152.9	152.9	147.3	3.77%	5.8		
41519	147.1	27.1	120.0	152.7	152.7	147.1	3.81%	5.6		
41579	147.0	27.1	119.9	152.5	152.5	147.0	3.77%	5.5		
41639	146.6	27.1	119.5	152.4	152.4	146.6	3.95%	5.8		
41699	146.4	27.1	119.3	152.2	152.2	146.4	3.98%	5.8		
41759	146.3	27.1	119.2	152.1	152.1	146.3	3.95%	5.8		
41819	145.9	27.1	118.8	151.9	151.9	145.9	4.12%	6.0		
41879	145.9	27.1	118.8	151.8	151.8	145.9	4.02%	5.9		
41940	145.5	27.1	118.4	151.6	151.6	145.5	4.20%	6.1		
FILL 1 hr		27.0		151.6	Model	Actual				
12	141.5	27.0	114.5	148.3	148.4	142.0	4.86%	6.9		
13	132.1	26.9	105.2	139.3	139.6	133.0	5.70%	7.5		
14	124.4	26.8	97.6	131.2	131.5	125.0	5.71%	7.1		
15	117.5	26.8	90.7	123.7	124.0	118.0	5.49%	6.5		

Heat Loss Model - Vers 1.1

16	111.3	26.7	84.6	116.7	116.9	111.0	5.07%	5.6		
17	105.4	26.7	78.7	110.2	110.4	105.0	4.78%	5.0		
18	100.1	26.7	73.4	104.2	104.4	100.0	4.30%	4.3		
19	95.1	26.7	68.4	98.6	98.8	95.0	3.89%	3.7		
20	90.5	26.8	63.7	93.4	93.6	90.0	3.43%	3.1		
21	86.4	26.8	59.6	88.6	88.8	87.0	2.76%	2.4		
22	82.4	26.9	55.5	84.1	84.3	82.0	2.32%	1.9		
23	78.5	27.0	51.8	80.0	80.2	79.0	1.75%	1.4		
24	75.5	27.0	48.5	76.2	76.3	75.0	1.11%	0.8		
25	72.5	27.0	45.5	72.6	72.8	72.0	0.39%	0.3		
26	69.8	27.0	42.8	69.4	69.5	69.0	-0.45%	-0.3		
27	66.8	27.0	39.8	66.3	66.4	66.0	-0.57%	-0.4		
28	64.3	27.0	37.3	63.5	63.6	64.0	-1.12%	-0.7		
29	61.8	27.0	34.8	60.8	60.9	62.0	-1.39%	-0.9		
30	59.8	27.0	32.8	58.4	58.5	60.0	-2.19%	-1.3		
31	57.7	27.0	30.7	56.1	56.2	58.0	-2.56%	-1.5		
32	55.7	27.0	28.7	54.0	54.1	56.0	-2.85%	-1.6		
33	54.1	27.0	27.1	52.1	52.2	54.0	-3.59%	-1.9		
34	52.3	27.0	25.3	50.3	50.3	52.0	-3.74%	-2.0		
35	50.6	27.0	23.6	48.6	48.7	50.0	-3.83%	-1.9		
36	49.1	27.0	22.1	47.0	47.1	49.0	-4.07%	-2.0		
37	47.7	27.0	20.7	45.6	45.7	48.0	-4.29%	-2.0		
38	46.3	27.0	19.3	44.3	44.3	46.5	-4.31%	-2.0		
39	45.0	27.0	18	43.0	43.1	45.0	-4.31%	-1.9		
40	43.8	27.0	16.8	41.9	41.9	43.0	-4.34%	-1.9		
41	42.7	27.0	15.7	40.8	40.8	42.0	-4.39%	-1.9		
42	41.7	27.0	14.7	39.8	39.8	41.0	-4.49%	-1.9		
43	40.7	27.0	13.7	38.9	38.9	40.0	-4.41%	-1.8		
44	39.6	27.0	12.6	38.0	38.0	40.0	-3.92%	-1.6		
45	39.1	27.0	12.1	37.2	37.2	39.0	-4.73%	-1.9		
46	38.4	27.0	11.4	36.5	36.5	38.5	-4.92%	-1.9		
47	37.5	27.0	10.5	35.8	35.8	38.0	-4.47%	-1.7		
48	36.6	27.0	9.6	35.2	35.2	37.0	-3.86%	-1.4		
49	36.1	27.0	9.1	34.6	34.6	36.0	-4.16%	-1.5		
50	35.4	27.0	8.4	34.0	34.1	35.0	-3.81%	-1.3		
51	34.8	27.0	7.8	33.5	33.5	35.0	-3.61%	-1.3		
52	34.3	27.0	7.3	33.1	33.1	34.0	-3.59%	-1.2		

Heat Loss Model - Vers 1.1

53	33.7	27.0	6.7	32.6	32.6	33.0	-3.17%	-1.1	*****			
54	33.4	27.0	6.4	32.2	32.2	33.0	-3.51%	-1.2				
55	32.6	27.0	5.6	31.8	31.8	32.0	-2.30%	-0.8				
56	32.1	27.0	5.1	31.5	31.5	32.0	-1.87%	-0.6				
57	31.8	27.0	4.8	31.2	31.2	32.0	-1.98%	-0.6				
58	31.6	27.0	4.6	30.9	30.9	31.0	-2.30%	-0.7				
59	31.2	27.0	4.2	30.6	30.6	31.0	-1.94%	-0.6				
60	31.1	27.0	4.1	30.3	30.3	31.0	-2.46%	-0.8				
61	30.6	27.0	3.6	30.1	30.1	31.0	-1.65%	-0.5				
62	30.4	27.0	3.4	29.9	29.9	30.0	-1.74%	-0.5				
63	30.1	27.0	3.1	29.7	29.7	30.0	-1.44%	-0.4				
64	29.9	27.0	2.9	29.5	29.5	30.0	-1.43%	-0.4				
65	29.6	27.0	2.6	29.3	29.3	30.0	-1.03%	-0.3				
66	29.4	27.0	2.4	29.1	29.1	29.0	-0.92%	-0.3				
67	29.3	27.0	2.3	29.0	29.0	29.0	-1.11%	-0.3				
68	29.3	27.0	2.3	28.8	28.8	29.0	-1.59%	-0.5				
69	29.2	27.0	2.2	28.7	28.7	29.0	-1.71%	-0.5				
70	29.1	27.0	2.1	28.6	28.6	29.0	-1.79%	-0.5				

THESIS - APPENDIX EIGHT

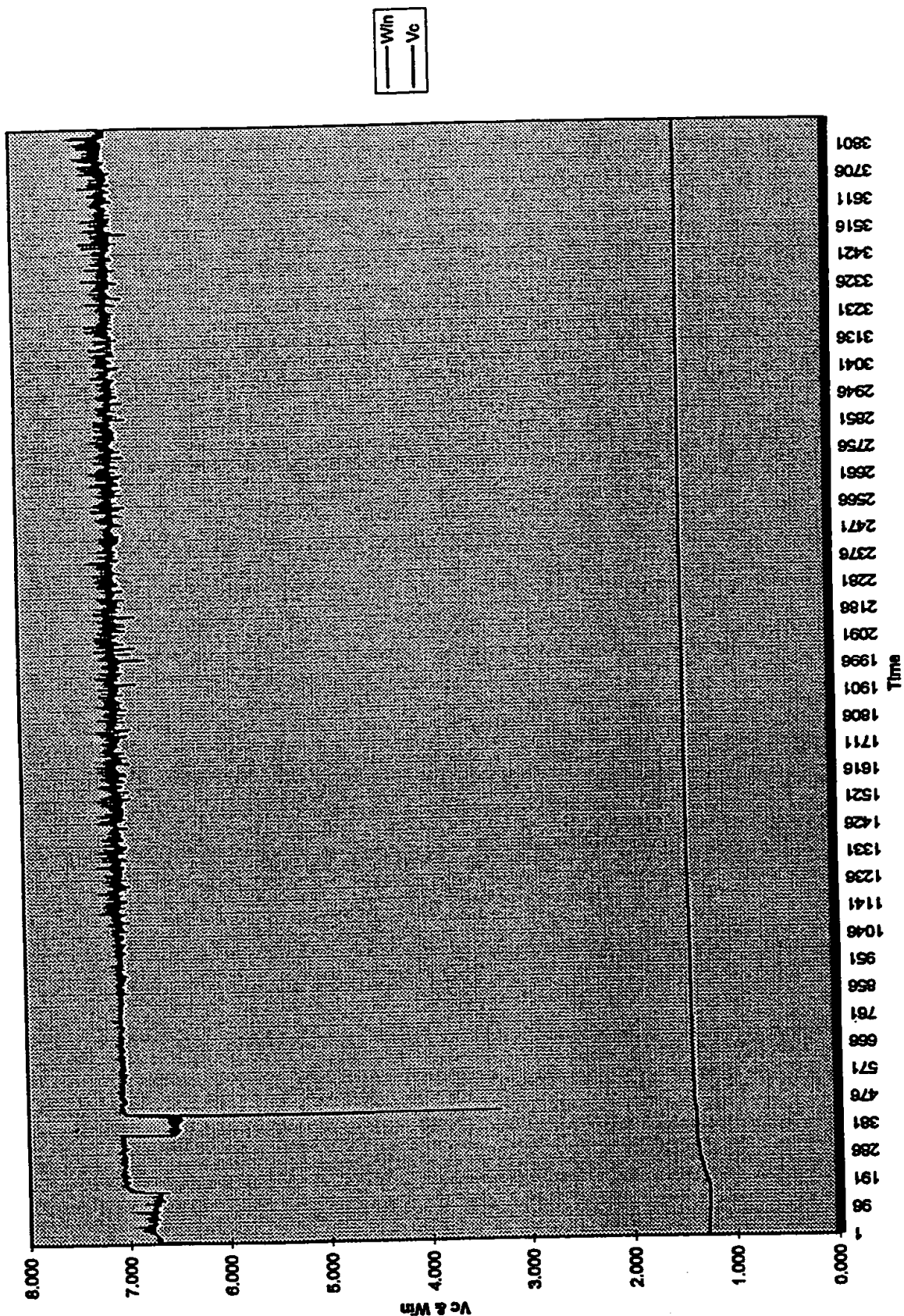


TP032787

Time [sec]	Vc	Vc'	x	Win	Vc	Statistics for Analysis are						
						for 1000 - 3892 [8.053 hrs]						
						Average	Std. Dev.	Min	Max			
57	1.274	0.255	0.134	6.710	1.274							
67	1.274	0.255	0.134	6.698	1.274							
77	1.274	0.255	0.134	6.706	1.274	Vc	1.453	0.013	1.422	1.477		
87	1.271	0.252	0.131	6.563	1.271	Win	7.084	0.057	6.755	7.405		
97	1.266	0.247	0.126	6.317	1.266							
107	1.274	0.255	0.134	6.681	1.274							
117	1.274	0.255	0.134	6.715	1.274							
127	1.274	0.255	0.134	6.703	1.274							
137	1.274	0.255	0.134	6.716	1.274							
147	1.274	0.255	0.134	6.708	1.274							
157	1.274	0.255	0.134	6.699	1.274							

Time [sec]	Vc	Vc'	x	WIn	Vc	Statistics for Analysis are			
						[for 2 - 3692 [10.832 hrs]			
						Average	Std. Dev.	Min	Max
57	1.274	0.255	0.134	6.710	1.274				
67	1.274	0.255	0.134	6.698	1.274				
77	1.274	0.255	0.134	6.706	1.274	Vc	0.048	1.262	1.477
87	1.271	0.252	0.131	6.563	1.271	WIn	0.129	3.307	7.405
97	1.268	0.247	0.126	6.317	1.268				
107	1.274	0.255	0.134	6.681	1.274				
117	1.274	0.255	0.134	6.715	1.274				
127	1.274	0.255	0.134	6.703	1.274				
137	1.274	0.255	0.134	6.716	1.274				

TP032797 Chart 1



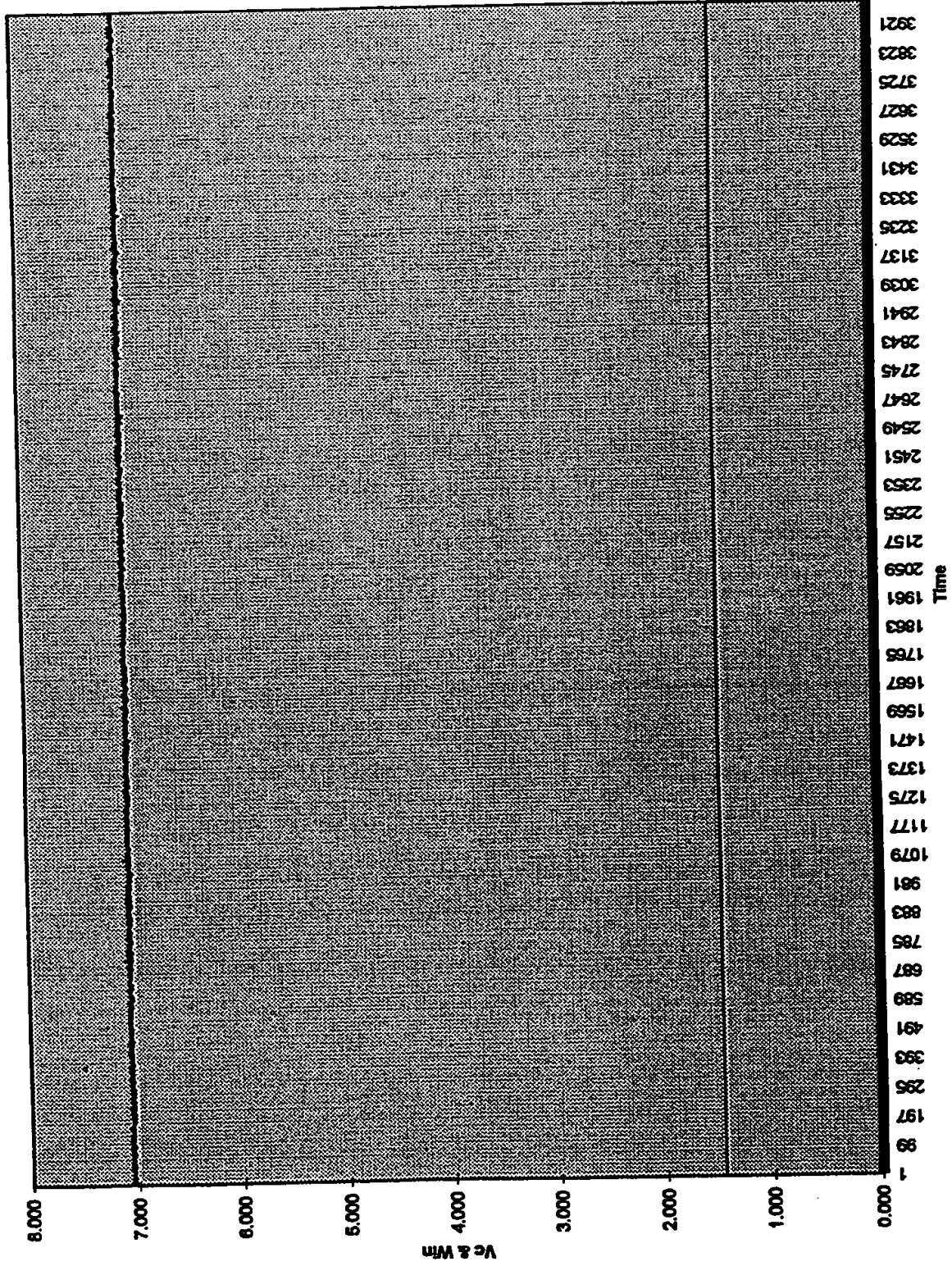
Time [sec]	Statistics for Analysis are									
	Vc		Vc'		x		Win		Vc	
	47	1.475	0.295	0.142	7.112	1.475	for 2 - 16384 [46.176 hrs]	Average	Std. Dev.	Min
57	1.475	0.295	0.144	7.208	1.475	1.464	1.475	1.464	0.001	1.475
67	1.475	0.295	0.143	7.131	1.475	7.083	0.021	7.009	0.021	7.250
77	1.475	0.295	0.143	7.150	1.475					
87	1.475	0.295	0.143	7.140	1.475					
97	1.475	0.295	0.143	7.168	1.475					
107	1.475	0.295	0.142	7.078	1.475					
117	1.475	0.295	0.142	7.083	1.475					
127	1.474	0.295	0.142	7.116	1.474					
137	1.474	0.295	0.141	7.088	1.474					
147	1.474	0.295	0.142	7.089	1.474					
157	1.474	0.295	0.142	7.115	1.474					
167	1.474	0.295	0.142	7.084	1.474					
177	1.473	0.295	0.141	7.068	1.473					
187	1.473	0.295	0.141	7.081	1.473					

TP033097

Time [sec]	Vc	Vc'	x	Win	Vc	Statistics for Analysis are						
						for 2 - 6361 [17.708 hrs]						
						Average	Std. Dev.	Min	Max			
65	1.445	0.289	0.140	6.997	1.445							
75	1.445	0.289	0.140	6.989	1.445							
85	1.445	0.289	0.140	6.995	1.445	Vc	0.002	1.445	1.454			
98	1.445	0.289	0.140	6.993	1.445	Win	0.015	6.958	7.055			
105	1.445	0.289	0.140	6.988	1.445							
115	1.445	0.289	0.140	6.982	1.445							
125	1.445	0.289	0.139	6.988	1.445							
135	1.445	0.289	0.139	6.988	1.445							
145	1.445	0.289	0.140	6.984	1.445							
155	1.445	0.289	0.141	7.029	1.445							
165	1.445	0.289	0.140	7.010	1.445							
175	1.445	0.289	0.140	6.995	1.445							
185	1.445	0.289	0.140	7.010	1.445							
195	1.445	0.289	0.140	7.007	1.445							
205	1.445	0.289	0.140	7.011	1.445							

Time [sec]	Vc	Vc'	x	Win	Vc	Statistics for Analysis are							
						for 2 - 8419 [23.438 hrs]							
						Vc	Average	Std. Dev.	Min	Max			
34	1.461	0.293	0.141	7.039	1.461								
44	1.461	0.293	0.141	7.050	1.461								
54	1.461	0.293	0.141	7.030	1.461								
64	1.461	0.293	0.141	7.040	1.461								
74	1.461	0.293	0.141	7.043	1.461								
84	1.461	0.293	0.141	7.044	1.461								
95	1.461	0.293	0.141	7.057	1.461								
104	1.461	0.293	0.141	7.049	1.461								
114	1.461	0.293	0.141	7.047	1.461								
124	1.461	0.293	0.141	7.045	1.461								
134	1.461	0.293	0.141	7.027	1.461								
144	1.461	0.293	0.141	7.062	1.461								
154	1.461	0.293	0.141	7.040	1.461								
164	1.461	0.293	0.141	7.044	1.461								
174	1.461	0.293	0.141	7.060	1.461								
184	1.461	0.293	0.141	7.050	1.461								

TP033197 Chart 1



Win
Vc

Time [sec]	Vc	Vc'	x	Win	Vc	Statistics for Analysis are							
						for 2 - 8446 [23.514 hrs]							
						Average	Std. Dev.	Min	Max				
51	1.471	0.294	0.141	7.027	1.471								
61	1.471	0.294	0.140	7.018	1.471								
71	1.472	0.294	0.140	7.019	1.472	Vc	1.452	0.003	1.457	1.472			
81	1.472	0.294	0.141	7.027	1.472	Win	7.034	0.016	6.985	7.287			
91	1.472	0.294	0.140	7.017	1.472								
101	1.471	0.294	0.141	7.043	1.471								
111	1.471	0.294	0.141	7.037	1.471								
121	1.471	0.294	0.140	7.025	1.471								
132	1.471	0.294	0.141	7.039	1.471								
141	1.471	0.294	0.140	7.018	1.471								
151	1.471	0.294	0.140	7.020	1.471								
161	1.471	0.294	0.141	7.035	1.471								
172	1.471	0.294	0.141	7.039	1.471								
182	1.471	0.294	0.141	7.037	1.471								
192	1.471	0.294	0.141	7.043	1.471								

TP040297

Time [sec]	Vc		Vc'	x	Win		Vc	Statistics for Analysis are for 2 - 8986 [25.018 hrs]					
	Vc							Average	Std. Dev.	Min	Max		
41	1.438		0.288	0.139	6.937	1.438							
51	1.438		0.288	0.139	6.931	1.438							
62	1.438		0.288	0.139	6.931	1.438	Vc	1.440	0.008	1.395	1.445		
71	1.438		0.288	0.139	6.942	1.438	Win	6.952	0.039	6.692	7.024		
81	1.438		0.288	0.139	6.966	1.438							
92	1.438		0.288	0.139	6.952	1.438							
102	1.438		0.288	0.139	6.940	1.438							
112	1.438		0.288	0.139	6.930	1.438							
122	1.438		0.288	0.138	6.920	1.438							
132	1.438		0.288	0.139	6.932	1.438							
142	1.438		0.288	0.139	6.950	1.438							
152	1.438		0.288	0.139	6.935	1.438							
162	1.438		0.288	0.139	6.940	1.438							

Time [sec]	Vc	Vc'	x	Win	Vc	Statistics for Analysis are			
						for 2 - 7697 [21.428 hrs]			
						Average	Std. Dev.	Min	Max
38	1.445	0.289	0.139	6.973	1.445				
48	1.446	0.289	0.139	6.981	1.446				
58	1.446	0.289	0.139	6.958	1.446	Vc	1.432	0.008	1.410
68	1.446	0.289	0.140	6.975	1.446	Win	6.967	0.034	6.708
78	1.446	0.289	0.139	6.971	1.446				
88	1.446	0.289	0.139	6.960	1.446				
98	1.445	0.289	0.139	6.972	1.445				
108	1.445	0.289	0.139	6.953	1.445				
118	1.445	0.289	0.139	6.974	1.445				
128	1.445	0.289	0.139	6.974	1.445				
138	1.445	0.289	0.139	6.955	1.445				
148	1.445	0.289	0.140	6.975	1.445				
158	1.445	0.289	0.139	6.963	1.445				

TP040497

Time [sec]	Vc	Vc'	x	Win	Vc	Statistics for Analysis are						
						for 2 - 16384 [45.618 hrs]						
						Average	Std. Dev.	Min	Max			
35	1.432	0.287	0.139	6.950	1.432							
45	1.432	0.287	0.139	6.943	1.432							
55	1.432	0.287	0.139	6.937	1.432	Vc	1.426	0.008	1.410	1.443		
65	1.432	0.287	0.139	6.932	1.432	Win	6.935	0.039	6.703	7.065		
75	1.432	0.287	0.139	6.935	1.432							
85	1.432	0.287	0.139	6.939	1.432							
95	1.432	0.287	0.139	6.941	1.432							
105	1.432	0.287	0.139	6.942	1.432							
115	1.432	0.287	0.139	6.934	1.432							
125	1.432	0.287	0.139	6.927	1.432							
135	1.432	0.287	0.139	6.929	1.432							
145	1.432	0.287	0.139	6.936	1.432							

Time [sec]	Vc	Vc'	x	Win	Vc	Statistics for Analysis are					
						for 2 - 8462 [23.558 hrs]					
						Average	Std. Dev.	Min	Max		
49	1.426	0.286	0.139	6.929	1.426						
59	1.426	0.286	0.139	6.930	1.426						
69	1.426	0.286	0.138	6.923	1.426	Vc	1.427	0.007	1.385	1.427	
79	1.426	0.286	0.138	6.910	1.426	Win	6.869	0.036	6.868	6.956	
89	1.426	0.286	0.139	6.944	1.426						
99	1.426	0.286	0.139	6.933	1.426						
109	1.426	0.286	0.139	6.934	1.426						
119	1.426	0.286	0.138	6.908	1.426						
129	1.426	0.286	0.139	6.930	1.426						
139	1.426	0.286	0.139	6.926	1.426						
149	1.427	0.286	0.138	6.919	1.427						
159	1.426	0.286	0.138	6.918	1.426						
169	1.426	0.286	0.139	6.928	1.426						
179	1.426	0.286	0.139	6.952	1.426						

TP040797

Time [sec]	Vc	Vc'	x	Statistics for Analysis are									
				for 2 - 8148 [22.684 hrs]									
				Win		Vc		Average			Std. Dev.	Min	Max
45	1.460	0.292	0.141	7.026	1.460								
55	1.459	0.292	0.140	7.020	1.459								
65	1.459	0.292	0.140	7.025	1.459			Vc	1.463	0.001	1.459	1.484	
75	1.459	0.292	0.141	7.027	1.459			Win	7.029	0.011	6.982	7.087	
85	1.459	0.292	0.141	7.028	1.459								
95	1.459	0.292	0.140	7.016	1.459								
105	1.459	0.292	0.141	7.025	1.459								
115	1.459	0.292	0.141	7.027	1.459								
125	1.460	0.292	0.141	7.035	1.460								
135	1.460	0.292	0.141	7.042	1.460								
145	1.460	0.292	0.141	7.033	1.460								
155	1.460	0.292	0.140	7.016	1.460								
165	1.460	0.292	0.140	7.023	1.460								
175	1.460	0.292	0.141	7.031	1.460								

Time [sec]	Vc	Vc'	x	Win	Vc	Statistics for Analysis are							
						for 2 - 8586 [23.904 hrs]							
							Average	Std. Dev.	Min	Max			
41	1.462	0.293	0.140	7.011	1.462								
51	1.462	0.293	0.140	7.016	1.462								
61	1.462	0.293	0.141	7.034	1.462	Vc	1.462	0.001	1.460	1.465			
71	1.462	0.293	0.141	7.035	1.462	Win	7.027	0.012	6.978	7.065			
81	1.462	0.293	0.140	7.023	1.462								
91	1.462	0.293	0.141	7.028	1.462								
102	1.462	0.293	0.141	7.037	1.462								
111	1.462	0.293	0.140	7.015	1.462								
121	1.462	0.293	0.140	7.011	1.462								
132	1.462	0.293	0.140	7.024	1.462								
142	1.462	0.293	0.141	7.027	1.462								
152	1.462	0.293	0.140	7.016	1.462								
162	1.462	0.293	0.140	7.018	1.462								

TP040997

Time [sec]	Vc	Vc'	x	Win	Vc	Statistics for Analysis are			
						for 2 - 6420 [17.972 hrs]			
						Average	Std. Dev.	Min	Max
43	1.456	0.292	0.140	7.005	1.456				
53	1.456	0.292	0.140	7.019	1.456				
63	1.456	0.292	0.140	6.996	1.456	Vc	1.464	0.003	1.456
73	1.457	0.292	0.140	7.012	1.457	Win	7.020	0.014	6.967
83	1.457	0.292	0.140	7.017	1.457				
93	1.457	0.292	0.140	7.010	1.457				
103	1.456	0.292	0.140	7.019	1.456				
113	1.456	0.292	0.140	7.025	1.456				
123	1.456	0.292	0.140	7.013	1.456				
133	1.456	0.292	0.140	7.022	1.456				
143	1.456	0.292	0.140	7.016	1.456				
153	1.456	0.292	0.140	7.018	1.456				
163	1.456	0.292	0.140	7.020	1.456				

GRAPHING of 20 CM Control Experimental Points							
Vc	Win	Vc-SD	Win-SD	Date	%-Vc-SD	%-Win-SD	
2.102	9.927	0.005	0.034	5-Mar	0.24%	0.34%	
2.355	11.085	0.012	0.013	6-Mar	0.51%	0.12%	
2.160	9.573	0.004	0.012	6-Mar	0.19%	0.13%	
2.453	10.808	0.006	0.011	7-Mar	0.24%	0.10%	
1.084	4.932	0.010	0.049	7-Mar	0.88%	1.00%	
1.299	6.009	0.001	0.008	8-Mar	0.08%	0.13%	
3.451	14.982	0.006	0.018	8-Mar	0.17%	0.12%	
3.664	15.885	0.005	0.012	9-Mar	0.14%	0.08%	
0.174	1.054	0.001	0.007	9-Mar	0.57%	0.66%	
0.000	0.050	0.000	0.001	10-Mar	0.00%	2.00%	

Prior to Added Insulation

Time [sec]	Vc	Vc'	x	Win	Vc	Statistics from 2589-4047 [8.12 hrs]							
						Average	Std Dev	Min	Max				
85	0.000	0.000	0.001	0.053	0.000	2.102	0.005	2.097	2.117				
105	0.000	0.000	0.001	0.059	0.000								
125	0.000	0.000	0.001	0.061	0.000	Vc		9.843	9.999				
145	0.000	0.000	0.001	0.063	0.000	Win							
165	0.000	0.000	0.003	0.161	0.000								
186	0.000	0.000	0.162	8.095	0.000								
205	0.011	0.002	0.199	9.947	0.011								
226	0.064	0.013	0.199	9.950	0.064								
245	0.129	0.026	0.199	9.928	0.129								
266	0.189	0.038	0.198	9.914	0.189								
286	0.241	0.048	0.198	9.903	0.241								
306	0.287	0.057	0.198	9.922	0.287								
326	0.329	0.066	0.199	9.928	0.329								
346	0.368	0.073	0.199	9.942	0.368								
366	0.406	0.081	0.199	9.938	0.406								
386	0.442	0.088	0.199	9.952	0.442								
406	0.477	0.095	0.199	9.952	0.477								
426	0.510	0.102	0.199	9.925	0.510								

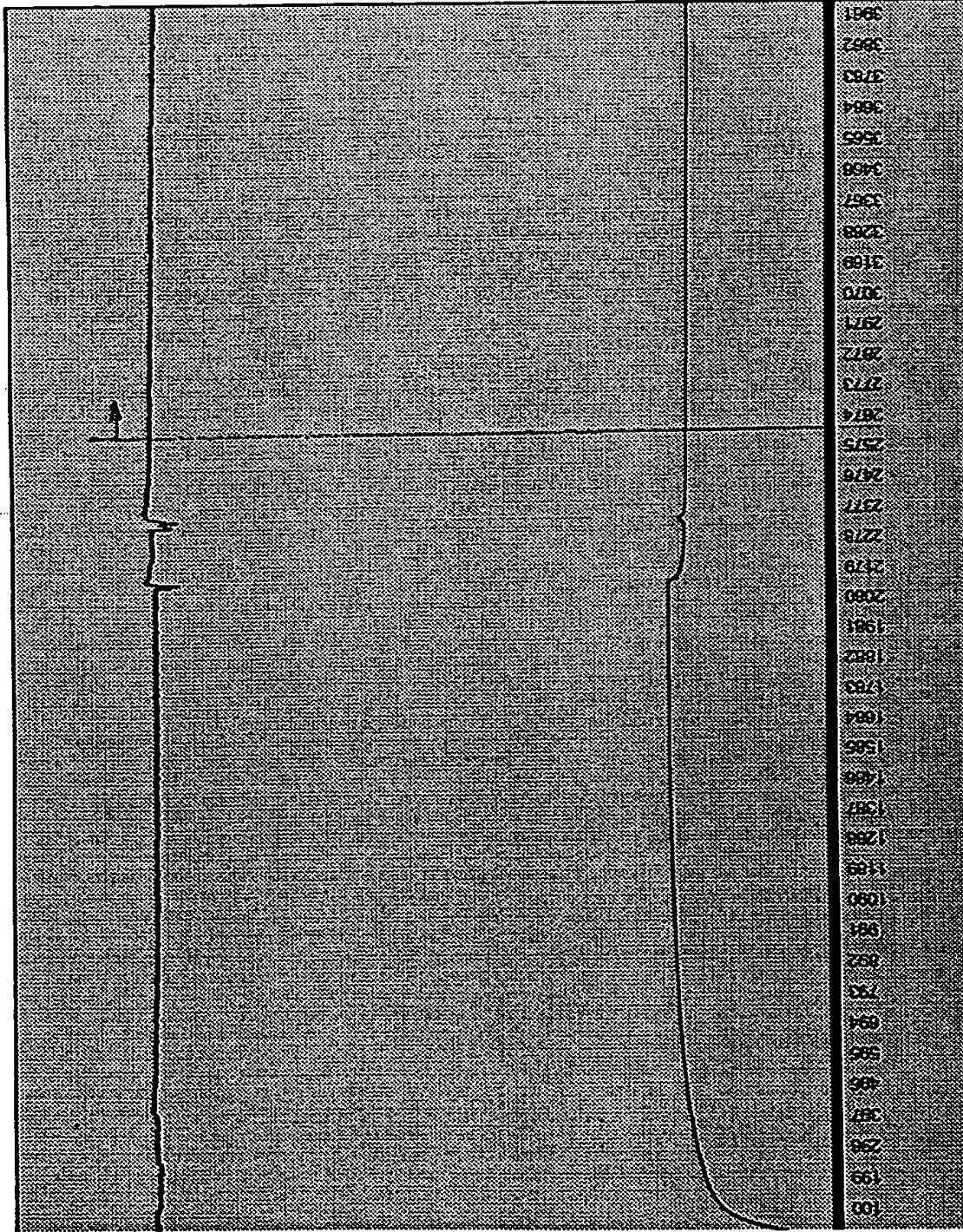
20 cm Control 10-watt point

 \bar{X} σ_n

Vc 2.102 0.005

Win 9.927 0.034

Prior to Additional Media



Time

Time [sec]	Vc	Vc'	X	Win	Vc	Statistics from 300-1350 [11 watt point]	and from 3000-3759 [10 watt point]	5.84 hrs
187	2.096	0.419	0.197	9.864	2.096			
207	2.096	0.419	0.197	9.860	2.096			
227	2.096	0.419	0.197	9.859	2.096			
247	2.096	0.419	0.204	10.213	2.096	11-watt	Average	Max
267	2.096	0.419	0.221	11.031	2.096	Vc	2.355	2.389
287	2.096	0.419	0.221	11.045	2.096	Win	11.085	11.126
307	2.099	0.420	0.221	11.045	2.099	10 watt		
327	2.103	0.421	0.221	11.050	2.103	Vc	2.160	2.168
347	2.109	0.422	0.221	11.050	2.109	Win	9.573	9.807
367	2.114	0.423	0.221	11.045	2.114			
387	2.120	0.424	0.221	11.052	2.120			
407	2.125	0.425	0.221	11.051	2.125			
427	2.130	0.426	0.221	11.046	2.130			
	2.135	0.427	0.221	11.073	2.135			

20 cm Centre /

11 watt

\bar{X} σ_n

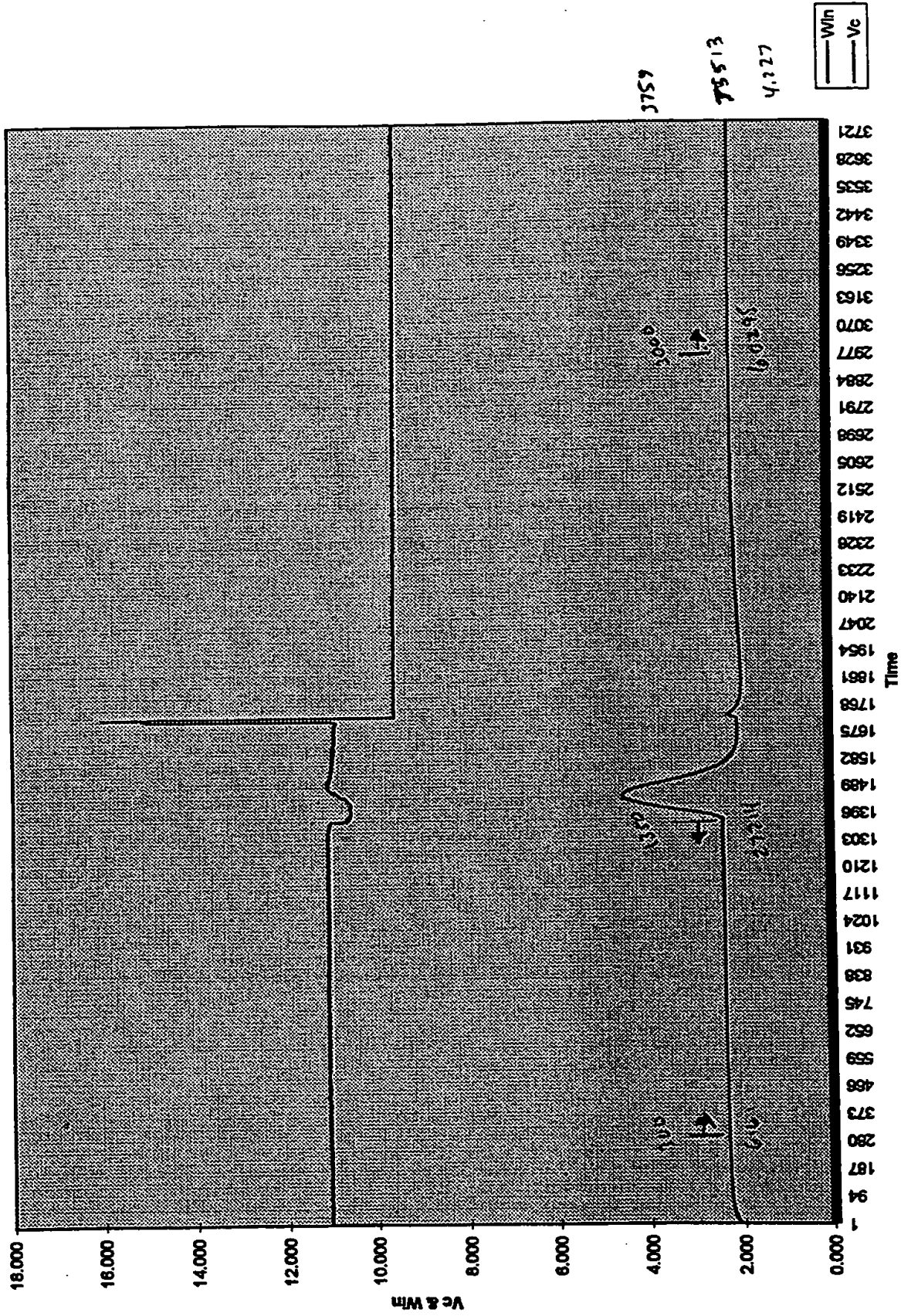
Vc 2.355 0.012

Win 11.085 0.013

10 watt

Vc 2.160 0.004

Win 9.573 0.012



TP030797

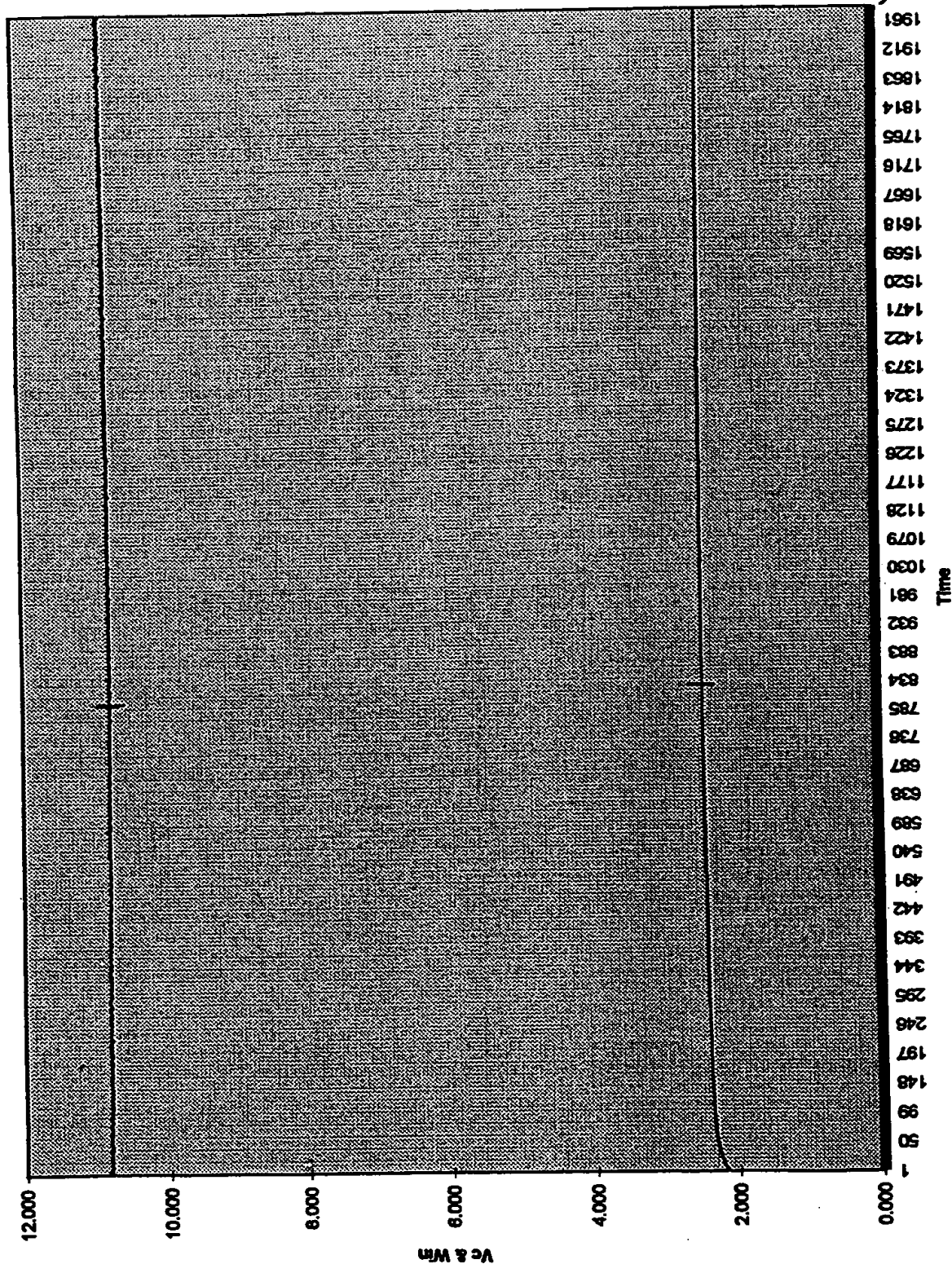
16961866 39317 6.35 hours

Time [sec]	Vc	Vc'	x	Win	Vc	Statistics from 834-1983				Min	Max
99	2.168	0.433	0.211	10.557	2.168	Average	Std Dev			2.439	2.464
119	2.170	0.434	0.217	10.847	2.170	2.453	0.00551			10.778	10.848
139	2.174	0.435	0.217	10.842	2.174	Vc					
159	2.179	0.436	0.217	10.840	2.179	Win					
179	2.184	0.437	0.217	10.838	2.184						
199	2.190	0.438	0.217	10.851	2.190						
219	2.195	0.439	0.217	10.833	2.195						
239	2.201	0.440	0.218	10.824	2.201						
259	2.208	0.441	0.217	10.834	2.208						
279	2.210	0.442	0.217	10.829	2.210						
300	2.214	0.443	0.217	10.830	2.214						
320	2.219	0.444	0.218	10.816	2.219						
340	2.222	0.444	0.218	10.807	2.222						
360	2.228	0.445	0.217	10.828	2.228						
380	2.230	0.448	0.218	10.818	2.230						

20cm control

11 watt point

\bar{V}_c 2.453
 \bar{W}_{in} 10.806
 $\sigma_{\bar{V}_c}$ 0.0055
 $\sigma_{\bar{W}_{in}}$ 0.0111



TP03797P

3 hours

Time (sec)	Vc	Vc'	x	Win	Time (hrs)	Vc	Win	Statistics from Hour 8-11			
								Sid. Dev.	Average	Min	Max
61	2.459	0.492	0.073	3.637	0.017	2.459	3.637	0.009543	1.084258	1.067	1.105
81	2.45	0.49	0.002	0.113	0.022	2.45	0.113	0.094	Vc		
101	2.421	0.484	0.002	0.094	0.028	2.421	0.094	0.081	Win		
121	2.381	0.476	0.002	0.081	0.034	2.381	0.081	0.066			
141	2.339	0.468	0.001	0.066	0.039	2.339	0.066	0.063			
161	2.298	0.46	0.001	0.063	0.045	2.298	0.063	0.071			
181	2.259	0.452	0.001	0.071	0.05	2.259	0.071	0.075			
201	2.221	0.444	0.002	0.075	0.058	2.221	0.075	0.079			
222	2.185	0.437	0.002	0.079	0.062	2.185	0.079	0.077			
241	2.15	0.43	0.002	0.077	0.067	2.15	0.077	0.074			
262	2.116	0.423	0.001	0.074	0.073	2.116	0.074	0.074			
281	2.084	0.417	0.001	0.074	0.078	2.084	0.074	0.073			
302	2.052	0.41	0.001	0.073	0.084	2.052	0.073	0.071			
322	2.022	0.404	0.001	0.071	0.089	2.022	0.071	0.081			
342	1.983	0.398	0.001	0.061	0.095	1.983	0.061	0.057			
362	1.965	0.393	0.001	0.057	0.1	1.965	0.057	0.051			
382	1.937	0.387	0.001	0.051	0.108	1.937	0.051				

20 cm. Control

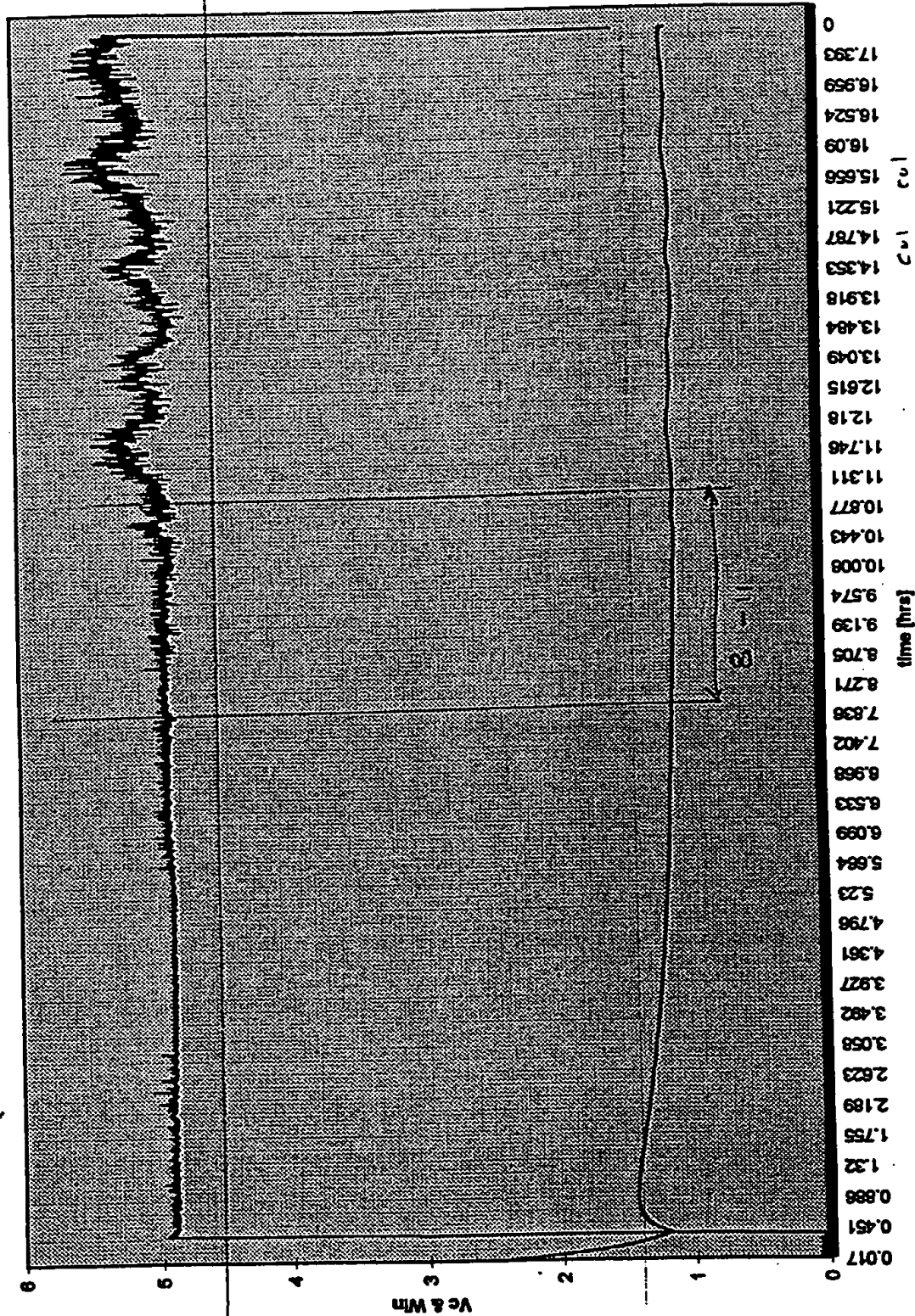
5 watt point

$$\frac{\sigma_n}{\bar{x}}$$

$$V_c = 1.084$$

$$W_{in} = 4.932$$

tp03797p



Row 1436
to 1974

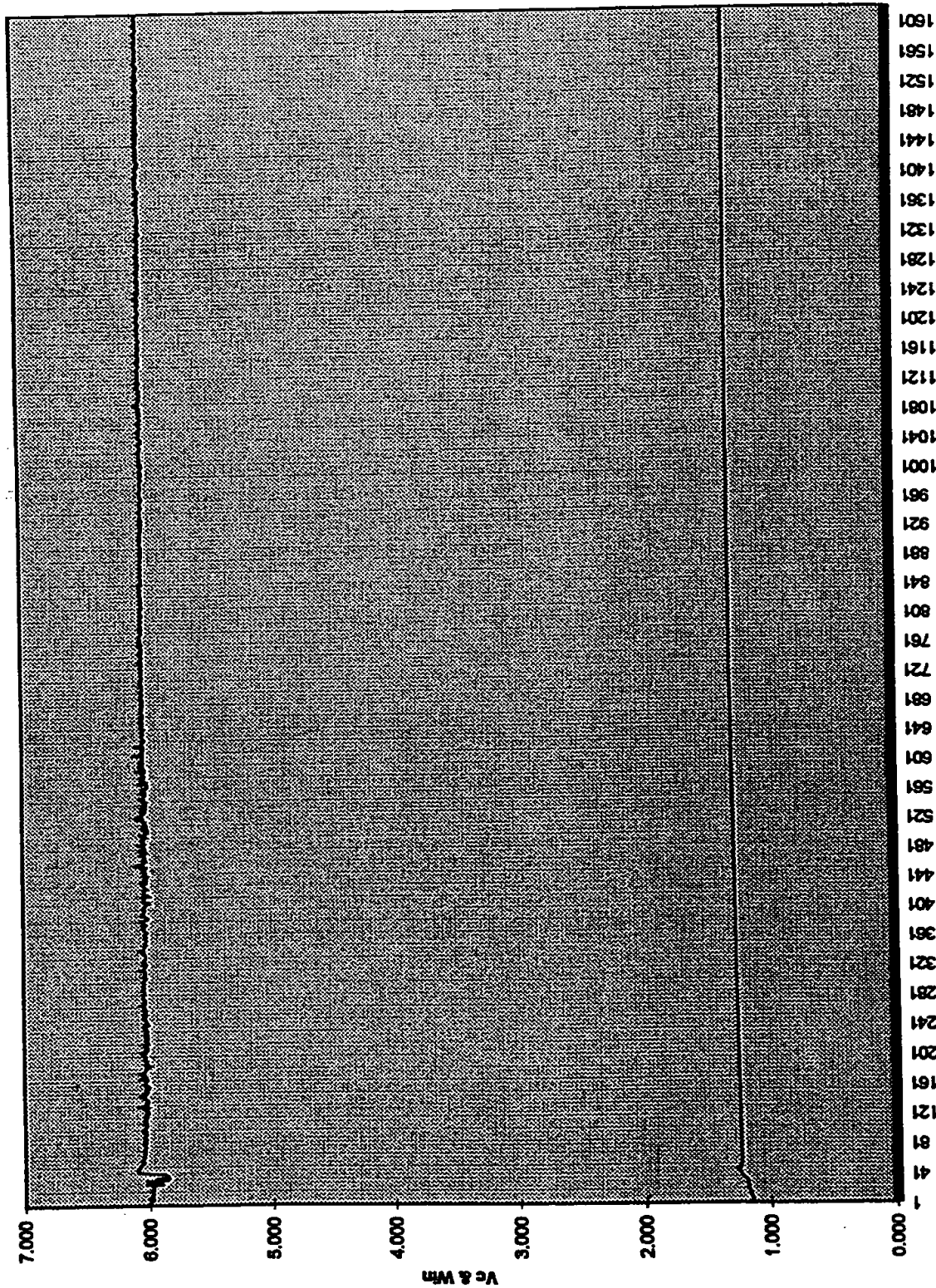
Col 1
Col 2

Col 3
Col 4

TP030897

Time [sec]	Vc	Vc'	x	Win	Vc	Statistics from 1419-1622 [1.13 hrs]				
						Average	Std Dev	Min	Max	
111	1.135	0.227	0.119	5.860	1.135	1.137				
131	1.137	0.227	0.120	6.009	1.137	1.139	0.001	1.297	1.301	
151	1.139	0.228	0.120	6.001	1.139	1.141	0.008	5.987	6.033	
171	1.141	0.228	0.120	5.992	1.141	1.144				
191	1.144	0.228	0.120	5.985	1.144					
211	1.146	0.229	0.120	6.002	1.146					
231	1.148	0.229	0.119	5.974	1.148					
251	1.150	0.230	0.119	5.974	1.150					
271	1.152	0.231	0.119	5.972	1.152					
291	1.154	0.231	0.120	5.982	1.154					
311	1.156	0.231	0.120	6.009	1.156					
331	1.158	0.232	0.120	5.980	1.158					
351	1.161	0.232	0.120	5.980	1.161					

20 cm control
 GwaH point
 \bar{X} 1.299
 σ_c 0.001
 V_c 6.009
 W_{10} 0.008



Time

1601
1561
1521
1481
1441
1401
1361
1321
1281
1241
1201
1161
1121
1081
1041
1001
961
921
881
841
801
761
721
681
641
601
561
521
481
441
401
361
321
281
241
201
161
121
81
41
1

1414
1622

28521
32541
4667 1.13

Page 1

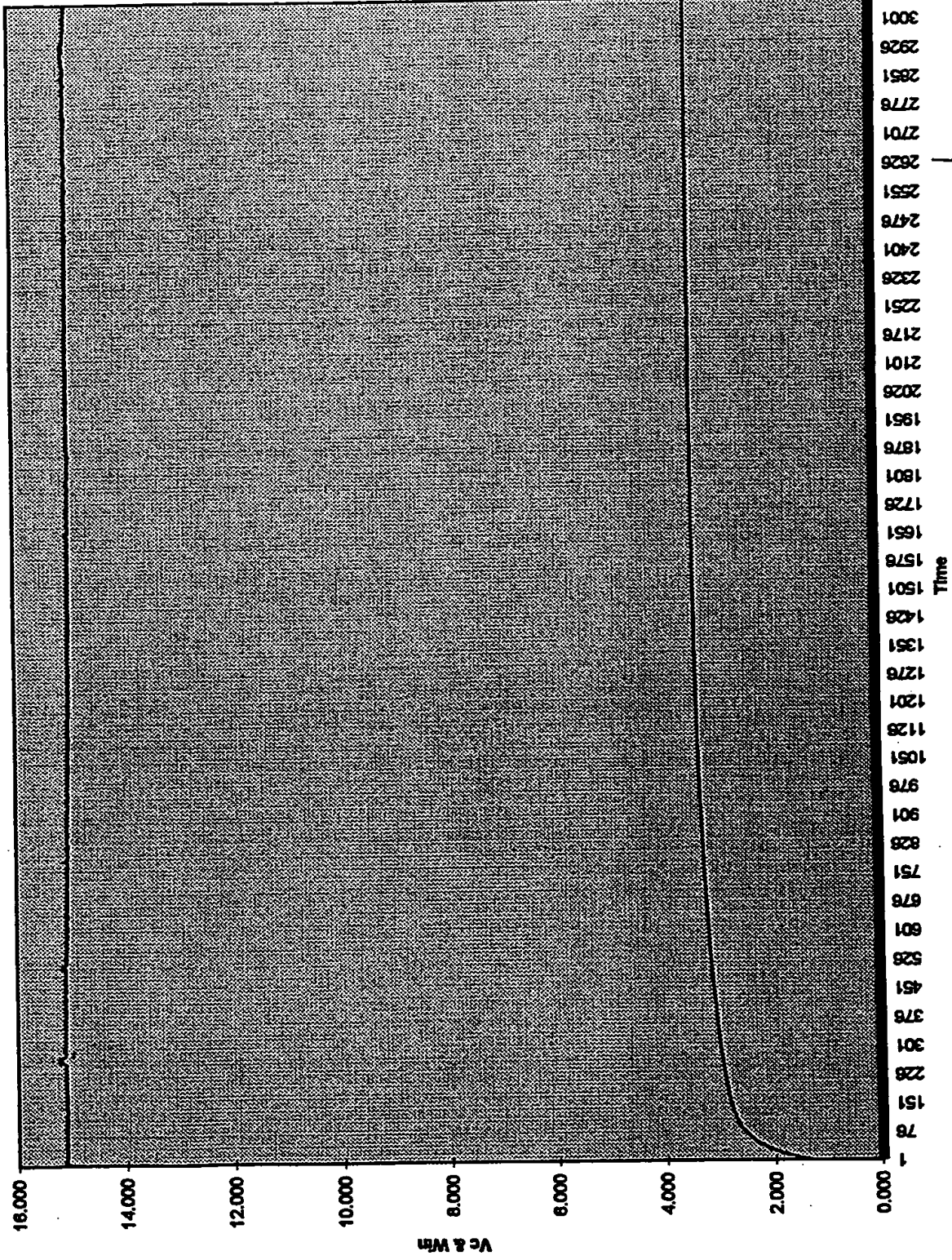
TP030897p

Time [sec]	Vc	Vc'	x	Win	Vc	Statistics from 2650-3059	2.278 Hrs		
64	1.301	0.260	0.294	14.686	1.301	Average	Std Dev	Min	Max
84	1.322	0.264	0.298	14.890	1.322	3.451	0.008	3.441	3.481
105	1.358	0.271	0.299	14.938	1.358	Vc			
124	1.397	0.279	0.298	14.951	1.397	Win	0.018	14.937	15.034
145	1.437	0.287	0.301	15.071	1.437				
164	1.475	0.295	0.302	15.104	1.475				
185	1.512	0.302	0.302	15.116	1.512				
205	1.548	0.310	0.303	15.128	1.548				
225	1.583	0.317	0.303	15.141	1.583				
245	1.616	0.323	0.303	15.145	1.616				
265	1.649	0.330	0.303	15.145	1.649				
285	1.679	0.336	0.303	15.146	1.679				
305	1.709	0.342	0.303	15.131	1.709				

20 cm Control
 15 watt point

$$\frac{\bar{x}}{V_c} = \frac{3.451}{0.006}$$

$$\frac{\sigma_n}{W_{in}} = \frac{14.982}{0.018}$$



3050 2650 5350
61356 8201 2.27

TP030997

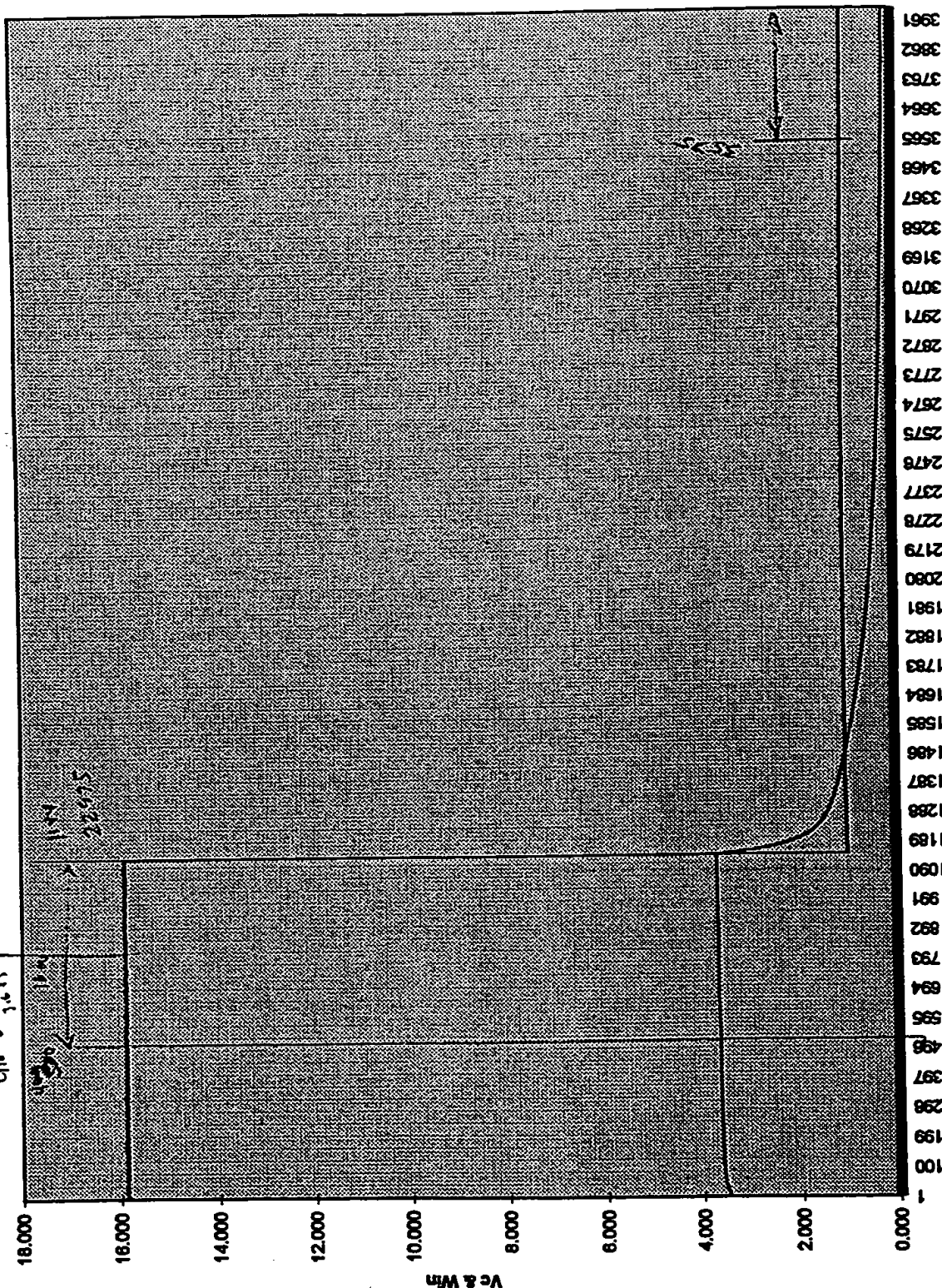
Time [sec]	Vc	Vc'	x	Win	Vc	Statistics from 770-1144 [1.944 hrs] for 16 watt point and from 4531-4789 [1.437 hrs] for 1 watt point			
						Average	Std Dev	Min	Max
79	3.453	0.691	0.316	15.791	3.453				
99	3.455	0.691	0.316	15.783	3.455				
119	3.459	0.692	0.316	15.809	3.459	16-watt			
139	3.463	0.693	0.317	15.834	3.463	Vc	3.664	0.005	3.671
159	3.466	0.693	0.317	15.835	3.466	Win	15.885	0.012	15.93
179	3.47	0.695	0.317	15.832	3.47	1 watt			
199	3.473	0.695	0.317	15.841	3.473	Vc	0.174	0.001	0.176
219	3.476	0.696	0.317	15.865	3.476	Win	1.054	0.007	1.078
239	3.479	0.696	0.318	15.878	3.479				
259	3.482	0.697	0.317	15.871	3.482		0.174	0.001	0.176
279	3.485	0.697	0.317	15.865	3.485		1.054	0.007	1.078
299	3.488	0.698	0.317	15.855	3.488				
319	3.49	0.698	0.318	15.875	3.49				
339	3.493	0.699	0.317	15.872	3.493				
360	3.495	0.699	0.318	15.885	3.495				

20 cm Control

16 watt \bar{X} σ_n
Vc 3.664 0.005
Win 15.885 0.012
1 watt
Vc 0.174 0.001
Win 1.034 0.007

TP030987 Chart 1

125477
31855
11944 hrs



Time

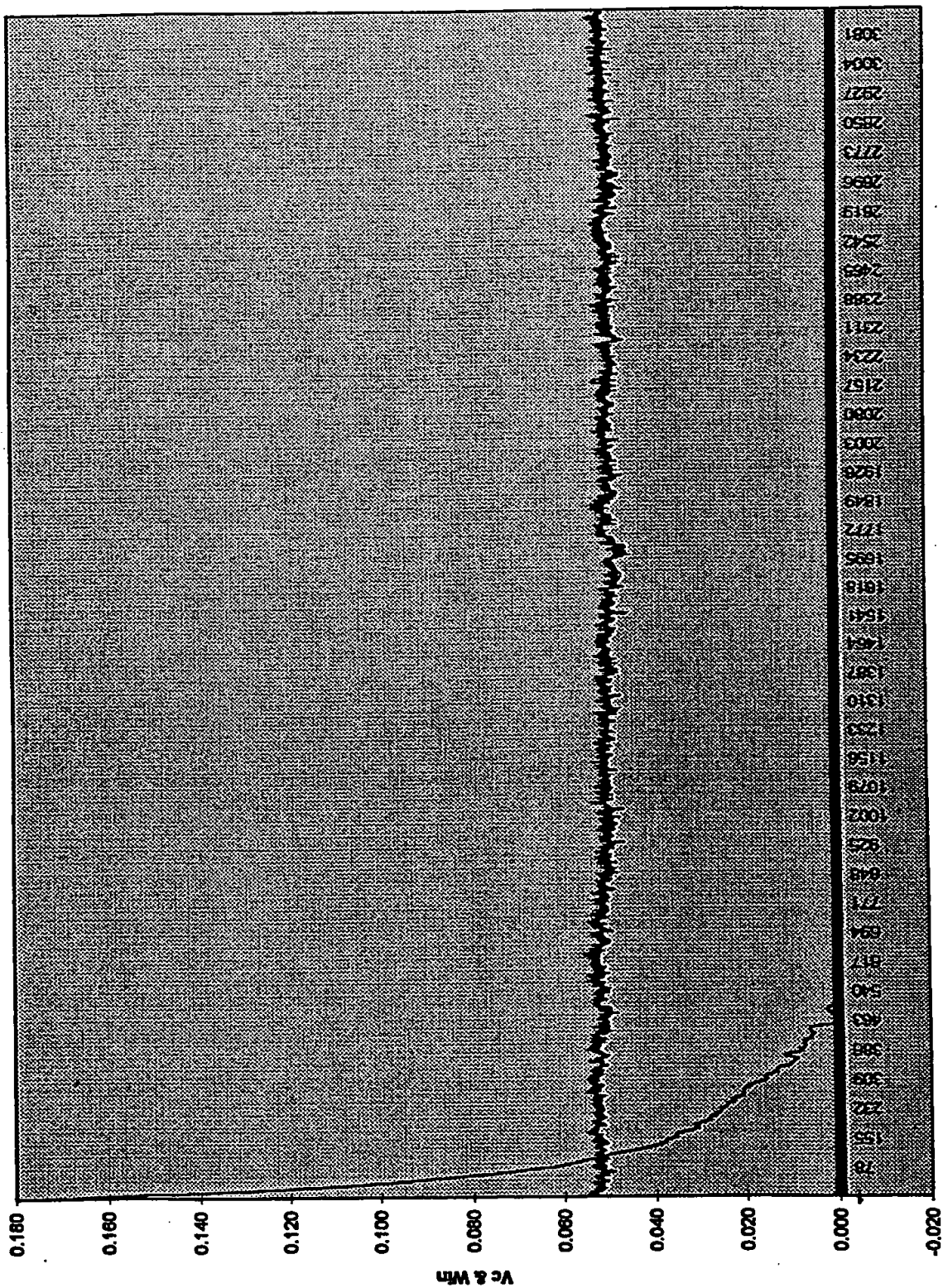
35754531, 4789
71715 96056
90883
176 .175
1.4371

Time [sec]	Vc	Vc'	x	Win	Vc	Statistics from 502-3147 [16.67 hrs]						
						Average	Std Dev	Min	Max			
87	0.174	0.035	0.001	0.048	0.174	0.000	0.000	0.000	0.001			
107	0.172	0.034	0.001	0.053	0.172	0.000	0.000	0.000	0.001			
127	0.169	0.034	0.001	0.054	0.169	0.000	0.001	0.044	0.055			
147	0.166	0.033	0.001	0.053	0.166	0.050	0.001					
167	0.163	0.033	0.001	0.054	0.163							
188	0.161	0.032	0.001	0.053	0.161							
207	0.158	0.032	0.001	0.055	0.158							
228	0.156	0.031	0.001	0.054	0.156							
247	0.153	0.031	0.001	0.053	0.153							
268	0.151	0.030	0.001	0.053	0.151							
288	0.148	0.029	0.001	0.054	0.148							
308	0.146	0.029	0.001	0.054	0.146							
328	0.143	0.028	0.001	0.054	0.143							
348	0.141	0.028	0.001	0.052	0.141							
368	0.139	0.028	0.001	0.053	0.139							

20 cm control

0 watt point

\bar{x} 0.000
 σ_n 0.000
 V_c 0.050
 W_{in} 0.001



[illegible][illegible]

Time [sec]	Vc	Vc'	x	Win	Vc	Statistics from 2825-3870 [5.82 hrs]							
						Average	Std Dev	Min	Max				
69	0.000	0.000	0.000	0.190	0.000	2.333	0.002	2.328	2.336				
89	0.000	0.000	0.000	0.190	0.000								
109	0.008	0.002	0.002	0.192	0.000	0.008	0.008	0.002	2.328				
129	0.032	0.006	0.006	0.194	0.000	0.032	0.012	0.012	9.647				
149	0.059	0.012	0.012	0.195	0.000	0.059							
169	0.088	0.017	0.017	0.196	0.000	0.088							
189	0.118	0.023	0.023	0.197	0.000	0.118							
209	0.149	0.030	0.030	0.198	0.000	0.149							
229	0.180	0.036	0.036	0.199	0.000	0.180							
249	0.212	0.042	0.042	0.199	0.000	0.212							
269	0.244	0.049	0.049	0.199	0.000	0.244							
289	0.277	0.055	0.055	0.199	0.000	0.277							
309	0.309	0.062	0.062	0.199	0.000	0.309							
330	0.341	0.068	0.068	0.200	0.000	0.341							
348	0.372	0.074	0.074	0.199	0.000	0.372							
370	0.403	0.080	0.080	0.199	0.000	0.403							
390	0.433	0.086	0.086	0.199	0.000	0.433							

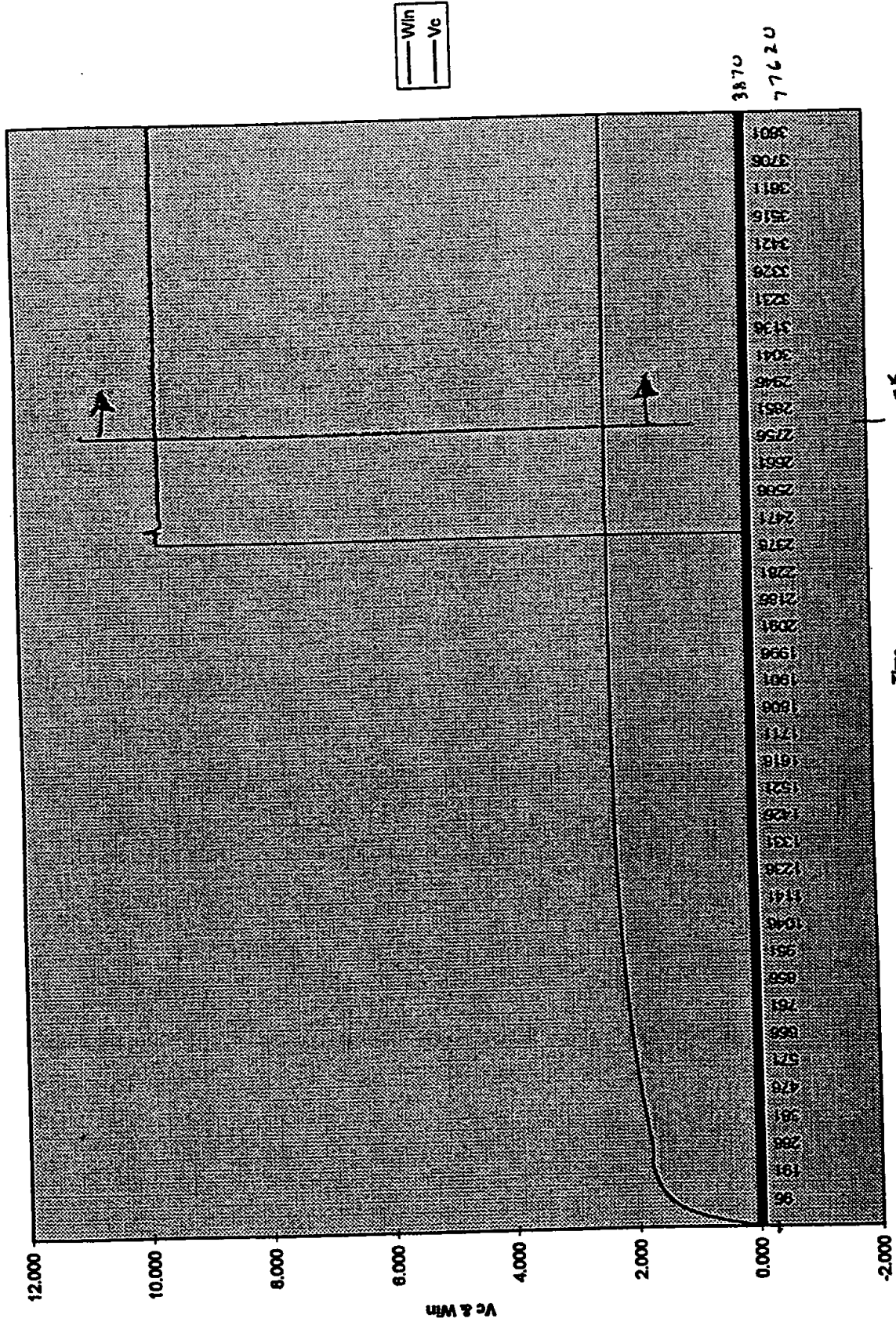
From Calibration Line

$$V_c = 2.333$$

≈ 10.260 watts expected

$$\text{excess watts} = \boxed{0.577}$$

TP031287 Chart 1



Time [sec]	Vc	Vc'	x	Win	Vc	Statistics from 2-2004 [5.575 hrs]							
						Average	Std Dev	Min	Max				
45	2.333	0.466	0.194	9.698	2.333	2.323	0.009	2.309	2.378				
55	2.333	0.467	0.194	9.694	2.333	9.880	0.060	9.657	9.998				
65	2.333	0.467	0.194	9.690	2.333								
76	2.333	0.467	0.194	9.686	2.333								
85	2.334	0.467	0.194	9.714	2.334								
98	2.334	0.467	0.194	9.693	2.334								
106	2.334	0.467	0.194	9.695	2.334								
116	2.334	0.467	0.194	9.692	2.334								
128	2.334	0.467	0.194	9.698	2.334								
136	2.334	0.467	0.194	9.678	2.334								
147	2.334	0.467	0.193	9.657	2.334								
158	2.334	0.467	0.194	9.694	2.334								
166	2.334	0.467	0.194	9.705	2.334								
176	2.334	0.467	0.194	9.694	2.334								
186	2.333	0.467	0.194	9.723	2.333								
196	2.333	0.467	0.194	9.708	2.333								
206	2.334	0.467	0.194	9.682	2.334								

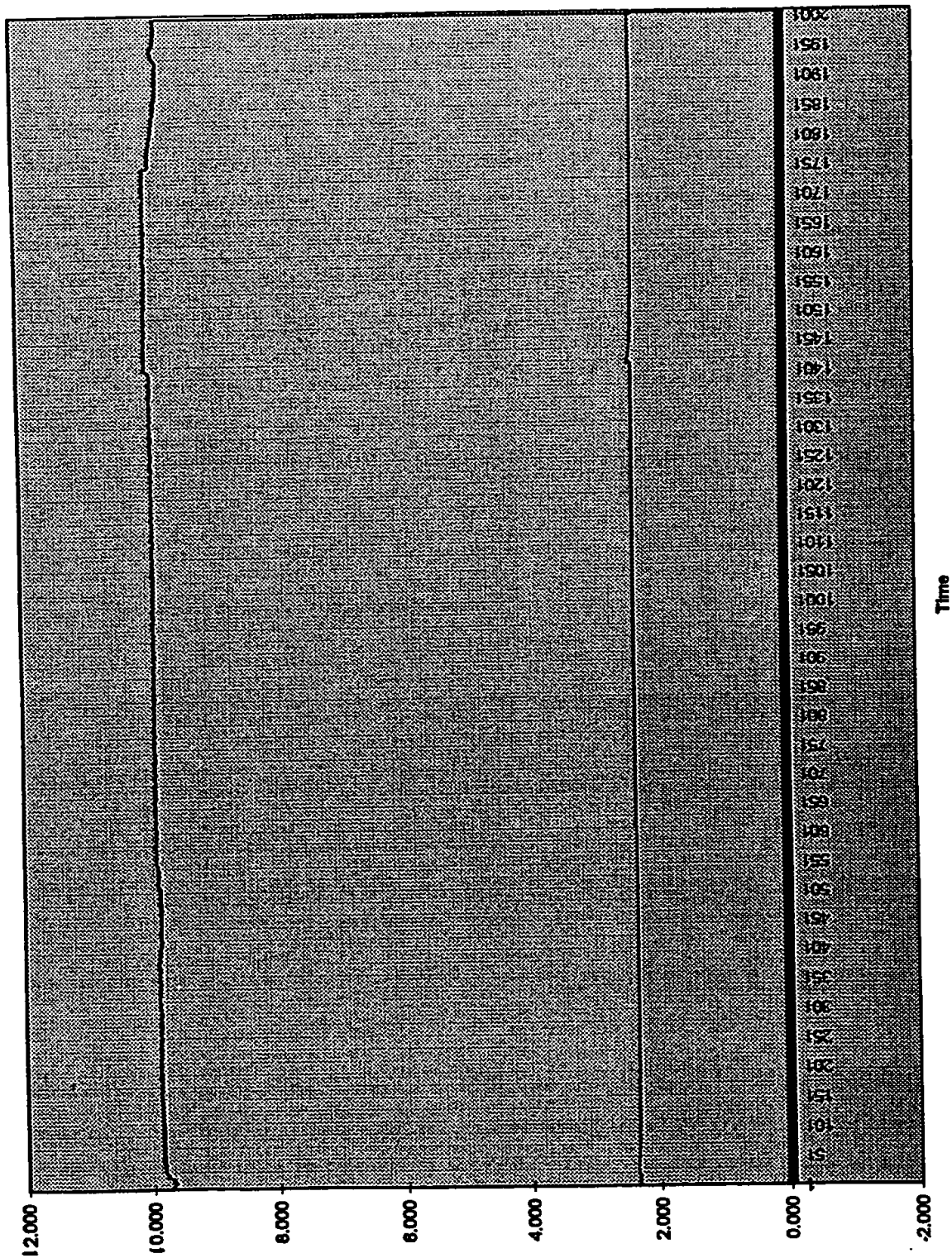
From Calibration Line

$$V_c = 2.323$$

$$= 10.217 \text{ watts expected}$$

$$\text{excess watts } \boxed{0.337 \text{ watts}}$$

TPO31397 Chart 1



Time

Time [sec]	Vc	Vc'	x	Win	Vc	Statistics from 5555 to 7089 [4.272 hrs]					
						Average	Std Dev	Min	Max		
49	0.000	0.000	0.011	0.000	0.000						
59	0.000	0.000	0.159	0.000	0.000			2.399	2.437		
69	0.000	0.000	0.198	0.000	0.000	Vc	0.010	9.671	9.945		
79	0.000	0.000	0.198	0.000	0.000	Win	0.056				
89	0.004	0.001	0.198	3.982	0.004						
99	0.023	0.004	0.198	3.951	0.023						
109	0.044	0.009	0.198	3.957	0.044						
119	0.067	0.013	0.197	9.858	0.067						
129	0.089	0.018	0.198	9.797	0.089						
139	0.111	0.022	0.198	9.816	0.111						
149	0.132	0.028	0.198	9.817	0.132						
159	0.152	0.030	0.198	9.815	0.152						
169	0.171	0.034	0.198	9.801	0.171						
179	0.189	0.038	0.198	9.809	0.189						
189	0.207	0.041	0.198	9.798	0.207						
199	0.224	0.045	0.194	9.724	0.224						

From Calibration Line

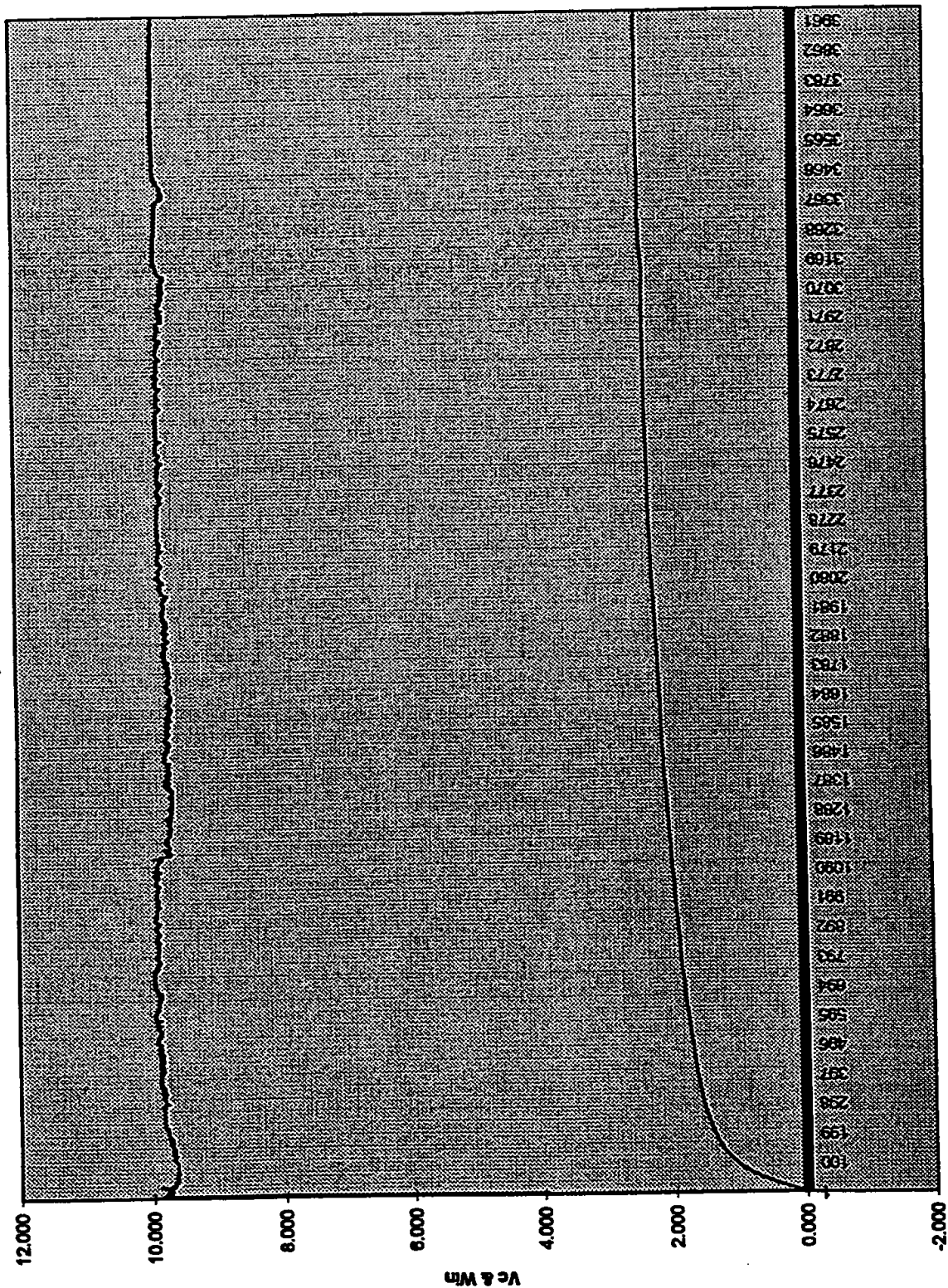
$$V_c = 2.419$$

$$= 10.628 \text{ watts expected}$$

$$\text{Excess Watts} = \boxed{0.804}$$

March 5 - March 10, 1997

Win	Predicted Vc	Given Vc=	Estimated	Watts Out	Actual =				
0	-0.0605	2.419							
1	0.1728								
2	0.4061			10.628	watts of power				
3	0.6394			9.824	watts of input power				
4	0.8727			0.804	excess watts of power produced				
5	1.106								
6	1.3393								
7	1.5726								
8	1.8059								
9	2.0392								
10	2.2725								
11	2.5058								
12	2.7391								
13	2.9724								
14	3.2057								
15	3.439								
16	3.6723								



Time

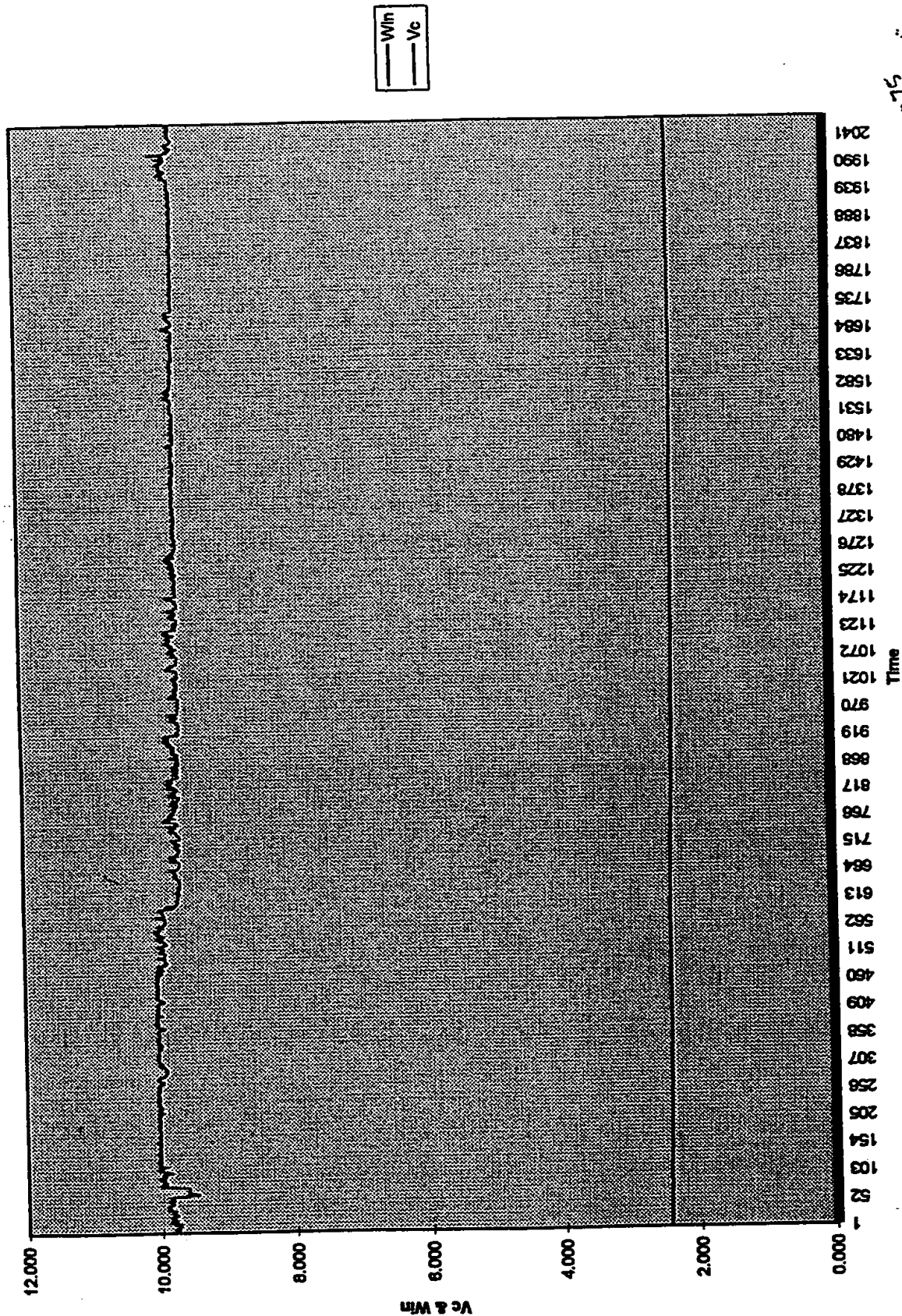
5555 55716 2.9
987,
End 7067 71094 2.1
9921

Time [sec]	Vc	Vc'	x	WIn	Vc	Statistics from 2 to 2076 [2.899 hrs]						
15	2.438	0.488	0.198	9.791	2.438	Average	Std Dev	Min	Max			
22	2.438	0.488	0.195	9.743	2.438	Vc	0.042	2.289	2.438			
25	2.438	0.488	0.198	9.777	2.438	Win	0.140	9.442	10.081			
30	2.438	0.488	0.195	9.761	2.438							
35	2.438	0.488	0.195	9.765	2.438							
40	2.438	0.488	0.198	9.799	2.438							
45	2.438	0.488	0.196	9.814	2.438							
50	2.438	0.487	0.195	9.753	2.438							
55	2.437	0.487	0.196	9.798	2.437							
60	2.437	0.487	0.196	9.780	2.437							
65	2.437	0.487	0.195	9.752	2.437							
70	2.436	0.487	0.195	9.756	2.436							
75	2.435	0.487	0.195	9.751	2.435							
80	2.435	0.487	0.194	9.716	2.435							
85	2.435	0.487	0.196	9.798	2.435							
90	2.434	0.487	0.198	9.815	2.434							
95	2.434	0.487	0.198	9.789	2.434							

March 5 - March 10, 1997

	Win	Predicted Vc						
	0	-0.0605		Given Vc=	2.350			
	1	0.1728		Estimated				
	2	0.4061		Watts Out	10.333	watts of power		
	3	0.6394		Actual =	9.765	watts of input power		
	4	0.8727			0.568	excess watts of power produced		
	5	1.106						
	6	1.3393						
	7	1.5726						
	8	1.8059						
	9	2.0392						
	10	2.2725						
	11	2.5058						
	12	2.7391						
	13	2.9724						
	14	3.2057						
	15	3.439						
	16	3.6723						

TP031697 Chart 1



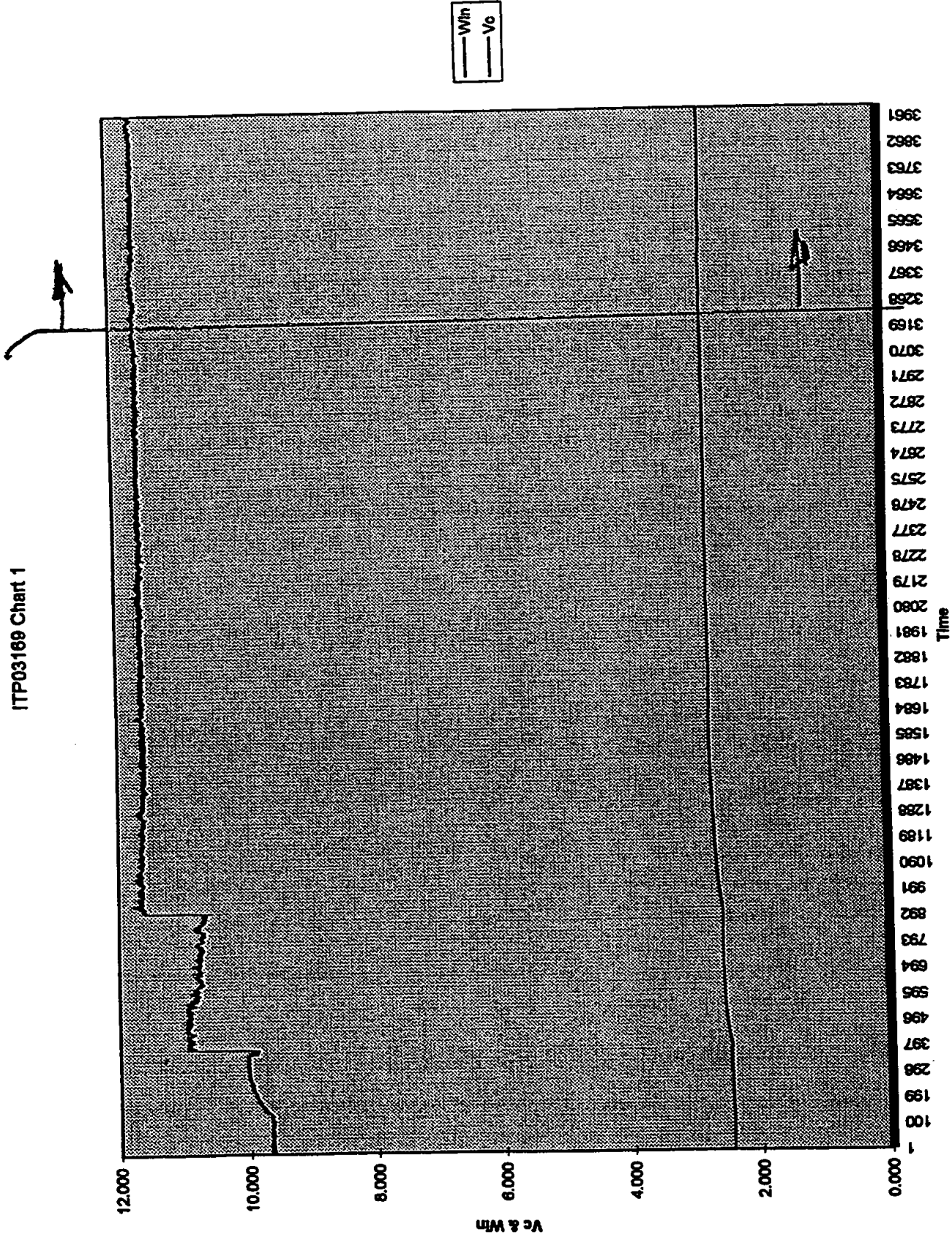
3E401
SL02, 2007

Time [sec]	Vc	Vc'	x	Win	Vc	Statistics from 3211 to 13017 [13.635 hrs]						
						Average	Std Dev	Min	Max			
39	2.434	0.487	0.193	9.847	2.434	2.793	0.016	2.767	2.827			
44	2.434	0.487	0.193	9.858	2.434							
49	2.434	0.487	0.193	9.880	2.434	Vc						
54	2.435	0.487	0.193	9.880	2.435	Win	11.624	11.531	11.787			
59	2.435	0.487	0.193	9.850	2.435							
64	2.435	0.487	0.193	9.885	2.435							
69	2.435	0.487	0.193	9.857	2.435							
74	2.435	0.487	0.194	9.884	2.435							
79	2.435	0.487	0.193	9.883	2.435							
86	2.435	0.487	0.193	9.858	2.435							
89	2.435	0.487	0.193	9.835	2.435							
94	2.435	0.487	0.193	9.843	2.435							
99	2.435	0.487	0.193	9.841	2.435							
104	2.435	0.487	0.193	9.852	2.435							
109	2.435	0.487	0.193	9.880	2.435							
114	2.435	0.487	0.194	9.880	2.435							
119	2.435	0.487	0.194	9.876	2.435							

March 5 - March 10, 1997

	Win	Predicted Vc						
	0	-0.0605	Given Vc=	2.793				
	1	0.1728	Estimated					
	2	0.4061	Watts Out	12.231	watts of power			
	3	0.6394	Actual =	11.624	watts of input power			
	4	0.8727		0.607	excess watts of power produced			
	5	1.106						
	6	1.3393						
	7	1.5726						
	8	1.8059						
	9	2.0392						
	10	2.2725						
	11	2.5058						
	12	2.7391						
	13	2.9724						
	14	3.2057						
	15	3.439						
	16	3.6723						

ITP03169 Chart 1

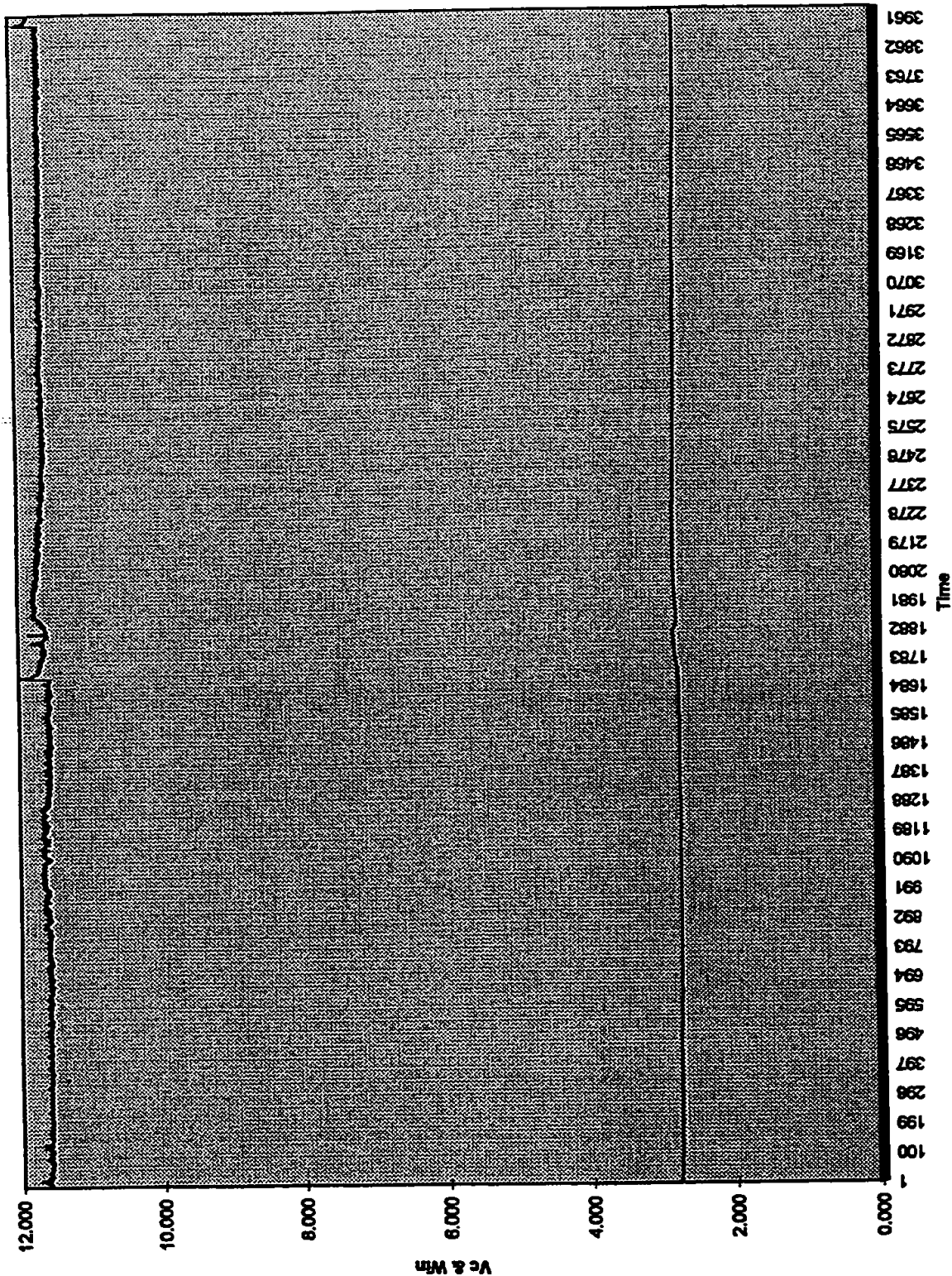


3211 16124 2.770
 13017 65275 2.777
 13.653 hrs

Time [sec]	Vc	Vc'	x	Win	Vc	Statistics from 2 to 5363 [7.464hrs]					
						Vc	Win	Average	Std Dev	Min	Max
27	2.773	0.555	0.233	11.627	2.773						
32	2.773	0.555	0.232	11.618	2.773						
38	2.773	0.555	0.233	11.64	2.773						
42	2.773	0.555	0.233	11.641	2.773						
48	2.773	0.555	0.232	11.619	2.773						
52	2.773	0.555	0.232	11.603	2.773						
57	2.773	0.555	0.232	11.624	2.773						
62	2.773	0.555	0.232	11.614	2.773						
67	2.773	0.555	0.232	11.607	2.773						
72	2.773	0.555	0.233	11.643	2.773						
77	2.773	0.555	0.233	11.625	2.773						
82	2.773	0.555	0.232	11.604	2.773						
87	2.773	0.555	0.233	11.643	2.773						
92	2.773	0.555	0.233	11.649	2.773						
97	2.773	0.555	0.234	11.676	2.773						
102	2.773	0.555	0.234	11.66	2.773						
107	2.773	0.555	0.233	11.668	2.773						
112	2.773	0.555	0.233	11.66	2.773						
117	2.773	0.555	0.233	11.64	2.773						

[illegible]

TP031797 Chart 1



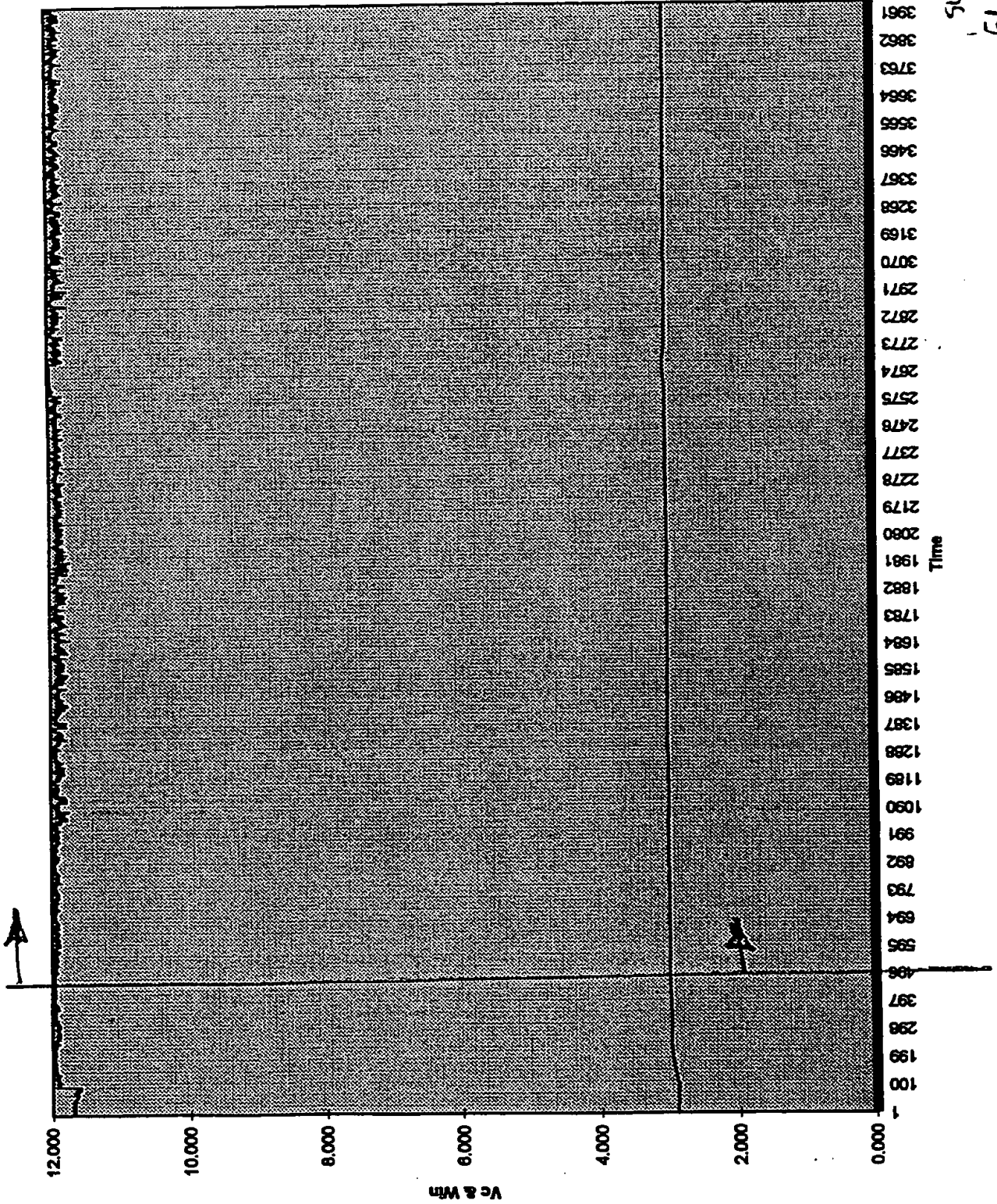
— Win
— Vc

Page 1

2	2.7	2.773	11.627
5363	2.6848	2.882	11.679
			7.464

Time [sec]	Vc	Vc'	x	Win	Vc	Statistics from 500 to 6686 [14.439 hrs]							
32	2.882	0.577	0.234	11.688	2.882	Average	Std Dev	Min	Max				
37	2.882	0.577	0.233	11.670	2.882	Vc	2.985	0.008	2.968	3.019			
42	2.882	0.577	0.233	11.669	2.882	Win	11.890	0.062	11.700	11.998			
47	2.882	0.577	0.234	11.684	2.882								
52	2.882	0.577	0.234	11.679	2.882								
25	2.882	0.577	0.234	11.680	2.882								
35	2.882	0.577	0.234	11.692	2.882								
45	2.882	0.577	0.234	11.703	2.882								
55	2.882	0.577	0.234	11.687	2.882								
65	2.883	0.577	0.234	11.686	2.883								
75	2.883	0.577	0.234	11.691	2.883								
85	2.883	0.577	0.234	11.681	2.883								
95	2.883	0.577	0.234	11.692	2.883								
105	2.883	0.577	0.234	11.690	2.883								
115	2.883	0.577	0.234	11.684	2.883								
126	2.883	0.577	0.233	11.667	2.883								

Win	Predicted Vc	Given Vc=	2.985
0	-0.0605	Estimated	
1	0.1728	Watts Out	13.054 watts of power
2	0.4061	Actual =	11.89 watts of input power
3	0.6394		1.164 excess watts
4	0.8727		
5	1.106		
6	1.3393		
7	1.5726		
8	1.8059		
9	2.0392		
10	2.2725		
11	2.5058		
12	2.7391		
13	2.9724		
14	3.2057		
15	3.439		
16	3.6723		



— Wm
— Vc

2.988
11.554
2.997
11.957

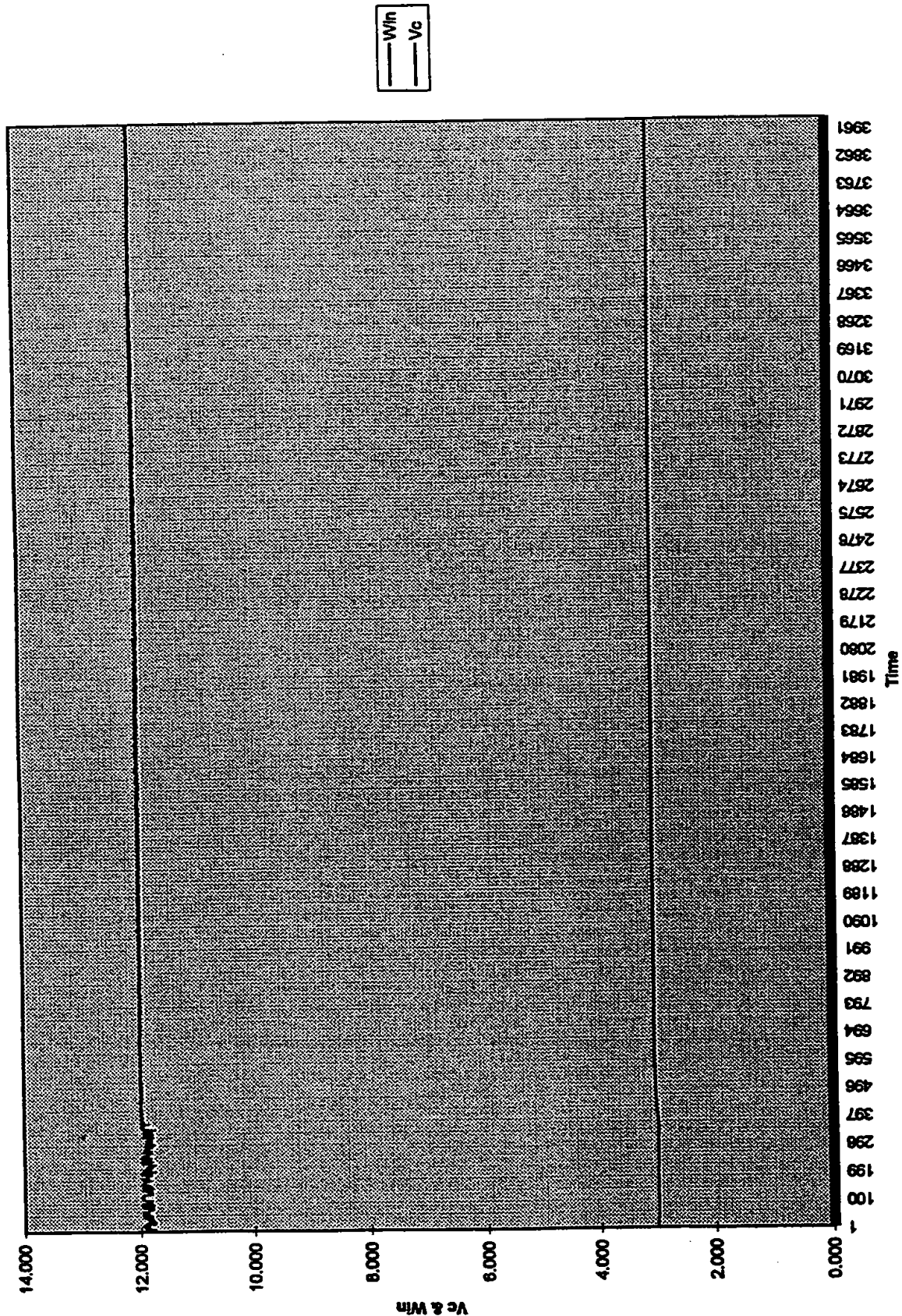
500 476.7
5685 5691.6

Time [sec]	Vc	Vc'	x	Win	Vc	Statistics from 2 to 1198 [31.194 hrs]					
						Average	Std Dev	Min	Max		
60	3.009	0.602	0.238	11.898	3.009						
70	3.009	0.602	0.238	11.876	3.009						
80	3.008	0.602	0.237	11.866	3.008						
90	3.008	0.602	0.238	11.876	3.008						
100	3.008	0.602	0.236	11.820	3.008						
110	3.007	0.602	0.237	11.866	3.007						
120	3.008	0.602	0.237	11.862	3.008						
131	3.005	0.602	0.236	11.787	3.005						
140	3.005	0.601	0.238	11.882	3.005						
150	3.004	0.601	0.238	11.807	3.004						
160	3.004	0.601	0.235	11.757	3.004						
170	3.003	0.601	0.235	11.752	3.003						
180	3.003	0.601	0.238	11.909	3.003						
190	3.002	0.601	0.239	11.931	3.002						
200	3.001	0.601	0.238	11.904	3.001						
210	3.001	0.601	0.238	11.893	3.001						
220	3.001	0.601	0.238	11.895	3.001						

March 5 - March 10, 1997

	Win	Predicted Vc						
	0	-0.0605	Given Vc=	2.999				
	1	0.1728	Estimated					
	2	0.4061	Watts Out	13.114	watts of power			
	3	0.6394	Actual =	11.883	watts of input power			
	4	0.8727		1.231	excess watts			
	5	1.106						
	6	1.3393						
	7	1.5726						
	8	1.8059						
	9	2.0392						
	10	2.2725						
	11	2.5058						
	12	2.7391						
	13	2.9724						
	14	3.2057						
	15	3.439						
	16	3.6723						

TP031897 Chart 1



2	60	11,840	3.007
11198	112300	11.619	2.861

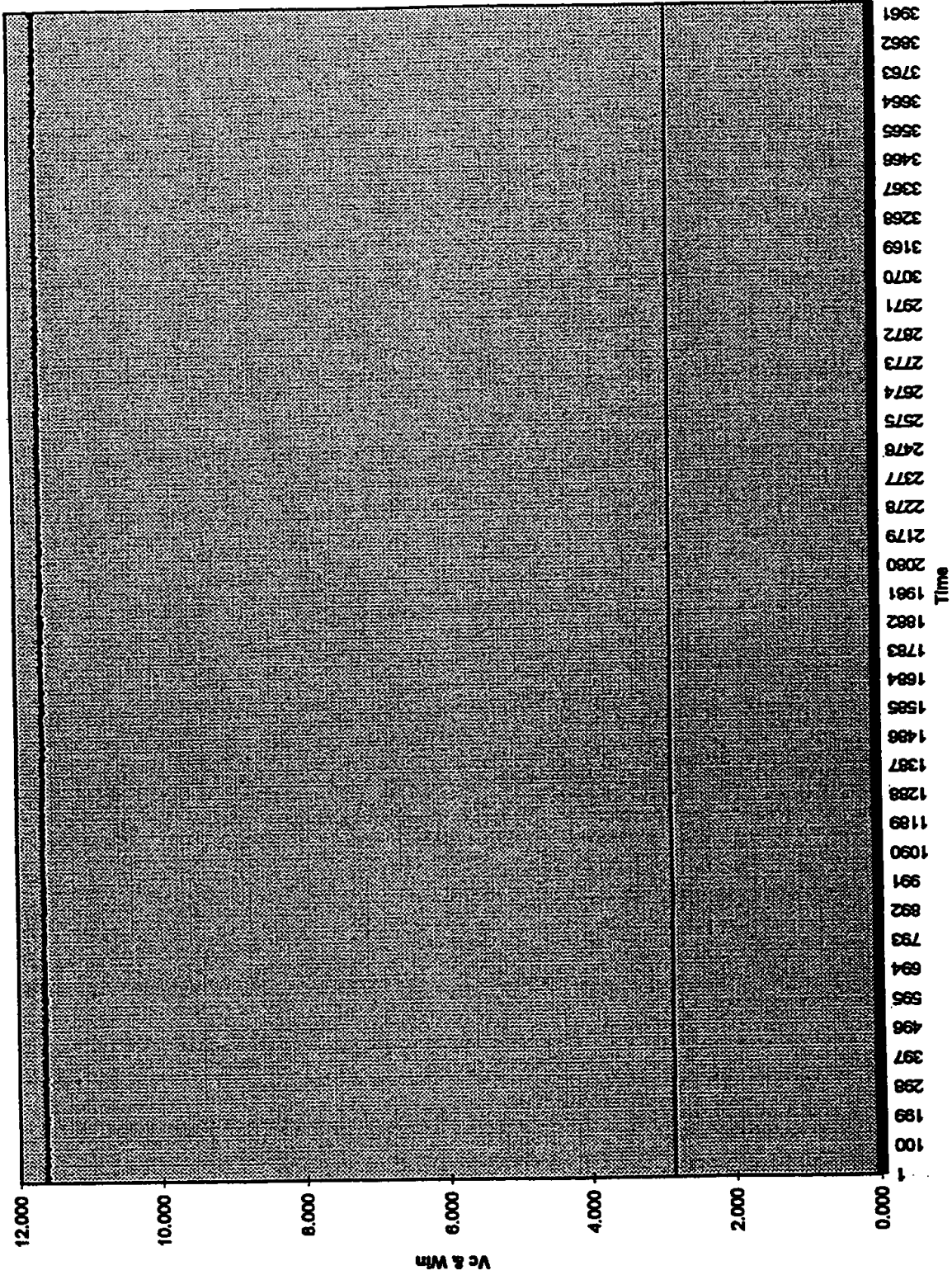
Time [sec]	Vc	Vc'	x	Win	Vc	Statistics from 2 to 5310 [14.761 hrs]				Statistics from 5311 to 6594 [3.576 hrs]			
35	2.861	0.573	0.232	11.583	2.861	Average	Std Dev	Min	Max				
45	2.861	0.573	0.232	11.608	2.861	Vc	0.004	2.847	2.862				
55	2.861	0.573	0.232	11.624	2.861	Win	0.024	11.533	11.779				
65	2.861	0.573	0.232	11.610	2.861								
75	2.861	0.573	0.232	11.597	2.861								
85	2.861	0.573	0.233	11.628	2.861								
95	2.861	0.573	0.233	11.632	2.861	Average	Std Dev	Min	Max				
105	2.861	0.573	0.233	11.631	2.861	Vc	0.001	2.842	2.849				
115	2.861	0.573	0.233	11.630	2.861	Win	0.011	11.874	11.982				
125	2.861	0.573	0.233	11.628	2.861								
135	2.861	0.573	0.233	11.645	2.861								
145	2.861	0.573	0.233	11.635	2.861								
155	2.861	0.573	0.233	11.654	2.861								
165	2.861	0.573	0.233	11.641	2.861								
175	2.860	0.573	0.233	11.642	2.860								
186	2.861	0.573	0.233	11.645	2.861								
195	2.861	0.573	0.232	11.577	2.861								

Win	Predicted Vc	Given Vc=	Estimated	Watts Out	Actual =	Watts of power	Watts of input power	excess watts
0	-0.0605	2.857						
1	0.1728							
2	0.4061			12.506				
3	0.6394			11.627				
4	0.8727			0.879				
5	1.106							
6	1.3393							
7	1.5726							
8	1.8059							
9	2.0392							
10	2.2725							
11	2.5058							
12	2.7391							
13	2.9724							
14	3.2057							
15	3.439							
16	3.6723							

March 5 - March 10, 1997

	<u>Win</u>	<u>Predicted Vc</u>					
	0	-0.0605		Given Vc=	2.843		
	1	0.1728		Estimated			
	2	0.4061		Watts Out	12.446	watts of power	
	3	0.6394		Actual =	11.909	watts of input power	
	4	0.8727			0.537	excess watts	
	5	1.106					
	6	1.3393					
	7	1.5726					
	8	1.8059					
	9	2.0392					
	10	2.2725					
	11	2.5058					
	12	2.7391					
	13	2.9724					
	14	3.2057					
	15	3.439					
	16	3.6723					

TP031997 Chart 1



5311 5324
6594 6611

Time [sec]	Vc	Vc'	x	Win	Vc	Statistics from 600 to 3067 [6.870 hrs]						
						Vc	Win	Average	Std Dev	Min	Max	
47	2.844	0.569	0.238	11.905	2.844			3.076	0.008	3.053	3.084	
57	2.844	0.569	0.238	11.908	2.844							
67	2.844	0.569	0.238	11.918	2.844							
77	2.844	0.569	0.254	12.711	2.844			13.040	0.021	12.961	13.090	
87	2.844	0.569	0.260	13.012	2.844							
97	2.845	0.569	0.260	13.023	2.845							
107	2.846	0.569	0.261	13.045	2.846							
117	2.848	0.570	0.261	13.056	2.848							
127	2.851	0.570	0.261	13.051	2.851							
137	2.854	0.571	0.261	13.045	2.854							
147	2.856	0.571	0.261	13.054	2.856							
157	2.859	0.572	0.261	13.046	2.859							
167	2.861	0.572	0.261	13.044	2.861							
177	2.863	0.573	0.261	13.046	2.863							
187	2.866	0.573	0.261	13.053	2.866							
197	2.868	0.574	0.261	13.043	2.868							
207	2.870	0.574	0.261	13.048	2.870							

Final report for period October-December 1996
In fulfillment of Service Contract with HydroCatalysis Power Corp. (now BlackLight Power, Inc.)

**REPORT ON CALORIMETRIC INVESTIGATIONS OF GAS-PHASE
CATALYZED HYDRINO FORMATION**

Submitted by
Prof. Jonathan Phillips*
and Julian Smith
Department of Chemical Engineering
Penn State University
University Park, PA 16802

Ph: (814) 863-4809
Fax: (814) 865-7846

Professor Stewart Kurtz
Department of Electrical Engineering
Penn State University
University Park, PA 16802

Ph: (814) 863-8407
Fax: (814) 863-8561


Jonathan Phillips


Julian Smith


Stewart Kurtz

*Corresponding Author



SUMMARY

Tests for heat production associated with hydrino formation were carried out with two types of calorimeters during the period October-December 1996. Experiments carried out in a modified Calvet system yielded extremely exciting results. Specifically, initial results are apparently completely consistent with the Mill's Hydrino formation hypothesis. In three separate trials between 10 and 20 K Joules were generated at a rate of 0.5 Watts, upon the admission of approximately 10^{-3} moles of hydrogen to the 20 cm³ Calvet cell containing a heated platinum filament and KNO₃ powder. This is equivalent to the generation of $1 \cdot 10^7$ J/mole of hydrogen, as compared to $2.5 \cdot 10^5$ J/mole of hydrogen anticipated from standard hydrogen combustion. Thus, the total heats generated appear to be two orders of magnitude too large to be explained by conventional chemistry, but the results are completely consistent with the Mill's model. It must be noted that although the results presented in this report are very exciting, they require further verification. Moreover, it should be noted that some control studies are not yet complete.

Also included is a brief report on an attempt to replicate the Calvet cell results on a larger scale using the water bath calorimeter (described in some detail in an earlier report). Unfortunately, no evidence of 'excess heat production' was found. This can be linked to a failure to maintain the catalyst ions (K⁺) in the vapor phase. Specifically, it is hypothesized that the KNO₃ catalyst evaporated from the containing pot at the reactor center, where the temperature is high, and deposited on the reactor walls, which are cold due to immediate contact with the calorimeter water bath. (That is, the catalytic material is 'cryo-pumped' by the cold walls.) Indeed, at the conclusion of the experiment, when the reactor was removed from the water bath, the walls of the quartz reactor were observed to be white in the general vicinity of the pot which contained the KNO₃.

INTRODUCTION

Experiments were conducted to test the hypothesis that in the gas phase potassium ions will catalyze the conversion of hydrogen atoms to hydrino atoms. These experiments were initially carried out in a Calvet cell as this type of calorimeter is highly sensitive and accurate. Moreover, the conditions of the calorimeter are controlled.

RM's theory of hydrino formation requires that both K^+ ions and H-atoms are present in the gas phase. In order to generate gaseous K^+ ions, KNO_3 is placed in a small (2cc) quartz 'boat' inside the calorimeter cell. The boat is heated, to increase the vapor concentration of KNO_3 , with a platinum filament, which is wound around the boat. A second function of the platinum filament is to generate H-atoms. It is well known that hydrogen molecules in contact with a heated filament will decompose, yielding a relatively high H-atom concentration in the boundary layer around the filament. Thus, according to RM's model, in a cell containing KNO_3 in the boat and vapor phase hydrogen, there is a small region in the boundary layer around the heated metal filament which should contain sufficient concentrations of both H-atoms and K^+ ions for hydrino formation to occur.

Calorimetric considerations require that a stable baseline exists before the heat generating process is initiated. Thus, signal change away from the baseline can be correlated to the onset of the process under investigation. In the present experiments the cell was run with KNO_3 in the boat and the filament fully 'powered'. The calorimeter was allowed to equilibrate until a steady baseline existed. The 'hydrino formation' process was initiated by then adding gaseous hydrogen. Good calorimetric practice also requires that adequate control studies be carried out. Also required are repeated electric calibrations.

In the present work, data is presented which indicates that significant heat evolved upon the introduction of hydrogen to the Calvet calorimeter cell. In contrast, no heat was evolved upon the admission of helium. Repeated calibrations were also conducted. Thus, it appears that The RM

hypothesis is supported by the present results. A more definitive statement must await repeats of these experiments, and the results of a few additional control experiments.

An attempt was also made to employ the water bath calorimeter (see previous report to HPC) to detect excess heat. Indeed, the positive results of the Calvet study present a staggering challenge to conventional physics. Challenges of this magnitude require enormous experimental support. Thus, evidence of excess heat production from a second type of calorimeter would be useful. Unfortunately, the experiment failed to yield any evidence of excess heat. However, there is reason to believe that catalyst concentration was low and thus the failure to observe excess heat does not disprove the Mill's hypothesis.

EXPERIMENTAL SYSTEM

Calvet Calorimeter. The Calvet-type calorimeter employed in this study is similar to one described in the literature (attached) and is also described in earlier reports to HPC (now BLP). In essence a stainless steel cup of almost exactly 20 cm³ volume is placed in a calorimeter well such that the cup is surrounded by thermopiles on its sides and bottom. The cup and calorimeter are surrounded by a thick layer of insulation, and the entire device is placed inside a commercial convection oven. In all cases experiments were conducted with the oven temperature set to 250 C.

Reaction cell. For these experiments the top of the calorimeter cup/reactor cell was fitted with a Conflat knife edge flange. The top element of the flange is connected to a gas supply system outside the convection oven with a 0.5 cm OD ss tube, and with two welded vacuum high current copper feedthroughs. The feedthroughs were connected on the cup side of the flange to a coiled section of 0.25 mm platinum wire approximately 18 cm in length. Fitted inside the coiled platinum was a small quartz boat into which 200 mg of powdered KNO₃ were placed.

Plumbing. On the outside of the oven the gas feed through is connected to a line leading to hydrogen and helium tanks, a pressure gauge, and a standard vacuum roughing pump. It is notable that the gas lines were all well insulated, both inside the oven, and for about 50 cm outside the oven.

The plumbing system was so arranged that the cell could be evacuated, and then isolated from the pump in such a way that hydrogen or helium could be added directly from high purity gas tanks. Great care was taken before the experiments were initiated to evacuate and flush the gas lines several times. It was also determined that the lines held gas pressure, with no loss in pressure, for several days. That is, there were no leaks.

Water Bath Calorimeter. This instrument is described in detail in the previous report to HPC. Two minor modifications were made for the present experiment. First, to facilitate the decomposition of hydrogen, the center section of the mandrel was wrapped with a 60 cm length (about 8 cm of mandrel) of 0.25 mm diameter platinum wire. Second, in the center of this section the same quartz boat (again filled with about 200 mg of catalyst) used in the Calvet system, wrapped with the same coil of platinum wire, was inserted into the circuit. (The experiment described was carried out after the completion of the Calvet system experiments.)

RESULTS

Calvet Calorimeter. The Calvet studies suggest large amounts of heat are generated upon the admission of hydrogen to the cell. In contrast, virtually no heat is observed upon admission of helium to the cell.

Calibration. The first tests performed on the Calvet system were electrical calibration experiments. The system was set-up for full experimentation: KNO_3 was in the boat, the system was evacuated, and 10 watts of steady power were supplied to the platinum coil. After a steady baseline was achieved (approximately 10 hours after the oven was adjusted to 250 C), the cell was isolated from the pump and the pressure allowed to equilibrate (approximately 100 Torr). This did not appear to impact the baseline in any fashion. The power supply was then adjusted to deliver an additional 1 watt (11 watt rather than 10) for a specified time period. The power was then returned to the original 10 watt setting. A typical response curve is shown in Figure 1. The area under the response curve can be used to obtain a calibration constant which relates signal area increase to the number of extra Joules delivered. This was done in four cases (Table I). As can be seen, there is some error (+/- 15%) in the calculated calibration constant.

Control Studies. Helium was admitted, approximately 10 psig, to the cell to test the impact of a change in pressure, and heat transfer characteristics on the response of the cell. The helium was admitted after the cell had been isolated from the pump for a considerable time and a steady pressure (approximately 100 Torr) achieved. As can be seen in Figure 2a, the response was a short-lived small increase in output signal, followed by a relatively short time period during which the signal gradually returns to the original baseline. Within an hour the signal returned to the original baseline, with some drift evident.

The response of the system is expected. The helium increases the rate of heat transfer away from the platinum filament, and heated boat. Thus, the initial addition of helium to the system results in a temporary increase in the amount of heat reaching the thermopiles. That is, the boat and the filament cool off, until such time as the boat and filament have reached their new steady state temperatures. The steady state temperature of boat and filament are a function of heat transfer mechanism. After the admission of helium most heat transfer is occurring by convection to the walls. Before the admission of helium a considerable fraction is by radiation. Radiative transfer of 10 watts requires a higher filament/boat temperature than does convective heat transfer.

Figure 2b illustrates again the impact of adding pressure, or removing gas, from the system. Upon the addition of helium there is a very short lived increase in heat reaching the thermopiles. Upon pumping there is a period of time, perhaps an hour, during which the heat signal goes below the baseline. This is consistent with the model in that pumping makes convective and diffusive heat transfer minimal. Virtually all heat transfer is by radiation, which requires that the filament/boat temperature increase. It takes some time for this new steady-state temperature to be reached.

Hydrogen Admission. Hydrogen admission was carried out in much the same fashion as helium admission. The cell reached an equilibrium pressure, approximately 100 Torr, and then hydrogen at 10 psig was admitted to the cell. The valve to the hydrogen source, which was a steel line 4 meters by 0.6 cm OD, was closed off by a valve in front of the regulator during admission. Moreover, it was open for only a couple of seconds in each case. This was done on three separate

occasions, and the signal that evolved in response to these three processes is recorded in Figures 3, 4 and 5. One other observation recorded was that the pressure decreased gradually over time, such that after about an hour the pressure returned to the original equilibrium pressure of the cell. It must also be noted that the heat production was ended deliberately in all three cases by pumping the system to 5×10^{-3} Torr. It is clear 'excess heat' evolution would have continued in all cases if the system had not been evacuated.

It is expected that in the absence of reaction that the response of the cell to the addition of hydrogen would be similar to that observed for helium. Indeed, given that pressure measurements suggest that most hydrogen is adsorbed, or in some other fashion removed from the cell after an hour, even heat transfer effects should be totally transitory. Even in the event of reaction no more than a small heat signal is expected. Indeed, a high end estimate is that 25 cm^3 of hydrogen at a temperature of 300 K and a pressure of 2 atmospheres entered the cell. This is equivalent to 2×10^{-3} moles of hydrogen. If all of that hydrogen interacted with oxygen to form water only 510 J would be generated. It is possible to imagine that the hydrogen could interact with nitrogen in KNO_3 to form ammonia. Even less energy would evolve from this process. Thus, the largest heat peak might be expected to be 0.5 watts for 1000 seconds (approx. 17 minutes). A block of this size is marked on Figure 3.

It is clear from figures 3, 4 and 5 that hydrogen admission to the cell apparently leads to far more energy evolution than can be explained by any conventional chemical process. It is interesting in this regard to graphically contrast the response of the system to helium admission to the response to that for hydrogen admission. This is done on Figure 6 in which Figure 3 and Figure 2a are superimposed.

Water Bath Calorimeter. Studies conducted with the water bath calorimeter do not indicate the evolution of any excess heat. As shown in Figure 7 the increase in temperature almost exactly parallels the increase predicted on the basis of the amount of energy added to the system and the known heat capacity of water.

Do the results of the experiment refute the RM hypothesis? No. At the conclusion of the experiment the large cell was removed from the water bath and a white coating was seen on the walls in the vicinity of the pot which contained the KNO_3 . This suggests that the KNO_3 was rapidly cryopumped by the walls, and that the gas phase concentration of catalyst was too low to be effective.

DISCUSSION

The evidence presented in this report clearly suggests that an extraordinary phenomenon takes place upon the admission of hydrogen to a cell containing a heated platinum filament and KNO_3 . This phenomenon appears to generate a tremendous amount of 'excess' heat. Still, the author of this report urges that a cautious approach be taken at present. Additional experimental work is required. A partial list of proposed additional experiments is given below:

- 1) A control experiment consisting of admission of hydrogen to a cell in which 10 watts of power is applied to a platinum filament, but no KNO_3 is present.
- 2) Hydrogen is admitted to a cell containing a platinum filament and KNO_3 in a boat, but no power is applied to the filament.
- 3) The experiments are run as described in the present report, but the boat containing KNO_3 is at the bottom of the cell, rather than in the center of the platinum coil.
- 4) The hydrogen admission experiments described above are repeated BUT continued for times sufficient to return the signal to the original baseline.

In addition, modifications in the apparatus should be made. First, insulation should be added to improve the stability of the baseline. Second, a quality pressure gauge should be attached to a known volume outside the oven such that all uncertainty regarding the number of moles of hydrogen admitted to the cell can be eliminated. Third, the plumbing should be re-arranged to facilitate 'capture' of gas for analysis using gas chromatography. Fourth, provision should be made to permit pressure to be recorded as a function of time.



Typical Calibration Experiment: 1 W Input, 20 Mins

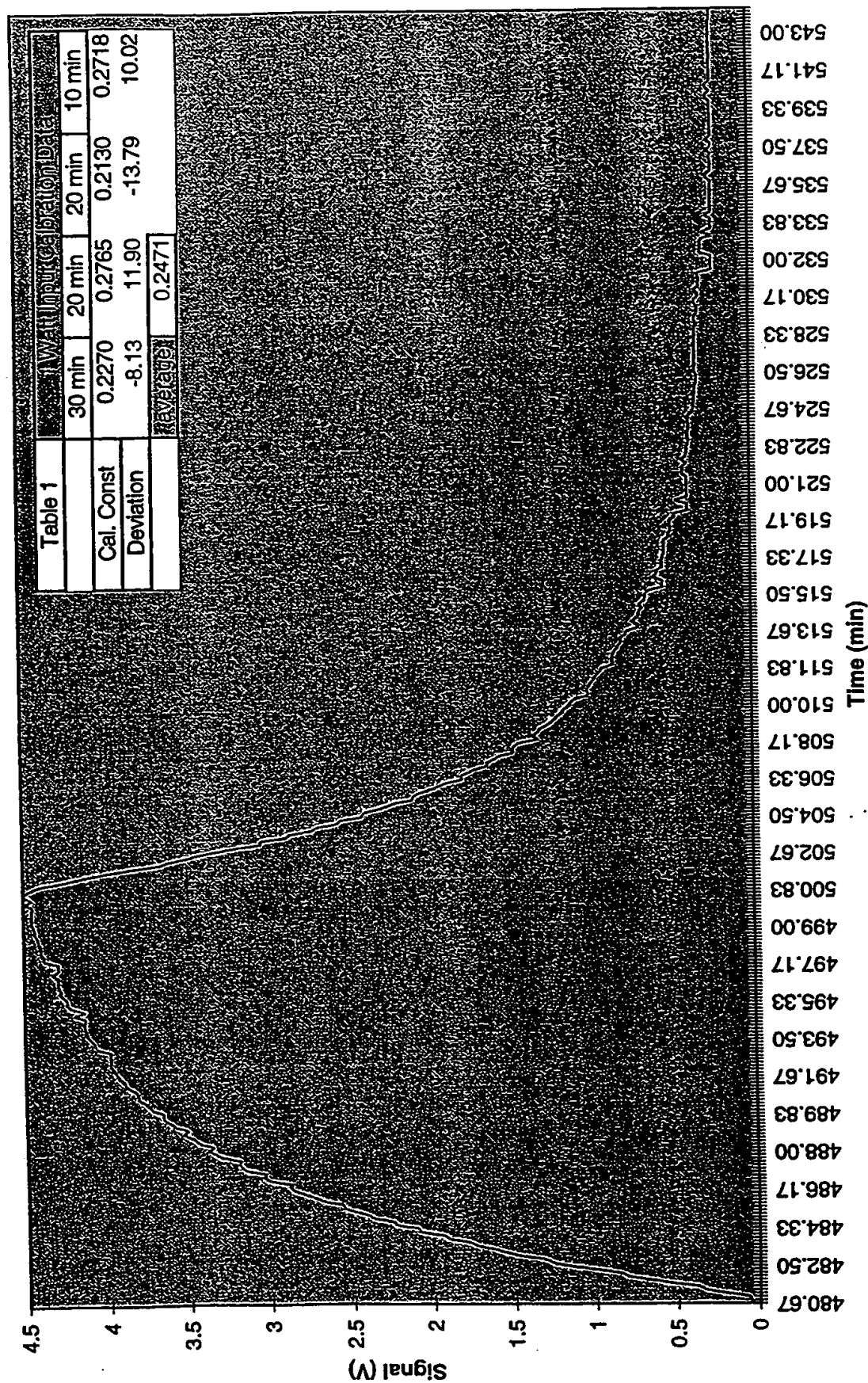


Figure 1

Heat Production, KNO3 w/ Helium Injection (BL1220A)

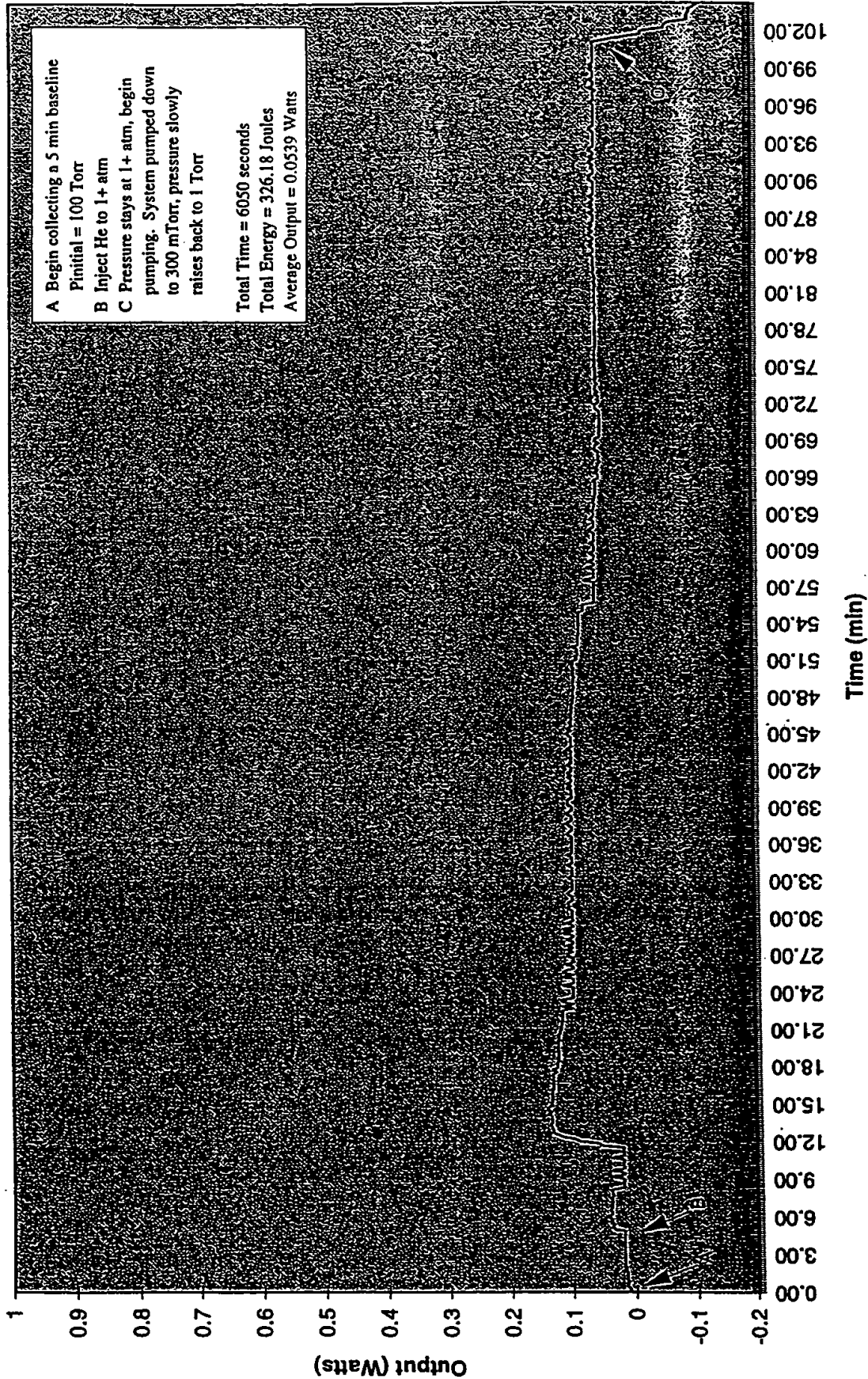


Figure 2A

Heat Production, KNO3 w/ Helium Injection (BL1219B)

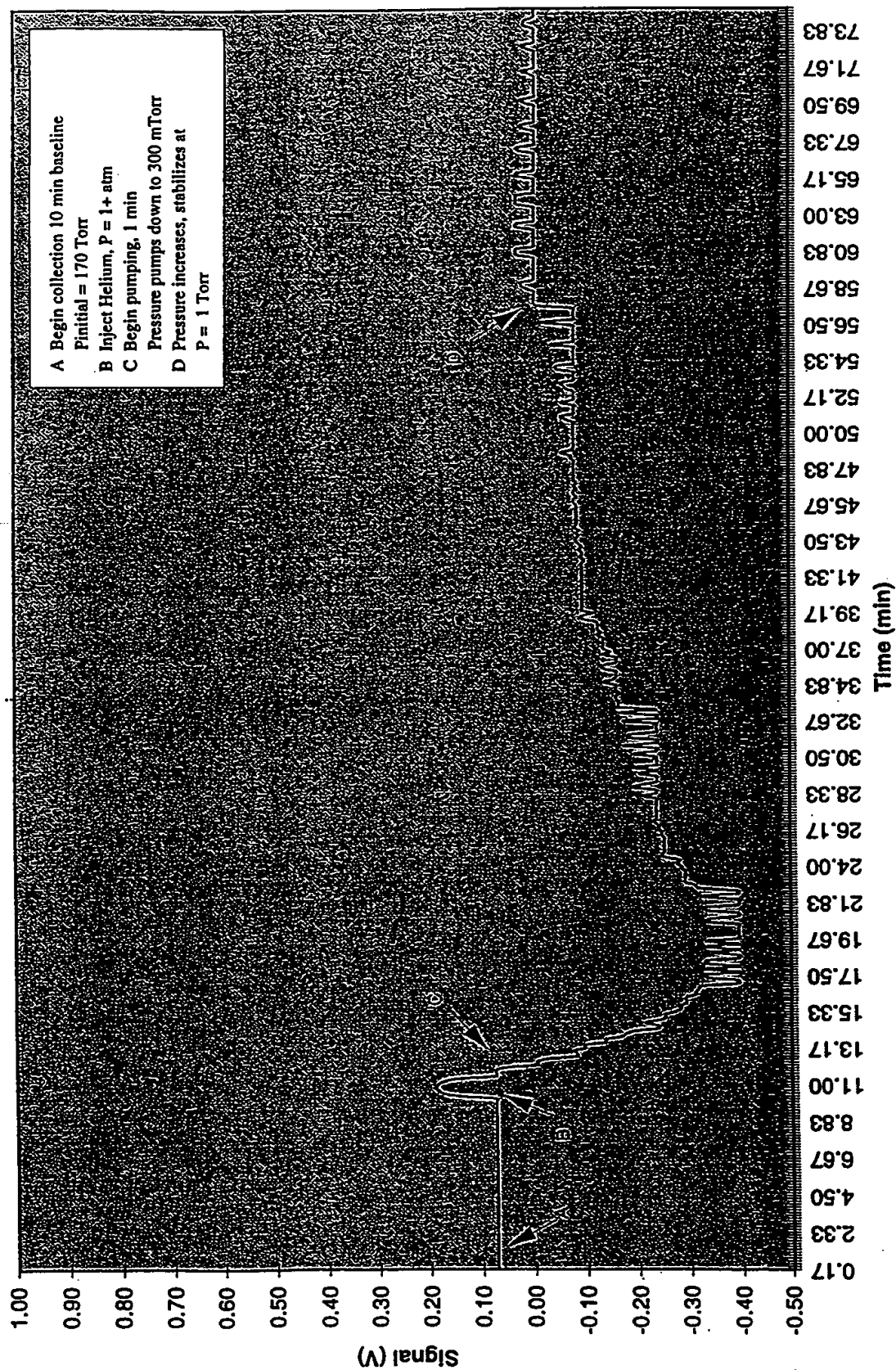
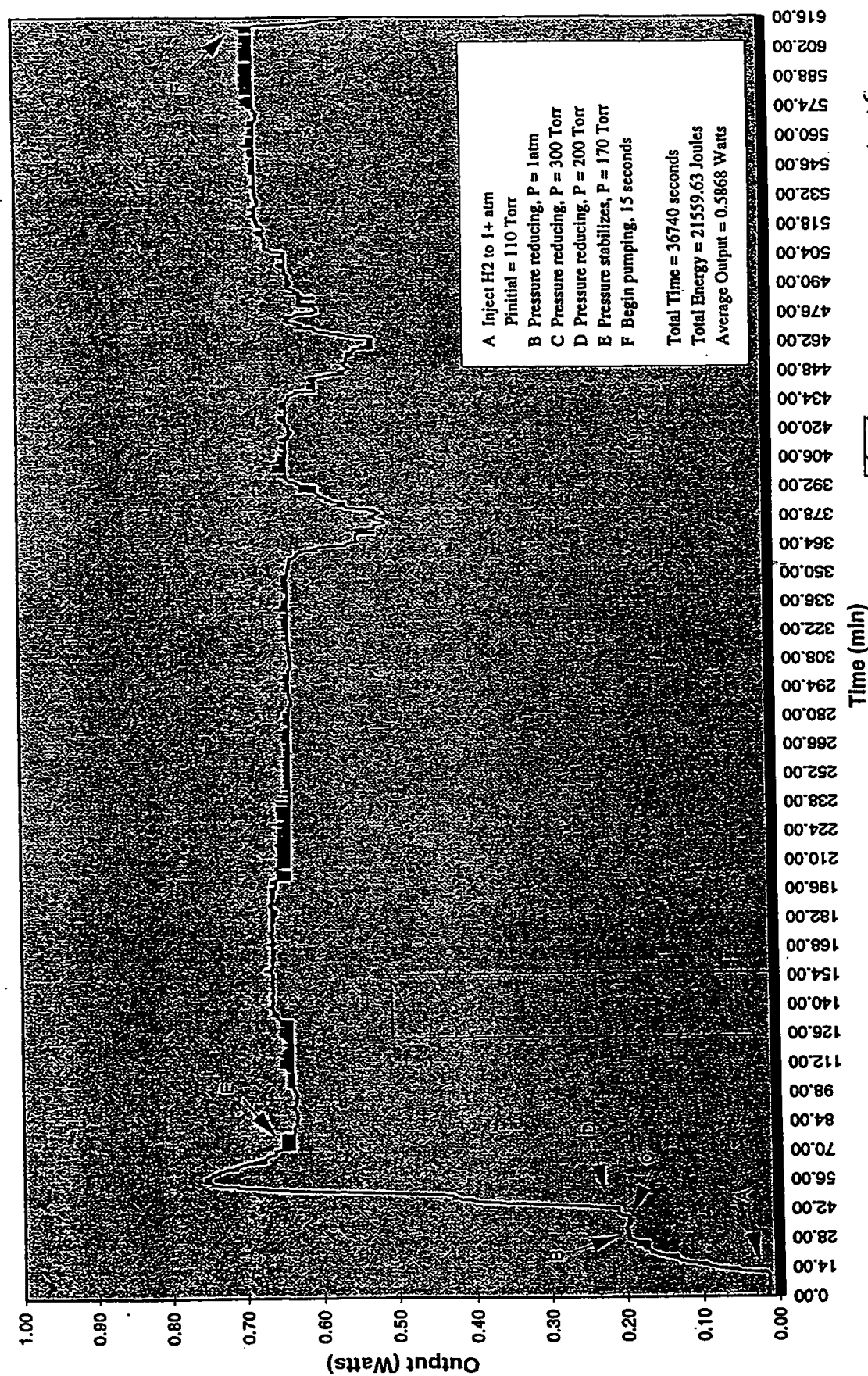


Figure 2B

Heat Production, KNO3 w/ H2 Injection (BL1218CD)





 - Peak area expected if
 all admitted H₂ reacts
 with O₂ to form H₂O.

Figure 3

Heat Production, KNO3 w/ H2 Injection (BL1220BC)

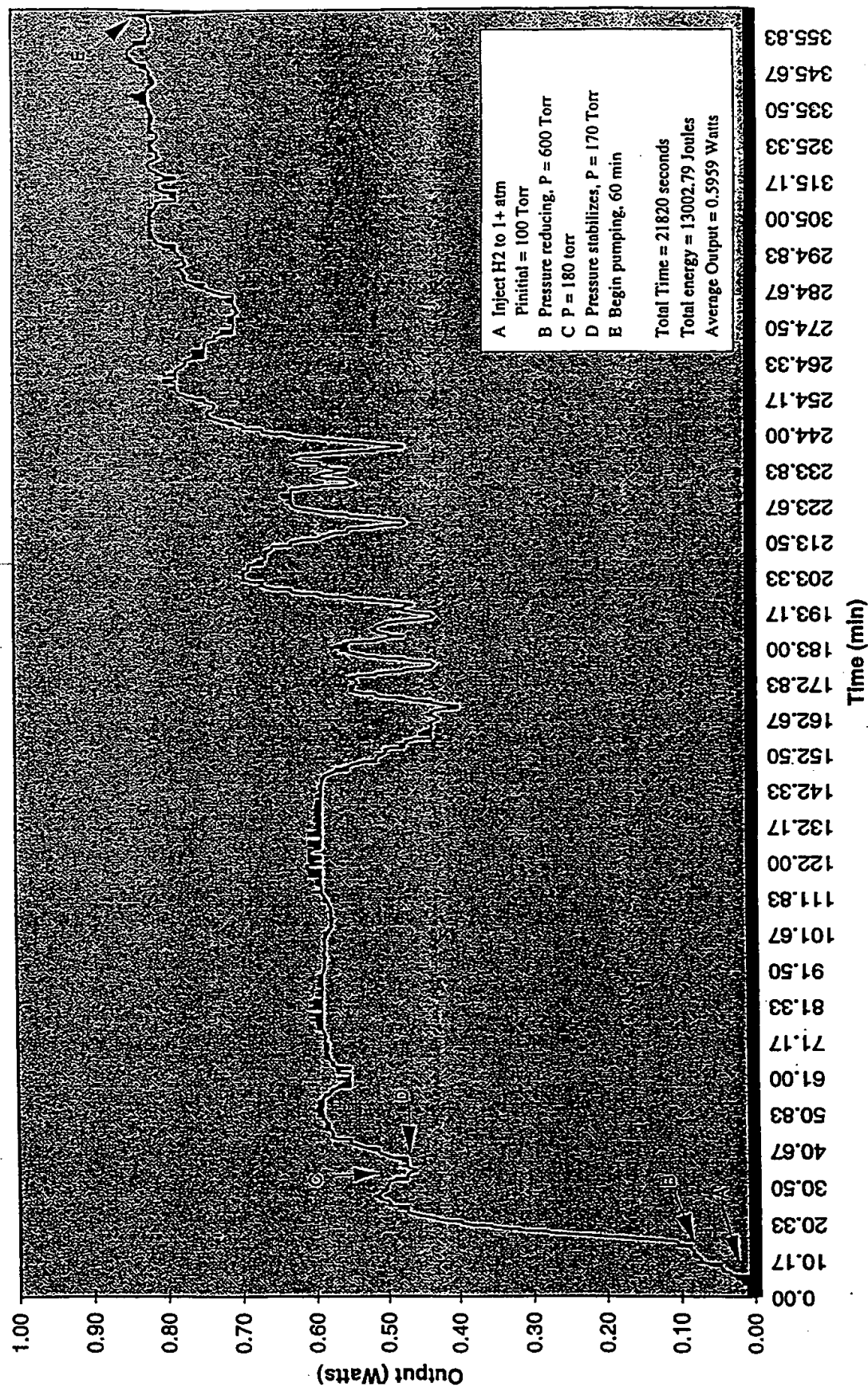


Figure 4

Heat Production, KNO3 w/ H2 Injection (BL1221AB)

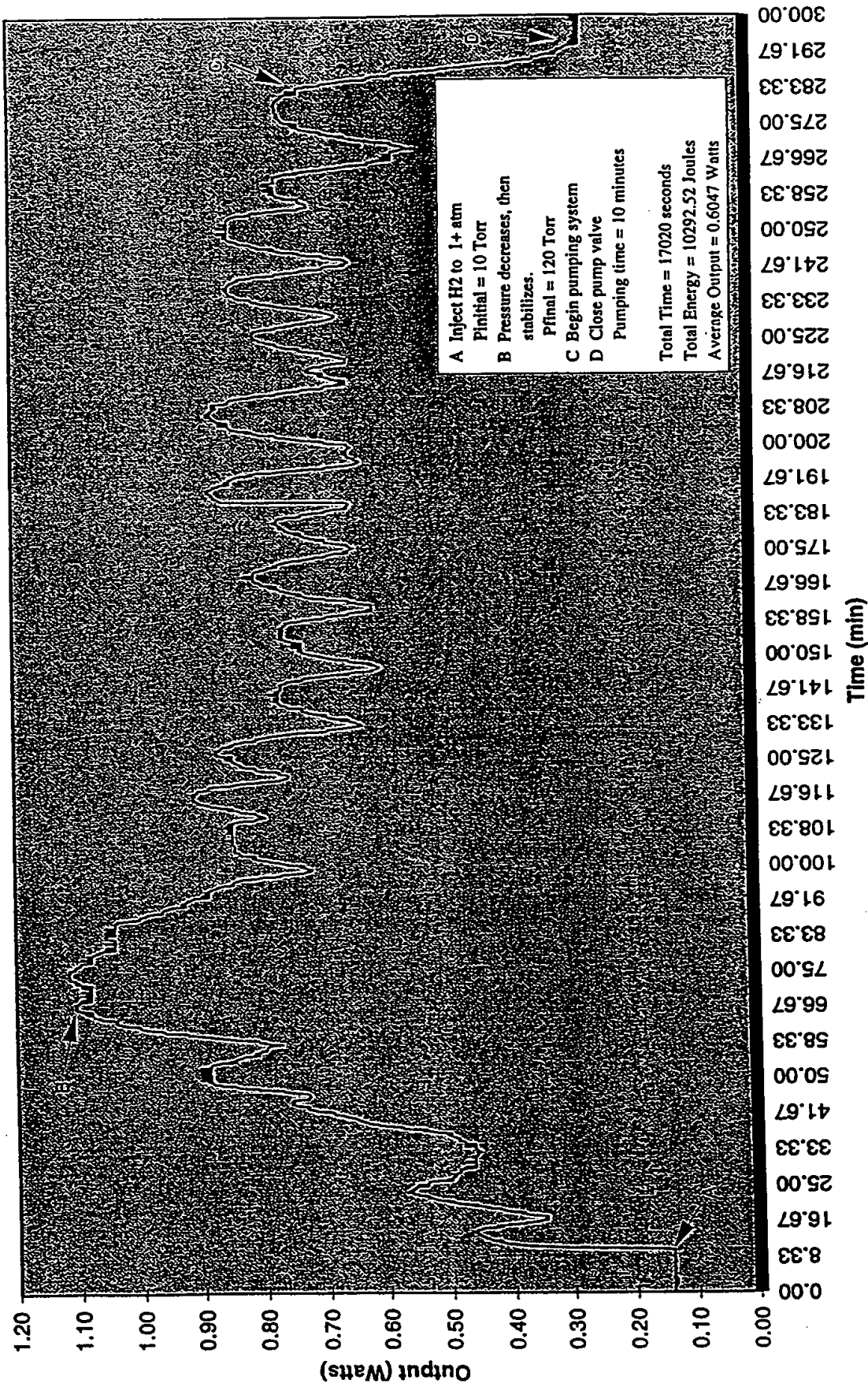


Figure 5

Heat Production, KNO3 w/ H2 and He Injection (BL1218CD,BL1219B)

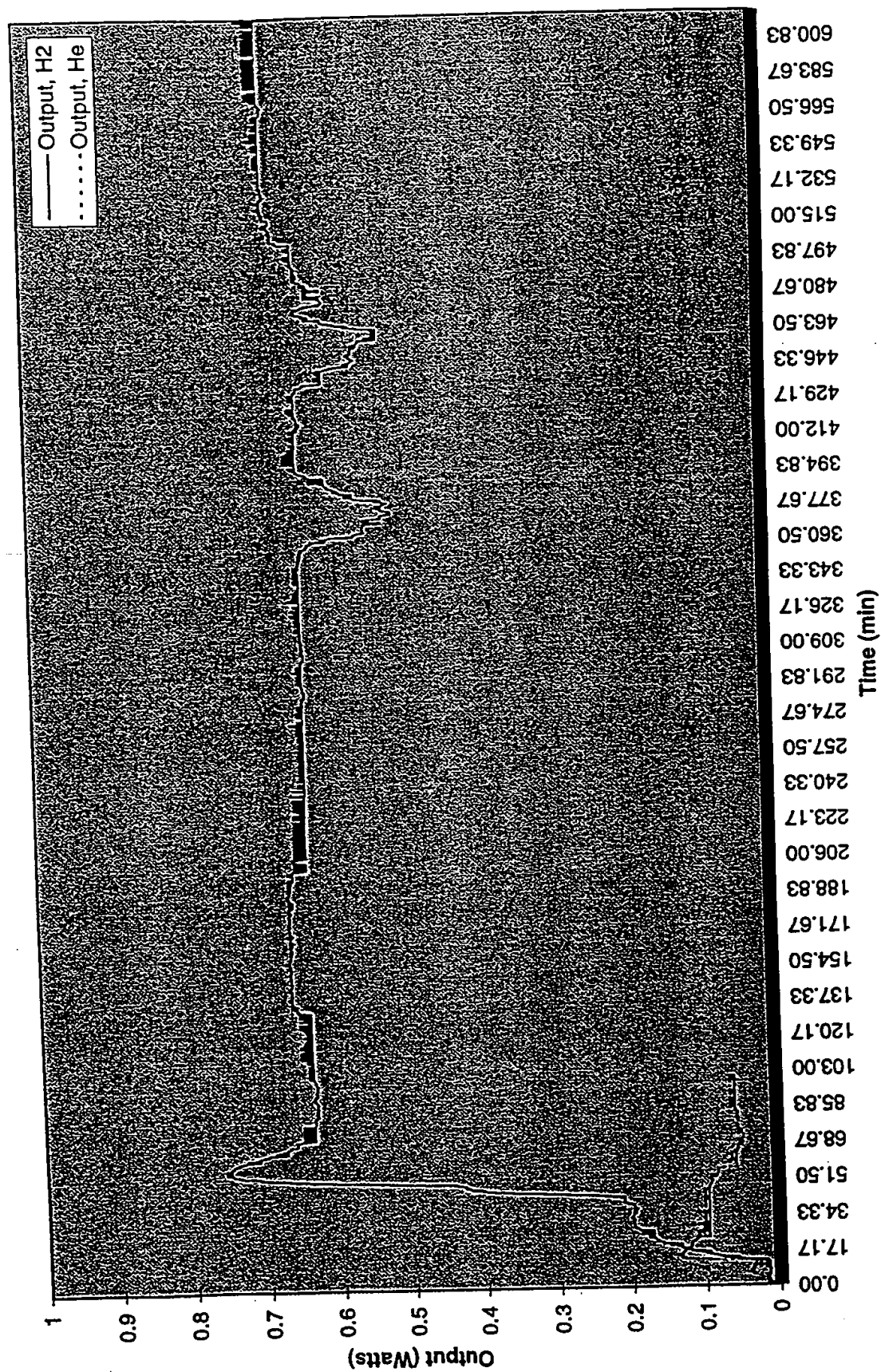


Figure 6



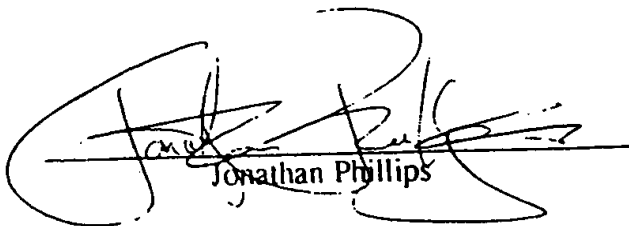
THIS PAGE BLANK (USPTO)

CONSULTING REPORT

January 1, 1996

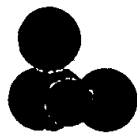
ADDITIONAL CALORIMETRIC EXAMPLES OF ANOMALOUS HEAT FROM
PHYSICAL MIXTURE OF K/CARBON AND PD/CARBON

By Jonathan Phillips and Hyunsip Shim
Department of Chemical Engineering
Penn State University
133 Fenske Lab
University Park, PA 16802
Ph: (814) 863-4809
e-mail: PWA@PSU.EDU



Jonathan Phillips

CONFIDENTIAL



INTRODUCTION

Repeatedly during the period from June to October 1995 apparent 'anomalous' heat was observed using one class of catalytic materials supplied by HCP corporation. Specifically, heats were observed, calorimetrically, of a magnitude not readily explained by conventional chemistry when pure hydrogen streams of about two atmosphere pressure were passed over the catalytic materials. The successful catalysts in all cases were physical mixtures of two materials: carbon supported potassium nitrate and carbon supported platinum.

The current report regards efforts to test four hypotheses. First, that HCP has mastered procedures which insure anomalous heat can be repeatedly obtained. Second, to illustrate that the choice of the carbon employed as a support has a small, but measurable, impact on the procedure for generating anomalous heat. Third, to demonstrate that the choice of noble metal can also marginally impact the process.

The fourth hypothesis is more complex. It is that the model of potassium transformation postulated in earlier reports is correct. That model consists of three parts. (i) Potassium nitrate is gradually reduced to potassium metal in the cell during the time that anomalous heat is observed. (ii) Once the potassium is fully reduced, heat evolution ceases. (iii) Potassium oxide (KO_2 or KOH) only forms upon air exposure. Tests were designed to allow the testing of this model using weight loss, calorimetric measurement of heat evolution from oxygen exposure after catalyst de-activation, and x-ray studies.

Three samples were studied. The first sample discussed in this report was different than those studied previously for two reasons: (i) the support was changed to a commercial 'charcoal', (ii) the noble metal in the mix was palladium rather than platinum. The other two samples were prepared on the 'standard' support material, Grade GTA Grafoil (Trademark, Union Carbide), a moderate surface area, high purity, graphitic material. However, changes were made in the composition of these catalytic mixtures as well. Carbon supported palladium, rather than carbon supported platinum, was mixed with these samples.

All three samples produced 'anomalous' heat. On the basis of these results it is clear that HCP has developed procedures which allow the repeated observation of 'anomalous' heat, which can be observed in different laboratories. Yet, it was found that the identity of the support material does impact the result. In order to obtain anomalous heat from a charcoal supported sample it was necessary to operate at a higher temperature. The use of palladium rather than platinum also appears to have some impact. The two graphite supported samples contained palladium almost immediately produced heat upon the introduction of hydrogen at 125 C. Generally with platinum containing mixtures there was a lengthy 'induction' period, and in most cases a temperature higher than 125 C was required to insure the observation of anomalous heat.

Some NOVEL tests were carried out with the two Grafoil supported samples to test the model of potassium transformation. Specifically, careful measures of weight loss and careful calorimetric measures of heat evolution (only one sample) during oxygen exposure of the deactivated catalyst were carried out. The values obtained were in close agreement with the postulated transformations. Specifically the weight loss and the heat observed during oxygen exposure of the deactivated catalyst were near values anticipated on the basis of the model and the x-ray results.

In sum, the present results contain two important findings. First, HCP can produce catalysts which repeatedly yield anomalous heat, and second, the model of potassium transformation is consistent with all measures. The latter finding has particular significance as it gives additional credence to the claim that anomalous heat is observed. Indeed, the heat anticipated for the over-all conversion of KNO_3 to KO_2 or KOH , even accompanied by the creation of water and ammonia, is only weakly exothermic. The actual heat observed was significantly more than that anticipated from conventional chemistry. If these findings can be repeated (twice) and if DIRECT evidence of the conversion of the potassium to a zero valent state during hydrogen flow can be obtained (e.g. *in situ* x-ray) these findings can be made the basis of an article for the peer-reviewed scientific literature.

It must be emphasized that calorimetric measures alone are somewhat ambiguous and that *in situ* x-ray studies are strongly advised before sending the material for publication. It is also recommended that 'control studies' be carried out. In the absence of a noble metal it is likely that potassium nitrate will follow the same decomposition course, but the process should yield an endotherm, rather than a strong exotherm.

Finally, it must be noted the results of even the most careful calorimetric, x-ray and weight change experiments will not serve as a proof of the existence of hydrinos. Results from our lab will only provide strong evidence that heats higher than predicted by conventional chemistry are observed in the dry HCP cells.

EXPERIMENTAL

All experimental procedures and equipment was identical to that described in earlier reports with two exceptions: (i) a new BLUE M furnace was employed, (ii) a gas sampling system on the exit line was employed. Neither change should have any impact on the calorimetric studies.

RESULTS

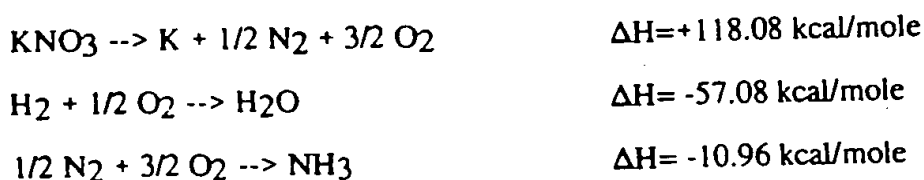
SAMPLE 111395A - The sample contains 5.9567 gms of total material, and was nominally 43 percent by weight potassium nitrate (2.56 gms or 0.0253 moles KNO_3). The support in this case was an activated charcoal obtained from Alpha Chemical. Charcoal loaded potassium made up 97% of the material, and the remaining 3% of the material was carbon supported palladium.

Previous experience with these samples at HCP indicated that heat is only observed at 200 C. Thus, after testing the calorimeter (Fig. 21-1) and baseline stabilization at 200 C in flowing helium (Fig. 21-2) hydrogen was introduced at 200 C. Almost immediately, a peak characteristic of hydride formation was detected (Fig. 21-3).

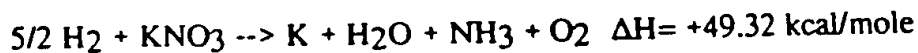
The signal decayed more gradually than usual for 'hydride' formation, and in fact, before reaching the original baseline the signal strength began a sharp climb in value. As shown in Figure

21-4 about 18 K seconds after hydrogen was first admitted the signal strength increased. In fact, about 24 K seconds after the increase began the signal saturated the amplifier (Figure 21-4). In fact, for almost 28 K sec. (approx. 7.5 hrs), the signal strength was higher than that computed for complete hydrogen conversion to water (0.24 Watts at a total flow rate of 2.16 ml/min at 300 K and 1 atmosphere of pressure). As usual, the signal gradually decayed to zero (Figs. 21-5,6,7).

The total heat produced before the signal decayed to zero was at least 23.4 kJ, or equivalently a minimum of 925 kJ was generated per mole of potassium. The actual heat generation was clearly higher as the amplifier saturated for about 6 K sec (Figure 21-4). Weight loss was also carefully determined. It was found to be 1.032 gms. Computations of the heat which would be generated by conventional chemistry were made. Only models consistent with the measured weight loss, and the x-ray analyses were considered. As discussed later the most likely set of reactions (Reaction Sequence I) is as follows:



For a sum reaction:

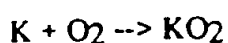


This 'most likely' chemistry indicates that the reduction of the nitrate to the metallic state is an ENDOTHERMIC process. Rather than observing heat evolution, heat should have been absorbed during the reduction process:

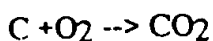
$$(49.32 \text{ Kcal/mol}) * (4.184 \text{ kJ/1 kcal}) * (0.0253 \text{ moles}) = 5.22 \text{ kJ}$$

Thus, there is a difference of more than 28 kJ between the observed process and the heat anticipated on the basis of the 'most likely' chemistry.

Not all of the data fully supported the Reaction Sequence I (RS I) model. First, the weight change was greater than predicted, and second the x-ray work showed that KO₂ (not potassium metal) was present after the reaction was completed and the sample exposed to air. Both findings can be partially explained by the fact that air exposure of fully reduced and well dispersed potassium should lead to a rapid exothermic process in which potassium metal is converted to KO₂ and concomitantly heat is generated. That is, following the formation of potassium metal it is likely two additional reactions (RS II) took place upon air exposure:



$$\Delta H = -68.1 \text{ kcal/mole}$$



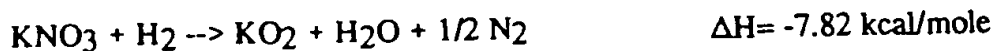
$$\Delta H = -94.05 \text{ kcal/mole}$$

If both RS I and II took place the mass loss associated with the net process would be that of one N atom and one O atom for each molecule of KNO₃ initially present. On this basis, and given the fact that 0.0253 mole of nitrate were initially present, the anticipated weight loss is: 0.76 gms. The measured weight change was -1.033 gms. (In fact, the above measure probably slightly overstates the weight loss as some sample is invariably lost during the two transfer processes between measurements: transfer to the calorimeter at the beginning, and transfer from the calorimeter at the end.) On this basis it is postulated that 0.273 gms were lost via the formation of carbon dioxide. The process of carbon dioxide formation that would use up 0.273 gms of carbon would yield a heat of 8.95 kJ.

In order to explain observed heats it is always reasonable to postulate chemistry different from the 'most likely' scenario (RS I). For example, if RS I and II both took place in the cell prior to air exposure (potassium oxide and carbon dioxide being the final products) a total of 10.94 kJ of heat would be generated. This is considerably less than that observed experimentally (23.4 kJ),

but not enough less that one could comfortably claim anomalous heat production. Moreover, this proposed sequence (I + II) is consistent with the x-ray data, as well as with the observed weight loss.

Other reaction processes are also consistent with the x-ray data. It appears that these other reactions ALL yield heats LESS THAN that for RS I plus RS II.. For example:



This reaction only yields 0.83 kJ for the number of moles of nitrate initially present. If this reaction occurred and carbon dioxide formation in the cell accounted for the remaining mass loss than a total of 9.78 kJ would be observed. Again, the computed total heat evolution is within a factor of 3 of that measured experimentally.

Given the composition of the catalyst, it is clear the greatest heat generation per gram would occur via the direct combustion of carbon. Indeed, if all the weight loss were associated with CO₂ formation the heat evolved would be 33.04 kJ for a weight loss of 1.03 gms. This would clearly account for all the observed heat, as well as the weight change. It is not consistent with the x-ray results, or gas phase chemical analysis reported by HCP.

As shown in the x-ray results the sample prior to treatment consists primarily of carbon and potassium nitrate. The 'Before' results do indicate the limitations of X-ray analysis. For example, even lines from palladium, an element known to be present, cannot be found. Still, the comment that carbon and potassium nitrate are the predominant species initially present is undoubtedly correct (21-8, 21-9, 21-10). It is also clear that following the deactivation of the catalyst and is subsequent exposure to air the predominant potassium phase is KO₂.

In sum, the above analysis indicates that additional data must be collected which limits the number of reasonable reaction sequences. The gas phase analysis conducted by HCP for example, tends to support the 'most likely' scenario above. That is, the discovery of NH₃ and no reports of

CO or CO₂ support this analysis. The discovery of some NO supports the suggestion that the process may even be more endothermic than that suggested by the 'most likely' scenario.

In the next couple of experiments efforts were made to eliminate CO₂ formation during air exposure, and to insure that the heat released during the reaction of oxygen with reduced metal was determined calorimetrically.

SAMPLE 113095A - The sample contains 8.3276 gms of total material, and was nominally 37 percent by weight potassium nitrate (3.08 gms or 0.0305 moles KNO₃). Grafoil loaded potassium made up 97% of the material, and the remaining 3% of the material was carbon supported palladium.

After the initial touch test (Fig. 22-1) the calorimeter temperature was raised to 125 C and held at that temperature in flowing helium for about 12 hours at which time it was determined the baseline was reasonably stable (Fig. 22-2). Hydrogen was introduced into the cell and almost immediately a moderate sized heat peak, generally considered to result from the formation of hydride, was observed (Fig. 22-3). About two hours after the 'hydride peak' reached its apex the signal began to rise significantly (Fig. 22-3). In fact, after about six hours the signal reached a value equivalent to the production of about 0.50 watts. Given a net input flow rate of 2.1 ml/min, and assuming a perfect stoichiometry of 2 hydrogen molecules per oxygen molecule, water formation would yield 0.24 watts. Assuming that all of the oxygen was 'free' and already present in the sample chamber (air leaks flowing inward against two atmosphere of hydrogen pressure assumed to be minimal), this flow rate of hydrogen completely converted to water would yield 0.35 watts. (In fact, there is no reason to believe there is any 'free' oxygen in the system. Any oxygen associated with a potassium oxide would yield scant heat upon potassium reduction and hydrogen oxidation. Reduction of carbon oxides would in fact be endothermic in most cases.) On the basis of the first calculation, it can be seen (22-4,5,6) that the rate of heat production exceeded that anticipated from the formation of water for 66 ksec (more than 18 hours). The catalyst clearly deactivated over the next 20 ksec (Figs. 22-6,7) until no heat at all was being produced. During

the period of heat production a total of more than 31 kJ of energy was evolved, or equivalently more than 1016 kJ/mole potassium initially present.

According to the model proposed by Phillips in earlier reports, the state of the fully deactivated catalyst should be metallic potassium. This suggestion was tested by exposing the deactivated sample to dry air (20% oxygen) slowly (approx. 20 cm³/min). A slow exposure to oxygen should prevent the type of rapid heating which conceivably can lead very high heating and concomitantly a limited amount of combustion of the carbon support. Unfortunately, due to a communication breakdown, no attempt was made to measure the amount of heat evolved.

A final measure of the weight loss of a sample which was handled in a fashion designed to eliminate post-deactivation combustion was quite revealing. The sample was found to lose 0.856 gms of weight. A net loss of one nitrogen and one oxygen per mole of nitrate initially present would lead to a weight loss of 0.915 gms. This suggests 'good' agreement between the model of potassium nitrate decomposition (RS I) and then potassium oxide (KO₂) formation during air exposure as outlined in the discussion of the previous sample above. According to that model at most 2.4 kJ could have been generated. This assumes there is no carbon dioxide formation. Indeed, given the weight loss there is no reason to believe carbon dioxide was formed.

If a worse case scenario is assumed, and all weight loss is attributed to the formation of carbon dioxide, we find that 28 kJ of total heat would be generated. This is close to the total amount of heat actually observed. Clearly it is important to unambiguously demonstrate that carbon monoxide and carbon dioxide are not generated to any extent during the 'reduction' cycle.

A 'best case' scenario may also be envisaged. Imagine that the decomposition process only produced potassium metal, oxygen and nitrogen (see first line in RSI). How many electron volts would be produced per atom of potassium initially present? That is, we assume that the 31 kJ observed is the net AFTER the heat required for the endothermic decomposition process is subtracted. This scenario requires that a total of 46 kJ were generated in an 'anomalous' fashion in order to account for the observed 31 kJ. Given the number of moles of

potassium initially present, this is equivalent to the generation of 15.7 eV/atom of potassium initially present.

Finally, it must be noted that analysis of this sample is not complete. X-ray study of the post treatment state of the potassium has not yet been carried out. The assumption that KO_2 is the final state of the potassium has not yet been demonstrated. As discussed with reference to sample 120495A (below), this is not always the case.

SAMPLE 120495A - The sample contains 8.82 gms of total material, and was nominally 37 percent by weight potassium nitrate (3.26 gms or 0.0323 moles KNO_3). Grafoil loaded potassium made up 97% of the material, and the remaining 3% of the material was carbon supported palladium.

After the initial touch test (Fig. 23-1) the calorimeter temperature was raised to 125 C and held at that temperature in flowing helium for about 12 hours at which time it was determined the baseline was reasonably stable (Fig. 23-2). Hydrogen was introduced into the cell and almost immediately a moderate sized heat peak, generally considered to result from the formation of hydride, was observed ((Fig. 23-3). About four hours after the 'hydride peak' reached its apex the signal began to rise significantly (Fig. 23-4). In fact, after about seven hours the signal reached a value equivalent to the production of about 0.50 watts. Given a net input flow rate of 3.3 ml/min, and assuming a perfect stoichiometry of 2 hydrogen molecules per oxygen molecule, water formation would yield 0.37 watts. Assuming that all of the oxygen was 'free' and already present in the sample chamber, this flow rate of hydrogen completely converted to water would yield 0.55 watts. (In fact, as explained with reference to sample 113095a there is no reason to believe there is any 'free' oxygen in the system.) On the basis of the first calculation, it can be seen (23-4,5,6) that the rate of heat production exceeded that anticipated from the formation of water for 55 ksec (more than 15 hours). The catalyst clearly deactivated over the next 40 ksec (Figs. 23-6,7) until no heat at all was being produced. During the period of heat production a total of more than 33 kJ of energy was evolved.

According to the model proposed by Phillips in earlier reports, the state of the fully deactivated catalyst should be metallic potassium. This suggestion was tested by exposing the deactivated sample to dry air (20% oxygen) slowly. The air was mixed with helium to insure the rate of heat evolution during the oxidation process could be measured. Also, a slow exposure to oxygen should prevent the type of rapid heating which conceivably can lead very high heating and concomitantly a limited amount of combustion of the carbon support. The composition of the oxygen containing mix was nominally that shown on Figure 23-8; however, there is reason to believe that the mix ratio was not precisely controlled. In any event, it is clear that heat did evolve upon the slow exposure of the sample to an oxygen containing mix for several days (Fig. 23-9 through 23-17). The total heat evolved during this period of time was about 10.5 kJ.

X-ray studies revealed that the primary product of the slow oxidation process was potassium hydroxide. There was evidence that KO_2 was present in limited amounts. In previous studies conducted in this laboratory the Grafoil supported deactivated samples were found to be primarily KO_2 with some KO_3 present. The reason that KOH formed in the present case probably relates to difference in the rate of oxidation. In previous studies oxygen exposure was rapid, probably leading to great increases in temperature, which probably favored more complete oxidation.

Weight loss can be used as a check on the x-ray analysis. The weight 'loss' anticipated for the net conversion of 0.0323 moles of KNO_3 to KOH is 1.45 gms. The observed weight loss was 1.20 gms. In contrast if 50% of the potassium nitrate converted to KOH and 50 % to KO_2 the expected weight loss would be 1.21 gms. This suggests that the later estimate is more reasonable. In any event, there is no reason to believe that any weight loss should be attributed to carbon combustion.

Given x-ray analysis showing KOH as the final product rather than KO_2 , an effort to convert KOH to KO_2 was undertaken. The sample was heated in air for four hours at 200°C . This caused the sample to gain weight, such that the NET weight loss was 1.02 gms (and not 1.20 gms). Given the number of moles initially present, the predicted weight loss for complete

conversion of KNO_3 to KO_2 is 0.97 gms. The measured weight loss is consistent with this model. X-ray studies to determine the final state of potassium are planned.

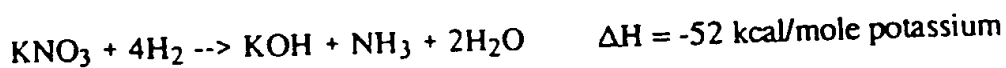
Given the assumption that potassium metal was present at the start of the oxidation process and the final composition of the potassium is a 50/50 mixture of KOH and KO_2 the heat evolved should be 11.3 kJ. This compares very well with the actual heat evolved of 10.5 kJ.

An alternative hypothesis is suggested by the x-ray revelation that the final state of the potassium was KOH (Figs 23 18-26). This suggests that a model must account for the presence of hydrogen in the final structure. One explanation is that the potassium state prior to oxygen exposure was KH and not K-metal . This would increase the expected heat to some extent. That is, we assume the following reactions take place in parallel during oxygen exposure:

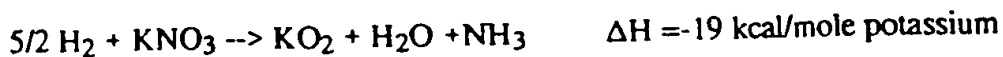


Next, we assume the same final disposition of the potassium (accounts for measured weight change) was a 1/1 mix of oxide and hydroxide. This would lead to the generation of 11.5 kJ. This is almost the same as that computed for the system assuming the final state of potassium was metallic.

It's revealing to compare the total heat evolved with the total heat anticipated simply from conventional chemistry. The conversion of 0.0323 moles of KNO_3 per the reaction below:



yields only 7 kJ for the amount of potassium originally present. Other scenarios yield even less heat. For example, if all the potassium were converted to oxide:



less heat would be produced. In fact only 2.6 kJ would be produced via this route. Thus, the MAXIMUM heat that can be accounted for by conventional routes for potassium nitrate conversion is 7 kJ. Other factors, for example the need to account for weight change, suggest even less heat should have been observed.

Even this maximum value for heat production from conventional chemistry is more than a factor of six less heat than observed experimentally. The observed experimental heat, greater than 43 kJ, is the sum of that released during hydrogen flow (>33kJ) and that measured during oxygen flow (>10kJ). In fact, the predicted heat is less than that observed during the oxidation process alone.

Finally, it is worth considering a worse case scenario. How much heat would be released if all the weight loss were due to carbon combustion? Given the weight loss of 1.02 gms, equivalent to less than 0.1 moles of carbon, we find 34 kJ would have been evolved to form CO₂. This value is uncomfortably close to the value actually measured. Yet this scenario is extremely unlikely. Indeed, where would 'free' oxygen come from during the hydrogen flow process? Why would it react to form carbon dioxide and not water? Moreover, carbon doesn't combust well at only 125 C. How do we explain the clear change in the crystal structure of the potassium without concomitant weight loss associated with that process?

SUMMARY/RECOMMENDATIONS

It is now clear that heat can be produced repeatedly from mixtures of potassium nitrate loaded carbon and noble metal carbon samples provided by HCP. It is also clear that there is a regular pattern: hydrogen flow leads to heat production, initially at a very high rate, but gradually decaying to yield a 'deactivated' catalyst. This deactivated catalyst releases additional heat during subsequent exposure to oxygen. Moreover, a final x-ray analysis indicates the crystal structure of

the potassium changes from a nitrate to an oxide during the process. Weight change can be attributed to changes in potassium crystal structure alone, if oxygen is admitted slowly.

It is also clear that there are many conventional chemical scenarios which lead from the initial nitrate structure to the final oxide structure. None of these can account for the observed heats.

It is clear that the model of potassium transformation accompanied by anomalous heat needs to be strengthened before this model is submitted to the scientific community. Specifically, three recommendations for further study are made. First, it is recommended that tests to confirm directly the postulated change in the potassium from nitrate to metal in flowing hydrogen be undertaken. If it can be verified that heat is released during a process which converts potassium nitrate to potassium metal, then the claim that anomalous heat has been observed is greatly strengthened. The change from nitrate to metal is ENDOTHERMIC. The best method for carrying out the proposed work is to employ *in situ* x-ray analysis.

Second, it is recommended that the heat release and crystal structure transformations of potassium nitrate on carbon in the absence of any noble metal be studied. In the absence of hydrogen atoms it is postulated that the same decomposition of the nitrate will take place. However, there should be no anomalous heat production. In fact, the overall transformation of the nitrate to a metallic state in flowing hydrogen at elevated temperature should be endothermic. Following the complete decomposition of the nitrate oxygen exposure should lead to significant heat release. The behavior of these samples should also be studied using both calorimetry and *in situ* x-ray diffraction.

One change in procedure is urged. Every effort should be made to study the composition of the off-gas during anomalous heat production. A clear certification that carbon oxides are not detected strengthens the argument that weight changes are related to changes in the structure of the potassium nitrate and not to the combustion of the support material.



Fig. 21-1
Touch Test (111395a)

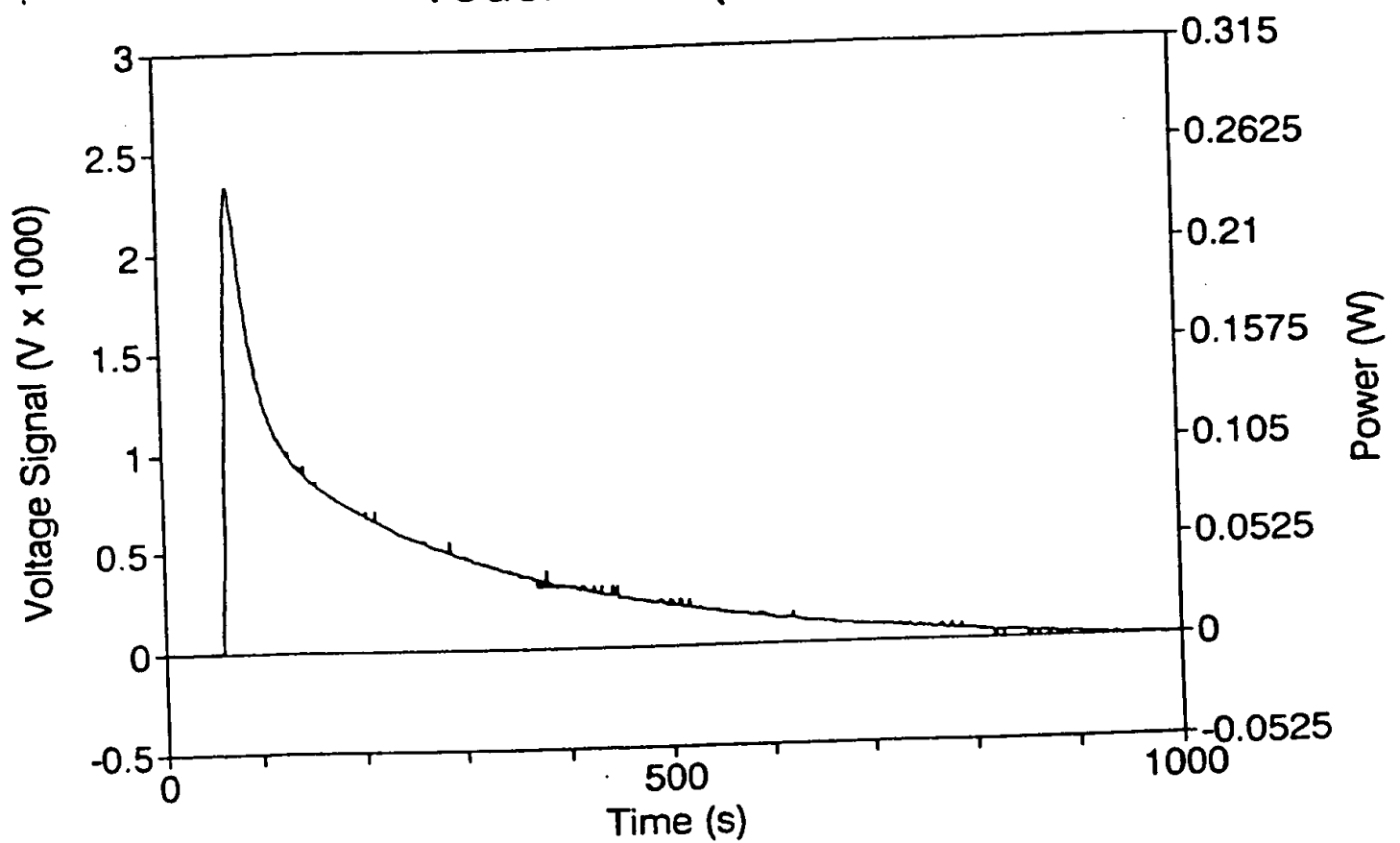


Fig. 21-2
Base Line 1 at 200 C (111395a)

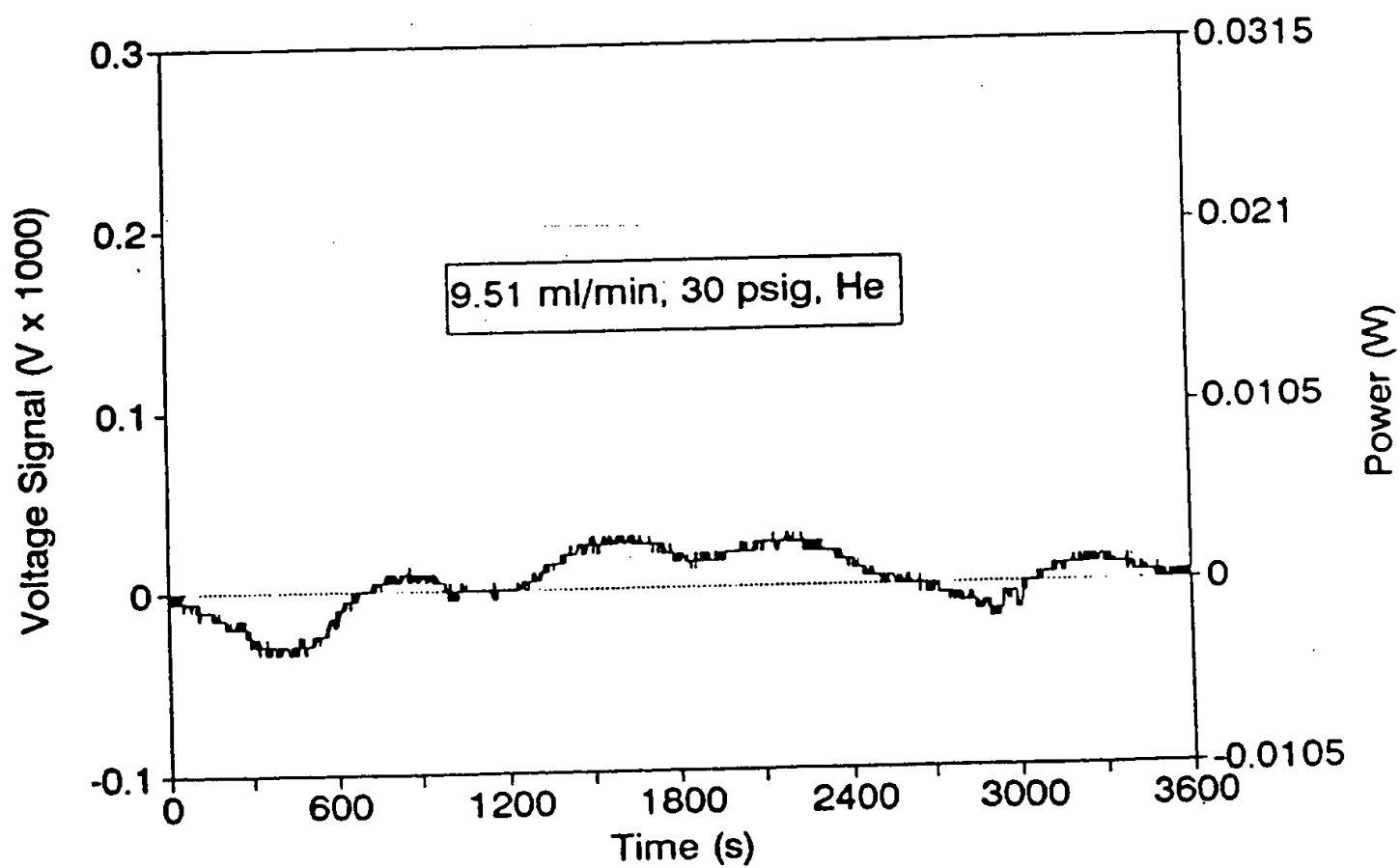


Fig. 21-3
Switch from He to H₂ at 200 C (111395a)

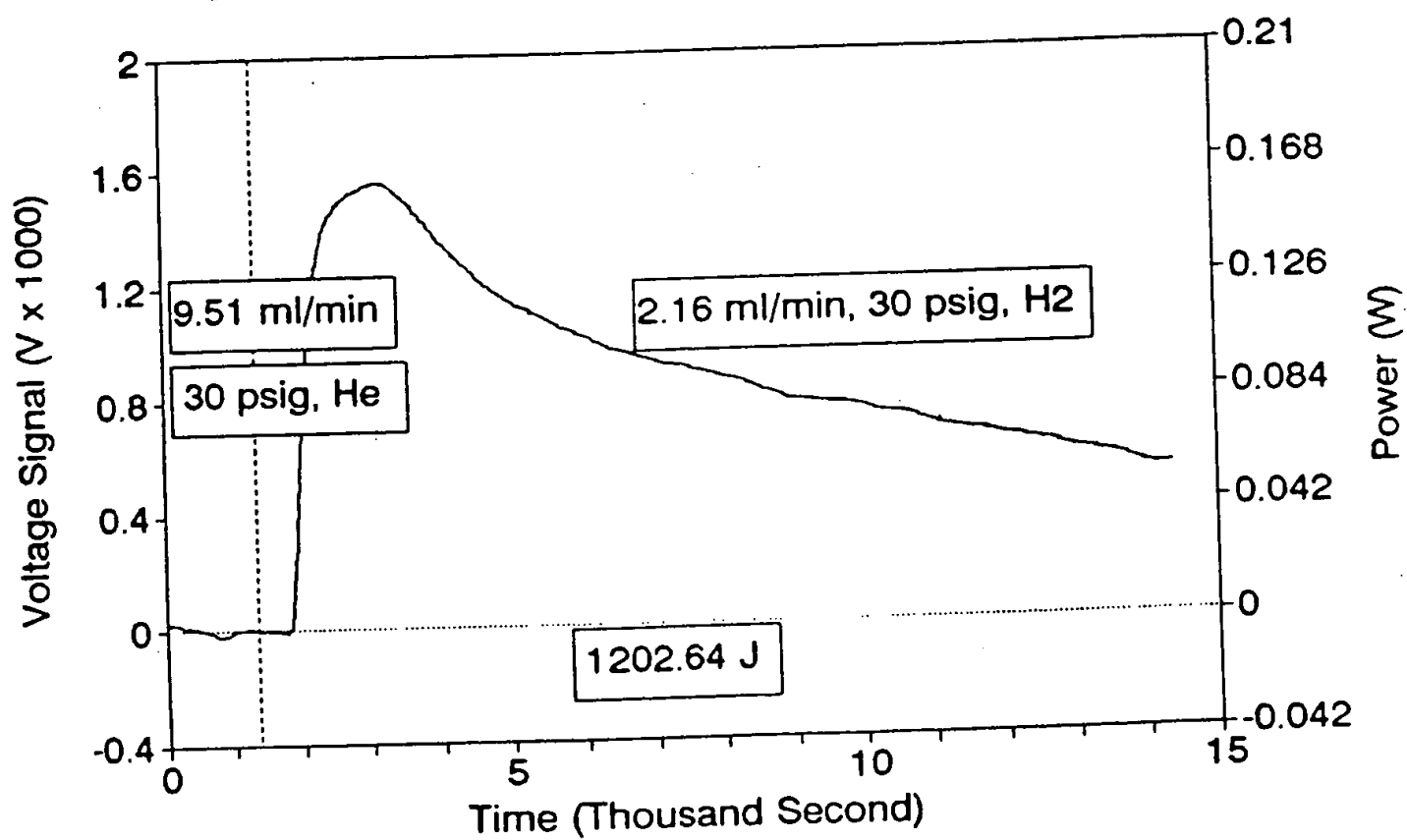


Fig. 21-4
H2 reaction 1 at 200 C (111395a)

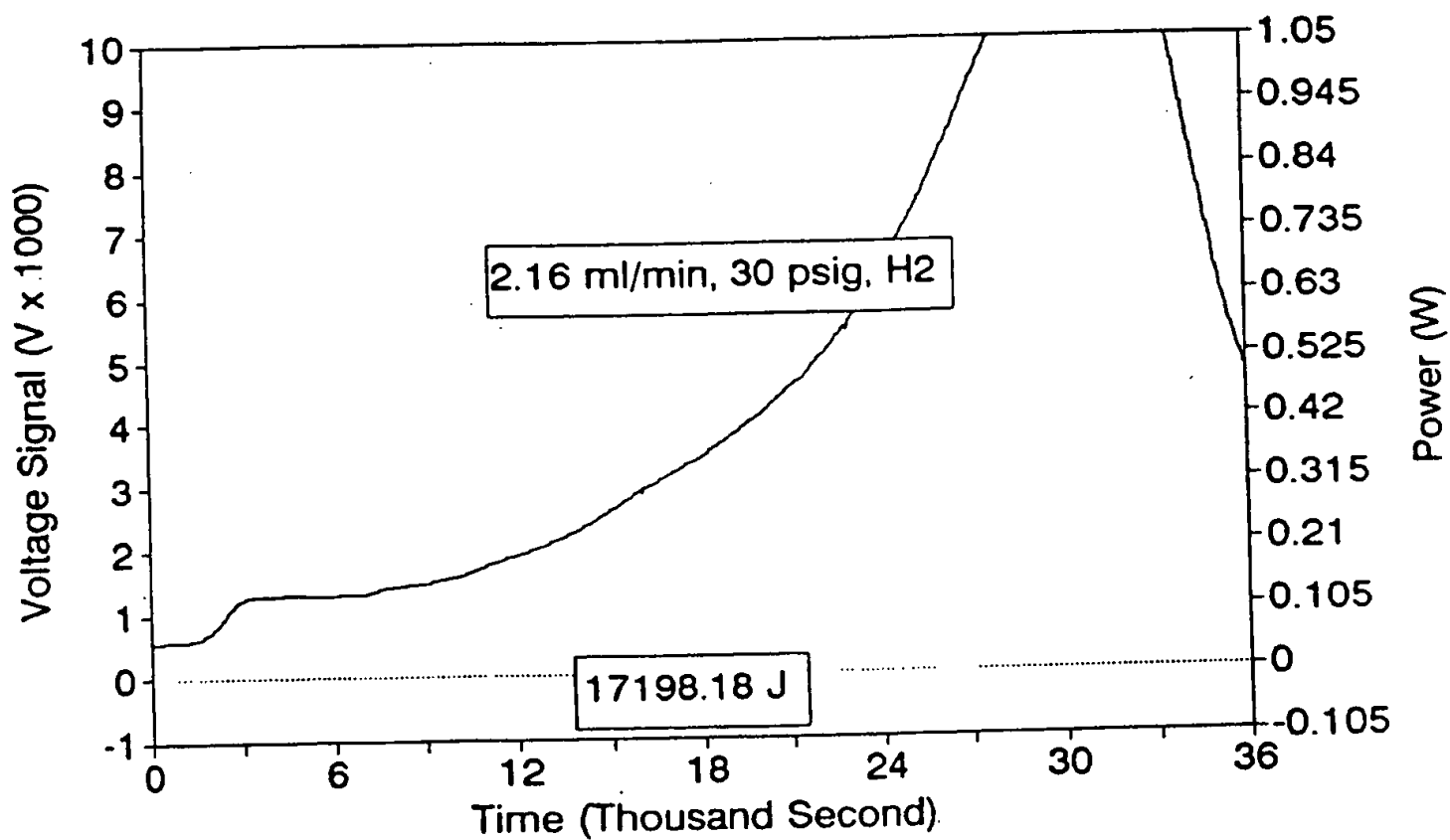


Fig. 21-5
H2 reaction 2 at 200 C (111395a)

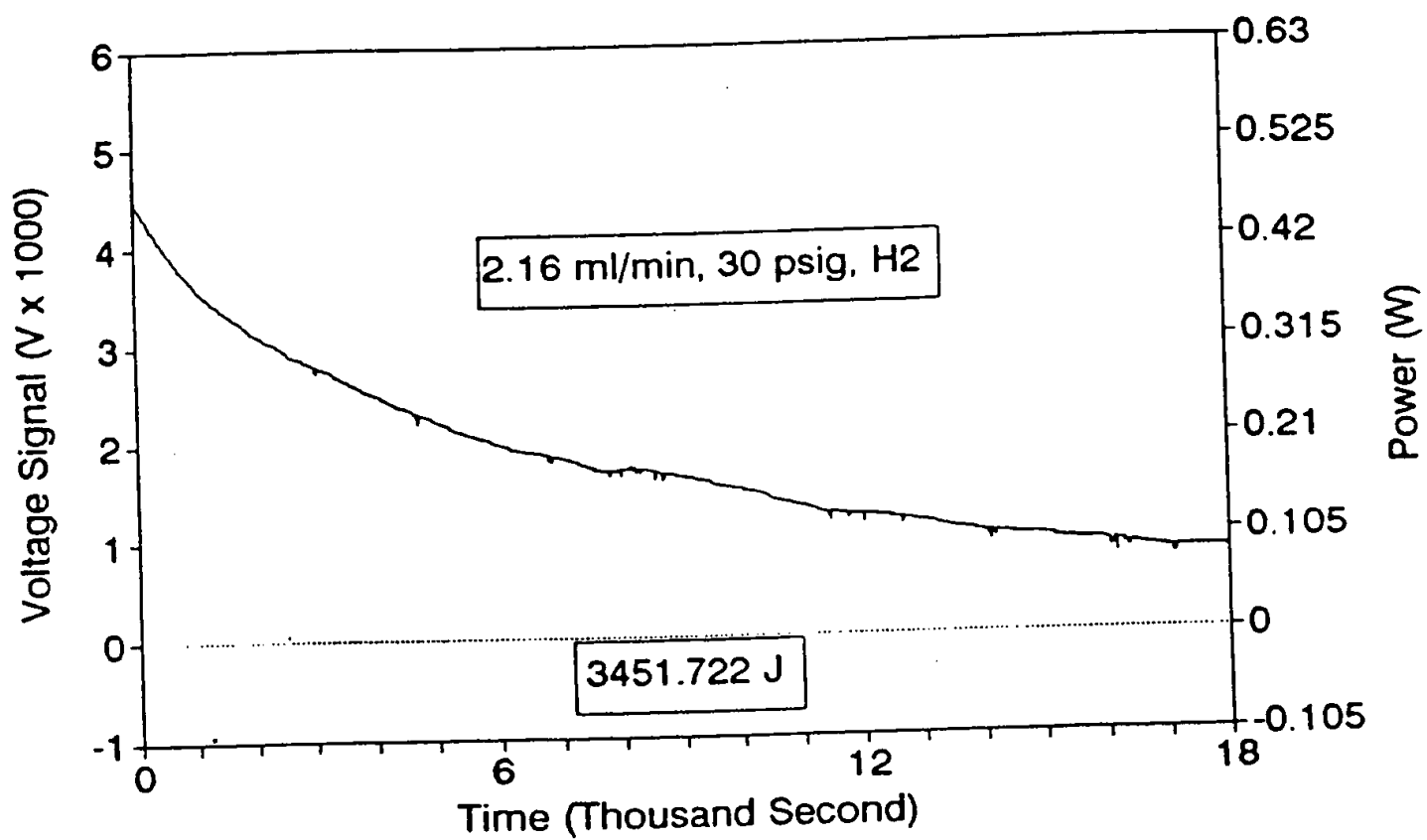


Fig. 21-6
H2 reaction 3 at 200 C (111395a)

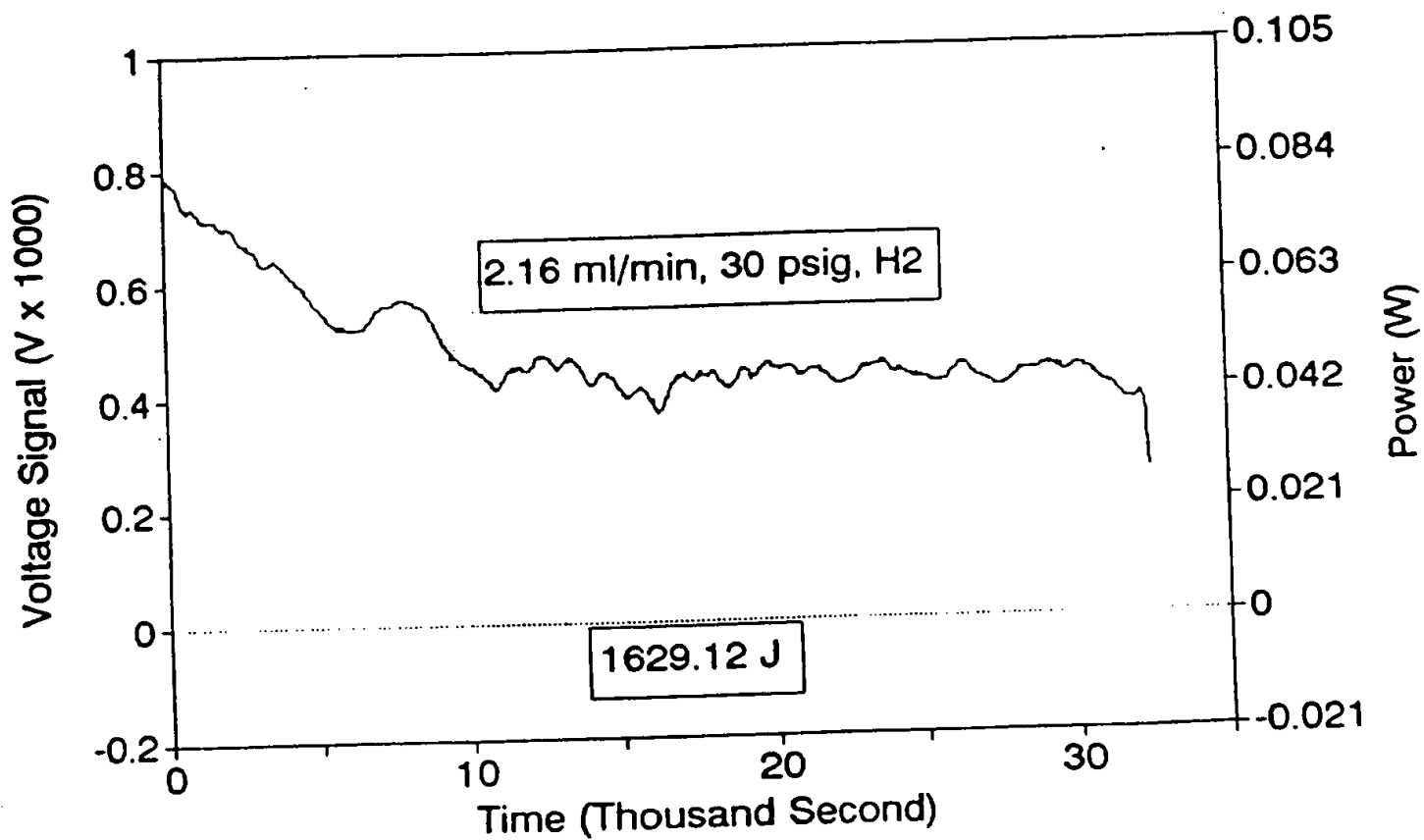
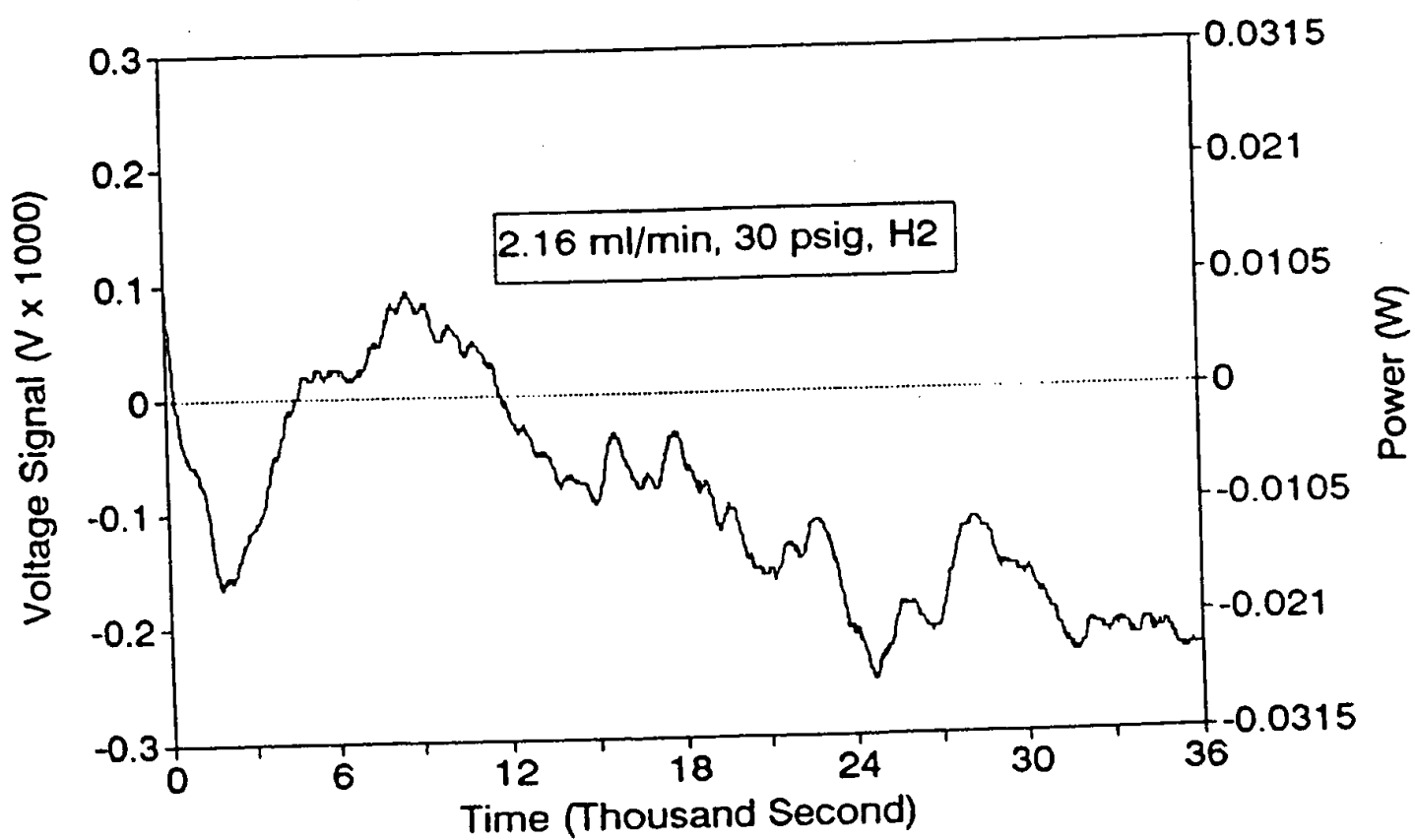
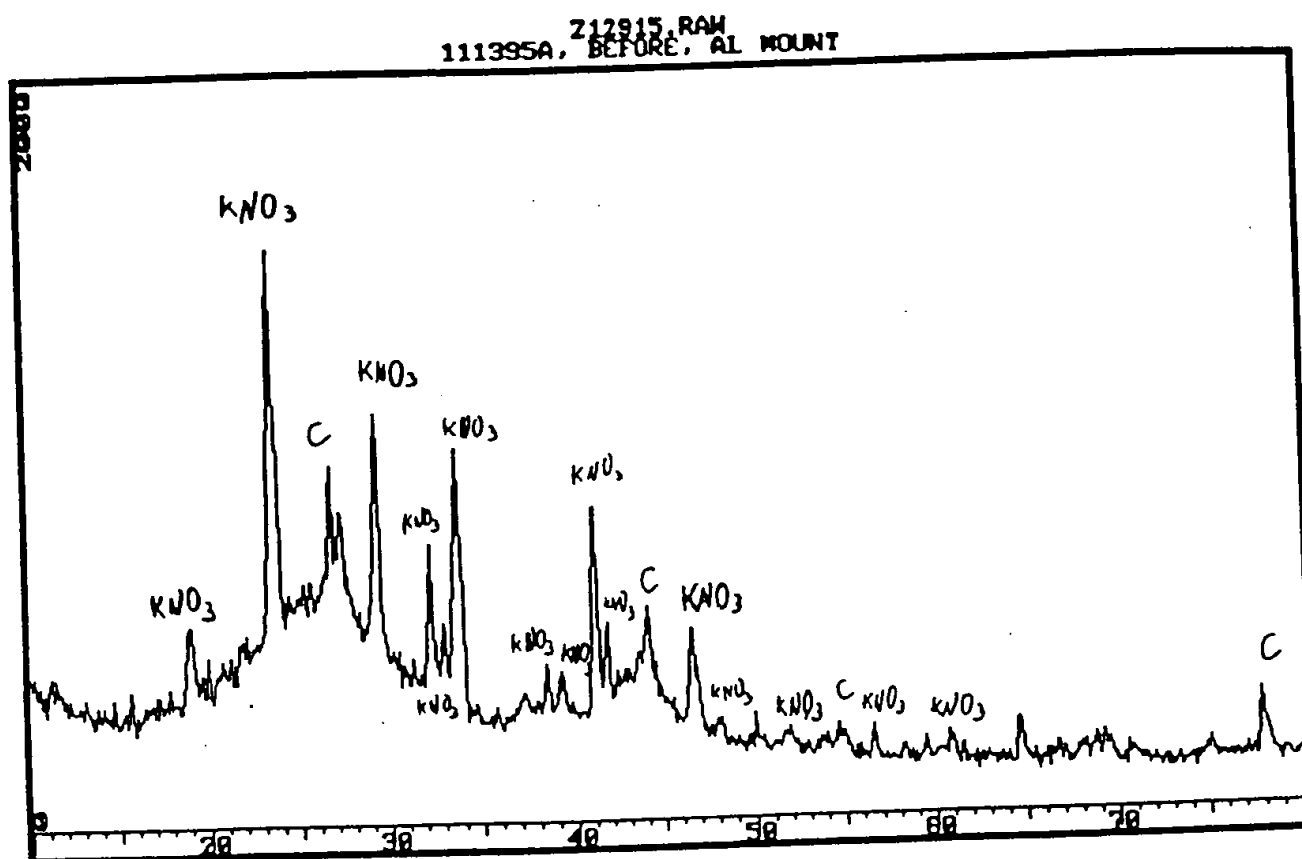


Fig. 21-7
H₂ reaction 4 at 200 C (111395a)



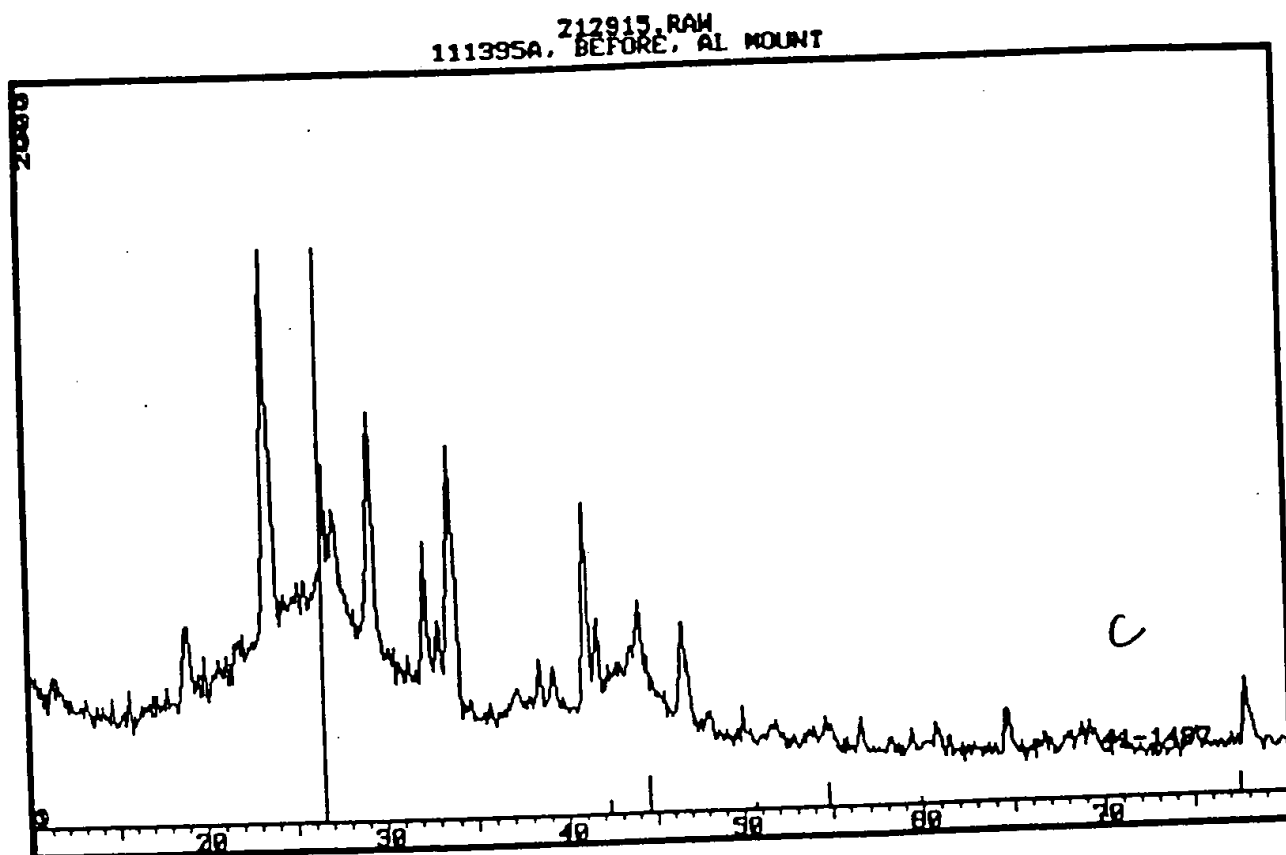
111395 A , Before



11/28

21-9

111 395 A, Before



21-10

111395A, BEFORE, AL MOUNT

2080

KNO₃

Fig. 22-1
Touch Test (113095a)

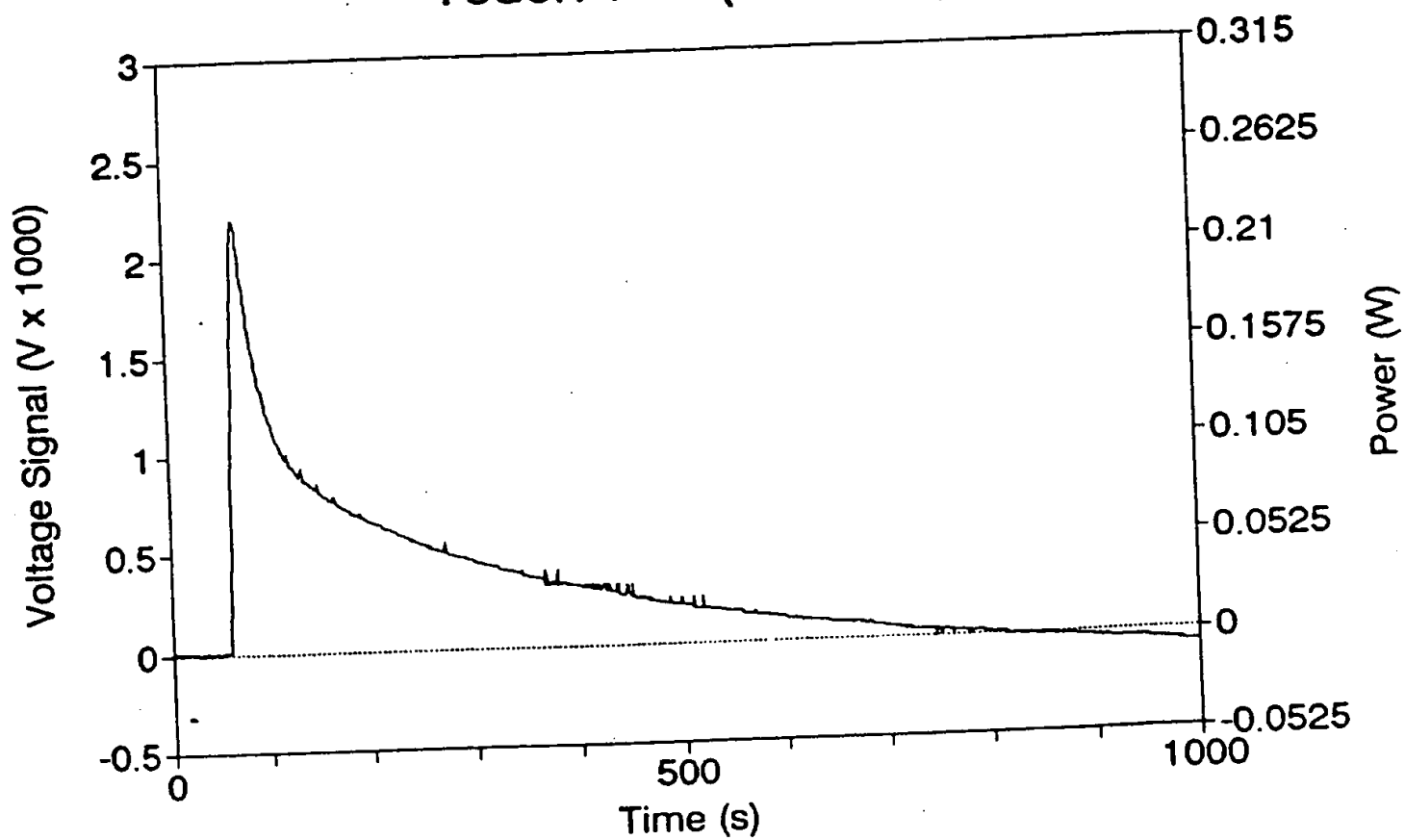


Fig. 22-2
Base Line 1 at 125 C (113095a)

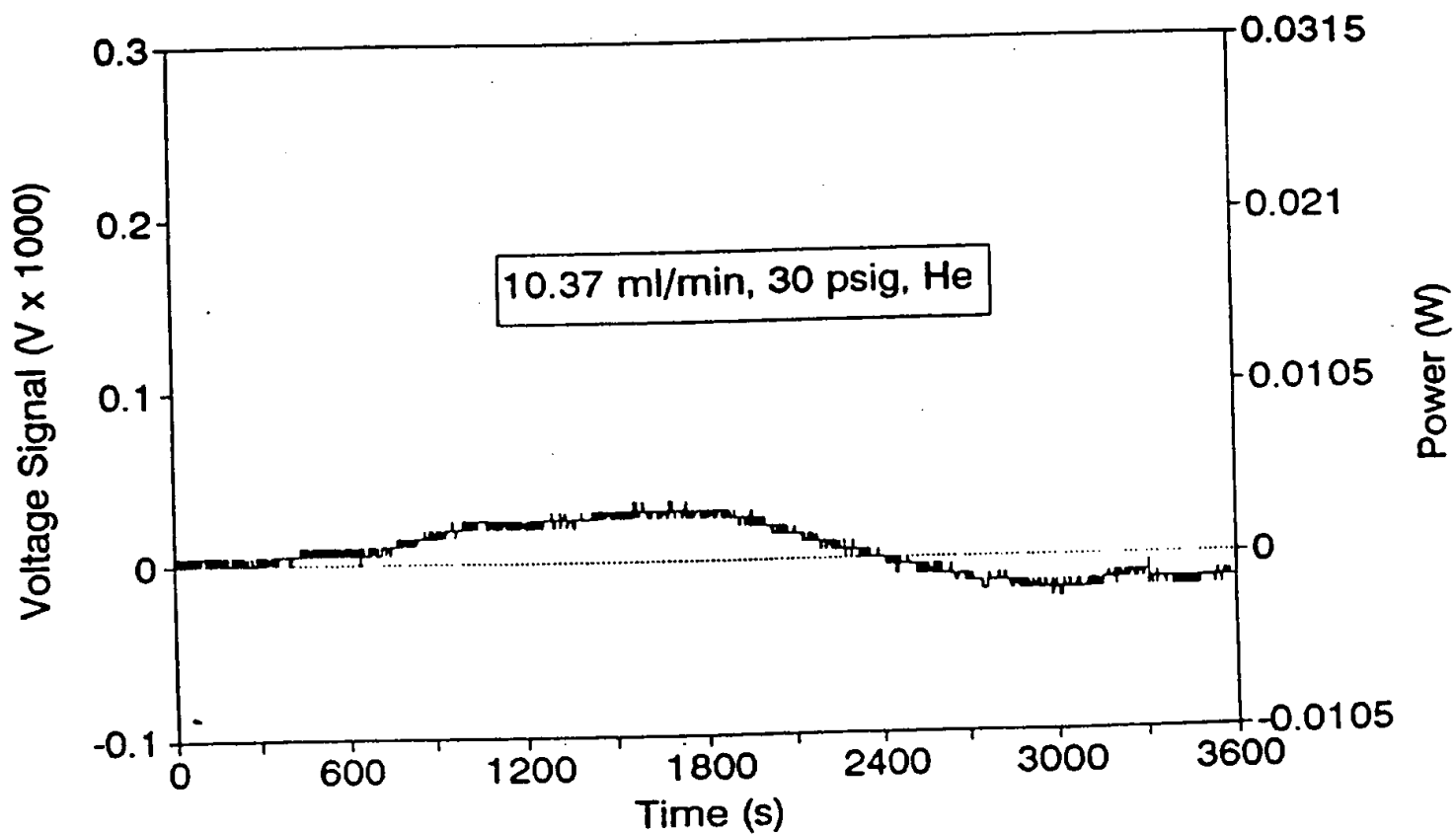


Fig. 22-3
Switch from He to H₂ at 125 C (113095a)

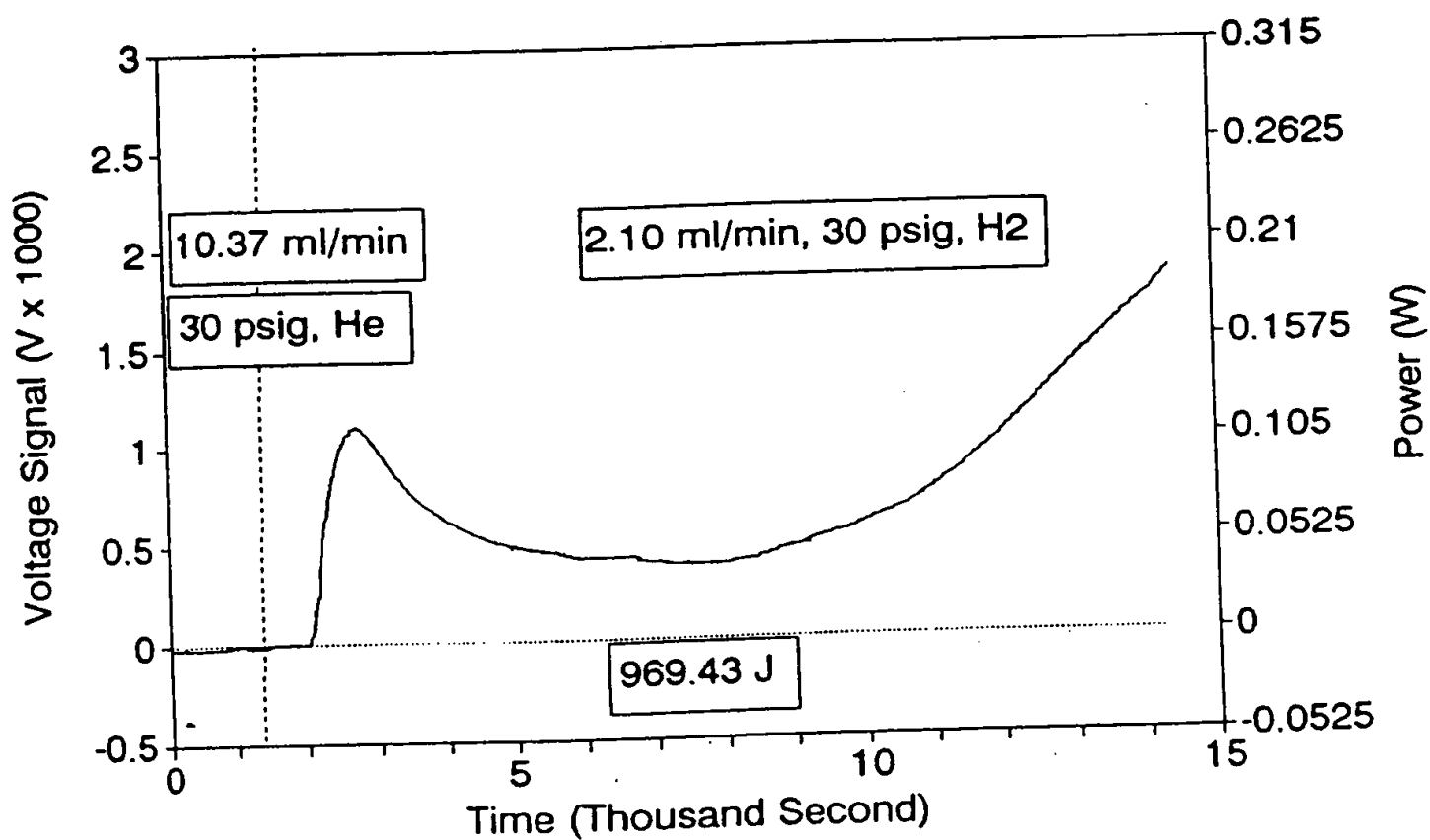


Fig. 22-4
H2 reaction 1 at 125 C (113095a)

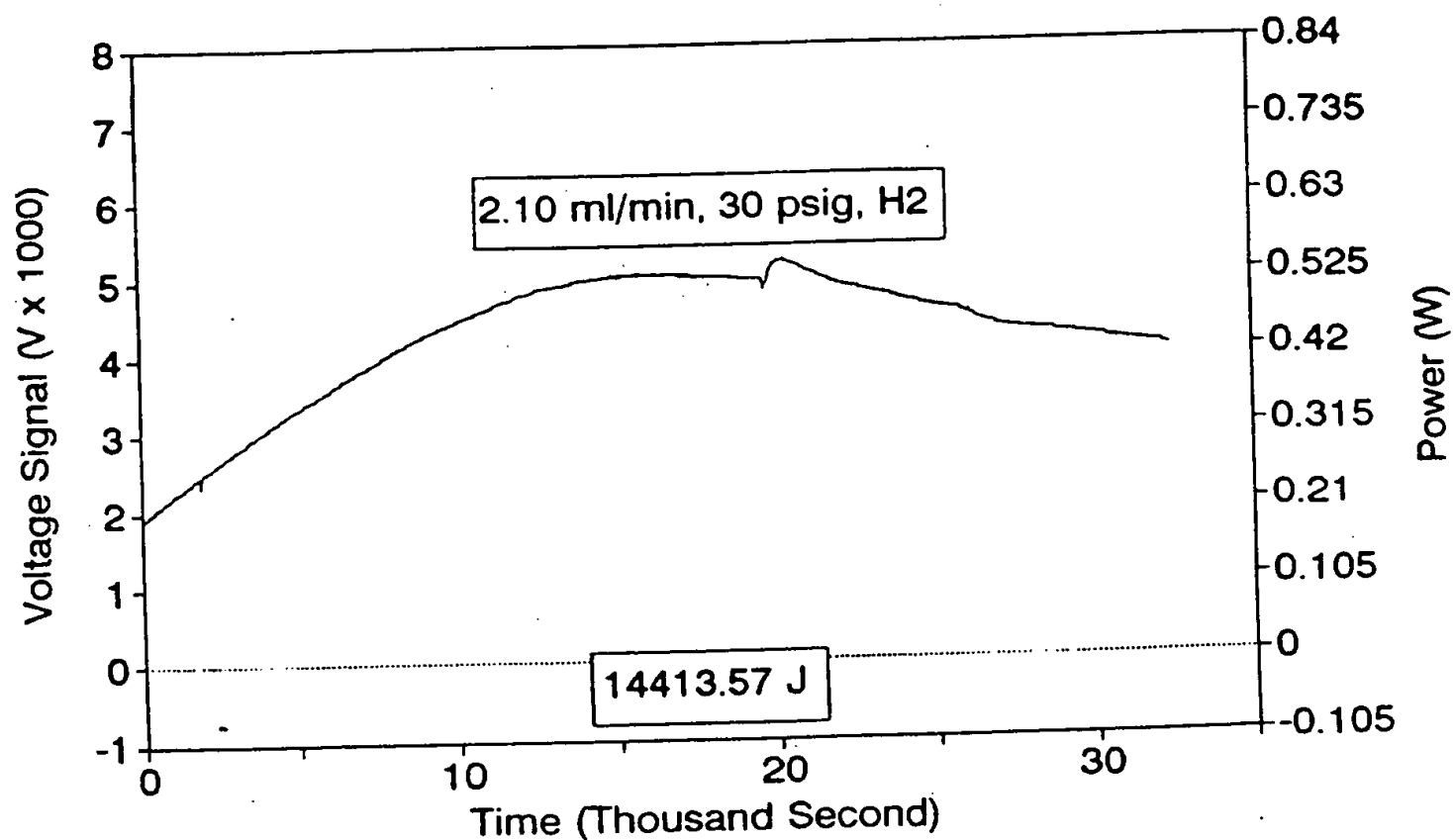


Fig. 22-5
H2 reaction 2 at 125 C (113095a)

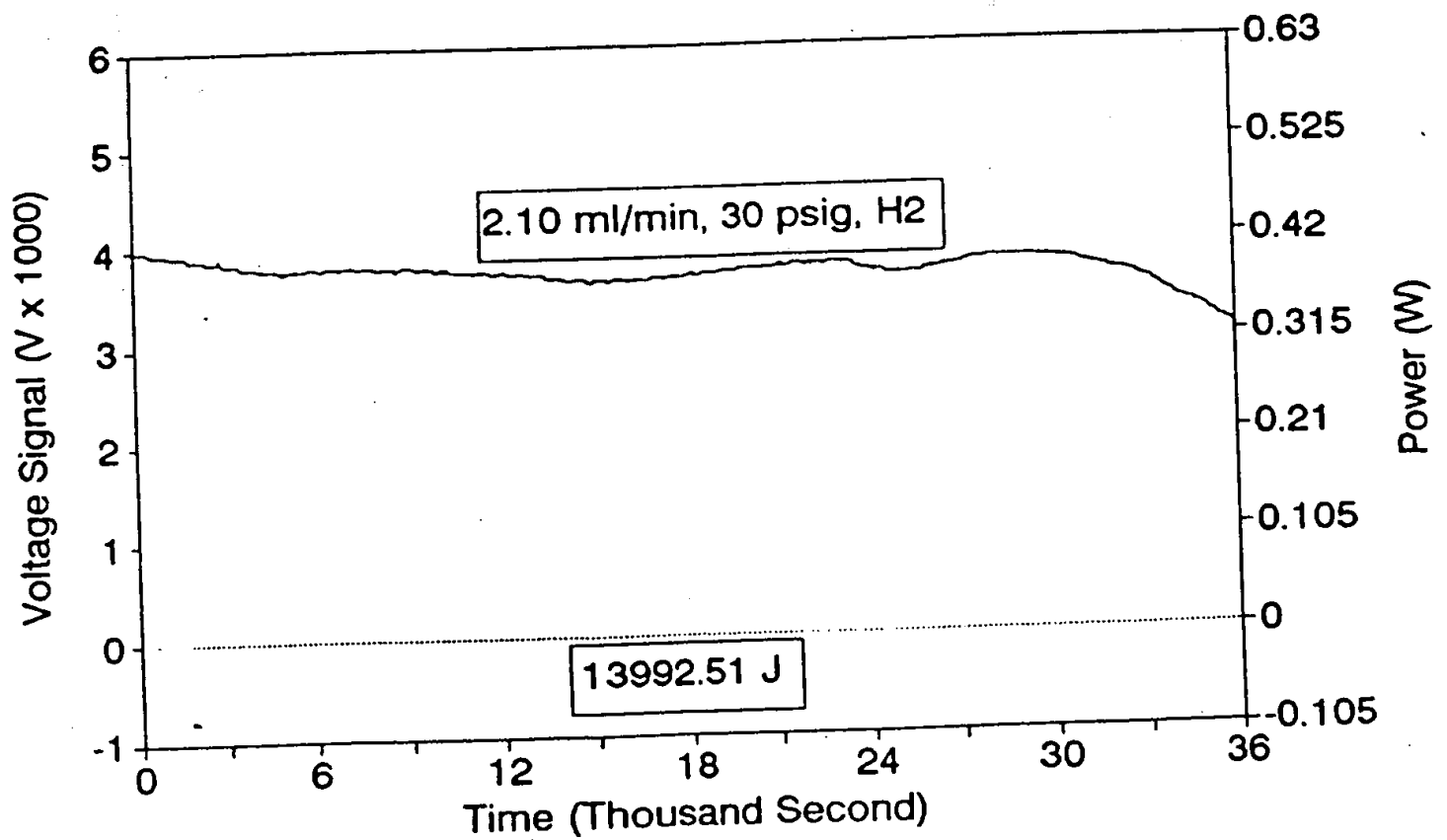


Fig. 22-6
H2 reaction 3 at 125 C (113095a)

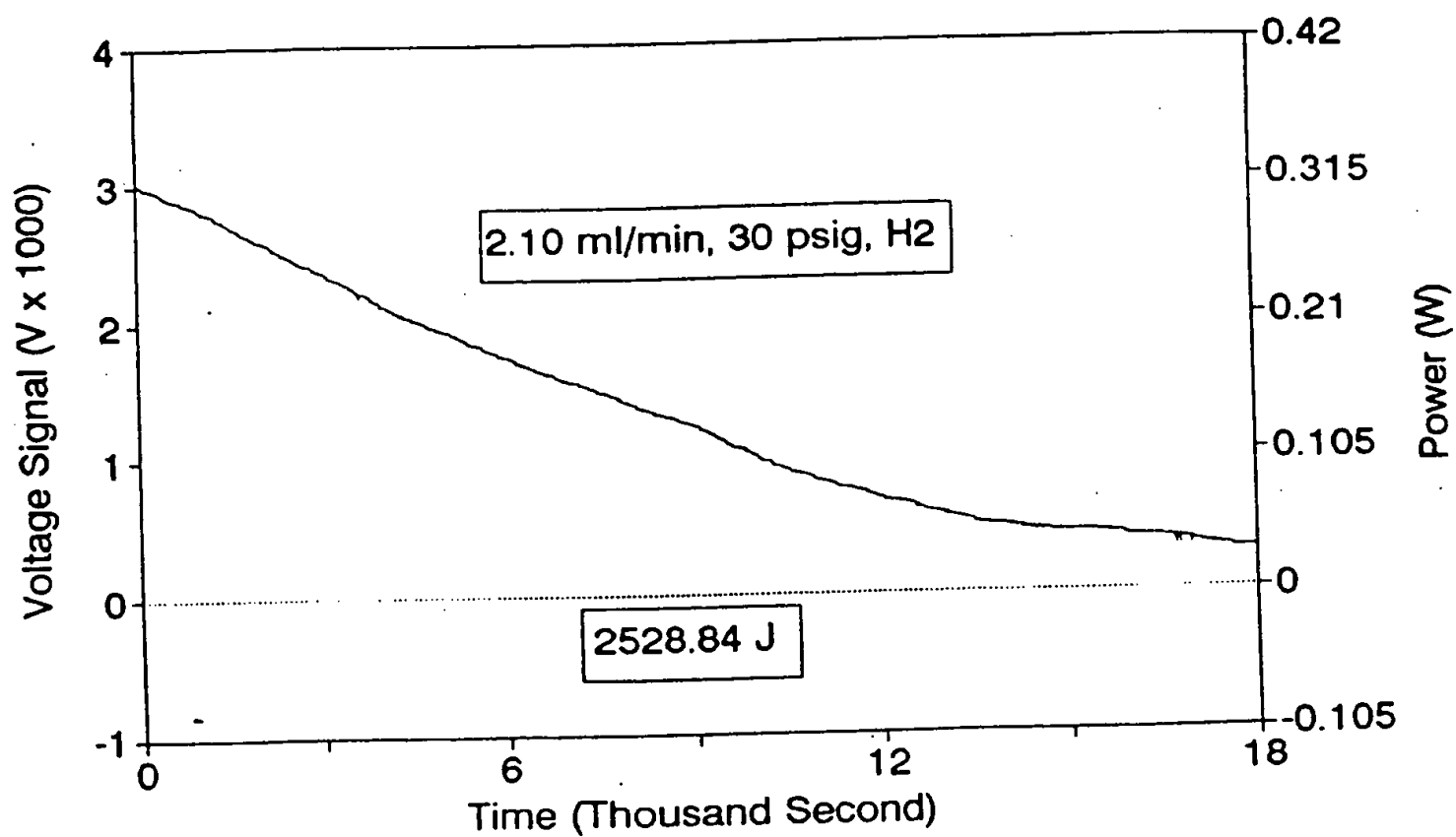


Fig. 22-7
H2 reaction 4 at 125 C (113095a)

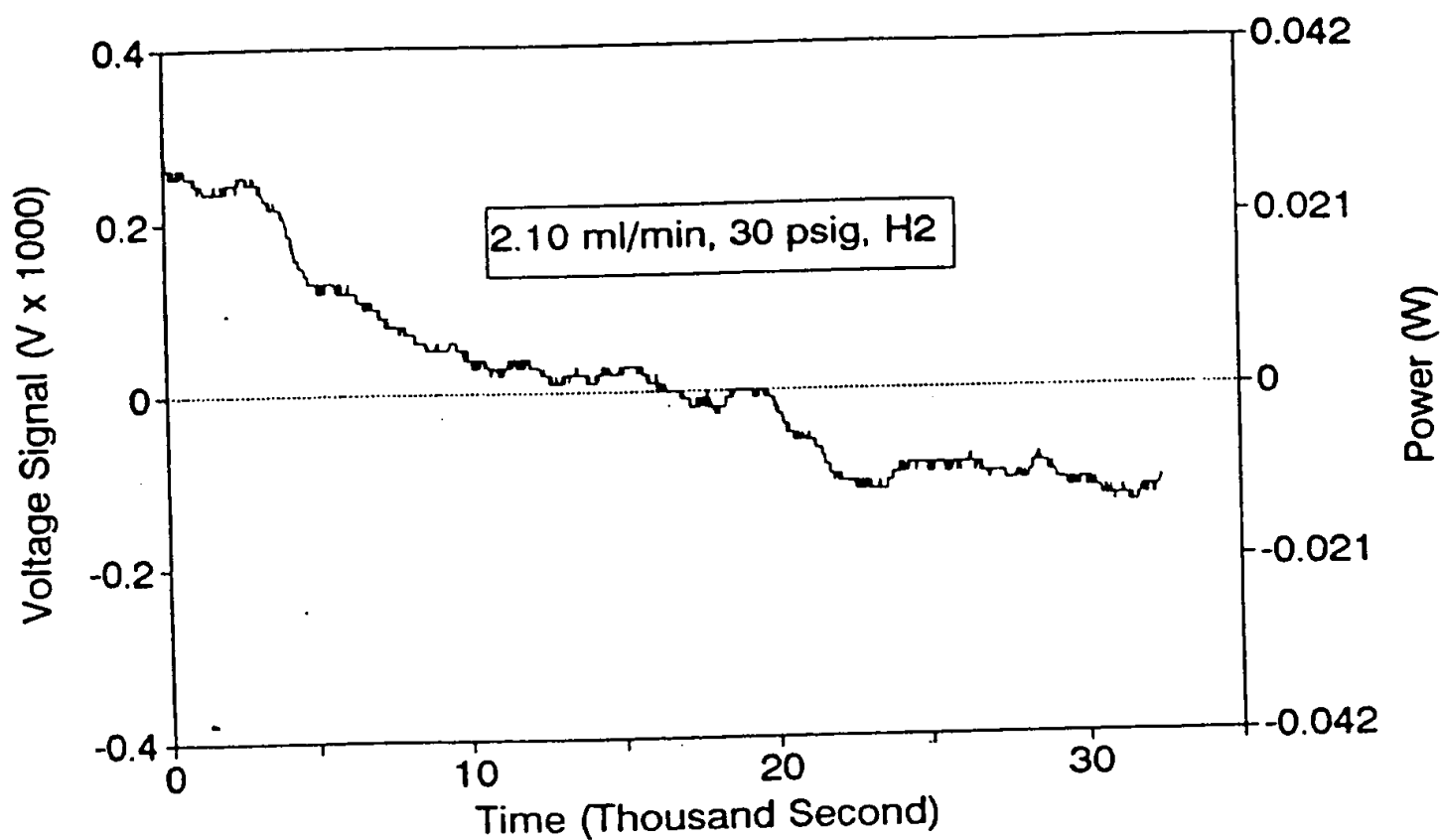




Fig. 23-1
Touch Test (120495a)

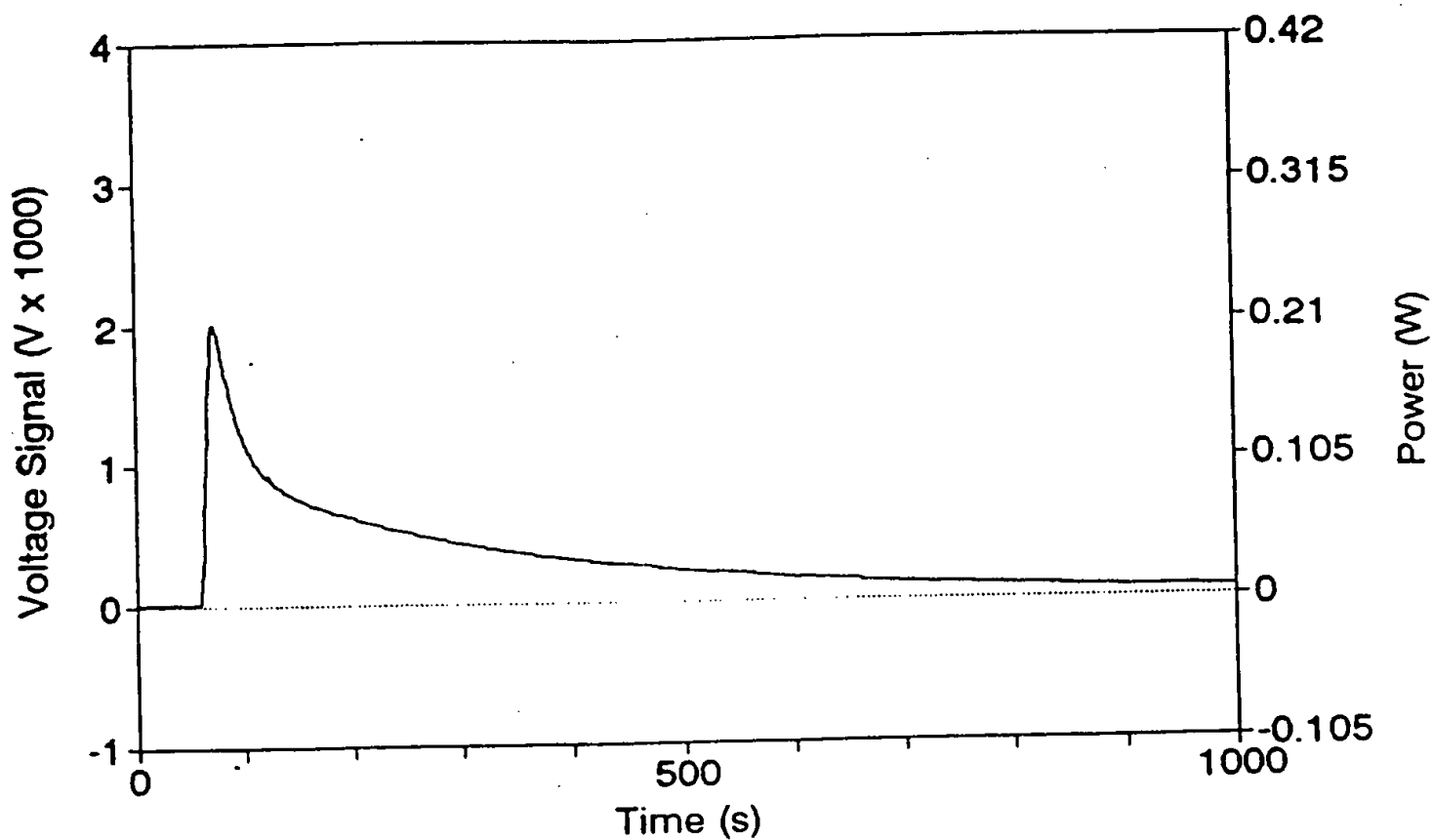


Fig. 23-2
Base Line 1 at 125 C (120495a)

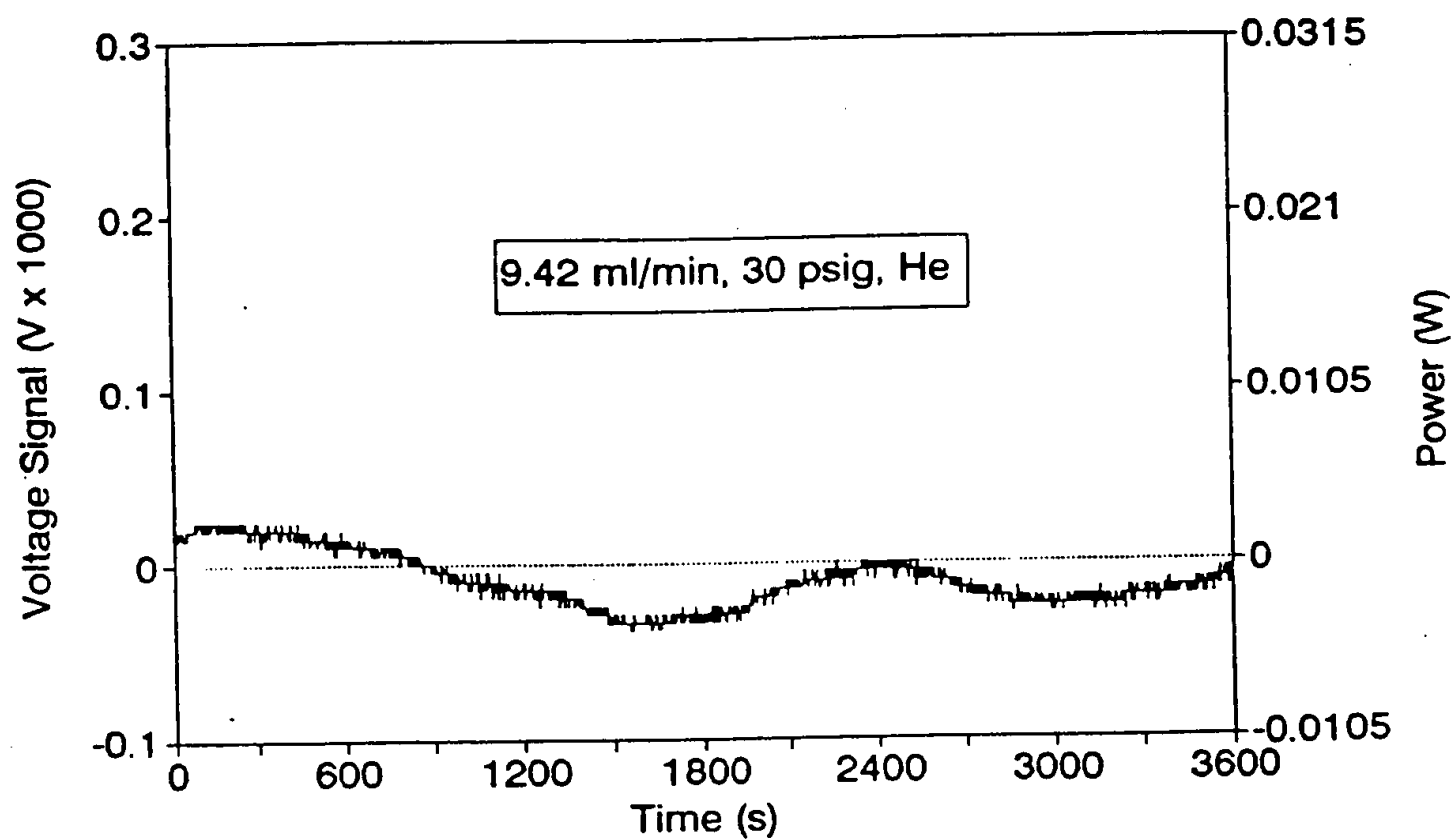


Fig. 23-3
Switch from He to H₂ at 125C (120495a)

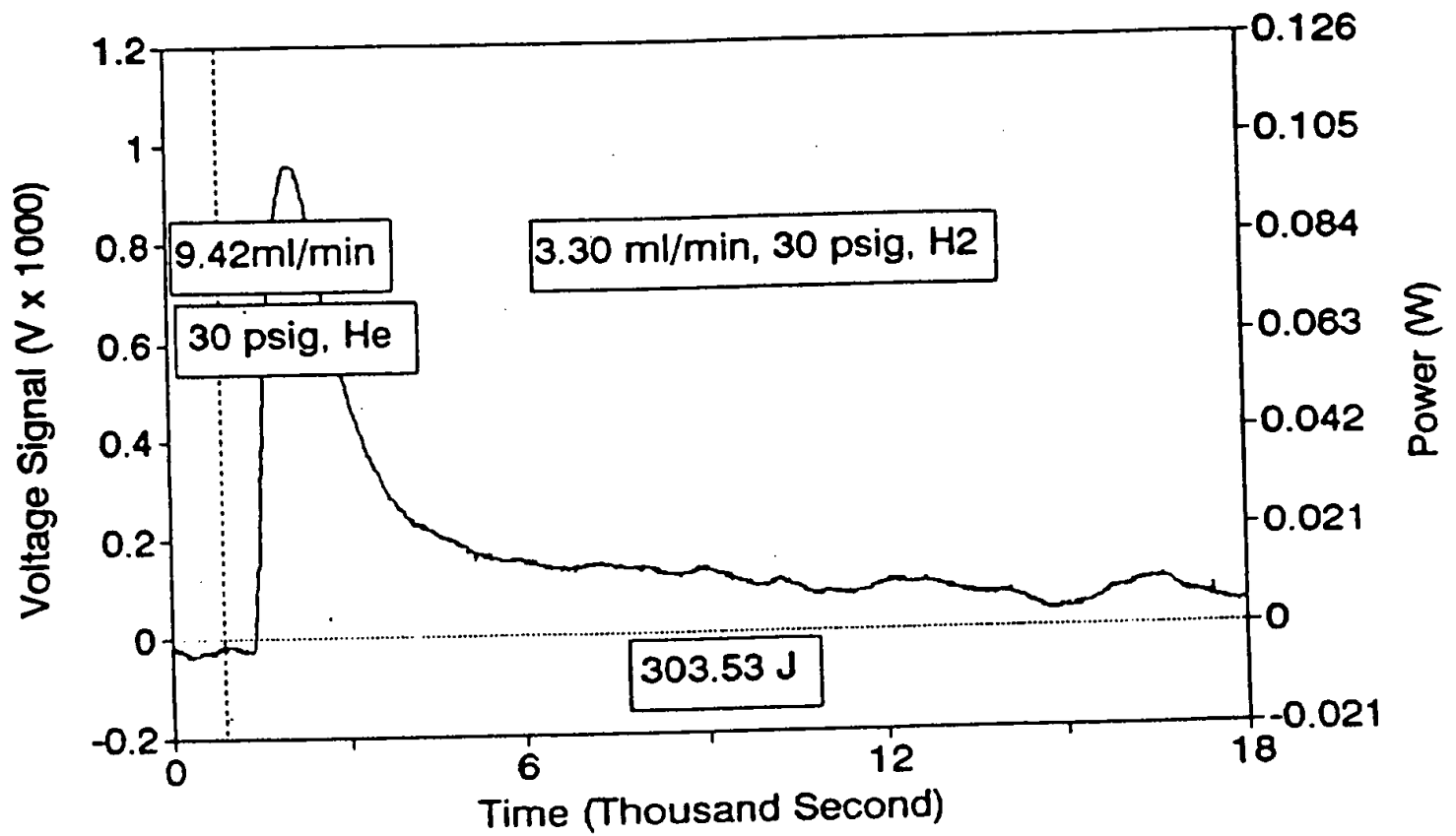


Fig. 23-4
H2 reaction 1 at 125 C (120495a)

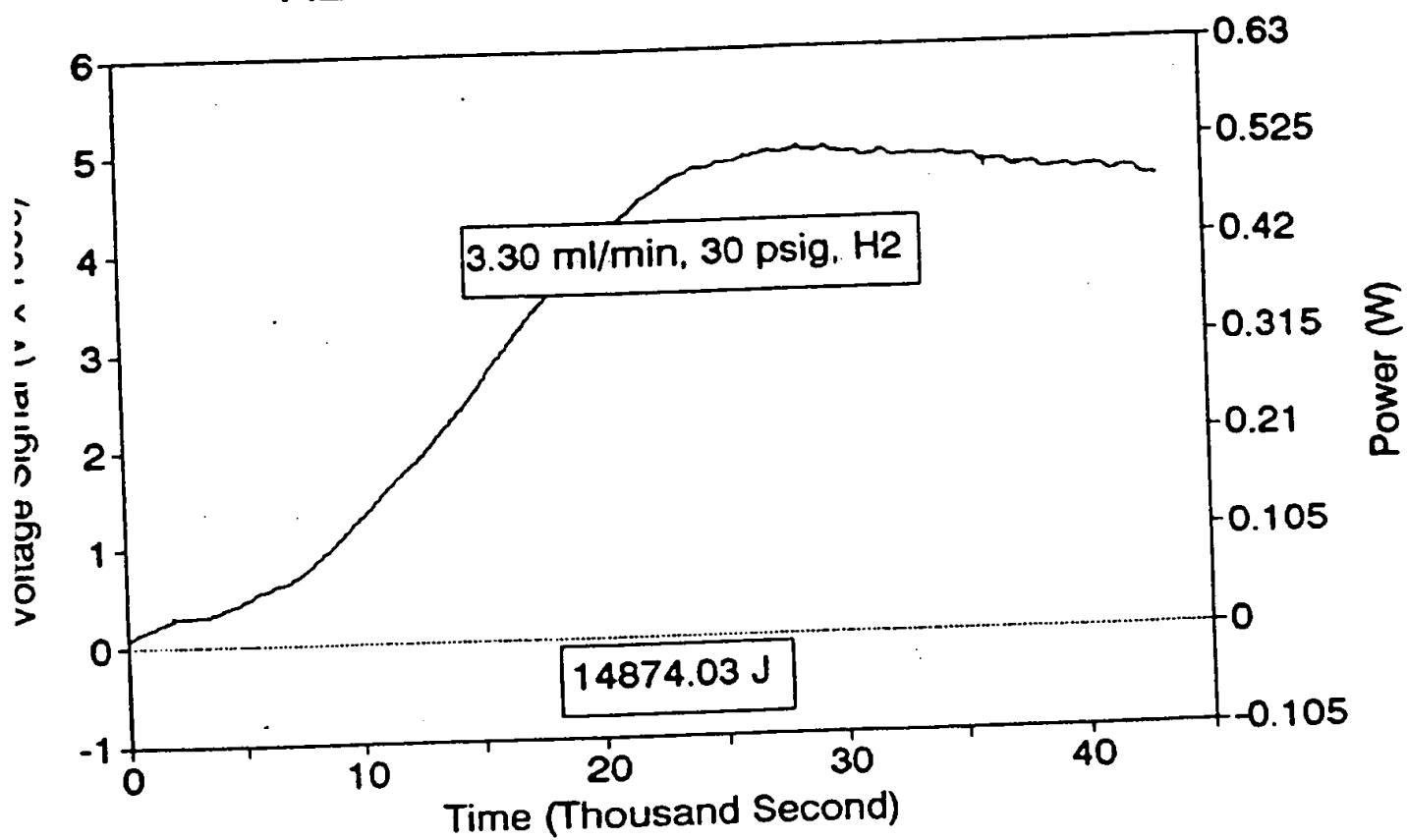


Fig. 23-5
H2 reaction 2 at 125 C (120495a)

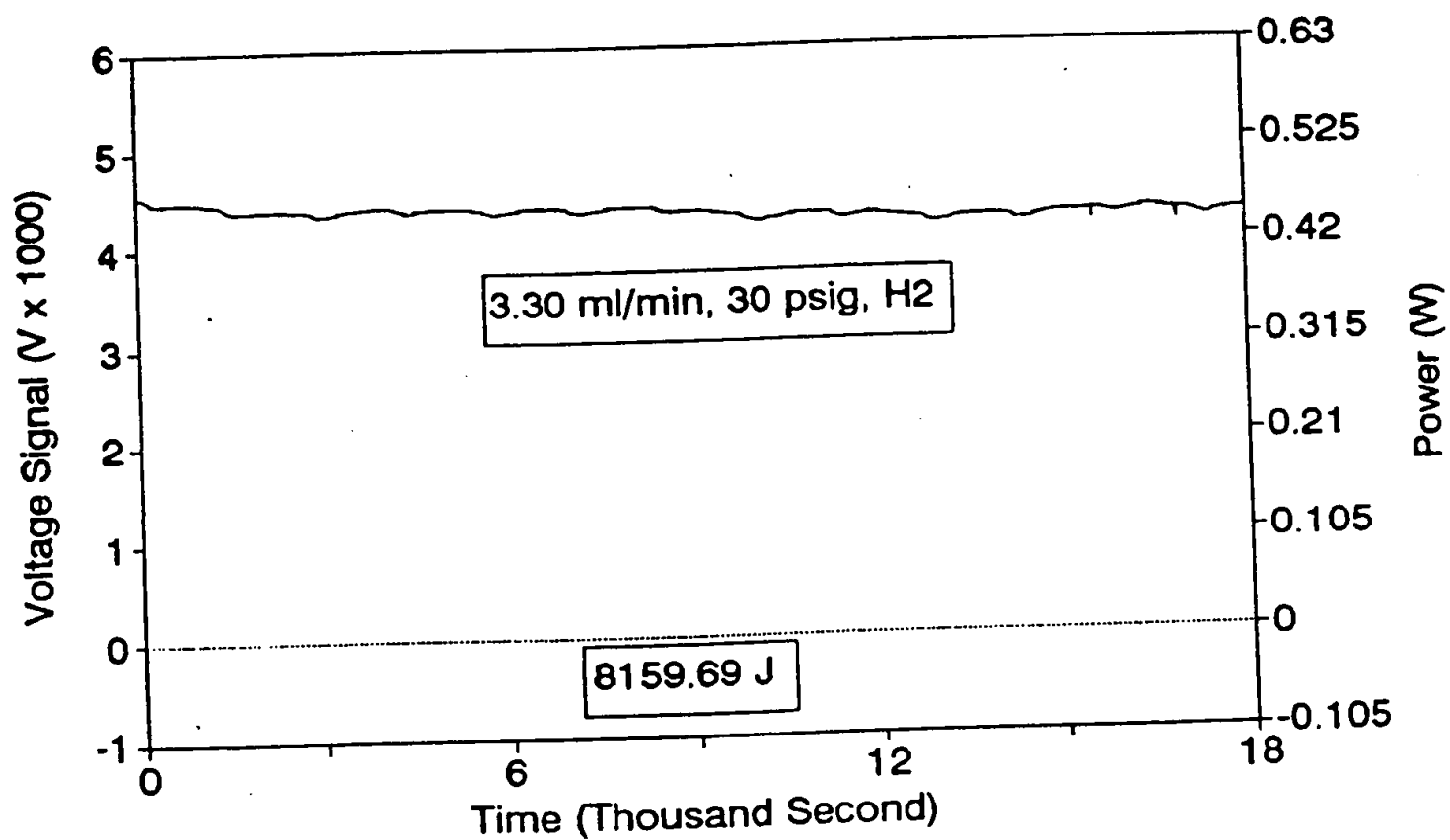


Fig. 23-6
H2 reaction 3 at 125 C (120495a)

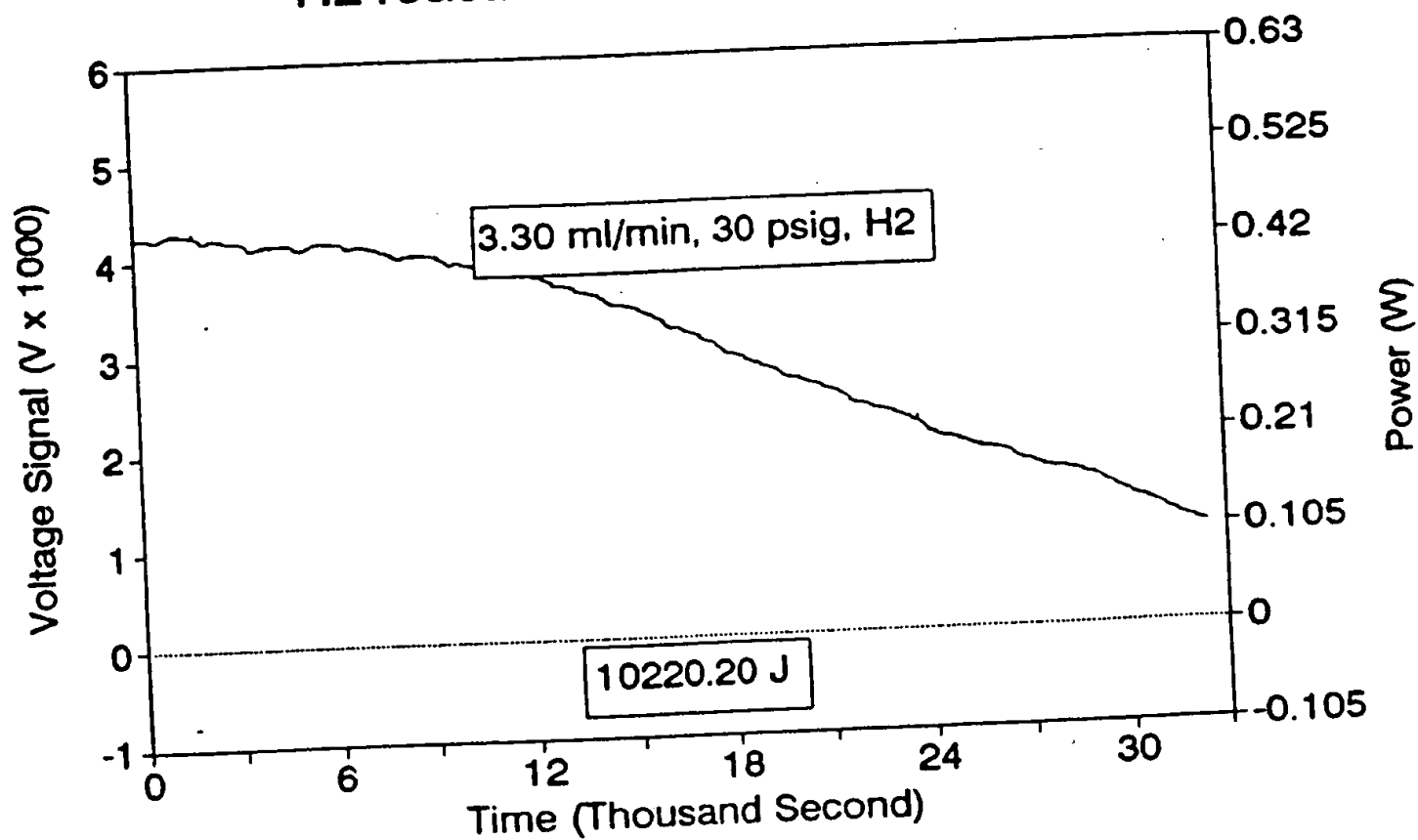


Fig. 23-7
H2 reaction 4 at 125 C (120495a)

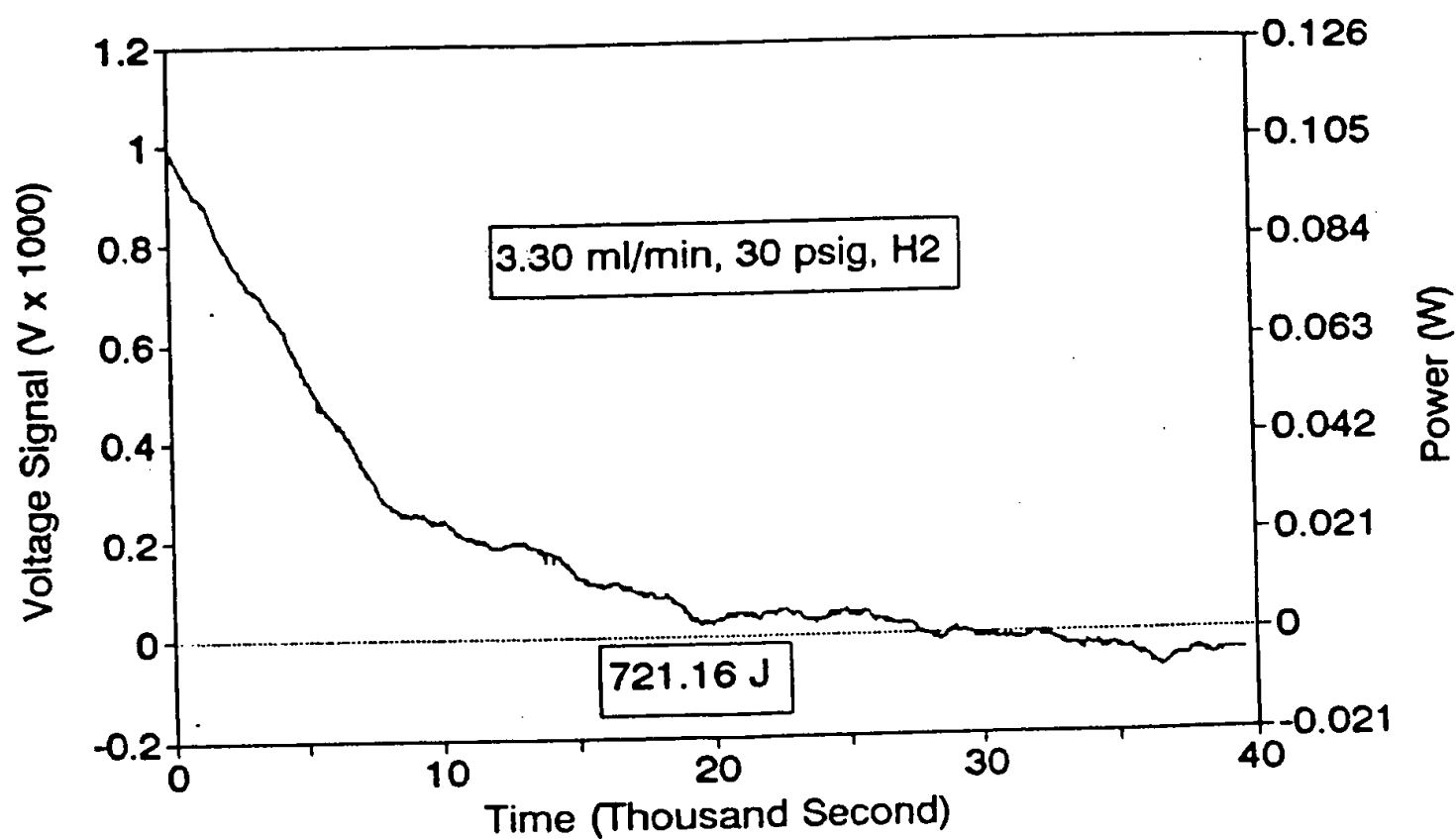


Fig. 23-8
Switch to (He+Air) at 125 C (120495a)

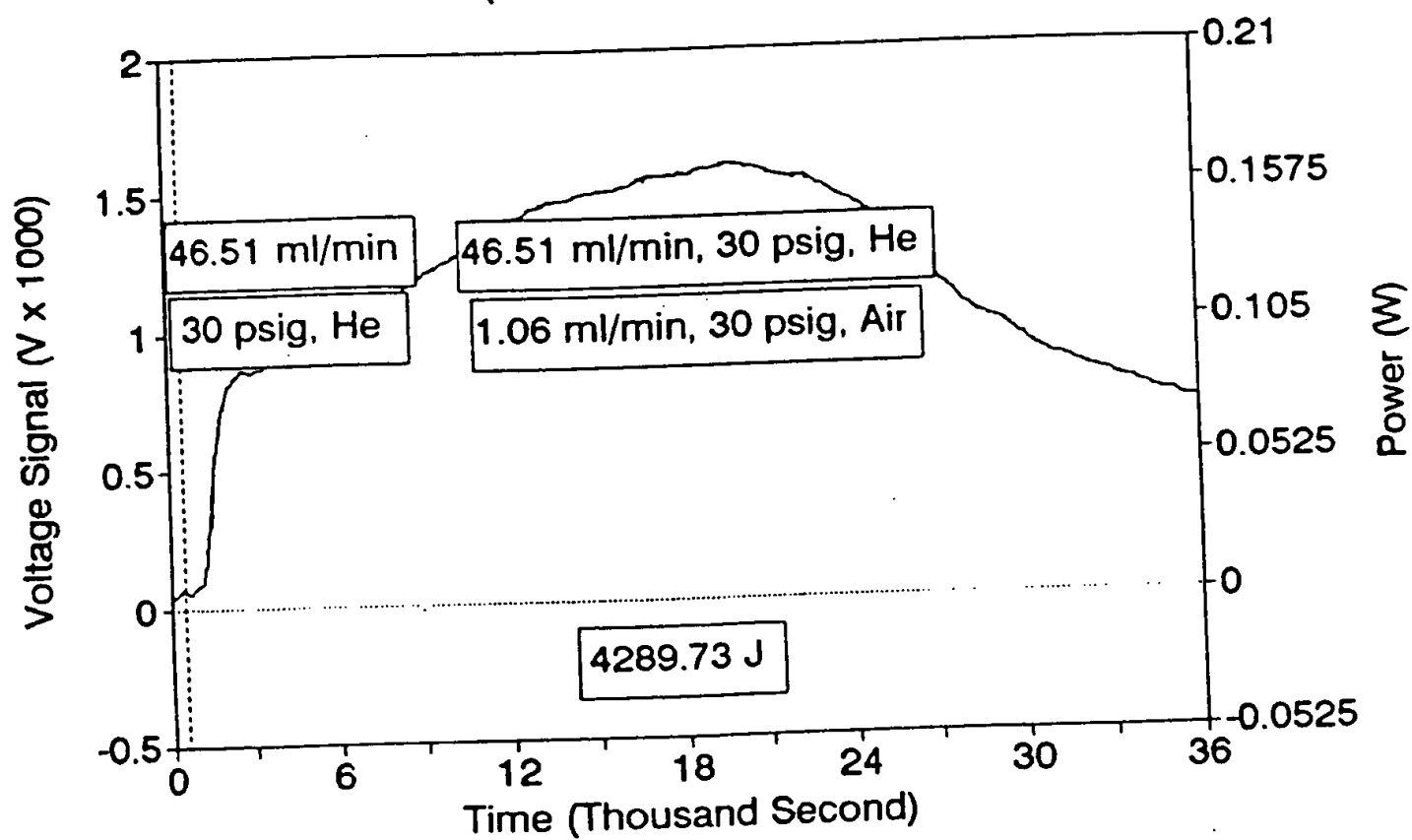


Fig. 23-9
Air reaction 1 at 125 C (120495a)

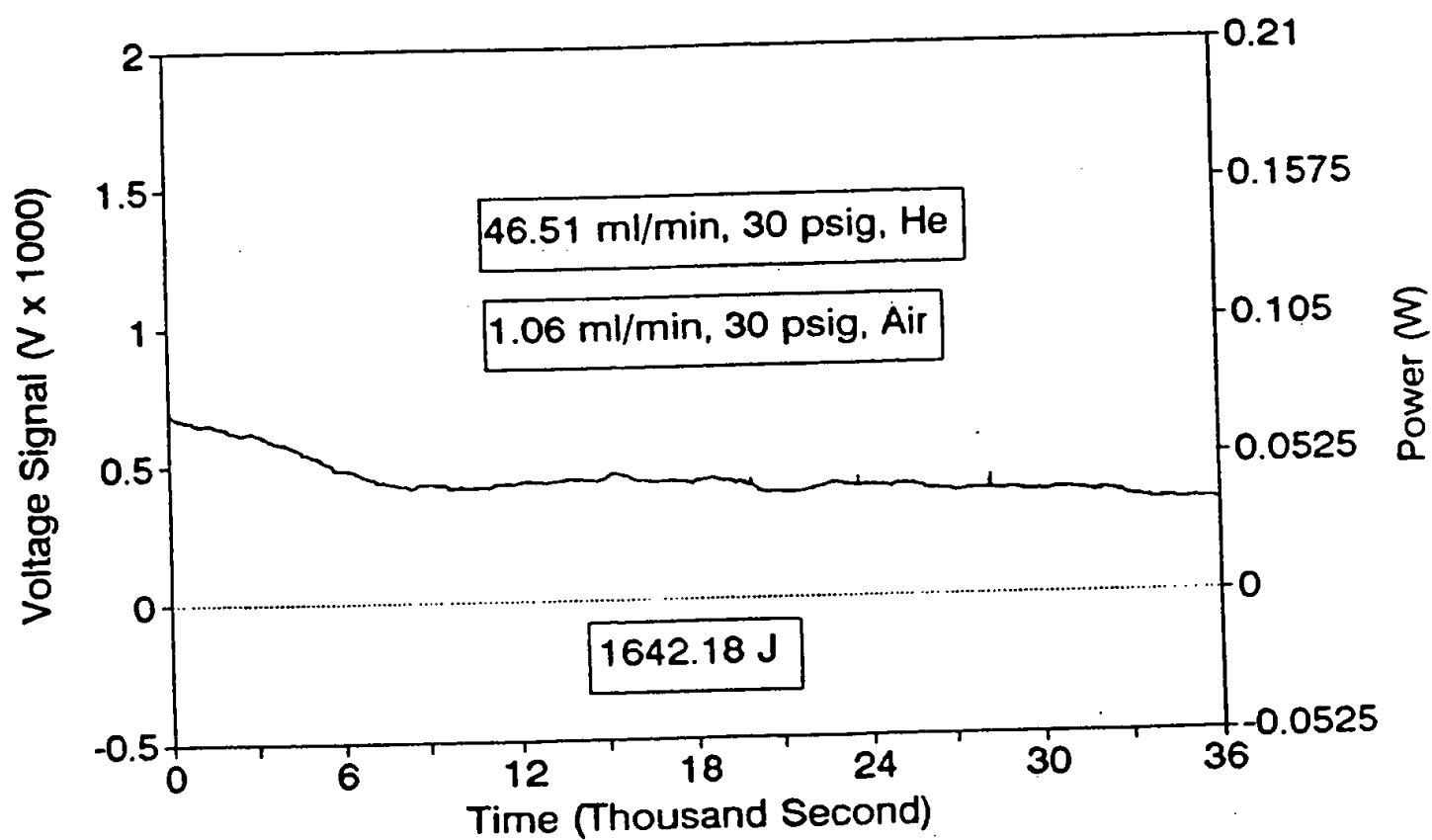


Fig. 23-10
Air reaction 2 at 125 C (120495a)

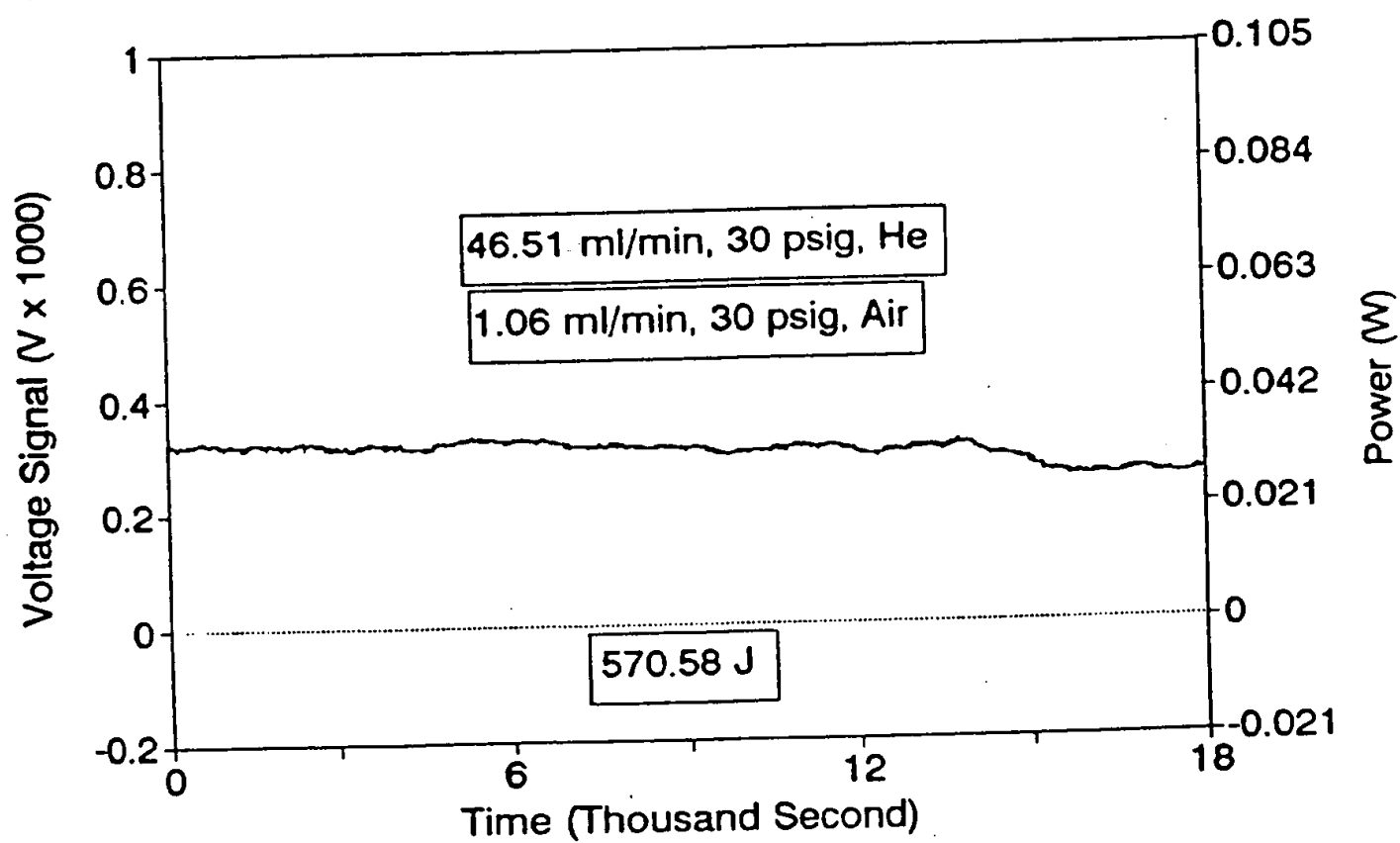


Fig. 23-11
Air reaction 3 at 125 C (120495a)

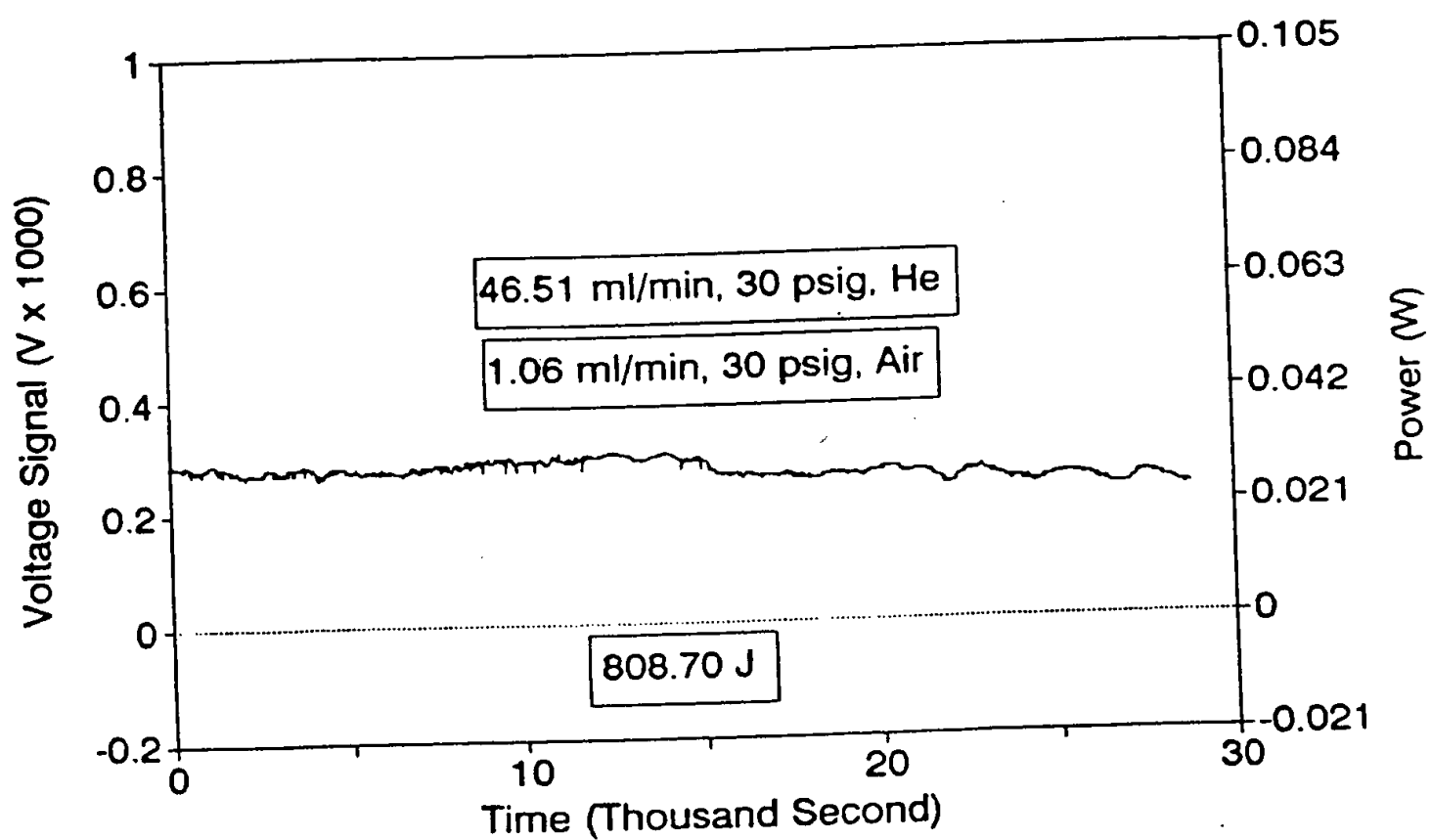


Fig. 23-12
Air reaction 4 at 125 C (120495a)

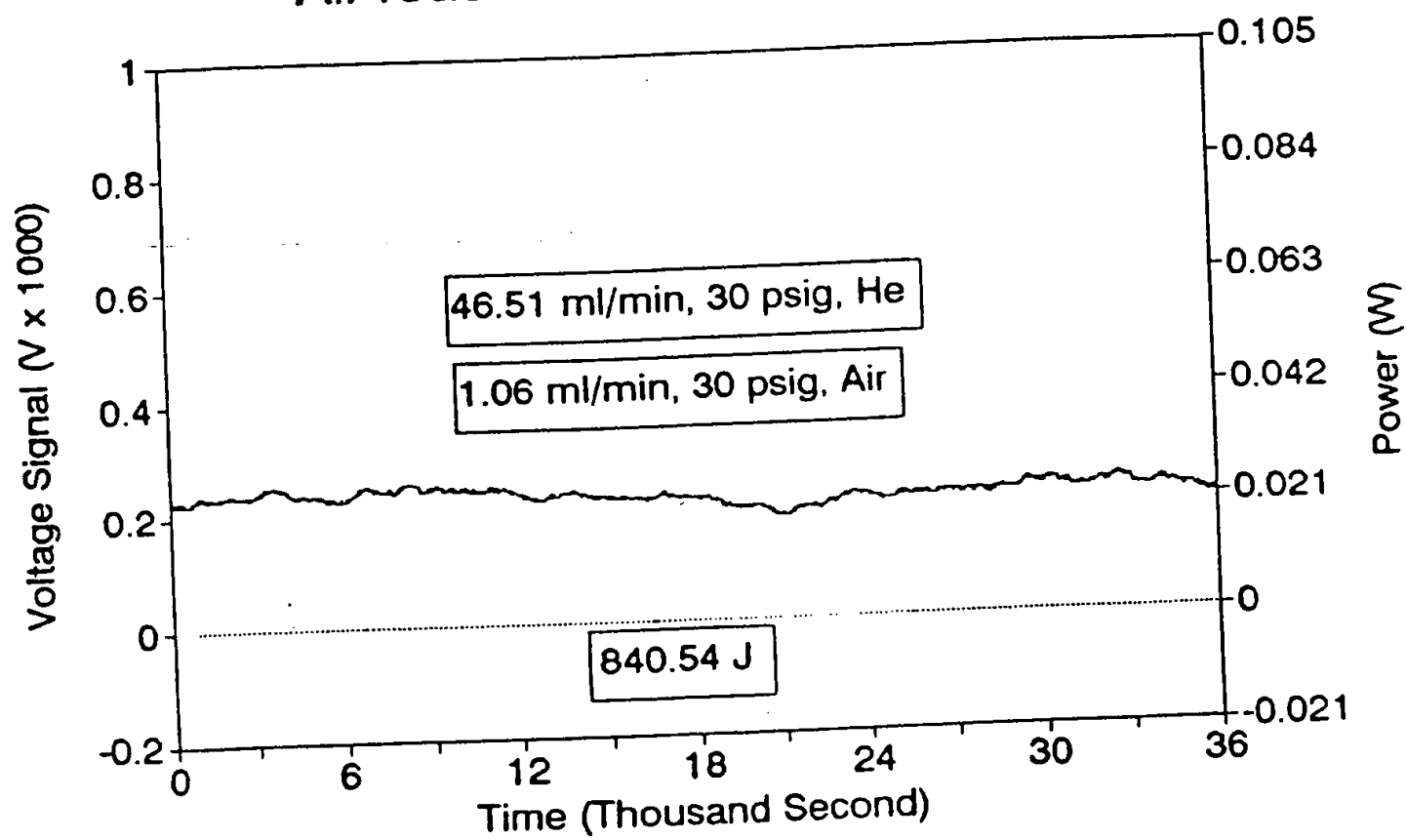


Fig. 23-13
Air reaction 5 at 125 C (120495a)

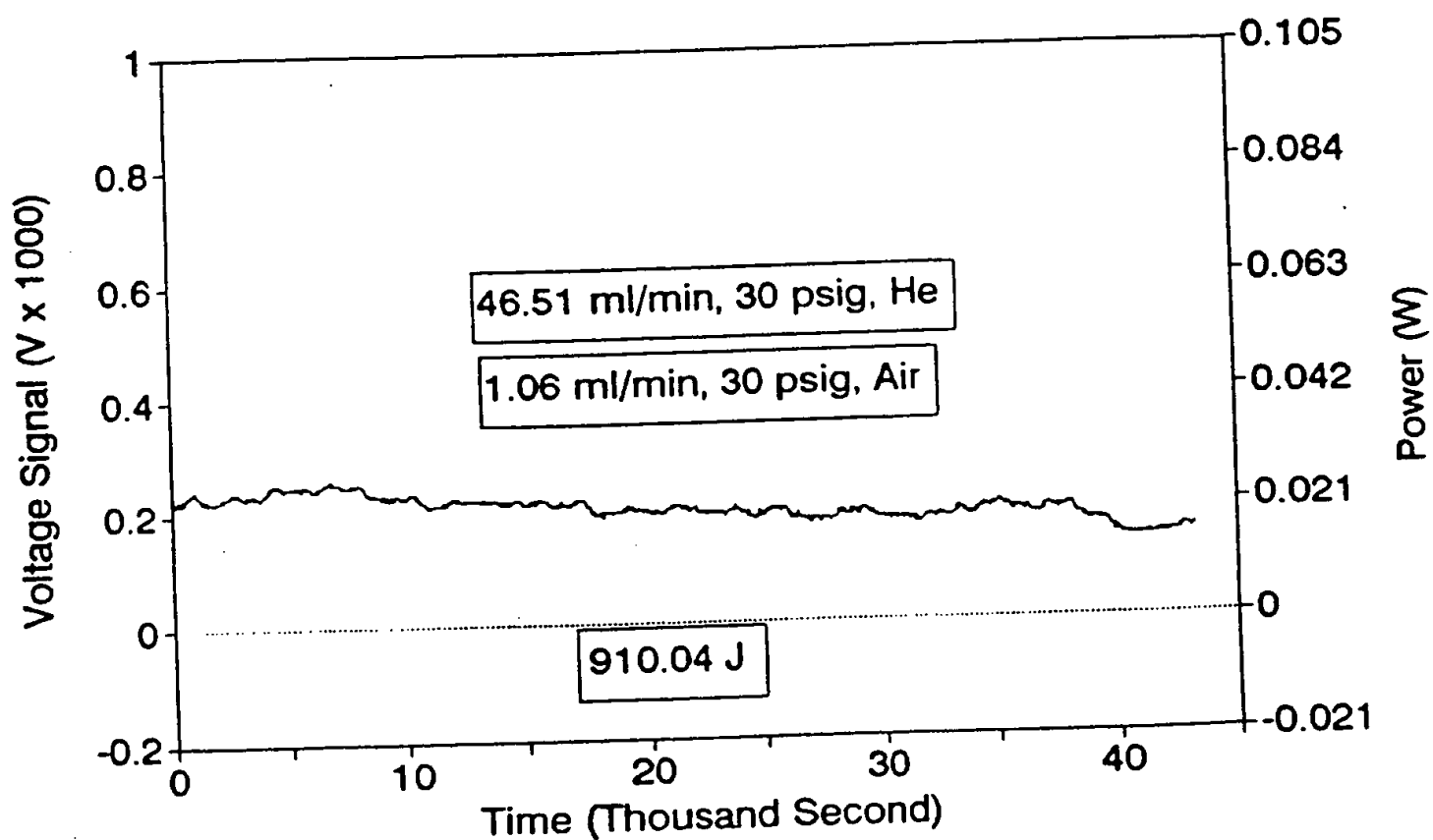


Fig. 23-14
Air reaction 6 at 125 C (120495a)

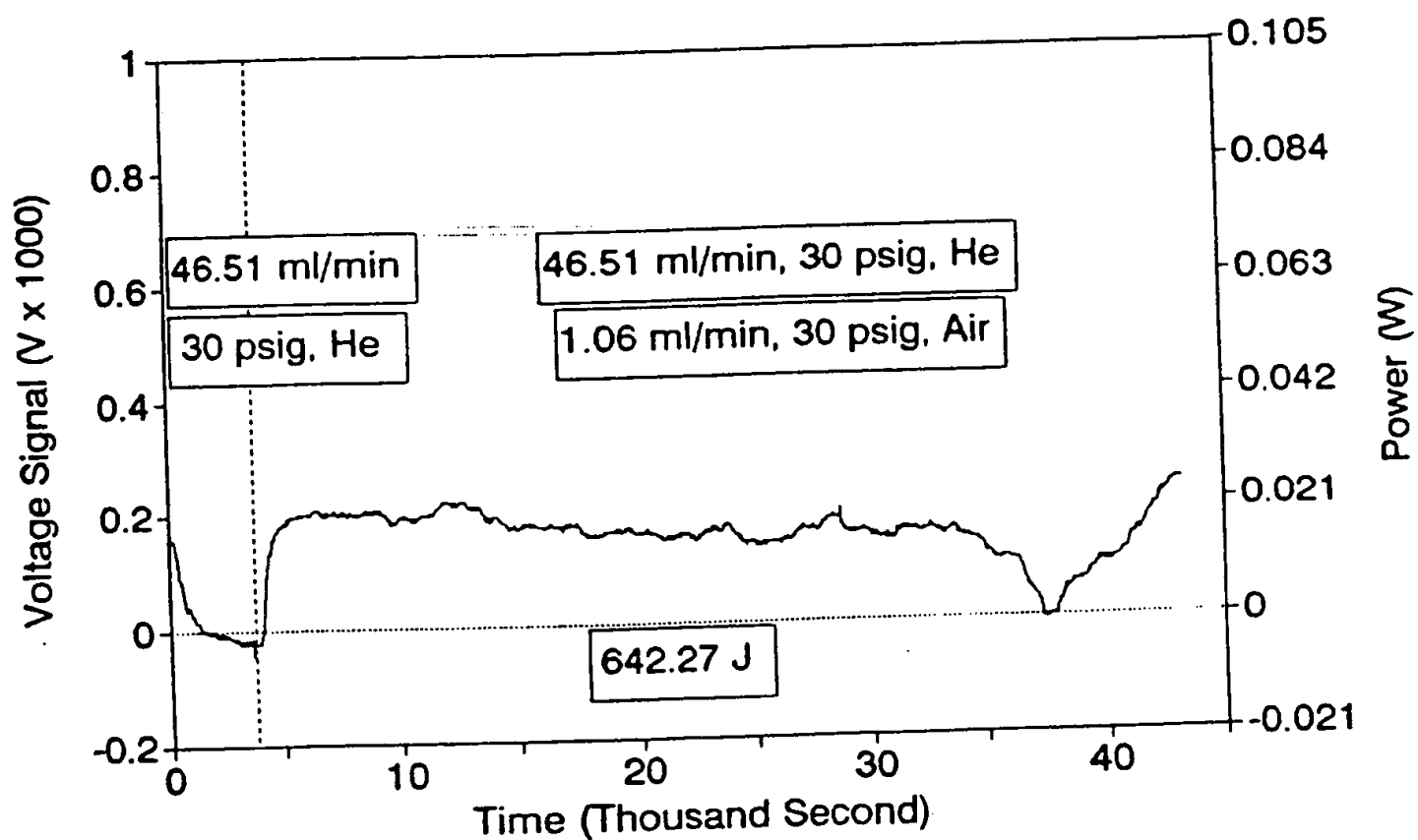


Fig. 23-15
Air reaction 7 at 125 C (120495a)

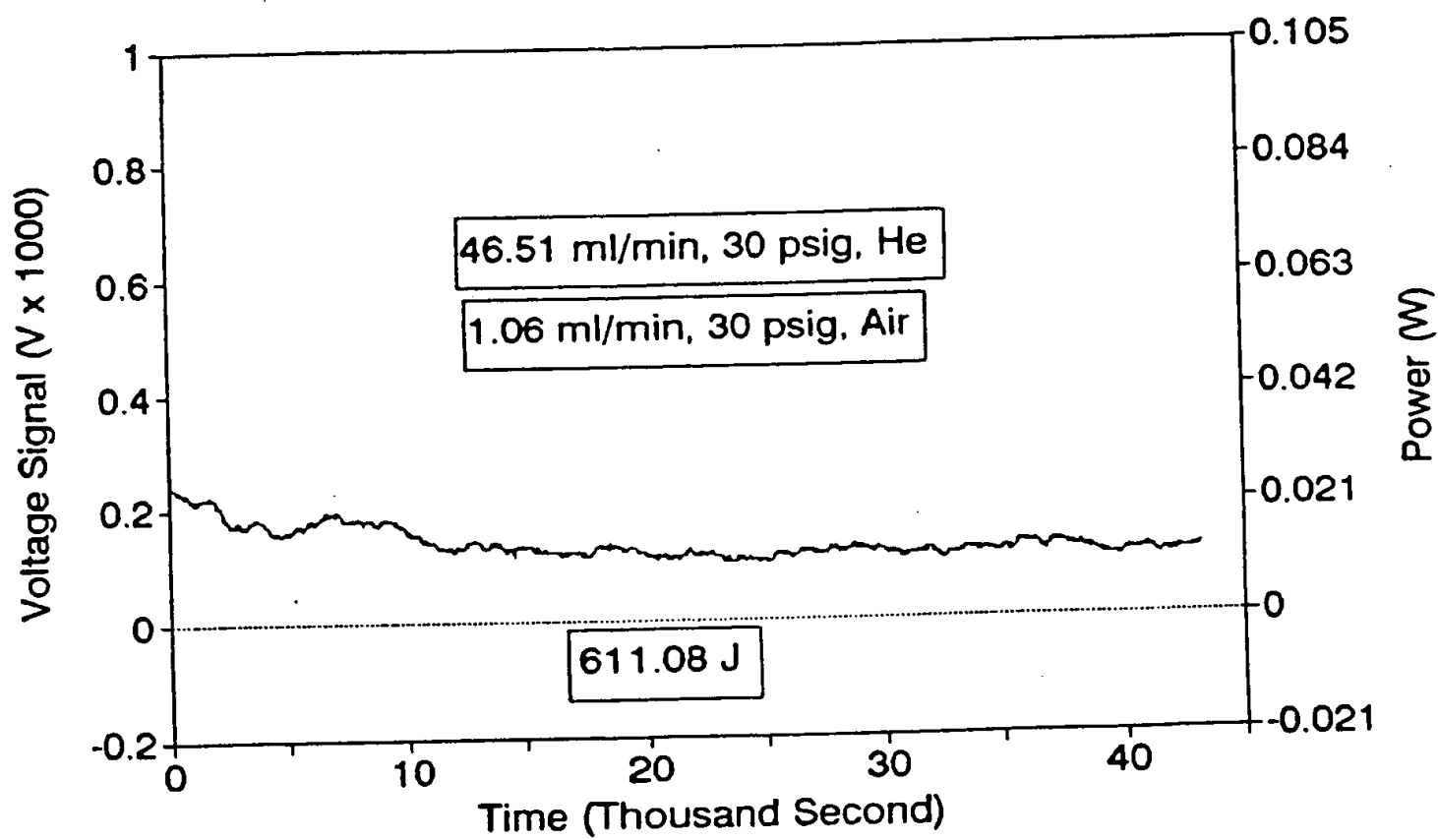


Fig. 23-16
Air reaction 8 at 125 C (120495a)

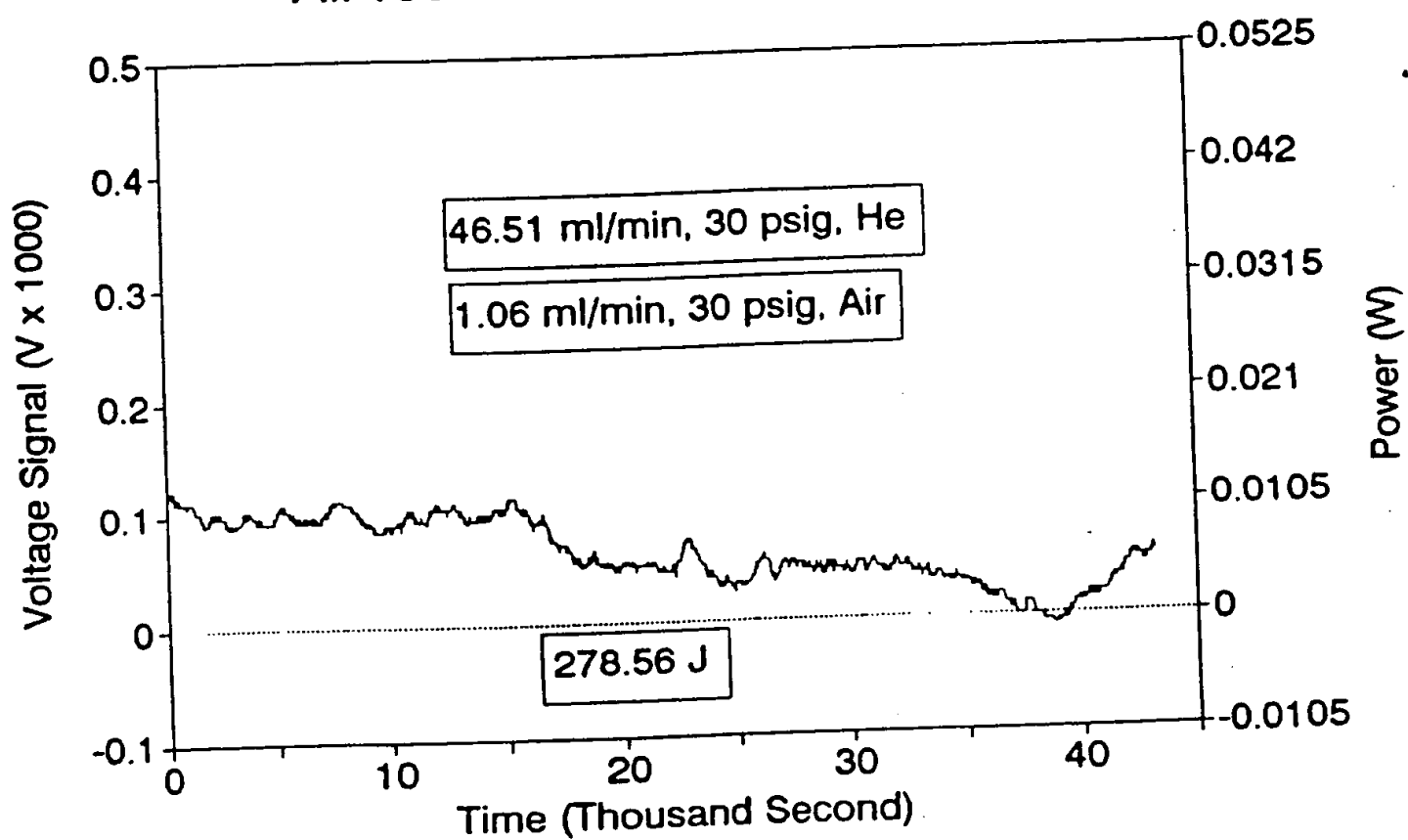
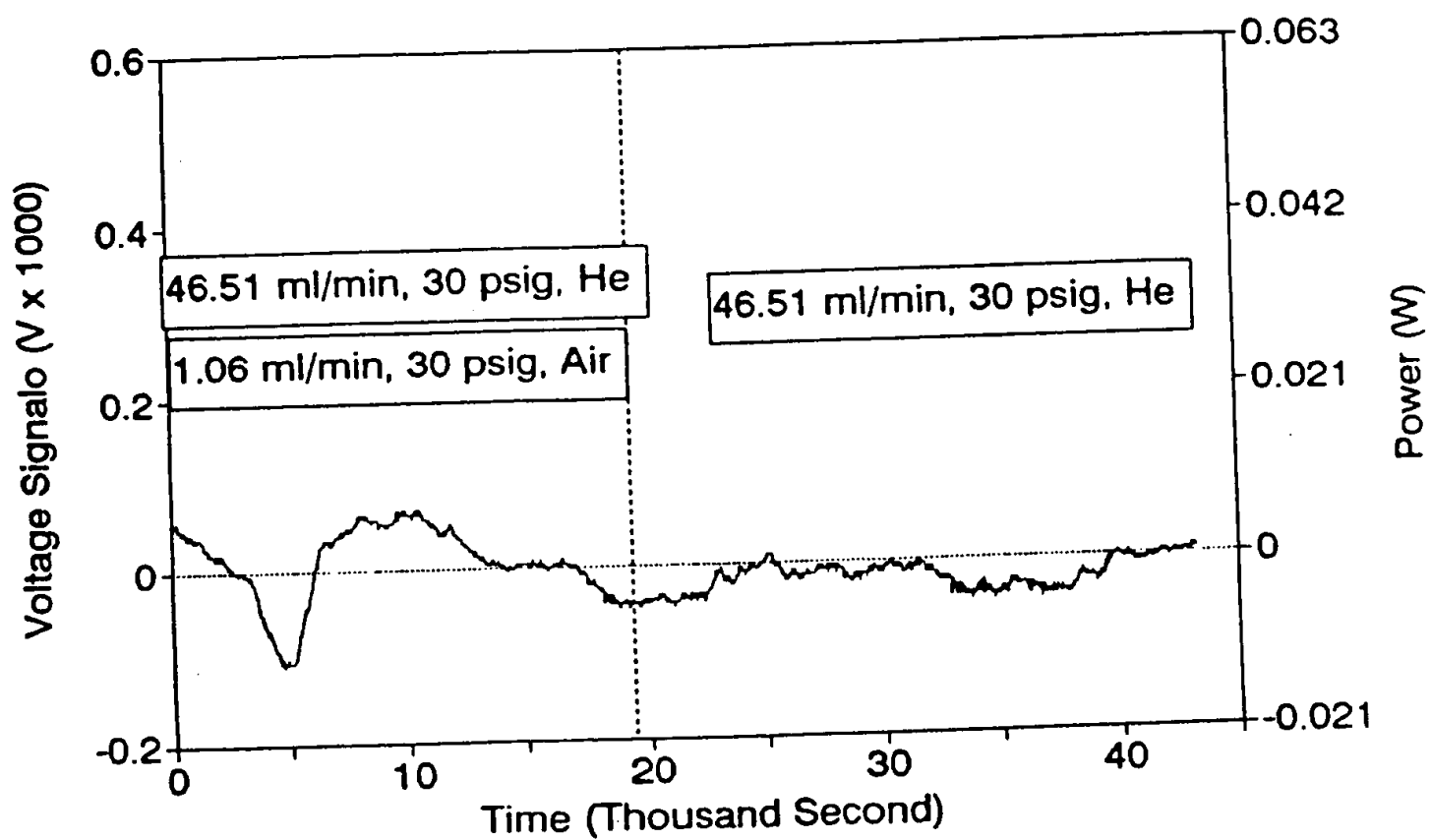


Fig. 23-17
Switch to He at 125 C (120495a)



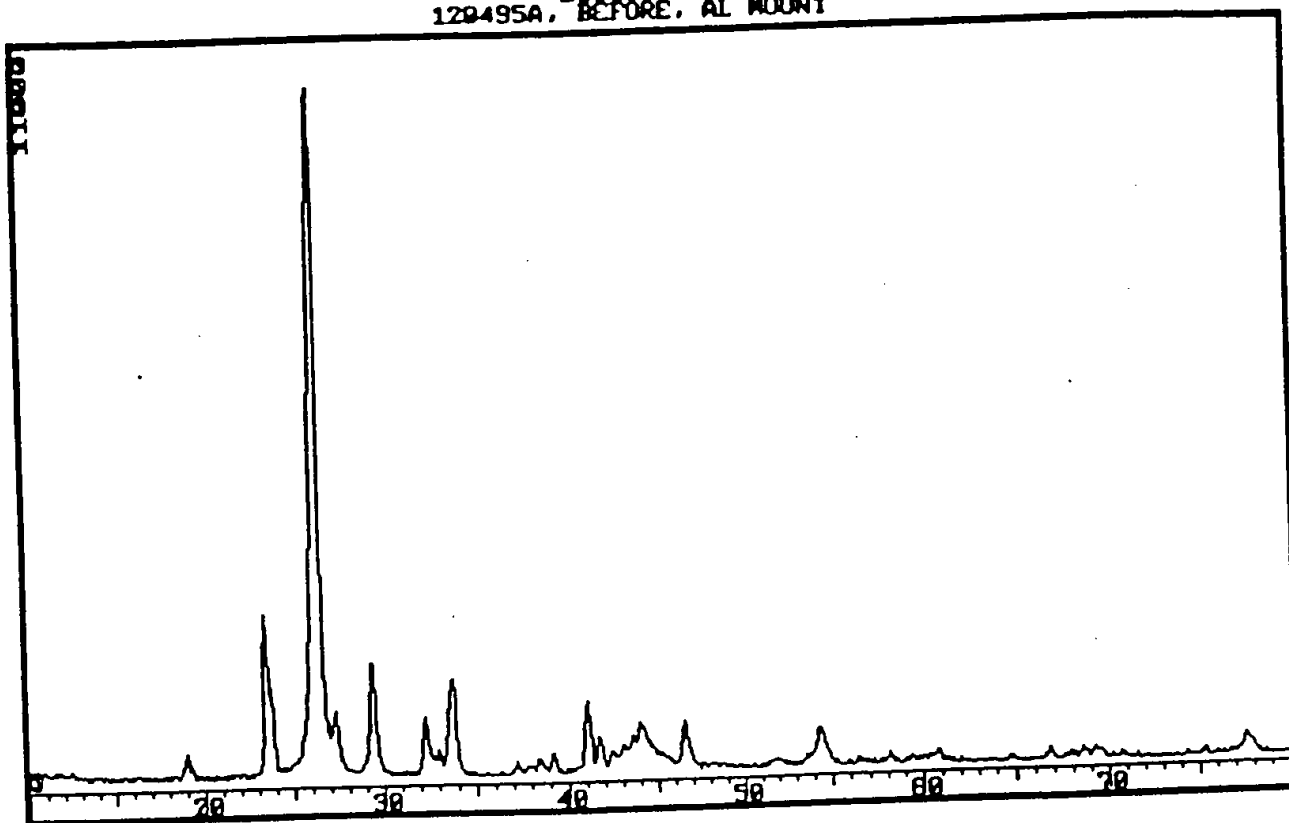
12/24 / 95

23-18

120495 A

Before

213156.RAW
120495A, BEFORE, AL MOUNT

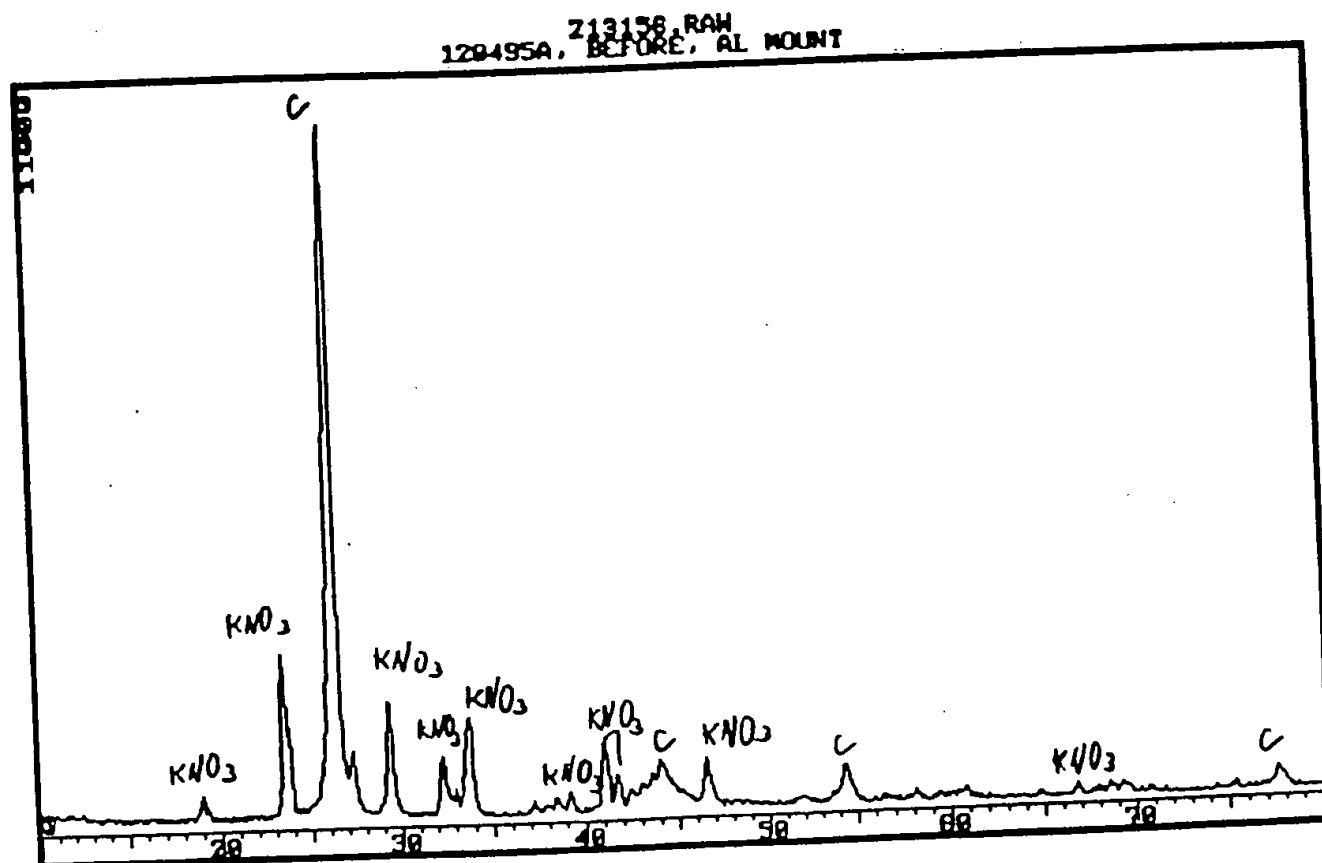


12/21/95

23-19

120496A

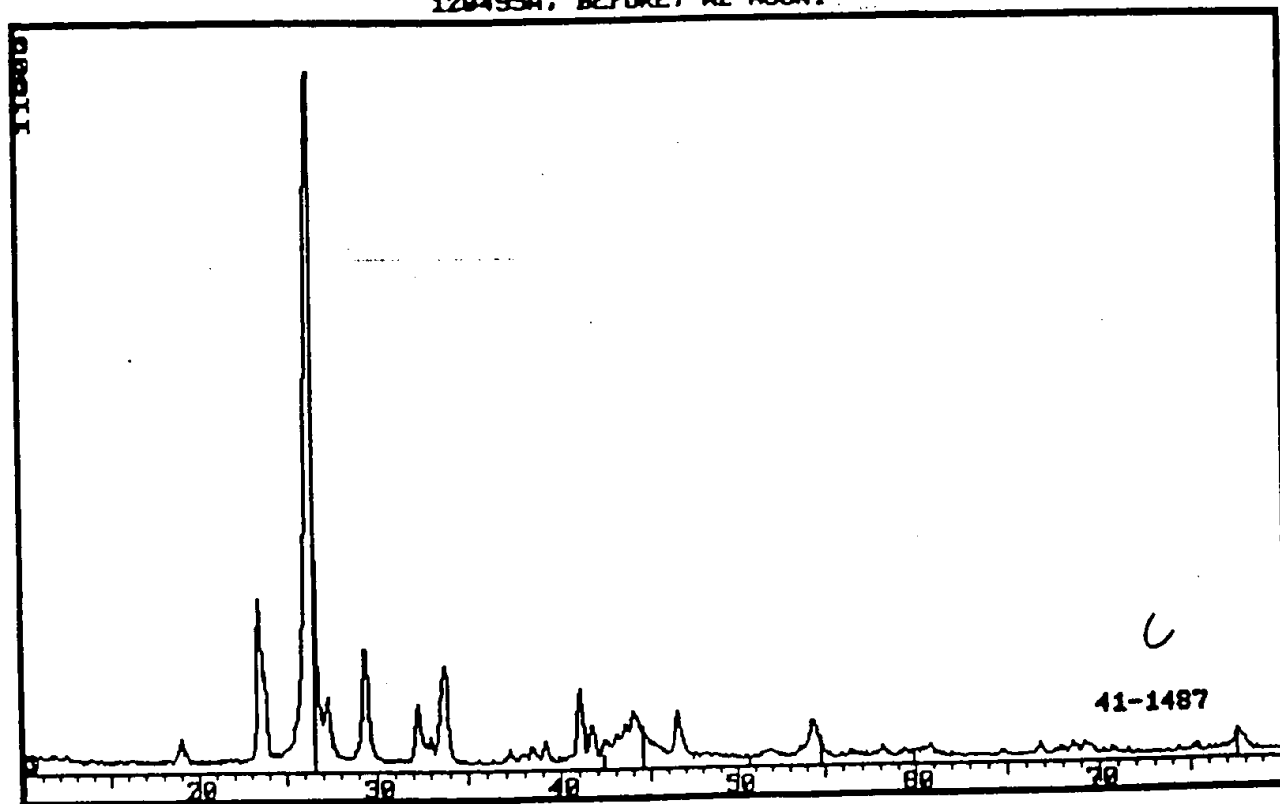
Before



12/21/95

23-20

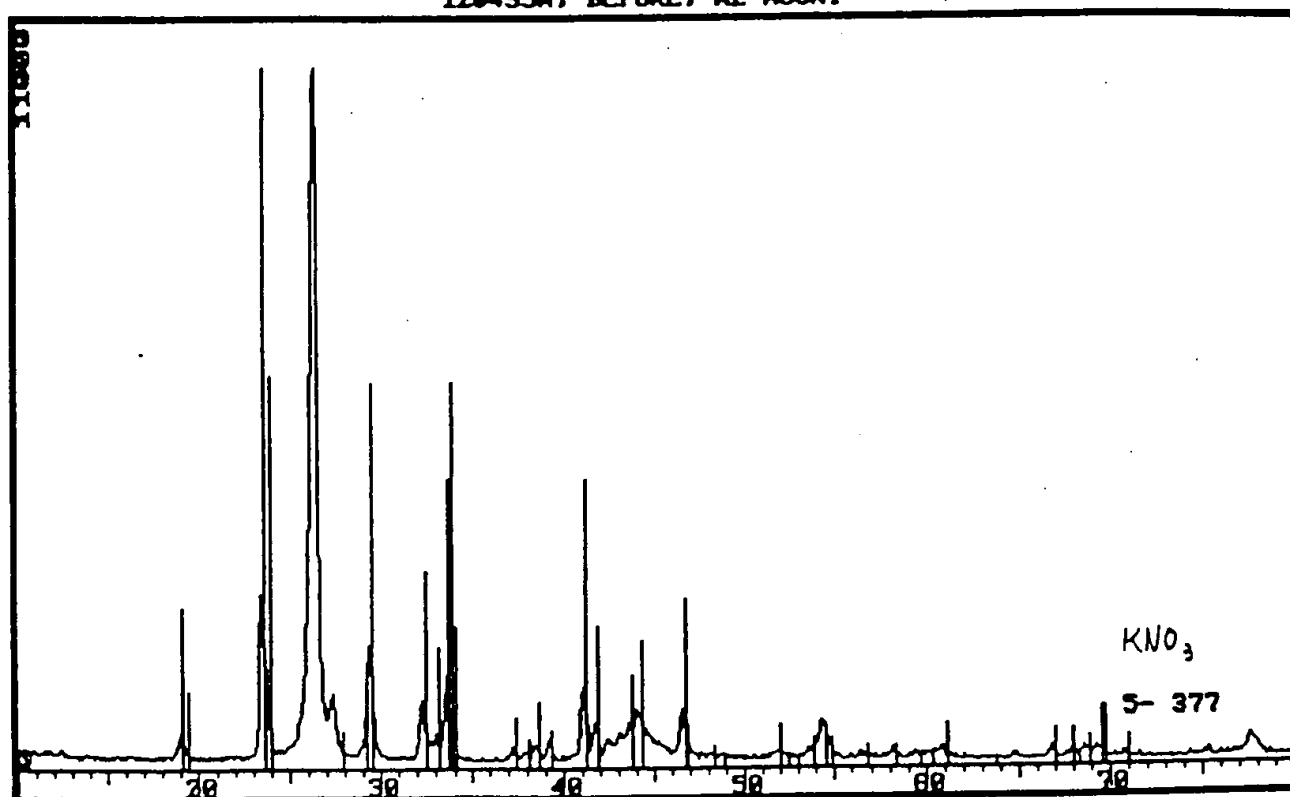
Z13156.RAW
120495A, BEFORE, AL MOUNT



12/21 195

22.21

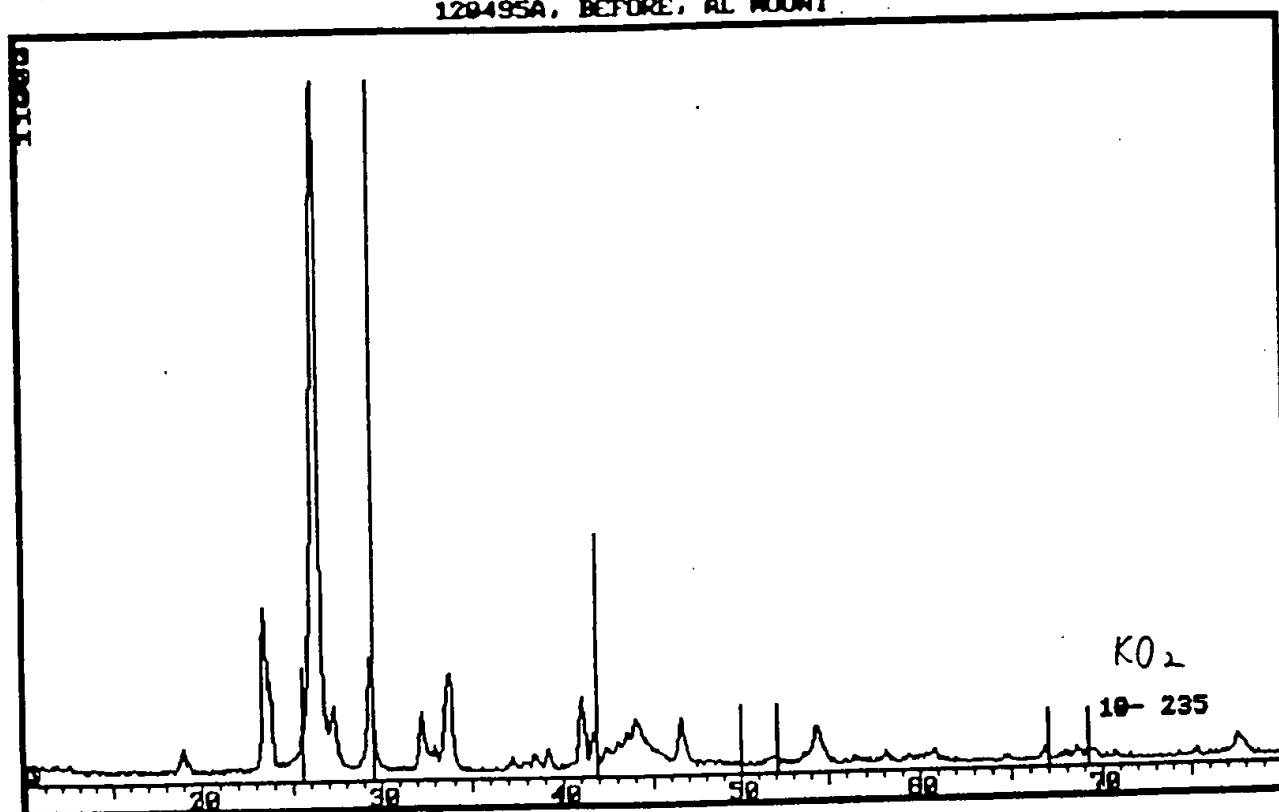
Z13178, RAM
120495A, BEFORE, AL MOUNT



23-22

12/21 / 95

219158.RAW
120495A. BEFORE, AL MOUNT



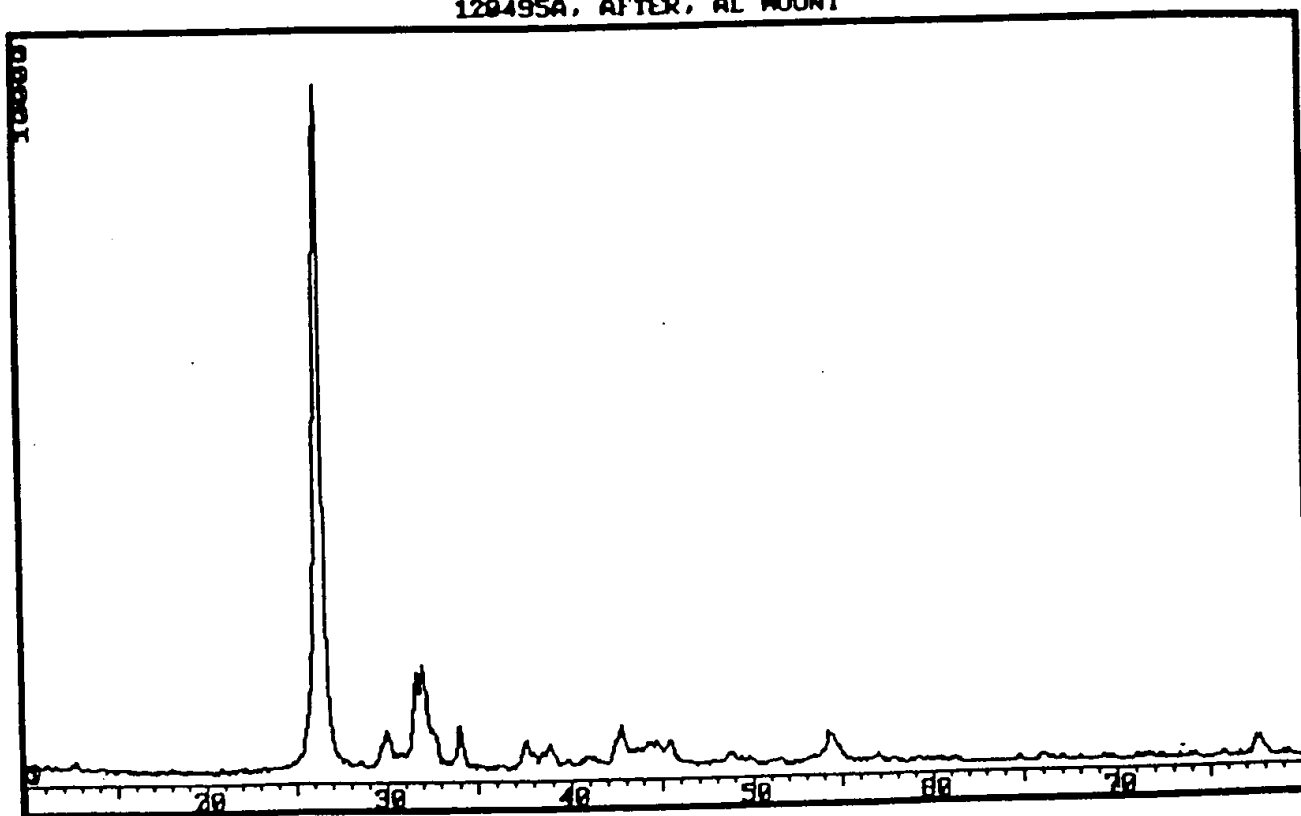
1 / 95

23-23

120495 A

After

213153.RAW
120495A, AFTER, AL MOUNT



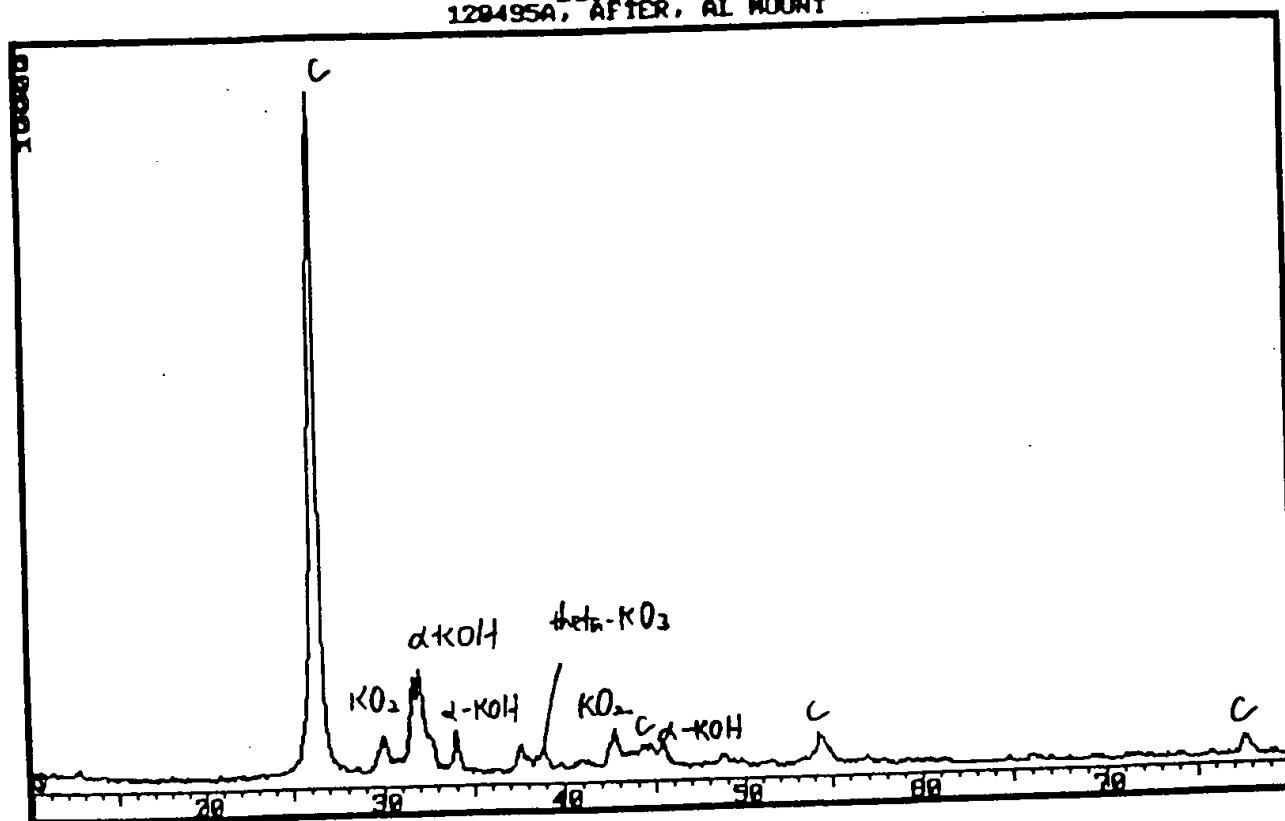
2/24/95

23-24

120495 A

After

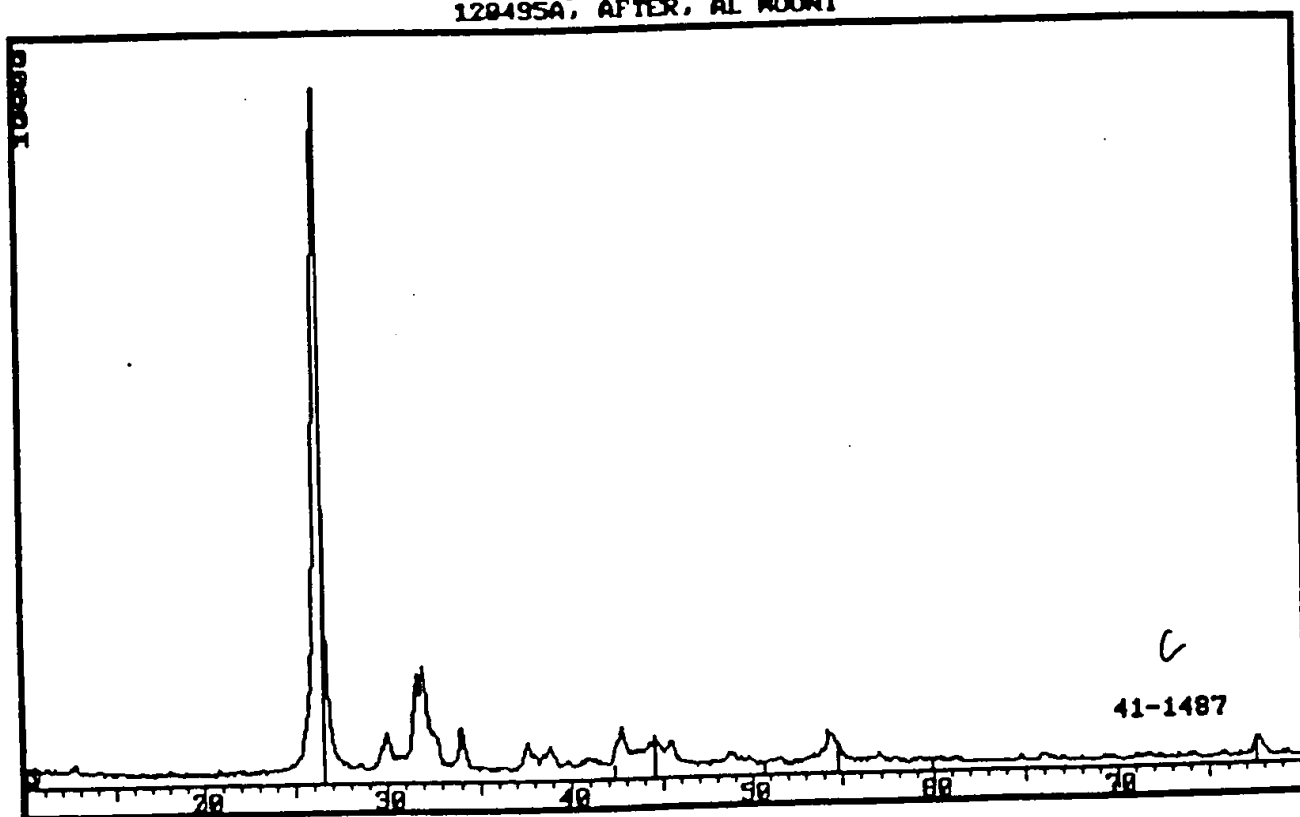
213155, RAW
120495A, AFTER, AL MOUNT



17/4/95

22-25

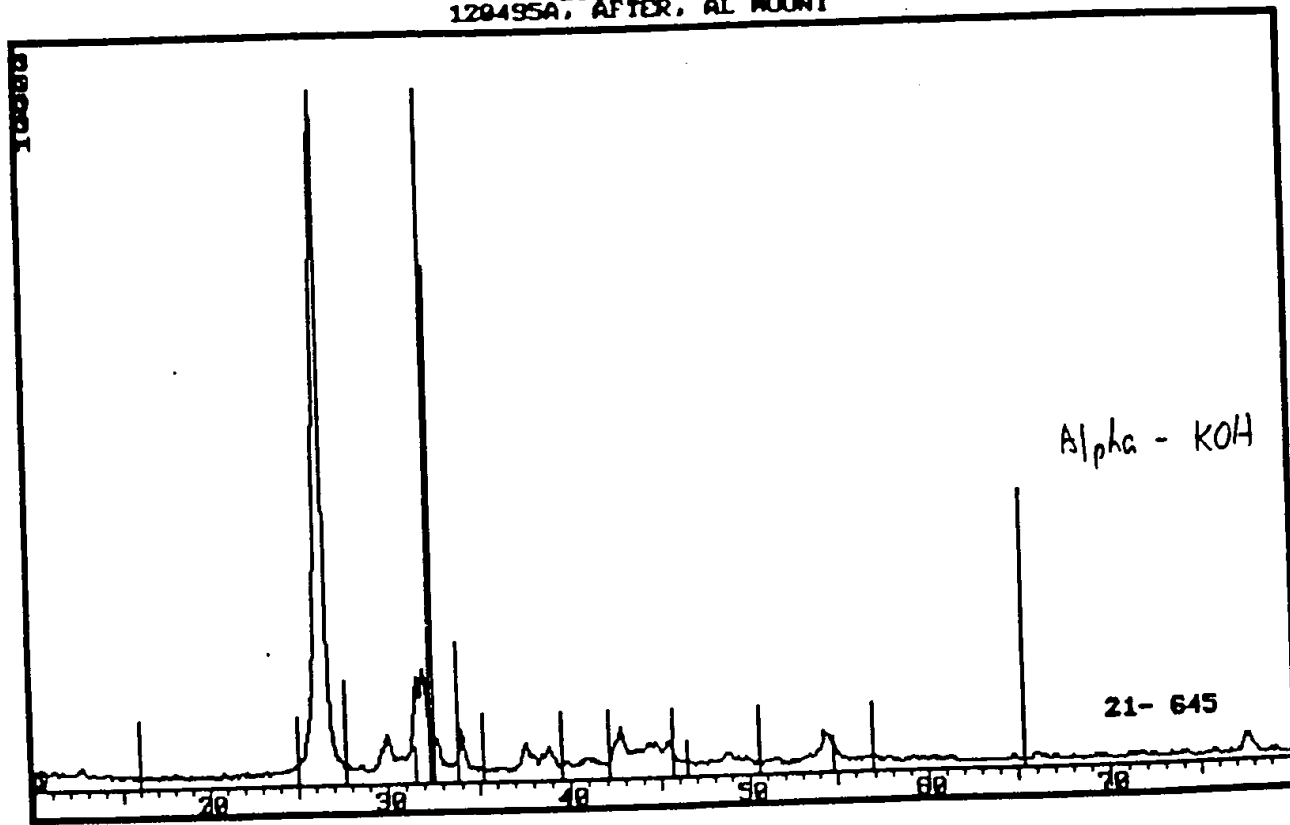
213153.RAW
120495A, AFTER, AL MOUNT



21 /95

23-23

Z19155, RAW
120495A, AFTER, AL MOUNT



THIS PAGE BLANK (USPTO)

THIS PAGE BLANK (USPTO)

CONFIDENTIAL

A Calorimetric Investigation
of the
Reaction of Hydrogen
with
Sample PSU#1

A
Confidential Report
submitted to
Hydrocatalysis Power Corporation

by

Michael C. Bradford, MS

11 September 1994



I. Experimental Methodology and Theory of Operation

Enclosed at the end of this technical report is a majority of Chapter III from my, Michael C. Bradford, Master of Science thesis at the Pennsylvania State University, entitled, "*A Calorimetric Investigation of the Lithium-Water and Lithium Hydride-Water Reaction Systems at Elevated Temperatures.*" Within this chapter is contained a schematic of the experimental apparatus, the theory by which it can be used to obtain thermodynamic data, and calibration data for the instrument. It also describes the capability of the system for quantifying pulses of gases, hydrogen and water, in an inert carrier gas stream.

II. Site Preparation and Installation of Equipment, 9 September 1994.

Ultra high purity (99.999%) helium and hydrogen were obtained from Matheson for use in the experiment. The schematic of the experimental apparatus, Figure III.2 in Chapter III, should be modified slightly to take the gas changes into consideration. The argon supply was removed and replaced by the hydrogen and helium supplies, connected to a common line through a three-way valve, which permitted instantaneous switching between hydrogen and helium. It should also be noted that the gases were further purified prior to entering the reactor by passing them through an oxygen trap (Alltech).

After installation of the equipment, a quick *touch* test of the calorimeter was performed at 298 K. Simply, the inner wall of the calorimeter was touched for a period of roughly 10 seconds. The resulting exotherm (Figure 1) was integrated, and the total amount of heat input into the calorimeter by my hand, roughly 21.5 Joules, was determined. This quick test verified the functionality and high sensitivity of the calorimeter.

The sample prepared by Hydrocatalysis Power Corporation, herein referred to as #1, was loaded into the reactor cell under a 40 psig UHP helium blanket to minimize any ambient contamination. The remainder of PSU#1 not loaded into the reactor cell was stored in a desiccator within the dry box under a helium blanket. The reactor cell was loaded into the experimental apparatus at 298 K under 1.5 ml/s helium purge, and the piping was leak tested with Snoop. After insulation was placed around the calorimeter, the oven was ramped to 523 K and allowed to thermally equilibrate for 24 hours prior to experimentation.

III. Experimental Data for the Reaction of Hydrogen with #1

On 10 September, the first data set at 523 K was obtained (Figure 2). This data is contained on a 1.44 M IBM diskette in ASCII format, DATA1.OUT, and as a Quattro Pro spreadsheet, DATA1.WQ1. After sampling the baseline (1 Hz) for 1 hr, the helium was switched to hydrogen at a constant flow rate of 1.5 ml/s. As Figure 1 indicates, there was essentially no indication of any exothermic processes taking place. The slight deviation in the baseline can be attributed to small thermal fluctuations, ± 0.5 K in the oven.

The second data set at 523 K was then obtained (Figure 3). This data is contained on a 1.44 M IBM diskette in ASCII format, DATA2.OUT, and as a Quattro Pro spreadsheet, DATA2.WQ1. At about $t = 0$ s, the hydrogen flow rate was increased to 4.5 ml/s. A new steady state, roughly at 0.03 W, was then obtained within about 1 hr. At this time, the hydrogen flow rate was then increased to 7.5 ml/s, during which a more substantial exotherm resulted. The new steady state, roughly 0.2 W, was reached in roughly 3 hr.

The third data set at 523 K was then obtained (Figure 4). This data is contained on a 1.44 M IBM diskette in ASCII format, DATA3.OUT, and as a Quattro Pro spreadsheet, DATA3.WQ1. At about $t = 0$ s, the hydrogen flow rate was increased to 13.5 ml/s. The heat output reached roughly 0.5 W after about 1 hr on stream. Before steady state was obtained, the hydrogen flow was switched back to helium. It is clear that a switch to helium resulted in an immediate cessation of heat production, as indicated by the exponential decay of the calorimetric signal. However, note that the new steady state for no reaction was now at roughly 0.25 W. This is a flow induced phenomena and is not yet fully understood. However, it has been documented clearly during past research (Michael C. Bradford, 26 March 1993, Notebook#1, page #80.).

The fourth data set at 523 K was then obtained (Figure 5). This data is contained on a 1.44 M IBM diskette in ASCII format, DATA4.OUT. The helium flow was reduced back to 1.5 ml/s to try to re-establish the original baseline. As the figure indicated, a decrease in helium flow resulted in an abrupt decay of the calorimetric signal toward the original baseline. The original baseline, 0.0 W was not reached in the figure because sufficient time was not allowed for equilibrium to be reached.

IV. Correction of Data for Baseline Drift and Flow Variation

Using the data in Figure 2 and Figure 4, it is clear that changing the helium flow from 1.5 ml/s to 13.5 ml/s resulted in a baseline shift from roughly 0.0 W to 0.25 W. This phenomenon corresponds to a flow correction factor of 0.0021 W/(ml/s). This correction factor permits a correction to be made to the obtained data.

Table I. Experimental Data.

v (H ₂) ml/s	P (W), raw	P(W), corrected
1.5	0.00	0.00
4.5	0.03	0.02
7.5	0.20	0.18
13.5	≈0.50	≈0.47

The values reported at 13.5 ml/s hydrogen are approximate because steady state had not been reached. Thus, the true heat production values at this flow condition must certainly be higher.

V. Conclusions

PSU#1 does substantially react with flowing hydrogen with considerable activity for extended periods of time. This reactivity was found to be dependent upon hydrogen flow rate. Thus, it is speculated that either the total pressure of hydrogen in the gas phase, or the diffusion of hydrogen through #1, strongly influences the sample reactivity.

Figure 1

Calorimeter Test at 298 K
9 September 1984

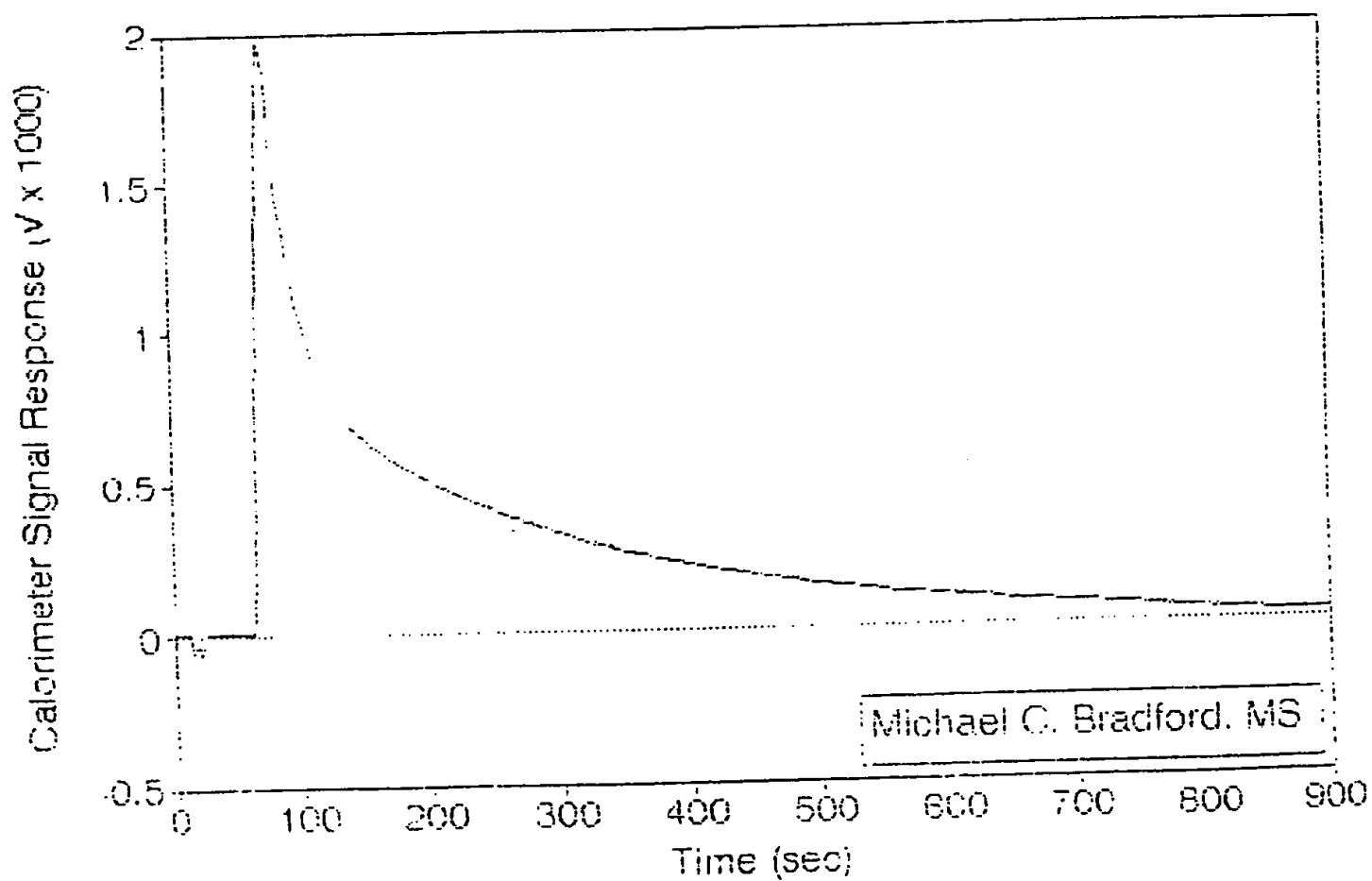


Figure 2

First Data Set at 523 K - DATA1.OUT
10 September 1994

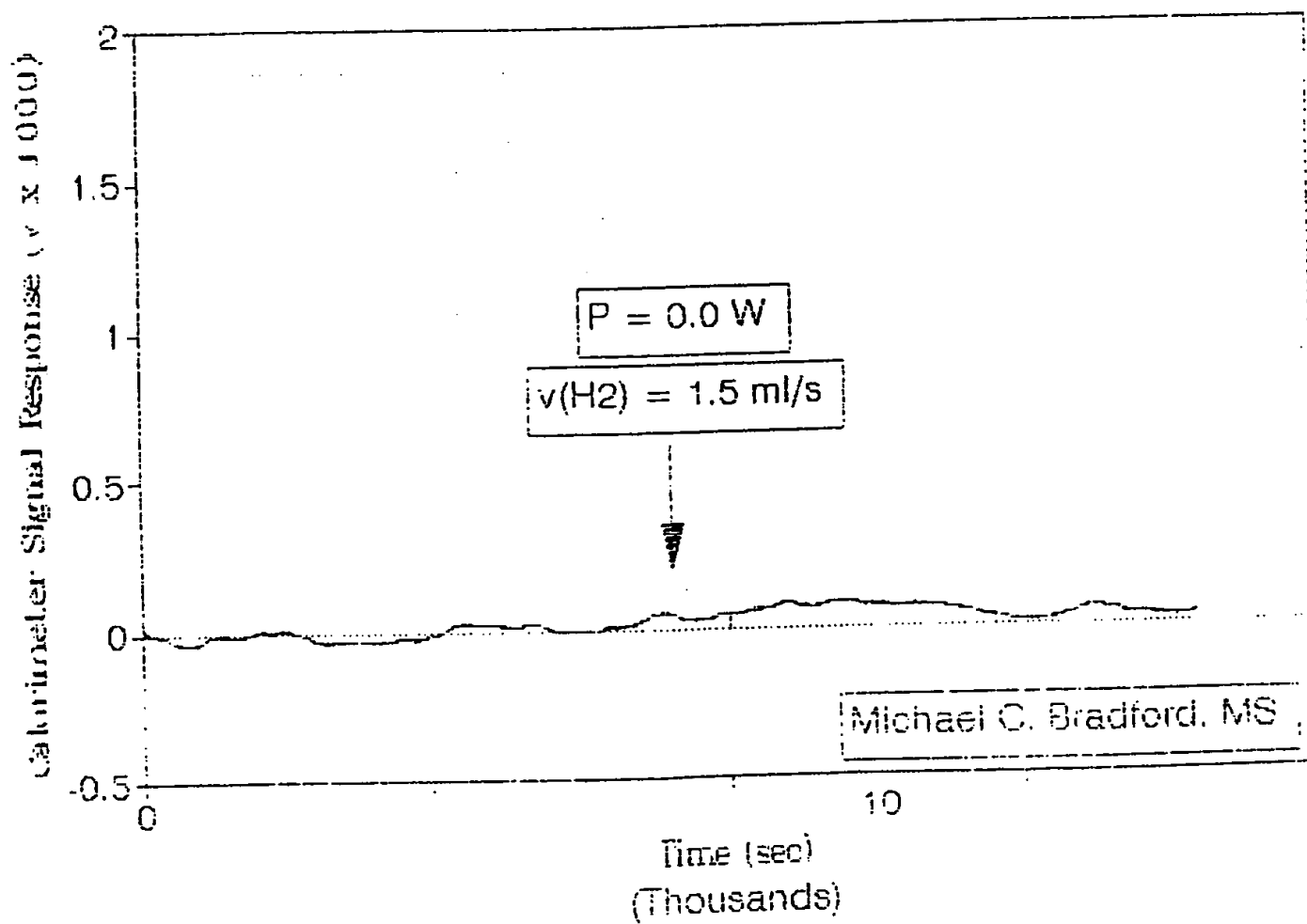


Figure 3

Second Data Set at 523 K - DATA2.OUT
10 September 1994

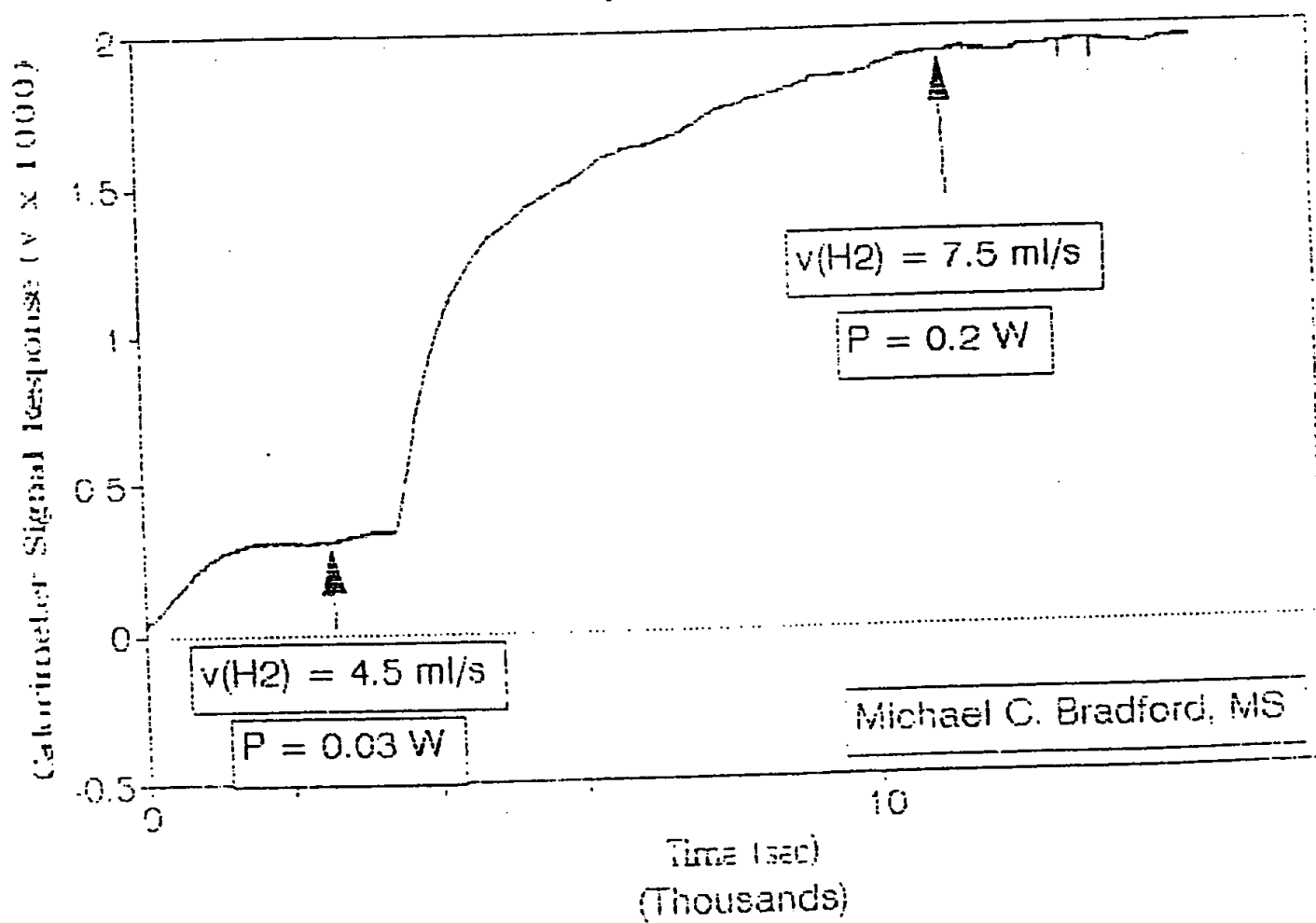


Figure 4

Third Data Set at 523 K - DATA3.OUT
10-11 September 1994

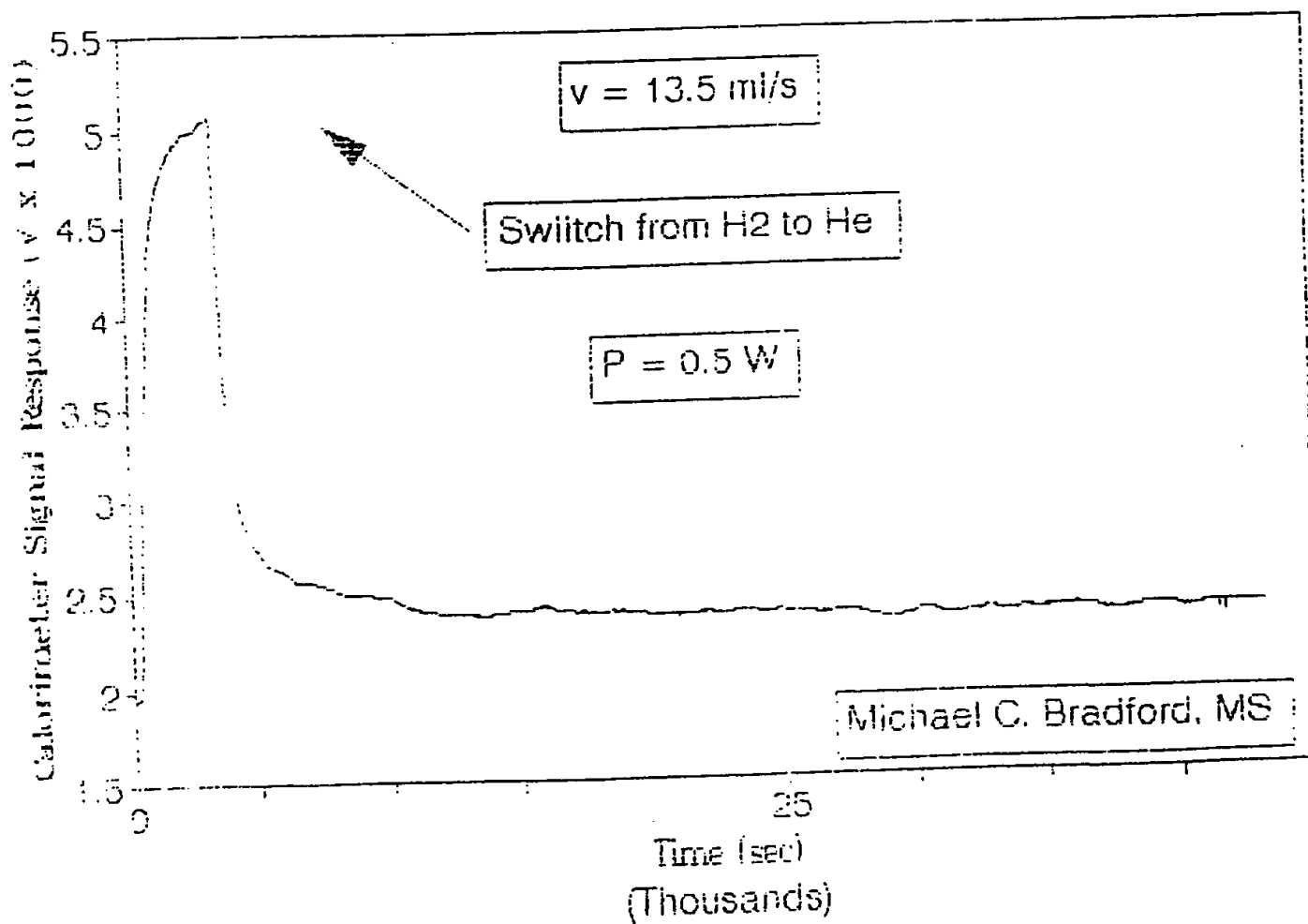


Figure 5

Fourth Data Set at 523 K - DATA4.OUT
11 September 1994

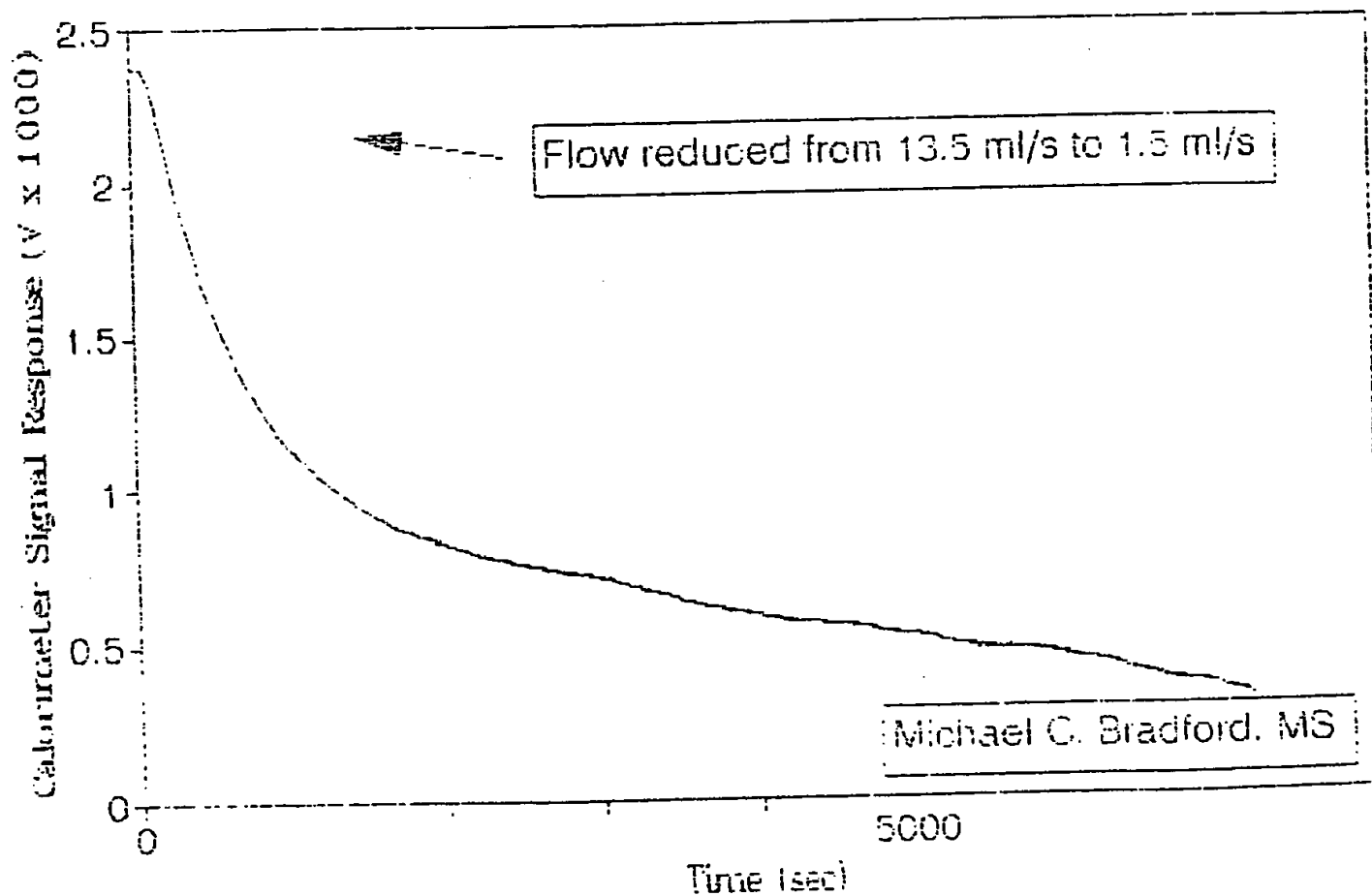
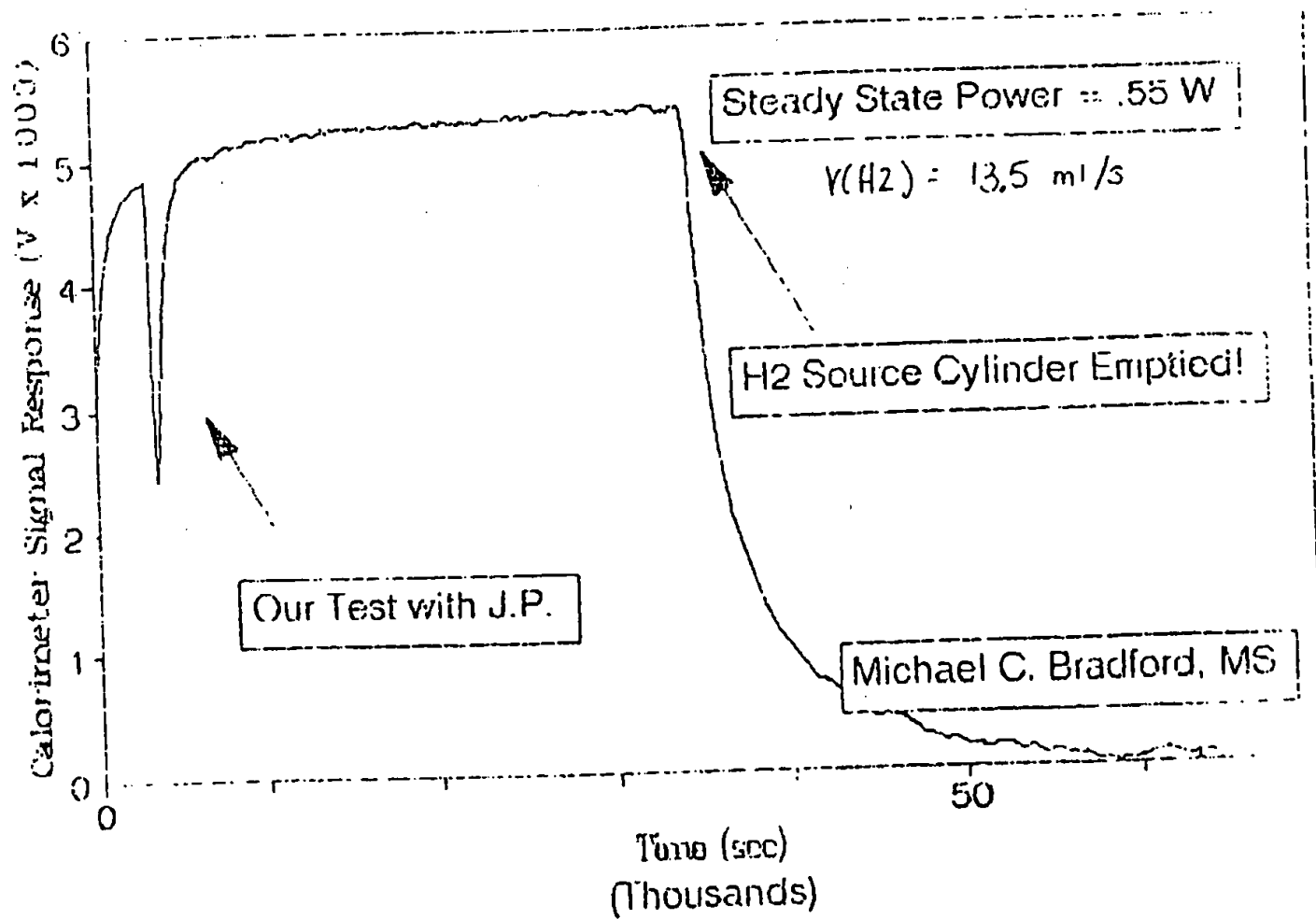


Figure 6

Fifth Data Set at 523 K - DATA5.OUT
12 September 1994



Chapter III Methodology

The initial step in the course of this investigation was to design an experimental apparatus which would adequately resemble a HYDROX fuel reactor (Chapter III.1). After this apparatus was constructed and the theory of the experimental measurement was understood (Chapter III.2), a calibration of the components of the apparatus was performed (Chapter III.3). A general experimental procedure (Chapter III.4) was then used to conduct two test experiments of known elementary reaction systems to validate the utility of the experimental apparatus (Chapter III.5).

III.1 Design

The main objective of the experimental design was to maximize the similarity of the experiment to an actual HYDROX fuel reactor. Thus the experimental apparatus had to be designed to operate at elevated temperatures, *ca* 588°K, and required the use of a cylindrical reactor, an open flow system, and an excess of fuel (lithium, lithium hydride, or lithium oxide).

There were several difficulties associated with the design of flow, Calvet reaction calorimeter for investigations at elevated temperatures.

- (1) Acceptable materials of construction had to be found. Today, most commercial thermopile insulating materials are not stable at temperatures above 530°K (32). Also, at high temperatures, lithium reacts with many materials, including silica and aluminum (14,44,77), which might ordinarily be used to construct the calorimeter shell.
- (2) A stable high temperature baseline had to be produced. Although some versions of the Calvet-type calorimeter have been constructed to operate at temperatures in excess of 1000°K, the baseline stability and inherent precision of these instruments has been reported as poor (78).
- (3) The calorimeter had to provide accurate heat of reaction data when operated with a constant gas flow, rather than when operated in the batch mode generally associated with Calvet-type calorimeters. Ketchen and Wallace (79) claim that in a flow calorimetric system, reaction heat is inevitably lost, thus necessitating

batch operation for the Calvet-type calorimeter.

- (4) A method of injecting constant, quantified doses of water vapor into the calorimeter had to be devised. It was also necessary to insure that the water enter the calorimeter at the calorimeter temperature.
- (5) The apparatus had to insure adequate mass transfer of the reacting species to minimize, or eliminate, bypass of water out of the reactor.
- (6) A method to analyze the reactor effluent stream for unreacted water and hydrogen had to be developed.

One of the large material concerns was overcome when recently, high temperature, high sensitivity thermopiles became available at reasonable prices, thus making the use of a Calvet-type calorimeter practical at elevated temperatures. A cylindrical heat flux microcalorimeter (International Thermal Instrument Co., Model CA-100-1) was used to measure the heat of reaction during this investigation. To avoid the complication of corrosion, a cylindrical reactor, machined from 304 stainless steel to fit inside of the calorimeter, was used to contain the fuel (Figure III.1).

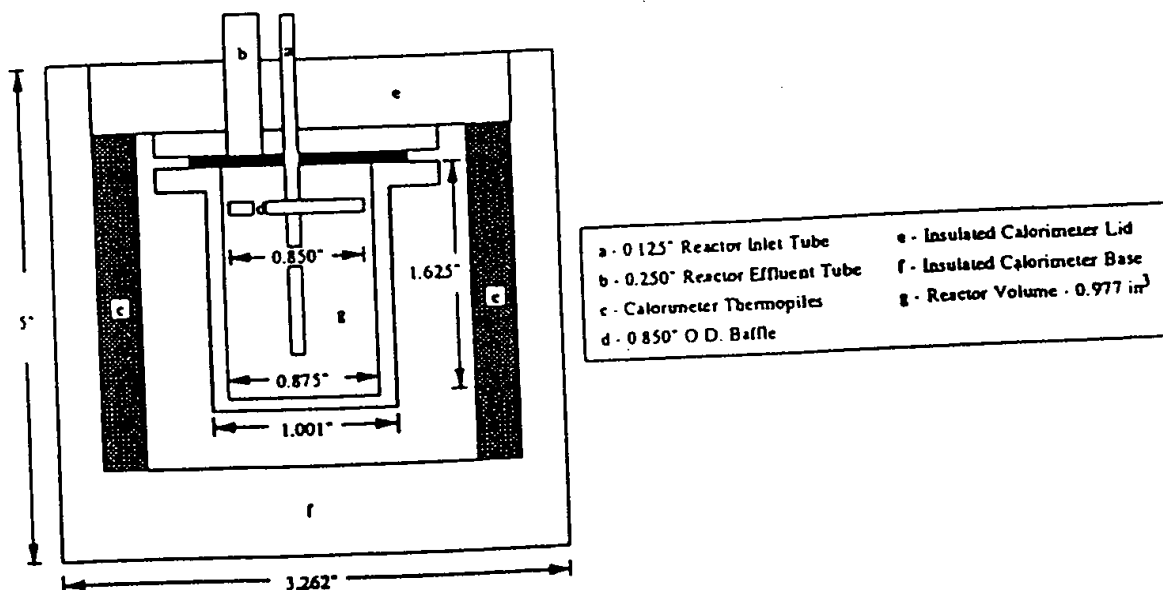


Figure III.1 : A schematic diagram of the reactor and the calorimeter.

Although the stainless steel does create an additional heat transfer resistance, it was needed to prevent corrosion of the calorimeter by the fuel. Lithium corrosion of stainless steels and ferritic alloys is negligible at temperatures below 723°K (14), and thus, stainless steel is frequently used and recommended for containment of lithium compounds (14,58,76,77). The additional heat transfer resistance created by the reactor to the calorimeter thermopiles was minimized by the use of thin reactor walls (0.16 cm). Although the maximum operating temperature of this calorimeter is 588°K, gradual sublimation of the thermopile insulating materials limited use of the calorimeter to approximately 2000 hours (31). Although this sublimation process did not affect the sensitivity of the calorimeter, it did require periodic manufacturer maintenance.

A schematic diagram of the entire experimental apparatus is outlined in Figure II.2. To address the operational issues mentioned previously, important support systems were installed (a) to maintain temperature control, (b) to introduce the water into the reactor, (c) to analyze the effluent gas, (d) and to enhance the reaction mass transfer.

To maintain an isothermal reaction system and improve baseline stability, the calorimeter was placed inside of a commercial convection oven (Despatch, Model LND 1-42-3), that could be operated from room temperature to 616°K. Also, the calorimeter and reactor were enclosed within a cubic insulated box, constructed of Durok (United States Gypsum Co.) and fiberglass, to further dampen thermal oscillations in the oven. The use of multiple *insulating* layers to dampen thermal perturbations in the infinite heat sink was demonstrated by Tian as early as 1923 (78), and can be easily illustrated using a basic heat transport model (Appendix B).

As mentioned previously, a flow, rather than a batch reaction process, was required for the experiment to resemble the HYDROX operating environment. Flow calorimeters have been used by other investigators to measure the heats of adsorption of liquids on porous solids temperatures up to 523°K (80,81,82). However, the use of a continuous gas flow can lead to a loss of heat, and thus a loss in accuracy of the experimental measurement. Barton (80) noticed during the calibration of his flow calorimeter that slight changes in flow rate altered the calibration constant by up to 20%. It was thus desirable to illustrate that gas flow rate would not significantly influence the experimental results of this investigation. Calibration experiments (Chapter III.3.4) conducted with an 18 Ω resistor (Mills Resistor Co.) and a fixed current (40-165 mA) source showed that the calibration constant of the calorimeter was not sensitive to the flow rate of gas, over the range of conditions which experiments were conducted. The argon

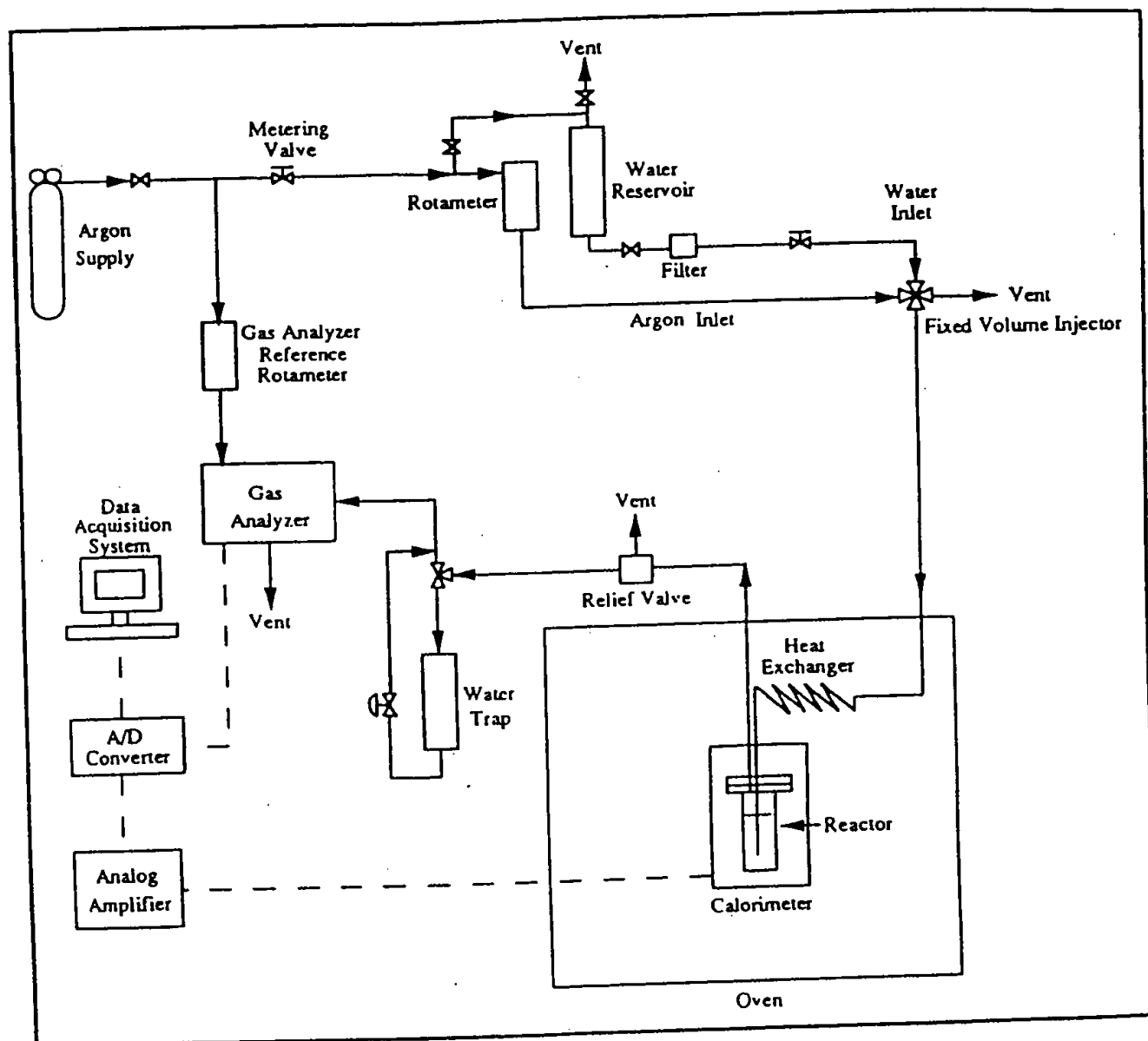


Figure III.2 : A schematic diagram of the experimental apparatus.

purge stream also served as a carrier gas, by providing a method for introduction of the limiting reagents (water or hydrogen) into the reactor.

The accurate step input of trace quantities of limiting reagent into the argon stream was accomplished using a four port fixed volume injector (Valco Instruments Co. Inc., Model No. CI4UWP) for water, and a six port fixed volume injector (Valco Instruments Co. Inc., Model No. C6WP) for hydrogen. The argon (MG Industries, 99.999% purity) purge stream was passed through an oxygen trap (Alltech, Catalog No. 4004), to remove any oxygen impurities, prior to entering the fixed volume injector. After sampling the limiting reagent, this stream then passed into the oven, and into a 300 cm x 0.241 cm ID teflon lined, stainless steel tubing coil, prior to entering the reactor. This tubing coil primarily functioned as a heat exchanger. Standard heat transfer calculations showed that it was of sufficient size to both vaporize the injected liquid water and bring the entire sample stream to the oven temperature (Appendix C).

During experiments, the reaction cell was loaded with the solid reagent as a packed bed of particles of less than 4 mm O.D. (Chapter III.4). To insure good mass transfer between the gaseous limiting reagent and the fuel, the gas was injected into the bottom of the packed bed, and forced to circumvent a horizontal baffle before exiting the reactor (Figure III.1). Experiments conducted with alternate reactor configurations did not sufficiently reduce channeling of the limiting reagent out of the reactor.

In this investigation, a method of gas analysis was required to quantify step inputs of hydrogen, produced during some reactions, and water vapor, channeled out of the reactor. The utility of in-situ gas chromatography (GC) to separate water and hydrogen mixtures has been demonstrated by Mindrup (83). However, because GC typically uses intermittent, periodic sampling to measure relative gas concentrations, it was not feasible to use in-situ GC in this investigation. Although there are many ex-situ GC methods for the quantification of trace quantities of water, including Karl Fischer Titration (84), the use of organic solvents (85,86), the use of calcium carbide (87,88), and the use of a Helium Ionization Detector (89), ex-situ methods for measuring water and hydrogen were not desirable in this investigation. A commercially available instrument, the *hygrometer*, is capable of accurate in-situ quantification of water in gas streams (90,91). Also, hydrogen adsorption on palladium films has been demonstrated as a viable candidate for in-situ hydrogen detection and quantification (92,93,94,95). However, budget constraints demanded the use of a single, economical instrument for both water and hydrogen analysis.

For this reason, an in-situ thermal conductivity-type gas analyzer (MSA, Model T-3 Type TC) was used to quantify hydrogen and water vapor in the reactor effluent stream. After the reactor effluent left the oven, it was passed through a 1.0 μm Nupro filter, to remove any entrained solid particulates, prior to entering the gas analyzer. Coincidentally, the optimal carrier gas for hydrogen detection using a thermal conductivity detector is argon (96), and fortunately, the gas analyzer is also sensitive to water vapor. In some experiments, to separate any unreacted water from hydrogen in the effluent stream, the reactor effluent was passed through a 13x molecular sieve (Alltech, Catalog No. 5269).

After the calorimeter signal was amplified, at 1000x magnification, the analog signals from the gas analyzer and the calorimeter were digitized with an Analog to Digital Converter (Real Time Devices, Model ADA1100) and sampled at a 5 Hertz frequency using standard data acquisition software (Real Time Devices, Atlantis) on a Swan 486 PC. All experimental data was converted to an ASCII format so that it could be imported into QBASIC for data analysis (see Appendix D for a listing of the data manipulation software).

III.2 Theory of Measurement

In this investigation, two in-situ measurements were made to quantify both the energy and material balances of the reacting systems. The heat of reaction was measured using a heat flux calorimeter, and both water bypass and hydrogen gas production were measured with a gas analyzer. The combination of the quantification of energy and material balances with basic reaction stoichiometry permitted determination of the overall reaction mechanism without the use of ex-situ analysis of solid reaction products.

III.2.1 Heat Flux Calorimetry

The cylindrical calorimeter walls contain a thermopile structure composed of two sets of thermoelectric junctions. One set of junctions is in thermal contact with the internal calorimeter wall, at temperature T_i , and the second set of thermal junctions is in thermal contact with the external calorimeter wall, at temperature T_e . Unless utilizing a twin calorimeter system, it is imperative for meaningful experimental results that T_e maintain constant throughout the duration of the experiment⁴.

⁴ Although, in this investigation, the oven maintained the infinite heat sink temperature to within $\pm 0.30\text{K}$, the calorimeter was sensitive to these slight thermal fluctuations. The insulating box surrounding

When heat is generated within a calorimetric cell, the calorimeter radially transfers a constant fraction of this heat, γ , into the surrounding heat sink⁵. As heat flows through the calorimeter walls, a temperature gradient, $(T_i - T_e)$, is established between the two sets of thermoelectric junctions. As stated by O'Neil et al. (97) this temperature gradient generates a voltage which can be mathematically represented by a series expansion.

$$\Delta V = C_1(T_i - T_e) + (C_2/2)(T_i - T_e)^2 + \dots \quad (\text{III.1})$$

If $(T_i - T_e)$ is negligibly small, then the series is adequately represented by the first term.

$$\Delta V = C_1 (T_i - T_e) \quad (\text{III.2})$$

The heat flux, (dQ/dt) , through the calorimeter walls is also directly proportional to this temperature gradient. Thus, the integrated value of the generated voltage, ΔV , produced in the thermopile over time is also directly proportional to the total heat produced, Q , by the reaction process (97).

$$Q = C \int_0^{\infty} \Delta V dt \quad (\text{III.3})$$

The proportionality constant, C , is typically determined experimentally during a calibration procedure (Chapter III.3.4). At a fixed temperature, if C is independent of the quantity of heat input, the calorimeter response is said to be *linear*. Typically however, the proportionality constant is a function of temperature. Failure to account for this temperature dependence has previously caused errors in data interpretation (97). The integral quantity, $\int \Delta V dt$, is the area of the experimental thermogram and was obtained, in this investigation, by direct numerical integration of the experimental data (Appendix D).

the calorimeter was added to dampen the oscillating thermal fluctuations of the infinite heat sink and to maintain a constant T_e (see Appendix B for a mathematical proof of this postulate). The insulation did *not* make the system adiabatic.

⁵ Typical thermal losses include axial conduction (which is minimized by internal calorimeter insulation), conduction losses through the calorimeter signal cable, radiation, and convection. Although it is safe to assume that radiation and conduction losses are negligible, it is not so easy to dismiss the possibility of convective heat loss in a flow system. However, a statistical analysis of the calibration constant data revealed that convective heat losses were indeed negligible in this experimental system (Chapter III.3.4).

Equation (III.3) is identical in form to the well known integrated Tian Equation (78,98,99).

$$Q = \frac{nk}{g\gamma} \int_0^{\infty} \Delta V dt \quad (\text{III.4})$$

Equation (III.4) provides a better intuitive look into the temperature dependence of the proportionality constant than equation (III.3) by providing a mathematical form for the proportionality constant.

$$C = \frac{nk}{g\gamma} \quad (\text{III.5})$$

where n is the number of thermoelectric junctions in the thermopile, k is the thermal conductivity of the thermopile, and g is an unknown function of n , the power of the thermoelectric junctions, and the amplification of the signal. Due to the unknown nature of g , the proportionality constant in Tian's equation must also be determined experimentally by a calibration.

However, during the course of this investigation, an improved theoretical form of equations (III.3) and (III.4) was rigorously derived using a straight forward heat transport model (Appendix A). The simplified result is

$$Q = \frac{Vk\pi^3}{3.88nSL^2} \int_0^{\infty} \Delta V dt \quad (\text{III.6})$$

The Seebeck Coefficient, S , is a thermal property of the thermoelectric junctions and is available for most known thermoelectric junctions over an extremely wide range of temperatures (100). The volume in which heat is generated, V , and the characteristic dimension of the calorimeter, L , are easily determined physical quantities. The thermal conductivity of the calorimeter, k , if not known, can be either measured or estimated with a suitable correlation (101-103).

Equation (III.6) predicts that the calorimeter response is independent of heat generation rate within the calorimeter, as observed experimentally (Chapter III.3.4), and permits the direct theoretical calculation of the calorimeter proportionality constant, provided that the physical and thermal properties of the calorimeter are well known.

A simplified form of the proportionality constant, obtained from the model in Appendix A for steady state heat generation within the calorimeter, defines the *intrinsic sensitivity* of a heat flux calorimeter.

$$C = \frac{P}{(\Delta V)_{ss}} \quad (\text{III.7})$$

P is the rate of heat generation, and $(\Delta V)_{ss}$ is the steady state voltage response to P. "The intrinsic sensitivity ...", numerically equivalent to the inverse of the calibration constant, "... is defined as the value of the steady emf that is produced by the thermoelectric elements when a unit of thermal power is dissipated continuously in the active cell of the calorimeter" (78). Equation (III.7) is established in the field of calorimetry as an experimental means of determining C, and can be derived by less rigorous mathematical treatment (104). Although the aforementioned mathematically derived results, equations (III.6) and (III.7), offer two significant theoretical improvements in heat flux calorimetry, determination of the proportionality constant is restricted to experimental calibration unless reliable thermal conductivity data for the complex structure of calorimeters becomes available.

The successful experimental applicability of equation (III.3)⁶ requires constant external wall temperature, T_e , and uniform radial symmetry of the thermal perturbations. It should also be noted that equation (III.3) is independent of the physical properties of the material inside of the calorimeter. Thus, all heat produced within the calorimeter must eventually flow into the infinite heat sink, regardless of the calorimeter contents. Although Gravelle (78) has suggested that equation (III.3) is not suitable for the analysis of thermograms produced by *rapid* heat input, due to the inherent thermal lag of the heat flow calorimeter, Evans (99) is convinced that this is not the case. Nonetheless, the proper method of determining the validity of equation (III.3) for the study of rapid reactions is through experimental determination of the *range of linearity* of the calorimeter response. The range of linearity is the range of heat quantity and input rate, at a fixed temperature, for which C is a constant, and is determined by an experimental calibration.

⁶ Equation (III.3) is herein considered to be equivalent to the general experimental forms of equations (III.4) and (III.6).

III.2.2 The Gas Analyzer

The gas analyzer was primarily used for the in-situ quantification of hydrogen production, and occasionally used for unreacted water quantification. The gas analyzer essentially consists of four electrically heated metal filaments suspended in a reference gas stream. These filaments are designed to maintain heat losses due to convection and radiation constant, and therefore are sensitive only to the difference in thermal conductivity of the sample stream and the reference stream (105). The change in thermal conductivity of the sample stream causes a change in the resistance of the filaments, thereby inducing a change in the output electrical signal. This transient signal is then sampled with the data acquisition software for analysis.

Because this instrument was designed to measure the *concentration* of a sample gas (S) in a flowing reference gas stream (R), the electrical output signal, $\Delta V dt$, is directly proportional to the concentration of S in R.

$$\Delta V dt \propto [S] \quad (III.8)$$

Using the following definition of concentration

$$[S] = \frac{\eta_S}{v_R} \quad (III.9)$$

where v_R is the volumetric flow rate of R and η_S is the molar quantity of S, equation (III.8) may be written as

$$\eta_S = C_S v_R \int_{t_i}^{t_f} \Delta V dt \quad (III.10)$$

where C_S is merely a proportionality constant dependent only on S, and t_i and t_f are the initial and final integration times, respectively. The validity of equation (III.10) was established experimentally for hydrogen and water vapor (Chapter III.3.3). The interesting result from equation (III.10) is that for constant η_S , the integral signal area increases for decreasing v_R . This empirical phenomenon influenced the choice of low reference flow rates in this investigation.

III.2.3 The Governing Experimental Equations

The governing equations used in this investigation for quantification of heat of reaction

$$Q = C \int_0^{\infty} \Delta V dt \quad (\text{III.3})$$

and quantification of gas in the effluent stream

$$\eta_S = C_S v_R \int_{t_i}^{t_f} \Delta V dt \quad (\text{III.10})$$

have identical mathematical forms and can be derived quasi-theoretically. The proper use of these two equations in this investigation required a statistically relevant calibration procedure to determine the calibration constants, C and C_S .

III.3 Apparatus Calibration

In this investigation, the accurate measurements of the heat of reaction, the amount of water bypass, and the quantity of hydrogen produced required the accurate determination of the limiting reagent volumes, the argon purge gas flow rate v_R , the calorimeter calibration constant, C , and the gas analyzer calibration constants, C_S . The numerical values of all calibration constants are reported with 95% confidence limits.

III.3.1 Limiting Reagent Volumes

A four port fixed volume injector was utilized for the introduction of liquid water into the argon purge stream. Because this injector was manufactured only to deliver reproducible fixed volumes *ca* 2 μl (106), it was necessary to calibrate the fixed volume injector. An HP5890 gas chromatograph with a six foot Chromosorb 102 packed column was utilized for this calibration procedure. Using 1.0 μl (SGE, Model 1BR-7) and 5.0 μl (SGE, Model 5BR-7) precision syringes, fixed volumes of n-hexane (Aldrich) were manually introduced into the chromatograph to calculate an n-hexane calibration constant,

$C_n = 2.00 \pm 0.05 \times 10^{-7} \mu\text{l} / \text{area unit}$. The four port fixed volume injector was then utilized to inject an *unknown* volume of n-hexane into the chromatograph. The mean integral area of the fixed volume injector areas, $A_m = 1.34 \pm 0.02 \times 10^7$ area units, was simply multiplied by C_n to determine the water sampling volume of the four port injector, $V_{\text{H}_2\text{O}} = 2.68 \pm 0.11 \mu\text{l}$.

A six port fixed volume injector with a nominal 2 ml sample loop was utilized for the introduction of hydrogen into the argon purge stream during the gas analyzer calibration. Because the manufacturer reported the volume range as $V = 2.0 \pm 0.2$ ml (106), the volume of the nominal 2 ml sample loop also needed to be calibrated. Using the experimental apparatus (Figure III.2), the sample loop was filled with liquid water at 298°K, and then emptied into a graduated cylinder of known mass. Using a Mettler AE100 balance, the mass of the water contained within the cylinder was then obtained. After five identical measurements, the mean mass of the water sample was determined to be $m = 2.195 \pm 0.005$ g. The volume of the six port injector sample loop was obtained by dividing the measured mass by the density of water at 298°K, $\rho = 0.9974 \text{ g/cm}^3$ (100). From this procedure, the volume of this sample loop, and thus the volume of hydrogen used during calibration of the gas analyzer, was determined to be $V_{\text{H}_2} = 2.201 \pm 0.005 \text{ cm}^3$.

III.3.2 Volumetric Flow Rate of the Argon Purge

The flow rate of the argon purge to the reactor was regulated with a rotameter and a metering valve (Figure III.2) and was determined from a standard *bubble-meter* calibration procedure. A schematic of this simple apparatus is provided in Figure III.3. Using the bubble-meter, a soap bubble was introduced into the reactor effluent. The volume, V , traveled by the soap bubble in the effluent was measured directly from the graduated markings on the pipette wall of the bubble meter. The duration of time, t , required for the soap bubble to travel V was measured with a single event stopwatch (Cole Parmer, Model 8668). The volumetric flow rate of argon, v_R , was then easily calculated. The measurement of v_R was performed at random, multiple times during an experiment to obtain a statistically relevant mean value and to monitor any possible abnormal deviations in flow rate. A typical value for v_R used in this investigation was $1.52 \pm 0.01 \text{ cm}^3/\text{sec}$.

III.3.3 The Gas Analyzer

Accurate knowledge of the limiting reagent volumes and the argon flow rate permitted the calibration of the gas analyzer over a wide range of v_R for hydrogen(g) and water(g). The entire experimental apparatus (Figure III.2) was used during this calibration procedure. At constant v_R , a known volume of limiting reagent was input into the argon stream using the appropriate fixed port injector. The limiting reagent then passed into the oven, through the empty reactor, and directly into the gas analyzer. The response of the gas analyzer to both hydrogen and water is illustrated in Figure III.4. The integral area of the gas analyzer signal response to the limiting reagent was then calculated numerically (Appendix D). To calculate the proportionality constants, CS , from the experimental data using equation (III.10), the volume of limiting reagents had to be converted to absolute molar quantities. The molar amount of water, η_{H_2O} , was calculated directly from the known calibration volume.

$$\eta_{H_2O} = \frac{\rho V_{H_2O}}{MW} \quad (III.11)$$

where ρ is the density of water at 298°K, and MW is the molecular weight of water. The molar amount of hydrogen, η_{H_2} , was calculated directly from the ideal gas law at 298°K.

$$\eta_{H_2} = \frac{PV_{H_2}}{RT} \quad (III.12)$$

The static hydrogen pressure, P , in the fixed volume injector was measured using the pressure gauge on the hydrogen source cylinder. The calibration constant for each limiting reagent is listed Table III.1 along with a range of v_R to which CS is restricted.

Table III.1
Gas analyzer calibration constants for the limiting reactants.

S	v_R (cm ³ / s)	CS (μmol/V cm ³)
hydrogen (g)	1.5 - 4.45	0.970 ± 0.006
water (g)	1.5 - 4.45	4.86 ± 0.23

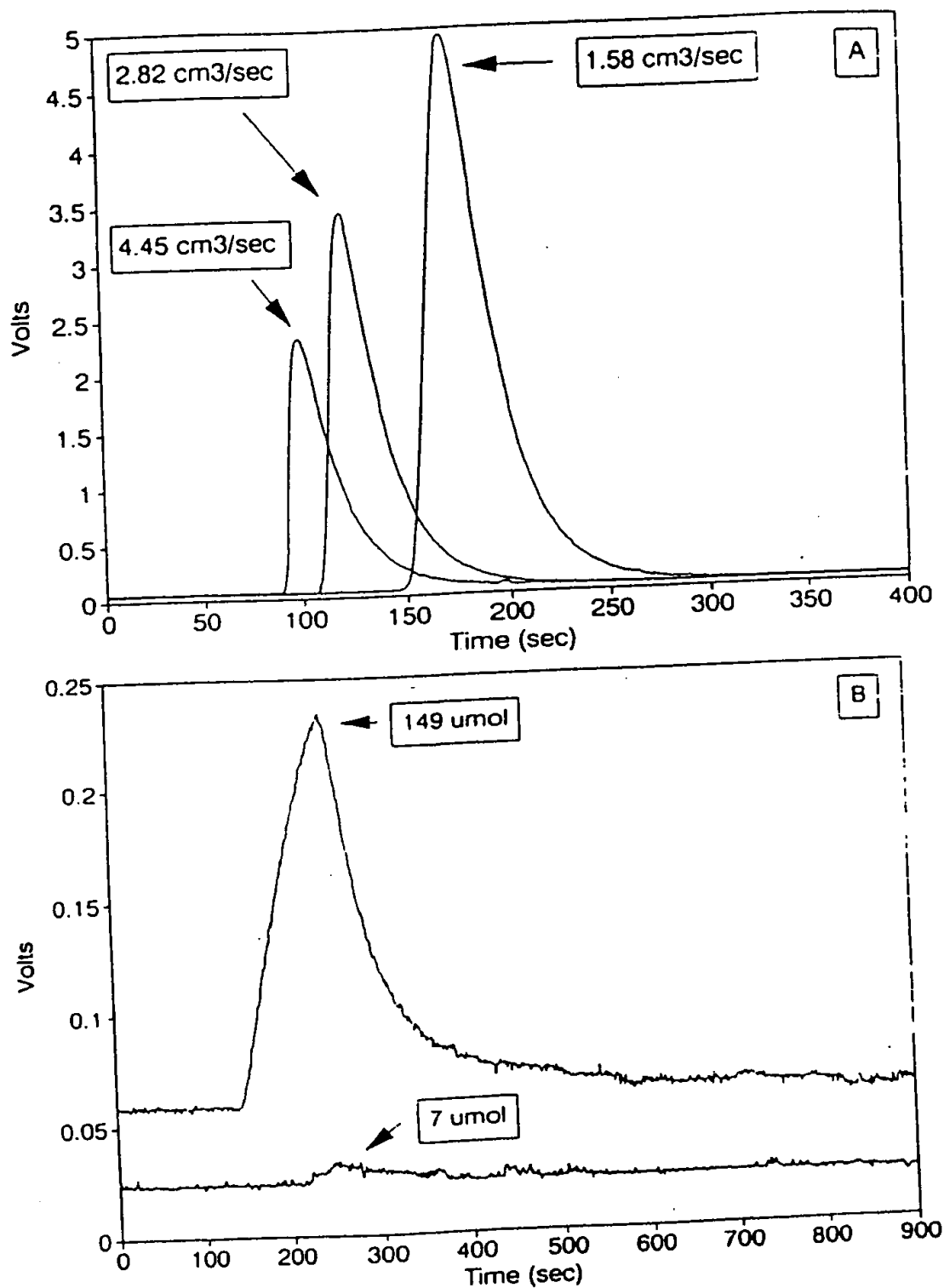


Figure III.3 : The gas analyzer signal response to (a) 274 μmol hydrogen gas at various gas flow rates, and (b) various amounts of water vapor at a flow rate of 1.58 cm^3/sec .

Because the thermal conductivity of hydrogen is much greater than that of water vapor (101), the gas analyzer is more *sensitive* to hydrogen. The sensitivity of the gas analyzer is the inverse of C_S and is a relative measure of the size of the integral signal response. The relatively larger deviation in CH_2O can be attributed to possible partial condensation of the water on the gas analyzer thermal filaments. The manufacturer of the gas analyzer has acknowledged that condensation of vapor can slightly alter the gas analyzer signal response (105).

III.3.4 The Heat-Flux Calorimeter

Quantitative experimental measurement of the heat of reaction with the calorimeter required a determination of the proportionality constant, C , in equation (III.3). Experimental determination of C was accomplished through a standard electrical calibration technique (78,107,108). A high precision beryllium core 18Ω resistor (Mills Resistor Co.) was placed within the reactor, inside of the calorimeter. The resistor, as part of a simple circuit, was connected to a constant current (40-165 mA) output source. A known quantity of current, I , flowing through a known resistance, R , for a known duration of time, t , produces a total amount of heat, Q , simply given by the expression

$$Q = I^2 R t = IVt \quad (III.13)$$

where V is the voltage. Both I and V were measured in-situ during all calibration experiments for an accurate determination of Q . Numerical integration of the calorimeter signal response curve corresponding to a known quantity of heat input, Q , permits calculation of the proportionality constant, C , of the calorimeter using the expression

$$C = \frac{IVt}{\int_{t_i}^{t_f} \Delta V dt} \quad (III.14)$$

The infinite integration limits have been replaced by t_i and t_f , the experimental initial and final integration times, respectively. For proper experimental use of equation (III.3), it was crucial to demonstrate that C , as calculated from equation (III.14), was independent of rate of heat generation, P , the total quantity of heat input, Q , and the flow rate of the argon

purge, v_R . The influence of infinite heat sink temperature, T , on C also needed to be determined. Thus, an appropriate test was devised to statistically ascertain the influence of P , Q , v_R and T on C .

For the calibration and statistical analysis it was necessary to write C as C_{ijk} , where i , j , and k are the numerical indices 1 or 2, referring to specific numeric values of P , v_R , and T , respectively (Table III.2).

Table III.2
Numerical values for C_{ijk} indices.

Indice #	i (W)	j (cm ³ /sec)	k (°K)
1	0.24	0	505
2	0.60	4.448	588

The combined indices ijk refer to the environmental conditions at which C_{ijk} was determined. A total of eight combinations of i , j , and k were used in this investigation.

During the electrical calibration procedure, a graph of $\int \Delta V dt$ vs Q was constructed at each temperature to demonstrate the linearity of the calorimeter response (Figure III.4). Although there is scatter in the data, the linearity of the curve indicated that the calorimeter signal response was independent of Q over the range of 10 to 75 Joules (This was also the range of heat observed in the actual reaction experiments). To determine the effect of rate of heat generation, P , and gas flow rate, v_R , on the calorimeter signal response, a standard statistical analysis was used.

Using each data point in Figure III.5, the individual C_{ijk} values were calculated directly from equation (III.14), and an average of the multiple *observations* of C_{ijk} was obtained (Table III.3). All reported C_{ijk} values include the calorimeter signal amplification of 1000x magnification.

An F-Test (109), at the $\alpha=0.05$ level of significance, was performed at each temperature to determine the effect of P and v_R on C_{ijk} . The first step was to postulate the *Null Hypothesis*, H_0 , at constant temperature (k).

$$H_0 : C_{11k} = C_{12k} = C_{21k} = C_{22k}$$

(III.15)

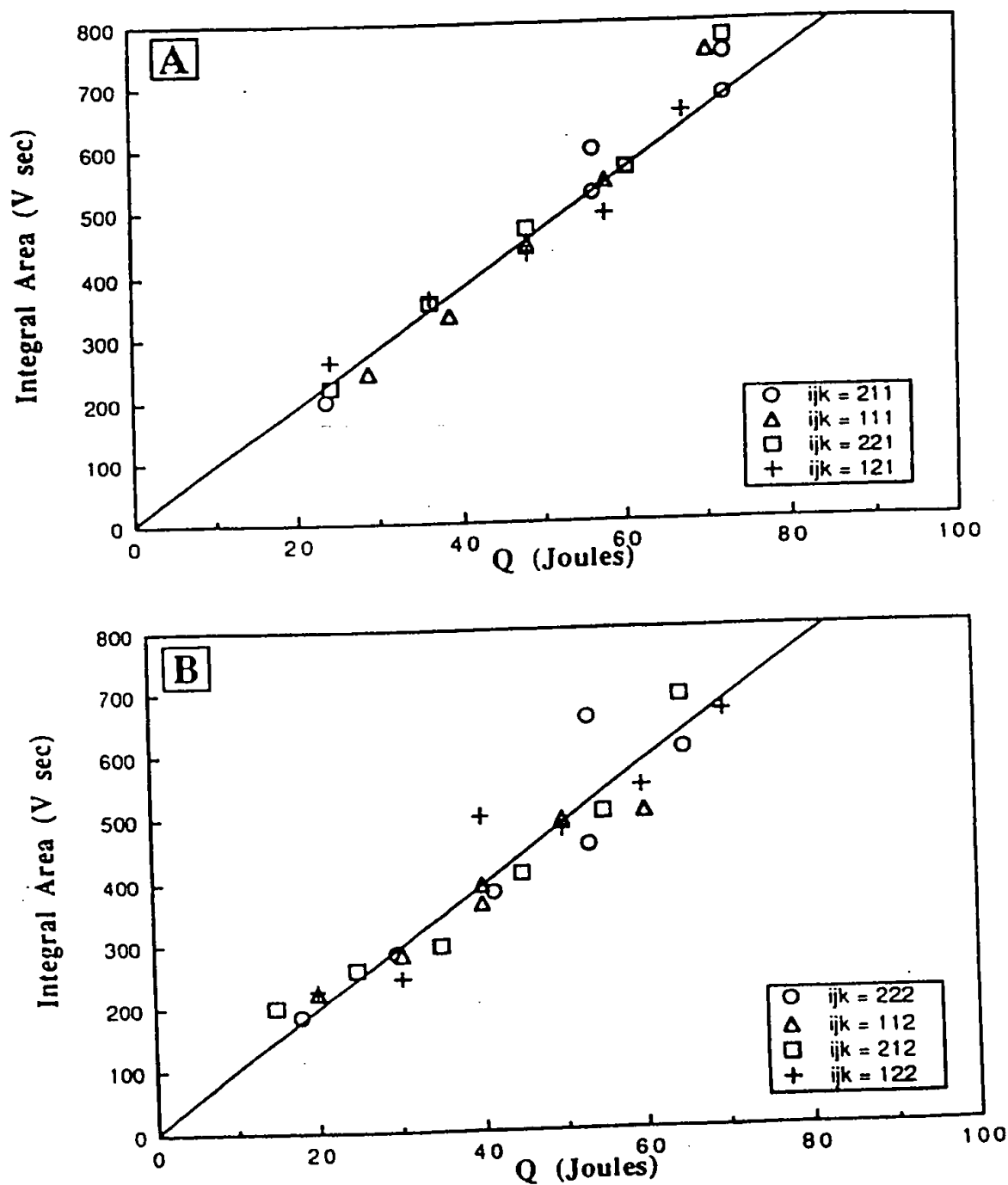


Figure III.4 : A plot of the integral calorimeter signal response, $\int \Delta V dt$, versus total heat input, Q , during the electrical calibration procedure at (a) 505°K and (b) 588°K.

Table III.3
Experimental values of C_{ijk} at 1000x magnification.

ij	C_{ij1} (J / V sec)	C_{ij2} (J / V sec)
11	0.108 ± 0.012	0.105 ± 0.010
12	0.109 ± 0.007	0.102 ± 0.017
21	0.104 ± 0.012	0.100 ± 0.017
22	0.103 ± 0.008	0.103 ± 0.013

The null hypothesis is merely a postulate that no statistical difference will be found between the inclusive means. Although "researchers rarely desire to prove the null hypothesis" (110), the validity of H_0 needed to be established for the purposes of this investigation. When validating H_0 it is important to minimize a *Type II error*, which is the probability of failing to reject H_0 when in fact there is a difference. The *Alternate Hypothesis*, H_a , at constant temperature (k)

$$H_a : C_{11k} \neq C_{12k} \neq C_{21k} \neq C_{22k} \quad (\text{III.16})$$

is a postulate that there is a statistical difference between the inclusive means. Although some researchers feel that the F-test is inadequate to test the validity of the *null hypothesis*, this procedure is outlined in Mickley et al. (111) and was recommended by *The Statistical Consulting Center* at The Pennsylvania State University. An L-test (111), at the $\alpha=0.05$ level of significance, was also performed to validate the implicit assumption in the F-test that the variance of each C_{ijk} is the same (109). Because the results of the F-test indicated that H_0 was valid at 505°K (k=1) and 588°K (k=2), a *grand mean* was calculated at each temperature from all the independent observations for C_{ijk} (Table III.4).

The preceding analysis, through verification of H_0 , permitted the conclusion that at a fixed temperature, the calorimeter signal response was independent of P and v_R . To determine the effect of temperature on the calorimeter signal response, an F-test was designed with the following hypothesis:

$$H_0 : C_{505} = C_{588} \quad (\text{III.17})$$

Table III.4

The grand means, C_k , of the calorimeter calibration constants, C_{ijk} .

Temperature ($^{\circ}\text{K}$)	C_k (J / V sec)
505	0.106 ± 0.004
588	0.103 ± 0.006

$$H_a : C_{505} \neq C_{588}$$

(III.18)

Because the results clearly showed that H_o was valid, it was reasonable to conclude that the calorimeter signal response was also independent of temperature, over the narrow range used in this investigation.

The preceding analysis of the calorimeter calibration constant, C , indicated that it was independent of rate of heat input, quantity of heat input, flow rate of argon gas, and temperature, with the limits of this investigation. However, because the manufacturer of the calorimeter indicated that C was slightly temperature dependent, it was decided to use the values for C determined at each temperature during reaction experiments, and not to lump them into another grand mean. The most important result of this analysis was that the flow rate of the argon gas, v_R , did not significantly alter C . This phenomenon required a physical interpretation.

During heat generation, heat is removed from the reactor within the calorimeter by either conduction through the thermopiles or by bulk transport with the exiting gas. Alternate avenues of heat loss are assumed to be constant and negligible (Chapter III.2.1). The conduction through the thermopiles is limited by the heat flux through the argon stream and the reactor wall. It was thus desirable to show that the rate of bulk heat removal by the flowing argon stream was negligible compared to the rate of heat removal to the thermopiles. Both of these processes are dependent upon the temperature difference, ΔT , which exists between the reactor within the calorimeter and the infinite heat sink.

The rate of bulk heat transfer, \dot{Q}_c , to the carrier gas can be written as

$$\dot{Q}_c = \rho v_R C_p \Delta T$$

(III.19)

where C_p is the heat capacity and ρ is the density of the carrier gas. The overall heat transfer coefficient, U , for the rate of heat removal to the thermopiles, \dot{Q}_h , can be defined as

$$\dot{Q}_h = UA\Delta T \quad (\text{III.20})$$

where A is the total internal surface area of the reactor. Note that the ratio of \dot{Q}_c / \dot{Q}_h

$$\frac{\dot{Q}_c}{\dot{Q}_h} = \frac{\rho v_R C_p}{UA} \quad (\text{III.21})$$

is only indirectly dependent on ΔT , through the possible dependence of U on ΔT . Using the data in Table III.5, the ratio of $\dot{Q}_c / \dot{Q}_h = 4.6\%$ was calculated from equation (III.21).

Table III.5
Data for the calculation of \dot{Q}_c / \dot{Q}_h .

Parameter	Value ⁷
$U (\text{W}/\text{cm}^2 \cdot \text{K})$	0.00116
$A (\text{cm}^2)$	36.55
$\rho (\text{g}/\text{cm}^3)$	8.51×10^{-4}
$C_p (\text{J}/\text{g} \cdot \text{K})$	0.5207
$v_R (\text{cm}^3/\text{sec})$	4.45

A minimum estimate of U , $0.00116 \text{ W}/\text{cm}^2 \cdot \text{K}$, was obtained directly from the literature as a mean value for free convection (103). The use of a minimum estimate of U maximizes the ratio of \dot{Q}_c / \dot{Q}_h , which can thus be taken as the upper limit to experimental error introduced by the argon purge. Including other avenues of heat transfer, such as radiation and forced convection, into the analysis would only increase the value of U .

⁷ The physical property data for argon was obtained from Lienhard (102).

Thus, because the rate of heat loss due to the argon purge, 4.6%, is essentially the same magnitude as the 95% confidence limit on the calorimeter calibration constant (Table III.4), heat loss due to the argon flow is within experimental measurement error. Thus, as determined experimentally using a statistical analysis of the calorimeter calibration data (Chapter III.3.4), the bulk rate of heat removal by the argon purge stream is negligible for the range of argon flow rates used in this study.

This preceding analysis introduces a general guideline to the design of flow calorimeters. It indicates that the error in measurement introduced by the carrier stream is negligible ($< 5\%$) if the carrier stream has a small heat capacity. Although Barton (80) used extremely small carrier flow rates (ca $0.06 \text{ cm}^3/\text{sec}$) in his flow calorimeter, he observed that the adjustment of carrier flow rate altered the calorimeter calibration constant by up to 20%. This phenomenon was most likely due to the large heat capacity of water (relative to argon), which he used as a carrier fluid.

It was not possible to ascertain the validity of the previous analysis for the presence of a solid reactant in the reactor. Calibration tests were not conducted with solid reagent present in the reactor because the calibrating resistor occupies a considerable fraction of the reactor volume, and would not fit within the reactor with a load of reactant present. However, the preceding physical interpretation suggests that the overall heat transfer coefficient should increase when solid reactant is present in the reactor, due to the improved conduction properties of metallic compounds over gases. Therefore, it is reasonable to conclude that with solid present in the reactor, the bulk rate of heat removal by the argon purge is also negligible.

III.4 Experimental Procedure

A general experimental procedure was followed for the two reactions used to test the apparatus (Chapter III.5), and the two fuel reactions of primary interest to this investigation (Chapter IV).

(1) The dry, solid reagent was loosely poured into the reactor in a dry box (Terra Universal, Model 1689-00) under a continuous blanket of argon at 298°K . A copper gasket was then placed on top of the test cell, and the reactor lid was fastened to the reactor with eight .375" stainless steel bolts. The bolts were coated with a small layer of high temperature anti-seize to minimize strain due to repeated thermal cycling. The inlet and

outlet pipes to the reactor were then sealed with swagelock fittings so that the reactor could serve as a temporary, batch, inert environment.

(2) The reactor was removed from the dry box and placed within the calorimeter. During this time, argon was continuously purged through the system and into the oven. The heat exchanger was then connected to the reactor inlet pipe, and the reactor outlet was connected to the effluent pipe. After securing the insulation around the calorimeter, the oven temperature was gradually ramped to the desired experimental temperature, either 505°K or 588°K. After thermal equilibrium was established, typically within 16 hours as indicated by a steady calorimeter baseline, the system was ready for experiment initiation.

(3) At time zero, the data acquisition system was activated for sampling data at 5 Hertz. The baseline was sampled for exactly 120 seconds, synchronized with a digital stopwatch, prior to the injection of limiting reagent into the argon stream to accurately determine the initial baseline voltage. Data acquisition was continued for approximately 3600 seconds after the injection of limiting reagent into the reactor. After the reaction terminated and thermal equilibrium was established, the data was saved in ASCII format for later analysis. Up to ten injections of limiting reagent into the reactor were performed during the course of one reaction investigation in order to obtain a statistically relevant sample size.

(4) At the completion of the reaction investigation, the system was cooled down to room temperature, the reactor was removed from the system, and then placed in the dry box. The solid contents of the reactor were removed under an argon blanket and saved in a calcium sulfate dessicator to minimize atmospheric contamination. The reactor was then removed from the dry box and submerged in a water bath to cleanse it of any lithium containing materials. After drying the reactor with acetone, it was ready for use in a new experiment.

III.5 Test Experiments

Prior to using the experimental apparatus to investigate the lithium-water and lithium hydride-water reaction systems, two test experiments were conducted to determine the extent of reliability of the experimental apparatus. Chemical reaction calibration is commonly used in microcalorimetry to independently verify the calibration constant of the calorimeter (107,108). Although the most common reaction in use is the reaction of sodium hydroxide with hydrochloric acid (107), the two following reactions

THIS PAGE BLANK (USPTO)

THIS PAGE BLANK (USPTO)

DECLARATION OF MICHAEL G. JACOX

I, Michael G. Jacox do hereby declare and say as follows:

1. I received a Bachelor of Science Degree in Nuclear Engineering from the Georgia Institute of Technology in 1985. I received a Masters of Science Degree in Nuclear Engineering from the University of Idaho in 1992.

2. From 1998 to the present, I have been employed as an Assistant Director for the Commercial Space Center for Engineering (CSCE), Texas A & M University, where I have developed a strategic plan for a newly created NASA commercial space center which resulted in an increase of NASA funding from \$500K to \$1M annually. I planned and executed the campaign for industry input and support of the CSCE. I led the development of the first integrated payload design center at Texas A & M University.

3. From 1996-1998, I was employed as a Program Manager at the Space Dynamics Lab, Utah State University, where I defined, promoted and managed the \$50M Solar Orbit Transfer Vehicle (SOTV) space experiment and technology development program. I also completed the first ever system-level ground test of the Integrated Solar Upper State (ISUS) on time and within the \$15M budget.

4. From 1994-1996, I was employed as a Systems Engineer at Lockheed-Martin Idaho Technologies, where I managed a team of more than 30 engineers and scientists from NASA, the Naval Research Lab, Air Force Research Lab and industry in a highly successful \$1M system definition study of the ISUS space power and propulsion concept. I also managed a joint DOD-DOE nuclear bimodal systems engineering team that evaluated concepts and developed preliminary designs of combined power and propulsion reactors.

5. From 1989-1994, I was employed as a Senior Scientist at EG&G Idaho, where I conceived the design and managed the development and testing of the first integrated thermionic/heat-pipe module for nuclear bimodal applications. The multi-million dollar effort resulted in successful prototype testing. I also managed the design and installation of a unique multi-million dollar hot hydrogen test facility at the Idaho National Engineering Lab. I further originated the design of the Small-Ex-core Heat Pipe Thermionic Reactor (SEHPTR), led the SEHPTR conceptual design team, and received a patent covering the SEHPTR. I also developed and benchmarked the first three-dimensional neutronics model of the Advanced Test Reactor.

6. From 1985-1989, I was employed as a Nuclear Research Officer at USAF Weapons Lab, where I led the Air Force's space nuclear power application studies resulting in significant national program modifications and the development of the Military Space Reactor Initiatives. I also installed advanced nuclear reactor analysis codes on in-house computers.

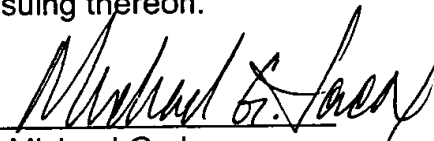
Declaration of Michael G. Jacox
Page 2 of 2

7. While employed at EG&G, I contracted for the Idaho National Engineering Laboratory (INEL) under a DOE contract. At INEL, I conducted three experiments in which hydrogen was reacted with a catalyst, (K^+ , K^+), generated from aqueous K_2CO_3 , in an electrolytic cell containing nickel and platinum electrodes. The test conditions and results are shown in the attached report. As can be seen from the test results, 20 to 30 watts of excess heat was observed and in one instance the ratio of excess power to input electrolysis joule heating power was 850%.

8. The evidence presented in the attached report clearly demonstrates that a phenomenon takes place upon the admission of hydrogen to an electrolytic cell containing aqueous KCO_3 . This phenomenon generates heat in excess of that expected from any known chemical process, given the content of the reactants in the cell. A detailed analysis of all constituents was conducted to ensure that no chemical reactions were occurring which could be generating the excess heat observed.

9. I declare further that all statements made herein of my own knowledge are true and that all statements made on information and belief are believed to be true; and further that these statements were made with the knowledge that willful false statements and the like so made are punishable by fine or imprisonment, or both, under Section 1001 of Title 18 of the United States Code and that such willful false statements may jeopardize the validity of the application or any patent issuing thereon.

By


Michael G. Jacox

Date:

25 July 00

Experimental Verification by Idaho National Engineering Laboratory

Methods

A search for excess heat during the electrolysis of aqueous potassium carbonate (K^+/K^+ electrocatalytic couple) was investigated using cells supplied by HydroCatalysis Power Corporation and a cell fabricated by Idaho National Engineering Laboratory (INEL). To simplify the calibration of these cells, they were constructed to have primarily conductive and forced convective heat losses. Thus, a linear calibration curve was obtained. Differential calorimetry was used to determine the cell constant which, was used to calculate the excess enthalpy. The cell constant was calculated during the experiment (on-the-fly-calibration) by turning an internal resistance heater off and on, and inferring the cell constant from the difference between the losses with and without the heater.

The general form of the energy balance equation for the cell in steady state is:

$$0 = P_{\text{appl}} + Q_{\text{htr}} + Q_{\text{xs}} - P_{\text{gas}} - Q_{\text{loss}} \quad (\text{III.1})$$

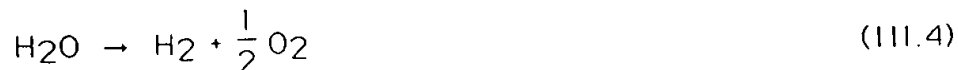
where P_{appl} is the electrolysis power; Q_{htr} is the power input to the heater; Q_{xs} is the excess heat power generated by the hydrogen "shrinkage" process; P_{gas} is the power removed as a result of evolution of H_2 and O_2 gases; and Q_{loss} is the thermal power loss from the cell. When an aqueous solution is electrolyzed to liberate hydrogen and oxygen gasses, the electrolysis power $P_{\text{appl}} (=E_{\text{appl}}I)$ can be partitioned into two terms:

$$P_{\text{appl}} = E_{\text{appl}}I = P_{\text{cell}} + P_{\text{gas}} \quad (\text{III.2})$$

An expression for $P_{\text{gas}} (=E_{\text{gas}}I)$ is readily obtained from the known enthalpy of formation of water from its elements:

$$E_{\text{gas}} = \frac{-\Delta H_{\text{form}}}{\alpha F} \quad (\text{III.3})$$

(F is Faraday's constant), which yields $E_{\text{gas}} = 1.48 \text{ V}$ for the reaction



The net faradaic efficiency of gas evolution is assumed to be unity; thus, Eq (III.2) becomes

$$P_{\text{cell}} = (E_{\text{appl}} - 1.48V)I \quad (\text{III.5})$$

The cell was calibrated for heat losses by turning an internal resistance heater off and on while maintaining constant electrolysis and by inferring

the cell constant from the difference between the losses with and without the heater where heat losses were primarily conductive and forced convective losses. When the heater was off, the losses were given by

$$c(T_c - T_b) = P_{\text{appl}} + 0 + Q_{\text{xs}} - P_{\text{gas}} \quad (\text{III.6})$$

where c is the heat loss coefficient; T_b is ambient temperature and T_c is the cell temperature. When a new steady state is established with the heater on, the losses change to:

$$c(T_c' - T_b) = P'_{\text{appl}} + Q_{\text{htr}} + Q'_{\text{xs}} - P'_{\text{gas}} \quad (\text{III.7})$$

where a prime superscript indicates a changed value when the heater was on. When the following assumptions apply

$$Q_{\text{xs}} = Q'_{\text{xs}}; P_{\text{appl}} = P'_{\text{appl}}; P_{\text{gas}} = P'_{\text{gas}} \quad (\text{III.8})$$

the cell constant or heating coefficient a , the reciprocal of the heat loss coefficient(c), is given by the result

$$a = \frac{T_c' - T_c}{Q_{\text{htr}}} \quad (\text{III.9})$$

In all heater power calculations, the following equation was used

$$Q_{\text{htr}} = E_{\text{htr}} I_{\text{htr}} \quad (\text{III.10})$$

LIGHT WATER CALORIMETRY EXPERIMENTS

INEL EXPERIMENT 1 (DC Operation)

The present experiments were carried out by observing and comparing the temperature difference, $\Delta T_1 = T(\text{electrolysis only}) - T(\text{blank})$ and $\Delta T_2 = T(\text{electrolysis plus resistor heating}) - T(\text{blank})$ referred to unit input power.

The cell comprised a 10 gallon (33 in. x 15 in.) Nalgene tank (Model # 54100-0010). Two 4 inch long by 1/2 inch diameter terminal bolts were secured in the lid, and a cord for a heater was inserted through the lid.

The cathode comprised 1.) a 5 gallon polyethylene bucket which served as a perforated (mesh) support structure where 0.5 inch holes were drilled over all surfaces at 0.75 inch spacings of the hole centers and 2.) 5000 meters of 0.5 mm diameter clean, cold drawn nickel wire (NI 200 0.0197", HTN36NOAG1, AI Wire Tech, Inc.). The wire was wound uniformly around the outside of the mesh support as 150 sections of 33 meter length. The ends of each of the 150 sections were spun to form three cables of 50 sections per cable. The cables were pressed in a terminal connector which was bolted to the cathode terminal post. The connection was covered with epoxy to prevent corrosion.

The anode comprised an array of 15 platinized titanium anodes (15 - Engelhard Pt/Ti mesh 1.6" x 8" with one 3/4" by 7" stem attached to the 1.6" side plated with 100 U series 3000). A 3/4" wide tab was made at the end of the stem of each anode by bending it at a right angle to the anode. A 1/4" hole was drilled in the center of each tab. The tabs were bolted to a 12.25" diameter polyethylene disk (Rubbermaid Model #2666) equidistantly around the circumference. Thus, an array was fabricated having the 15 anodes suspended from the disk. The anodes were bolted with 1/4" polyethylene bolts. Sandwiched between each anode tab and the disk was a flattened nickel cylinder also bolted to the tab and the disk. The cylinder was made from a 7.5 cm by 9 cm long x 0.125 mm thick nickel foil. The cylinder traversed the disk and the other end of each was pressed about a 10 A / 600 V copper wire. The connection was sealed with

Teflon tubing and epoxy. The wires were pressed into two terminal connectors and bolted to the anode terminal. The connection was covered with epoxy to prevent corrosion.

Before assembly, the anode array was cleaned in 3 M HCl for 5 minutes and rinsed with distilled water. The cathode was cleaned in 3% H_2O_2 / 0.57 M K_2CO_3 and rinsed with distilled water. The anode was placed in the cathode support and the electrode assembly was placed in the tank containing electrolyte. The power supply was connected to the terminals with large cables.

The electrolyte solution comprised 28 liters of 0.57 M K_2CO_3 (Alfa K_2CO_3 99%) in the case of the MC 3 cell or 28 liters of 0.57 M Na_2CO_3 (Alfa Na_2CO_3 99%) in the case of the MC 2 cell.

The heater comprised a 57 ohm 1500 watt Incoloy coated cartridge heater which was suspended from the polyethylene disk of the anode array. It was powered by a regulated power supply. The voltage was measured with a digital meter, and the current was measured as a voltage across a precision resistor with a digital meter.

The stirrer comprised a 1 cm diameter by 43 cm long glass rod to which an 8 cm by 2.5 cm Teflon half moon paddle was fastened at one end. The rod passed through a bearing hole in the tank lid and through a bearing hole in the center of the anode array disk. The other end of the stirrer rod was connected to a variable speed stirring motor. The stirrer shaft was rotated at 4 Hz. With the stirrer connected, the stirrer motor drew 4.7 W. With the stirrer disconnected, the stirrer drew 4.4 W; thus, 0.3 W was the stirrer power.

Electrolysis was performed at 39.5 amps constant current with a constant current power supply. The cells were operated in the environmental chamber in the INEL Battery test Laboratory. The chamber maintained the average temperature of the cell surroundings within 1 °C. The bottom of the cell rested on a 1/2 inch thick sheet of Styrofoam.

The temperature was recorded with a series of Teflon-coated Type E thermocouples inserted in several places. The ambient temperature reference was a closed one-liter container of water

with a thermocouple nominally in the center of the water volume.

Data from thermocouples, voltages, and currents were logged by one of the Battery Lab's computer based data systems and recorded at 5 minute intervals. The delta temperature ($\Delta T = T(\text{electrolysis only}) - T(\text{blank})$) and electrolysis power were plotted. The heating coefficient was determined "on the fly" by the addition of heater power. The delta temperature $\Delta T_2 = T(\text{electrolysis} + \text{heater}) - T(\text{blank})$ and the electrolysis power and heater power were plotted.

Mass spectroscopy of the gasses evolving from the MC 3 (K_2CO_3) cell was performed using a VG Instruments model SXP-50 high -precision mass spectrometer with 0.01-amu mass resolution and 6 decade sensitivity.

A 100 ml sample of the 0.57 M K_2CO_3 electrolyte of the MC 3 (K_2CO_3) cell was removed after 20 days of cell operation, and a chemical analysis was performed on the electrolyte using an Inductively Coupled Plasma-Atomic Emission Spectrometer.

RESULTS

Light Water Calorimetry

The results of the electrolysis for INEL cell runs MC 2 and MC 3 at 39.5 A constant current appear in Figure 1 (hand plot of data by INEL scientists). As shown in Figure 1, the MC 3 (K_2CO_3) cell intercepts the Total Input Power axis at 35 W; whereas, the MC 2 (Na_2CO_3) cell intercepts the Total Input Power axis at 59 W. The input power to electrolysis gases given by Eqs. (III.2-III.5) is $(39.5)(1.48) = 58.5$ W. The production of excess enthalpy of 25 W is observed with the MC 3 (K_2CO_3) cell, and energy balance is observed with the MC 2 (Na_2CO_3) cell.

Mass spectroscopic analysis of the gasses evolved by the MC 3 (K_2CO_3) cell showed that a significant fraction of the sample was air with standard constituents. When the spectrum associated with air was removed, the residue showed a majority of diatomic hydrogen and oxygen gases in approximately the 2:1 proportion expected from the electrolysis and residual water vapor. There were no hydrocarbons, no metallic constituents or other anomalies except that a slightly higher than expected hydrogen to oxygen ratio was observed. No

tritium or deuterium measurements above normal background were observed.

Chemical analysis of an electrolyte sample from the MC 3 (K_2CO_3) cell after 20 days of operation found the following components at levels above the background levels in the water used to fill and replenish the cell: 1.7 ppm silicon, 1.1 ppm sulfur, and 46.5 ppm sodium in addition to the K_2CO_3 salt. Small quantities of silicon are known impurities in the nickel wire and may have also come from the glassware used in various processes. Sulfur is a common impurity in the salt, and it may have come from the resin beds used for water deionization. Sodium is a probable salt impurity, and it may also have come from hand contact with the system. The potassium was measured at 43,000 $\mu\text{g/ml}$ corresponding to a salt molarity of 0.55 M (within measurement error of the initial 0.57 molarity determined by weighing the salt and measuring the water for the initial charge). The electrolyte retained its molarity. The cell potential characteristics were essentially unchanged over the duration of operation. There were no nickel or other metallic compounds present in the electrolyte. A visual inspection of the cell showed that all of the structural components were intact. The cell comprised about 155 moles of nickel in the cathode, about 6.5 moles of titanium in the anodes, and about 13.7 moles of K_2CO_3 . The only material consumed in the cell was nano-pure deionized water.

INEL EXPERIMENT II (Pulsed Power Operation)

The MC 3 (K_2CO_3) cell was wrapped in a one-inch layer of urethane foam insulation about the cylindrical surface. The top was not insulated. The bottom of the cell rested on a 1/2 inch thick sheet of Styrofoam.

The cell was operated in a pulsed power mode. A current of 10 amperes was passed through the cell for 0.2 seconds followed by 0.8 seconds of zero current for the current cycle. The cell voltage was about 2.4 volts, for an average input power of 4.8 W. The electrolysis power average (Eq. (III.5)) was 1.84 W, and the stirrer power was measured to be 0.3 W. Thus, the total average net input power was 2.14 W. The cell was operated at various resistance heater settings, and the temperature

difference between the cell and the ambient as well as the heater power were measured.

RESULTS

Light Water Calorimetry

The results of the excess power as a function of cell temperature with the MC 3 cell operating in the pulsed power mode at 1 Hz with a cell voltage of 2.4 volts, a peak current of 10 amperes, and a duty cycle of 20 % appears in Figure 2.

Figure 2 shows that the excess power is temperature dependent for pulsed power operation, and the maximum excess power shown in Figure 2 is 18 W for an input electrolysis joule heating power of 2.14 W. Thus, the ratio of excess power to input electrolysis joule heating power is 850 %.

INEL EXPERIMENT III (Forced Convection Calorimetry Of INEL Cell)

INEL scientists constructed an electrolytic cell comprising a nickel cathode, a platinized titanium anode, and a 0.57 M K_2CO_3 electrolyte. The cell design appears in Appendix I. The cell was operated in the environmental chamber in the INEL Battery test Laboratory at constant current, and the heat was removed by forced air convection in two cases. In the first case, the air was circulated by the environmental chamber circulatory system alone. In the second case, an additional forced air fan was directed onto the cell.

The cell was equipped with a water condensor, and the water addition to the cell due to electrolysis losses was measured.

RESULTS

Light Water Calorimetry

The data of the forced convection heat loss calorimetry experiments during the electrolysis of a 0.57 M K_2CO_3 electrolyte with the cell appears in Table 1 and Figure 3. The comparison of the calculated and measure water balance of the INEL cell appears in Table 2 and Figure 4.

The intercept of the Net Input Power (calculated using Eq. (III.5)) axis of Figure 3 for both cases of forced convection is 13 W. Thus, 13 W of excess power was produced by the INEL cell. This excess power can not be attributed to recombination of the hydrogen and oxygen as indicated by the

equivalence of the calculated and measured water balance as shown in Figure 4.

FIGURE 1.

THERMAL CONDUCTANCE CALIBRATION (11/25)

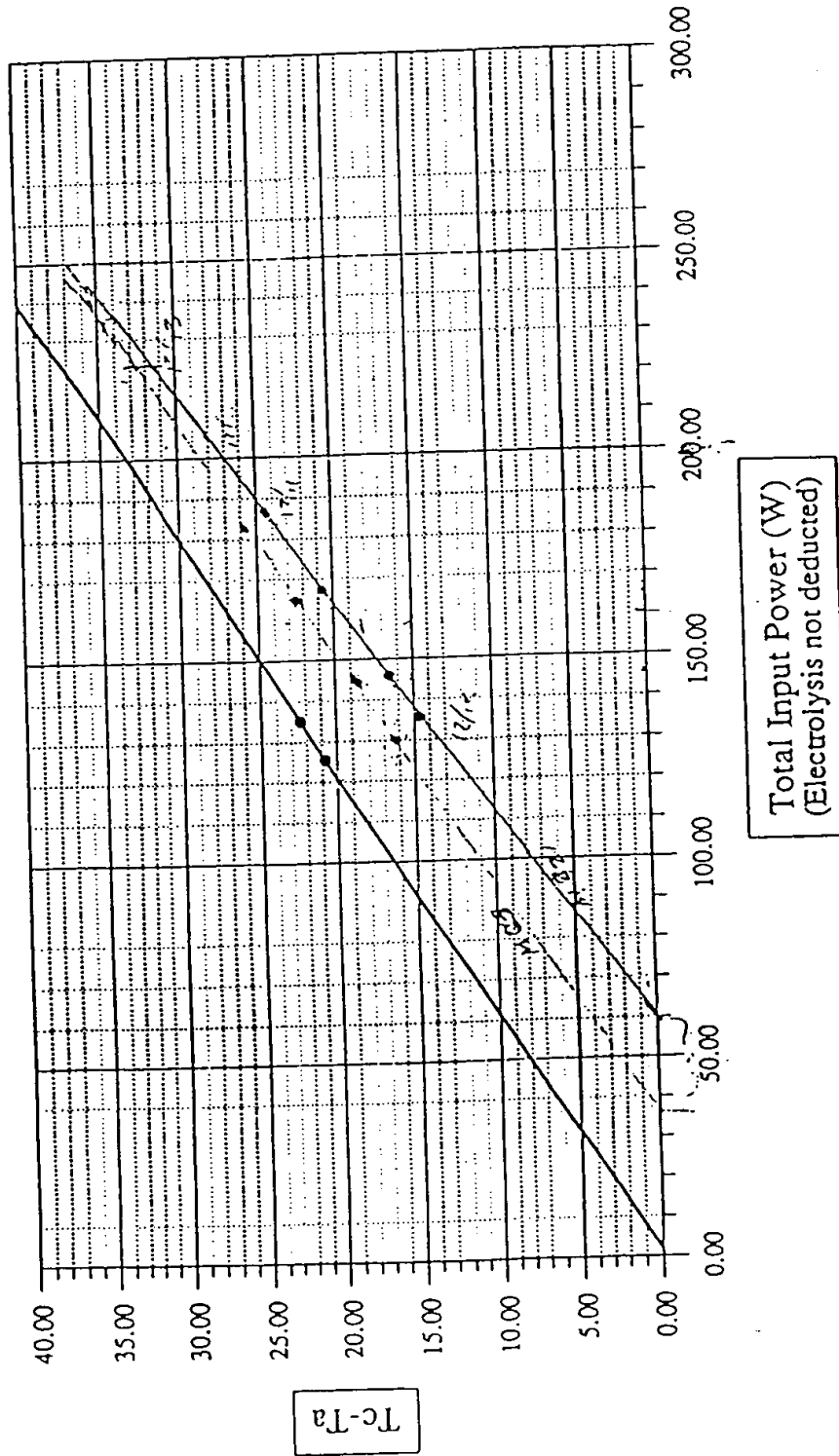


Figure 2.

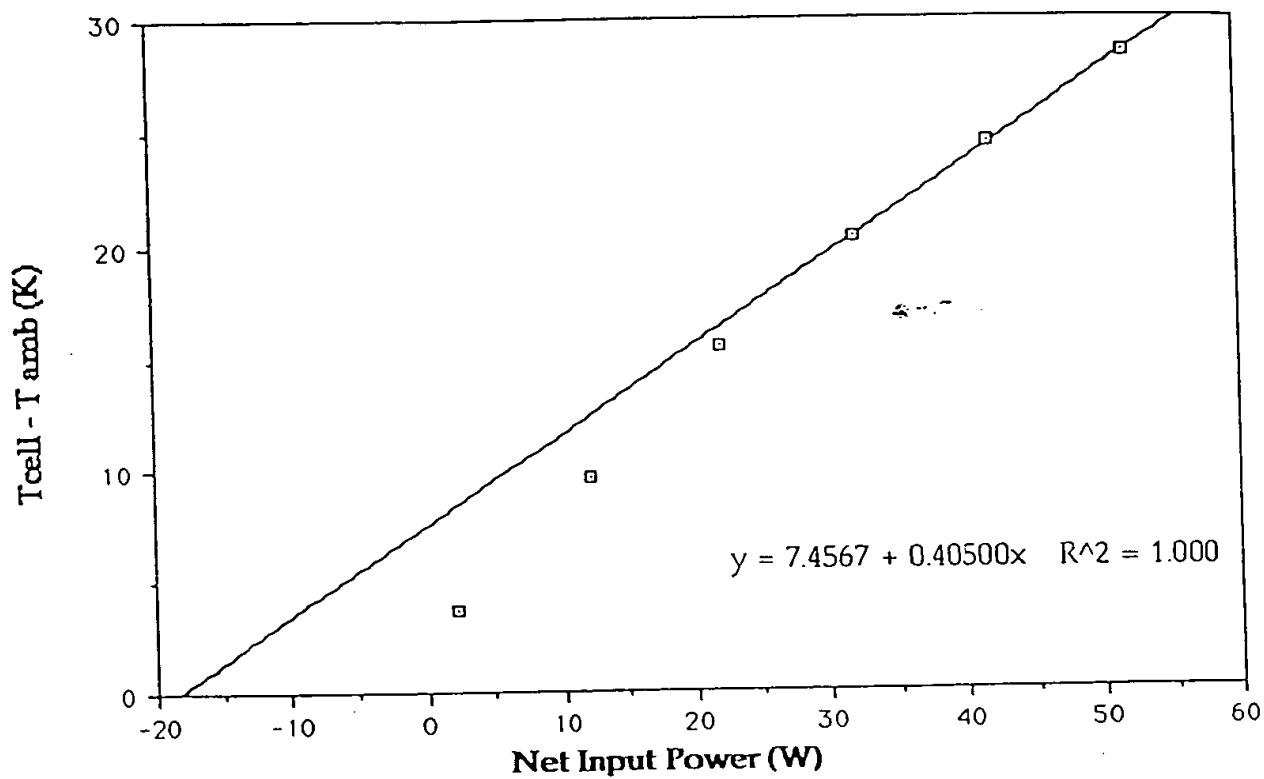
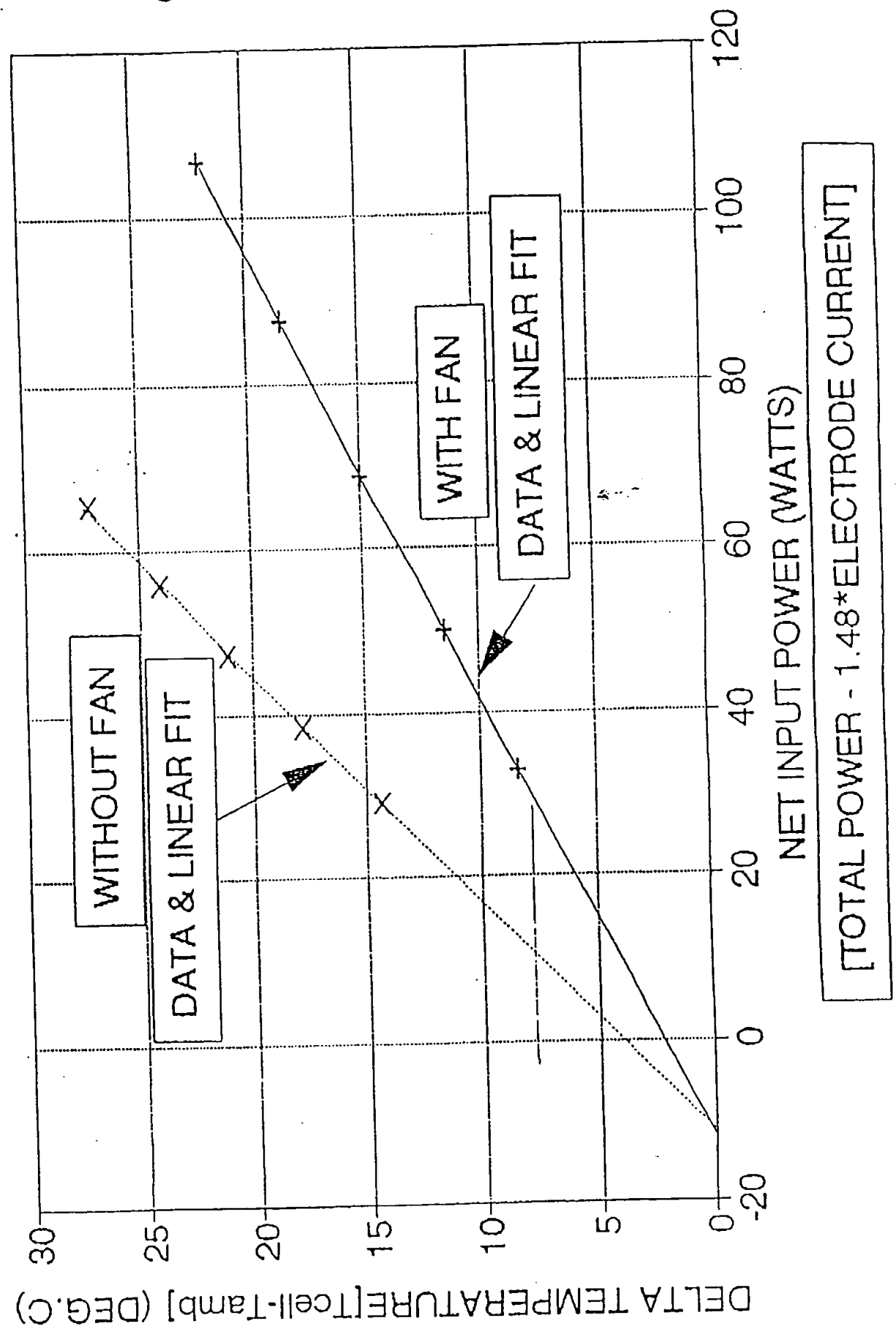


Figure 3.

IC1 T99 THRU T103 & T105 THRU T109



IC1 WATER ADDITION

1/9/93 THRU 1/29/93

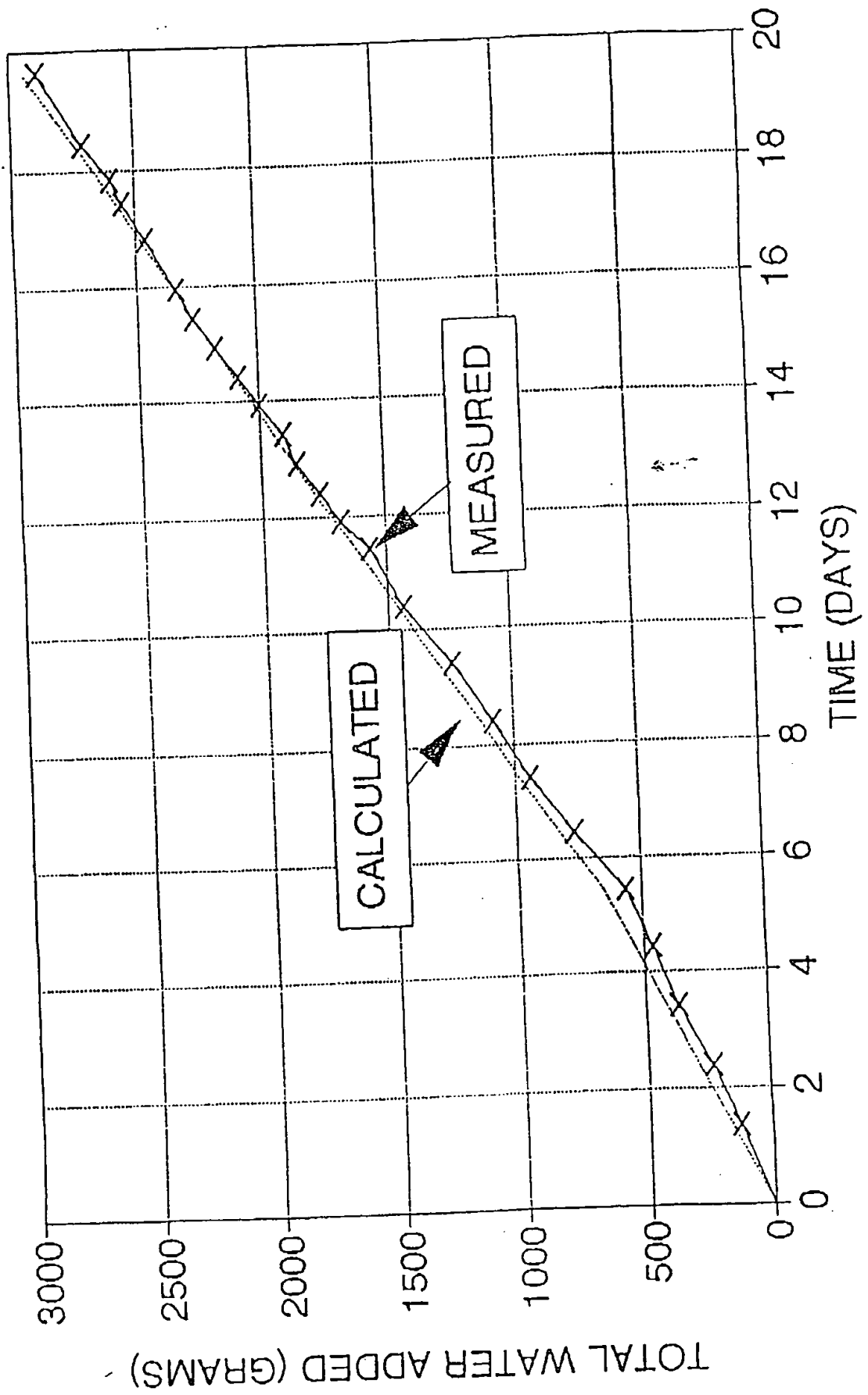


Table 1.
FILE IC1

TEST NO.	TOTAL POWER	DELTA TEMP	LF DT	DELTA TEMP	LF DT	PWR-A*1.48
T99	94.8	27.2	27.36265			65.2962
T100	85.2	24.05	23.93155			55.6962
T101	76.8	21.05	20.92933			47.2962
T102	67.8	17.75	17.71267			38.2962
T103	58.57	14.3	14.4138			29.0662
	18.24		-0.00042			-11.2638
T105	136.07			21.95	21.94573	106.6662
T106	117.05			18.42	18.42674	87.5462
T107	98.25			14.95	14.94844	68.7462
T108	79.45			11.47	11.47015	49.9462
T109	62.58			8.35	8.348937	33.0762
	17.45				-0.00082	-12.0538

Table 2.
ICI WATER ADDITION ;FILE ICIWAT

DATE	HOURS	TIME MINUTES	SECONDS	OPRO TIME	OPRO DATE+TIM	DATE-START DAYS	ELECTRO AMPS	WATER GRAMS	WATER TOTAL	WATER CALC	TOTAL CALC	ADDED/CALC
01/09/93	21	30	0	0.885833	33978.9	-0.00416667	16	0	0	0	0	
01/11/93	7	15	0	0.302063	33980.3	1.402083333	13	131	131	189.9935	189.9935	0.77061781
01/12/93	7	10	0	0.298611	33981.3	2.398611111	16	108	239	120.4645	290.468	0.82863844
01/13/93	7	20	0	0.311808	33982.31	3.411806556	14.84	131	370	121.9893	412.4473	0.89706429
01/14/93	7	55	0	0.330556	33983.33	4.430556556	14.94	89	469	122.6582	535.1085	0.8577747
01/15/93	7	50	0	0.326389	33984.33	5.426388889	14.93	102	581	118.8168	654.9243	0.8566875
01/16/93	8	20	0	0.351369	33985.35	6.461388889	18.93	205	786	164.6302	819.5648	0.93463404
01/17/93	8	19	0	0.346828	33986.36	7.446827778	18.93	168	954	169.8341	979.3887	0.9358891
01/18/93	7	42	0	0.320833	33987.32	8.420833333	18.94	160	1084	158.5665	1135.955	0.98428301
01/19/93	7	32	0	0.313886	33988.31	9.413888889	19.93	164	1238	158.4995	1293.488	0.96664903
01/20/93	7	25	0	0.309028	33989.31	10.40902778	18.84	194	1432	159.9145	1455.369	0.98394292
01/21/93	7	42	0	0.320833	33990.32	11.420833333	19.93	133	1666	162.511	1617.88	0.98731826
01/21/93	19	28	0	0.811111	33990.81	11.811111111	19.93	110.5	1875.5	78.7489	1896.628	0.89754899
01/22/93	7	32	0	0.313889	33991.31	12.413888889	19.93	83	1758.6	80.76369	1777.379	0.98937791
01/22/93	19	37	0	0.817361	33991.82	12.817361111	19.93	92	1860.6	80.88519	1855.245	0.9968323
01/23/93	7	32	0	0.313889	33992.31	13.413888889	19.94	48	1898.5	79.78976	1938.034	0.97856882
01/23/93	19	18	0	0.804861	33992.6	13.804861111	18.93	102	1998.8	78.86744	2018.892	0.99088111
01/24/93	7	23	0	0.311111	33993.31	14.411111111	19.93	84	2082.5	81.31128	2098.203	0.99281693
01/24/93	19	20	0	0.805556	33993.81	14.805556556	19.93	93	2175.8	79.41613	2177.818	0.99602727
01/26/93	7	38	0	0.318054	33994.32	15.41805556	19.93	94	2269.5	82.31512	2250.933	1.00423318
01/25/93	20	-1	0	0.834028	33994.83	15.83402778	19.93	86	2334.5	82.87261	2342.806	0.99645461
01/26/93	16	31	0	0.888184	33995.89	16.788184444	18.93	122	2456.5	137.1919	2478.998	0.98052498
01/27/93	7	46	0	0.322817	33996.32	17.42281667	18.93	96	2552.5	101.9468	2581.944	0.9858824
01/27/93	17	35	0	0.732939	33996.73	17.83293889	18.94	55	2608.8	86.8408	2684.784	0.98516331
01/28/93	7	47	0	0.324306	33997.32	18.42430556	18.93	107	2716.6	95.03047	2742.815	0.99004131
01/29/93	12	50	0	0.634722	33998.53	19.63472222	18.94	171	2888.5	194.5085	2937.323	0.98269741

Appendix I.

DATE: December 15, 1992
TO: Richard Deaton MS 4139, Ext. 6-2016, FAX 6-2681
FROM: R. L. Drexler MS 3123, Ext. 6-1789
SUBJECT: INEL CELL CATHODE ESTIMATE

Attached are the following sketches and revised sketches:

Cathode Assembly for INEL CELL	12/15/92
Narrow Cathode Strap for INEL CELL	12/15/92
Cathode C-1 INEL CELL	12/2/92
Mandrel - Cathode Winding	12/8/92
Electrode Bus Ring INEL CELL	12/15/92

Would you please give us a firm estimate for fabrication of two "identical" cathode assemblies per the 12/15/92 sketch, and two Electrode Bus Rings per the 12/15/92 sketch.

The cathode windings could be made on a mandrel per the sketch 12/8/92 or similar suitable arrangement.

These cathodes and bus rings are similar to those previously fabricated except:

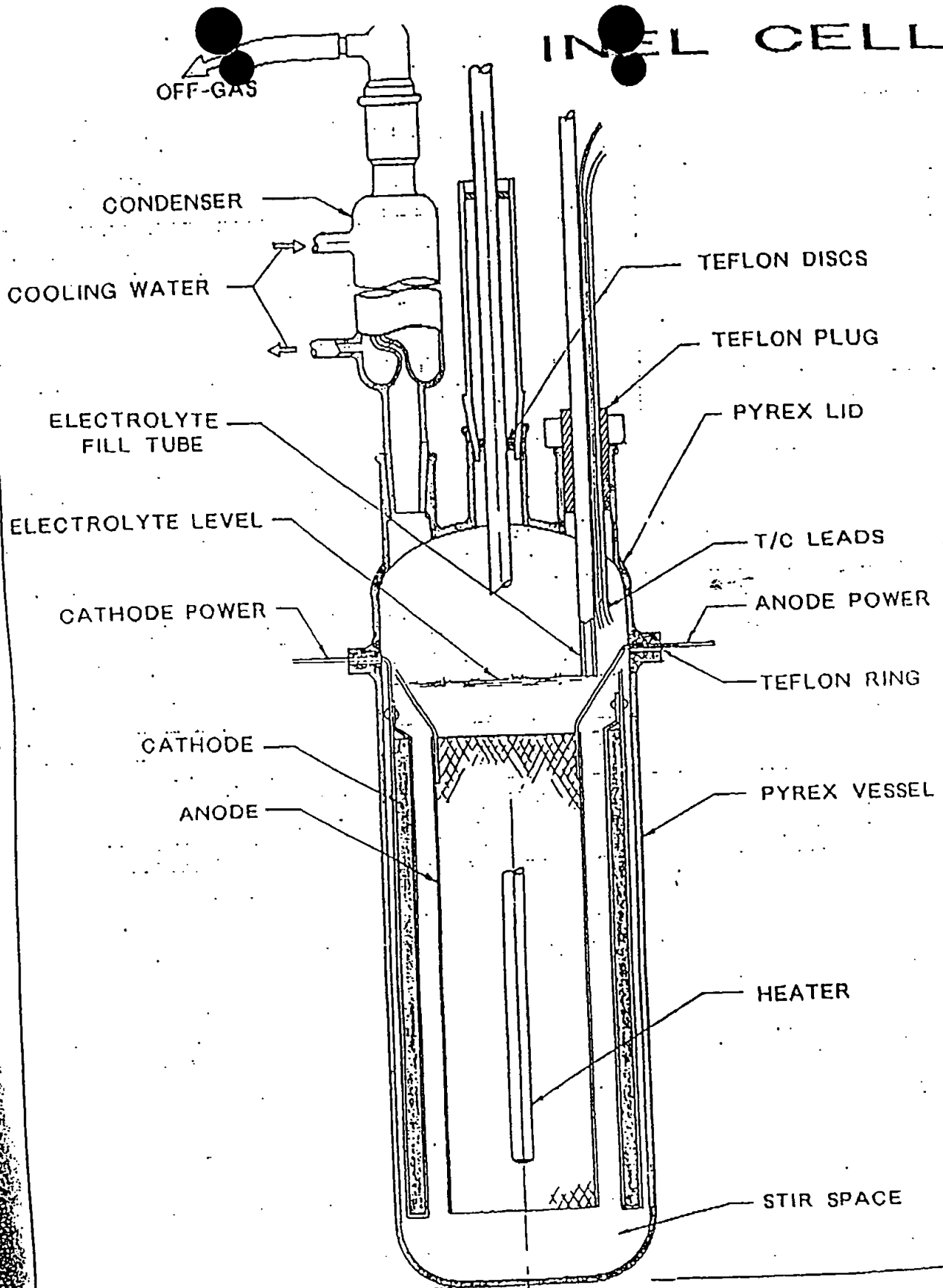
1. The straps are 0.5 in. wide rather than 1.0 in. wide. These narrower straps would be flat rather than arched to fit the winding curvature.
2. There are no secondary straps as were added to the windings of the first cathode assembly.
3. Windings would be less dense than the first winding. A much steeper pitch is probably necessary to achieve the more open wind.
4. Weight of the NI-200 wire of each winding should be very close to 3.33 pounds, and both windings should have the same weight as closely as possible.
5. Slots in the Teflon Bus Ring for the cathode straps would be 0.50 wide rather than the 1.0 width of the first ring.

FEB 04 '93 05:11PM OSTA

P.3/6

INEL CELL

INEL CELL

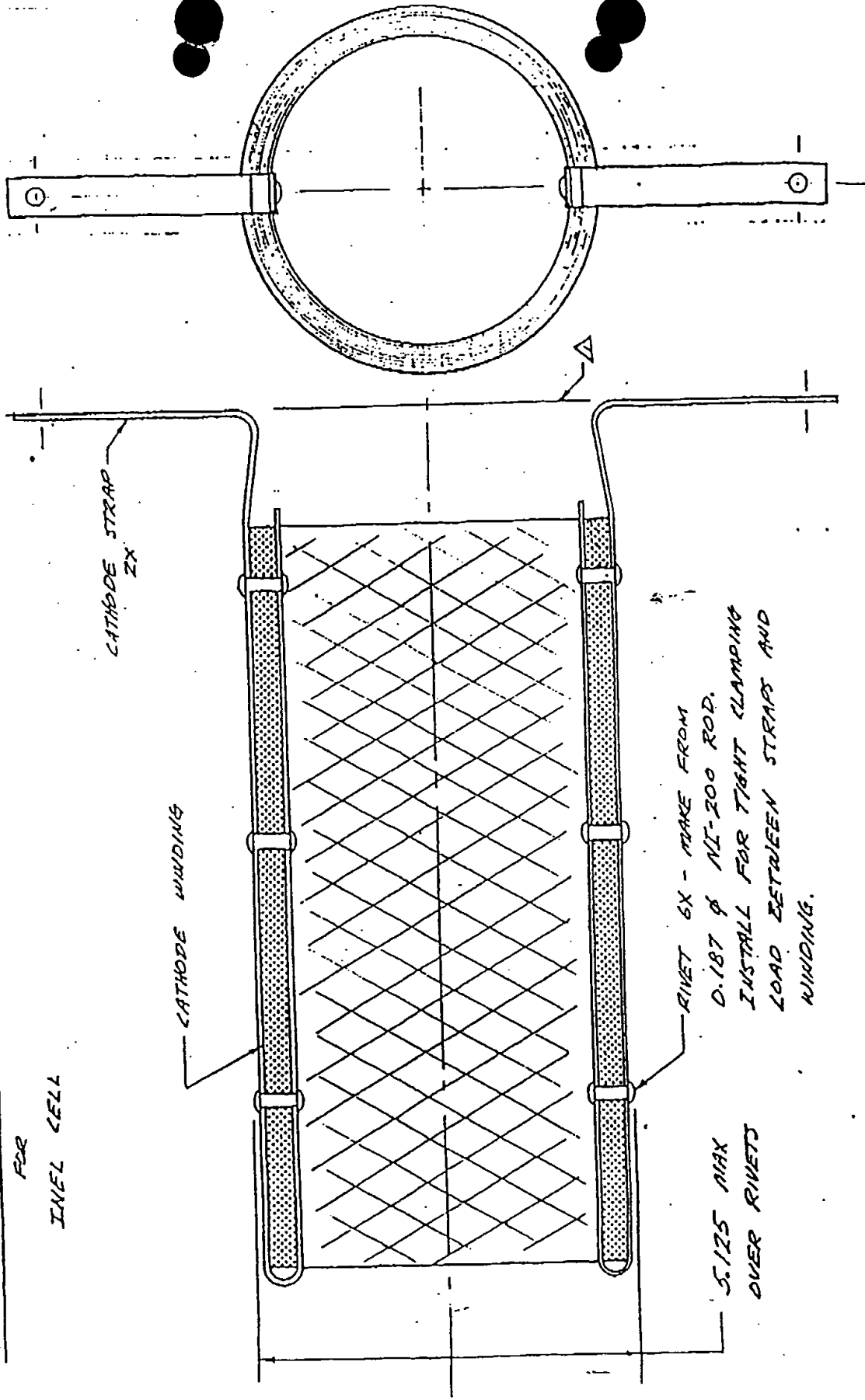


0 1 2 3 4 5 6
INCHES

RLD
 11-25-92
 12-15-92

CATHODE ASSEMBLY

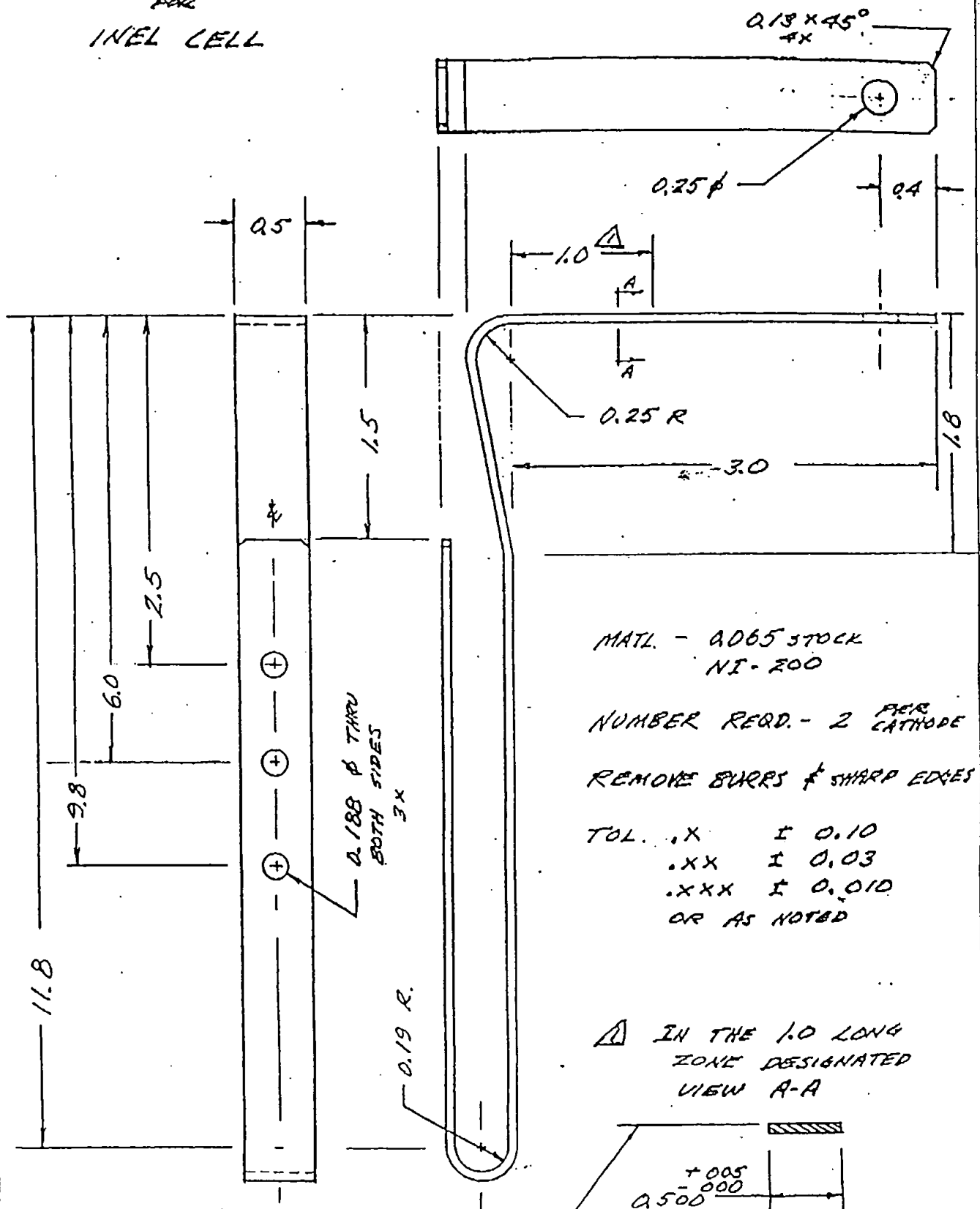
FOR INEL CELL



△ ALIGN BOTH STRAPS
 IN PLANE AT 90°
 WITH WINDING &

12-15-92

FOR
INEL CELL



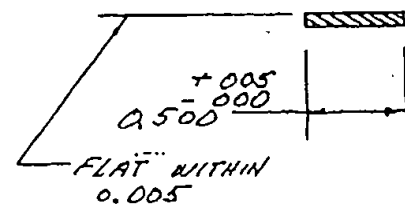
MATL - 2065 STOCK
NI-200

NUMBER REQD. - 2 PER CATHODE

REMOVE BURRS & SHARP EDGES

TOL. .X I 0.10
.XX I 0.03
.XXX I 0.010
OR AS NOTED

A IN THE 1.0 LONG
ZONE DESIGNATED
VIEW A-A



7-2-92
10-19-92
10-21-92
12-2-92

CATHODE C-1

INEL CELL

NI-200
CATHODE
STRAP -
TWO AT
180°

WINDING
NI-200
WIRE
0.010 DIAM
3.33 LB
0.2 SOLID WRAP

10.0"

NUMBER RECD. — ONE PER CELL

THIS PAGE BLANK (USPTO)



HPC
Confidential
Information

EVALUATION OF HEAT
PRODUCTION FROM LIGHT
WATER ELECTROLYSIS
CELLS OF HYDROCATALYSIS
POWER CORPORATION

S. H. Peterson
Technology Development

February 25, 1994

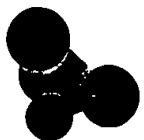
"DRAFT"

APPROVED:

Dale L. Keairns, Manager
Environmental Technologies



Westinghouse STC
1310 Beulah Road
Pittsburgh, Pennsylvania 15235-5098



ABSTRACT

An experimental study was undertaken to evaluate heat production in electrolysis cells designed and set up by Hydrocatalysis Power Corporation (HPC). Results show 50% more heat production in cells with an "active electrolyte" of 0.57 molar K_2CO_3 , compared to a cell with a control electrolyte of 0.57 molar Na_2CO_3 . Other calorimetric data are presented. Evidence for the mechanism proposed by HPC is discussed, along with an alternative mechanism proposed by Arnold Isenberg. Critical experiments to resolve the question of heat production are proposed.



1. Introduction

Hydrocatalysis Power Corporation (HPC) has developed electrolysis cells that are reported to produce excess power, as heat, during electrolysis of a potassium carbonate electrolyte with a nickel cathode. This may be loosely associated with "Cold Fusion" although HPC claims an advanced quantum theory that provides a purely chemical explanation for the heat production. The effect occurs in cells containing only normal water, arguing against any nuclear phenomenon. An investigation of this heat production was undertaken to determine if there is an effect that could be the basis of advanced power generation, or if the claimed effects can be attributed to poor calorimetry or other experimental artifacts.

Following an exchange of information about requirements and facilities, Mr. William Good, of HPC, came to STC on December 7, 1993 to set up four cells for our evaluation. Experiments were conducted until December 23. This letter report is a brief summary of experiments conducted and their results.

2. Conclusions

1. Electrolysis cells provided by Hydrocatalysis Power Corporation demonstrated 50% excess heat with K_2CO_3 electrolyte, compared to a control cell containing Na_2CO_3 electrolyte.
2. Comparison of heating due to resistance of electrolysis current to heating from an immersed auxiliary heater was consistent, in some instances, with the excess heat observed with electrolyte comparison. However, design problems with the HPC cell make power balance comparisons uncertain. The design problems include the high operating temperature of the cells, and the variation of operating temperature with operating conditions.
3. Evidence for the mechanism leading to the observed anomalous heat is sparse. Data provided by HPC were unconvincing when reviewed by STC experts. In an independent experiment, Arnold Isenberg demonstrated an alternative, chemical mechanism that would not provide a basis for power production.
4. A basis for improved cell design and more significant experimental characterization of the HPC thermal effects was established by these experiments. Critical experiments were identified.

3. Recommendations

1. It is essential to determine if the anomalous heat observed in the HPC cells was due to the difference in Faraday efficiency of electrolytic gas generation between the K_2CO_3 and Na_2CO_3 electrolytes, as Isenberg observed with a different cell geometry. If the anomalous heat is only due to difference in Faraday efficiency, there is no effect worth further investigation.
2. If the heat anomaly survives the determination of Faraday efficiency, further studies should be directed at determination of scaling effects. Improved cell design features have been identified for such studies. These are described in the discussion.
3. HPC has developed a gas phase cell that does not require an electrolyte or electrolysis. These cells merit further attention.

4. Experimental:

4.1 HIGH TEMPERATURE CELLS

Initially, three cells were set up identically in 2 liter dewars. Each had a cathode made up of 500 m of 0.38 mm diameter Ni wire (ALFA, .99999 pure), giving 0.6 M^2 surface area. The cathodes were wound loosely on porous teflon forms. The anode of each cell was Pt deposited on a Ti mesh, approximately 14 cm long by 4 cm wide, folded back on itself about 6 cm. Two such pieces were used for each cell, for an approximate area of 200 cm^2 .

The cells were constructed by placing the cathode in the dewar, placing the anode down the center of the teflon form, and also placing an auxiliary heater and a thermocouple in a glass tube down the center of the teflon form. All three cells were connected in series with a common power supply. This was to ensure that equal electrolysis was done in each cell.

The components of each electrolysis cell were prepared by following a protocol established by HPC, appendix 1. Each of these first three cells was set up by Bill Good.

The cells were polarized and electrolyte, $0.57 \text{ M K}_2\text{CO}_3$, was added to permit electrolysis current to flow. This step was done as quickly as possible to ensure that no cathode was exposed to the highly basic, corrosive electrolyte without undergoing electrolysis, for more than the minimum time necessary. Initially, 1.5 l of electrolyte was added to each cell, to bring the electrolyte level to the top of the electrode assembly. Later, after the electrolyte had heated up and expanded, it was necessary to remove 100 ml of solution, leaving a charge of 1.4 l of electrolyte in each cell. The power supply was adjusted to provide a nominal electrolysis current of 3 amperes. This initial set up was somewhat rushed because Bill Good had only 3 days available at STC.

A plastic foam lid was made for each cell. The lids had some thermal insulation value, but were definitely not gas tight. Lead wires penetrated for the electrodes and for the auxiliary heater. Additional penetrations permitted insertion of the thermocouple and a small funnel that allowed for addition of water to compensate for the water lost to electrolysis, calculated to be 25 ml/day for electrolysis at 3 A.

A data collection system was set up, based on a Molytek data recorder acquired for this purpose. It was set up to measure the following parameters:



Series current

Room Temperature (measured in a dummy dewar cell containing distilled water).

For each cell:

Voltage drop

Cell temperature

Heater voltage

Heater current, measured as voltage drop across a 0.01 ohm, 1% precision resistor.

The Molytek allows channels to be used for calculations based on the information in other channels. So, for instance, the heater power was calculated for each cell. By the time the fourth cell was on line, all 32 channels of the data logger were in use.

Initial experiments were performed with 0.57 M K_2CO_3 in all 3 cells. They were run at 3 A until they reached thermal equilibrium. At these equilibrated conditions the three cells were at the following temperatures: Cell A, 68.1 °C; Cell B, 68.8 °C; and Cell C, 69.4 °C. Since the room temperature was 23.7 °C, that meant the three cells were showing very similar response, about 45 °C above ambient temperature.

The power being delivered to each cell was determined by measuring the voltage drop across each cell. The total power is then the product $I_{series} V_{cell}$ into each cell, but the power available for heating the cell is less due to the loss of heat from evolution of electrolysis gases. HPC assumes 100% Faraday efficiency for electrolysis gas evolution, so the power available for cell heating is reduced by the enthalpy of formation of the gases from water, which corresponds to 1.48 volts. Then the heating power into the cell, assuming 100% Faraday efficiency of gas formation, is

$$W_{el} = I_{series}(V_{cell} - 1.48)$$

Auxiliary heaters were placed in each cell, to permit "on-the-fly" calibration of the power balance in the cells at conditions close to any given set of operating conditions. A series of experiments were performed in which combinations of electrolysis power and heater power were applied, and the equilibrium temperatures of the cells determined. These experiments are summarized in figures 1 to 3, which show the conditions of operation summarized as the

electrolysis heating power, W_{el} , auxiliary heater power, W_{htr} , $W_{total} = W_{el} + W_{htr}$, and the heating coefficient for those conditions. Figures 4 to 6 show the temperature rise for each cell at the same conditions.

On December 20, cell A was switched from the K_2CO_3 electrolyte to Na_2CO_3 to provide a control experiment. Na_2CO_3 is not expected to be catalytic for extracting energy from H atoms, and HPC routinely use it as a control. Prior to the electrolyte switch, all three cells were again equilibrated at 3 A electrolysis current with no auxiliary heat, and were still showing similar behavior with temperatures ranging from 66.4 to 73.8 °C. After the electrolyte switch, Cell A equilibrated at 49.9 °C, while Cells B and C were at 69.2 and 74.9 °C.

4.2 LOW TEMPERATURE CELL

The high operating temperatures of the first three cells caused several problems, such as

- At such high temperature, the vapor pressure of water is approximately 0.5 atm, and the variation with temperature is significant. The gases lost through electrolysis will thus carry off an approximately equal volume of water vapor, and this loss is temperature dependent. This makes it difficult to interpret thermal effects associated with changes in power to the cell which result in operation at various temperatures.
- The resistance of the electrolyte to current flow is temperature dependent. When the heat loss coefficient of a cell is as low as that for these dewar cells, resulting in a heating coefficient of $>10^\circ C/watt$, each change in cell conditions produces a different heating effect due to operation at a different temperature.
- Water was added to each cell periodically to make up for the gases lost through electrolysis. However, the additional loss due to evaporation was significant and more difficult to compensate. When this effect became evident, one cell (B) was put on a balance to provide daily weight information. However, since this effect is temperature dependent, the same correction did not apply to all cells. Furthermore, periodic addition of cold water is equivalent to a power loss that is not considered in the power balance calculation. Adding the same amount of water to each cell balanced the



power effect, but did not adequately compensate to maintain constant electrolyte composition.

- Because of the high cell temperature, addition of auxiliary heat required the heater to run at even higher temperature. Heat conduction through the lead wires was probably significant, reducing heat into the solution and causing the heating coefficient for auxiliary heat to be low.

A fourth cell was set up, using another set of electrodes provided by HPC. Instead of a dewar, the cell was made with a 2 gallon high density polyethylene pail with a tight fitting lid. The cell setup was essentially the same as the three smaller volume dewar cells, except that the pail had enough room on the bottom to use a magnetic stirrer off to one side to provide additional stirring to supplement the mixing due to bubbles from the electrolysis. A larger (but unfiltered) power supply permitted running this cell at a higher current, up to 7 amps. This cell was filled with 7 liters of 0.57 M K_2CO_3 . Initial heating with only the auxiliary heater, at power up to 6.1 W heated this cell up to only about 1 °C above ambient. When electrolysis was begun, it was set at 7 amps, with a voltage drop across the cell of 4.2 volts, giving net electrolysis heat of about 19 W. The cell equilibrated at about 32 °C, 9.5 °C above ambient, giving a heating coefficient of 0.5 deg/W. An attempt was made to reduce the electrolysis power to 10 W and replace that power with auxiliary heat, but under these conditions the daily variation in room temperature was larger than any other observed effect.

4.3 Results

4.3.1 Experiments with K_2CO_3 electrolyte

Initial results showed approximately 11-13 degrees/watt of heating when the cells were run with only electrolysis. When the auxiliary heaters were used in addition to the electrolysis heat, the additional heat rise was equivalent to about 8 deg/watt. Thus, the "excess heat" from electrolysis seemed to be about 50%, based on the assumption of 100% Faraday efficiency of electrolytic gas production. Other tests were designed to further check this initial observation. These consisted of various settings of electrolysis and auxiliary heater powers, illustrated by figures 1 to 3, which show the various power

levels and the observed heating coefficients for cells A, B, and C, respectively. Figures 4 to 6 show the same power data, along with the observed temperature rise for these cells. In all these figures, each point represents equilibrated behavior at the indicated conditions, based on at least several hours of stable traces observed on the chart recording of the data logger. In most cases, multiple points were recorded and plotted at constant conditions, to illustrate the reproducibility and stability of the experiments.

In figure 1, the heating coefficient for cell A is shown for electrolysis at 3 amps, with three levels of auxiliary heating of 0, 0.54 and 1.2 W. Each time the heater power is increased, the heating coefficient decreases. However, as figure 4 shows, the temperature of the cell does increase as the power is increased. Some more subtle effects are also apparent. The electrolysis power decreases a little each time the auxiliary heat is increased. This is because the conductivity of the electrolyte increases with temperature, so at constant current the voltage drops and the power decreases slightly.

Following the experiments at 1.2 W of auxiliary heat, an attempt was made to provide the same total power with electrolysis alone. The heating coefficient did increase a little, as would be expected if there is an anomalous heat source associated with electrolysis. However, as mentioned above, loss of heat from the heater through the electrical leads would also cause the same effect.

Finally, the electrolysis current was set at 3 amps again to establish the equilibrium behavior before changing the electrolyte in cell A to Na_2CO_3 . The temperature rise and heating coefficient were very close to those observed in the initial 3 A electrolysis with no auxiliary heating.

Cells B and C showed effects similar to those observed for cell A, except that their auxiliary heater levels were set at other values to get more information on the effects of auxiliary heat. However, cell C consistently had the highest temperature of the three cells, and thus was susceptible to the largest loss of water from evaporation. This became apparent when the temperature was observed to continue a slow increase under steady operating conditions, illustrated by data from Dec. 14 and 15 in figure 6. Cell resistance kept dropping and the temperature kept rising as the salt concentration increased.

25 ml of water was being added daily to each cell to replace the calculated loss due to electrolysis. However, it became clear that this was inadequate due to the likely

evaporative loss. A high capacity balance was then obtained and placed under cell B (chosen because it was intermediate in temperature). The weight change over 24 hours was about 50 g, consistent with the expectation of 25 g for electrolysis and an equal amount of evaporation if the vapor pressure of water is 0.5 atm. Accordingly, the daily water addition was changed to 50 ml per cell. This would still be expected to slightly overcompensate in cell A, the coolest cell, and undercompensate in cell C, the hottest cell. In the end, when the cells were shut down and dismantled, the volume of electrolyte in each cell was measured. Cell C was down to 1000 ml, showing a net loss of about 400 ml of water over the duration of the experiments. Cell B contained 1300 ml of electrolyte, showing that it had been fairly well replenished once the weight change information was available. Cell A had 1350 ml, but it had been changed over to Na_2CO_3 electrolyte only a few days earlier.

The electrolyte stability was a matter of concern once the evaporative loss problem was recognized. Accordingly, samples were extracted from each cell for Total Inorganic Carbon (TIC) analysis. For these electrolytes, TIC should be a direct measurement of CO_3^{2-} concentration. On 12/20, the three cells showed the following values of TIC:

<u>Cell</u>	<u>TIC</u> <u>molar</u>
A	0.46
B	0.47
C	0.44

Thus there seems to be some loss or destruction of carbonate under the cell operating conditions.

4.3.2 Control Experiment with Na_2CO_3 Electrolyte

Because Cell C was more erratic than the other two, and because Cells A and B were very similar, it was decided to change the electrolyte in cell A to 0.57 molar Na_2CO_3 for a control, since Na_2CO_3 is not expected to be catalytically active for hydrogen shrinking. An objective of this test was to adjust the electrolyte concentration to match the resistance of cells A and B, and thus to run them at the same input power. Since the concentration of CO_3^{2-} had changed,

according to the TIC measurement, the resistances were expected to be different. However, when the cells approached equilibrium and the resistance stopped changing with temperature, they turned out to be very close, so no adjustment was needed. This meant that the cells were running with nearly identical electrical input power, 3.42 W for Cell A and 3.79 W for Cell B. With a heating coefficient of 12 deg/W, one would expect cell A to be about 5 degrees cooler than cell B under these conditions. However, the equilibrated cell temperatures were A: 50° C, and B: 69° C. Cell C was at 75° C. Thus it seems that there is anomalous heat in cell B that causes >15° additional heating. If cell A is a true control, and its temperature represents the effect of resistance heating, then the true heat coefficient is about 8 deg/W, and the anomalous heat in cell B is about 50% greater. The effect of switching electrolytes is illustrated in figure 7.

Considering that the time for these experiments allowed only a few characterization tests, and no real optimization, the 50% excess heat with K_2CO_3 compared to Na_2CO_3 electrolyte seems to be the effect predicted by HPC. The actual temperature difference of 15° C is large enough to give confidence that trivial measurement errors are not the cause of the effect. However, two additional sources of information have added doubt about the HPC mechanism and to the question of whether such cells represent a source of useful heat.

4.3.3 Isenberg's Check of Faraday Efficiency

Arnold Isenberg was an interested and very helpful observer of these experiments. When I had the opportunity to describe the final results, especially the difference between the K_2CO_3 and Na_2CO_3 electrolytes, he raised a potential alternative mechanism based on the formation of percarbonates due to the reaction of dissolved oxygen with the carbonate in the electrolyte. He requested, and received, permission to conduct a brief experiment experiment, described in attachment 2, to see if this might indeed cause the observed difference in temperature rise for the two electrolytes. As he describes, the Faraday efficiency of electrolysis gas evolution in the two electrolytes was different, and the presence of peroxy species was demonstrated.

4.3.4 Byers' Review of ESCA Data

HPC has conducted a search for the "shrunk hydrogen" product of the electrode reaction that produces excess energy in these reactions. If the existence of shrunk hydrogen, at the energy levels of the Mills theory, could be proven, a promising new energy source could be assured and further development would be clearly warranted. Unfortunately, Art Byers'

evaluation of the Electron Spectroscopy for Chemical Analysis (ESCA) data presented by HPC is that the evidence is not convincing (see attachment 3).

4.3.5 Other Factors for Consideration

As will be discussed below, the cells presented for evaluation by HPC performed as expected, showing excess energy when K_2CO_3 was used for the electrolyte, compared to a control cell filled with Na_2CO_3 electrolyte. However, the time available did not allow for much parametric investigation. The data represent certain experimental conditions, but no optimization studies were performed.

Other factors should be examined before final decisions are made about this technology. In particular, the following seem worthy of consideration:

- HPC claims observation of cells that produce more heat than the total input electrolysis power. If such claims can be substantiated, alternative mechanisms involving chemicals such as percarbonates would not explain the observations.
- After a discussion of cathode preparation between Bill Good and John Jackovitz, John provided a sample of Ni felt, annealed under hydrogen at $1100^\circ C$. Initial response from HPC was that with this cathode material, a cell drawing 80 amp, with voltage drop of 2.2V, for total electric power input of 0.176W, produced 0.250W of heat. They requested 7 additional sheets of the Ni felt, to produce a cell that would develop 120W of excess heat. The effect of this cathode material could be evaluated at STC. The results of HPC tests are not known at this time.
- HPC has also described energy production in cells that use gaseous hydrogen, and which do not involve electrolysis. In these cells, high pressure H_2 is applied to a cell prepared with a coating of the catalytic K_2CO_3 , and high rates of heat production are observed. In fact, it is reported that excess energy production continues after input energy is terminated, for significant periods of time.

5. Discussion

In general, the cells provided by HPC performed as they were expected to. The heat generated by resistance to electrolysis current, assuming 100% Faraday efficiency of electrolysis gas generation, was greater than the heat generated by the pure resistance heating of the auxiliary heaters. Furthermore, the heat production was greater with K_2CO_3 than with Na_2CO_3 electrolyte, by about 50%. On the basis of these results, HPC feels that this demonstration was successful.

Unfortunately, several factors reduce one's confidence that these cells have identified an attractive heat source that could be developed for power generation purposes. These will be discussed below.

The first factor to be considered in discussion of these experiments is problems with the heat measurements. Part of the problem was that these cells operated at quite a high temperature; higher than was anticipated. The operating temperature was difficult to predict because the heat loss coefficient for this size and design of cell was unknown. When these cells turned out to equilibrate around $70^\circ C$, it caused at least three problems:

- At this temperature, the vapor pressure of water is about 0.5 atm, and it varies significantly with temperature. Thus, changing operating conditions in a way that changed temperature changed the heat loss due to evaporation of water. Furthermore, there was uncertainty about how much water to add to a cell each day for replacement of water loss due to electrolysis.
- The effect of the auxiliary heaters was difficult to interpret. The heater had to get quite hot to generate significant heating at the cell conditions. Power loss through the heater wires could be significant, and difficult to estimate. This could explain the low heating coefficient for the auxiliary heaters relative to the heating due to electrolysis.
- Finally, there was loss of inorganic carbon during the experiments, perhaps from thermal breakdown of carbonate ion, or perhaps due to aerosol formation and transport. This is evidence for chemical reactions that are not accounted for in the HPC model; how the power balances of the cells are affected is unknown.

Another feature of the heat effects was that the heating coefficient decreased any time a change was made that increased the cell temperature. This includes changes such as increasing the electrolysis current, as well as changes such as adding auxiliary heating at constant electrolysis current. This effect is probably due to increased evaporation loss, but it makes interpretation of the heat measurements more difficult.

An attempt was made to minimize the effect of temperature change by operating the cells at the same total input power by varying both heater and electrolysis powers. The equilibrated results are shown in the figures for data of 12/18 to 12/19. These results are not very conclusive; the cell temperature and heating coefficient are determined mostly by the total input power, and not on how the power is partitioned between electrolysis current and auxiliary heater. This was also the case when the same thing was tried with cell D, operating at much lower temperature.

If the temperature measurements do not show a clear heating anomaly, the effect of changing electrolyte from K_2CO_3 to Na_2CO_3 was remarkable. The intent was to change electrolyte in one cell, and to match the power input for the two cells (A and B) connected in series. This worked out quite well, and the Na_2CO_3 cell equilibrated at a temperature $20^\circ C$ lower than the cell containing the K_2CO_3 electrolyte. At first, this looked like clear confirmation of the HPC effect.

Isenberg's measurement of the difference of Faraday efficiency for the two electrolytes raises quite a different possibility for the difference in temperature between the K and Na electrolytes. He observed Faraday efficiency of 57% for K_2CO_3 in the temperature range of $55-65^\circ C$, and 69% for Na_2CO_3 at $50-55^\circ C$. This 12% difference, scaled to the 3A electrolysis current, would account for about half of the observed temperature anomaly. Given the difference in geometries of the experiments, it is not clear how to compare them. Isenberg's setup had the anode and cathode concentric with a thin insulator between them, giving maximum opportunity for the recombination reaction. In the cells described in this report, the electrode separation was much greater, but there was sufficient agitation of the electrolyte solution that when the cells were opened on 12/23, the electrolyte was very uniformly filled with tiny bubbles. This was good in terms of providing sufficient agitation to provide uniform temperature in the cell, but possibly also of promoting recombination.

In contrast to Isenberg's experiment, the daily weight loss in Cell B indicated loss of 50 g of water/day. This is fully consistent with 100% Faraday efficiency plus loss of an equal

amount of water due to evaporation at the 0.5 atm vapor pressure of water at the cell temperature. Alternatively, the 50 g/day loss could result from lower Faraday efficiency and evaporative loss if there is significant formation and transport of aerosol from the cells.

5.1 Additional Studies

Some additional experiments, based on these preliminary observations, should be able to resolve the issues raised here. The following approach is suggested:

1. It is essential to determine if the depolarization observed by Isenberg, attributed to chemical reactions leading to the formation of percarbonates, caused the difference in temperature between cells when Na was substituted for K in the electrolyte. The principle change in our setup required would be to use a sealed lid on the cell with a vent for gas release, which would permit the evolved gases to be measured and characterized. Hard plastic lids that would meet this need were machined, but there was not time to use them.
2. The sealed cell configuration of test 1 would also permit examination of the effect of increased agitation to assure uniform temperature distribution in the cell, and a test of a mechanism proposed by Gene Struhl (Baltimore, retired). He has proposed that the heat observed results from chemical reaction of the hydrogen formed at the cathode, and that the effect could be enhanced by sparging with oxygen, or diminished by sparging with nitrogen. Sparging would provide a way of varying the agitation in the cell, as well as a way to investigate the effect of the sparging gas on cell heat production.

The results of these tests 1 and 2 would determine the Faraday efficiency of electrolytic gas production in our cells. If it is shown that the observed temperature anomaly is a result of differing Faraday efficiencies for the two electrolytes, there would be no reason to pursue further experiments at this time. However, it would be desirable to continue to monitor developments that might indicate true anomalous heat production, particularly in gas phase cells in which the problems associated with electrolysis do not arise.



If the observed heat anomaly survives the Faraday efficiency test, there are a number of additional tests that should be considered as a sound development program. These include the following:

- It will be very valuable to establish a mode of operation that will permit separation of the cell temperature from the cell power. This can be done by operating a flow cell in which flowing electrolyte is introduced into the cell at a preset (variable) temperature, and the temperature rise in the cell is determined. In such a flow cell, the temperature rise can be controlled by controlling the flow rate. Shorter residence time in the cell should also minimize electrolyte destruction, and permit determination of electrolyte stability. Experimental parameter variations will be under much better, controlled conditions. Jim Bauerle has considered the design of a flow calorimeter for such experiments, and his input will be invaluable in designing and carrying out these tests.
- The cooperation between John Jackovitz and Bill Good has identified Ni mesh, annealed under H_2 at $1100^\circ C$ as a cathode material with the potential to produce true excess energy greater than the product of cell voltage times current. This electrode material should be employed in our well designed flow cell.
- HPC recommends understanding electrolysis cells before trying experiments with gas cells. However, the gas cells provide a possible route to the high temperature operation needed for power generation, without the problems associated with carrying out electrolysis in aqueous solution at temperatures above the boiling point of water. An objective of advanced testing should be to test and characterize gas cells, including use of the $1100^\circ C$, H_2 annealed Ni felt as the catalytic surface.

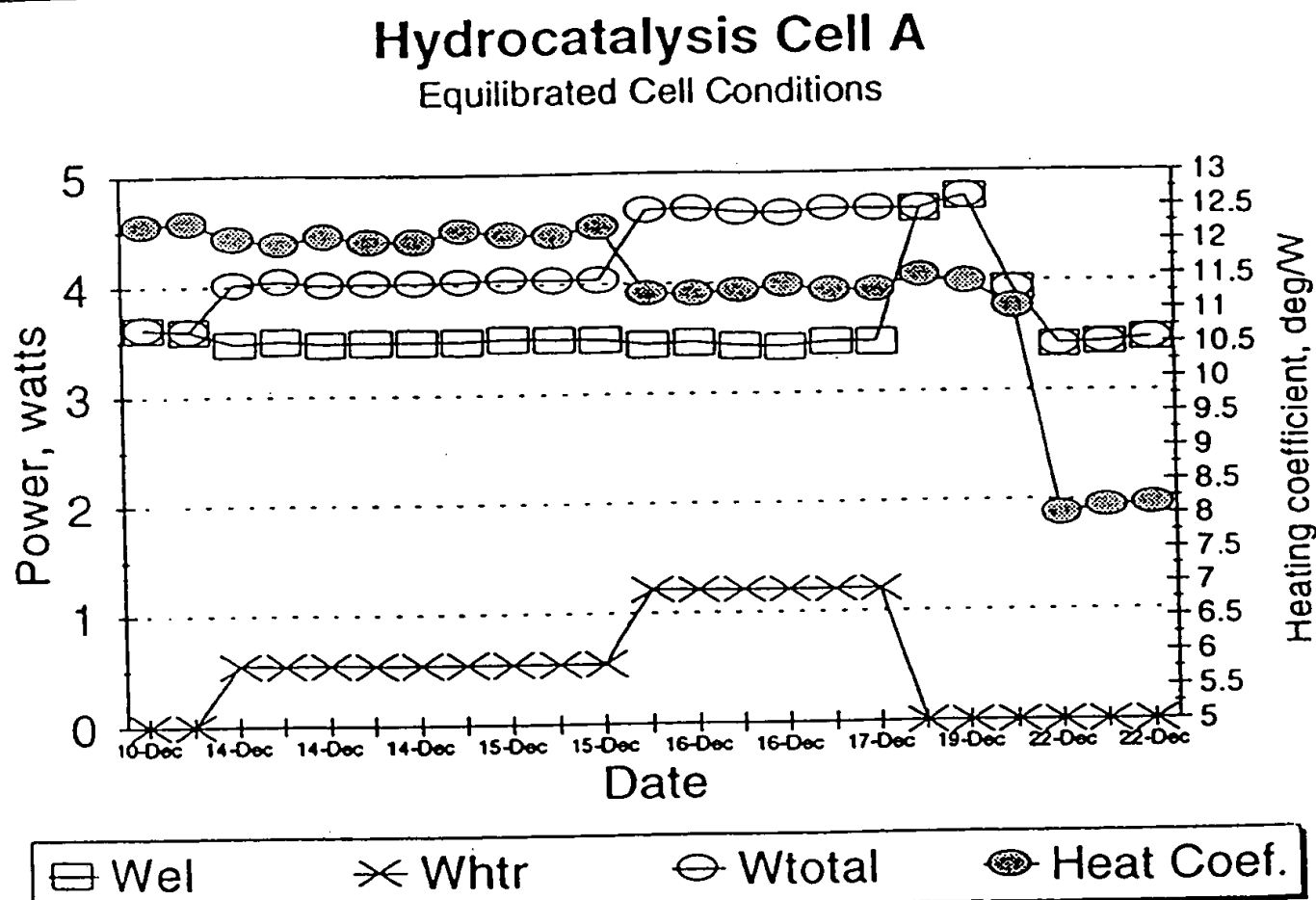


Figure 1.

Equilibrated values for heating coefficient of cell A at various conditions of input power. Points before 12/22 are with K_2CO_3 electrolyte; last three points are with Na_2CO_3 electrolyte.

Hydrocatalysis Cell B

Equilibrated Cell Conditions

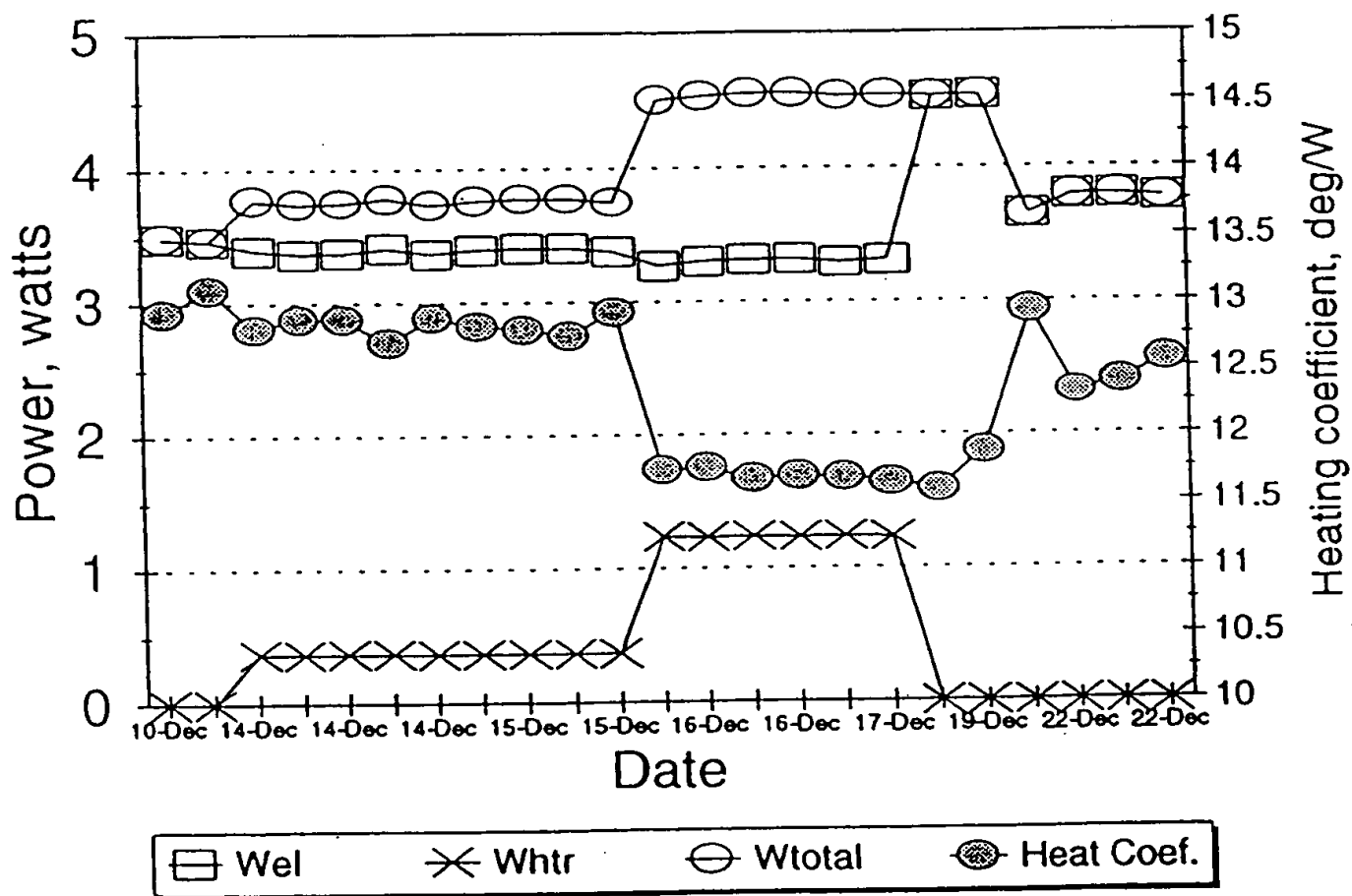


Figure 2. Equilibrated values for heating coefficient of cell B at various conditions of input power. All points are with K_2CO_3 electrolyte.

Hydrocatalysis Cell C

Equilibrated Cell Conditions

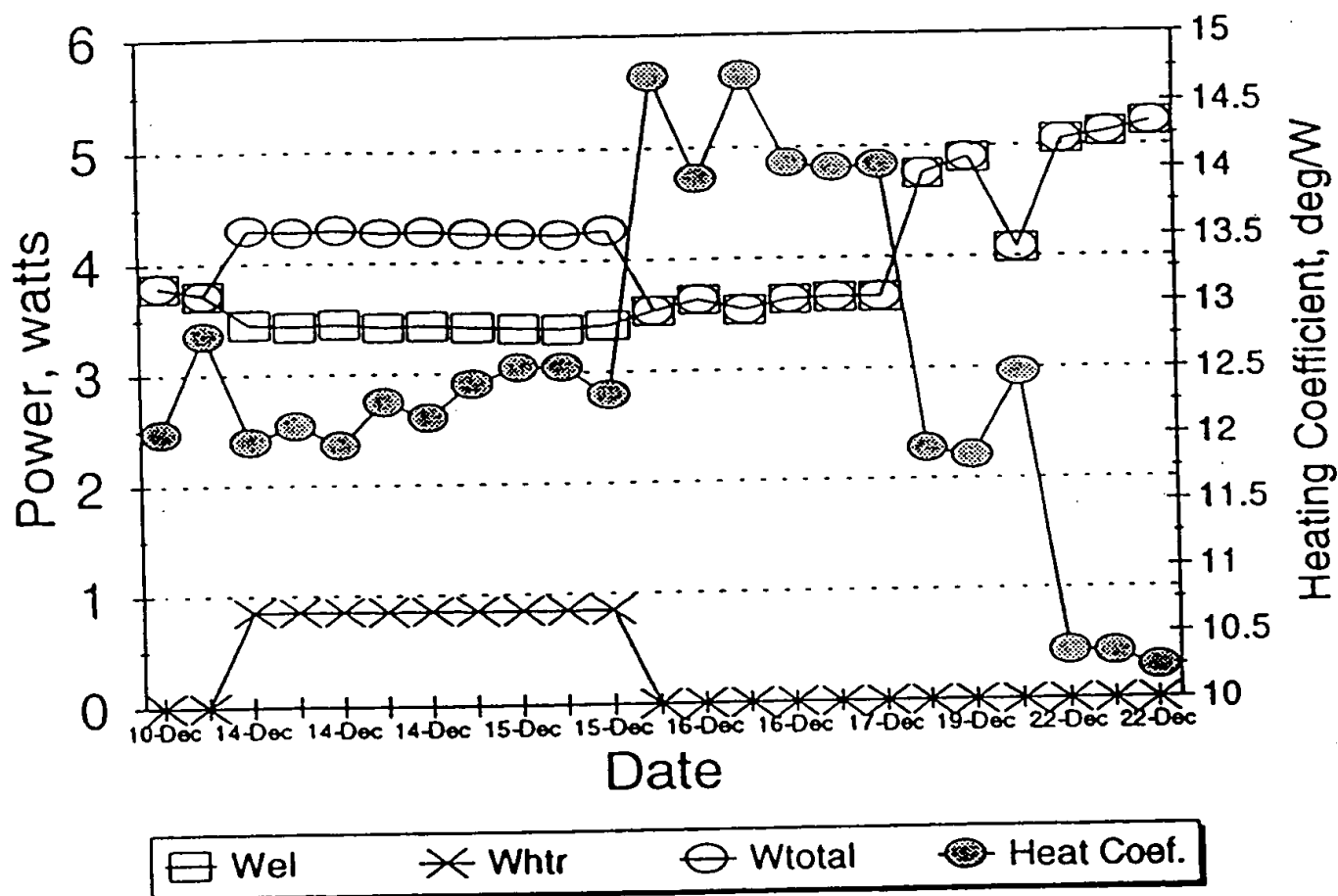


Figure 3. Equilibrated values for heating coefficient of cell C at various conditions of input power. All points are with K_2CO_3 electrolyte.

Hydrocatalysis Cell A

Temperature rise vs input power

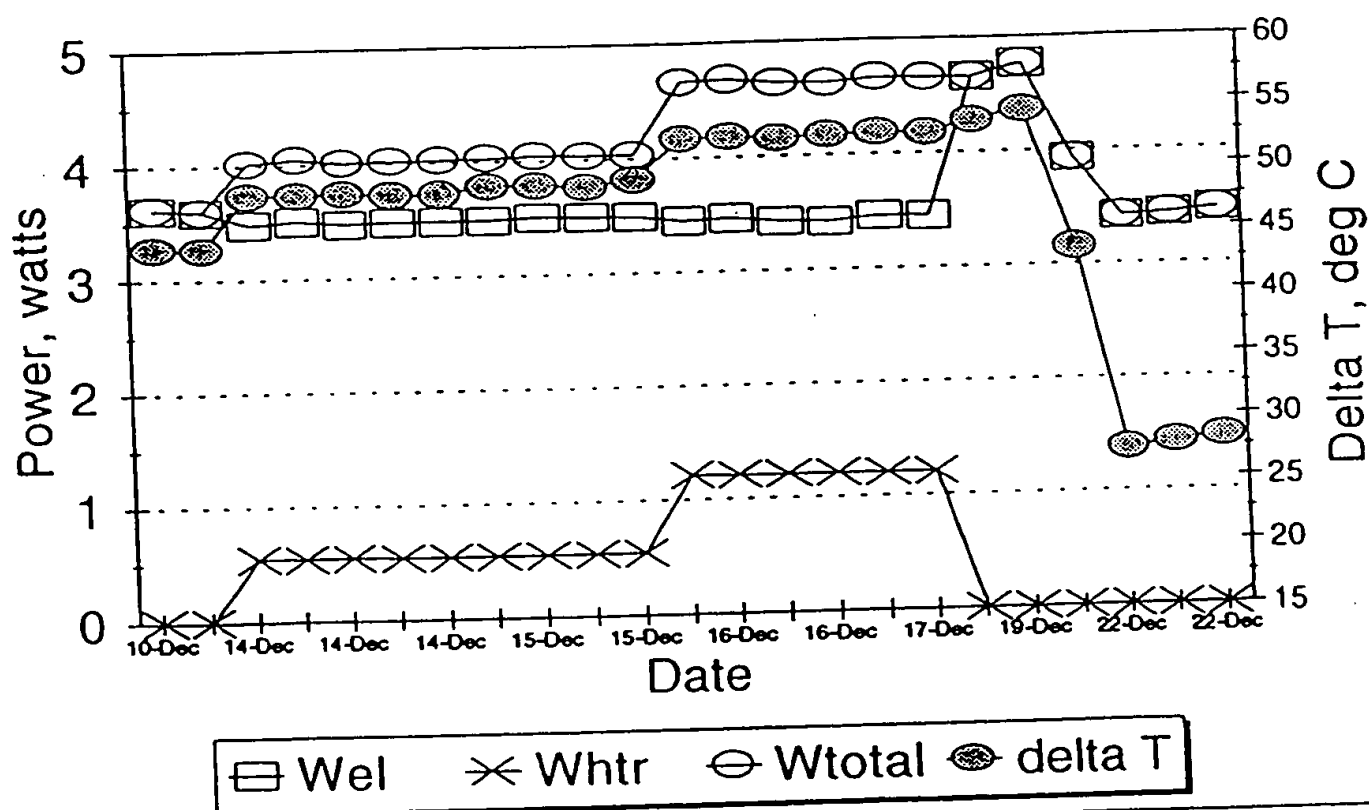


Figure 4. Equilibrated values for temperature rise (ΔT) of cell A at various conditions of input power. Points before 12/22 are with K_2CO_3 electrolyte; last three points are with Na_2CO_3 electrolyte.

Hydrocatalysis Cell B

Temperature rise vs input power

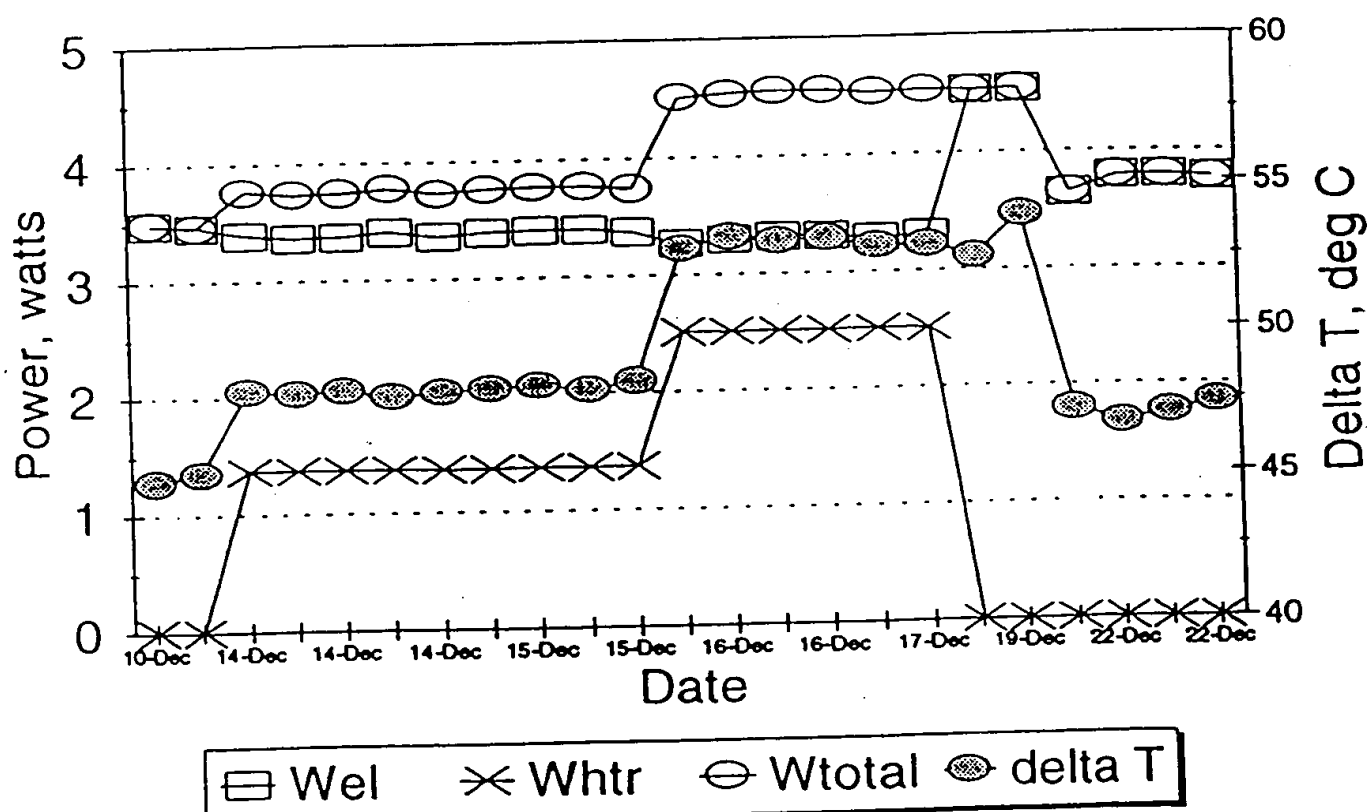


Figure 5.

Equilibrated values for temperature rise (ΔT) of cell B at various conditions of input power. All points are with K_2CO_3 electrolyte.

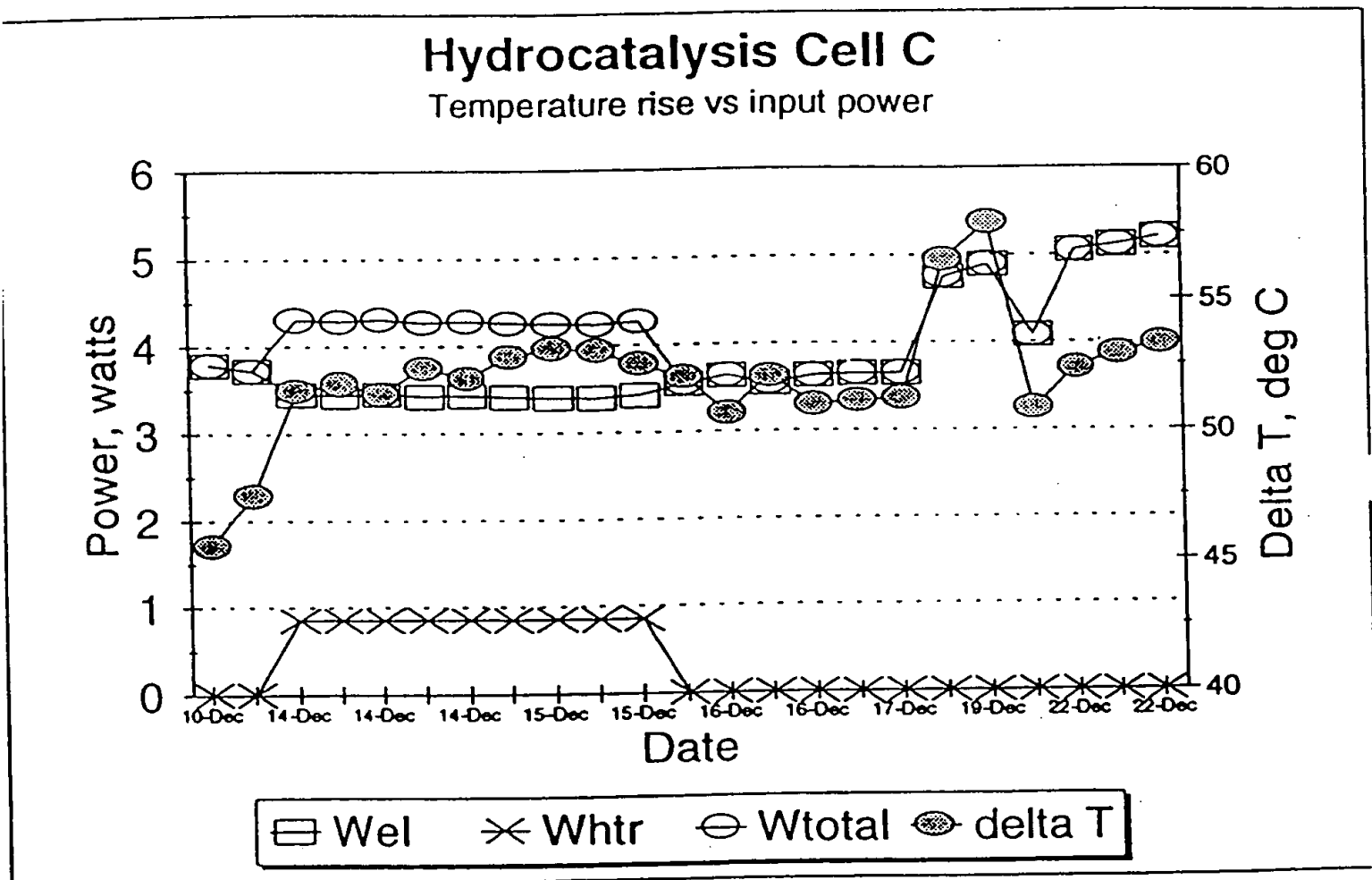


Figure 6. Equilibrated values for temperature rise (ΔT) of cell C at various conditions of input power. All points are with K_2CO_3 electrolyte.

Hydrocatalysis Data

Effect of Na_2CO_3 in Cell A

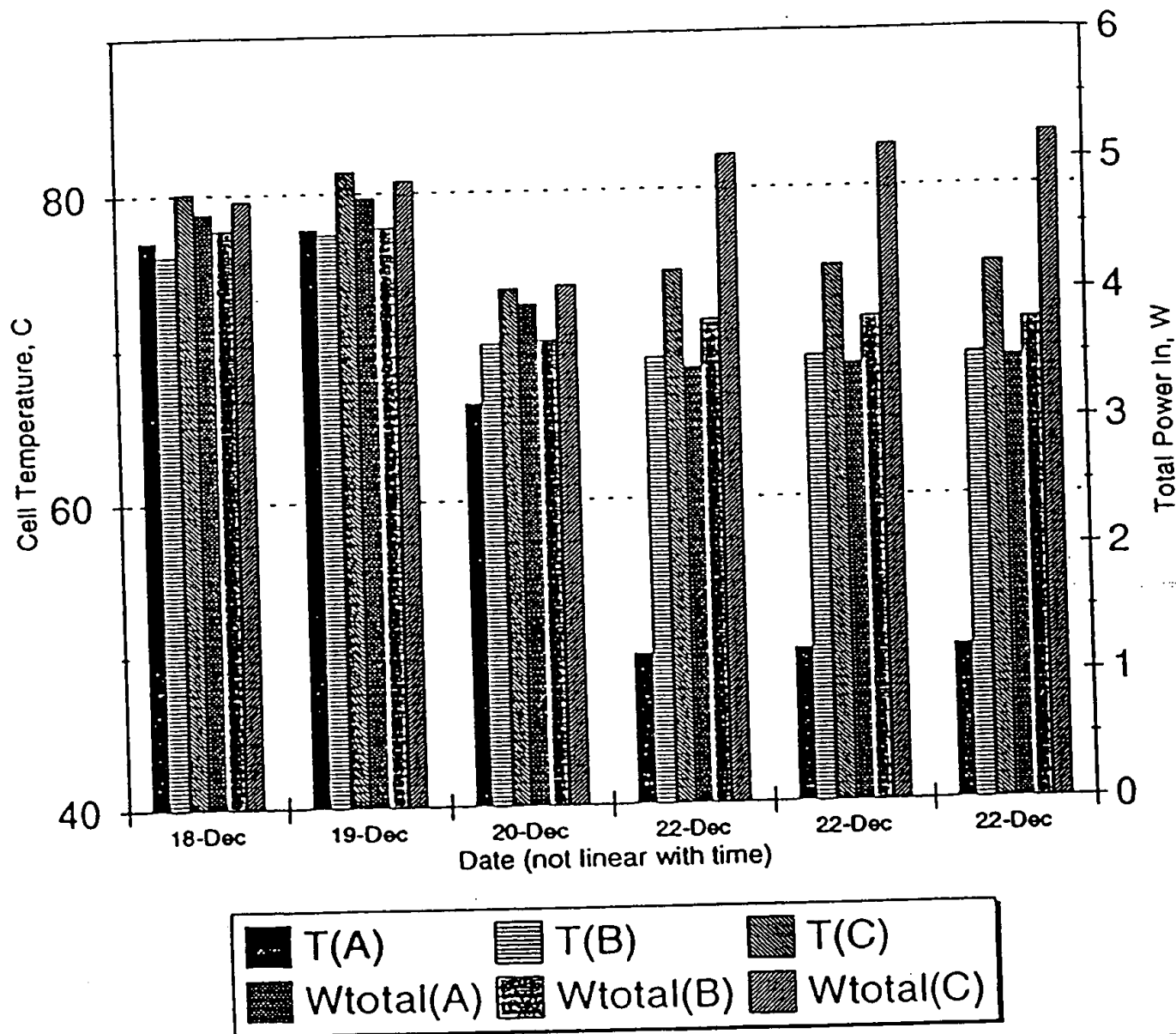


Figure 7.

Effect of changing electrolyte in cell A from K_2CO_3 (before 12/22) to Na_2CO_3 . Bars show equilibrated temperature for various input power conditions.





Attachment 1

HPC Experimental Protocol



Attachment 2
Isenberg's Determination of Faraday Efficiency



From: Science & Technology Center
WIN: 236-2157
Date: January 14, 1994
Subject: Thermal Effects in Electrolysis of Aqueous K_2CO_3 -Solutions

To: S. H. Peterson 501-3E17
cc: W. J. Dollard 501-2W59
S. D. Harkness 801-3C54C
J. A. Spitznagel 801-3C54D
P. R. Emlage 501-2B32

Recently you conducted some nice calorimetric measurements on electrochemical cells during the electrolysis of potassium- and sodium-carbonate solutions, in order to verify data that had been obtained by R. L. Mills and W. R. Good of HydroCatalysis Power Corporation using anode/cathode hardware; that they provided to you. As you informed me, you confirmed that the thermal effects during the electrolysis of K_2CO_3 solutions were significantly more exothermic than in Na_2CO_3 solution as electrolyte.

Mills and Good have observed this effect and explained it through a rather bizarre theory involving new energy states of hydrogen. The thermal effects, in my view, needed an immediate rational explanation. Therefore, I conducted several electrochemical measurements that can explain higher exothermal reactions during the electrolysis of aqueous K_2CO_3 -solutions as compared to Na_2CO_3 -solutions. In the interpretation of enthalpy measurements as proposed by Mills and Good, the assumptions are made that the faradaic efficiency with respect to gas evolution is 100%. This assumption enters into the computation as a loss of energy from the calorimetric system. However, when electrochemical side reactions take place, gas evolution rates may be reduced and the side reactions can contribute to exothermic effects within the calorimeter. Computations, therefore, must take such thermal effects into account.

I electrolyzed aqueous solutions of K_2CO_3 and Na_2CO_3 within the confines of a 500 ml gas burette, in order to measure the total volume of gas evolving from anode and cathode. The rate of gas evolution was measured and pressure, temperature, and humidity corrections were made. No special pretreatment (purification) of electrodes or electrolyte were made. I suspected anodic side reactions could involve the formation of percarbonates (adducts of hydrogen peroxide and carbonates). These compounds would depolarize (be reduced at) the cathode and lead to a lower than theoretical rate of gas evolution (<10.45 ml gas per ampere minute).

The presence of percarbonates can be detected by acidifying the electrolyte and by subsequent reaction of the solution with potassium iodide. The presence of H_2O_2 (from percarbonate) will lead to the formation of free iodine which is colorimetrically detected with a starch indicator. Both electrolyte solutions did show a strong iodine reaction after electrolysis had been performed, thus, explaining the low efficiency in observed gas evolution.

The essential experimental data are summarized in Table 1 and the simple electrolysis apparatus is shown in Figure 1.

Following observations have been made:

- Gas evolution in both electrolytes is significantly below 100%.
- Higher efficiency of gas evolution is observed in the Na_2CO_3 -electrolyte, which explains higher enthalpy values in an otherwise "mirror" K_2CO_3 system.
- Increased electrolyte temperature decreases gas evolution efficiency in both electrolyte solutions significantly.

The last observation was not expected because H_2O_2 is less stable at higher temperature. This would indicate that the cathode depolarization reaction rate determines the gas evolution efficiency. This rate would be expected to go up with temperature.

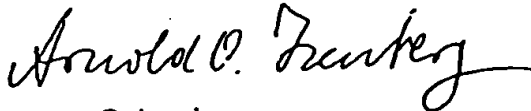
Conclusions:

- Comparison of thermal effects in the electrolysis of K_2CO_3 and Na_2CO_3 can only be made if careful gas evolution and gas composition analysis is conducted in addition to the calorimetric measurements.
- Anodic/cathodic side reactions in the two electrolysis systems are expected to depend very much on the geometry of the electrochemical cell, current density, temperature, electrolyte volume, and power supply current profiles.
- The experimental apparatus of this study underestimates gas evolution inefficiencies because of a relative low current (as compared to 3A in your calorimetric experiment), higher dilution of anodic by-products (2 liter electrolyte), and partial removal of anodic by-products from the electrolysis cell active region by the increasing gas column in the gas burette/electrolysis cell envelope.

The latter point is demonstrated by comparison of experiment 1 and 2 in Table 1. Before the start of the second experiment, the electrolyte had been enriched with anodic by-products from the first experiment. Then, the electrolyte column in the

burette was raised to the top and during the second experiment the electrodes operated in an environment of accumulated anode by-products. This explains the lower gas evolution rate under otherwise similar conditions.

Please feel free to use this information in the interpretation of your carefully executed calorimetric measurements.



Arnold O. Isenberg
Consulting Scientist
Advanced Energy Conversion Division

dk

Attachments

P.S.: One could tell the "hydrino theoreticians" to use sodium or potassium borate solutions as electrolyte. The expected anodic by-product concentrations would be even higher (perborates) and the expected "unexplainable" thermal effects would be even more exothermic (if one conveniently assumes 100% gas evolution efficiency). Sorry, there is a little bit of a nasty streak to me!



Table 1

Efficiency of Gas Evolution in
Alkaline Carbonate Electrolysis Cells

Experiment #	Electrolyte Type	Electrolyte Temperature °C	Current A	Collected Gas Volume ml, S.T.P	Gas Evolution Rate ml/min	Gas Evolution Efficiency %
1	0.57m K_2CO_3	19	1.00	216.7	7.01	67.1
2	0.57m K_2CO_3	19	1.00	260.9	6.74	64.5
3	0.57m Na_2CO_3	22	1.00	256.3	7.92	75.8
4	0.57m Na_2CO_3	50-55	1.00	250.3	7.18	68.8
5	0.57m K_2CO_3	55-65	1.00	252.0	5.98	57.2
6	0.57m K_2CO_3	65-70	1.00	251.5	5.89	56.4

WESTINGHOUSE ELECTRIC CORPORATION

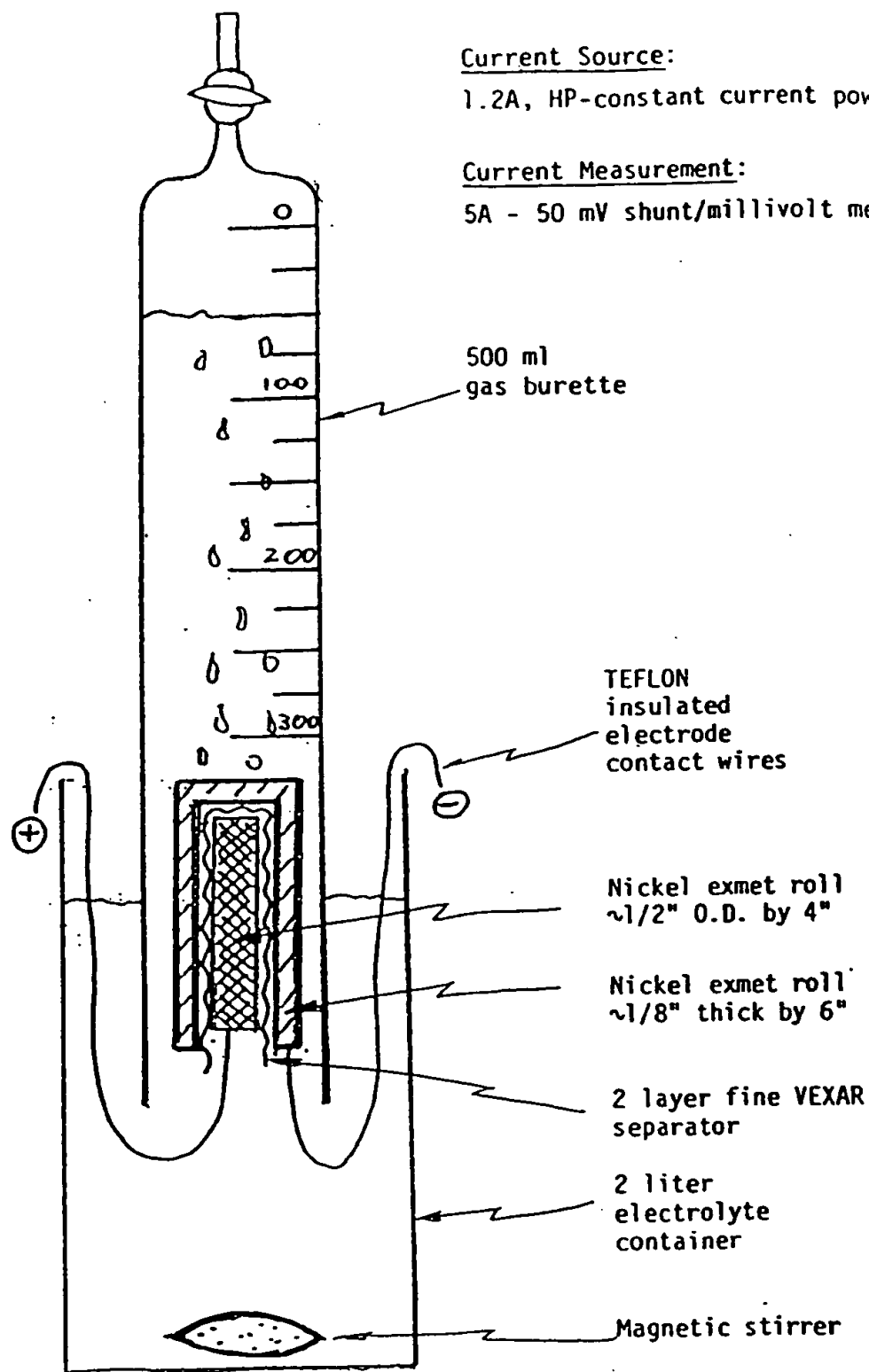


Fig. 1 - Gas meter - electrolysis cell.

Attachment 3
Byers' Review of ESCA Evidence for the
Existence of "Shrunken Hydrogen"



From: SCIENCE & TECHNOLOGY CENTER
WIN: 236-1678
Date: January 18, 1994
Subject: *Review of ESCA Evidence for Fractional Quantum Energy Levels of Hydrogen*

To: STC
John Spitznagel

cc: S. H. Peterson
A. Isenberg
R. J. Jacko
W. G. Clark, Jr.

I have reviewed the paper by Randell L. Mills and William R. Good on the evidence for fractional quantum energy levels of hydrogen. This paper proposes the creation "hydrino" atoms on nickel electrodes during the electrolysis of aqueous potassium carbonate. The proposed hydrino atoms are hydrogen atoms which have dropped into a new electronic ground state where $n=1/2$. The existence of this fractional quantum level is used to explain the production of heat in electrolysis experiments which was previously attributed to cold fusion. ESCA characterization of the nickel electrodes was used to support the hydrino theory.

The ESCA evidence consisted of a broad peak at 55 eV binding energy in a spectrum from an electrode in which excess heat was observed. This is the binding energy which was predicted for an electron in a hydrino atom. The authors state that "There is no known atom which has an electron with a binding energy in this region that was present in the electrolytic cell." While it is true that none of the elements which were intentionally added to the cell have electrons with binding energies in this area, the possibility of the presence of trace impurity elements must be considered. A cathodic electrode will concentrate even ultratrace elements to levels detectable by ESCA.

A search of the NIST XPS database identified a number of compounds which had elements with photoelectron transitions in this area. The most common are compounds of iron. The binding energy for Fe 3p electrons ranges between 52.8 and 57.95 eV depending on the oxidation state of the iron. The broad peak which was observed is common for iron compounds of mixed valence state or for iron

oxide mixtures. The presence of iron could be confirmed by looking at the more intense 2p photoelectron peak which have a binding energy near 710 eV. The ESCA scan in the Mills paper went no higher than 310 eV. Compounds of lithium and osmium could also have produced peaks in the 55 eV region. The authors would have built a more convincing argument for a new quantum state had they addressed the impurity issue.

Another consideration which sheds doubt on the authors interpretation of the ESCA results is that the lightest elements are very difficult to detect. The minimum detection limit for lithium is typically near 10 atomic %, and hydrogen cannot be detected at all under normal conditions. The expected poor detection limit for the hydrino atom requires that it be present at high concentration at the nickel electrode surface. This is unlikely because of the high vacuum required for ESCA.

In summary, the ESCA data presented by Mills and Good does not provide strong evidence for fractional quantum states of hydrogen.

Art Byers

W. A. Byers
Corrosion Technology

HYDROCATALYSIS POWER CORPORATION

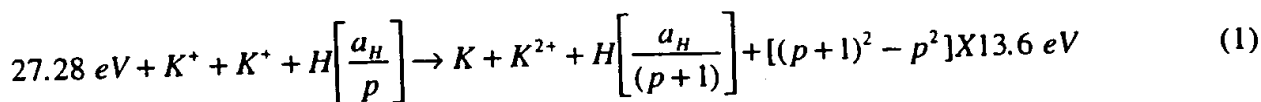
Comments to Confidential Draft Report from Westinghouse STC, "Evaluation of Heat Production From Light Water Electrolysis Cells of HydroCatalysis Power Corporation", February 25, 1994

Light Water Calorimetry Experiments

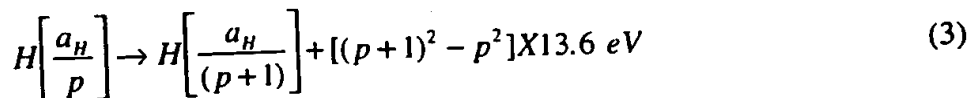
Westinghouse scientists report that excess heat was observed during the electrolysis of aqueous potassium carbonate (K^+/K^+ electrocatalytic couple); whereas, no excess heat was observed during the electrolysis of aqueous sodium carbonate.

The data of the temperature of the cell minus the ambient temperature shows that when potassium carbonate replaced sodium carbonate in the same cell with the same input electrolysis power, the potassium experiment was twice as hot as the sodium carbonate experiment for the duration of the experiment, one month. The present experimental results are consistent with the release of heat energy from hydrogen atoms where pairs of potassium ions (K^+/K^+ electrocatalytic couple) induce the electrons of hydrogen atoms to relax to quantized energy levels below that of the "ground state" by providing a net enthalpy equal to an integer-multiple of 27.2 eV which stimulate these transitions. The balanced reaction is given by Eqs. (1-3) below. Excess heat was observed only when Na_2CO_3 was replaced by K_2CO_3 . For two sodium ions, no comparable reaction with a net enthalpy equal to an integer multiple of 27.2 eV is possible. (see Eq.(4) below). The excess energy could not be explained by recombination or known chemistry.

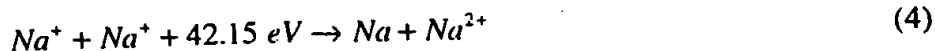
Theoretical Explanation An efficient catalytic system that hinges on the coupling of three resonator cavities involves potassium. For example, the second ionization energy of potassium is 31.63 eV. This energy hole is obviously too high for resonant absorption. However, $K(I)$ releases 4.34 eV when it is reduced to K . The combination of $K(I)$ to $K(II)$ and $K(I)$ to K , then, has a net energy change of 27.28 eV.



And, the overall reaction is



For two sodium ions, no comparable reaction with a net enthalpy equal to an integer multiple of 27.2 eV is possible. For example, 42.15 eV of energy is absorbed by the reverse of the reaction given in Eq. (2.14), where Na^+ replaces K^+ :



Faraday Efficiency

A Westinghouse research scientist proposes that the excess energy may be due to recombination (burning of the evolving hydrogen and oxygen) or some exotic chemical reaction of the counterion of the electrolyte which consumes some of the current that otherwise would electrolyze water.

The general form of the energy balance equation for the cell in steady state is:

$$0 = P_{in} + P_{xs} - P_{loss} \quad (5)$$

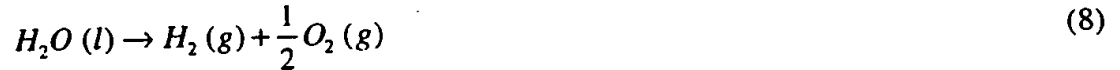
where P_{in} is the input power; P_{xs} is the excess power generated (the source of this power is given by Eqs. (1)-(3) above); and P_{loss} is the thermal power loss from the cell. In these experiments, the applied voltage, V_{appl} , and the current, I , were constant. Thus, the input power is given by

$$P_{in} = V_{appl} I \quad (6)$$

When an aqueous solution is electrolyzed to liberate hydrogen and oxygen gases, the input power can be partitioned into two terms:

$$P_{in} = P_{ohm} + P_{gas} \quad (7)$$

where P_{ohm} is the ohmic power that heats the cell and P_{gas} is the power needed to produce the H_2 and O_2 gases.



An expression for $P_{gas}(= V_{gas} I)$ is readily obtained from the known enthalpy of formation of water ($\Delta H_f = -286 \text{ kJ/mole}$):

$$V_{gas} = -\frac{\Delta H_f}{\alpha F} = -\frac{-286 \times 10^3 \text{ J/mole}}{2 \times 96484 \text{ C/mole}} = 1.48 \text{ volts} \quad (9)$$

where α is the number of moles of electrons involved in the reaction and F is the Faraday constant. The net Faraday efficiency of gas evolution is assumed to be unity. Thus, the ohmic power is given by

$$P_{ohm} = (V_{appl} - 1.48) I \quad (10)$$

The experimentally observed rise in temperature of the potassium experiment was twice that of the sodium experiment. The temperature rise cannot be attributed to a hypothesis that the net faraday efficiency of gas evolution is not unity, because it was **experimentally measured to be unity** by weighing the experiment to determine that the expected rate of water consumption was observed, and the output power exceeded the total input power. This further overcomes the hypothesis of Isenberg that an extremely unusual chemical reaction of the carbonate ion was responsible for consuming the current. Furthermore, the hypothesis of Isenberg is highly improbable, for the following reasons:

- The chemical reactions proposed by Isenberg would be expected to occur to the same extent in the sodium control experiment, which showed no excess, heat because they both potassium and sodium cells contained equivalent amounts of carbonate and were operated under identical conditions.
- Production of percarbonate from carbonate **consumes** energy, as opposed to **producing** energy.
- The carbonate concentrations of all of the experiments was analyzed following their completion, and the final carbonate concentration in all cases was about the same as the starting concentration. The slight decrease in carbonate over the length of the experiments is attributed to the very slow conversion of carbonate to carbon dioxide and hydroxide at the anode at elevated temperature as given by Itskovich ["Electrolysis of aqueous potassium carbonate solutions in a model electrolytic cell", Itskovich, A. R.; Merenkov, P. T., (Inst. Khim., Tashkent, USSR). *Dokl. Akad. Nauk Uzb. SSR* 1968, 25(7)].
- Electrochemical reactions which consume the electrolyte can be ruled out because any proposed electrochemical reactant would be completely consumed over the duration of these experiments.

In the case of the last point above, the current of each experiment was 3 A, and each experiment contained 1.5 liters of 0.57 molar electrolyte. Thus, the total number of moles of electrolyte was

$$0.57 \text{ moles/liter} \times 1.5 \text{ liters} = 0.85 \text{ moles} \quad (11)$$

According to Faraday's Law, a current of 3 amperes consumes one mole equivalent in 8.9 hours.

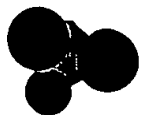
$$\frac{96484 \text{ coulombs / mole equivalent}}{3 \text{ coulombs / second}} = 32,161 \text{ seconds} = 8.9 \text{ hours} \quad (12)$$

The duration of the experiment was **one month**, and the excess energy was **constant** over the duration of the experiment.

Summary

The data clearly indicate that excess heat was generated in each electrolytic cell experiment using potassium carbonate. The experiments were permitted to operate for weeks, and the excess heat remained relatively constant. What is the source of this excess enthalpy? Electrochemical reactions which consume the electrolyte can be ruled out, because any proposed electrochemical reactant would be completely consumed over the duration of these experiments. The Faraday efficiency was measured to be 100% for both electrolytes. The results are consistent with the release of heat energy from hydrogen atoms where the K^+/K^+ electrocatalytic couple induces the electrons of hydrogen atoms to relax to a quantized potential energy level below that of the "ground" state, by providing a redox energy-energy hole (27.28 eV) resonant with this transition. The balanced reaction is given by Eqs. (1-3).

No excess heat was observed until K_2CO_3 replaced by Na_2CO_3 . For two sodium ions, no comparable reaction with a net enthalpy equal to an integer multiple of 27.2 eV is possible as given by Eq. (4).



THIS PAGE BLANK (USPTO)

EXCESS ENERGY CELL FINAL REPORT

25 APRIL 1995

C. W. HALDEMAN, E. D. SAVOYE, G. W. ISELER, H. R. CLARK

OUTLINE

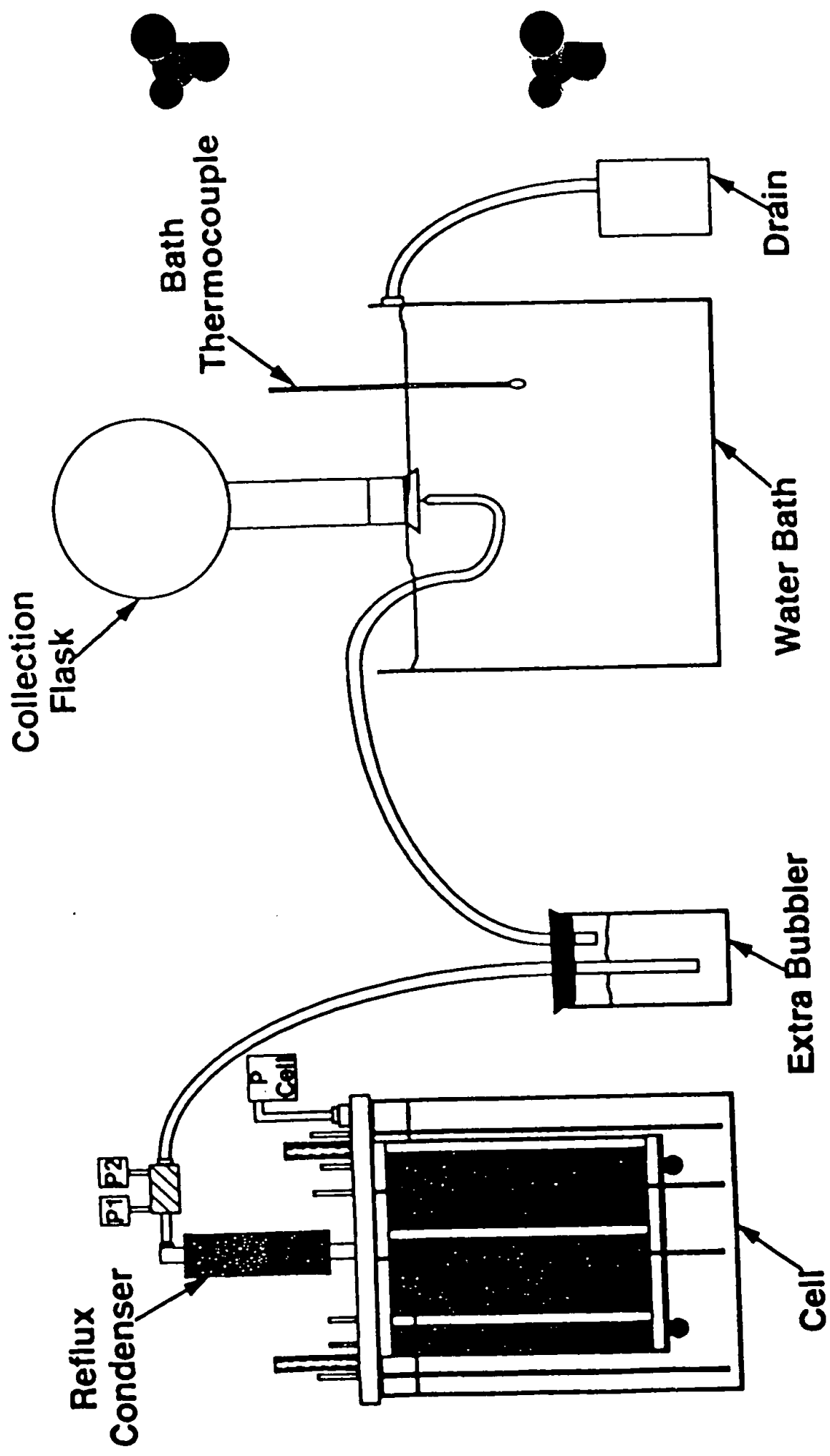
- REVIEW
- CHANGES SINCE LAST REPORT
 - RETURN TO ROOM THERMAL ENVIRONMENT
 - RE-WOUND CELL
 - RESIDUAL GAS ANALYSIS
- ENERGY MEASUREMENTS
- GAS MEASUREMENTS
- CONCLUSIONS

APPENDIX A

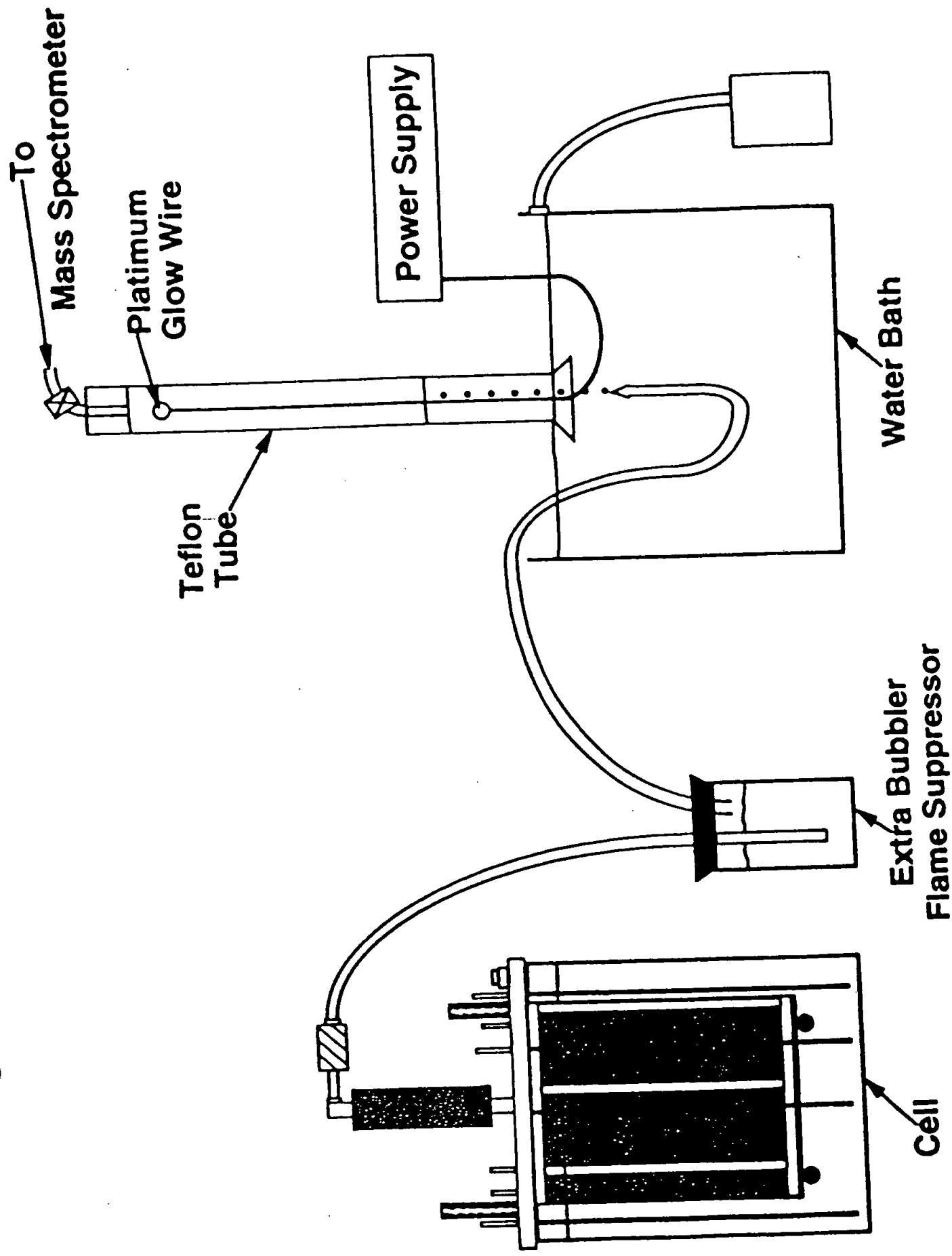


•ec/•chuck/4/20

Sealed Cell Layout



Gas Collection With Combustion Tube



SUMMARY OF CELLS ASSEMBLED

<u>CELL #</u>	<u>CATHODE</u>	<u>ANODE</u>	<u>C/A RATIO</u>	<u>RESULTS</u>
1	ANNEALED #41 NICKEL 1.8 lbs 52000 cm ²	PLATINIZED Ti 100 cm ²	520: 1	NO EXCESS ENERGY
1A	SAME WIRE HEAT TREATED IN H ₂ 770°C	SOFT NICKEL SHEET 3000 cm ² PLATINIZED Ti 100 cm ²	17: 1	NO EXCESS ENERGY
2	HARD DRAWN 0.5 mm NICKEL 16,000 cm ²	SAME	5: 1	5 → 10% EXCESS ENERGY
2A	NEW WINDING HARD DRAWN 0.5 cm ² NICKEL 15,000 cm ²	PLATINIZED Ti SHEET 3100 cm ²	5: 1	5 → 30% EXCESS ENERGY
3	HARD DRAWN - SCRATCHED #44 NICKEL 190,000 cm ² (0.002 in.) 0.05 cm dia.	SAME	61: 1	20 → 50% EXCESS ENERGY
4	#46 HARD DRAWN SMOOTH NICKEL WIRE 240,000 cm ²	SAME	75: 1	20 → 1400% EXCESS ENERGY 4 x VI INPUT



soce/y/chuck/4/21

OCTOBER 1994 PLANS

1. USE SEALED SYSTEM RECOMBINER / CONDENSER
TO COLLECT GAS
2. REWIND CELL WITH SMOOTH #46 WIRE
3. USE WET CHEMICAL GAS ANALYZER
4. CONTINUE TO LOOK FOR HIGHER EXCESS ENERGY
AND CHARACTER OF RESIDUAL GAS



p1/chuck/4/24

RE-WOUND CELL

- CATHODE - 4.7 lbs #46 NICKEL WIRE
Dia. (0.00157 inch) 0.00399 cm

SURFACE AREA 240,000 cm²
CURRENT DENSITY 41 μ a/cm² @ 10a

- ANODE - 5 FOLDED SHEETS Pt PLATED Ti
15.2 x 20.3 cm

SURFACE AREA 3200 cm²
CURRENT DENSITY 32 ma/cm² @ 10a
75:1 CATHODE: ANODE RATIO

- ELECTROLYTE - 16l 0.6 M K₂ CO₃
IN LAB DI WATER



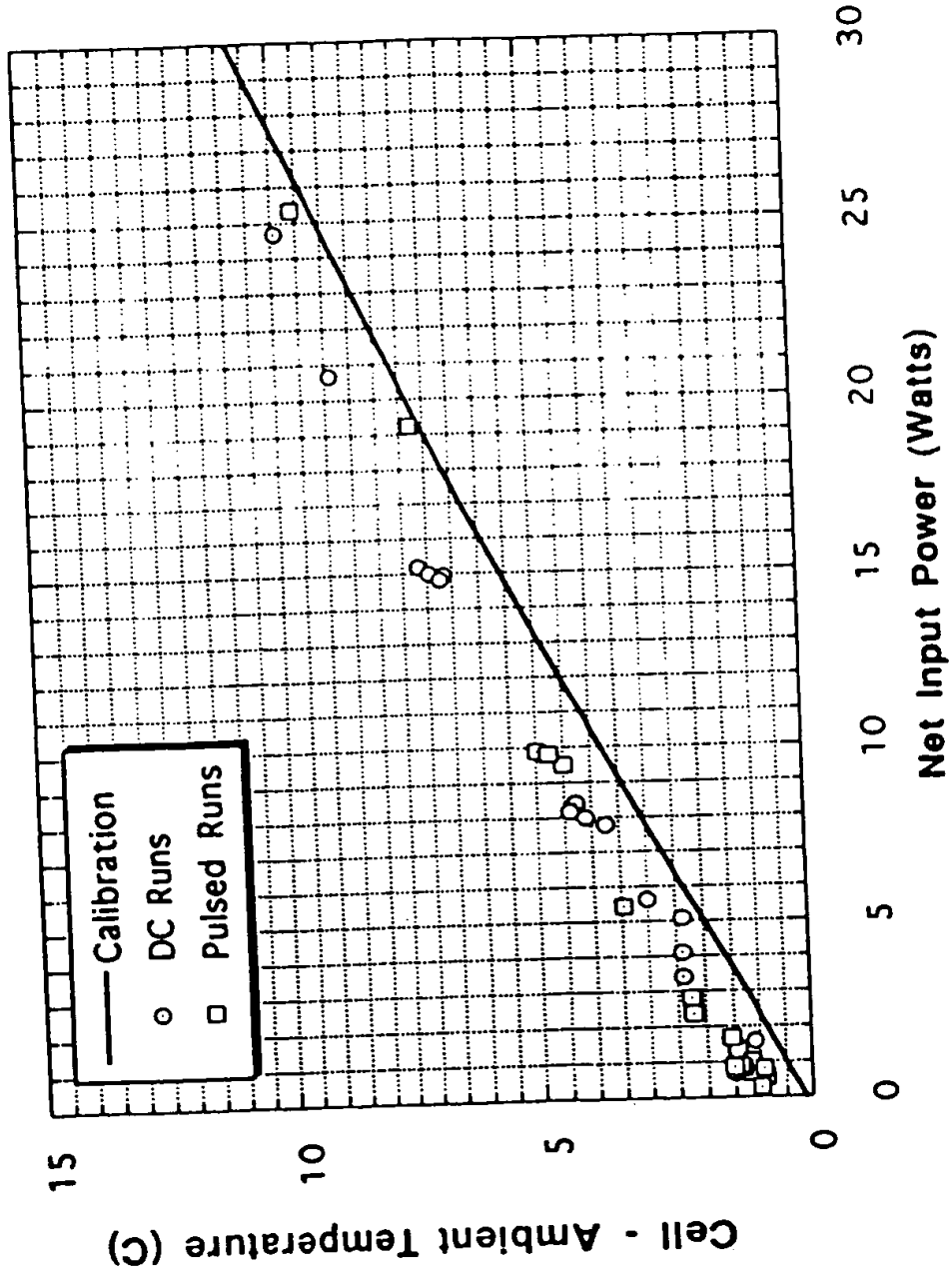
rc/Chuck/4/20

GAS FLOW ABSOLUTE MEASUREMENT

- **DIRECT WATER DISPLACEMENT**
 - 2000 \pm 0.5 cc VOLUMETRIC FLASK
- **WATER BATH TEMPERATURE \pm 0.1°C**
- **TIME MEASUREMENT \pm 0.02 sec**
- **BAROMETRIC PRESSURE**
 - NATIONAL WEATHER SERVICE BAROMETER - CORRECTED
FOR TEMPERATURE AND LATITUDE \pm 0.1 mm
- **MEASURED VOLUME CORRECTED FOR**
 - TEMPERATURE
 - PRESSURE
 - WATER VAPOR CONTENT



Electrolytic Cell Data Results



4/20/95

Immunobias

Electrolytic

Electrode																	Overall (times)
File Name Run No.	V (Volts)	I (Amps)	P (Watts)	Duty Cycle	Freq (Hz)	Pos Peak V (Volts)	Cell (C)	Ambient (C)	ΔT (C)	H ₂ O Power Correction (watts)	P _{in} (watts)	Output Power (watts)	Δ Power (watts)	Output/P _{in} (F=1)	Output/P _{in} (F=1)	Output/P _{in} (F=1)	
Run285	2.830	4.995	14.136	100%	0	0	24.159	20.406	3.753	0.0796	7.776	10.379	2.603	133.5%	155.1%	0.73	
Run286	2.893	5.014	14.505	100%	0	0	23.789	19.656	4.113	0.1125	7.992	11.365	3.393	142.5%	161.9%	0.76	
Run287	2.758	5.126	14.136	100%	0	0	28.913	20.202	8.711	0.1761	7.994	cal check	N/A	N/A	N/A		
Run288	2.740	5.217	14.295	100%	0	0	31.453	20.648	10.805	0.3006	7.658	cal check	N/A	N/A	N/A		
Run289	2.745	5.761	15.786	100%	0	0	34.92	20.73	14.19	0.2325	8.401	cal check	3.607	145.3%	166.0%	0.81	
Run290	2.920	4.999	14.597	100%	0	0	23.682	19.597	4.285	0.1331	8.169	11.866	4.386	121.2%	134.1%	0.74	
Run291a	3.367	10.010	33.704	100%	0	0	28.682	19.75	8.912	0.1709	20.674	25.06	N/A	N/A	N/A		
Run292	3.359	10.009	33.620	100%	0	0	30.52	20.637	9.883	0.2416	20.394	28.043	3.362	113.6%	122.8%	0.70	
Run293	3.468	11.500	40.112	100%	0	0	30.455	20.52	9.935	0.3851	24.681	12.2	4.032	149.4%	170.6%	0.84	
Run294	2.919	4.998	14.589	100%	0	0	24.184	19.78	4.404	0.0417	8.168	12.208 W heaters ad	N/A	N/A	N/A		
Run295	2.758	4.645	12.535	100%	0	0	28.013	19.852	8.161	0.1097	6.806	1.718 W heaters ad	N/A	N/A	N/A		
Run296a	2.869	4.768	13.679	100%	0	0	24.726	20.36	4.366	0.2800	7.308	6.58	3.179	193.5%	207.9%	0.90	
Run297	2.830	2.768	7.775	100%	0	0	21.9	19.516	2.384	0.1158	3.401	2.232 W heaters ad	N/A	N/A	N/A		
Run298	2.669	2.879	6.825	100%	0	0	22.629	19.854	2.875	0.1212	3.250	4.803 W heaters ad	N/A	N/A	N/A		
Run299	2.533	2.876	6.525	100%	0	0	23.908	19.871	4.336	0.0993	3.299	1.076 W heaters ad	N/A	N/A	N/A		
Run300	2.564	2.676	6.802	100%	0	0	22.487	19.825	2.862	0.1172	3.351					0.79	
Run301 - Data Lost due to computer failure																	
Run302	3.226	7.908	25.497	100%	0	0	26.803	19.604	7.199	0.0700	16.166	20.119	4.924	132.4%	147.2%	0.77	
Run303	3.220	7.903	25.448	100%	0	0	28.617	19.545	8.972	0.1148	14.994	19.47	4.476	129.9%	142.9%	0.77	
Run304-low P	1.919	2.309	2.000	20%	6	2.6	21.089	19.669	1.42	0.0356	0.660	3.928	3.259	587.3%	N/A	1.86	
Run304-High P	1.923	2.259	2.000	20%	6	2.6	21.165	19.662	1.503	0.0035	0.738	4.155	3.417	563.1%	N/A	2.08	
Run305	2.080	3.712	4.809	20%	6	3.3	22.158	19.917	2.241	0.0303	2.795	6.185	3.390	221.3%	136.4%	0.72	
Run306a	3.188	8.066	25.691	100%	0	0	27.004	20.336	6.666	0.0761	14.936	19.801	3.863	124.5%	N/A	1.51	
Run307	2.046	3.214	4.037	20%	6	2.8	21.991	19.775	2.216	0.0094	2.354	6.116	3.782	259.8%	N/A	1.63	
Run308	1.867	2.626	2.207	10%	6	2.6	21.481	20.004	1.457	0.0050	1.293	4.029	2.736	311.5%	N/A	1.82	
Run309	1.933	2.226	2.462	20%	6	2.6	21.268	19.849	1.439	0.0081	1.329	3.98	2.851	298.6%	N/A	2.43	
Run310	1.802	1.808	1.373	10%	6	2.6	21.798	20.594	1.202	0.0039	0.884	3.33	2.646	487.0%	N/A	N/A	
Run311	1.794	1.853	1.428	10%	6	2.6	22.395	20.182	2.213	0.0036	0.811	2.491	1.941	452.9%	N/A	2.19	
Run312	1.787	1.828	1.137	10%	6	2.6	21.503	20.608	0.895	0.0029	0.550	2.923	2.216	413.1%	625.3%	1.50	
Run313	1.950	0.999	1.948	100%	0	0	20.89	19.837	1.053	0.0084	0.707	2.005	1.671	1498.8%	3382.6%	4.26	
Run314	1.894	0.278	0.470	100%	0	0	19.934	19.217	0.717	0.0017	0.134	2.005	N/A	N/A	N/A	N/A	
Run315a	1.882	0.276	0.467	100%	0	0	21.151	19.398	1.753	0.0015	0.186	1.908 W heaters ad	N/A	N/A	N/A	N/A	
Run316	1.880	0.276	0.466	100%	0	0	21.785	19.300	2.485	0.0015	0.202	3.068 W heaters ad	N/A	N/A	N/A	N/A	
Run317	2.150	2.002	4.304	100%	0	0	21.353	20.247	1.106	0.0142	1.589	3.068	1.479	193.1%	230.2%	0.71	
Run318	2.526	3.880	9.840	100%	0	0	22.06	19.689	2.391	0.0266	4.102	6.599	2.497	180.9%	177.8%	0.73	
Run319	3.957	20.000	79.140	100%	0	0	38.979	20.499	18.48	0.3847	53.007	64.021	1.014	101.9%	110.8%	0.86	
Run320	2.543	3.167	8.054	100%	0	0	21.943	19.574	2.389	0.0162	5.090	6.539	1.449	128.5%	195.4%	0.81	
Run321	2.776	3.999	11.097	100%	0	0	23.815	20.801	3.014	0.0309	5.631	8.324	2.693	147.8%	161.7%	0.75	
Run322	1.812	2.084	1.897	10%	6	2.6	21.321	19.635	1.488	0.0046	0.656	4.109	3.254	480.6%	N/A	2.42	
Run323	1.834	2.168	1.783	10%	12	2.6	20.673	19.488	1.175	0.0035	1.018	3.256	2.238	319.7%	N/A	1.86	
Run324	1.809	2.016	1.601	10%	4	2.6	21.05	19.698	1.366	0.0046	0.794	3.749	2.856	472.0%	N/A	2.34	
Run325	1.824	2.129	1.700	10%	6	2.6	21.143	19.748	1.397	0.0040	0.674	3.866	2.991	442.1%	N/A	2.27	
Run326	1.936	3.087	2.875	10%	6	3.0	21.298	19.782	1.644	0.0068	1.877	4.268	2.591	254.6%	N/A	1.48	
Run326a	2.169	6.218	7.901	10%	6	4.0	23.383	19.931	3.462	0.0115	5.430	8.541	4.111	175.7%	N/A	1.21	
Run327	2.326	8.809	13.418	10%	6	4.6	24.601	19.61	4.991	0.0163	9.866	13.940	3.963	140.1%	N/A	1.03	
Run328 - This run no. accidentally skipped																	
Run329	1.828	2.034	1.600	10%	6	2.6	21.27	20.328	0.942	0.0041	0.780	2.819	1.829	331.6%	N/A	1.84	
Run330	3.744	8.032	30.072	100%	0	0	26.298	19.727	6.569	0.0391	17.238	18.319	1.081	106.3%	112.7%	0.61	
Run331/ver 1ld																	

Electrolytic Cell Data Reduction Table
 The Following Runs are the Start of Experiments with the new Smooth Nickel wire Cathode on 10/27/84

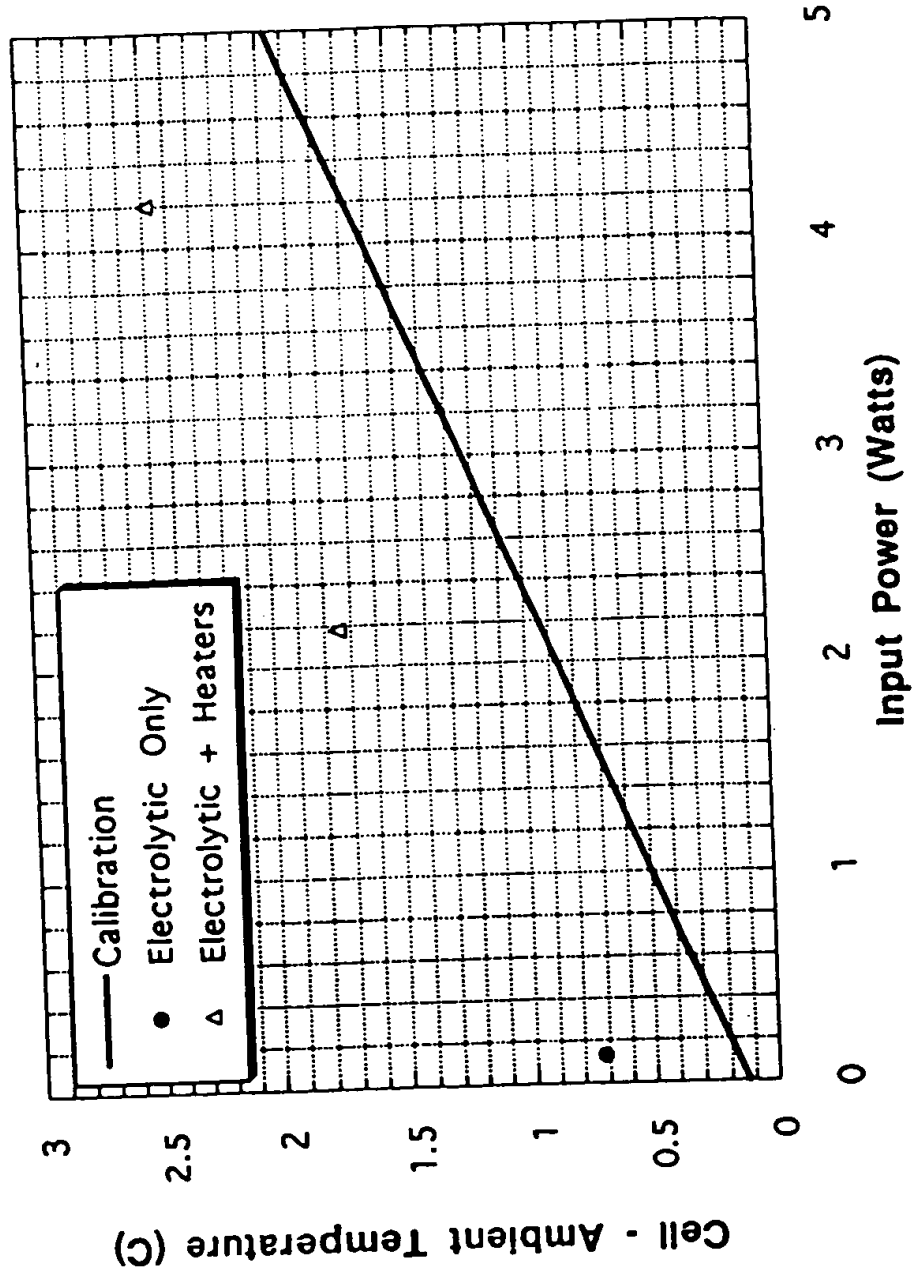
Run Name (Run No.)	Bar. Pressure (Torr)	Bar. Pressure (calibrated)	P _{cell} (psig)	P ₁ (psig)	P ₂ (psia)	P ₃ (psig)	P ₄ (psia)	P ₅ (psig)	P ₆ (psia)	Flowrate (cc/min) (fully corr.)	Faraday Efficiency	Data Taken Over Time Range (min)
Run285	767.20	759.66	0.6032	0.6013	15.27	0.4896	15.15	0.1117	20.541	47.20	84.29%	1250-1350
Run286	766.82	759.30	0.7183	0.7202	15.37	0.6555	15.31	0.0647	19.747	48.11	85.60%	3200-3600
Run287	745.81	759.31	0.7753	0.7777	15.05	0.7161	14.98	0.0616	20.031	44.81	77.98%	2000-2200
Run288	766.65	759.33	0.9375	0.9405	15.60	0.8714	15.53	0.0691	20.522	47.58	81.36%	1650-1700
Run289	767.68	760.32	0.7066	0.7093	15.38	0.6445	15.32	0.0648	20.443	53.68	83.27%	1050-1100
Run290	751.43	751.43	0.7775	0.7604	15.28	0.7218	15.22	0.0586	19.740	47.31	84.42%	3600-3700
Run291a	771.05	763.58	0.5429	0.5451	15.28	0.4612	15.20	0.0839	19.725	95.90	85.48%	7200-7500
Run292	765.75	756.48	0.8049	0.8072	15.25	0.4805	15.12	0.1267	20.856	98.83	88.30%	1300-1400
Run293	773.76	768.16	0.7184	0.7208	15.51	0.5830	15.37	0.1379	20.577	111.98	88.86%	1250-1350
Run294	774.90	767.26	0.4375	0.4396	15.25	0.3757	15.18	0.0838	19.962	47.95	85.58%	2000-2100
Run295	774.00	767.25	0.8714	0.8737	15.48	0.3951	15.40	0.0788	19.868	42.26	82.93%	2500-3000
Run296a	756.79	749.85	1.1130	1.1160	15.59	1.0383	15.51	0.0777	20.500	45.81	85.71%	950-1030
Run297	779.70	771.87	1.0230	1.0260	15.92	0.9491	15.85	0.0769	19.680	28.35	91.43%	5000-6000
Run298	762.46	765.20	1.0890	1.0720	16.85	0.9943	15.57	0.0777	20.291	24.55	84.92%	1230-1315
Run299	761.11	761.69	0.9829	0.9859	15.87	0.8848	15.59	0.0811	19.845	23.58	81.68%	1800-2200
Run300	770.82	763.14	1.0940	1.0970	15.83	1.0263	15.75	0.0707	19.979	23.64	81.90%	3500-4000
Run301 - Data Lost due to computer failure												
Run302	765.09	757.83	1.3088	1.3110	15.94	1.2235	15.85	0.0875	19.833	76.57	88.40%	1900-2200
Run303	775.04	767.39	-2.5190	-2.5200	12.29	-2.5824	12.25	0.0424	19.960	77.38	87.34%	1150-1250
Run304-low P	779.86	772.02	-8.2870	-8.2870	8.61	-8.4183	8.48	0.1313	19.969	9.77	37.75%	5000-6150
Run304-High P	756.59	749.86	6.9990	7.0210	21.49	6.8748	21.34	0.1464	20.095	9.49	37.48%	2400-2800
Run305	779.36	771.53	-5.7390	-5.7360	9.15	-5.8589	9.03	0.1209	20.183	14.87	35.74%	1000-2000
Run306a	773.07	765.50	0.9063	0.9071	15.68	0.8700	15.64	0.0371	20.681	79.90	88.48%	1272-1325
Run307	773.04	765.47	0.3967	0.4207	15.19	0.4176	15.19	0.0031	20.110	12.52	34.75%	1800-2000
Run308	755.91	749.01	0.4164	0.4155	14.87	0.4135	14.87	0.0020	20.270	6.79	23.98%	2600-2900
Run309	771.98	764.48	0.4091	0.4091	15.16	0.4071	15.16	0.0020	20.184	6.47	33.94%	3280-3680
Run310	766.86	758.38	0.4140	0.4144	15.05	0.4130	15.05	0.0014	21.043	6.15	25.41%	800-800
Run311	757.22	750.27	0.4143	0.4146	14.69	0.4134	14.69	0.0012	20.422	4.60	22.15%	650-750
Run312	775.36	767.70	0.4157	0.4163	15.23	0.4155	15.23	0.0008	20.964	3.99	23.32%	980-1040
Run313	758.38	751.38	0.4158	0.4224	15.09	0.4219	15.09	0.0005	19.422	9.12	81.45%	3200-3600
Run314	787.17	759.93	0.3937	0.3946	15.28	0.3943	15.28	0.0003	19.535	2.32	80.95%	7500-8000
Run316a	779.08	771.27	0.4106	0.4116	15.22	0.4115	15.22	0.0001	19.405	2.08	88.86%	1520-1720
Run316	775.02	767.37	0.4158	0.4168	15.12	0.4123	15.11	0.0045	19.453	1.97	63.31%	800-1000
Run317	769.10	761.86	0.4158	0.4168	15.19	0.3991	15.16	0.0108	19.767	19.55	87.11%	1350-1500
Run318	762.60	755.44	0.8085	0.8099	15.19	0.5991	15.16	0.0108	19.767	34.30	85.47%	3200-3600
Run319	760.92	763.82	0.2108	0.2115	14.76	0.4079	14.60	0.1636	20.295	189.00	84.30%	2450-2750
Run320	765.02	748.16	0.7814	0.7829	15.22	0.8805	15.12	0.1024	19.779	22.18	62.48%	3600-3800
Run321	758.18	761.19	0.6103	0.6116	15.11	0.4812	14.98	0.1308	20.746	37.54	83.74%	1200-1500
Run322	761.75	754.82	0.2201	0.2211	14.70	0.2186	14.76	0.0025	19.978	6.28	26.88%	1600-2200
Run323	769.86	761.26	0.8840	0.8860	15.58	0.8837	15.58	0.0023	19.701	5.47	26.88%	3000-3500
Run324	762.80	746.83	0.2817	0.2817	15.28	0.8836	15.28	0.0024	19.910	6.02	26.60%	2000-2200
Run325	764.88	767.44	1.2460	1.2460	16.87	1.2448	16.88	0.0022	19.927	6.16	26.61%	1600-2000
Run326a	758.18	751.19	0.3682	0.3684	14.86	0.3641	14.86	0.0023	19.978	6.89	25.94%	400-800
Run327	767.84	750.90	2.5690	2.5680	17.08	2.5849	17.08	0.0031	20.149	18.04	25.88%	2000-2200
Run328 - This run no. accidentally skipped												
Run329	762.80	766.73	3.1290	3.1280	17.71	3.1212	17.71	0.0048	19.799	25.46	26.51%	4000-4500
Run330	774.31	768.68	0.8036	0.8089	16.70	0.8038	16.70	0.0023	20.687	8.08	28.63%	3000-3200
Run331/next lid	766.27	768.00	7.1170	7.1410	21.77	7.1358	21.77	0.0054	19.946	82.27	91.37%	4800-8200

4/20/85

File Name Run No.)	V (Volts)	I (Ampe)	P (Watts)	Duty Cycle	Freq (Hz)	Peak V (Volts)	Call (C)	Ambient (C)	ΔT (C)	ISO Power Correction (watts)	P _{in} (watts)	Output Power (watts)	$\Delta Power$ (watts)	Output/P _{in} (F=1)	Output/P _{in} (times)
un332wet lid	3.576	7.032	25.146	100%	0	0	25.716	19.046	5.77	0.0472	13.965	16.049	2.084	114.9%	121.1%
un333wet lid	3.531	7.019	24.784	100%	0	0	25.159	19.567	5.571	0.0355	13.831	15.486	1.655	112.0%	119.9%
un335wet lid	1.950	0.991	1.932	100%	0	0	20.774	20.176	0.598	0.0064	0.464	1.661	1.217	362.0%	365.3%
un328 - This run no. accidentally shipped															
un337wet lid	2.051	3.162	3.947	20%	6	2.9	21.336	19.754	1.582	0.0096	2.069	4.372	2.303	211.3%	N/A
un338wet lid	2.229	4.907	7.188	20%	6	3.3	22.352	19.987	2.365	0.0167	4.192	6.563	2.391	157.0%	N/A
un339wet lid	2.493	7.969	14.130	20%	6	4.0	23.96	19.725	4.235	0.0308	9.418	11.73	2.312	124.6%	N/A
un340wet lid	2.139	5.819	7.211	10%	6	4.0	21.684	19.615	2.269	0.0099	4.957	8.28	1.303	126.3%	N/A
un341	2.998	11.266	26.364	40%	6	4.0	27.271	19.977	7.294	0.0693	19.221	20.391	1.170	106.1%	N/A
un342	1.799	2.027	1.599	10%	6	2.6	21.325	19.601	1.624	0.0040	0.846	4.213	3.367	496.2%	N/A
un343	2.479	8.110	14.362	20%	6	3.6	24.323	19.627	4.496	0.0317	9.508	12.458	2.950	131.0%	N/A
un344	2.494	8.103	14.370	20%	6	3.6	24.927	20.065	4.762	0.0265	9.796	13.205	3.407	134.8%	N/A
un345	2.906	14.927	34.014	20%	6	5.0	29.859	20.266	9.591	0.0732	25.335	27.037	1.702	106.7%	N/A
un346	1.711	0.639	0.700	20%	6	1.6	21.208	20.198	1.01	0.0023	0.275	2.805	2.530	1019.6%	N/A
Run348	3.233	8.001	25.867	100%	0	0	27.298	20.542	6.756	0.0652	14.825	18.652	4.027	127.2%	155.7%

4/20/85		Measured															
File Name	Bar. Pressure (Torr)	Bar. Pressure (calibrated)	P. cell (psig)	P1 (psig)	P1 (psia)	P2 (psig)	P2 (psia)	P. cell (psig)	P2 (psia)	P. cell (psig)	P2 (psia)	P. cell (psig)	P2 (psia)	I1 (C)	Flowrate {cc/min) (fully corr.)	Paradey Efficiency	Data Taken Over Time Range (min)
Run332/next lid	768.86	761.83	3.7160	3.7100	18.22	3.6900	18.20	0.0200	20.186	73.11	92.75%	3300-3800					
Run333/next lid	778.38	768.88	5.8730	5.8710	20.71	5.8552	20.69	0.0158	19.833	71.51	90.88%	2000-2500					
Run335/next lid	767.86	759.88	1.8180	1.8200	18.31	1.8165	18.31	0.0035	20.443	10.85	97.67%	6600-7200					
Run336 This run just a temp run-no data																	
Run337/next lid	760.10	772.25	0.7219	0.7238	15.83	0.8300	15.53	0.0938	20.087	14.01	39.28%	3000-3800					
Run338/next lid	767.89	760.52	0.8398	0.8416	15.32	0.5442	15.22	0.0974	20.235	22.20	40.36%	3200-3500					
Run339/next lid	770.28	762.82	0.0534	0.0548	14.78	0.0428	14.77	0.0120	19.908	34.52	38.64%	2500-2800					
Run340/next lid	765.41	758.14	2.2250	2.2320	18.86	2.2289	18.86	0.0031	19.849	16.51	25.31%	3400-3600					
Run340b/next lid	764.55	767.31	0.4369	0.4415	15.08	0.4193	15.04	0.0222	20.010	66.78	52.86%	1800-2000					
Run341	762.89	756.72	0.6187	0.6151	15.20	0.5845	15.17	0.0308	20.088	5.62	24.73%	1900-2000					
Run342	768.43	761.04	0.2439	0.2458	14.93	0.2382	14.93	0.0076	20.102	35.80	39.16%	3400-3600					
Run343	763.41	758.22	0.6468	0.6482	15.44	0.8410	15.44	0.0072	20.341	33.34	36.70%	2500-2800					
Run344a	772.93	766.38	0.4704	0.4724	15.24	0.4625	15.22	0.0189	20.466	61.89	36.87%	4180-4250					
Run346	776.32	767.88	0.3388	0.3381	15.16	0.3388	15.16	0.0023	20.509	3.19	33.94%	2800-2800					
Run348																	
Run347 This run just a temp run-no data																	
Run348	766.38	759.07	0.4389	0.4323	16.08	0.4001	16.05	0.0322	20.714	82.04	91.47%	6000-6500					

0.278 Ampere Data



MASSACHUSETTS INSTITUTE OF TECHNOLOGY
LINCOLN LABORATORY

2 May 1995

TO: Ad Hoc Committee Distribution
FROM: C. W. Haldeman *CWH*
SUBJECT: Additional Material

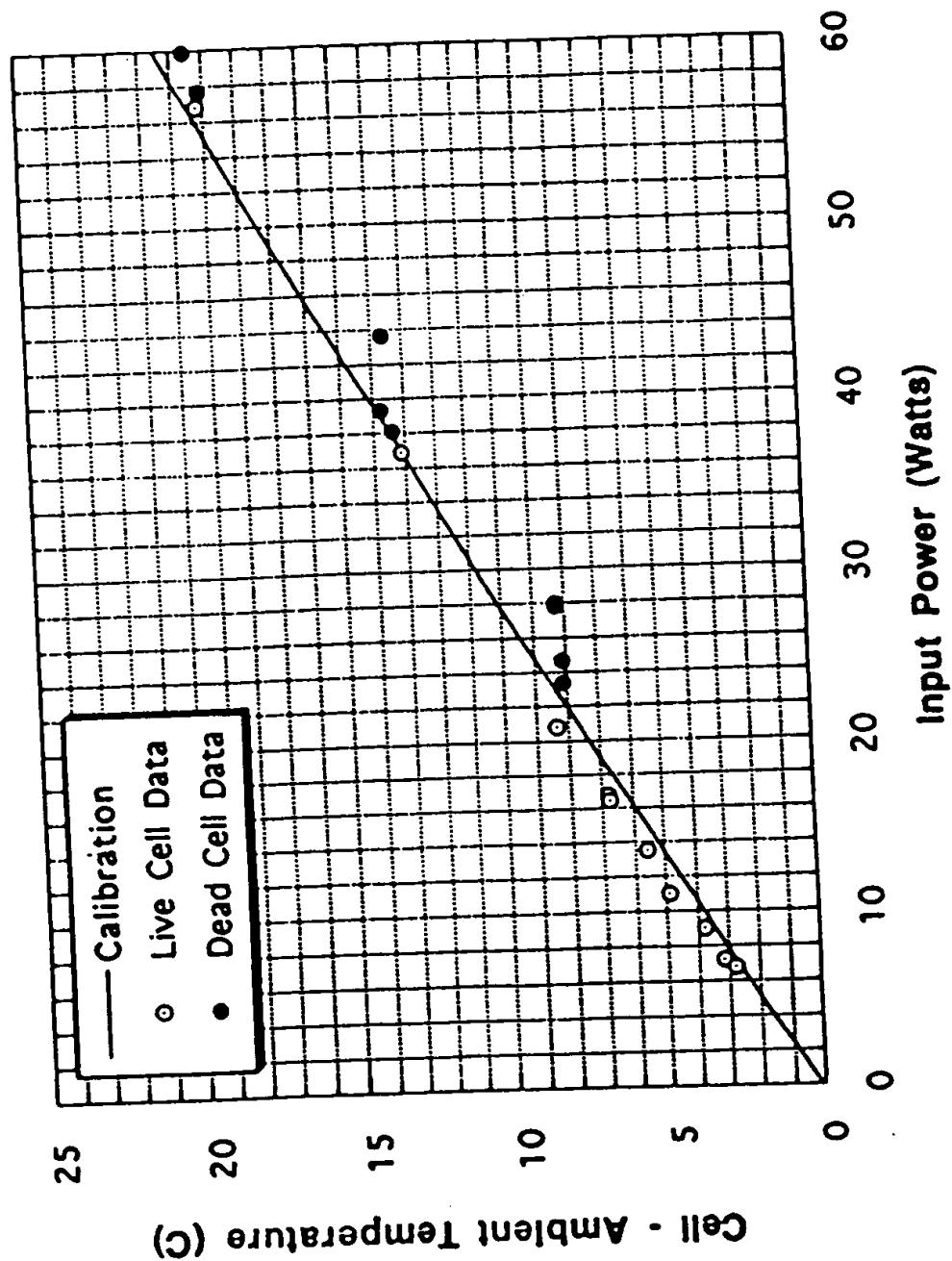
You should have all received my viewgraphs from the 25 April meeting. At that meeting Marv and Ron requested that I replot the data from the new cell (Cell 4) in terms of excess power vs. net input power. This has been done and is attached. The large scatter seems to indicate that the excess power is not a function of net input or at least has a stronger dependence on some variable not controlled. Also requested and included is the old data from Cell 3 which includes data before and after the power failure. The calibration curve is the same for both windings of the cell and includes both calibration and recalibration results.

Since the data now includes both Cell 3 and 4, I replotted the Cell 4 results to avoid confusion. This is the same plot in the presentation which was entitled "Electrolytic Cell Data Results." Please add these figures to the package.

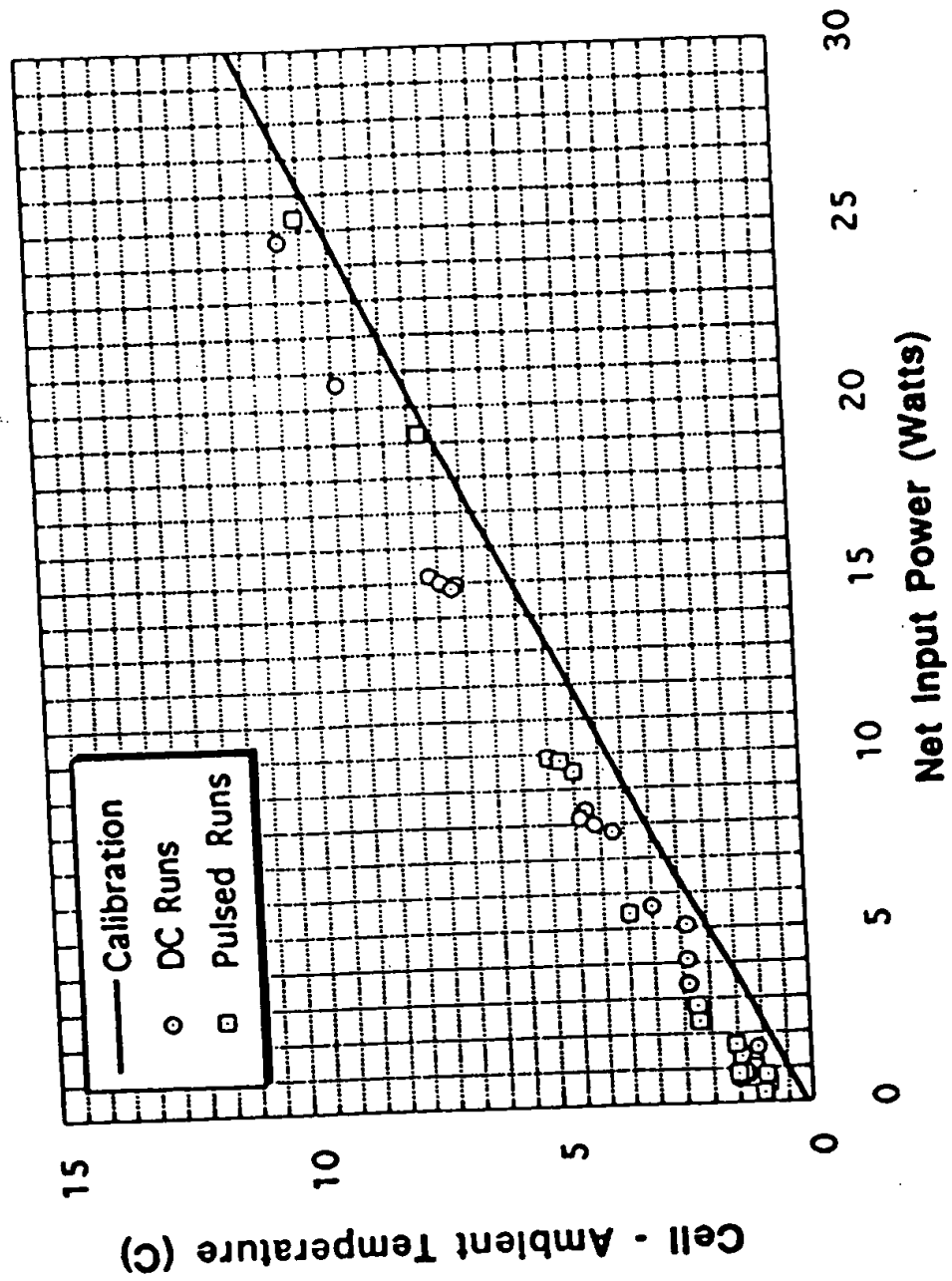
CWH:jf
Attachments

FOR LABORATORY USE ONLY

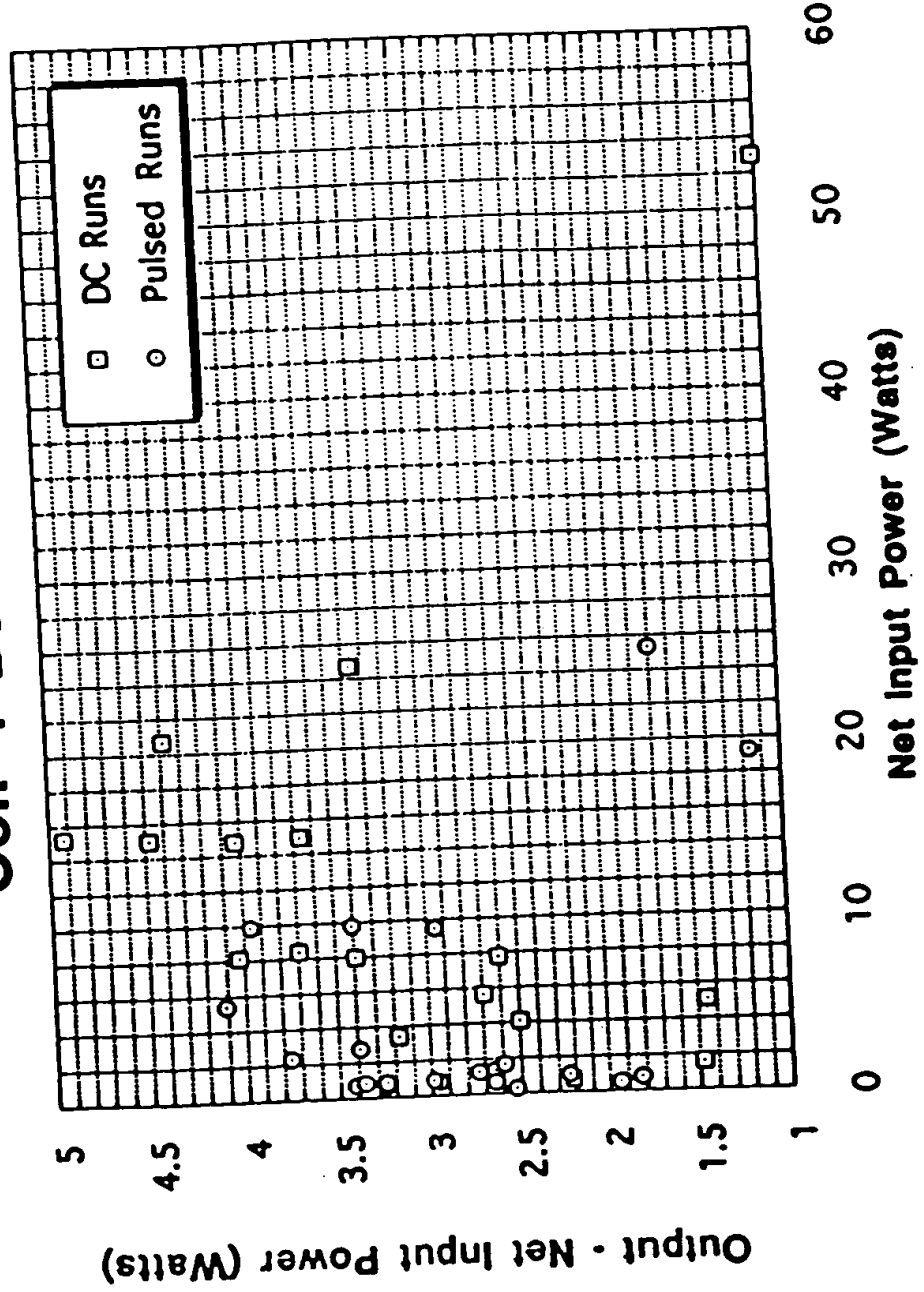
Cell 3 Data Results



Cell 4 Data Results



Cell 4 Data Results



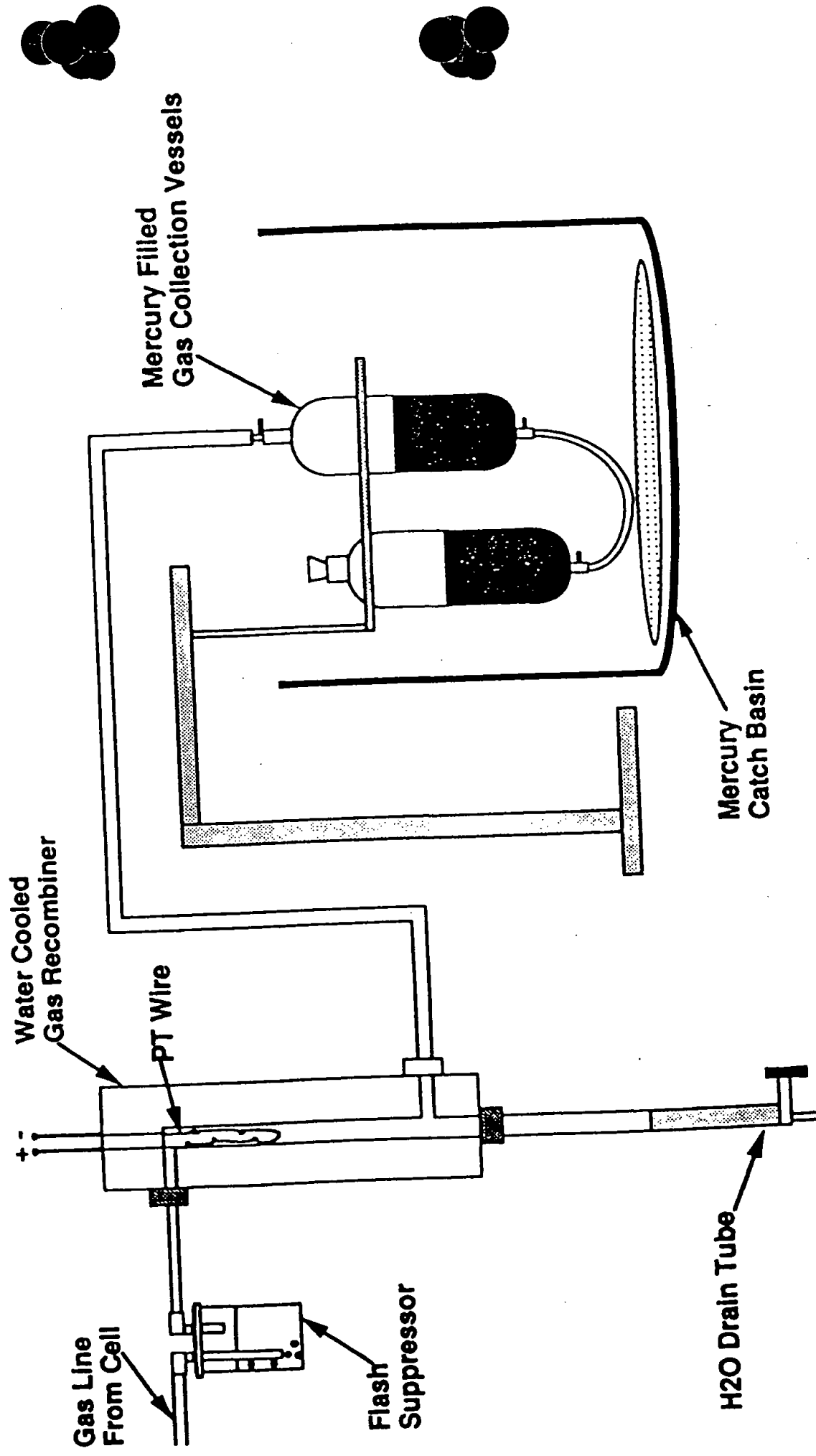
GAS MEASUREMENTS

- **CHEMICAL ABSORPTION**
 - BURRELL WET ANALYZER
- **MASS SPECTROMETER**
 - INFICON QUADRAPOLE - 102 VOLT ENERGY
- **CRYO CONDENSATION**

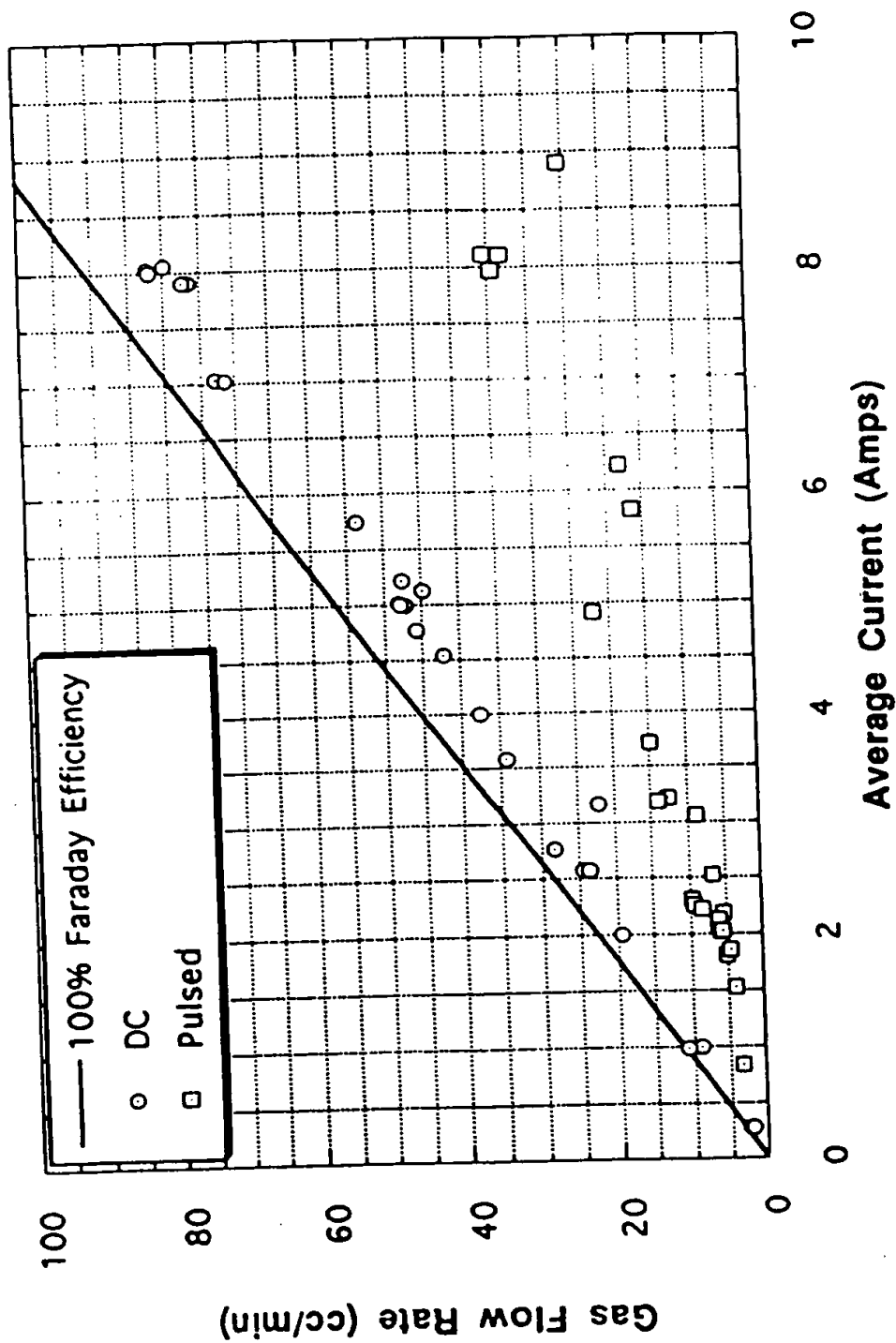


gmj/chuck 4/20

Electrolytic Cell Current Gas Collection System



Cell Gas Production



GAS WET ANALYSIS
BURRELL ABSORPTION TUBE ANALYZER

GAS TESTED FOR	ABSORBENT
CO_2	KOH sol
O_2	CrCl_2 sol
H_2	HOT (300°C) CuO

WET ANALYSIS RESULTS

PERCENT

SAMPLE

CO₂ O₂

H₂

RESIDUE

AIR

0

21

0

79

RAW CELL GAS

0

32

67

01

RECOMBINED CELL GAS
MANY SAMPLES

0

18 → 22

0 → 0.2

BALANCE 78 → 82
CALLED PROCESSED
CELL GAS

MASS SPEC ANALYSIS OF PROCESSED CELL GAS SHOWS
N₂, A, H₂O

HYDRO-CATALYSIS CLAIMS TO HAVE FOUND 1-2% H₂



Wat/Chuck/4/20

RECOMBINER RESULTS

- GAS GENERATION 2 TO 100 cc/minute
 2.8 TO 144 l/day

- RECOMBINED WATER CHECKS OUT GAS MEASUREMENT
- $\pm 1\%$

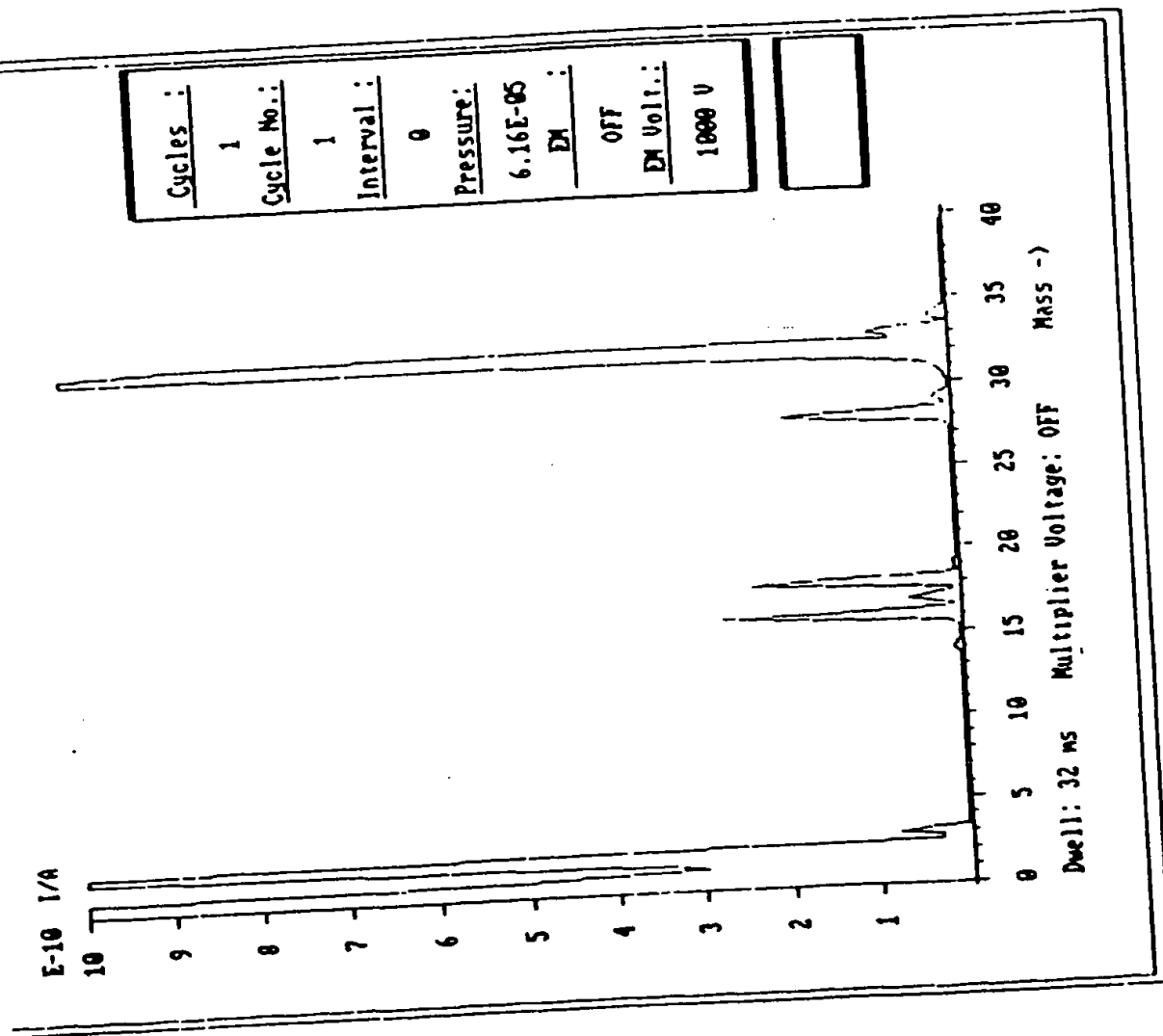
- RESIDUAL GAS FROM RECOMBINER - 50 \rightarrow 100 cc/day
 - 1.8% TO 0.1% OF TOTAL GAS FLOW
 - NEARLY 100% CONDENSED OVER LN₂



rrf/chuck/4/20

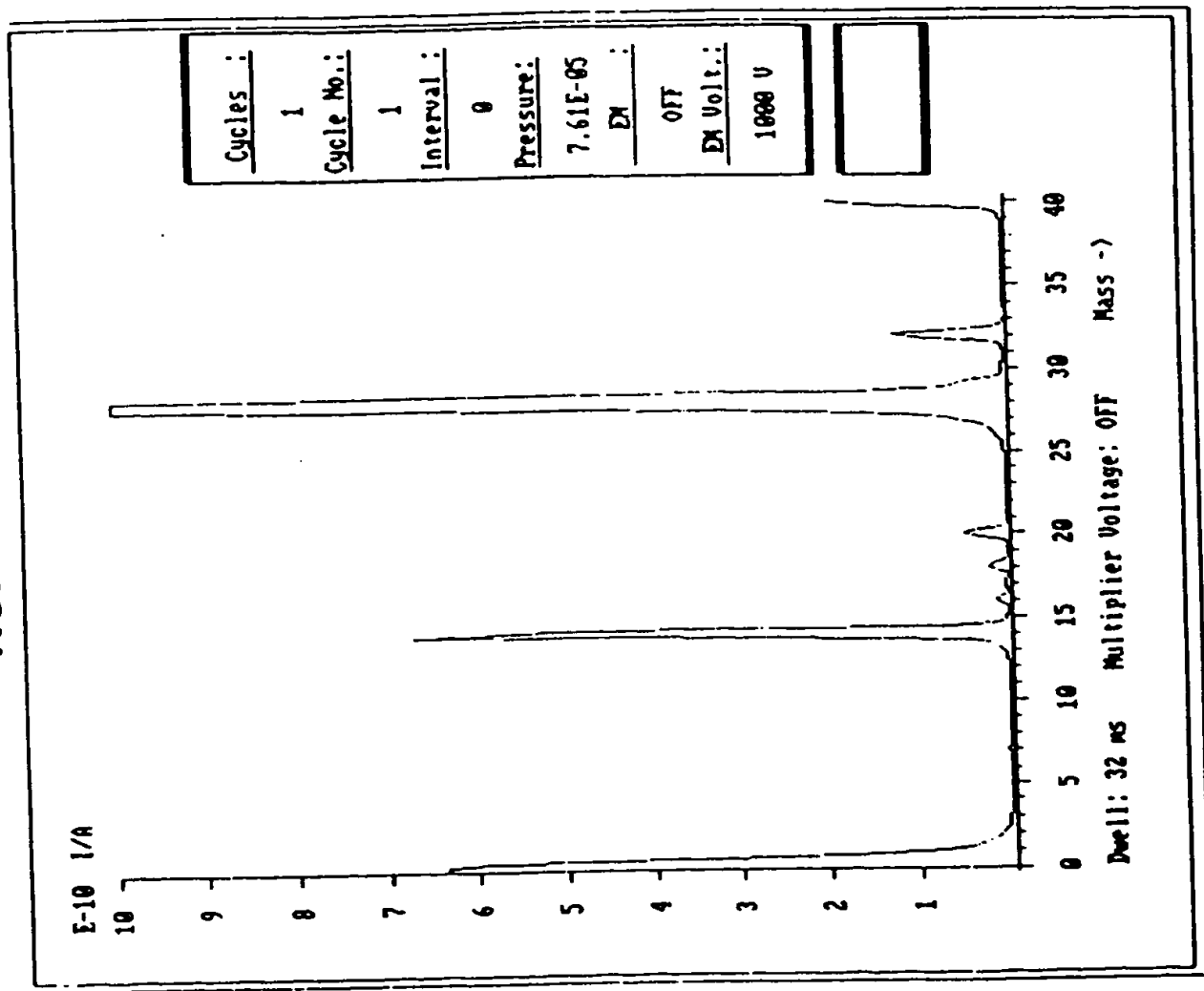
"RAW CELL GAS"

RUN 334

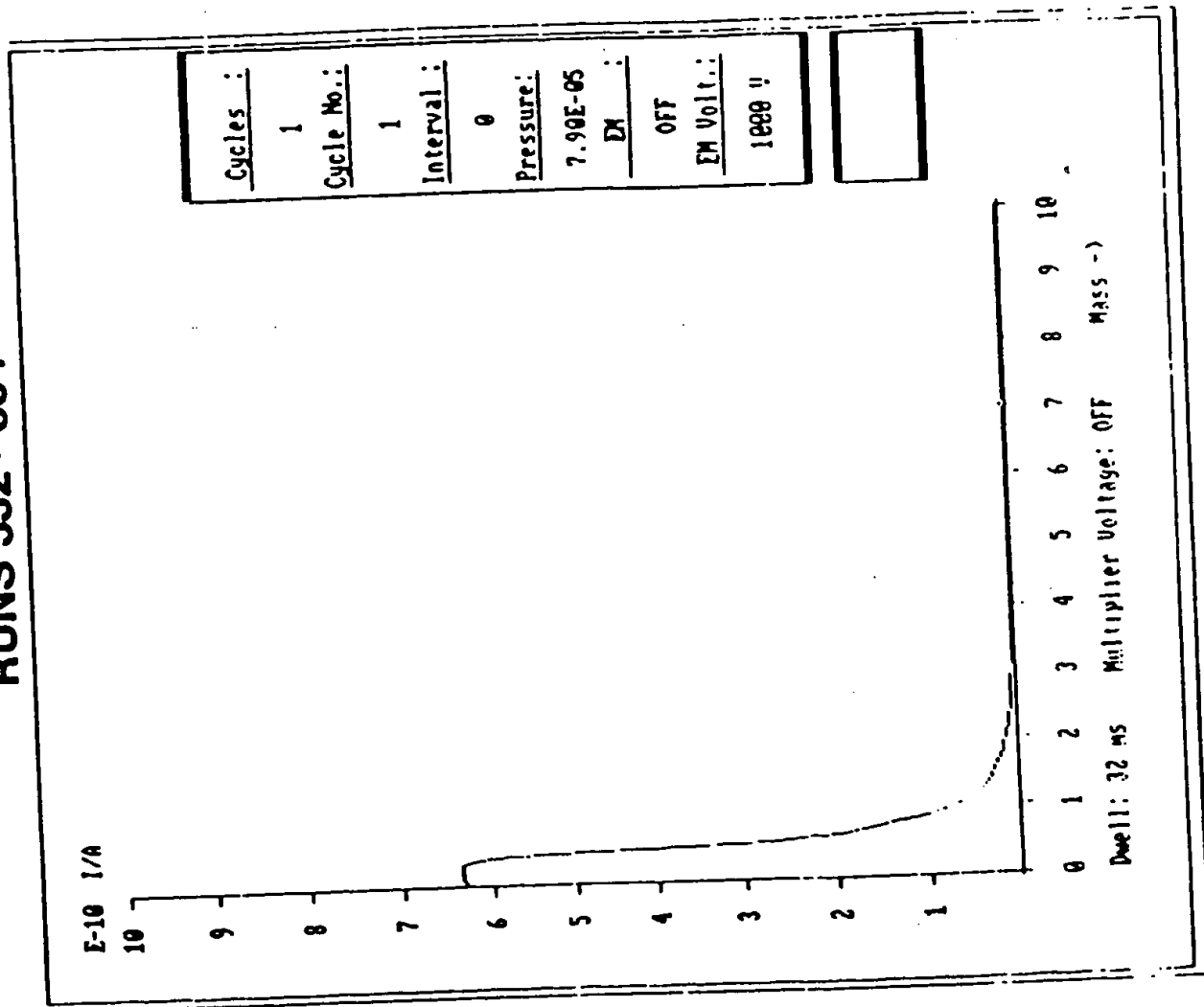


"PROCESSED CELL GAS"

RUNS 332 - 334



"PROCESSED CELL GAS RUNS 332 - 334



ISOTOPIC RATIOS - HD/H₂

SAMPLE	TEST PRESSURE TORR	3/2 RATIO
BOTTLE HYDROGEN	1.3 x 10 ⁻⁴	0.052
LAB DI WATER	9.8 x 10 ⁻⁵	0.035
CELL GAS	9.7 x 10 ⁻⁵	0.025
RECOMBINER WATER	8.9 x 10 ⁻⁵	0.031
CELL ELECTROLYTE	9.9 x 10 ⁻⁵	0.044



WHAT TO DO NEXT FOR HIGHER ENERGY

- STUDY GAS CELL WHICH HAS MUCH HIGHER ENERGY DENSITY
 - HYDROCATALYSIS WILL PAY -- CRDA ?
- TEST PALLADIUM - SILVER COATED NICKEL WIRE WITH D_2O SYSTEM ACC CONTINUATION ?
- INVESTIGATE TUBULAR REACTOR USING PALLADIUM - SILVER



CONCLUSIONS

- EXCESS ENERGY IS PRESENT AT 0.5 TO 5 W LEVEL
0.5 TO 2.5° ABOVE CALIBRATION

TEMPERATURE CALIBRATIONS $\pm .02^{\circ}\text{C}$

- GAINS ARE HIGH 5 TO 14 x NET INPUT
1.5 TO 4 x GROSS VI INPUT

BUT ONLY AT 1-4 W EXCESS

- SOURCE IS NOT DETERMINED

- LOWER STATE HYDROGEN WAS NOT FOUND - WHY ?
 - A) NOT THERE
 - B) CHEMICALLY MORE REACTIVE THAN REPORTED
EASILY ABSORBED IN METAL

- ISOTOPIC RATIOS CONSISTENT WITH ELECTROLYTIC CELL
DECOMPOSITION OF WATER

- CANNOT PROVE OR DISPROVE POSSIBLE EXPLANATIONS
FOR EXCESS HEAT



cf/chuck/4/20